

Lecture Notes in Civil Engineering

David Bienvenido-Huertas  
Juan Moyano-Campos *Editors*

# New Technologies in Building and Construction

Towards Sustainable Development

 Springer

# Lecture Notes in Civil Engineering

Volume 258

## Series Editors

Marco di Prisco, Politecnico di Milano, Milano, Italy

Sheng-Hong Chen, School of Water Resources and Hydropower Engineering,  
Wuhan University, Wuhan, China

Ioannis Vayas, Institute of Steel Structures, National Technical University of  
Athens, Athens, Greece

Sanjay Kumar Shukla, School of Engineering, Edith Cowan University, Joondalup,  
WA, Australia

Anuj Sharma, Iowa State University, Ames, IA, USA

Nagesh Kumar, Department of Civil Engineering, Indian Institute of Science  
Bangalore, Bengaluru, Karnataka, India

Chien Ming Wang, School of Civil Engineering, The University of Queensland,  
Brisbane, QLD, Australia

**Lecture Notes in Civil Engineering (LNCE)** publishes the latest developments in Civil Engineering - quickly, informally and in top quality. Though original research reported in proceedings and post-proceedings represents the core of LNCE, edited volumes of exceptionally high quality and interest may also be considered for publication. Volumes published in LNCE embrace all aspects and subfields of, as well as new challenges in, Civil Engineering. Topics in the series include:

- Construction and Structural Mechanics
- Building Materials
- Concrete, Steel and Timber Structures
- Geotechnical Engineering
- Earthquake Engineering
- Coastal Engineering
- Ocean and Offshore Engineering; Ships and Floating Structures
- Hydraulics, Hydrology and Water Resources Engineering
- Environmental Engineering and Sustainability
- Structural Health and Monitoring
- Surveying and Geographical Information Systems
- Indoor Environments
- Transportation and Traffic
- Risk Analysis
- Safety and Security

To submit a proposal or request further information, please contact the appropriate Springer Editor:

- Pierpaolo Riva at [pierpaolo.riva@springer.com](mailto:pierpaolo.riva@springer.com) (Europe and Americas);
- Swati Meherishi at [swati.meherishi@springer.com](mailto:swati.meherishi@springer.com) (Asia - except China, and Australia, New Zealand);
- Wayne Hu at [wayne.hu@springer.com](mailto:wayne.hu@springer.com) (China).

**All books in the series now indexed by Scopus and EI Compendex database!**

More information about this series at <https://link.springer.com/bookseries/15087>

David Bienvenido-Huertas · Juan Moyano-Campos  
Editors


# New Technologies in Building and Construction

Towards Sustainable Development

 Springer



*Editors*

David Bienvenido-Huertas   
Department of Building Construction  
University of Granada  
Granada, Spain

Juan Moyano-Campos  
Department of Graphical Expression  
and Building Engineering  
University of Seville  
Seville, Spain

ISSN 2366-2557

ISSN 2366-2565 (electronic)

Lecture Notes in Civil Engineering

ISBN 978-981-19-1893-3

ISBN 978-981-19-1894-0 (eBook)

<https://doi.org/10.1007/978-981-19-1894-0>

© The Editor(s) (if applicable) and The Author(s), under exclusive license to Springer Nature Singapore Pte Ltd. 2022

This work is subject to copyright. All rights are solely and exclusively licensed by the Publisher, whether the whole or part of the material is concerned, specifically the rights of translation, reprinting, reuse of illustrations, recitation, broadcasting, reproduction on microfilms or in any other physical way, and transmission or information storage and retrieval, electronic adaptation, computer software, or by similar or dissimilar methodology now known or hereafter developed.

The use of general descriptive names, registered names, trademarks, service marks, etc. in this publication does not imply, even in the absence of a specific statement, that such names are exempt from the relevant protective laws and regulations and therefore free for general use.

The publisher, the authors and the editors are safe to assume that the advice and information in this book are believed to be true and accurate at the date of publication. Neither the publisher nor the authors or the editors give a warranty, expressed or implied, with respect to the material contained herein or for any errors or omissions that may have been made. The publisher remains neutral with regard to jurisdictional claims in published maps and institutional affiliations.

This Springer imprint is published by the registered company Springer Nature Singapore Pte Ltd. The registered company address is: 152 Beach Road, #21-01/04 Gateway East, Singapore 189721, Singapore

# Preface

This book presents contributions on new technologies in building and construction. Buildings are complex elements that impact environment significantly. The sustainability of this sector requires a holistic and multidisciplinary approach that allows adequate strategies to be established to reduce its environmental impact. This heterogeneity is represented in these chapters, which have been developed by researchers from different countries. The book is divided into three parts: (i) analysis, (ii) design and modeling, and (iii) solutions.

In the analysis part, techniques and methodologies are included to characterize different building variables. In this regard, the techniques related to thermal characterization, sealing, energy performance, and the assessment of indirect issues, such as energy poverty, are grouped together. The use of the techniques allows the building to appropriately continue with the aspects mentioned in the next sections.

In the design and modeling part, research studies on the use of new digitization technologies in buildings are collected. The use of these technologies in historic buildings constitutes a great challenge, especially if the goal is to develop BIM models to propose future action measures. In this sense, the chapters analyze aspects such as the use of digitization techniques, the introduction of data in the models, and the generation of predictive models. Thus, the analysis of the buildings through the techniques described in the first part allows to generate the model of the building.

Finally, in the solution part, research studies present improvements in building processes. The proposed solutions contribute to dealing with the sustainability of the analyzed and modeled buildings. In this regard, measures including the use of more sustainable materials, the design of better facilities, and the more sophisticated use of BIM are proposed.

The 23 chapters of the book represent an advance in current knowledge about new technologies in building and construction, which is crucial for academics, researchers, architects, engineers, and professionals from the sector.

Granada, Spain  
Seville, Spain

David Bienvenido-Huertas  
Juan Moyano-Campos

# Contents

## Analysis

<b>Application of Qualitative and Quantitative Infrared Thermography at Urban Level: Potential and Limitations</b> .....	3
Blanca Tejedor, Elena Lucchi, and Iole Nardi	
<b>Temperature-Based Approach for In Situ Evaluation of Thermal Transmittance of Building Walls</b> .....	21
Mihaela Domazetović and Hrvoje Krstić	
<b>Combining Characterization Tests of Building Envelope Thermal Transmittance with the Acoustic Characterization Through Data Mining Approaches</b> .....	37
Krizia Berti, Blanca Tejedor, Joaquín Durán, and David Bienvenido-Huertas	
<b>Methodology for the Evaluation of an Energetic Model of Thermal Transmittance in a Window by Means of Horizontal Aggregation (HA) from Short-range Photogrammetry for Model Digital Twin</b> .....	47
María Fernández-Alconchel, Juan E. Nieto-Julián, Manuel J. Carretero-Ayuso, and Juan Moyano-Campos	
<b>Comparative Analysis of the Influence of the Convective Term in the Quantitative Assessment by Infrared Thermography</b> .....	67
David Bienvenido-Huertas, Blanca Tejedor, David Marín-García, and Joaquín Durán	
<b>In Situ Methodology to Assess the Action of Water-Wind on Building Windows</b> .....	89
Manuel J. Carretero-Ayuso, David Bienvenido-Huertas, and Carlos E. Rodríguez-Jiménez	

<b>Outdoor Microclimate Influence on Building Performance: Simulation Tools, Challenges, and Opportunities</b> .....	103
Victoria Patricia López-Cabeza, Jesus Lizana, Eduardo Diz-Mellado, Carlos Rivera-Gómez, and Carmen Galán-Marín	
<b>Identifying and Describing Energy-Poor Household Groups. A Comparison Between Two Different Methods: Conventional Statistical Characterisation and Artificial Intelligence-Driven Clusterisation</b> .....	123
Ana Sanz Fernández, Miguel Núñez Peiró, José Antonio Iglesias Martínez, Agapito Ismael Ledezma Espino, Carmen Sánchez-Guevara Sánchez, and Marta Gayoso Heredia	
<b>Design and Modelling</b>	
<b>BIM Technology in Green Buildings: Integrating BIM with Greenery Systems</b> .....	141
Mitra Manouchehri, Mercedes Valiente López, and Joaquín Santiago López	
<b>New Trends in Laser Scanning for Cultural Heritage</b> .....	167
Jesús Balado, Ernesto Frías, Silvia M. González-Collazo, and Lucía Díaz-Vilariño	
<b>Technological Paradigms for Cultural Heritage. A Scan To BIM Methodology for the Description of Historical Architecture</b> .....	187
Cesare Verdoscia, Michele Buldo, Antonella Musicco, and Riccardo Tavolare	
<b>Laser Scanning Intensity Fingerprint: 3D Visualisation and Analysis of Building Surface Deficiencies</b> .....	207
Daniel Antón, Manuel J. Carretero-Ayuso, Juan Moyano-Campos, and Juan E. Nieto-Julián	
<b>The Semantic Discretization of Architectural Heritage as the Basis of a HBIM Restoration and Conservation Project</b> .....	225
Juan E. Nieto-Julián, Javier Farratell, Manuel Bouzas Cavada, and Juan Moyano-Campos	
<b>Integrating Artificial Intelligence Approaches for Quantitative and Qualitative Analysis in H-BIM</b> .....	243
David Bienvenido-Huertas, Blanca Tejedor, Manuel J. Carretero-Ayuso, Carlos E. Rodríguez Jiménez, and Marta Torres-González	

**Solutions**

**Properties of Gypsum Mortars Dosed with LFS for Use in the Design of Prefabricated Blocks** ..... 265  
 Isabel Santamaría-Vicario, Álvaro Alonso-Díez, Mathieu Horgnies, and Ángel Rodríguez-Saiz

**Lightweight Recycled Polyurethane Mortar Placement: A Case of Success** ..... 283  
 Verónica Calderón, Lourdes Alameda Cuenca-Romero, Sara Gutiérrez-González, and Raquel Arroyo

**Earth as a Sustainable Construction Material. Characterization of Different Mixtures and Implementation Using the Projected Earth System** ..... 299  
 Ignacio Valverde-Palacios, Raquel Fuentes-García, Ana Cervilla-Maldonado, and Ignacio Valverde-Espinosa

**Sustainability Challenges in Outdoor Swimming Pools** ..... 321  
 Miguel José Oliveira, Fátima Farinha, Armando Inverno, Jânio Monteiro, Cristiano Cabrita, and Adelino Venturinha

**Reality of Photovoltaic Technology Applied to Homes not Connected to the Grid Connected Using Lithium Batteries Without Generator Set Support** ..... 337  
 David Marín-García

**Extracting Energy from Flooded Coal Mines for Heating and Air-Conditioning of Buildings: Opportunities and Challenges** ..... 353  
 Amin Al-Habaibeh, Bubaker Shakmak, Anup Athresh, Keith Parker, and Omar Hamza

**Towards a Simple Cold Box Adapted to Warm Climates: A Case Study in Mediterranean Climate** ..... 367  
 David Bienvenido-Huertas, Manuel J. Carretero-Ayuso, David Marín-García, and Joaquín Durán

**Information Systematisation Towards Rational Building Maintenance Decisions** ..... 379  
 Clara Pereira, Ana Silva, Cláudia Ferreira, Jorge de Brito, Inês Flores-Colen, and José D. Silvestre

**Integrated Design of Building Projects: From BIM to Additive Manufacturing** ..... 421  
 Eric Forcael, Rodrigo García-Alvarado, Jaime Soto-Muñoz, and Jesús Alberto Pulido-Arcas

# Analysis

# Application of Qualitative and Quantitative Infrared Thermography at Urban Level: Potential and Limitations



Blanca Tejedor, Elena Lucchi, and Iole Nardi

**Abstract** In recent years, the usefulness of infrared thermography (IRT) has been extended to multiple scenarios, due to several benefits: rapid inspection, multi-point detection, real-time monitoring, etc. However, the range of applicability can vary from the single building inspection to the analysis of municipalities. This chapter outlines the most common techniques based on qualitative and quantitative infrared thermography (IRT) for the diagnosis of elements at urban level, assessing different types of instrumentation (i.e., drones, vehicles, and portable cameras) for three representative investigated objects: building envelopes, PV panels, and urban heat island (UHI) effect.

**Keywords** Infrared thermography · Building envelopes · Urban heat island (UHI) · Photovoltaics (PV)

## 1 Introduction

Infrared thermography (IRT) allows to detect the infrared radiation (IR) emitted by a body and to convert it into the temperature of the body itself, providing its temperature pattern (thermal image).

This is a technique born for military purposes and spread to several fields of investigation: human and veterinary medicine, cultural heritage preservation, and botany to mechanical engineering. Its history has been recalled in [1], and it is strictly linked to the development and production sensors capable of offering a higher

---

B. Tejedor (✉)

Department of Project and Construction Engineering, Group of Construction Research and Innovation (GRIC), Universitat Politècnica de Catalunya (UPC), C/Colom, 11, Ed. TR5, 08222 Terrassa (Barcelona), Spain  
e-mail: [blanca.tejedor@upc.edu](mailto:blanca.tejedor@upc.edu)

E. Lucchi

Institute for Renewable Energy, EURAC Research, Viale Druso 1, I-39100 Bolzano, Italy

I. Nardi

ENEA Casaccia Research Center, via Anguillarese, 301, S.M. Di Galeria, I 00123 Rome, Italy

resolution with lower cost [2]. The different fields of IRT usefulness lead to a wide range of employment scenarios [3], which differ in: (i) the approaches (passive or active); (ii) the relative motion of camera and object (static or dynamic); (iii) the energy source; (iv) excitation form; (v) the way energy is transferred or generated (transmission, reflection or internal); and (vi) scanning way. The thermal resolution of an IR camera is influenced by a series of features and properties, which is summarized in Fig. 1.

Building and construction is probably among the fields that mostly benefited from the introduction, development, and employment of this non-destructive, non-invasive, and contactless technique. These characteristics add up to the real-time investigation, multi-point detection, and digital image collection [4]. The need for rapid inspection of wide areas has led the development of technologies and instrumentation that could facilitate this task over the years.

Indeed, the applicability of IRT ranges from the single building inspection to the analysis of sets of buildings or neighborhoods (Fig. 2), implementing different types of instrumentation (i.e., drones, vehicles, and portable cameras). This can involve the assessment of several targets: built quality of envelopes and preventive maintenance (i.e., detection of anomalies like heat losses, thermal bridges, and moisture); PV panels faults through corrective maintenance; and urban heat island (UHI) effect among others.

<i>Feature</i>	<i>Operative description</i>	<i>Property</i>
<b>SPECTRAL RESOLUTION</b>	Portion of the electromagnetic spectrum to which the IR camera sensor (detector) is sensible (generally, for building and construction sector, it is referred to long wavelength infrared radiation (8–14 μm))	Wavelength
<b>SPATIAL RESOLUTION</b>	The smallest discernable target measurable by the detector.	IFOV
<b>RADIOMETRIC RESOLUTION</b>	The smallest temperature difference that can be perceived by the camera pixels.	NEDT
<b>TEMPORAL RESOLUTION</b>	Image refresh frequency in the camera	

**Fig. 1** IR camera features and properties

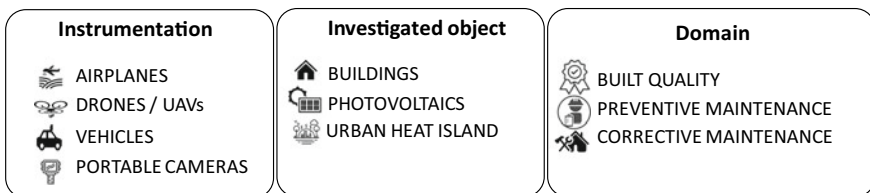


**Fig. 2** IRT instrumentation



Within this context, the following sections pretend to overview the aspects mentioned above, highlighting the current state of IRT instrumentation and the most common investigated objects at urban level.

## 2 Instrumentation

Information provided by IRT become even more useful when they are coupled with those from other techniques: visual inspection, heat flow meter method, moisture measurement, and city geometry models among others. When techniques are fused and mixed, their strength points are enhanced by a multi-disciplinary approach, whose aim is to provide a depiction of the investigated object as much complete as possible, avoiding misinterpretations and errors. By way of example, some studies are reported below. Fox et al. [4] proposed a useful classification of the passive technique. Lucchi et al. [1] reviewed the employment of IRT in energy audits. Later, Kirmat et al. [5] pointed out the main differences between passive and active approaches. Morrison et al. [6] analyzed the IRT at urban level to investigate the variability of surfaces temperature of several building and of vegetation and grass, coupling with modeling of urban geometries or materials properties. The work, besides focusing on the importance of camera sensors and their positioning, and of materials properties, aimed to highlight the importance of shadows in the temperature reading.

According to these works, the following methodologies (briefly described in the following) can be outlined: (i) aerial surveys; (ii) automated fly-past surveys; (iii) street pass-by surveys; (iv) walk-around surveys; (v) walk-through survey; (vi) repeat survey; and (vii) time-lapse survey. Such techniques differ in execution time, post-process time, cost, spatial resolution, need for specialized personnel, urban level at which they are employed, etc. (Fig. 3).

**Aerial thermography** (aIRT) is carried out when an airplane (or a helicopter as well) is equipped with an IR camera, and it flies over the area to be investigated. Normally, several flights are needed to have a proper depiction of the area. Given the survey typology, the portion investigated is the unique that faces the sky. Therefore, building roofs, PV panels, and vegetation foliage can be detected. From this kind of approach, even energy models of cities can be retrieved [7]. The flight altitude can be 350–450 m, and from that, distance images could not have the proper spatial resolution. It can somehow be included in this category also the investigations carried out from satellites that acquire with good quality information on the Earth surface, including thermal pattern. It is worth noting that, given the high distance between sensor and object, the spatial resolution is quite high in these cases (about 1 km<sup>2</sup>) [8], so data must be validated with point measurements. The complexity of this method is clearly shown in [9], where the principles of infrared machine vision are exposed, as well as the application of deep learning.

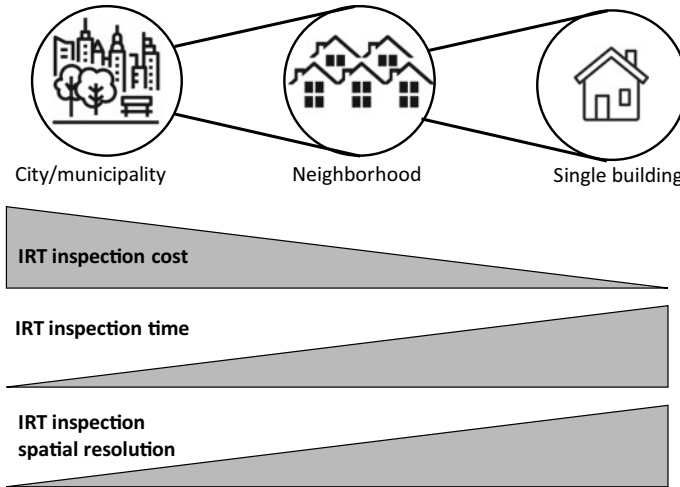


**Fig. 3** IRT characteristics at different urban levels

**Automated fly-past** employs the same principle, by using drones or small aircrafts, whose flight altitude is lower (50–100 m). Unmanned aerial systems (UAS) or vehicles (UAV) are employed very frequently in combination with thermographic inspection. An interesting review on their application has been recently proposed [10], where it emerged that the 29% of the considered publications (which account for a total of 92 on the topic) are referred to the building science. In fact, it has been also presented a decision tree for the UAS literature investigation, where importance is given to the drone flight path planning, that concerns not only the survey location but also the audit focus (windows, roof, landscape, etc.) and the flight path pattern (distance from surface, bearing angle, and altitude). The costs of such apparatuses are quite high, so some researchers are looking for less expensive solution. It is the case of [11], who self-assembled a low-cost drone with IR camera. Nevertheless, some encouraging results have been recently proposed, as widely illustrated in [12] where machine learning is employed. In that work, a review on thermal measurement technique is carried out, by grouping according to type (passive/active—qualitative/quantitative), method, application (overall building evaluation, insulation, thermal bridge or air leakage assessment, moisture detection) and quantification index (like the overall thermal transfer value—OTTV). Moreover, a data-driven framework has been used for estimating the energy loss by employing thermal images from UAS. Then, machine learning has been used to post-process data images and retrieve the U-value of different building elements (window, wall, and roof). In [13], unmanned aerial vehicles (UAVs) were implemented for quantitative analysis of the thermal properties of building envelopes (i.e., measurement of the thermal transmittance or U-value via IRT). Results have been compared with heat flow measurement (HFM) method, and a sensitivity analysis has also been conducted, showing the influence of the radiosity of the test object, the background reflection, and air temperature.

The frontiers of drones in construction sector are multiple, ranging from the integration of the retrieved information with the building energy model (BEM) for the identification of the more suitable energy renovation strategies of maintenance interventions [14], to the calibration of outdoor microclimate simulation models [15], to the inspection of structures difficult to be accessed like decks [16, 17].

Of course, more common vehicles can be used as mobile support for an IR camera. That is how the **street pass-by** thermography originates. This is a useful way to rapidly investigate a multitude of building facades and structures, and to assess the thermal bridges or air leakages that might occur. The principle is similar to that of “Google Map” cars, where the thermal images of the surroundings are acquired. Although this kind of vehicle runs the street at low speed (to sketch details), this technique is still not enough precise to retrieve quantitative information. The object or wall emissivity should be properly set to have reliable quantitative results. In addition, the viewing angle plays a key role in the final image.

Another application of IRT is the man-based one, meaning that physically an operator, equipped with an IR camera, shoots the building or object of interest. Hence, the thermal images are acquired at pedestrian level but might also sketch relevant portion of buildings when perspective angles are employed. This approach is referred to as **walk-around**, since the object is observed from outside, by walking around it. Otherwise, when it is possible (or needed) to enter the building, the IR is called **walk-through**, meaning that the inspection is acquired from both side of the building. Regarding the walk-around thermography, it must be pointed out that on one hand it provides thermal information on façades human height, i.e., where they are not sketched by aerial or automated fly-past devices. Moreover, this method has lower costs, and it overcomes the inconvenience of a flight plan (needed for satellite, aerial, or airborne devices). On the other hand, some inconvenience arises, like the perspective of the thermal images. In this sense, a pixel-by-pixel rectification can be carried out [18]. This method can be also correlated to other techniques, like imaging from satellites, as also reported in [19]. The walk-through approach requires to access to the building and to possibly interfere with the normal activities inside it. To give an example, if a school façade is inspected by the indoor environment, thermal images of wall might include whiteboard, drawing, maps, and similar. Furthermore, this approach is quite time-consuming when several rooms or spaces must be analyzed. However, the information provided can be more accurate, since sky conditions and boundary conditions are more stable. In this case, the spatial resolution is high, given the fact that objects can be observed by a short distance.

Being the IRT a non-invasive and non-destructive technique, it can be employed as many times as needed, even on the same investigation object. This could be helpful, for instance, to monitor over the time the variations or modifications occurred to the object. Hence, there is the need to **repeat survey**, that is, to carry out an IR campaign on the same object from the same viewing angle at the same (or quite same) conditions at fixed time intervals (order of months or years). This helps to identify possible incoming damages before they become serious. Hence, IR is used for predictive maintenance to verify the health of the built environment [5], and of the technical plants that serve it, and for condition monitoring [20]. Repeated survey

can also be useful to assess the quality and effectiveness of interventions once they are realized. For instance, IR repeat survey can be applied for assessing materials aging [21, 22], weathering [23, 24], faults [25, 26], detachment [27, 28], moisture [29, 30], degradation [31, 32], and so on.

The aforementioned methodologies referred to the analysis of thermal images that “freeze” the IR emission of the bodies into a thermal image. Despite this, there might be the need of assessing the dynamic behavior of materials. That is the birth of the **time-lapse** method that allows to see the transient phenomena over the decided time interval. Some works refer to time-lapse active thermography, but when buildings are concerned, the passive method is preferable. The time-lapse method consists in acquiring a series of thermal images at fixed acquisition rate, to visualize the changes in thermal pattern due to phenomena that change over time that might be incoming moisture, heat releases, etc. Some IR cameras have the possibility of recording videos; others involve the post-processing of a series of thermal images. The time-lapse survey allows to have both qualitative and quantitative information, according to the purpose and to the post-processing method. The time-lapse approach suffers for the variability of boundary conditions during the acquisition. The different approaches hereby mentioned differ for the cost (equipment plus survey), for the time taken by the survey, and also for the sizes of the investigated area, that often compensate with the spatial resolution. In Fig. 4, methods are qualitatively compared, while repeat survey and time-lapse are not reported since the concern the way methods can be applied.

Given the characteristics of the methods, several investigated objects can be distinguished at urban context (i.e., building façade, roof, pavement, photovoltaic installations, etc.). In Fig. 5, a summary of the methods is reported, for the analysis of the elements deepened in the following sections.





	Cost	Time	Investigated area	Spatial resolution
Aerial survey 	●●●●	●○○○	●●●●	●○○○
Automated fly-past 	●●●○	●○○○	●●●○	●●○○
Street pass-by 	●○○○	●●●○	●●●○	●●●○
Walk-around 	●○○○	●●●●	●●○○	●●●●

Fig. 4 IRT methods for surveys at urban level

	Aerial	Automated fly-past	Street pass by	Walk-around
Façade	✗	✓	✓	✓
Roof	✓	✓	✗	✗
Pavement	✓	✓	✓	✓
Photovoltaics	✗	✓	✗	✓
UHI	✗	✓	✗	✓

Fig. 5 Methods for investigated objects

### 3 Investigated Object

#### 3.1 Building Envelope

IRT has been widely employed to assess possible thermal anomalies and damages on the building envelope. Qualitative and quantitative analyses can be conducted to determine: (i) thermal characterization of building surfaces; (ii) thermal bridges; (iii) detachments; (iv) U-value measurements; (v) air leakages; (vi) moisture or rising damp; and (vii) cracks [1, 33–37].

Initially, mainly ground-based IRT, such as walk-around and walk-through survey, was applied in a qualitative way for the thermal characterization of building surfaces concerning wall thicknesses, presence of different building components, surface properties (especially the thermal emissivity, also called  $\epsilon$ -value), and energy problems related to layering technique [1]. This survey follows specific standard procedures, which requires the control of weather, boundary conditions, and environmental conditions [1]. Besides, thermal bridges, defined as additional heat losses in the building façade, might be due to structural elements (beams) or to geometry (like corners) and, in general, those points where a discontinuity causes an increase in heat flow. Therefore, they appear as hotter zone [38]. Detachments, instead, are those points where the plaster (or covering or coating) is separated from the wall. The air that is entrapped into the detachment causes an alteration on the heat flow, and it can be revealed by thermal inspection. The explanation of this phenomenon can be applied to moisture or rising damp: the water that goes from the ground to the wall appears as a colder region of the thermal image. The same applies to seepages, when drainpipes cause the water to flow along the wall or when there are voids, holes of discontinuity in the ceiling materials that allow water penetration. In a qualitative approach, even cracks and structural detachment can be revealed, especially to older buildings (like historical buildings) or churches or bridges. The quantitative approach, instead, entails the need to quantify the energy losses, by providing the capability of the investigated object of transferring heat [23, 39]. Different building elements can be assessed, from thermal bridges [37, 40] to entire façades [36, 41, 42]. Regarding the vertical opaque wall, different approaches are proposed in literature,

depending on the need to access the building for the inspection. This applies both for the current wall and for the thermal bridges. In general, methods that do not require to access the building suffer for the variability of the boundary conditions (weather, sky radiation, humidity, direct solar radiation, wind speed, and direction), while those approached that are performed from indoor overcome these issues but require the permission of the occupants, and might require to move furniture or paintings and, in general, those objects and stuff that prevent a good image [36].

More recently, an IRT and automated fly-past in building inspections was performed for visualizing the thermal patterns within the envelope and the heat movements through and across different materials [10]. UAS and UAV, particularly, are low-cost and highly productive solutions for a large range of applications related to inspections and fault detection that requires non-destructive testing capabilities [4]. This approach reduces the manual workflow of processing and post-processing, also speeding the surveys on large buildings at reduced costs [10]. Besides, it imaging aids in client communications [43]. Also, physical risks, costs, limitations, and psychological impacts of human-UAV interactions have been deeply analyzed for identifying a road map to advance their knowledge [43]. The main sectors for their application are: (i) heat and water flow detection; (ii) thermal bridges; and (ii) U-value measurements. Heat flow detection refers to the identification of heat losses or/and water leakages on large building façades and roofs. Only few studies have been realized. To this purpose, Entrop et al. [44] developed a real-time approach that combines IRT with UAV for detecting remotely heat/water leakages in building structures to solve time and cost problems. Limitations of this approach are connected to the difficulties of sensing every portion of a large or complex building and saving and recording the IR images on 3D maps. Benefits are related to the accurately and rapidly examination of large areas reducing costs and safety risks. Besides, Benz et al. [45] introduced a general framework for the conventional qualitative assessments of thermal bridges and air leakages through a UAS-based assessment of IR thermograms. Otherwise, Bayomi et al. [14] identified a series of information on material deterioration and heat losses thanks to the thermal anomalies captured by a drone equipped with an IR camera. On the contrary, several studies estimated the U-value of the building envelope from UAV data. In general, the U-value is estimated using air temperature difference between outdoor and indoor conditions recorded simultaneously, respectively, with UAV and indoor-held IR camera. To this purpose, Sadhukhan et al. [12] and Bayomi et al. [14] installed thermocouples to verify the surface temperatures of the IR images, and internal and external sensors to measure air temperature. Besides, Benz et al. [45] mounted an external thermal sensor for each thermogram and matched this value with the temperature produced by the sensor spot to calibrate the U-value estimation. Several suggestions have been defined for improving the accuracy of the U-value measurements with IRT. First, the UAS flight should be planned in thermally steady phase of the façade and during precise measurement of the environmental conditions [45]. Better conditions are cloudy morning or evening hours, without precipitation and with stable temperatures [10]. A difference of 10 K between indoor and outdoor temperature is suggested [10]. Also, to reduce the error incorporated by the view angle, the orthogonal orientation of thermograms and the

surface should be maintained [45]. Besides, the effects of solar irradiance must be avoided [12].

The challenges found for remotely piloted aircrafts in building inspection include [10]: (i) limitations in global positioning system (GPS) positioning and battery power, (ii) interferences with UAS and possible crashing, (iii) difficulties to reach building components for aIRT and UAS size and navigation; (iv) operation vibrations; and (v) risks in signal acquisition and interpretation. Like other applications, also in the energy audit, the accuracy of the drone flight depends on the accuracy of the GPS and inertial navigation system (INS). The root mean square error specifically is less with onboard GPS than with ground control points [10]. The technological advance in the automation sector is moving through the reduction of dimensions, weights, and costs of drones, also increasing stability, payload capabilities, automated obstacle avoidance, and connectivity assurance [10]. A benefit is related to the safety of workers that can operate remotely also under critical circumstances thank to the onsite presence of drones [46]. The application of automated fly-past passive thermal inspection in the energy audit sector needs further experimentation-based research and standardizations for fault detection [10, 47]. Standardized procedures or equations particularly should be interest optimal distances of flight paths, flight speed for clarity, geometry analysis, and automated post-processing [10].

### 3.2 *PV Inspection*

Temperature distribution is an empirical way for detecting defects on PV modules and roofs. It is expected that well-performing PV cells or modules have uniform temperature distribution during normal operating conditions [48]. Defective PV systems produce temperature differences ( $\Delta T$ ) or thermal anomalies. For this reason, passive IRT (automated fly-past surveys, walk-around surveys) and active IRT (time-lapse survey) are used in a qualitative way for quality control [48]. Defects detectable on PV systems concern optical degradation (e.g., delamination, discoloration of the encapsulate, micro-cracks, front cover breakage, soiling/dust accumulation), electrical mismatches and degradation (e.g., lifetime stress, hot spot browning, cell cracks/fracture, inactive or disconnected strings, completely or partially inactive modules, corrosion, junction boxes, ribbons or connections breakage, poor soldering, shunts and short-circuited cells, snail trails, solder bond failures, shading), and non-classified imperfections (defective/short-circuited bypass diode, open-circuited submodule, loss of adhesion, anthropogenic impacts) [26, 47, 49–52]. These problems cause a reduction in module efficiency and represent an electrical risk for the operators [52].

In general, IR images for PV inspections are captured in the mid-wave (about 3–5  $\mu\text{m}$ ) or long-wave (7–14  $\mu\text{m}$ ) that considered a trade-off between data availability, measuring conditions of IR sensors, and costs [53]. PV inspections can be performed with ground-based and remotely piloted aircrafts IRT approaches. In both cases, they are more efficient combining RGB and IRT cameras, allowing a simultaneous



comparison of data to understand better the presence of shadow and specificities [47, 51].

Ground-based IRT uses handheld IR cameras on ground (called also walking method) or lifting platforms (called also crane/lift method) [54]. These methods are used for identifying and locating PV degradation and faults. In both cases, accurate PV inspections requires the selection of appropriate resolution and weight of the IR camera [54]. Camera resolution determines the monitoring distance and the accuracy of the surface temperature values [54]. Thus, high values should be chosen. Besides, low-weight cameras should be preferred as they influence the duration of the survey. The inclination of the camera lens influences the results of the survey. In both cases, the lens angle of the IR camera should be perpendicular to tilted module surface for acquiring adequate results. Walk-around surveys is high affected by the module inclination that should not less than  $15^\circ$  while crane/lift method that is less affected by module angles [54]. The first method is time-consuming and labor-intensive for the involvement of personnel walking the length of the array [48, 51]. The second one takes shorter times, but requires additionally footage to investigate some faults [54]. In both cases, the monitoring accuracy is prone to human error and competences [48].

The usage of remotely piloted aircrafts IRT in PV inspections grows considerably in the last decade to overcome the major drawbacks of the ground-based IRT, especially for utility-scale and large-scale PV power plants as well as for roof-mounted PV with limited access [47–52, 55]. They have multiple advantages, such as ability to reach difficult-access areas, large angles of vision, cost saving, increment of operator safety, reduction of data collection time, and operational risks [49]. Significantly reductions of inspection time (85%) have been found [48]. Otherwise, weaknesses refer to the lower image resolutions than ground-based IRT methods [51], sensitivity to environmental conditions [48], inaccuracy in hot-spots and micro-cracks detection and complexity and redundancy of IR image and data [48]. In this case, IRT measurements are performed outdoors, under steady-state illumination (i.e., clear-sky or maximum 2 non-cumulus cloud coverage) and maximum power-point conditions [26]. Mainly, UAS and drones are used for recognizing PV degradation and faults as well as problems caused by environmental events on PV roofs, such as windstorms, hailstorms, air turbulence, sunlight reflection, and lightning [51]. Similar to the ground-based IRT, the most important aspect for selecting the IR camera is resolution and weight, battery flight time, and lens type [51]. The resolution of the camera particularly determines the maximum flight height, strongly influencing the duration of the inspection [51]. This is a critical point for large-scale PV power plants, because normally the minimum irradiance conditions last around six hours per day [51]. In addition, stability of the system, flight duration, maximum payload, and compatibility between devices impacts on the quality and the cost of the inspection [51]. Various problems have been defined for remotely piloted aircrafts IRT on PV systems [26, 50, 53]: (i) other parts absorbed the incident radiation contributing to module heating (e.g., back sheet segment between the cells); (ii) high-temperature diffusion rate due to environmental conditions; (iii) absence of thermal stability for the changes in environmental conditions; and (iv) difficulties in detect defects that



do not act as local heat sources. To overcome many of these problems, the ideal conditions need the presence of constant and perpendicular orientation of the UAV-mounted or drone-mounted IRT sensor to the PV modules and a flight altitude at least of five meters to prevent self-shading [51]. Also, the inspection should carry out on cloudless, bright, and dry days, with reduced wind speed ( $<4$  m/s), a direction of the sun perpendicular to the PV modules, and an irradiance over  $600$  W/m<sup>2</sup> on the plane of the inspected PV array [51]. Actually, there is a lack of interpreting the defects of different PV technologies and their impact on the output power generation, especially when PV systems operate under changing environmental conditions [48]. In parallel, image processing is an important role in an IRT of PV panels. An accurate interpretation of a 3-dimensional (3D) ortho-mosaic for each single rooftop requires high overlapping rates between the images, which must contain azimuth, and tilts of the PV panels [56]. This situation is hard to reach for an autopilot operated pre-flight route setting for a specific area. Normally, unnecessary noise is generated on the thermal values and the exterior orientation parameters, such as the measurement of distances, angles, and PV areas [56]. This causes serious data redundancy. Thus, the importance of the interpretation of the thermal images and the correlation between performance degradation, fault types, and thermal signatures of PV modules is largely introduced [47, 50, 51]. To overcome this problematic, Hwang et al. [56] developed a 3D video stream-based ortho-mosaic for widely scattered PV roofs. Despite this, the processing phase requires standard specifications to reduce computational complexities and assessment error in the identification of PV defects [48]. In addition, several studies displayed the potential of automated inspections for increasing the speed of the survey and generating a great number of images. The models developed for the automatic detection of PV module defects using deep learning techniques obtained an average accuracy of 99% [47, 52, 57–59].

### 3.3 *Urban Heat Island (UHI)*

UHI effect is defined as an increase of temperatures in urban areas in comparison with rural areas [60–63]. It is estimated that the ambient air temperature can grow between  $3.6$  and  $5$  °C in the canopy layer due to UHI effect [64]. Consequently, the energy consumption of cooling systems is greater in cities [61, 62, 64, 65], reaching values between 18 and 43% over the reference load [66]. This phenomenon often occurs in crowded cities and small cities (i.e., Rome [64]; Barcelona [67]; Beijing [66]; Tehran [63]), which are characterized by public spaces where the thermophysical properties of historical buildings amplify the UHI as well [64, 68].

In most cities, 50–60% of urban areas are comprised of roof and pavement [62], and some materials present a significant temperature sensitivity (i.e., asphalt concrete pavement) [62, 64]. According to Lassandro et al. [69], building façades should have an adaptive capacity at short-term and long-term, to ensure functionality under unpredictable conditions such as heat waves. Within this context, United States Environment Protection Agency (USEPA) suggested to use “cool pavement.” In contrast to

the conventional material, cool pavement has a greater reflectance. Indeed, the pavement surface temperature can decrease 6 °C, if the increase of total reflectance/albedo is 0.1 [62]. This could help to reduce several significant parameters: citizens' thermal stress [61, 70], primary energy demand [61–63], and surface temperature and heat release [71]. Consequently, an improvement of the urban microclimate and outdoor thermal comfort of the population could be achieved [15].

However, few studies evaluated the optical properties of reflective pavement coatings (i.e., spectral full scales, pigments of the sample), and green and cool materials for pavements or walls are still in development [62]. Li et al. [72] assessed the seasonal effects of albedo or solar reflectivity on the thermal behavior of pavements, using a portable solar reflectometer and dual pyranometer with automatic data collection system. The authors demonstrated that the measured albedo was high in the early morning and in the evening, while it was low and constant in the mid-day. In addition, peak solar radiation intensity was positively correlated with the cooling effect. Sham et al. [60] quantified the sensible heat release generated by building fabrics in hot and cold seasons. The CSTM technique was implemented to capture a sequence of thermal images of a larger sample of buildings simultaneously. The findings suggested that finish materials (i.e., ceramic, granite, or aluminum), building features (i.e., orientation), and seasonal change could affect the cooling pattern. By way of example, the sensible heat release change presented lower percentages (6.7–9.7%) for granite and aluminum walls, regardless the season. Furthermore, the ratio between sensible heat release and global solar radiation was slightly similar in hot and cold season. Salata et al. [64] analyzed three mitigation strategies of UHI on 27 buildings of Sapienza University (Rome) during a heat wave: (i) urban greening; (ii) cool pavement; and (iii) cool roofs. To quantify the impact of such strategies, numerical simulations were computed using ENVI-met Software. This made possible to obtain the Mediterranean Outdoor Comfort Index (MOCI) as well as the hourly values of the ambient air temperature and the mean radiant temperature. The researchers extrapolated that the optimum solution was the combination of all strategies, since the health risk could be decreased between 60 and 80%. Nevertheless, the solution did not have a high influence on pedestrians. Aguerre et al. [70] compared a sequence of thermograms with simulated thermal models of a real urban district using finite element method (FEM), to evaluate the spatial distribution of the radiation emitted by urban surfaces and the influence on the outdoor thermal comfort. The authors stated that changing the reflectance of southern façades could lead to temperature differences of up 10 °C. Xie et al. [62] applied infrared thermography to assess temperature distribution and thermal performance of reflective coating samples. The researchers concluded that solar reflectance can be increased by pavement coatings doped with chrome and nano-pigments. Furthermore, the most influential reflectance values ranged from 400 to 1100 nm. Carpio et al. [73] carried out a bibliometric analysis about UHI from 1990 to 2019. The findings showed that the topic presented an increasing trend in relation to laboratory experiments and new techniques to evaluate concrete elements with infrared-reflective pigments. In addition, the authors noted that building fabrics, urban planning, and climate zone could be causal factors of UHI. Hence, mitigation strategies cannot be generalized across

the cities. It is required to adapt national building codes to local regulations. Fabbri et al. [15] considered that existing studies compared simulation results with punctual experimental measurements of ambient air temperature and mean radiant temperature. For this reason, the authors used infrared thermography to collect images of an urban area of Medicina (Italy) and subsequently, to calibrate holistic outdoor microclimate numerical models by ENVI-met Software. Overall, measured and simulated surface temperatures fitted well. The only limitation was given in areas with dense vegetation.

## 4 Conclusions

The International Energy Agency [IEA 2021] stated that cities are responsible for 75% of global energy use. For this reason, the diagnosis is essential at urban level (cities, neighborhood and single buildings). IRT is a non-invasive and accurate technique that provides real-time data in both qualitative and quantitative way. In fact, this chapter pointed out a wide range of instrumentation (i.e., drones, vehicles, and portable cameras), analyzing some key aspects: time of inspection, investigated area, cost and spatial resolution. It can be extrapolated that most of quantitative IRT applications are still ongoing. Some examples are exposed below. Data taken from neighborhoods and building with IR cameras installed on drones or vehicles cannot be directly integrated in building energy models (BEMs), and a calibration of model related to outdoor microclimate is required. Besides this, the incorporation a larger sensor network presents a high cost and post-processing time. Concerning PV panels, recent studies based on IRT and machine learning facilitated the tasks of preventive and corrective maintenance. Nevertheless, there is a gap for some research questions, such as correlation between defects and output power, additional noise in the measured parameters, technical problems of piloted aircrafts, etc. Regarding the UHI effect, IRT makes possible to identify and determine the most optimum mitigation strategy in cities, taking into account: building fabrics, urban planning, and climate zone. However, few studies were developed, and the analysis could be a challenging task in heavily vegetated areas.

## References

1. Lucchi E (2017) Applications of the infrared thermography in the energy audit of buildings: a review. *Renew Sustain Energ Rev* 0–1. <https://doi.org/10.1016/j.rser.2017.10.031>
2. Rogalski A (2012) History of infrared detectors. *Opto-Electron Rev* 20:279–308. <https://doi.org/10.2478/s11772-012-0037-7>
3. Ibarra-Castanedo C, Tarpani JR, Maldague XPV (2013) Nondestructive testing with thermography. *Eur J Phys* 34. <https://doi.org/10.1088/0143-0807/34/6/S91>

4. Fox M, Coley D, Goodhew S, De Wilde P (2014) Thermography methodologies for detecting energy related building defects. *Renew Sustain Energy Rev* 40:296–310. <https://doi.org/10.1016/j.rser.2014.07.188>
5. Kiritmat A, Krejcar O (2018) A review of infrared thermography for the investigation of building envelopes: advances and prospects. *Energ Build* 176:390–406. <https://doi.org/10.1016/j.enbuild.2018.07.052>
6. Morrison W, Kotthaus S, Grimmond S (2021) Urban surface temperature observations from ground-based thermography: intra- and inter-facet variability. *Urban Clim* 35:100748. <https://doi.org/10.1016/j.uclim.2020.100748>
7. Bitelli G, Conte P, Csoknyai T, Franci F, Girelli VA, Mandanici E (2015) Aerial thermography for energetic modelling of cities. *Rem Sens* 7:2152–2170. <https://doi.org/10.3390/rs70202152>
8. Irani Rahaghi A, Lemmin U, Sage D, Barry DA (2019) Achieving high-resolution thermal imagery in low-contrast lake surface waters by aerial remote sensing and image registration. *Rem Sens Environ* 221:773–783. <https://doi.org/10.1016/j.rse.2018.12.018>
9. He Y, Deng B, Wang H, Cheng L, Zhou K, Cai S, Ciampa F (2021) Infrared machine vision and infrared thermography with deep learning: a review. *Infrared Phys Technol* 116:103754. <https://doi.org/10.1016/j.infrared.2021.103754>
10. Rakha T, Gorodetsky A (2018) Review of Unmanned Aerial System (UAS) applications in the built environment: towards automated building inspection procedures using drones. *Autom Constr* 93:252–264. <https://doi.org/10.1016/j.autcon.2018.05.002>
11. Kayan H, Eslampanah R, Yeganli F, Askar M (2018) Heat leakage detection and surveillance using aerial thermography drone. In: 2018 26th IEEE signal processing and communications applications conference (SIU), pp. 1–4. <https://doi.org/10.1109/SIU.2018.8404366>
12. Sadhukhan D, Peri S, Sugunaraaj N, Biswas A, Selvaraj DF, Koiner K, Rosener A, Dunlevy M, Goveas N, Flynn D, Ranganathan P (2020) Estimating surface temperature from thermal imagery of buildings for accurate thermal transmittance (U-value): a machine learning perspective. *J Build Eng* 32:101637. <https://doi.org/10.1016/j.jobe.2020.101637>
13. Patel D, Schmiedt JE, Röger M, Hoffschmidt B (2018) Approach for external measurements of the heat transfer coefficient (U-value) of building envelope components using UAV based infrared thermography. 1–8. <http://www.qirt2018.de/portals/qirt18/doc/Fr.2.C.1.pdf>
14. Bayomi N, Nagpal S, Rakha T, Fernandez JE (2021) Building envelope modeling calibration using aerial thermography. *Energ Build* 233:110648. <https://doi.org/10.1016/j.enbuild.2020.110648>
15. Fabbri K, Costanzo V (2020) Drone-assisted infrared thermography for calibration of outdoor microclimate simulation models. *Sustain Cities Soc* 52:101855. <https://doi.org/10.1016/j.scs.2019.101855>
16. Omar T, Nehdi ML (2017) Remote sensing of concrete bridge decks using unmanned aerial vehicle infrared thermography. *Autom Constr* 83:360–371. <https://doi.org/10.1016/j.autcon.2017.06.024>
17. Biscarini C, Catapano I, Cavalagli N, Ludeno G, Pepe FA, Ubertini F (2020) UAV photogrammetry, infrared thermography and GPR for enhancing structural and material degradation evaluation of the Roman masonry bridge of Ponte Lucano in Italy. *NDT E Int* 115:102287. <https://doi.org/10.1016/j.ndteint.2020.102287>
18. Acuña Paz y Miño J, Dupont N, Beckers B (2021) Pixel-by-pixel rectification of urban perspective thermography. *Rem Sens Environ* 266:112689. <https://doi.org/10.1016/j.rse.2021.112689>
19. Hartz D, Prashad L, Hedquist BC, Golden J, Brazel AJ (2005) Linking satellite and hand-held infrared thermography to observed neighborhood climate conditions
20. Bagavathiappan S, Lahiri BB, Saravanan T, Philip J, Jayakumar T (2013) Infrared thermography for condition monitoring—a review. *Infrared Phys Technol* 60:35–55. <https://doi.org/10.1016/j.infrared.2013.03.006>
21. Kaplani E (2012) Detection of degradation effects in field-aged c-Si solar cells through IR thermography and digital image processing. *Int J Photoenergy* 2012. <https://doi.org/10.1155/2012/396792>

22. Nardi I, de Rubeis T, Perilli S (2016) Ageing effects on the thermal performance of two different well-insulated buildings. *Energy Procedia*. <https://doi.org/10.1016/j.egypro.2016.11.133>
23. Nardi I, De Rubeis T, Taddei M, Ambrosini D, Sfarra S (2017) The energy efficiency challenge for a historical building undergone to seismic and energy refurbishment. *Energy Procedia* 133:231–242. <https://doi.org/10.1016/j.egypro.2017.09.357>
24. Evangelisti L, Guattari C, Fontana L, De Lieto Vollaro R, Asdrubali F (2022) On the ageing and weathering effects in assembled modular facades: on-site experimental measurements in an Italian building of the 1960s. *J Build Eng* 45:103519. <https://doi.org/10.1016/j.job.2021.103519>
25. Schirripa Spagnolo G, Del Vecchio P, Makary G, Papalillo D, Martocchia A (2012) A review of IR thermography applied to PV systems. *IEEE*
26. Tsanakas JA, Ha L, Buerhop C (2016) Faults and infrared thermographic diagnosis in operating c-Si photovoltaic modules: a review of research and future challenges. *Renew Sustain Energy Rev* 62:695–709. <https://doi.org/10.1016/j.rser.2016.04.079>
27. De Freitas SS, De Freitas VP, Barreira E (2014) Detection of façade plaster detachments using infrared thermography—a nondestructive technique. *Constr Build Mater* 70:80–87. <https://doi.org/10.1016/j.conbuildmat.2014.07.094>
28. Lourenço T, Matias L, Faria P (2017) Anomalies detection in adhesive wall tiling systems by infrared thermography. *Constr Build Mater* 148:419–428. <https://doi.org/10.1016/j.conbuildmat.2017.05.052>
29. Edis E, Flores-Colen I, de Brito J (2015) Quasi-quantitative infrared thermographic detection of moisture variation in facades with adhered ceramic cladding using principal component analysis. *Build Environ* 94:97–108. <https://doi.org/10.1016/j.buildenv.2015.07.027>
30. Barbosa MTG, Rosse VJ, Laurindo NG (2021) Thermography evaluation strategy proposal due moisture damage on building facades. *J Build Eng* 43:102555. <https://doi.org/10.1016/j.job.2021.102555>
31. Kordatos EZ, Exarchos DA, Stavrakos C, Moropoulou A, Matikas TE (2013) Infrared thermographic inspection of murals and characterization of degradation in historic monuments. *Constr Build Mater* 48:1261–1265. <https://doi.org/10.1016/j.conbuildmat.2012.06.062>
32. Menezes A, Glória Gomes M, Flores-Colen I (2015) In-situ assessment of physical performance and degradation analysis of rendering walls. *Constr Build Mater* 75:283–292. <https://doi.org/10.1016/j.conbuildmat.2014.11.039>
33. Paoletti D, Ambrosini D, Sfarra S, Bisegna F (2013) Preventive thermographic diagnosis of historical buildings for consolidation. *J Cult Herit* 14:116–121. <https://doi.org/10.1016/j.culher.2012.05.005>
34. Lerma C, Mas A, Gil E, Vercher J, Peñalver MJ (2014) Pathology of building materials in historic buildings. Relationship between laboratory testing and infrared thermography. *Mater Constr* 64:1–11. <https://doi.org/10.3989/mc.2013.06612>
35. Di Maio R, Piegari E, Mancini C (2015) Quantitative analysis of pulse thermography data for degradation assessment of historical buildings. *Eur Phys J Plus* 130. <https://doi.org/10.1140/epjp/i2015-15105-6>
36. Tejedor B, Casals M, Gangoellés M, Roca X (2017) Quantitative internal infrared thermography for determining in-situ thermal behaviour of façades. *Energy Build* 151:187–197. <https://doi.org/10.1016/j.enbuild.2017.06.040>
37. Tejedor B, Barreira E, Almeida RMSF, Casals M (2020) Thermographic 2D U-value map for quantifying thermal bridges in building façades. *Energy Build* 224:110176. <https://doi.org/10.1016/j.enbuild.2020.110176>
38. Mayer Z, Heuer J, Volk R, Schultmann F (2021) Aerial thermographic image-based assessment of thermal bridges using representative classifications and calculations
39. Nardi I, Lucchi E, de Rubeis T, Ambrosini D (2018) Quantification of heat energy losses through the building envelope: a state-of-the-art analysis with critical and comprehensive review on infrared thermography. *Build Environ* 146:190–205. <https://doi.org/10.1016/j.buildenv.2018.09.050>

40. Barreira E, Almeida RMSF, Ferreira JPB (2017) Assessing the humidification process of lightweight concrete specimens through infrared thermography. *Energy Procedia* 132:213–218. <https://doi.org/10.1016/j.egypro.2017.09.757>
41. Nardi I, Paoletti D, Ambrosini D, de Rubéis T, Sfarra S (2016) U-value assessment by infrared thermography: a comparison of different calculation methods in a Guarded Hot Box. *Energy Build* 122:211–221. <https://doi.org/10.1016/j.enbuild.2016.04.017>
42. Tejedor B, Casals M, Macarulla M, Giretti A (2019) U-value time series analyses: evaluating the feasibility of in-situ short-lasting IRT tests for heavy multi-leaf walls. *Build Environ* 159:106123. <https://doi.org/10.1016/j.buildenv.2019.05.001>
43. Jeelani I, Gheisari M (2009) Safety challenges of UAV integration in construction: conceptual analysis and future research roadmap. *Coast Estuar Process* 1–360. <https://doi.org/10.1016/j.ssci.2021.105473>
44. Entrop AG, Vasenev A (2017) Infrared drones in the construction industry: designing a protocol for building thermography procedures. *Energy Procedia* 132:63–68. <https://doi.org/10.1016/j.egypro.2017.09.636>
45. Benz A, Taraben J, Debus P, Habte B, Oppermann L, Hallermann N, Voelker C, Rodehorst V, Morgenthal G (2021) Framework for a UAS-based assessment of energy performance of buildings. *Energy Build* 250:111266. <https://doi.org/10.1016/j.enbuild.2021.111266>
46. Irizarry J, Gheisari M, Walker BN (2012) Usability assessment of drone technology as safety inspection tools. *Electron J Inf Technol Constr* 17:194–212
47. Stegner C, Dalsass M, Luchscheider P, Brabec CJ (2018) Monitoring and assessment of PV generation based on a combination of smart metering and thermographic measurement. *Sol Energy* 163:16–24. <https://doi.org/10.1016/j.solener.2018.01.070>
48. Rahaman SA, Urmee T, Parlevliet DA (2020) PV system defects identification using remotely piloted aircraft (RPA) based infrared (IR) imaging: a review. *Sol Energy* 206:579–595. <https://doi.org/10.1016/j.solener.2020.06.014>
49. García Márquez FP, Segovia Ramírez I (2019) Condition monitoring system for solar power plants with radiometric and thermographic sensors embedded in unmanned aerial vehicles. *Meas J Int Meas Confed* 139:152–162. <https://doi.org/10.1016/j.measurement.2019.02.045>
50. Waqar Akram M, Li G, Jin Y, Chen X, Zhu C, Zhao X, Aleem M, Ahmad A (2019) Improved outdoor thermography and processing of infrared images for defect detection in PV modules. *Sol Energy* 190:549–560. <https://doi.org/10.1016/j.solener.2019.08.061>
51. Kirsten Vidal de Oliveira A, Aghaei M, Rüther R (2020) Aerial infrared thermography for low-cost and fast fault detection in utility-scale PV power plants. *Sol Energy* 211:712–724. <https://doi.org/10.1016/j.solener.2020.09.066>
52. Manno D, Cipriani G, Ciulla G, Di Dio V, Guarino S, Lo Brano V (2021) Deep learning strategies for automatic fault diagnosis in photovoltaic systems by thermographic images. *Energy Convers Manag* 241:114315. <https://doi.org/10.1016/j.enconman.2021.114315>
53. Akram MW, Li G, Jin Y, Chen X, Zhu C, Ahmad A (2020) Automatic detection of photovoltaic module defects in infrared images with isolated and develop-model transfer deep learning. *Sol Energy* 198:175–186. <https://doi.org/10.1016/j.solener.2020.01.055>
54. Cubukcu M, Akanalci A (2020) Real-time inspection and determination methods of faults on photovoltaic power systems by thermal imaging in Turkey. *Renew Energy* 147:1231–1238. <https://doi.org/10.1016/j.renene.2019.09.075>
55. Du B, He Y, He Y, Zhang C (2020) Progress and trends in fault diagnosis for renewable and sustainable energy system based on infrared thermography: a review. *Infrared Phys Technol* 109:103383. <https://doi.org/10.1016/j.infrared.2020.103383>
56. Hwang YS, Schlüter S, Il Park S, Um JS (2021) Comparative evaluation of mapping accuracy between UAV video versus photo mosaic for the scattered urban photovoltaic panel. *Rem Sens* 13. <https://doi.org/10.3390/rs13142745>
57. Fernández A, Usamentiaga R, de Arquer P, Fernández MÁ, Fernández D, Carús JL, Fernández M (2020) Robust detection, classification and localization of defects in large photovoltaic plants based on unmanned aerial vehicles and infrared thermography. *Appl Sci* 10. <https://doi.org/10.3390/app10175948>



58. Henry C, Poudel S, Lee SW, Jeong H (2020) Automatic detection system of deteriorated PV modules using drone with thermal camera. *Appl Sci* 10:1–16. <https://doi.org/10.3390/app1013802>
59. Huerta Herraiz Á, Pliego Marugán A, García Márquez FP (2020) Photovoltaic plant condition monitoring using thermal images analysis by convolutional neural network-based structure. *Renew Energ* 153:334–348. <https://doi.org/10.1016/j.renene.2020.01.148>
60. Sham JFC, Memon SA, Tommy, Lo Y (2013) Application of continuous surface temperature monitoring technique for investigation of nocturnal sensible heat release characteristics by building fabrics in Hong Kong. *Energ Build* 58:1–10. <https://doi.org/10.1016/j.enbuild.2012.11.025>
61. Golasi I, Salata F, de Lieto Vollaro E, Coppi M, de Lieto Vollaro A (2016) Thermal perception in the mediterranean area: comparing the Mediterranean Outdoor Comfort Index (MOCI) to other outdoor thermal comfort indices. *Energies* 9:1–16. <https://doi.org/10.3390/en9070550>
62. Xie N, Li H, Abdelhady A, Harvey J (2019) Laboratorial investigation on optical and thermal properties of cool pavement nano-coatings for urban heat island mitigation. *Build Environ* 147:231–240. <https://doi.org/10.1016/j.buildenv.2018.10.017>
63. Sedaghat A, Sharif M (2022) Mitigation of the impacts of heat islands on energy consumption in buildings: a case study of the city of Tehran, Iran. *Sustain Cities Soc* 76:103435. <https://doi.org/10.1016/j.scs.2021.103435>
64. Salata F, Golasi I, Petitti D, de Lieto Vollaro E, Coppi M, de Lieto Vollaro A (2017) Relating microclimate, human thermal comfort and health during heat waves: an analysis of heat island mitigation strategies through a case study in an urban outdoor environment. *Sustain Cities Soc* 30:79–96. <https://doi.org/10.1016/j.scs.2017.01.006>
65. Pisello AL, Castaldo VL, Pignatta G, Cotana F, Santamouris M (2016) Experimental in-lab and in-field analysis of waterproof membranes for cool roof application and urban heat island mitigation. *Energ Build* 114:180–190. <https://doi.org/10.1016/j.enbuild.2015.05.026>
66. Cui Y, Yan D, Hong T, Ma J (2017) Temporal and spatial characteristics of the urban heat island in Beijing and the impact on building design and energy performance. *Energy* 130:286–297. <https://doi.org/10.1016/j.energy.2017.04.053>
67. Salvati A, Coch Roura H, Cecere C (2017) Assessing the urban heat island and its energy impact on residential buildings in mediterranean climate: Barcelona case study. *Energ Build* 146:38–54. <https://doi.org/10.1016/j.enbuild.2017.04.025>
68. Ambrosini D, Galli G, Mancini B, Nardi I, Sfarra S (2014) Evaluating mitigation effects of urban heat islands in a historical small center with the ENVI-Met® climate model. *Sustain* 6:7013–7029. <https://doi.org/10.3390/su6107013>
69. Lassandro P, Di Turi S (2019) Multi-criteria and multiscale assessment of building envelope response-ability to rising heat waves. *Sustain Cities Soc* 51:101755. <https://doi.org/10.1016/j.scs.2019.101755>
70. Aguerre JP, Nahon R, Garcia-Nevaldo E, La Borderie C, Fernández E, Beckers B (2019) A street in perspective: thermography simulated by the finite element method. *Build Environ* 148:225–239. <https://doi.org/10.1016/j.buildenv.2018.11.007>
71. Aboelata A (2021) Reducing outdoor air temperature, improving thermal comfort, and saving buildings' cooling energy demand in arid cities—cool paving utilization. *Sustain Cities Soc* 68:102762. <https://doi.org/10.1016/j.scs.2021.102762>
72. Li H, Harvey J, Kendall A (2013) Field measurement of albedo for different land cover materials and effects on thermal performance. *Build Environ* 59:536–546. <https://doi.org/10.1016/j.buildenv.2012.10.014>
73. Carpio M, González Á, González M, Verichev K (2020) Influence of pavements on the urban heat island phenomenon: a scientific evolution analysis. *Energ Build* 226:110379. <https://doi.org/10.1016/j.enbuild.2020.110379>

# Temperature-Based Approach for In Situ Evaluation of Thermal Transmittance of Building Walls



Mihaela Domazetović and Hrvoje Krstić

**Abstract** Currently, there are several common measurement techniques to measure the thermal transmittance (U-value) of external building walls. Existing literature review identified so far, some advantages, disadvantages, and limitations of practical application of those existing methods. Due to observed limitations of the commonly used standardized and non-standardized methods, new methods are developing aiming at improvement of the accuracy and reliability of in situ measurements. This chapter deals with possibilities of using temperature-based method (TBM) and further development of this method due to reported promising results. This method is relatively new and relies on the Newton's law of cooling. Method itself is simple to use, inexpensive, and accurate when compared to standardized methods of measurements and results are easy to obtain and to interpret. The aim of research presented in this chapter was to improve the accuracy of the in situ measurement of building façades with low thermal transmittance values by using the TBM.

**Keywords** Thermal transmittance · Temperature-based method · Walls

## 1 Introduction

In last two decades, significant effort was made on improving energy efficiency of buildings in European Union (EU). All member countries obliged to ensure achievement of the EU energy and environmental goals. In order to implement the goals set, the first version of the Energy Performance of Buildings Directive (EPBD), Directive 2002/91/EC, was approved on December 16, 2002, and entered into force on January 4, 2003 [1]. This and later directives on the energy efficiency of buildings promote policies that will help [2]:

- Achievement of the highly energy efficient and decarbonized building stock by 2050,

---

M. Domazetović (✉) · H. Krstić  
Faculty of Civil Engineering and Architecture Osijek, Josip Juraj Strossmayer  
University of Osijek, Osijek, Croatia  
e-mail: [mdomazetovic@fos.hr](mailto:mdomazetovic@fos.hr)



- Creation of the stable environment for investment decisions,
- Consumers and businesses to make more informed choices to save energy and money.

Since then, legislation framework on improving energy efficiency of existing and new buildings was adjusted in all member countries to comply with the requirements that were set in the directives. Another significant year in energy efficiency of the buildings was year 2010 when the term Nearly Zero Energy Buildings (nZEB) was introduced in revised version of the EPBD. The obligation to design and build nZEB buildings now applies to all new buildings. But existing buildings, both public and residential, continue to waste enormous amount of energy until they are renovated in terms of improving their energy performance and/or introducing renewable energy sources. This issue was revised in Energy Performance of Buildings Directive 2018/844/EU which sets a framework for a long-term renovation of existing building stock [3].

When it comes to renovation of existing building stock with unsatisfactory energy performance, it is important to determine the actual energy consumption and design energy demands. This is important for buildings owners when it comes to making the decision about measures to be applied to improve energy efficiency. Building owners usually seek to apply measures with short payback period of investment. Usually at this stage, the energy performance gap occurs where can be noticed how actual and design energy needs of the buildings are substantially different, according to some authors in the range from 1 to 120% [4].

For researchers, policy decision makers, and owners of those buildings, it is important to understand where this energy performance gap is coming from? The actual building energy demand depends on various factors—the thermal characteristics of the building envelope (thermal properties and thickness of the envelope layers, type of joinery and type of glazing...), installed Heating, Ventilation, and Air Conditioning (HVAC), climate at the building location, and building usage regime [5]. If the testing of the thermal characteristics of the building envelope is performed in environment controlled by the researchers, the only variable that can cause the energy performance gap is building envelope condition. Studies conducted in 1990s proved existence of the energy performance gap between actual and design energy demands [6–13] and as more important the gap between actual and design thermophysical properties of the building envelope elements [14–22]. Research conducted later in [8, 12] showed that even slight changes in thermal transmittance value (U-value) of building envelope elements—as one of the very sensitive parameters in predicting design energy demand—result in a considerable change in actual energy demand.

Determination of real thermal properties is fundamental for the correct design of energy efficient buildings. Therefore, it is important to verify actual values of thermal transmittance as one of the most influencing parameters of the accuracy of energy simulations of heat loss during the design phase. Based on the literature review, in situ measurements of facades with low U-values represent a challenging task since no matter which method is used, measured U-values deviate in some cases more than 100% compared to theoretical (design) U-values [16, 19, 23–25].

There are several methods for measuring the U-value of building envelope; they are heat flow meter method (HFM), infrared thermography (IRT), temperature-based method (TBM), natural convection and radiation method (NCaR), and simple hot box–heat flow meter method (SHB–HFM) [26]. The main difference between the methods is that the HFM and SHB–HFM methods are using heat flow meter for measurements of the U-value, and other methods are based on a measured or assumed surface heat transfer coefficient without direct measurements of heat flow.

A brief comparison between methods used for measuring U-values of building envelope is presented in Table 1. Comparison is made regarding the year when the method was introduced, standardization of the method, accuracy of the method, and short lists of main advantages and disadvantages. Comparison is made for three mostly used methods—heat flow meter method (HFM), infrared thermography (IRT), and temperature-based method (TBM).

Based on the data in Table 1 and the importance of proper determination of U-value when it comes to lowering energy performance gap in buildings, this chapter deals with possibilities of using TBM and further development of this method due to the promising results demonstrated so far.

Based on the literature review, research papers regarding this method date back to year 2016 when Cuerda et al. in 2016 [27] assessed and compared measurement results of thermally insulated solid brick wall obtained with TBM to calculated results based on Spanish regulation and databases during summer period and obtained deviation of 31%. Buzatu et al. in 2017 [28] compared measured U-values using TBM to theoretical calculation—MC001/2009 and obtained deviation of 40 and 44% for the case studies analyzed. Andújar Márquez et al. in 2017 [29] compared measurement results obtained with TBM to results measured using HFM method and obtained deviation of the results of 2%.

Bienvenido-Huertas et al. in 2018 [30] did comparison of the measurement results using TBM with ones obtained using calculation method according to ISO 6946 during winter, summer, and autumn season and obtained deviations of 4%–37%, 7%–62%, and 19%–83%, respectively. Kim et al. in 2018 [31] compared measurement results using TBM to ones obtained with HFM method according to ISO 9869-1 [14] during winter season and obtained deviation between results from 6 to 17%.

Generally, based on the literature review, it can be seen that when measurement results of U-value by the means of TBM were compared to theoretical U-values, higher deviations were obtained than when compared to results measured using HFM method.

Even though research results of conducted measurements found in literature showed good agreement between measured and theoretical U-values, there is still a lack of research in which TBM is used. Therefore, to improve the reliability of the method, further studies are still needed for different types of walls in different temperature conditions.

In this chapter, the viability of the TBM for in situ U-value assessment of real size external wall with low U-value was analyzed since generally, in situ U-value measurement of external walls with low U-values represents a challenging task. No

**Table 1** Brief comparison between methods used for measuring U-vale of building envelope

Method	Year method was introduced	Standard used for method	Accuracy of the method (Range [%]) [26]	Main advantages	Main disadvantages
HFM	1970s	ISO 9869-1:2014 Thermal insulation—Building elements—In situ measurement of thermal resistance and thermal transmittance—Part 1: Heat flow meter method	0–163% (45–142% <sup>a</sup> ) Avg. 24% (90% <sup>a</sup> )	Standardized method Non-destructive method Numerous HFM method studies	Limitations with respect to the test season Requires steady-state conditions Time delay in the thermal response of walls with a higher thermal mass Measurement duration High cost Complex instrumental setup
IRT	1990s	ISO 9869-2:2018 Thermal insulation—Building elements—In situ measurement of thermal resistance and thermal transmittance—Part 2: Infrared method for frame structure dwelling	0–162% (1–286% <sup>a</sup> ) Avg. 19% (55% <sup>a</sup> )	Standardized method Non-destructive method Considerable amount of research IRT is a useful tool	Method is prescribed for building components with a relatively small heat capacity per unit area Highly influenced by outside weather conditions and effects Evacuation of the building occupants Needs qualified experienced personnel Measurement duration High cost Complex instrumental setup

(continued)

**Table 1** (continued)

Method	Year method was introduced	Standard used for method	Accuracy of the method (Range [%]) [26]	Main advantages	Main disadvantages
TBM	2000s	Non-standardized alternative method	4–37% (2–62% <sup>a</sup> ) 0.3–17% <sup>b</sup>	Non-destructive method Low cost Simple instrumental setup Measurement duration Promising results	Estimation of real heat transfers between the environment and wall Requires steady-state conditions Lacks accuracy evaluation and research

<sup>a</sup>Deviations obtained for measurements performed in summer conditions and

<sup>b</sup>Percentage difference compared to U-values obtained using HFM method [26]

matter which method is used, high deviations between measured and calculated U-values of walls with low U-value are reported. For this purpose, an in-depth analysis of the influence of the temperature difference and the test duration on measurement results was conducted. The U-value of a brick wall thermally insulated with 10 cm of mineral rock wool wall was evaluated in a test chamber under different internal temperature conditions.

## 2 The Main Principles of Temperature-Based Method for in Situ Thermal Transmittance Measurements

Temperature-based method (TBM), also called thermometric method (THM) [30, 32] or air–surface temperature ratio (ASTR) method [33], is a non-destructive method for the in situ U-value assessment. It is based on monitoring of inside wall surface temperature and the temperatures of the environment on both sides of the wall.

The methodology of TBM is based on Newton’s law of cooling [34] that in terms of buildings wall U-value can be expressed as

$$U = h_i \frac{T_i - T_w}{T_i - T_e}$$

where  $h_i$  [W/(m<sup>2</sup>K)] is the internal heat transfer coefficient,  $T_w$  [K] is the indoor surface temperature, and  $T_i$  and  $T_e$  [K] are the indoor and outdoor air temperature, respectively. Therefore, two temperature sensors, a data logger, and surface temperature sensors are required to perform measurements.

To decrease and avoid single point measurement error, it is recommended to use three surface temperature sensor placed to the internal side of the wall at the distance of 10–15 cm between them, 1.5 m high [35, 36], and 2 cm away from mortar joints between bricks [37]. If the location of mortar joints cannot be identified by IRT, probes should be mounted not horizontally or vertically aligned [37]. The air temperature sensors should be placed at the same height as surface temperature sensors and 30–40 cm away from the wall to avoid convective effects [35, 36].

TBM has widely been used in practice due to its advantages of being quick, simple, and less expensive compared to standardize methods. Since TBM is not a standardize method, guidelines for installing the equipment and conducting in situ measurement of U-value are only given by the manufacturers of the equipment [35] and by researchers who performed studies dealing with the feasibility of the method [30, 31, 33]. Furthermore, most of the guidelines for conducting measurements comply with the requirements and guidelines for heat flow meter method set out in ISO 9869-1 [14] such as avoiding direct solar radiation, required test duration, performing measurements during the night, and using IRT to avoid placement of sensors in the vicinity of thermal bridges or other non-homogeneities.

According to the manufacturers and results of studies found in literature, it is recommended that measurements are conducted under steady-state conditions, while the minimal temperature difference when performing the measurement should be at least equal to 15 °C [30, 35]. As stable meteorological conditions are difficult to achieve, long-term measurements and measurements during the night are recommended, which in a way simulate stable meteorological conditions.

It is recommended to record measured data for post-processing at fixed intervals long enough to facilitate data processing and avoid loss of information [36]. So far, progressive average method has been used for the analysis of data obtained by TBM. In literature, authors performed data analysis to either to entire data set obtained during the measurement period [29, 31, 33] or filtered one [30].

### 3 Experimental Research

In order to analyze the influence of the temperature difference, the test duration, and the accuracy of equipment on measurement results, in situ experimental research of a wall with low U-value was performed in a test chamber with plan dimensions of 3.65 m × 4.55 m. To simulate outside temperature conditions during the measurements and to control and avoid impacts of direct solar radiation, precipitation, and wind velocity, the test chamber was built inside an unheated building. Impact of direct solar radiation was avoided by shading all openings of the unheated building.

Inside temperature conditions in test chamber were controlled by a programmable HVAC unit that was used for heating.

The exterior walls of chamber were made of 30 cm-thick lightweight concrete thermal blocks thermally insulated with 10 cm of expanded polystyrene (EPS). Two opposite sides of the chamber facing East and West were constructed in such a way to allow testing of different type of walls as shown in Fig. 1. The ceiling of the chamber was made from lightweight concrete blocks with thermal insulation of 10 cm of EPS.

In this study, in situ measurements of U-value using TBM were performed on a brick wall thermally insulated with 10 cm of mineral rock wool. According to studies by Givoni [38], examined wall was constructed in the length of 2.2 m to decrease edge effect. Table 2 summarizes main characteristics and thermal properties of tested wall together with theoretical U-value calculated according to international standard ISO 6946:2017 building components and building elements—thermal resistance and thermal transmittance—calculation methods [39].

The measuring equipment used for the U-value assessment by TBM consisted of a data logger (Testo 435-4), three surface temperature sensors for measuring surface temperature of a wall, and two temperature sensors for measuring the internal and external temperature. An infrared camera has been used prior to the test in order to avoid placement of sensors in the vicinity of thermal bridges or other non-homogeneities. Surface temperature sensors were mounted at a height of 1.5 m. Temperature sensors for measuring the internal and external temperature were placed 30 cm away from the examined wall at the same height as surface temperature sensors. The main technical specifications of equipment used for measurement are given in Table 3.



**Fig. 1** Test chamber (left) and tested brick wall before installation of thermal insulation (right)

**Table 2** Main properties of tested wall

Wall	Material layer	$d$ [mm]	$\lambda$ [W/(mK)]	$U$ [W/(m <sup>2</sup> K)]
Brick wall (BW)	Mortar plaster	20	0.66	0.29
	Full brick	250	0.80	
	Mineral rock wool	100	0.035	

**Table 3** Main specifications and accuracy of equipment

Equipment	Measured quantity	Measuring range	Resolution	Accuracy
Data logger with Thermocouples type K Thermocouple type K	Surface and internal air temperature	-20 to +70 -20 to +70	0.1 °C 0.1 °C	±0.1 ±0.3
	External air temperature			
Infrared camera FLIR E60bx	Field of view (FOV)	25° × 19°		
	Spectral range	7.5–13 μm		
	Thermal sensitivity	<0.05–30 °C		

Experimental research was performed under real outside air temperatures during the heating season. Tests in different conditions were conducted for the purpose of evaluating the method and comparing the obtained values.

To analyze the influence of different temperature conditions, the designated level of internal temperature was varied. First, measurement was performed varying the internal temperature, moving away from steady-state conditions (case BW1). Internal temperature was varied based on external temperature in order to maintain an average temperature difference of 15 °C between inside and outside air. The latter was achieved using programmable HVAC system. In the second measurement period, the internal temperature,  $T_i$ , was set all the time at 30 °C and kept as constant as possible during the measurement period (case BW2).

During both measurement periods, indoor surface, internal and external temperatures were continuously monitored. Each test lasted for 7 days with an acquisition time step equal to 10 min.

## 4 Data Analysis

Acquired measurement data in this research was processed by using the progressive average procedure according to the following expression:

$$U_m \left[ \frac{\text{W}}{\text{m}^2\text{K}} \right] = h_i \frac{\sum_{j=1}^n T_{i(j)} - T_{w(j)}}{\sum_{j=1}^n T_{i(j)} - T_{e(j)}}$$

where the index  $j$  enumerates the individual measurements. Internal heat transfer coefficient was taken as a fixed value of 7.69 W/(m<sup>2</sup>K) according to ISO 6946:2017 [39].

In order to assess the accuracy of the measurement results obtained by the TBM, uncertainty considering the accuracy of the equipment was calculated. Since the measured U-value is obtained from the values of three independent quantities (internal temperature ( $T_i$ ), external temperature ( $T_e$ ) and internal wall surface temperature ( $T_w$ )), the uncertainty of the measurement result is expressed as a combined standard uncertainty,  $u_c$ . The combined standard uncertainty of measurements was

calculated according to the ISO/IEC Guide 98-3:2008 [40]:

$$u_c^2(U) = \left(\frac{\delta U}{\delta T_i}\right)^2 \cdot u_c^2(T_i) + \left(\frac{\delta U}{\delta T_e}\right)^2 \cdot u_c^2(T_e) + \left(\frac{\delta U}{\delta T_w}\right)^2 \cdot u_c^2(T_w)$$

where  $u_c(T_i)$  is the uncertainty associated with the internal temperature measuring equipment,  $u_c(T_e)$  is the uncertainty associated with the outdoor temperature measuring equipment, and  $u_c(T_w)$  is the uncertainty associated with the internal surface wall temperature measuring equipment.

To access the influence of the achieved temperature differences during the test on the accuracy of the results, measurement results were analyzed by each day of a measurement period using cumulative values. Measurements were classified into four intervals of temperature difference between inside and outside air. For each interval mean, U-values were calculated. For the purpose of results evaluation, for the presented mean U-values by intervals, the proportion of data in relation to the total number of data obtained during the measurement was analyzed. The accuracy of results was analyzed calculating absolute values of the relative difference between theoretical and measured U-values:

$$\sigma(\%) = \left| \frac{U_m - U_t}{U_t} \right| * 100$$

To determine the reliability of the obtained measured U-values, the criterion proposed in ISO 9869-1 was used. According to ISO 9869-1 [14], the deviation higher than 20% between measured U-values and calculated U-values according to ISO 6946:2017 [39] was taken as significant.

The influence of the test duration on the accuracy of the measured U-values was analyzed in relation to the theoretical U-values. The criteria proposed in ISO 9869-1 [14] have been applied to determine the required measurement time. According to ISO 9869-1 [14], it is recommended that measurements are carried out for at least three days, and the measurement can be completed if the U-value at the end of the test does not deviate by more than  $\pm 5\%$  from the value measured 24 h earlier. To determine the duration of the test, mean daily cumulative U-values were observed, and the variability of the results was analyzed by calculating the coefficient of variation according to:

$$V(\%) = \sqrt{\frac{\sum_{i=1}^n (U_{mi} - \bar{U}_m)^2}{n - 1}} \cdot \frac{1}{\bar{U}_m} \cdot 100$$

where  $U_m$  is the average of measured U-values of the wall, and  $n$  is the total number of data in the sample.



## 5 Results and Discussion

U-value and temperature data trend observed during both measurement periods are shown in Figs. 2 and 3. It can be seen that during both measurement periods, similar average external temperature is observed while average internal temperature significantly differs as a result of set inside temperature conditions. In the first measurement period when internal temperature was adjusted based on external temperature in order to maintain an average temperature difference of 15 °C between inside and outside air, average internal temperature obtained was 18.46 °C. In the second measurement period, internal temperature was set to constant value of 30 °C during the whole test, and therefore, average internal temperature was significantly higher with an average of 29.26 °C while external average temperature was 2.99 °C.

Based on the data obtained by in situ measuring of wall under two different temperature regimes, the mean U-values with measurement uncertainties according to the average method were calculated and shown in Table 4. The results show that

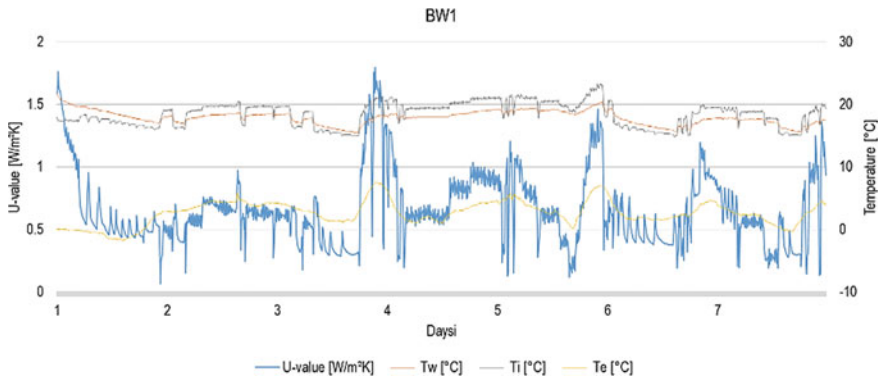


Fig. 2 Measured U-values, surface, internal and external temperature, case BW1

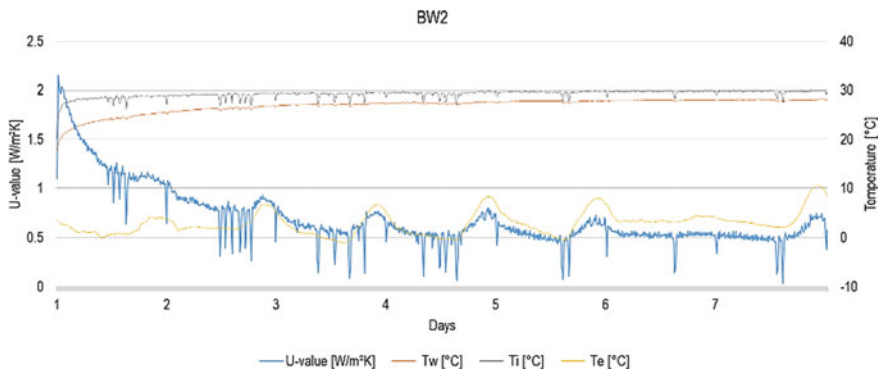
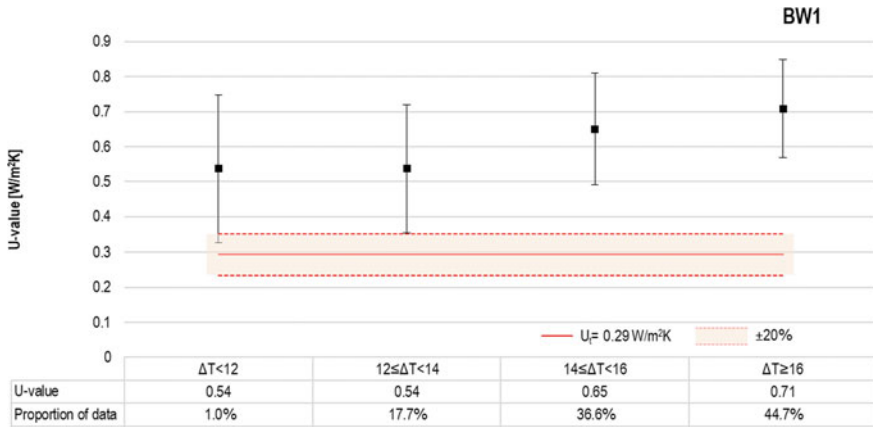


Fig. 3 Measured U-values, surface, internal and external temperature, case BW2

**Table 4** Measured and theoretical U-values

Case	Wall	Duration [days]	Conditions	$\Delta T_{avg}$	$U_m$ [W/m <sup>2</sup> K]	$U_t$ [W/m <sup>2</sup> K]	$\sigma$ [%]
1	BW	7	$\Delta T = 15 \text{ }^\circ\text{C}$	15.8	$0.65 \pm 0.15$	0.29	125.8
2	BW	7	$T_i = 30 \text{ }^\circ\text{C}$	26.3	$0.70 \pm 0.09$	0.29	141.4



**Fig. 4** Measured U-values for achieved intervals of temperature difference between inside and outside air, case BW1

regarding temperature conditions, the obtained mean U-values after seven days of testing differ by only 7.7%. However, measurement uncertainty is much higher when inside temperature is varied.

The mean U-values and their associated combined uncertainty in four intervals of temperature differences between inside and outside air and for both measuring campaigns are shown in Figs. 4 and 5. It can be seen that in the second measuring campaign, obtained temperature difference during the entire measurement period was above 16 °C, while in the first one, temperature difference varied from 10 °C to above 16 °C. In both measuring campaigns and in all intervals of temperature difference, measured mean U-values are significantly higher than estimated ones which agrees with the published results of in situ monitoring of walls with low U-value found in literature [16, 19, 23–25]. The temperature difference above 16 °C led to highest deviation between measured and theoretical U-values, while uncertainties of measurements decreased as temperature difference increased. Comparing measured U-values of two measurement campaigns, in the interval of temperature difference above 16 °C, it can be seen that obtained results at the end of the test deviate by only 1.4%.

For more detailed analysis, data was filtered by observing only intervals with minimum of 43% of the data. The 43% of data were considered according to ISO 9869-1 [14] which represents the minimum test duration of three days. Therefore, for both case studies, only interval of temperature difference above 16 °C was analyzed.

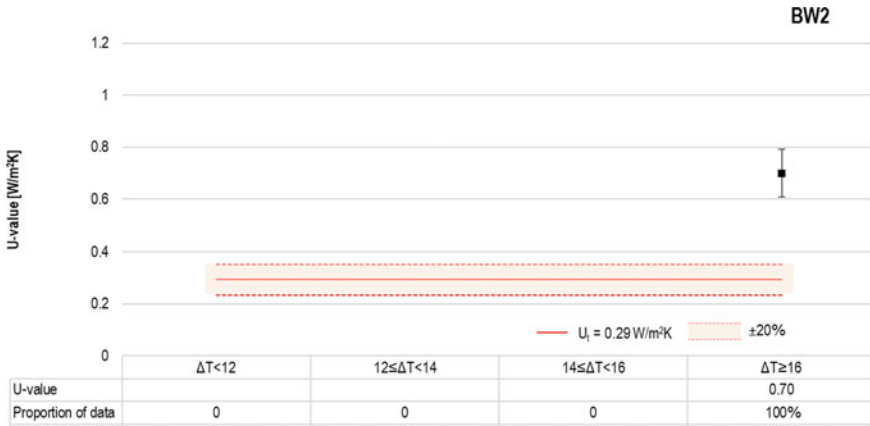


**Fig. 5** Measured U-value for achieved intervals of temperature difference between inside and outside air, case BW2

Measured mean U-values ( $U_m$ ) and their associated uncertainties, the absolute values of the relative difference between theoretical and measured U-value ( $\sigma$ ), proportion of data ( $n$ ), and the coefficients of variation ( $V$ ) are summarized in Table 4 for each day of a measurement using cumulative values. The proportion of data is reported by each day considering total number of data obtained during the measurement.

According to the results presented in Table 5, in the first measurement case (BW1) when the temperature difference was above 16 °C, the test could be stopped after the third day, since the coefficient of variation of the results was lower than 5%, with a deviation between theoretical and measured U-values of 144.4%. In the second

**Table 5** Summarized description of measured U-values and their associated combined standard uncertainties, deviation between theoretical and measured U-value, daily proportion of data and coefficient of variation of the measured thermal transmittance

	BW1				BW2			
	$\Delta T \geq 16$				$\Delta T \geq 16$			
Duration (days)	$U_m$	$\sigma$	$n$	$V$	$U_m$	$\sigma$	$n$	$V$
	W/(m <sup>2</sup> K)	%	%	%	W/(m <sup>2</sup> K)	%	%	%
1	0.73 ± 0.14	151.3	11.7	—	1.31 ± 0.09	351.1	14.3	—
2	0.71 ± 0.14	146.4	12.6	0.17	1.06 ± 0.09	265.5	28.6	9.5
3	0.71 ± 0.14	144.4	13.1	0.31	0.91 ± 0.09	214.0	42.9	7.1
4	0.74 ± 0.14	155.8	26.4	11.57	0.82 ± 0.09	183.8	57.1	3.4
5	0.74 ± 0.14	153.8	37.7	1.89	0.77 ± 0.09	164.9	71.4	1.0
6	0.74 ± 0.14	153.9	38.1	0.14	0.73 ± 0.09	151.2	85.7	0.2
7	0.71 ± 0.14	144.1	44.7	1.42	0.70 ± 0.09	141.4	100.0	0.1

measurement case (BW2) for the same temperature difference, the test could be stopped after fourth day, with a deviation between theoretical and measured U-values of 183.8%. It can be seen that in the second measurement case, deviations between theoretical and measured U-values are higher in the first days of test, and as the test evolves, U-values tend to decrease. On the contrary, in the first measurement case, there is no significant influence of test duration on measured U-values since measured U-values differ by maximum of 4% during seven days of testing. It is worth noting that preliminary results of this study show how test duration can be shortened if the temperature difference of 16 °C between inside and outside air is maintained.

## 6 Conclusions

New approaches for in situ assessment of thermal transmittance have proven to be very effective and promising. However, there is still a lack of comprehensive research that would enable to draw more profound conclusions about the reliability and applicability of such methods. One of the new methods widely used in practice is TBM. However, only few researchers have studied the actual behavior of the built wall in real conditions using this method, and the accuracy of the wall U-value measurement is not yet clearly verified.

In this direction, this research tends to improve the accuracy of the in situ measurement of external walls with low U-value using the TBM. Therefore, in-depth analysis of the influence of the temperature difference and the test duration on measurement results was conducted. In situ U-value measurement was performed in the test chamber on the insulated external brick wall with low U-value. Two tests were performed under different temperature conditions; varying internal temperature to obtain average temperature difference of 15 °C between inside and outside air and maintaining constant internal temperature of 30 °C. Both tests lasted seven days.

Even though it is recommended to perform in situ measurement under steady-state conditions, preliminary results of this study show that it is possible to obtain same level of U-value under varying indoor temperature conditions as long as the temperature difference between inside and outside air during the test is higher than 16 °C. This is crucial cognition for wider application of method in practice when designing the measures of improving energy efficiency of existing buildings. Regardless of the operational conditions, the results of the both measurements are significantly higher than the corresponding calculated U-values which is in agreement with the published results of in situ monitoring of walls with low U-value reported in literature. High indoor air temperature is not needed to acquire data on the U-value, and therefore, unnecessary losses of energy during testing can be avoided. The temperature difference above 16 °C led to highest deviation between measured and theoretical U-values. When observing the whole data set, slightly lower measured U-value is obtained in the first measurement campaign, i.e., maintaining an average temperature difference of 15 °C between inside and outside air. However, variation of internal temperatures

results in higher measurement uncertainties. Generally, measurement uncertainties decrease as the temperature difference increase.

Furthermore, this research preliminary results show how test duration can be shortened if the internal temperature is adjusted based on external temperature, maintaining temperature difference of 16 °C between inside and outside air.

Nowadays, the use of façades with very low U-values is increasing. Since overestimation of U-values can result in misguided assessment of energy saving measures and therefore in lower than expected improvements in thermal performance, future research should consider larger sample of different types of external walls with very low U-value. Also, there is a significant gap in the literature when it comes to performing in situ measurements during the occupancy periods. Therefore, in order to improve the reliability of the method, future research should analyze the results obtained taking into account occupancy behavior parameters.

## References

1. The Energy Performance of Buildings Directive (EPBD). 2021 [cited 2021 1.12.2021]. Available from <https://epb.center/epb-standards/energy-performance-buildings-directive-epbd/>
2. Energy performance of buildings directive. 2019 [cited 2021. 1.12.2021]. Available from [https://ec.europa.eu/energy/topics/energy-efficiency/energy-efficient-buildings/energy-performance-buildings-directive\\_en](https://ec.europa.eu/energy/topics/energy-efficiency/energy-efficient-buildings/energy-performance-buildings-directive_en)
3. Directive (EU) 2018/844 of the European Parliament and of the Council of 30 May 2018 amending Directive 2010/31/EU on the energy performance of buildings and Directive 2012/27/EU on energy efficiency. 2018, Official Journal of the European Union
4. Jack R et al (2018) First evidence for the reliability of building co-heating tests. *Build Res Inform* 46(4):383–401
5. Bauwens G, Roels S (2014) Co-heating test: a state-of-the-art. *Energ Build* 82:163–172
6. Branco G et al (2004) Predicted versus observed heat consumption of a low energy multifamily complex in Switzerland based on long-term experimental data. *Energ Build* 36(6):543–555
7. Burman E, Mumovic D, Kimpian J (2014) Towards measurement and verification of energy performance under the framework of the European directive for energy performance of buildings. *Energy* 77:153–163
8. Majcen D, Itard L, Visscher H (2013) Actual and theoretical gas consumption in Dutch dwellings: what causes the differences? *Energ Policy* 61:460–471
9. de Wilde P (2014) The gap between predicted and measured energy performance of buildings: a framework for investigation. *Autom Constr* 41:40–49
10. Sunikka-Blank M, Galvin R (2012) Introducing the prebound effect: the gap between performance and actual energy consumption. *Build Res Inform* 40(3):260–273
11. Norford LK et al (1994) Two-to-one discrepancy between measured and predicted performance of a 'low-energy' office building: insights from a reconciliation based on the DOE-2 model. *Energ Build* 21(2):121–131
12. Majcen D, Itard LCM, Visscher H (2013) Theoretical vs. actual energy consumption of labelled dwellings in the Netherlands: discrepancies and policy implications. *Energ Policy* 54:125–136
13. Demanuele C, Tweddell T, Davies M (2010) Bridging the gap between predicted and actual energy performance in schools. In: World renewable energy congress XI, UAE Abu Dhabi
14. International Organization for Standardization. Thermal insulation—Building elements—In-situ measurement of thermal resistance and thermal transmittance—Part 1: Heat flow meter method (ISO 9869-1:2014)

15. Standard UNI 10351 (1994) Materiali da costruzione. Conduttività termica e permeabilità al vapore [Construction materials: Thermal conductivity and vapour permeability]
16. Albatici R, Tonelli AM, Chiogna M (2015) A comprehensive experimental approach for the validation of quantitative infrared thermography in the evaluation of building thermal transmittance. *Appl Energ* 141:218–228
17. Lucchi E (2017) Thermal transmittance of historical brick masonries: a comparison among standard data, analytical calculation procedures, and in situ heat flow meter measurements. *Energ Build* 134:171–184
18. Desogus G, Mura S, Ricciu R (2011) Comparing different approaches to in situ measurement of building components thermal resistance. *Energ Build* 43(10):2613–2620
19. Asdrubali F et al (2014) Evaluating in situ thermal transmittance of green buildings masonries— a case study. *Case Stud Constr Mater* 1:53–59
20. Evangelisti L et al (2015) In situ thermal transmittance measurements for investigating differences between wall models and actual building performance. *Sustainability* 7(8):10388
21. Gaspar K, Casals M, Gangolells M (2016) A comparison of standardized calculation methods for in situ measurements of façades U-value. *Energ Build* 130:592–599
22. Evangelisti L, Guattari C, Asdrubali F (2018) Influence of heating systems on thermal transmittance evaluations: simulations, experimental measurements and data post-processing. *Energ Build* 168:180–190
23. Nardi I et al (2015) A comparison between thermographic and flow-meter methods for the evaluation of thermal transmittance of different wall constructions. *J Phys Conf Ser* 655:012007
24. Bros-Williamson J, Garnier C, Currie JI (2016) A longitudinal building fabric and energy performance analysis of two homes built to different energy principles. *Energ Build* 130:578–591
25. Flood C, Scott L, Architects C (2016) In situ thermal transmittance of case studies in Dublin. In: *Sustainable ecological engineering design for society*, Leeds Beckett University, p 13
26. Teni M, Krstić H, Kosiński P (2019) Review and comparison of current experimental approaches for in-situ measurements of building walls thermal transmittance. *Energ Build* 203:109417
27. Cuerda E et al (2016) Evaluation and comparison of building performance in use through on-site monitoring and simulation modelling. In: *Proceedings of the 3rd IBPSA-England conference BSO 2016*, Great North Museum, Newcastle
28. Buzatu G et al (2017) Thermal transmittance determination for different components of buildings. In: *2017 international conference on optimization of electrical and electronic equipment (OPTIM) and 2017 international Aegean conference on electrical machines and power electronics (ACEMP)*
29. Andújar Márquez JM, Martínez Bohórquez MA, Gómez Melgar S (2017) A new metre for cheap, quick, reliable and simple thermal transmittance (U-Value) measurements in buildings. *Sensors (Basel, Switzerland)* 17(9)
30. Bienvenido-Huertas D et al (2018) Determining the U-value of façades using the thermometric method: potentials and limitations. *Energies* 11(2):360
31. Kim S-H et al (2018) The feasibility of improving the accuracy of in situ measurements in the air-surface temperature ratio method. *Energies* 11(7):1885
32. David Bienvenido-Huertas CR-B (2021) Optimization of the characterization of the thermal properties of the building envelope analysis of the characterization of the façades using artificial intelligence, 1st ed. *SpringerBriefs in Applied Sciences and Technology*
33. Kim S-H et al (2018) Reliability field test of the air-surface temperature ratio method for in situ measurement of U-values. *Energies* 11(4):803
34. Çengel YA (2004) *Heat transfer: a practical approach*. McGraw-Hill, New York
35. Testo AG (ed) (2014) *U-value measurement using the Testo 635*. Testo AG, Lenzkirch, Germany
36. Bienvenido-Huertas D et al (2019) Review of in situ methods for assessing the thermal transmittance of walls. *Renew Sustain Energ Rev* 102:356–371
37. Meng X et al (2015) Factors affecting the in situ measurement accuracy of the wall heat transfer coefficient using the heat flow meter method. *Energ Build* 86:754–765

38. Givoni B (1998) Effectiveness of mass and night ventilation in lowering the indoor daytime temperatures. Part I: 1993 experimental periods. *Energy Build* 28(1):25–32
39. International Organization for Standardization. Building components and building elements—Thermal resistance and thermal transmittance—Calculation methods (ISO 6946:2017)
40. International Organization for Standardization. ISO/IEC Guide 98-3:2008—Uncertainty of Measurement—Part 3: Guide to the Expression of Uncertainty in Measurement (GUM:1995). International Organization for Standardization, Geneva, Switzerland

# Combining Characterization Tests of Building Envelope Thermal Transmittance with the Acoustic Characterization Through Data Mining Approaches



Krizia Berti, Blanca Tejedor, Joaquín Durán, and David Bienvenido-Huertas

**Abstract** Climate change has forced many sectors to establish measures to achieve decarbonisation. Building is amongst these sectors with the greatest challenge. To achieve decarbonisation, energy improvement measures should be established. These improvement measures depend on an appropriate characterization of the existing buildings. For this purpose, there are many experimental tests based on measuring envelope variables, such as surface temperature and heat flow. Thus, thermal parameters of envelopes could be accurately known. In view of this circumstance, the question arises as to whether it is possible to know other envelope parameters additionally, such as sound insulation. The previous studies have shown the feasibility of characterizing envelope variables through artificial intelligence predictive models. Thus, this study characterizes sound insulation by using these predictive models with the variables obtained from the thermal monitoring of an envelope through thermal transmittance tests.

**Keywords** Artificial intelligence · Thermal transmittance tests · Acoustic characterization · Overall sound reduction index A

## 1 Introduction

Reducing building energy consumption is amongst the main challenges of today's society. The European Union's roadmap towards a low-carbon economy aims at reducing emissions to the atmosphere by 90% in comparison with the levels from 1990 [1]. Thus, reducing building energy consumption is crucial to achieve that goal.

---

K. Berti

Department of Building Construction II, University of Seville, Seville, Spain

B. Tejedor

Department of Project and Construction Engineering, Group of Construction Research and Innovation (GRIC), Universitat Politècnica de Catalunya (UPC), Barcelona, Spain

J. Durán · D. Bienvenido-Huertas (✉)

Department of Building Construction, University of Granada, Granada, Spain

e-mail: [dbienvenido@ugr.es](mailto:dbienvenido@ugr.es)



Building energy consumption is mainly based on the use of HVAC systems [2, 3]. In this regard, knowing the thermal performance of building envelopes is essential to accurately know its energy demand and to establish energy saving measures [4, 5]. Many research studies on the thermal characterization of envelopes have been recently developed, and most focus on experimental characterization [6].

Likewise, wall thermal transmittance could be experimentally characterized through various procedures. The heat flow metre method (HFM) and the thermometric method (THM) are the most used (see Fig. 1). HFM is developed by ISO 9869-1 [6] and consists in measuring the heat flow and indoor and outdoor air temperature in façades in periods of time from 3 to 7 days. Some studies have shown some limitations and requirements that should be considered when monitoring façades with this method. For instance, Cesaratto et al. [7], Desogus et al. [8], and Trethowen [9] found that one of the main error contributions of the method was based on the heat flow measurement. In this regard, Meng et al. [10] established that the error related to the placing of the heat flux plate could reach 26%. Moreover, the need for ensuring a high thermal gradient [8, 11], the orientation of the wall [12], and the presence of condensations [13] or freezes [14] has been reported to guarantee the representation of results [8, 11].

THM is a variation of the HFM. THM is a method that replaces heat flow measurement by surface temperature measurement [15, 16] due to the error sources related to the heat flow when determining thermal transmittance [9, 10]. Its theoretical foundation is based on the Newton's cooling and considers that heat transfer by convection is equivalent to heat transfer by radiation and convection in steady state. Both HFM and THM have been widely used at a scientific and professional level [6]. However, the characteristics of the methods could be limited, thus preventing from using them appropriately. In this regard, one of the limitations is the validation of experimental results. For this purpose, ISO 9869-1 indicates that experimental results should be validated by analyzing the percentage deviation between the value obtained by the

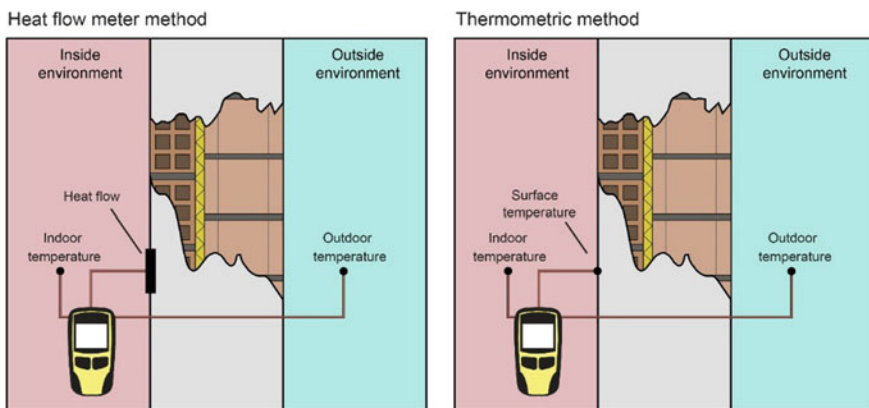


**Fig. 1** Schemes of both the heat flow metre method and the thermometric method

results and the theoretical value obtained through ISO 6946 [17]. The limitation of this aspect is that ISO 6946 requires to know the layers and thermal properties of façades previously, so its use is very limited in existing buildings [18]. A recent study therefore suggested the possibility of characterizing the thermal transmittance from ISO 6946 through statistical techniques based on artificial intelligence (AI) and by using the data obtained from the monitoring [19]. The goal was to use AI models to determine the theoretical value of the wall without knowing its composition and properties, thus validating experimental results. The AI models developed led to estimate with both a determination coefficient greater than 99.55% and an average error lower than 0.05 W/(m<sup>2</sup>K). Based on these results, Bienvenido-Huertas et al. [20] analyzed the possibility of using AI models to predict periodic thermal properties of façades successfully, such as the periodic thermal transmittance or the thermal admittance.

However, the possibility of characterizing acoustic thermal properties through the data obtained by monitoring thermal transmittance has not been previously studied or evaluated. For this reason, this study suggests the possibility of characterizing the overall sound reduction index  $A$  ( $R_A$ ) of façades by using the data monitored by HFM or THM. For this purpose, this study is based on the mathematical formulation approach included in the Spanish Technical Building Code, and  $R_A$  was appropriately estimated by using a dataset of 22,820 tests simulated in façades (obtained by combining 163 actual monitoring with 140 façades designs).

## 2 Methodology

### 2.1 Dataset Creation

One of the main requirements to apply appropriately approaches of predictive models with AI is having a large dataset that guarantees the correct learning of models. As conducting a great sample of tests requires much time and limits the use of this kind of approach, two-dimensional transitory simulations were designed to generate the dataset required. These simulations were performed by using the HTFlux software.

Simulations were based on the combination of actual tests with simulated façade models (Fig. 2). For this purpose, 140 typologies of façades were modelled. These typologies were designed based on both the walls included in the Constructive Elements Catalogue (Instituto de Ciencias de la Construcción Eduardo Torroja, 2010) and those obtained from several cataloguing studies on façades of the Spanish building stock [22, 23]. Thus, the models correspond to typologies of façades from the building periods of the Spanish building stock. As for the walls built in the building periods after the NBE-CT-79, insulating materials were several, including expanded polystyrene, mineral wool, polyurethane, and extruded polystyrene. As walls were designed in the simulation process, their layers (i.e. the type of material, thickness, and thermal properties of each layer) were therefore accurately known.

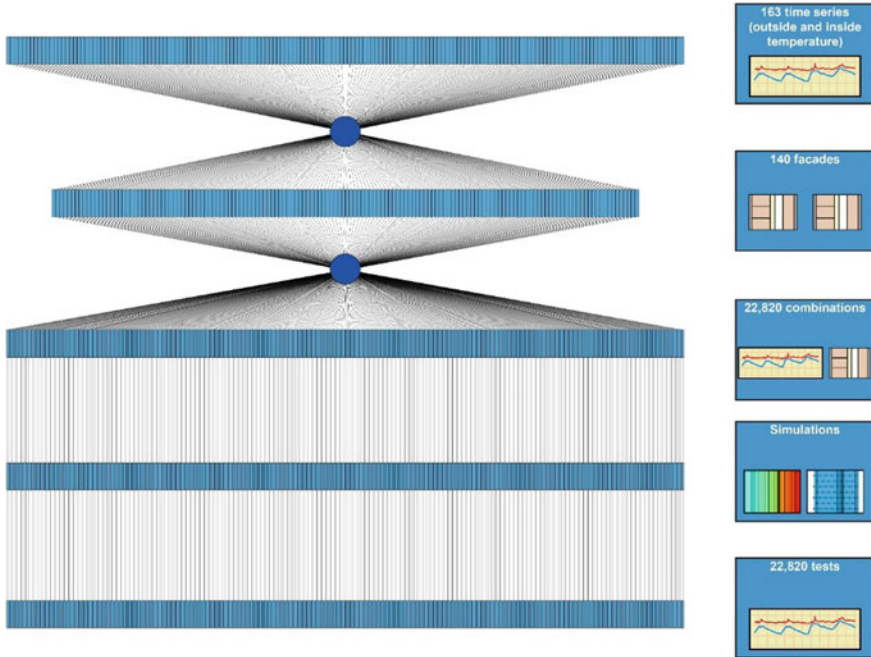


Fig. 2 Workflow of the simulation process

Thus, a dataset with accurate knowledge of  $R_A$  was available. To determine  $R_A$ , the two approach expressions included in the Spanish Technical Building Code were used:

$$R_A = 16.6 \log(m) + 5 \quad \text{if } m \leq 150 \text{ kg/m}^2 \quad (1)$$

$$R_A = 36.5 \log(m) - 38.5 \quad \text{if } m > 150 \text{ kg/m}^2 \quad (2)$$

Each of the 140 typologies of façades was combined with a set of 163 time series of indoor and outdoor air temperature obtained in Campaign 1. A total of 22,820 combinations between the typologies of walls and the time series was therefore obtained. These measurements were conducted under several test conditions. There were monitoring under favourable and unfavourable conditions, thus including a wide variety of test conditions.

Two-dimensional transitory simulations were performed in each combination to obtain two variables: the surface temperature and the heat flow. As for boundary conditions, the surface thermal resistances established by ISO 6946:2007 for horizontal heat flows were used:  $0.13 \text{ m}^2\text{K/W}$  for indoor conditions and  $0.04 \text{ m}^2\text{K/W}$  for outdoor conditions. This was due to the fact that ISO 6946:2007 recommends these surface thermal resistance values for typical envelope buildings and under

normal performance conditions (i.e. with an indoor temperature within acceptable thermal comfort ranges). Likewise, these surface thermal resistance values have been used in other similar research studies on thermal characterization through transitory simulations [19].

Likewise, monitoring from Campaign 1 lasted between 3 and 7 days. Thus, the time corresponding to each time series was considered as the simulation time. Other aspects related to the simulation process were data acquisition time and the location of the probe of both the surface temperature and the heat flow. On the one hand, intervals of 15 min were applied, coinciding with those used to measure indoor and outdoor air temperatures. On the other hand, the variables measured were at a height of 1.50 m above the floor to avoid two-dimensional effects on the heat flow due to the junction with the slab. This criterion is in accordance with the operational criteria included in the existing studies on thermal transmittance methods.

Likewise, the measurements of the surface temperature and the heat flow from 163 actual tests were available and used to validate the simulated data, thus guaranteeing the representation of the data used. At the end of the simulation process, 22,820 tests were available. Figure 3 represents several examples of the data obtained. Moreover, the use of these tests in the various AI models varied according to the study's needs. The 75% of the 22,820 tests was used as the training dataset (with 17,115 instances), and the remaining 25% was used for the testing dataset (with 5705 instances).

## 2.2 AI Algorithm: Random Forest

The AI algorithm used was the random forest. Random forest is an evolution of classification and regression trees. The algorithm creates a set of classification and regression tree models by removing some of their limitations, such as the overfitting or the influence of atypical values [24, 25], thus reducing the variance and the bias of the model [26, 27]. Likewise, it is an algorithm used to develop effective models by using large datasets; moreover, it is not influenced by atypical values [28]. The number of trees considered in the algorithm significantly influences the performance of the random forest model [29]. To train a RF model, the training subset is divided into  $N$  samples [27]. Each sample generates a tree model. The estimate given by the random forest model ( $\hat{Y}_{\text{RF}}$ ) is obtained from the average of the estimates given by each tree ( $\hat{Y}_t$ ):

$$\hat{Y}_{\text{RF}} = \frac{1}{T} \sum_{t=1}^T \hat{Y}_t \quad (3)$$

where  $T$  is the number of trees.

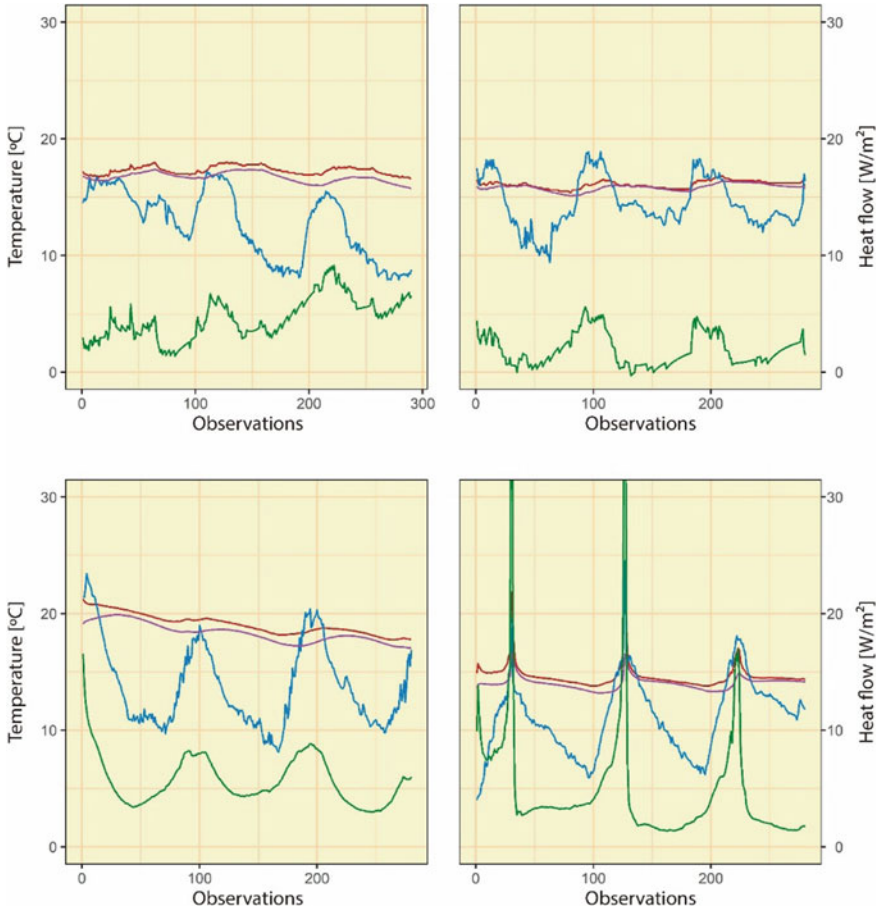


**Fig. 3** Example of several time series simulated. The graphs represent the indoor air temperature (in red), the outdoor air temperature (in blue), the indoor surface temperature (in purple), and the heat flow (in green)

### 3 Results and Discussion

First, the optimal number of trees of each random forest model was selected to optimize their performance. For this purpose, the performance obtained by the models with numbers of trees between 2 and 150 was analyzed through both the determination coefficient ( $R_2$ ) and the average error obtained. The analysis showed that random forest models with a number of 54 and 56 trees and with data obtained by HFM and THM were the most appropriate options. Table 1 summarizes the results obtained by the statistical parameters. Performances were satisfactory in the training phase, although the performance obtained with the HFM approach was the most appropriate. To analyze the error associated with each instance of the testing dataset, Figs. 4 and 5

**Table 1** The results obtained by the statistical parameters in the training phase with an optimal tree configuration

Approach	Number of trees	$R_2$ (%)	Average error
HFM	54	97.09	0.4469
THM	56	95.70	0.6041

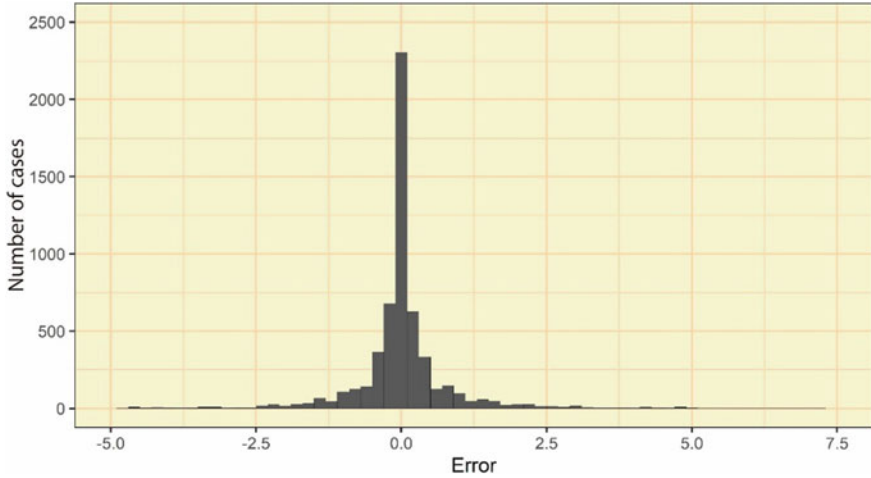


**Fig. 4** Histogram of the error obtained in the estimate of the A-weighted overall sound reduction index with the random forest model of the HFM approach

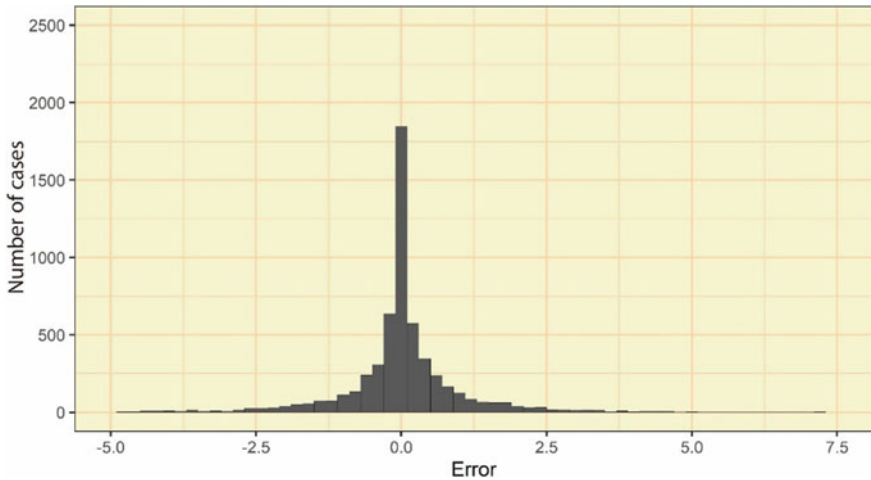


**Fig. 5** Histogram of the error obtained in the estimate of the A-weighted overall sound reduction index with the random forest model of the THM approach

include the histograms of the error obtained in the testing. The percentage of instances with a low error was high. In this regard, in the HFM approach, the 69.79% of the instances obtained an error lower than 0.4 dBA, whereas in the THM approach, the percentage was 60.35%. Likewise, the approach was limited to a certain extent, since some instances obtained high errors. Nonetheless, the low percentage of cases of the instances for the testing dataset (13.21% in HFM and 18.7% in THM) guarantees the reliability of the approach to characterize  $R_A$  by monitoring thermal transmittance tests.

## 4 Conclusions

Thermal transmittance tests are crucial to know the existing built environment accurately and to establish energy conservation measures. As these tests could be widely used, the use of variables monitored to obtain greater information is an important aspect that should be analyzed. The previous studies have assessed the possibility of determining thermal variables (e.g. the periodic thermal transmittance), although there are other variables from other characteristics that could be obtained. For this reason, this study analyzed the possibility of determining acoustic variables.

The results of this chapter have shown the feasibility of characterizing the A-weighted overall sound reduction index by monitoring thermal transmittance tests. For this purpose, having prediction models using the random forest algorithm is essential. The use of monitoring variables of the main thermal transmittance tests (i.e. ISO 9869-1 or thermometric method) allowed low errors to be obtained in the estimates of the A-weighted overall sound reduction index. Thus, it would be possible to obtain knowledge on this variable through thermal transmittance tests. This would provide thermal transmittance tests with a great potential. The advantage of having combined analysis procedures to characterize different variables or properties of building envelopes would guarantee greater information of the existing building stock, as well as greater profitability in performing these tests as more results would be obtained. Thus, the results obtained by the tests could be used to design energy conservation measures to improve users' acoustic comfort conditions.

## References

1. European Commission (2011) A roadmap for moving to a competitive low carbon economy in 2050. Brussels, Belgium
2. Kurekci NA (2016) Determination of optimum insulation thickness for building walls by using heating and cooling degree-day values of all Turkey's provincial centers. *Energy Build* 118:197–213. <https://doi.org/10.1016/j.enbuild.2016.03.004>
3. Vine EL, Kazakevicius E (1999) Residential energy use in Lithuania: the prospects for energy efficiency. *Energy* 24:591–603. [https://doi.org/10.1016/S0360-5442\(99\)00013-4](https://doi.org/10.1016/S0360-5442(99)00013-4)

4. Invidiata A, Lavagna M, Ghisi E (2018) Selecting design strategies using multi-criteria decision making to improve the sustainability of buildings. *Build Environ* 139:58–68. <https://doi.org/10.1016/j.buildenv.2018.04.041>
5. Rubio-Bellido C, Perez-Fargallo A, Pulido-Arcas JA (2016) Optimization of annual energy demand in office buildings under the influence of climate change in Chile. *Energy* 114:569–585. <https://doi.org/10.1016/j.energy.2016.08.021>
6. Bienvenido-Huertas D, Moyano J, Marín D, Fresco-Contreras R (2019) Review of in situ methods for assessing the thermal transmittance of walls. *Renew Sustain Energy Rev* 102:356–371. <https://doi.org/10.1016/j.rser.2018.12.016>
7. Cesaratto PG, De Carli M, Marinetti S (2011) Effect of different parameters on the in situ thermal conductance evaluation. *Energ Build* 43:1792–1801. <https://doi.org/10.1016/j.enbuild.2011.03.021>
8. Desogus G, Mura S, Ricciu R (2011) Comparing different approaches to in situ measurement of building components thermal resistance. *Energ Build* 43:2613–2620. <https://doi.org/10.1016/j.enbuild.2011.05.025>
9. Trethowen H (1986) Measurement errors with surface-mounted heat flux sensors. *Build Environ* 21:41–56. [https://doi.org/10.1016/0360-1323\(86\)90007-7](https://doi.org/10.1016/0360-1323(86)90007-7)
10. Meng X, Yan B, Gao Y, Wang J, Zhang W, Long E (2015) Factors affecting the in situ measurement accuracy of the wall heat transfer coefficient using the heat flow meter method. *Energ Build* 86:754–765. <https://doi.org/10.1016/j.enbuild.2014.11.005>
11. Gaspar K, Casals M, Gangolells M (2018) In situ measurement of façades with a low U-value: avoiding deviations. *Energ Build* 170:61–73. <https://doi.org/10.1016/j.enbuild.2018.04.012>
12. Ahmad A, Maslehuddin M, Al-Hadhrani LM (2014) In situ measurement of thermal transmittance and thermal resistance of hollow reinforced precast concrete walls. *Energ Build* 84:132–141. <https://doi.org/10.1016/j.enbuild.2014.07.048>
13. Litti G, Khoshdel S, Audenaert A, Braet J (2015) Hygrothermal performance evaluation of traditional brick masonry in historic buildings. *Energ Build* 105:393–411. <https://doi.org/10.1016/j.enbuild.2015.07.049>
14. Grubeša IN, Teni M, Krstić H, Vračević M (2019) Influence of freeze/thaw cycles on mechanical and thermal properties of masonry wall and masonry wall materials. *Energies* 12:1–11. <https://doi.org/10.3390/en12081464>
15. Bienvenido-Huertas D, Rodríguez-Álvaro R, Moyano JJ, Rico F, Marín D (2018) Determining the U-value of façades using the thermometric method: potentials and limitations. *Energies* 11:1–17. <https://doi.org/10.3390/en11020360>
16. Kim S-H, Lee J-H, Kim J-H, Yoo S-H, Jeong H-G (2018) The feasibility of improving the accuracy of in situ measurements in the air-surface temperature ratio method. *Energies* 11:1–18. <https://doi.org/10.3390/en11071885>
17. International Organization for Standardization (2007) ISO 6946:2007—Building components and building elements—Thermal resistance and thermal transmittance—Calculation method. Geneva, Switzerland
18. Ficco G, Iannetta F, Ianniello E, D’Ambrosio Alfano FR, Dell’Isola M (2015) U-value in situ measurement for energy diagnosis of existing buildings. *Energ Build* 104:108–121. <https://doi.org/10.1016/j.enbuild.2015.06.071>
19. Bienvenido-Huertas D, Rubio-Bellido C, Pérez-Ordóñez JL, Oliveira MJ (2020) Automation and optimization of in-situ assessment of wall thermal transmittance using a Random Forest algorithm. *Build Environ* 168. <https://doi.org/10.1016/j.buildenv.2019.106479>
20. Bienvenido-Huertas D, Rubio-Bellido C, Solís-Guzmán J, Oliveira MJ (2020) Experimental characterisation of the periodic thermal properties of walls using artificial intelligence. *Energy* 203. <https://doi.org/10.1016/j.energy.2020.117871>
21. Eduardo Torroja Institute for Construction Science (2010) Constructive elements catalogue of the CTE
22. Kurtz F, Monzón M, López-Mesa B (2015) Energy and acoustics related obsolescence of social housing of Spain’s post-war in less favoured urban areas. The case of Zaragoza. *Inf La Construcción* 67:m021. <https://doi.org/10.3989/ic.14.062>



23. Domínguez-Amarillo S, Sendra JJ, Oteiza I (2016) La envolvente térmica de la vivienda social. El caso de Sevilla, 1939 a 1979. Editorial CSIC, Madrid
24. Dudoit S, Fridlyand J, Speed TP (2002) Comparison of discrimination methods for the classification of tumors using gene expression data. *J Am Stat Assoc* 97:77–87
25. Larivière B, Van Den Poel D (2005) Predicting customer retention and profitability by using random forests and regression forests techniques. *Exp Syst Appl* 29:472–484. <https://doi.org/10.1016/j.eswa.2005.04.043>
26. Breiman L (1996) Bagging predictors. *Mach Learn* 24:123–140
27. Breiman L (2001) Random forests. *Mach Learn* 45:5–32. <https://doi.org/10.1023/A:1010933404324>
28. Assouline D, Mohajeri N, Scartezzini JL (2018) Large-scale rooftop solar photovoltaic technical potential estimation using Random Forests. *Appl Energ* 217:189–211. <https://doi.org/10.1016/j.apenergy.2018.02.118>
29. Zhou Y, Qiu G (2018) Random forest for label ranking. *Exp Syst Appl* 112:99–109. <https://doi.org/10.1016/j.eswa.2018.06.036>

# Methodology for the Evaluation of an Energetic Model of Thermal Transmittance in a Window by Means of Horizontal Aggregation (HA) from Short-range Photogrammetry for Model Digital Twin



María Fernández-Alconchel, Juan E. Nieto-Julián,  
Manuel J. Carretero-Ayuso, and Juan Moyano-Campos

**Abstract** One of the great challenges in the architecture, engineering, and construction (AEC) industry is data communication and its development in modelling techniques. The development of 5G techniques, with the Internet of things (IoT), artificial intelligence (AI), amongst others, is developing significant advances for staging of data integration in the so-called digital twins (DTs). Undoubtedly, the DTs intend to synchronize the real physical data with a digital world that experiences successive changes that occur throughout the life cycle of the system. In this context, this work experiments with a horizontal integration methodology to evaluate the U-value of a window frame from structure from motion (SfM) photogrammetry data, as part of a digital twin. The “in situ” evaluation of the thermal transmittance of a common aluminium window frame that is being used in existing buildings in the 1960s and that reached constructions of the 1980s is addressed. The experimental results apply simulation analysis using two-dimensional software. Thermal transmittance measurement equipment was used through a thermal flow meter plate, and the variations in thermal behaviour were analyzed according to the geometry of the frame. The results show different Uf-value data between the simulation and the in situ measurement with a dispersion variability of 1.5 W/m<sup>2</sup>K between the models. The essence and originality of the experimentation lie in the integration of horizontal aggregates (HA) as a basis in the simulation, measurement, and reverse engineering processes to an energy model of the DT system.

**Keywords** Structure from motion (SfM) · Digital twins · Window frame · U-value · Horizontal aggregates

---

M. Fernández-Alconchel · J. E. Nieto-Julián · J. Moyano-Campos (✉)  
Department of Graphical Expression and Building Engineering, University of Seville, Seville,  
Spain  
e-mail: [jmoyano@us.es](mailto:jmoyano@us.es)

M. J. Carretero-Ayuso  
Department of Architecture, University of Alcalá, Alcalá de Henares, Spain

## 1 Introduction

The United Nations Framework Convention establishes as a priority agreement to work on reinforcing the response to climate change, in which there is also a double aspect of mitigation in search of sustainability and investment towards a digital transition economy [1]. The Summit of World Leaders in Convection (UNFCCC) is not new, recently the one held in Glasgow (UK) and its precedent in the Paris Summit in 2020. In this global context, there are two aspects that are closely related that are; the mitigation of the energy consumed in buildings, and on the other hand, the increase in new paradigms in digital technology platforms, including virtual ones, sustainability procedures, and effective interaction of project stakeholders. The ecological transition is supported by regulation (EU) 2020/852 for the mitigation of climate change.

In the global context, buildings represent rates around 40% of global energy consumption [2]. This means that due to the fact that most of the energy consumed during the use of the building comes from non-renewable resources, it is necessary to reduce the energy consumption of existing buildings [3, 4]. This causes unfavourable situations for users, such as energy poverty [5–7] or energy inequalities between regions [8–10]. Also, the current situation of monetary poverty is creating problems for citizens to meet the energy bill [11–13]. For this reason, it is essential to improve the energy performance of existing buildings. For this, although the use of adaptive strategies may be interesting [14–16], the ideal is to implement energy conservation measures [17, 18].

Windows are elements that form an integral part of the building envelope and therefore are responsible for the exchanges of heat and light between interior spaces [19]. The energy performance of windows significantly influences the energy demand and represents a fundamental question for evaluating the energy loss of buildings. Windows as elements are considered energy efficient if they have a low-thermal transmittance (U-value). These values in Spain, where this study is focussed, and according to the UNI EN ISO-10077-2 [20] standard, provide a methodology to evaluate the thermal behaviour of the frame and also establish the criteria that validate a numerical model. The index that characterizes the thermal flux of the windows is the thermal transmittance  $K$  designated with the letter or factor  $U$  ( $W/m^2K$ ). The thermal behaviour of the openings depends on the design, technology, and materials of the frame profiles and the door or window leaf.

In another sense, there is the digitization process that seeks to enhance the infrastructures, skills, and technologies for a digital society. The new dynamic approach based on digital twins (DTs) allows for real-time evaluation and control of parameters in a quantitative sustainability assessment. Obtaining a digital twin (DT) supports decision processes related to energy aspects. The digital twin is the collection link for the relevant digital artefacts [21], including engineering, operational, and descriptive data. Therefore, simulation technology offers the opportunity to integrate physical data and merge the real and virtual world.

The term digital twins (DTs) have several meanings, thus Al-Sehrawy and Kumar [22] determined up to 18 different definitions, defined in three aspects; identity and nature, objective and purpose, and finally the third in the main constituents, elements, and components. Of all of them, the digital twin was found as a construction of digital information on a physical system, an element defined by Grieves and Vickers [23]. In this sense, Grieves presented DT for the first time at a conference in 2002 at the University of Michigan. From then in, NASA incorporated this term on satellites that were not accessible for research inspections. This new concept requires generating precision in the measurements and obtaining results related to new physical models. Therefore, converting the analysis case studies of this project using BIM models into a digital twin allows (i) collection, (ii) analysis, and (iii) visualization of the data, that is, the monitoring of the gradients of temperature, humidity, and flows of water heat in a digital model. Advances in digital twins can serve as enabling technologies. Tao et al. [24] worked on the six important points to build a digital twin. One of the main steps is the reconstruction of a virtual representation and incorporating data to facilitate design decisions and simulations of virtual systems. Digital twins therefore monitor the life cycle of a process by reproducing its operation in a virtual model. Angjeliu et al. [25] in a reduced term speaks of a digital replica of physical reality. Hence, the importance of reconstructing the case studies in BIM models that, in addition to representing the complex geometric structures, can control the semantic content.

In this line, the objective of this work is to implement the transfer systems for a horizontal aggregation (HA) that adds value to the changes of a digital model and that have to do with the mitigation of the energy consumption of buildings, in what the strategy is geared towards the green and digital transition.

## 2 Related Work

The importance of financing institutions for the economic progress of the digitized construction industry is essential to reduce the ecological and environmental footprint [26]. Both digital twins and the Internet of things (IoT) pay close attention to information management solutions in both established and emerging areas [27]. The DTs allow the integration of three modalities; on the one hand, they contain real-time data records in real time, reliable, and resistant to changes [28], they also allow automated optimization protocols through IoT, they also allow automated optimization protocols through IoT, and thirdly, they allow monitoring in a chain of blocks [29]. Of these three lines in which the DT participates in, the flow of information towards a BIM level 3 increases in the automatic processes of data acquisition techniques such as photogrammetry (SfM) or terrestrial laser scanner (TLS), for which there is an opportunity to migrate digital interface wallets [10]. Wong et al. [30] state in this sense that the current industry 4.0 is interested in technological ecosystems that include digital twins as the work process on the asset life cycle of assets.

The four categories of the research go through the incorporation of the real capture through photogrammetry or optical laser, evaluating the dispersion between both techniques, passing the model to a BIM generator, and third, the applicability of the IoT, network technologies. Sensors and monitoring through software that recognizes the energy analysis of the digital model. Monitoring the frame of a window is a task that can be thought of as simple but seeing the particularities of the process of evaluating and capturing horizontal aggregation as monitoring in a digital twin has not been done yet. One of the most widely used and researched applications is the determination of the thermal transmittance of walls [31]. In this sense, in recent years, studies of the thermal characterization of walls have addressed four fundamental aspects: (i) the optimization of quantitative infrared thermography methods, through studies carried out by Tejedor et al. [32, 33] and Bienvenido-Huertas et al. [34, 35]; (ii) the improvement and limitations of the heat flow metre method [36–38]; (iii) the application of artificial intelligence [39, 40]; and (iv) the application in historic buildings [41, 42].

With respect to windows, the studies are more focussed and with respect to the improvement of the thermal transmittance of window frames. Malvoni et al. [43] established a two-dimensional numerical method for the evaluation of thermal behaviour in the sections of the frame according to UNI EN ISO 10077-2, in which the characteristics of the use of different materials inside the frame are validated through software. Lechowska et al. [44] propose two different ways to decrease the thermal transmittance of the window frame without modifying its geometry. The evaluation is also done through CFD. And Baldinelli and Bianchi [45] performed a comparative analysis by thermography from a 2D and 3D simulation. Characterizing the thermal transmittance of the envelope is closely linked to the study of walls, windows, and homogeneous elements, and in addition to the heat flux method HFM according to ISO 9869-1 [46], infrared thermography (IRT) in its two aspects of analysis both qualitative and quantitative [47] helps to characterize the surface that involves possible heat transfer phenomena [48].

### 3 Methodology and Horizontal Aggregation

An experimental work is carried out, where through the installation of several temperature sensors, sensors that measure the speed of the external wind, heat flow transducer plates and others, the in situ measurement of the thermal transmittance of the window frames. In addition, the results of the thermal transmittance simulation of the window frame are verified using Psi-Therm 2D software [49]. The integration of the experimental data allows us to evaluate in real time the monitoring of the digital twin. In this reporting process, it will be possible to determine the HA that can be incorporated into a BIM model, with the aim of adding value to the digital twin in the energy behaviour and in the future scenario of the building. The use of BIM in horizontal aggregates allows one to establish an original path in the monitoring process of parametric elements not currently used in the energy field.

### 3.1 Data Acquisition and Measurement Verification

3D modelling and reconstruction have been considered as a digital representation that contemplates the geometric and simplified properties of a building, or architectural object (Fig. 1). They are models that provide an immediate representation of the designed architecture in three dimensions. Progress in the digital BIM platform involves introducing semantic components, represented as digital objects with relationships, attributes, and properties [50]. Although the parametric objectives contained in the BIM platforms are closely related to the objects provided by the manufacturers of the commercial houses, for example, doors, windows, and accessories that are part of the envelope. The platforms allow the creation of parametric objects extracted from the design process and that can incorporate the desired semantic components. But the initial phase to obtain correct geometric properties is scanning, whether optical, photogrammetric, or through LIDAR. And here appear the data acquisition techniques, which in this case has been chosen for SfM.

The topographic survey technique was carried out from a sequence of convergent photographs using a NIKON D80 digital reflex camera with a 12 MP sensor of size: 23.6–15.6 mm, Nikon DX AF-S NIKKOR 18–135 mm f lens./3.5–5.6 G ED. The focal length used was 18 mm, optical image stabilizer, and exposure (fixed) 1/400 sf 3.5. The CCD sensor is 23.6 mm  $\times$  15.8 mm, distributed over 3872  $\times$  2592 pixels for maximum resolution in NEF RAW format. ISO was set at 200 at 9 m altitude (relative to the starting altitude). Four visible control points were set at the various positions to create a reference ( $x, y, z$ ) coordinate system. The control points are taken through a calliper that has millimetre precision, that is, 0.1 E–3. The results obtained from the photogrammetry is a cloud of points with the exact geometric properties that will define the digital replica. The insertion in the BIM platform is immediate to obtain the characteristics and properties of the elements in the 3D reconstruction.

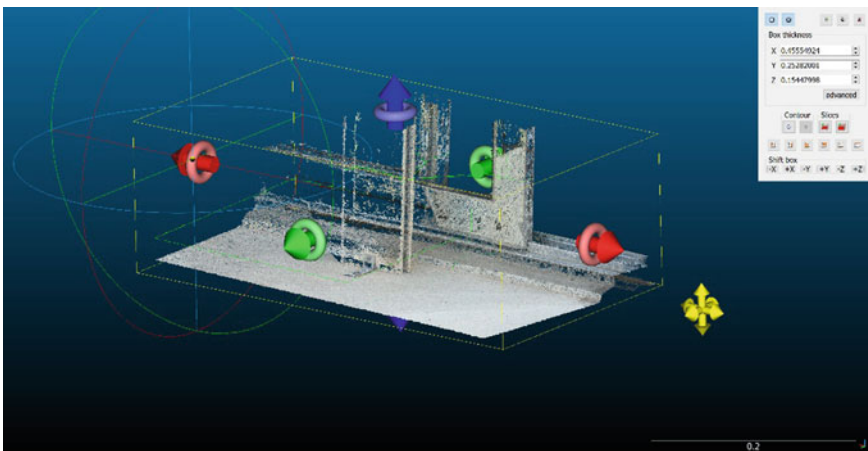


Fig. 1 3D model from the photogrammetry of the aluminium window

### 3.2 Experimental Validation of “in Situ” U Measurements

In the study, a detailed analysis of the enclosure and carpentry is carried out to obtain experimental tests. The “in situ” measurements of the thermal transmittance measurements (U-value) in an aluminium window frame containing dimensions of 1.80 m × 1.90 m. The window is located on the fourth floor of an office of the Higher Technical School of Building Engineering of the University of Seville. The Ahlborn Almemo 2590-4AS (Ahlborn Mess—und Regelungstechnik GmbH, Deutschland) data acquisition equipment consists of a 20 mm × 80 mm flexible heat flux plate and also has thermocouples that measure contact or ambient temperature and outside temperature and interior of the different elements that make up the experimental campaign. The equipment has been used for monitoring in a calibrated camera system by Lechowska et al. [44] and to measure enclosures other than Bienvenido-Huertas et al. [51, 52]. Accompanying this equipment, a CR1000KD was used to make some measurements of the data and have a more exact value in the outdoor temperature records. The data analysis was performed with a frequency of 10 min per record for a total of three days. Two experimental campaigns have been carried out in a Mediterranean region where the climatic limitations are based on cold winters with little rain and very hot summers with no rain. A period in the month of April characterized by very mild temperatures with high temperatures at noon and in which a thermal jump of more than 8 °C is not achieved and in the winter phase. And another measurement phase in the month of December where a thermal gradient of at least 12 °C has been achieved, with which it can be estimated as the most appropriate measurements to obtain the  $U_f$ -value.

The thermal transmittance of the frame section  $U_f$  [W/m<sup>2</sup> K] is defined according to the UNI EN ISO 10077-2 standard and according to Eq. 1:

$$U_f = \frac{L_f^{2D} - U_p b_p}{b_f} \quad (1)$$

where

- $L_f^{2D}$  [W/mK] is the thermal conductance of the frame section;
- $U_p$  [W/m<sup>2</sup>K] is the thermal transmittance of the central area of the panel;
- $b_p$  [m] is the visible width of the panel;
- $b_f$  [m] is the width of the frame section.

The results obtained both the interior temperature with two thermocouples and the exterior temperature. In addition, the heat flux of the frame is obtained, and the results obtained are graphed in Fig. 2.

In this study, other physical factors such as heat, light, and sound have not been analyzed, which are also factors that guarantee the comfort of users, since the objective is shown as a determination of the possible controls and analysis of a used

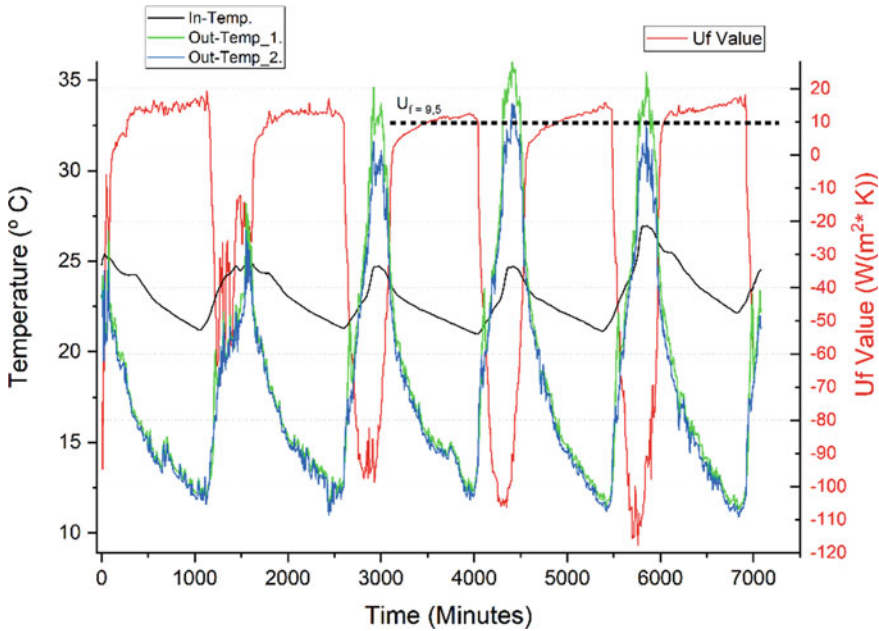


Fig. 2 Graph of the comparison between the data collected by Almemo and CR1000KD

carpentry. Frequently, in all homes catalogued between the 1960s and 1980s in the Mediterranean area of southern Spain and in other regions of Europe.

### 3.3 Simulation and Distribution of Window Frame Temperatures

For modelling, a single type of configuration has been made on the aluminium frame that supports a simple glass, and according to the stipulations of the Spanish Community in aluminium windows and the technical building code CTE 2009 establishes the thermal transmittance with a theoretical value of  $5.7 \text{ (W/m}^2\text{K)}$ . The 3D model is obtained with elements that are very precise in their dimensions, hence the originality added to this research, which is why the exact geometry of the element has been acquired through the photogrammetric study. In this sense, the scientific community knows that the geometry and characteristics of the cavities influence the general performance of the frame [43]. The modelling of the window, being a discontinued carpentry and not having a type of manufacturer profiles, requires the necessary geometric analysis to take it to the simulation model. It is an aluminium carpentry (high-thermal conductivity:  $K = 160 \text{ W/mK}$ ) and an air space between the window profile (Table 1). Typical carpentry in the European Union of the constructive



**Table 1** Materials used in the simulation

Materials used						
Material	$\lambda$ W/(mK)	$C$ J/(kg K)	$\rho$ kg/m <sup>3</sup>	$\mu$	Obj	Comments
PVC	0.17	960	1390	50,000	2	ISO 10077-2 validation material; $\lambda$ according to ISO 10077-2; $C\rho, \rho, \mu$ are typical values but not relevant for the validation
Glass	1	750	2200	1,000,000	1	ISO 10077-2 validation material; $\lambda$ according to ISO 10077-2; $C\rho, \rho, \mu$ are typical values but not relevant for the validation
Aluminium	160	880	2800	1,000,000	1	ISO 10077-2 validation material; $\lambda$ according to ISO 10077-2; $C\rho, \rho, \mu$ are typical values but not relevant for the validation

typologies of the years 1960–1980. The boundary conditions have been established according to ISO 10077-2 [53]. For the modelling, two scenarios were established, setting the air temperature at  $-5\text{ }^\circ\text{C}$  for the external environment and  $20\text{ }^\circ\text{C}$  for the interior environment (Tables 2, 3, and 4). The second scenario has been to establish the maximum and minimum values of the real registers. The process has been through the implementation of numerical simulations in two- and three-dimensional domains with the CFD code through the Psi-THERM 2D software [49] (Figs. 3 and 4).

**Table 2** Limits set in the simulation

Limits			
Limits	$T\text{ }^\circ\text{C}$	RH (%)	Objects
Internal climate	20	50	1
Internal climate reduced	20	50	3
External climate	0	80	1

**Table 3** Heat transfer resistance

Heat transfer resistance			
Name	$R$ (m <sup>2</sup> K)W	of the material	to the material
dyn1	0.13	All	Internal climate
dyn2	0.2	All	Internal climate reduced
dyn3	0.04	All	External climate

**Table 4** Boundary conditions and heat fluxes

Boundary conditions and heat fluxes				
Name	Temp (°C)	$R_{si}/R_{se}$	Length (m)	Heat fluxes W/m
R1			10.79	
R2	-5	0.04	1.84	-150.13
R3	-5	0.04	0.2	-2.799
R4	-5	0.04	0.24	-15.006
R5	-5	0.04	2.48	-215.131
R6	20	0.13	2.48	211.228
R7	20	0.13	0.24	17.942
R8	20	0.13	0.21	5.053
R9	20	0.13	1.83	148.844

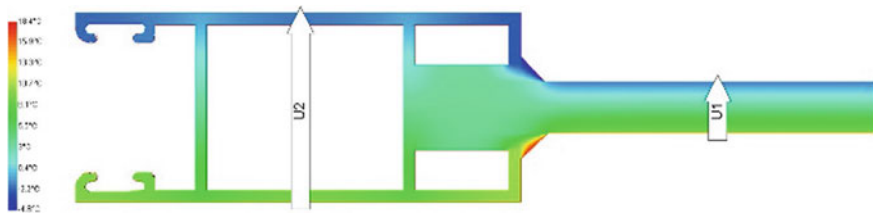


**Fig. 3** Temperature contour simulation

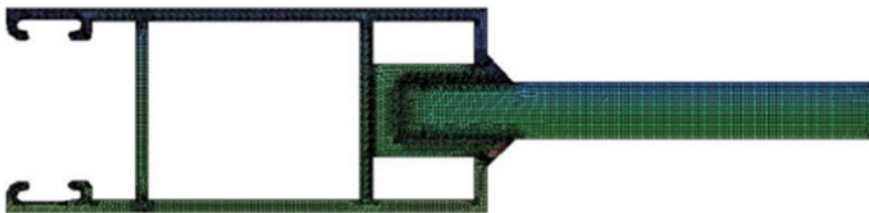


**Fig. 4** Heat flow contour simulation

The thermal bridge loss coefficient of the window obtained a linear thermal transmittance value of  $\psi = +14,217 \text{ W/(mK)}$ .

### 3.4 Application of Infrared Thermography Technique

We know that the infrared thermography technique (ITT) technology is widely used to evaluate heat losses, associated with thermal bridges [54, 55] or in general, in

buildings [56]. Therefore, it is essential that there is an energy analysis as a horizontal aggregate where heat losses from the environment of the window elements are examined according to Figs. 5 and 6.

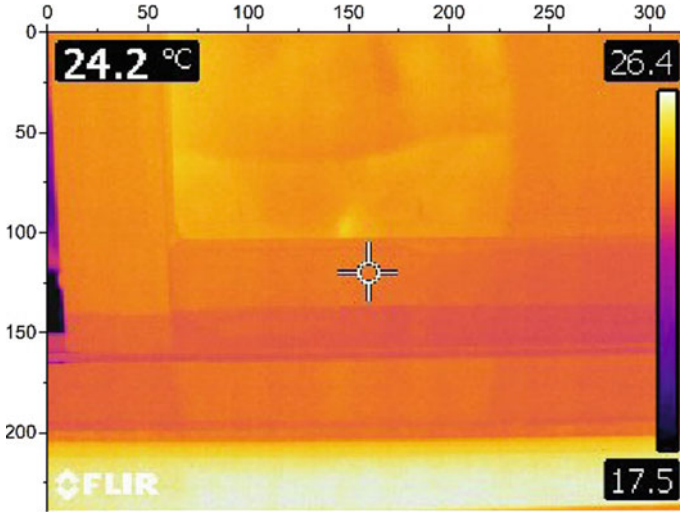


Fig. 5 Thermal image of the aluminium window

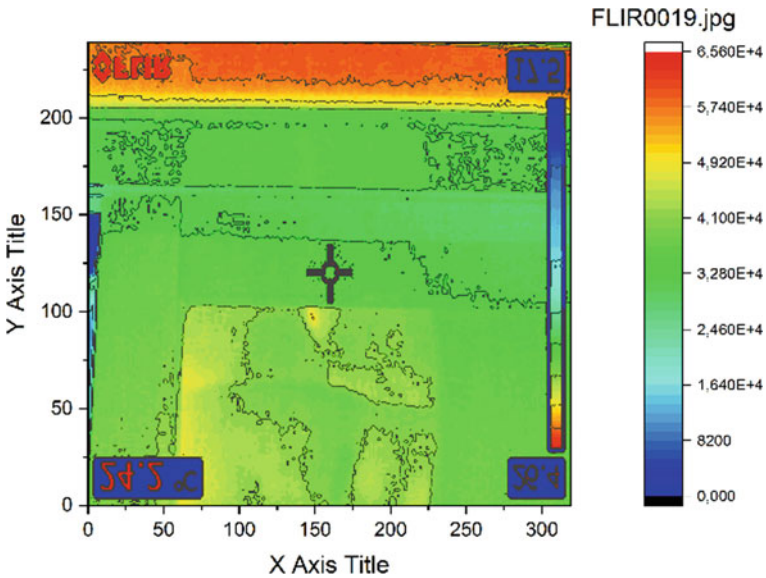
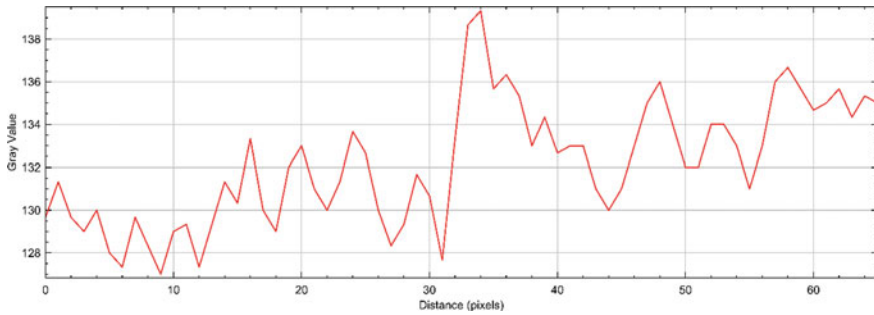


Fig. 6 Temperature differential image



**Fig. 7** Image of the thermogram analysis on a profile that cuts the window frame

To observe the temperatures that have been recorded on the internal and external surface of the frame, they have been measured with a FLIR E60bx infrared camera, with a measurement range of  $-10$  to  $105$  °C, FOV of  $25^\circ \times 19^\circ$ , and IFOV of  $1.036$  m rad. The spectral range of the camera is  $7.5\text{--}13$   $\mu\text{m}$ , and the thermal sensitivity is less than  $0.05$  °C at  $30$  °C. The camera was placed on a tripod, at a perpendicular distance of  $1.5$  m from the camera. Wall and with a  $20^\circ$  tilt angle of  $20^\circ$  to avoid reflections on the wall. These temperature measurements can be contrasted with the datalogger records and verify the results obtained. For the partial sector of the window and view from the inside, a series of thermograms are made, and subsequently, the image is post-processed through specialized software that gives a matrix of  $300 \times 240$  temperature values. The basic principle of IRT is that all bodies emit thermal radiation that depends on their temperature and emissivity. IRT allows the infrared radiation of an object to be captured without the need for it to be illuminated. Figure 5 shows an example of the application of these non-destructive testing techniques. The images can be processed to obtain the greatest variability of exchanges and heat sources in Fig. 7 and to appreciate different ranges depending on the interest of the researcher.

Studies that determine the problems that thermal bridges can pose, and even for components as small as windows [54], assume that IRT can develop different approaches when active lines are used, as is the case for the image in Fig. 7. In this case, as can be seen from the image, the change in pitch from the frame to the glass can be determined through the pixels. The EN ISO 10077-2 standard deals with numerical calculations for window and door frames. Actually, the thermal bridge between glass and glass is minimal in this type of carpentry. Therefore, the quantitative thermographic image allows the validation of simulations of the energy loss analysis and the evaluation of the energy performance, as well as the global energy losses of the construction elements.

## 4 Insertion of Reports to BIM

Most of the applicability of DT has to do with the aeronautical industry and especially with the maintenance of jet engines. But in the field of the energy sector and the cultural heritage sector, there is little research, and its applicability is almost nil. One of the causes is that buildings have a very long useful life, and this is complex in practice [25]. The new term found as a paradigm in the production of industry 4.0 is called DT, and the concept, despite being defined by Glaessgen and Stargel [57] as a probabilistic, multiphysics, and multiscale simulation, actually allows the integration of significant advances in monitoring in a replica of the product. The improvement in the digital model according to Angjeliu et al. [25] could include (i) geometric data enhancements, (ii) materials characterization, (iii) contour data enhancements, and (iv) prediction. In essence, the structure is composed of a physical model, information data container and that the model can obtain simulation reports, it is a structure undoubtedly applied to structural elements of a building, and therefore, the essence of this area is to establish models of adjustment according to the specific areas of knowledge. The structural model goes through phases different from an energy model. For example, Kang et al. [58] proposed an implementation of six phases in bridge structures and that by applying them, the reality of the real world can be predicted and the optimal operating conditions of the virtual environment can be analyzed. It is necessary to design a DT model considering the information that can be extracted from the process and the usability of the system for its application. Kang et al. [58] they insist that to implement a digital twin model, attributes based on data and simulations must be used, these attributes are what we call in this research horizontal aggregates (HA). In our case in the creation of an energetic digital twin, the design of the method has been based on a BIM platform, where the HAs are incorporated into the parametric digital model. Building information models (BIMs) are relational and parametric in nature [59] and their benefits have to do with implementation costs and time. Instead, here, the model emerges as an information container and a database that can be updated in real time. The interest that digital twins have shown comes from the obtaining and availability of data groups that monitor physical entities. But the methodology for creating digital twins does not yet have a fixed standard or standards. Integrating the experimental physical reality and analysing the responses of energy reports and their preventive maintenance operations is an original case in this research. The objective achieved is to reduce the discrepancy between numerical and experimental results and create complex and to intelligent simulation models [25].

Many of the building information modelling (BIM) studies with energy simulation work to establish IFC database schemas with common gbXML formats from Green Building [60], these are processes that keep being aggravated in a two-phase connectivity to the real world. The PassivBIM Java tool that allows connectivity to design parameter transfer decisions [61] can process geometry from IFC files, optimizing energy performance. In Fig. 8, the digital model is built from the base of a DT\_energetic. BIM platforms can be subject to a hybrid model that combines

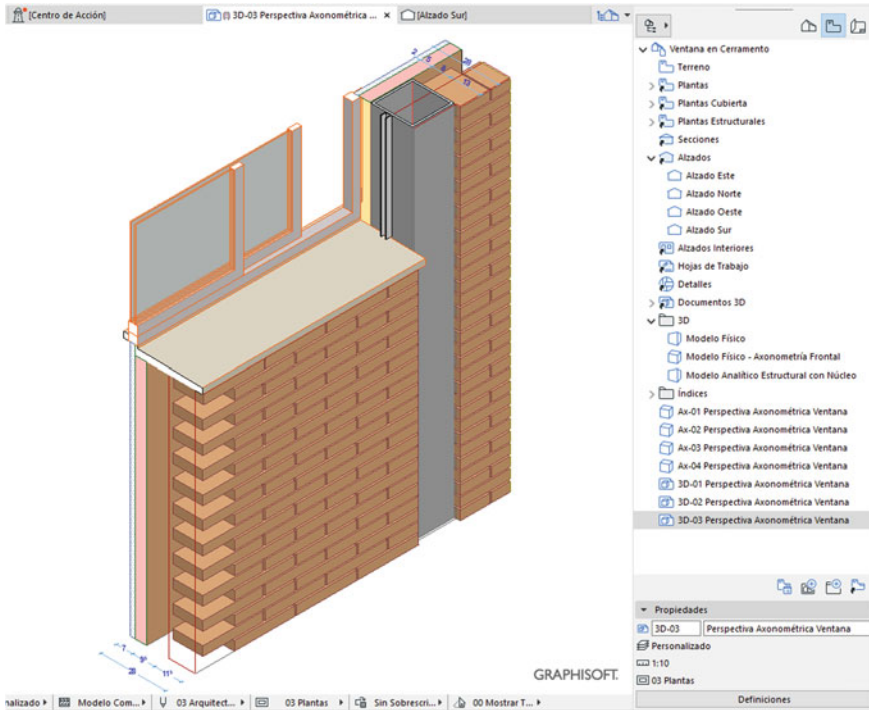


**Fig. 8** BIM modelling of the hollow insert of the window frame

energy reports over time and continuous geometric models, where three-dimensional modifications can be expressed in parametric objects.

In this discussion of the model that a digital twin is not about a BIM with sensors, Zhang et al. [62] bet on the possibility that a DT can be derived from a building information model. Khajavi et al. [63] compared a digital twin with BIM, and the main difference is that the DT administrators in the building cycle phase to improve its operation. Although the application software in engineering through DT Predix [64] may be different from those of building, BIM can be contextualized to acquire DT processes.

## 5 Results and Discussion

The energy policies that the large developed countries are carrying out, as well as the actions aimed at reducing energy consumption, require an integrating plan where most sectors become aware of the importance of reducing energy consumption. But this integrative plan requires optimization of energy performance, based on an integrative design approach by the administrations and interdisciplinary teamwork that

optimizes energy use and the quality of the interior environment of the building [65], with current uses and new construction buildings. The recent emergence of BIM platforms and the numerous applications of the Internet of things (IoT) offer new knowledge and capabilities to adapt new models that inform the study and decisions on the life cycle of the building. At present, a new term DT arises for the built environment, digital twins, whose objective is the synchronization of the real world with the digital platform for the management of construction processes [66]. Currently, there are European projects such as the SPHERE project that provides a BIM-based digital twin platform as a service to optimize the life cycle of the building and reduce costs and improve energy efficiency. But the main question that researchers are asking is how does a physical world integrate with a digital world? Deng et al. It tries to answer this question through a development of five-level taxonomies to reflect the evolution from BIM to DT. It includes the simulations compatible with BIM, the integration of the IoT, the applicability of artificial intelligence environments to establish predictions, and finally, the ideal DTs. Really called in this work, horizontal aggregation (HA) those systems that complement a digital twin through these taxonomies based especially on a hierarchical structure.

Firstly, during the design or manufacturing phase, the digital twin is created, through reverse engineering for existing buildings, and in the case of prototypes based on a first design cycle. In this case, the 3D reconstruction of a window element has been modelled and considered as a digital representation that considers the geometric and simplified properties. Therefore, the HA would be a three-dimensional object in a perfectly measurable and precise coordinate system ( $x, y, z$ ). In the results that have been obtained, distances greater than 2 mm in thickness have been detected between the use of massive data capture systems (MDCSs) techniques and the manual dimensioning procedure. The second aggregate (HA) will be the massive energy data components, that is, monitoring through temperature and humidity probes and thermal flow plates. We determined that based on the ISO 10077-2 standard that deals with numerical calculations of window and door frames, the specifications of an aluminium window frame thermal transmittance value is 5.7 U (W/m<sup>2</sup>K), but the results of the values obtained in the “in situ” measurement are really different, obtaining a  $U_f$  result of 9.5 U (W/m<sup>2</sup>K). In these types of aggregations (HA), we can distinguish different phases of operations that have to do with the monitoring of probes, be they external, internal, or analysis. The next aggregation will be the simulation phase. Apply interactive simulation models based on models of real buildings. In our case, the process has been through the implementation of numerical simulations in two- and three-dimensional domains, the CFD code through the Psi-THERM 2D software, which has given results where the little thermal transmittance that this window has can be determined and that, in addition, confirmed with the data obtained by the datalogger. The elements and their composition have very poor insulation, and the energy losses are really very notable, with thermal temperature variations of around two or three degrees of difference. The next horizontal addition would be the analysis of thermogram studies from photographs of a FLIR E60bx camera. It is possible to determine and monitor the temperature distribution in surface units in an interior environment where sensitive changes can be determined because of

thermal bridges between the window frame and the glass as it passes through the elastic band that separates both elements. The graph between units 30 and 40 makes a change in unit change. The utility of DTs in the built environment can be considerably increased by real-time decision-making of the scenarios analyzed within the framework of the energy study. IDP speaks of requirement hierarchies following the ISO 19650 standard, based on information requirements of the interested parties, contracts, and deliverables, and that in turn horizontal aggregations of modification of the digital twin are carried out to enrich it. It would only be necessary to establish the predictive conditions that are done through artificial intelligence (AI).

## 6 Conclusions

Most of the scientific and experimental studies of U-value transfer in windows are taken from the hot box test in laboratory tests, where the conditions in stationary state are the most optimal, but it is difficult to find studies like the one presented in this manuscript in which a complete analysis of energy studies outside the laboratory is analyzed and in which it is one of the most important elements in the building envelope, such as the window frame. The appearance of BIM is a new opportunity to integrate a DT in a 3D reconstruction and to be able to annex the horizontal aggregations that have been seen in this research to a BIM model. Accessibility to information data tries to put an open BIM that transmits the data that are registered in an open standard format such as the Industry Foundation Classes (IFC) considering all the particularities of the building and its environment.

These aspects will favour a sustainable transition of the built environment to the decarbonisation objectives set by organizations such as the European Union. The use of these models will not only allows to have a database on the current state of the thermal properties of existing windows in a three-dimensional model, but it may be the starting point for the design of energy conservation measures. This aspect will acquire great relevance, but it takes into account the expected transformation in the energy performance of buildings with climate change [67, 68], with a loss of efficiency in heating saving measures [69]. In any case, the results shown in this chapter constitute a starting point that should be progressively improved in the future studies. Several questions arise when addressing the next steps of the investigation. Thus, the use of artificial intelligence techniques [70] obtaining more accurate digital models [71] and the use of other modelling technologies [72] should be addressed in the future work.

## References

1. CMNUCC, Acuerdo de París, COP21. 21930 (2015) 40. <http://unfccc.int/resource/docs/2015/cop21/spa/109s.pdf>



2. Pérez-Lombard L, Ortiz J, Pout C (2008) A review on buildings energy consumption information. *Energy Build* 40:394–398. <https://doi.org/10.1016/j.enbuild.2007.03.007>
3. Bienvenido-Huertas D, Rubio-Bellido C, Pérez-Fargallo A, Pulido-Arcas JA (2020) Energy saving potential in current and future world built environments based on the adaptive comfort approach. *J Clean Prod* 249. <https://doi.org/10.1016/j.jclepro.2019.119306>
4. Sánchez-García D, Bienvenido-Huertas D, Pulido-Arcas JA, Rubio-Bellido C (2020) Analysis of energy consumption in different European cities: the adaptive comfort control implemented model (ACCIM) considering representative concentration pathways (RCP) scenarios. *Appl Sci* 10:1–24. <https://doi.org/10.3390/app10041513>
5. Bienvenido-Huertas D, Sánchez-García D, Rubio-Bellido C (2020) Analysing natural ventilation to reduce the cooling energy consumption and the fuel poverty of social dwellings in coastal zones. *Appl Energy* 279. <https://doi.org/10.1016/j.apenergy.2020.115845>
6. Bienvenido-Huertas D, Sánchez-García D, Rubio-Bellido C (2021) Adaptive setpoint temperatures to reduce the risk of energy poverty? A local case study in Seville. *Energy Build* 110571. <https://doi.org/10.1016/j.enbuild.2020.110571>
7. Pérez-Fargallo A, Bienvenido-Huertas D, Rubio-Bellido C, Trebilcock M (2020) Energy poverty risk mapping methodology considering the user's thermal adaptability: the case of Chile. *Energy. Sustain Dev* 58:63–77. <https://doi.org/10.1016/j.esd.2020.07.009>
8. Bienvenido-Huertas D, Sánchez-García D, Rubio-Bellido C, Pulido-Arcas JA (2020) Analysing the inequitable energy framework for the implementation of nearly zero energy buildings (nZEB) in Spain. *J Build Eng.* <https://doi.org/10.1016/j.jobe.2020.102011>
9. Bienvenido-Huertas D, Marín-García D, Carretero-Ayuso MJ, Rodríguez-Jiménez CE (2021) Climate classification for new and restored buildings in Andalusia: analysing the current regulation and a new approach based on k-means. *J Build Eng* 43:102829. <https://doi.org/10.1016/j.jobe.2021.102829>
10. Bienvenido-Huertas D, Oliveira M, Rubio-Bellido C, Marín D (2019) A comparative analysis of the international regulation of thermal properties in building envelope. *Sustainability* 11:5574. <https://doi.org/10.3390/su11205574>
11. Bienvenido-Huertas D (2021) Do unemployment benefits and economic aids to pay electricity bills remove the energy poverty risk of Spanish family units during lockdown? A study of COVID-19-induced lockdown. *Energy Policy* 150. <https://doi.org/10.1016/j.enpol.2020.112117>
12. Bienvenido-Huertas D (2021) Influence of the type of thermostat on the energy saving obtained with adaptive setpoint temperatures: analysis in the current and future scenario. *Energy Build* 244:111024. <https://doi.org/10.1016/j.enbuild.2021.111024>
13. Bienvenido-Huertas D, Sánchez-García D, Rubio-Bellido C, Oliveira MJ (2020) Influence of adaptive energy saving techniques on office buildings located in cities of the Iberian Peninsula. *Sustain Cities Soc* 53:101944. <https://doi.org/10.1016/j.scs.2019.101944>
14. Bienvenido-Huertas D, Sánchez-García D, Rubio-Bellido C, Pulido-Arcas JA (2021) Applying the mixed-mode with an adaptive approach to reduce the energy poverty in social dwellings: the case of Spain. *Energy* 237. <https://doi.org/10.1016/j.energy.2021.121636>
15. Bienvenido-Huertas D, Sánchez-García D, Pérez-Fargallo A, Rubio-Bellido C (2020) Optimization of energy saving with adaptive setpoint temperatures by calculating the prevailing mean outdoor air temperature. *Build Environ* 170. <https://doi.org/10.1016/j.buildenv.2019.106612>
16. Bienvenido-Huertas D, Sánchez-García D, Rubio-Bellido C, Marín-García D (2021) Potential of applying adaptive strategies in buildings to reduce the severity of fuel poverty according to the climate zone and climate change: the case of Andalusia. *Sustain Cities Soc* 73. <https://doi.org/10.1016/j.scs.2021.103088>
17. Bienvenido-Huertas D, Sánchez-García D, Rubio-Bellido C (2020) Comparison of energy conservation measures considering adaptive thermal comfort and climate change in existing Mediterranean dwellings. *Energy* 190. <https://doi.org/10.1016/j.energy.2019.116448>
18. Bienvenido-Huertas D (2020) Analysis of the relationship of the improvement of façades and thermal bridges of Spanish building stock with the mitigation of its energy and environmental impact. *Energies* 13. <https://doi.org/10.3390/en13174499>

19. Gastines M, Pattini A (2019) Propiedades energéticas de tecnologías de ventanas en Argentina. *Rev. Hábitat Rev. Sustentable*. 9:47–57
20. E.I. 10077-2 (2003) Thermal performance of windows, doors and shutters—calculation of thermal transmittance—numerical method for frames
21. Rosen R, Boschert S, Sohr A (2018) Next generation digital twin. *Atp Mag* 60:86–96. <https://doi.org/10.17560/ATP.V60I10.2371>
22. Al-Sehrawy R, Kumar B (2020) Digital twins in architecture, engineering, construction and operations. A brief review and analysis. *Lect Notes Civ Eng* 98:924–939. [https://doi.org/10.1007/978-3-030-51295-8\\_64](https://doi.org/10.1007/978-3-030-51295-8_64)
23. Grieves M, Vickers J (2017) Digital twin: mitigating unpredictable, undesirable emergent behavior in complex systems. In: *Transdisciplinary perspectives on complex systems*, pp 85–113. [https://doi.org/10.1007/978-3-319-38756-7\\_4](https://doi.org/10.1007/978-3-319-38756-7_4)
24. Tao F, Sui F, Liu A, Qi Q, Zhang M, Song B, Guo Z, Lu SC-Y, Nee AYC (2018) Digital twin-driven product design framework. 57:3935–3953. <https://doi.org/10.1080/00207543.2018.1443229>
25. Angjeliu G, Coronelli D, Cardani G (2020) Development of the simulation model for Digital Twin applications in historical masonry buildings: the integration between numerical and experimental reality. *Comput Struct* 238:106282. <https://doi.org/10.1016/J.COMPSTRUC.2020.106282>
26. Wong JKW, Li H, Wang H, Huang T, Luo E, Li V (2013) Toward low-carbon construction processes: the visualisation of predicted emission via virtual prototyping technology. *Autom Constr* 33:72–78. <https://doi.org/10.1016/J.AUTCON.2012.09.014>
27. Götz CS, Karlsson P, Yitmen I (2020) Exploring applicability, interoperability and integrability of Blockchain-based digital twins for asset life cycle management. *Smart Sustain Built Environ*. <https://doi.org/10.1108/SASBE-08-2020-0115/FULL/PDF>
28. Macchi M, Roda I, Negri E, Fumagalli L (2018) Exploring the role of digital twin for asset lifecycle management. *IFAC-PapersOnLine* 51:790–795. <https://doi.org/10.1016/J.IFACOL.2018.08.415>
29. Moin S, Karim A, Safdar Z, Safdar K, Ahmed E, Imran M (2019) Securing IoTs in distributed blockchain: analysis, requirements and open issues. *Futur Gener Comput Syst* 100:325–343. <https://doi.org/10.1016/J.FUTURE.2019.05.023>
30. Wong JKW, Ge J, He SX (2018) Digitisation in facilities management: a literature review and future research directions. *Autom Constr* 92:312–326. <https://doi.org/10.1016/J.AUTCON.2018.04.006>
31. Teni M, Krstić H, Kosiński P (2019) Review and comparison of current experimental approaches for in-situ measurements of building walls thermal transmittance. *Energ Build* 203:109417. <https://doi.org/10.1016/j.enbuild.2019.109417>
32. Tejedor B, Casals M, Gangolells M (2018) Assessing the influence of operating conditions and thermophysical properties on the accuracy of in-situ measured U-values using quantitative internal infrared thermography. *Energ Build* 171:64–75. <https://doi.org/10.1016/j.enbuild.2018.04.011>
33. Tejedor B, Casals M, Gangolells M, Roca X (2017) Quantitative internal infrared thermography for determining in-situ thermal behaviour of façades. *Energ Build* 151:187–197. <https://doi.org/10.1016/j.enbuild.2017.06.040>
34. Bienvenido-Huertas D, Bermúdez J, Moyano J, Marín D (2019) Comparison of quantitative IRT to estimate U-value using different approximations of ECHTC in multi-leaf walls. *Energ Build* 184:99–113. <https://doi.org/10.1016/j.enbuild.2018.11.028>
35. Bienvenido-Huertas D, Bermúdez J, Moyano JJ, Marín D (2019) Influence of ICHTC correlations on the thermal characterization of façades using the quantitative internal infrared thermography method. *Build Environ* 149:512–525. <https://doi.org/10.1016/j.buildenv.2018.12.056>
36. Evangelisti L, Guattari C, Gori P, Bianchi F (2017) Heat transfer study of external convective and radiative coefficients for building applications. *Energ Build* 151:429–438. <https://doi.org/10.1016/j.enbuild.2017.07.004>

37. Evangelisti L, Guattari C, Asdrubali F (2018) Influence of heating systems on thermal transmittance evaluations: simulations, experimental measurements and data post-processing. *Energy Build* 168:180–190. <https://doi.org/10.1016/j.enbuild.2018.03.032>
38. Ficco G, Iannetta F, Ianniello E, D'Ambrosio Alfano FR, Dell'Isola M (2015) U-value in situ measurement for energy diagnosis of existing buildings. *Energy Build* 104:108–121. <https://doi.org/10.1016/j.enbuild.2015.06.071>
39. Bienvenido-Huertas D, Rubio-Bellido C, Pérez-Ordóñez JL, Oliveira MJ (2020) Automation and optimization of in-situ assessment of wall thermal transmittance using a Random Forest algorithm. *Build Environ* 168. <https://doi.org/10.1016/j.buildenv.2019.106479>
40. Bienvenido-Huertas D, Rubio-Bellido C, Solís-Guzmán J, Oliveira MJ (2020) Experimental characterisation of the periodic thermal properties of walls using artificial intelligence. *Energy* 203. <https://doi.org/10.1016/j.energy.2020.117871>
41. Lucchi E, Roberti F, Alexandra T (2018) Definition of an experimental procedure with the hot box method for the thermal performance evaluation of inhomogeneous walls. *Energy Build* 179:99–111. <https://doi.org/10.1016/j.enbuild.2018.08.049>
42. Lucchi E (2017) Thermal transmittance of historical brick masonries: a comparison among standard data, analytical calculation procedures, and in situ heat flow meter measurements. *Energy Build* 134:171–184. <https://doi.org/10.1016/j.enbuild.2016.10.045>
43. Malvoni M, Baglivo C, Congedo PM, Laforgia D (2016) CFD modeling to evaluate the thermal performances of window frames in accordance with the ISO 10077. *Energy* 111:430–438. <https://doi.org/10.1016/j.energy.2016.06.002>
44. Lechowska AA, Schnotale JA, Baldinelli G (2017) Window frame thermal transmittance improvements without frame geometry variations: an experimentally validated CFD analysis. *Energy Build* 145:188–199. <https://doi.org/10.1016/j.enbuild.2017.04.002>
45. Baldinelli G, Bianchi F (2014) Windows thermal resistance: infrared thermography aided comparative analysis among finite volumes simulations and experimental methods. *Appl Energy* 136:250–258. <https://doi.org/10.1016/J.APENERGY.2014.09.021>
46. International Organization for Standardization, ISO 9869-1:2014—Thermal insulation—Building elements—In situ measurement of thermal resistance and thermal transmittance. Part 1: Heat flow meter method, Geneva, Switzerland, 2014
47. Soares N, Martins C, Gonçalves M, Santos P, da Silva LS, Costa JJ (2019) Laboratory and in-situ non-destructive methods to evaluate the thermal transmittance and behavior of walls, windows, and construction elements with innovative materials: a review. *Energy Build* 182:88–110. <https://doi.org/10.1016/j.enbuild.2018.10.021>
48. Fokaides PA, Kalogirou SA (2011) Application of infrared thermography for the determination of the overall heat transfer coefficient (U-Value) in building envelopes. *Appl Energy* 88:4358–4365. <https://doi.org/10.1016/j.apenergy.2011.05.014>
49. B. Software, Psi-Therm GmbH (2020)
50. Osello A (2012) The future of drawing with BIM for engineers and architects-. Dario Flaccovio Ed. Srl.
51. Bienvenido-Huertas D, Moyano J, Rodríguez-Jiménez CE, Muñoz-Rubio A, Bermúdez Rodríguez FJ (2020) Quality control of the thermal properties of superstructures in accommodation spaces in naval constructions. *Sustainability* 12:4194. <https://doi.org/10.3390/su12104194>
52. Bienvenido-Huertas D, Pérez-Ordóñez JL, Moyano J, Seara-Paz S (2020) Towards an in-situ evaluation methodology of thermal resistance of basement walls in buildings. *Energy Build* 208:109643. <https://doi.org/10.1016/j.enbuild.2019.109643>
53. N.I.I. 10077-2 (2012) Thermal performance of windows, doors and shutters—Calculation of thermal transmittance—Part 2: Numerical
54. Asdrubali F, Baldinelli G, Bianchi F (2012) A quantitative methodology to evaluate thermal bridges in buildings. *Appl Energy* 97:365–373. <https://doi.org/10.1016/j.apenergy.2011.12.054>
55. O'Grady M, Lechowska AA, Harte AM (2017) Infrared thermography technique as an in-situ method of assessing the heat loss through thermal bridging. *Energy Build* 135:20–32. <https://doi.org/10.1016/j.enbuild.2016.11.039>

56. Scheuer C, Boot E, Carse N, Clardy A, Gallagher J, Heck S, Marron S, Martinez-Alvarez L, Masarykova D, Mcmillan P, Murphy F, Steel E, Van Ekdorn H, Vecchione H (1978) Application of aerial infrared thermography to the measurement of building heat loss. *Build Syst Des* 75:24–26. <https://doi.org/10.2/JQUERY.MIN.JS>
57. Glaessgen EH, Stargel DS (2012) The digital twin paradigm for future NASA and U.S. Air force vehicles. Collect technical paper—AIAA/ASME/ASCE/AHS/ASC structures, structural dynamics and materials conference. <https://doi.org/10.2514/6.2012-1818>.
58. Kang JS, Chung K, Hong EJ (2021) Multimedia knowledge-based bridge health monitoring using digital twin. *Multimed Tools Appl* 80:34609–34624. <https://doi.org/10.1007/S11042-021-10649-X/FIGURES/11>
59. Stanley R, Thurnell D (2014) The benefits of, and barriers to, implementation of 5D BIM for quantity surveying in New Zealand, Australas. *J Constr Econ Build* 14(1):105–117. <https://doi.org/10.3316/INFORMIT.200817347855487>
60. Kim JB, Jeong W, Clayton MJ, Haberl JS, Yan W (2015) Developing a physical BIM library for building thermal energy simulation. *Autom Constr* 50:16–28. <https://doi.org/10.1016/J.AUTCON.2014.10.011>
61. Cemesova A, Hopfe CJ, McLeod RS (2015) PassivBIM: enhancing interoperability between BIM and low energy design software. *Autom Constr* 57:17–32. <https://doi.org/10.1016/J.AUTCON.2015.04.014>
62. Zhang X, Shen J, Saini PK, Lovati M, Han M, Huang P, Huang Z (2021) Digital twin for accelerating sustainability in positive energy district: a review of simulation tools and applications. *Front Sustain Cities* 3:35. <https://doi.org/10.3389/FRSC.2021.663269/BIBTEX>
63. Khajavi SH, Motlagh NH, Jaribion A, Werner LC, Holmstrom J (2019) Digital twin: vision, benefits, boundaries, and creation for buildings. *IEEE Access* 7:147406–147419. <https://doi.org/10.1109/ACCESS.2019.2946515>
64. G. Digital(2022) GE Predix Platform | Industrial IoT Platform | GE Digital
65. Trebilcock M (2021) Proceso de Diseño Integrado: nuevos paradigmas en arquitectura sustentable. *Arquitectura Rev* 5:65–75. <https://doi.org/10.4013/arq.2009.52.01>
66. Ruikar K, Kotecha K, Sandbhor S, Thomas A (eds), Deng M, Menassa CC, Kamat VR (2021) From BIM to digital twins: a systematic review of the evolution of intelligent building representations in the AEC-FM industry, *ITcon Vol. 26, Special Issue Next Generation ICT—How distant is ubiquitous computing*, pp 58–83, <http://www.itcon.org/2021/5>. <https://doi.org/10.36680/J.ITCON.2021.005>.
67. Bienvenido-Huertas D, Pulido-Arcas JA, Rubio-Bellido C, Pérez-Fargallo A (2020) Influence of future climate changes scenarios on the feasibility of the adaptive comfort model in Japan. *Sustain Cities Soc* 61:102303. <https://doi.org/10.1016/j.scs.2020.102303>
68. Bienvenido-Huertas D, Sánchez-García D, Rubio-Bellido C (2022) Influence of the RCP scenarios on the effectiveness of adaptive strategies in buildings around the world. *Build Environ* 208. <https://doi.org/10.1016/j.buildenv.2021.108631>
69. Bienvenido-Huertas D, Rubio-Bellido C, Marín-García D, Canivell J (2021) Influence of the Representative Concentration Pathways (RCP) scenarios on the bioclimatic design strategies of the built environment. *Sustain Cities Soc* 72:103042. <https://doi.org/10.1016/j.scs.2021.103042>
70. Bienvenido-Huertas D, Nieto-Julián JE, Moyano JJ, Macías-Bernal JM, Castro J (2019) Implementing artificial intelligence in H-BIM using the J48 algorithm to manage historic buildings. *Int J Archit Herit* 1–13. <https://doi.org/10.1080/15583058.2019.1589602>
71. Andriasyan M, Moyano J, Nieto-Julián JE, Antón D (2020) From point cloud data to building information modelling: an automatic parametric workflow for heritage. *Rem Sens* 12. <https://doi.org/10.3390/rs12071094>
72. Moyano J, Nieto-Julián JE, Antón D, Cabrera E, Bienvenido-Huertas D, Sánchez N (2020) Suitability study of structure-from-motion for the digitisation of architectural (Heritage) spaces to apply divergent photograph collection. *Symmetry (Basel)* 12:1–25. <https://doi.org/10.3390/sym12121981>

# Comparative Analysis of the Influence of the Convective Term in the Quantitative Assessment by Infrared Thermography



David Bienvenido-Huertas, Blanca Tejedor, David Marín-García, and Joaquín Durán

**Abstract** Envelope thermal transmittance strongly influences building energy consumption, so there is a significant interest in using methods that assess it accurately. The quantitative infrared thermography method is among the most studied methods to assess thermal transmittance as this method could be used to analyse building envelopes qualitatively and quantitatively. However, its main limitation is the great variety of approaches. Their greater differences are the convective heat transfer coefficient and the place from which the measurement is carried out. This chapter comparatively analyses the experimental results obtained in previous studies. The analysis showed that the approaches from the interior using expressions of adimensional numbers allow accurate characterizations of thermal transmittance to be obtained.

**Keywords** Thermal transmittance · Infrared thermography method · Convective term · Wall

---

D. Bienvenido-Huertas (✉) · J. Durán  
Department of Building Construction, University of Granada, Granada, Spain  
e-mail: [dbienvenido@ugr.es](mailto:dbienvenido@ugr.es)

B. Tejedor  
Department of Project and Construction Engineering. Group of Construction Research and Innovation (GRIC), Universitat Politècnica de Catalunya (UPC), Barcelona, Spain

D. Marín-García  
Department of Graphical Expression and Building Engineering, University of Seville, Seville, Spain

## 1 Introduction

The existing building stock is characterized by envelopes with poor thermal performance [1]. Furthermore, this becomes more important in façades as façades are the elements with the greatest surface in contact with the external air [2], so they constitute the place where the greatest energy losses take place. Thus, most building stock is characterized by both high energy consumption and indoor conditions with a high probability of being inappropriate for most of the year.

The thermal behaviour of these façades is deficient due to both their design and the ageing of materials [3]. It is estimated that the improvement of the thermal performance of façades would reduce the heat losses in buildings between 10 and 45% [4]. As a result, the reduction of these heat losses would reduce energy consumption, as the results obtained in the comparative study of the regulations of the various countries have shown.

In short, determining appropriately thermal transmittance is crucial to not overestimate energy consumption. In addition, obtaining an erroneous thermal transmittance value of a wall influences the calculation of other aspects related to energy rehabilitation (e.g. the range of thermal comfort hours), thus implying to propose measures not adapted to reality, with an increase in periods of economy amortization.

Thus, architects, engineers, quantity surveyors and other professionals responsible for works related to the energy improvement of the existing building stock should correctly characterize thermal transmittance to reduce both energy consumption and CO<sub>2</sub> emissions in accordance with the new goals and priorities of today's society. This property could be determined by various procedures, such as theoretical calculation methods or in-situ tests. Quantitative infrared thermography methods (QIRT) are those recently emerging. As for the field of energy audit, infrared thermography has usually been used to qualitatively analyse building envelopes [5–8] for many purposes: to detect thermal anomalies, thermal bridges, and air infiltrations, among others.

In the last fifteen years, however, a series of studies have been focused on the analysis of the use of the method to determine thermal transmittance. The method uses infrared thermography to measure mainly surface temperature, emissivity, and the reflected apparent temperature, although other variables could also be measured, such as the indoor and outdoor air temperature [9].

This type of method has the advantage of being non-destructive and quick and, at the same time, walls can be qualitatively analysed. Thus, thermal transmittance could be assessed without the risk of wrongly assessing an area affected by thermal bridges, unlike other methods.

In addition, tests can be performed in a short period of time, so the monitoring time is reduced in comparison with other methods, such as HFM or THM. Recent research studies have been focused on the proposal and analysis of various methods, which could be divided into two categories: methods from the interior and methods from the exterior of the wall. Each approach is different from the point of view of both test execution and data analysis.

The first study was conducted in 2008, in which Madding [10] proposed to calculate thermal transmittance by using the internal convective contribution and the radiative contribution expressed as a linearization of the Stefan–Boltzmann law:

$$U = \frac{4\varepsilon\sigma\left(\frac{T_{s,\text{in}}+T_{\text{refl}}}{2}\right)^3(T_{s,\text{in}} - T_{\text{refl}}) + h_{\text{in}} \cdot (T_{s,\text{in}} - T_{\text{in}})}{T_{\text{in}} - T_{\text{ext}}} \quad (1)$$

where  $\varepsilon$  [adimensional] is the emissivity of the wall,  $\sigma$  is the Stefan–Boltzmann constant, and  $T_{\text{refl}}$  [K] is the reflected apparent temperature.

A similar formulation was proposed by Fokaides and Kalogirou [11], but, instead of using the third power of the mean of indoor surface and reflected temperatures, it is only used for the surface temperature, obtaining the following expression:

$$U = \frac{4 \cdot \varepsilon \cdot \sigma \cdot T_{s,\text{in}}^3 \cdot (T_{s,\text{in}} - T_{\text{refl}}) + h_{\text{in}} \cdot (T_{s,\text{in}} - T_{\text{in}})}{T_{\text{in}} - T_{\text{ext}}} \quad (2)$$

The convective coefficients used for Eqs. (1) and (2) are different according to the authors: the correlations of Holman [12] and Earle [13] are used for Eq. (1), and the tabulated value from ISO 6946:2007 is used for Eq. (2).

Both Eqs. (1) and (2) are considered to measure from the interior. However, there are three approaches to perform tests from the exterior. One of the approaches was formulated by Albatici et al. [9, 14, 15] by applying the heat balance on the external side of the façade. For the external convective contribution, the authors used a Jürges' correlation published by Watanabe [16], but simplifying the equation by removing the constant term from the linear regression:

$$U = \frac{\varepsilon \cdot \sigma \cdot (T_{s,\text{ext}}^4 - T_{\text{ext}}^4) + 3.8054 \cdot v \cdot (T_{s,\text{ext}} - T_{\text{ext}})}{T_{\text{in}} - T_{\text{ext}}} \quad (3)$$

where  $v$  [m/s] is the local wind speed.

Likewise, Dall'O et al. [17] applied a thermal balance that was different from that of Eq. (3), since the equivalence between the heat flux of the wall and the heat flux by convection exchanged with the exterior was considered (Eq. (4)). For  $h_{\text{ext}}$ , the convection correlation published by Watanabe was used, but with no simplification.

$$U = \frac{(5.8 + 3.8054 \cdot v) \cdot (T_{s,\text{ext}} - T_{\text{ext}})}{T_{\text{in}} - T_{\text{ext}}} \quad (4)$$

Recently, a new proposal was given for the method from the interior. Tejedor et al. [18] proposed a new approach on the convection and radiation flows based on the equivalence of the heat flux (Eq. (5)). The main difference between this approach and that of Eqs. (1) and (2) is the convective coefficient used as it is an approach by using adimensional numbers.



$$U = \frac{\varepsilon \cdot \sigma \cdot (T_{\text{refl}}^4 - T_{s,\text{in}}^4) + \frac{k \left\{ 0.825 + \frac{0.387 \text{Ra}_L^{1/6}}{[1 + (0.492/\text{Pr})^{9/16}]^{8/27}} \right\}^2}{L} (T_{\text{in}} - T_{s,\text{in}})}{T_{\text{in}} - T_{\text{ext}}} \quad (5)$$

where  $\text{Ra}_L$  [adimensional] is the Rayleigh number,  $\text{Pr}$  [adimensional] is the Prandtl number,  $k$  is the thermal conductivity of the air [W/(m K)], and  $L$  is the height of the wall [m].

In the same study, Tejedor et al. [18] proposed a simplification of Eq. (24) by considering that, under typical test conditions, the internal temperature oscillates between 20 and 25 °C, so a fixed value can be given to the Prandtl number. This simplification led to the following equation:

$$U = \frac{\varepsilon \cdot \sigma \cdot (T_{\text{refl}}^4 - T_{s,\text{in}}^4) + \frac{k \cdot \{0.825 + 0.325 \cdot \text{Ra}_L^{1/6}\}^2}{L} \cdot (T_{\text{in}} - T_{s,\text{in}})}{T_{\text{in}} - T_{\text{ext}}} \quad (6)$$

Thus, there is no consensus among the publications on a theoretical proposal adapted to all the case studies analysed as the convection correlations used by the authors were established for certain test conditions, so their use therefore presents limitations regarding elements with other characteristics, such as the surface of the finish (smooth or rough), wind direction (windward or leeward), etc.

Thus, the great variety of proposals in the scientific literature could make the choice of the approach difficult. The main difference of the analysis of the equations of the proposals is the correlation used for the convective term. For this reason, it is necessary not just a comparative analysis of the proposals to determine that with the greatest robustness in view of both boundary conditions and several case studies, but also to widen the comparative analysis to more expressions for the convective term that are emerging from the beginning of the twentieth century. In this regard, the richness of the expressions is different as there are more than 90 correlations which are dependent on wind speed, the surface temperature or adimensional numbers.

Thus, the goal of this chapter is to determine the convection correlation, both external and internal, better adapted to quantitative infrared thermography methods. For this purpose, the results obtained in previous studies that applied QIRT from the exterior and the interior in several case studies are comparatively analysed.

## 2 Methodology

The experimental campaign and the results compared in this chapter were obtained in previous studies [19, 20]. The methodology used in the tests is summed up in the next subsections.



## 2.1 Experimental Campaign

The experimental campaign consisted in applying the approaches related to infrared thermography to characterize the thermal transmittance of three walls. Each wall belonged to a different building period: case study A ( $U$ -value =  $1.10 \text{ W}/(\text{m}^2 \text{ K})$ ), case study B ( $U$ -value =  $0.79 \text{ W}/(\text{m}^2 \text{ K})$ ), and case study C ( $U$ -value =  $0.58 \text{ W}/(\text{m}^2 \text{ K})$ ).

Tests were divided into two monitoring according to the infrared thermography approach: exterior and interior (Fig. 1). A total of 4 tests were carried out in each wall for each approach. Thus, 8 tests were conducted in each wall. Tests lasted 2 h and 30 min and were performed in consecutive days. Other aspects to be stressed are as follows:

- Tests were performed with no rain during both the measurement and the 48 previous hours.
- Wind speed during tests was always lower than 1 m/s.
- Tests were performed under constant conditions, so the thermal dynamic parameters were not analysed in these cases. To guarantee this aspect, tests were performed in winter, between the hours before and after dawn. Likewise, a temperature difference between 10 and 15 °C was guaranteed between the internal and external air in all monitoring by using heating systems.

Table 1 includes the equipment used for the tests. All probes were placed at a height of 1.5 m from the floor. Likewise, external air temperature sensors were placed as much aligned as possible from the internal temperature sensor and separated 20 cm



**Fig. 1** Examples of the external and internal monitoring conducted in Campaign 2

**Table 1** List of the equipment used in tests

Equipment	Variable	Measurement range	Resolution	Accuracy
FLIR E60bx infrared camera	FOV	25° × 19°		
	Spectral range	7.5–13 μm		
	Thermal sensitivity	<0.05–30 °C		
PCE-423 hot-wire anemometer	Wind speed	0–25 m/s	0.01 m/s	±5%
ALMEMO 2590-4AS data logger				
with T 190-3	Temperature	–10 to 105 °C	0.1 K	±0.05 K ±0.05%
with T 190-10	Temperature	–200 to 205 °C	0.1 K	±0.05 K ±0.05%
with plate FQA018C	Heat flux	±2000 W/m <sup>2</sup>	–	5%
TESTO 435-2 data logger				
with 0614 1635	Temperature	–20 to 70 °C	0.1 °C	±0.1 °C
with 0632 9735	Temperature	–20 to 70 °C	0.1 °C	±0.3 °C

from the external side of the wall [21]. In addition, the hot-wire anemometer was placed with a perpendicular separation of 10 cm from the façade [15, 22].

The infrared camera was placed in a tripod, at a perpendicular distance of 1.5 m from the façade and with an inclination angle of 20° to avoid reflections on the façade [18]. A reflector foil was also placed to measure the reflected temperature.

Before starting tests, the emissivity of walls was determined by an adhesive tape certified according to ASTM E1933-14 [23]. It was only determined at the beginning of the tests as this is a fixed value with no variations due to the common environmental temperature oscillations in buildings [24].

## 2.2 Data Analysis

As indicated above, the goal of this chapter was to analyse and determine the convection correlation that is best adjusted to infrared thermography approaches, as there are many expressions for the convective term due to both experimental correlations with a certain variable and adimensional numbers. Studies on quantitative methods through infrared thermography have used some of these expressions with no justification. Thus, the correlations indicated in the next two subsections have been considered in the analyses performed with infrared thermography. The expressions concerning external convective heat transfer coefficient ( $h_{ext}$ ) were applied to Eq. (7), and the expressions concerning internal convective heat transfer coefficient ( $h_i$ ) were applied to Eq. (8).

$$U = \frac{h_{\text{ext}}(T_{s,\text{ext}} - T_{\text{ext}}) + \varepsilon\sigma(T_{s,\text{ext}}^4 - T_{\text{ext}}^4)}{T_{\text{in}} - T_{\text{ext}}} \quad (7)$$

$$U = \frac{h_{\text{in}} \cdot (T_{\text{in}} - T_{s,\text{in}}) + \varepsilon\sigma(T_{\text{refl}}^4 - T_{s,\text{in}}^4)}{T_{\text{in}} - T_{\text{ext}}} \quad (8)$$

### 2.2.1 Experimental Correlations of the External Convective Term

The use of the set of Jürges' equations was based on adjusting the external convective heat transfer coefficient for a copper plate heated in a wind tunnel [25]. However, Cole and Sturrock [26] highlighted several problems related to the results of the wind tunnel experiments, so the measured external convective heat transfer coefficient of a small flat plate has disadvantages to be applied to construction surfaces at great scale [25]. Moreover, Watmuff et al. [27] indicated that the convection correlation indicated by Jürges has a radiation component, so its use in the formulation proposed by Albatici and Tonelli could increase more the prevalence of the radiation component. Moreover, the dependence of the external convective heat transfer coefficient on wind speed depends on the position of the measurement and the size of the wall [25].

For this reason, the use of a unique value for the external convective heat transfer coefficient due to a correlation with wind could present difficulties to be applied in various case studies because of the height of the wall, the proximity to corners, etc. There are many expression of correlations, some of them compiled by many authors [25, 28, 29].

When analysing these studies, some aspects should be considered when comparing the correlation equations proposed in the results. On one hand, the height at which wind speed is measured is different (e.g. wind speed in roofs, local wind speed or wind speed in a countryside). On the other hand, the perpendicular separation distance from vertical surfaces where wind is measured is not usually indicated. For this reason, applying the equations used in these experiments could be something of a challenge as a wind flow pattern around a building significantly fluctuates, thus implying that the wind profile is highly dependent on the distance from the building envelope. Likewise, other aspects, such as the existing differences in the convective term between the mean point and the edge of a vertical surface [25] are not included in most studies.

Table 2 includes a list of the many correlations of the external convective heat transfer coefficient due to the local wind speed used in the study. These correlations make distinctions according to the type of roughness of the vertical surface, wind direction, and even wind speed. Most distinctions are made for the expressions included in the same study. Table 3 includes the correlations for adimensional numbers.

**Table 2** Approaches of the external convective heat transfer coefficient due to correlations with wind speed

Equation		Comments (m/s)	Reference
$h_{\text{ext}} = 5.8 + 3.95v$	(9)	$v < 5$	Nusselt and Jürges [30]
$h_{\text{ext}} = 7.31v^{0.78}$	(10)	$5 < v < 24$	Nusselt and Jürges [30]
$h_{\text{ext}} = 7.11v^{0.775}$	(11)	Smooth surfaces, $5 < v < 24$	Jürges [31]
$h_{\text{ext}} = 7.52v^{0.784}$	(12)	Rough surfaces, $5 < v < 24$	Jürges [31]
$h_{\text{ext}} = 5.7 + 3.8v$	(13)	Smooth surfaces, $v < 5$	McAdams [32]
$h_{\text{ext}} = 7.2v^{0.78}$	(14)	Smooth surfaces, $v > 5$	McAdams [32]
$h_{\text{ext}} = 7.6v^{0.78}$	(15)	Rough surfaces, $v > 5$	McAdams [32]
$h_{\text{ext}} = 6.2 + 4.3v$	(16)	Rough surfaces, $v > 5$	Davies [33]
$h_{\text{ext}} = 6.97v^{0.666}$	(17)	–	Sogin [34]
$h_{\text{ext}} = 6.05 + 4.08v$	(18)	Rough surfaces, $v \leq 5$	Schaak [35]
$h_{\text{ext}} = 7.82 + 3.50v$	(19)	Smooth surfaces, with no speed limit	Jennings [36]
$h_{\text{ext}} = 10.7 + 4.96v$	(20)	Smooth brick, with no speed limit	Jennings [36]
$h_{\text{ext}} = 5.7 + 6v$	(21)	Heating	Sturrock [37]
$h_{\text{ext}} = 6.60v^{0.6}$	(22)	–	Mitchell [38]
$h_{\text{ext}} = 18.65v^{0.605}$	(23)	–	Lokmanhekim [39]
$h_{\text{ext}} = 5.8 + 2.9v$	(24)	Windward	Ito [40]
$h_{\text{ext}} = 8.7 + 9.4v$	(25)	Leeward, $v > 4$	Ito [40]
$h_{\text{ext}} = 11.4 + 5.7v$	(26)	Heating, normal surface, $v < 5$	Cole and Sturrock [26]
$h_{\text{ext}} = 5.7v$	(27)	Heating, leeward surface, $v < 5$	Cole and Sturrock [26]
$h_{\text{ext}} = 2.8 + 3.0v$	(28)	Correction of Eq. (30), $v < 5$	Watmuff et al. [27]
$h_{\text{ext}} = 4.7 + 7.6v$	(29)	–	Kimura [41]
$h_{\text{ext}} = 7.55 + 4.35v$	(30)	–	Nicol [42]
$h_{\text{ext}} = 4.5 + 2.9v$	(31)	Smooth surfaces	Lunde [43]
$h_{\text{ext}} = 8.55 + 2.56v$	(32)	–	Test et al. [44]
$h_{\text{ext}} = 5.1 + 1.7v$	(33)	$0.5 < v < 20$	Sharples [45]
$h_{\text{ext}} = 6.47 + 6.806v$	(34)	–	Yazdanian and Klems [46]
$h_{\text{ext}} = 2.38v^{0.89}$	(35)	Forced convection, windward	Yazdanian and Klems [46]
$h_{\text{ext}} = 2.86v^{0.617}$	(36)	Forced convection, leeward	Yazdanian and Klems [46]
$h_{\text{ext}} = 4.955 + 1.444v$	(37)	–	Jayamaha et al. [47]

(continued)

**Table 2** (continued)

Equation		Comments (m/s)	Reference
$h_{\text{ext}} = 8.91 + 2.00v$	(38)	Windward	Loveday and Taki [48]
$h_{\text{ext}} = 4.93 + 1.77v$	(39)	Leeward	Loveday and Taki [48]
$h_{\text{ext}} = 16.15v^{0.397}$	(40)	Windward, $0.5 < v < 9$	Loveday and Taki [48]
$h_{\text{ext}} = 16.25v^{0.503}$	(41)	Leeward, $0.5 < v < 9$	Loveday and Taki [48]
$h_{\text{ext}} = 16.21v^{0.452}$	(42)	Windward and leeward	Loveday and Taki [48]
$h_{\text{ext}} = 14.82v^{0.42}$	(43)	Windward, $0 < v < 10$	Taki and Loveday [49]
$h_{\text{ext}} = 15.06v^{0.53}$	(44)	Leeward, $0 < v < 4.5$	Taki and Loveday [49]
$h_{\text{ext}} = 4.47 + 10.21v$	(45)	$0.5 < v < 3$	Hagishima and Tanimoto [50]
$h_{\text{ext}} = 4 + 4v$	(46)	–	ISO 6946:2007
$h_{\text{ext}} = 7.4 + 3.8v$	(47)	Rough surfaces, $v < 15$	Mirsadeghi et al. [51]
$h_{\text{ext}} = 6.5 + 3.6v$	(48)	Smooth surfaces, $v < 15$	Mirsadeghi et al. [51]
$h_{\text{ext}} = 16.7v^{0.5}$	(49)	–	Mirsadeghi et al. [51]
$h_{\text{ext}} = 5.8 + 4.1v$	(50)	–	CIBSE [52]
$h_{\text{ext}} = 3.32 + 6.31v$	(51)	Windward, $0 < v < 3.5$	Liu and Harris [53]
$h_{\text{ext}} = 3.19 + 5.03v$	(52)	Leeward, $0 < v < 3.5$	Liu and Harris [53]
$h_{\text{ext}} = 5.56 + 4.48v$	(53)	Rough surfaces, $v < 5$	Xie et al. [54]

**Table 3** Approaches of the external convective heat transfer coefficient due to correlations with adimensional numbers

Equation		Comments	Reference
$h_{\text{ext}} = \frac{k(0.10\text{Re}^{0.666})}{L}$	(54)	Windward	Nusselt and Jürges [30]
$h_{\text{ext}} = \frac{k(0.20\text{Re}^{0.666})}{L}$	(55)	Leeward	Nusselt and Jürges [30]
$h_{\text{ext}} = \frac{k(0.42\text{Re}^{0.6})}{L}$	(56)	–	Jürges [31]
$h_{\text{ext}} = \frac{k(0.931\text{Re}^{0.5}\text{Pr}^{0.333})}{L}$	(57)	–	Jürges [31]
$h_{\text{ext}} = \frac{k(0.93\text{Re}^{0.5}\text{Pr}^{0.333})}{L}$	(58)	–	McAdams [32]
$h_{\text{ext}} = \frac{k(0.86\text{Re}^{0.5}\text{Pr}^{0.333})}{L}$	(59)	–	McAdams [32]
$h_{\text{ext}} = \frac{k(0.0253\text{Re}^{0.8+3})}{L}$	(60)	–	McAdams [32]
$h_{\text{ext}} = \frac{k(0.664\text{Re}^{0.5}\text{Pr}^{0.33})}{L}$	(61)	Laminar flow	Davies [33]
$h_{\text{ext}} = \frac{k(0.037\text{Re}^{0.8}\text{Pr}^{0.33})}{L}$	(62)	Turbulent flow	Sogin [34]

### 2.2.2 Experimental Correlations of the Internal Convective Term

Like the external convective term, there are many expressions for the internal convective term. Studies that apply the quantitative infrared thermography from the interior have been characterized by using a greater variety of expressions for the internal convective transfer coefficient. In this regard, whereas the approaches from the exterior have only used the Jürges correlation published by Watanabe [16], 6 various expressions have been used in the internal approaches, from the use of experimental correlations to the allocation of theoretical values.

However, the existing expressions have not been included due to the variety of expressions used by the authors in their studies. There are many experimental correlation expressions due to the temperature differences, some of them compiled by several review papers [55–58].

Table 4 includes a list of the correlations of the internal convective heat transfer coefficient due to the temperature differences analysed in the study. The approach used for each correlation varies according to the research, thus existing certain correlations according to the similarity of the heat transfer by convection of a vertical surface of a room with that of an insulated flat plate or according to the tests performed in close rooms with certain HVAC systems.

It is worth stressing that these correlations of the internal convective heat transfer coefficient do not consider the effect that the flank elements cause to the vertical surface, gaps or the room itself [58]. Thus, the use of a fixed correlation for all the case studies of the internal convective heat transfer coefficient could vary thermal transmittance results.

As for the correlations of the internal convective heat transfer coefficient using adimensional numbers, there are many correlations apart from Churchill and Chu's proposal and used in the research studies by Tejedor et al. [18]. Table 5 includes the correlations selected for this study due to their suitability to be used on façades.

## 3 Results and Discussion

The results were used to analyse the wide variety of formulations to characterize thermal transmittance. There are two types of approaches: (i) the approaches that consider the convective term as the total term of heat transfer; and (ii) the approaches that use both the convection and radiation term. In addition, the approach of simplified convection and radiation are included in the external methods.

Thus, all approaches were analysed by using the equations included in Tables 2, 3, 4 and 5. However, before discussing the results, the great variety of expressions were simplified through the cluster analysis, thus reducing the volume of expressions used and easing the interpretation of the results. This analysis also reflected some similarity patterns among the various equations that show the limitations of the restriction criteria of each equation when used in other applications.

**Table 4** Approaches of the internal convective heat transfer coefficient due to correlations with temperature differences

Equation <sup>1</sup>		Comments	Reference
$h_{in} = 3.05 \cdot (\Delta T_{si})^{0.12}$	(63)		Wilkes and Peterson [59]
$h_{in} = 2.5 \cdot (\Delta T_{si})^{0.25}$	(64)		Giesecke [60]
$h_{in} = 1.368 \cdot \left(\frac{\Delta T_{si}}{L}\right)^{0.25}$	(65)	Laminar flow regime	Min et al. [61]
$h_{in} = 1.973 \cdot (\Delta T_{si})^{0.25}$	(66)	Turbulent flow regime	Min et al. [61]
$h_{in} = 1.664 \cdot (\Delta T_{si})^{0.27}$	(67)		Min et al. [61]
$h_{in} = 1.776 \cdot (\Delta T_{si})^{0.25}$	(68)		Min et al. [61]
$h_{in} = 1.517 \cdot (\Delta T_{si})^{0.33}$	(69)		Min et al. [61]
$h_{in} = \frac{0.0257}{L} \cdot (0.825 + 7.01 \cdot (\Delta T_{si})^{1/6} \cdot L^{3/6})^2$	(70)		Churchill and Chu [62]
$h_{in} = (0.134 \cdot (L)^{-0.5} + 1.11 \cdot (\Delta T_{si})^{0.17})^2$	(71)	Simplification of the Churchill and Chu correlation	ESDU [63]
$h_{in} = \left\{ \left[ 1.5 \cdot \left(\frac{\Delta T_{si}}{L}\right)^{1/4} \right]^6 + \left[ 1.23 \cdot (\Delta T_{si})^{1/3} \right]^6 \right\}^{1/6}$	(72)		Alamdari and Hammond [64]
$h_i = 1.31 \cdot \left(\frac{\Delta T_{si}}{L}\right)^{0.33}$	(73)	Laminar flow regime	Earle [13]
$h_i = 1.8 \cdot (\Delta T_{si})^{0.25}$	(74)	Turbulent flow regime	Earle [13]
$h_{in} = 3.08 \cdot (\Delta T_{si})^{0.25}$	(75)		Li et al. [65]
$h_{in} = 2.88 \cdot (\Delta T_{si})^{0.25}$	(76)		Li et al. [65]
$h_i = 1.42 \cdot \left(\frac{\Delta T_{si}}{L}\right)^{0.25}$	(77)	Laminar flow regime	Holman [12]
$h_i = 1.31 \cdot (\Delta T_{si})^{0.25}$	(78)	Turbulent flow regime	Holman [12]
$h_{in} = 1.98 \cdot (\Delta T_{si})^{0.32}$	(79)	Wall close to a radiator	Khalifa and Marshall [66]
$h_{in} = 2.3 \cdot (\Delta T_{si})^{0.24}$	(80)	Wall with a radiator below the window	Khalifa and Marshall [66]
$h_{in} = 2.92 \cdot (\Delta T_{si})^{0.25}$	(81)	Wall in front of a radiator	Khalifa and Marshall [66]

(continued)

<sup>1</sup> To simplify the reading of Table 4, the variable  $\Delta T_{si}$  was used. This variable refers to the difference between the internal surface temperature and the internal temperature.

**Table 4** (continued)

Equation		Comments	Reference
$h_{in} = 2.03 \cdot (\Delta T_{si})^{0.14}$	(82)	Insulated wall with a large surface	Khalifa and Marshall [66]
$h_{in} = 1.57 \cdot (\Delta T_{si})^{0.31}$	(83)		Hatton and Awbi [67]
$h_{in} = \frac{1.823}{L^{0.127}} \cdot (\Delta T_{si})^{0.293}$	(84)		Awbi and Hatton [68]
$h_{in} = 1.332 \cdot \left(\frac{\Delta T_{si}}{L}\right)^{1/4}$	(85)	Laminar flow regime	Fohanno and Polidori [69]

**Table 5** Approaches of the internal convective heat transfer coefficient due to correlations with adimensional numbers

Equation		Comments	Reference
$h_{in} = k \cdot \frac{0.555 \cdot (Ra)^{0.25}}{L}$	(86)	$10^3 < Ra < 10^8$	Jakob [70]
$h_{in} = k \cdot \frac{0.129 \cdot (Ra)^{0.33}}{L}$	(87)	$10^8 < Ra < 10^{12}$	Jakob [70]
$h_{in} = k \cdot \frac{0.56 \cdot (Ra)^{0.25}}{L}$	(88)	Laminar flow regime	Fishenden and Saunders [71]
$h_{in} = k \cdot \frac{0.12 \cdot (Ra)^{0.33}}{L}$	(89)	Turbulent flow regime	Fishenden and Saunders [71]
$h_{in} = k \cdot \frac{0.548 \cdot (Ra)^{0.25}}{L}$	(90)	Laminar flow regime	McAdams [32]
$h_{in} = k \cdot \frac{0.52 \cdot (Ra)^{0.25}}{L}$	(91)	$Ra < 3 \cdot 10^8$	McAdams [32]
$h_{in} = k \cdot \frac{0.59 \cdot (Ra)^{0.25}}{L}$	(92)	$10^4 < Ra < 10^9$	McAdams [32]
$h_{in} = k \cdot \frac{0.13 \cdot (Ra)^{0.33}}{L}$	(93)	$2 \cdot 10^9 < Ra < 10^{12}$	McAdams [32]
$h_{in} = k \cdot \frac{0.48 \cdot (Gr)^{0.25}}{L}$	(94)	Laminar flow regime	CIBSE [72]
$h_{in} = k \cdot \frac{0.119 \cdot (Gr)^{0.33}}{L}$	(95)	Turbulent flow regime	CIBSE [72]
$h_{in} = k \cdot \frac{0.516 \cdot (Ra)^{0.25}}{L}$	(96)	Laminar flow regime	Wong [73]
$h_{in} = k \cdot \frac{0.021 \cdot (Ra)^{0.25}}{L}$	(97)	$10^{10} < Ra < 10^{12}$	Wong [73]
$h_{in} = k \cdot \frac{0.555 \cdot (Ra)^{0.25}}{L}$	(98)	Laminar flow regime	Welty [74]
$h_{in} = k \cdot \frac{0.021 \cdot (Ra)^{0.40}}{L}$	(99)	Turbulent flow regime	Welty [74]
$h_{in} = k \cdot \frac{0.508 \cdot \frac{Pr^{0.5} \cdot Gr^{0.25}}{(0.952 + Pr)^{0.25}}}{L}$	(100)	Laminar flow regime	Welty [74]
$h_{in} = k \cdot \frac{0.678 \cdot \frac{Pr^{0.5} \cdot Gr^{0.25}}{(0.952 + Pr)^{0.25}}}{L}$	(101)	Laminar flow regime	Welty [74]
$h_{in} = k \cdot \frac{0.10 \cdot (Ra)^{0.33}}{L}$	(102)		Holman [12]
$h_{in} = k \cdot \frac{0.54 \cdot (Ra)^{0.25}}{L}$	(103)	$1.15 \cdot 10^5 < Ra < 2 \cdot 10^9$	Al-Arabi and Sakr [75]



Tables 6 includes a summary of the clusters obtained by each type of correlation. The analysis was conducted according to the value obtained for the convective heat flux in each test. Moreover, the values used for the convection term in the existing studies on the quantitative infrared thermography method were also analysed (Albatici et al., Dall'O et al., Madding, Fokaides and Kalogirou, and Tejedor et al.).

In this regard, there are several interesting aspects of the results of the cluster analysis. The first aspect is related to the group of both wind correlations or temperature differences that establish opposite application criteria. These criteria, as Tables 2, 3, 4 and 5 have shown, depended on several aspects, such as wind direction or the type of surface finish of the wall. Likewise, the equations related to a certain type of flow (laminar or turbulent) were grouped. Secondly, most experimental correlations that use a characteristic length presented similarities among them. Thus, these results showed that the criteria defined by the authors who published the correlations could present discrepancies when are compared with correlations that establish opposite criteria. This aspect could start the discussion on the operational definitions that each correlation should have. Most of these definitions are based on the metrological criteria that the authors followed for the tests (e.g. the tests in wind tunnel).

After conducting the cluster analysis of the various expressions, the results were analysed. As for the external methods, the value obtained by each test was considered, whereas in the internal method a total result was assessed at the end of the tests. The reason was the great variability of the external results mainly due to the reading of both the local wind speed and the external surface temperature. This aspect showed one of the main weaknesses of the external methods in comparison with the internal methods because of the great influence of external climate conditions, which could vary the expression of the external convective term.

Great differences among the two methods were seen by comparing the results obtained. To provide readers with some information on this aspect, the percentage deviations shown in Figs. 2, 3 and 4 between the measured value and the referential value are summarized (the figures represent the percentage deviation in comparison with the value of the method from ISO 9869-1:2014).

External methods are characterized by presenting both high percentage deviations and a great variation in the oscillation of results. In this regard, the correlations with wind speed and adimensional numbers obtained deviations greater than 20% in comparison with the referential value, both in the convection approaches and in the convection and radiation approaches. The percentage contributions of the correlations were different according to the equation.

There were significant deviations in both approaches and the contributions varied from one equation to another, so the existing limitations to determine the radiation contribution were stressed. In this regard, some previous studies have mentioned the difficulties to determine the radiation component from the exterior. However, the fact that the convection approaches had a low number of representative results showed the difficulties to apply the external method.

As for the approach of simplified convection and radiation, the results were similar to that of the cluster t in the approach of convection and radiation because of the null

**Table 6** Groups of the experimental correlations of the convective term obtained with the cluster analysis

Exterior				Interior			
Wind speed		Adimensional numbers		Temperature differences		Adimensional numbers	
Cluster	Equations	Cluster	Equations	Cluster	Equations	Cluster	Equations
a	(42), (43)	a	(54), (61)	a	(72)	a	(97)
b	(41), (49)	b	(62)	b	(65), (73), (77), (85)	b	(5), (6), (87), (93), (95)
c	(40)	c	(57), (58), (59)	c	(78)	c	(89)
d	(23), (44)	d	(6) (adapted to the exterior)	d	(70), (71)	d	(92)
e	(4), (9), (13), (21), (24), (50), (53)	e	(55), (56)	e	(68), (74)	e	(100)
f	(29), (45)	f	(60)	f	(67), (69), (83), (84)	f	(86), (88), (90), (98), (101), (103)
g	(16), (18), (48)			g	(75)	g	(99)
h	(34)			h	(63), (76), (81)	h	(91), (94), (96), (102)
i	(51), (52)			i	(66), (79), (82)		
j	(28)			j	(64)		
k	(31), (46)			k	(2)		
l	(33), (37), (39)			l	(80)		
m	(32), (38)						
n	(25)						
o	(19), (30), (47)						
p	(26)						
q	(20)						
r	(17), (22)						
s	(10), (11), (12), (14), (15)						
t	(3), (27), (35), (36)						

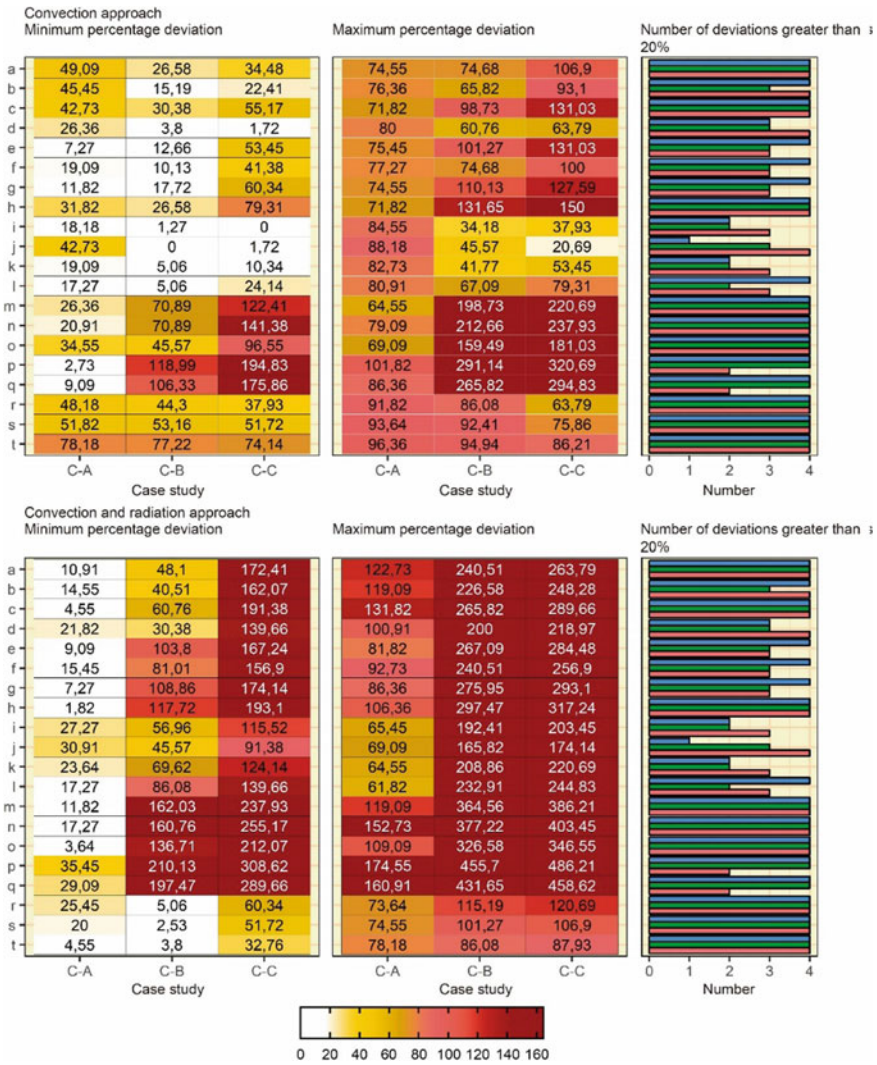


**Fig. 2** Percentage deviations obtained by the methods from the exterior that use wind speed correlations. The number of the valid results obtained in each case study is represented in the graphs on the right. *Source* Own elaboration

percentage contribution of the convective heat flux in the total flow in the approach of simplified convection. Different results were only obtained in those in which there was a greater percentage contribution of the convective term.

Likewise, there were significant differences in the results according to the type of wind speed used in calculations (average wind speed during the whole test or

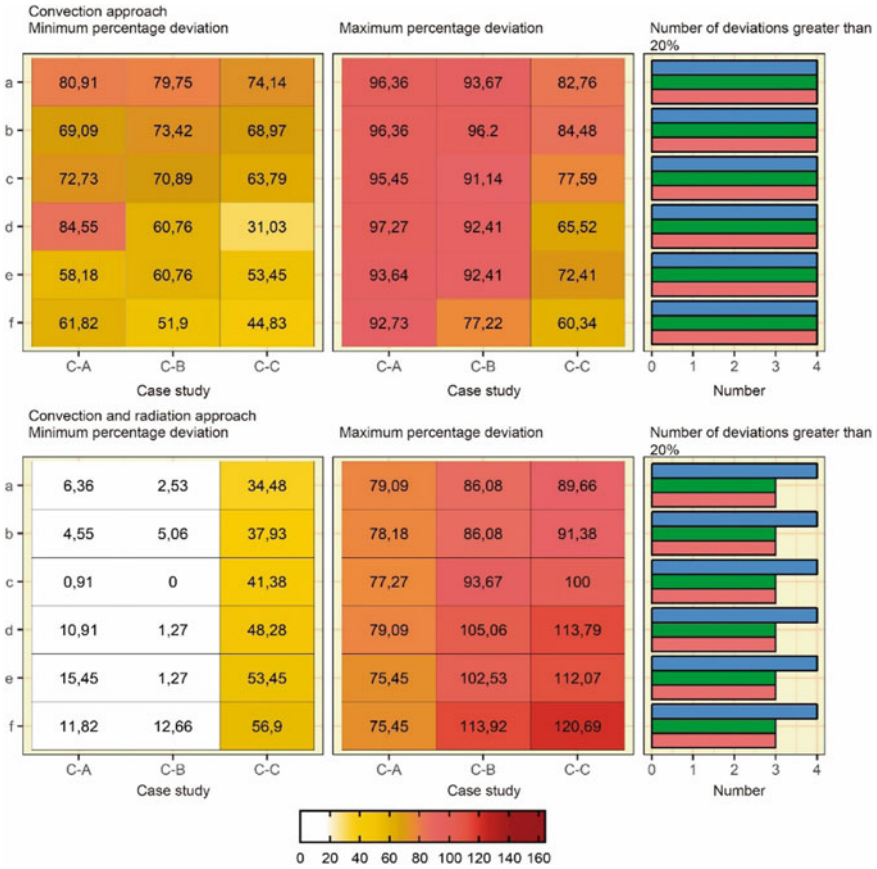


**Fig. 3** Percentage deviations obtained by the external methods that use correlations of adimensional numbers. The number of the valid results obtained in each case study is represented in the graphs on the right. *Source* Own elaboration

instantaneous speeds). This aspect, which has been scarcely developed, seems to show a limitation to use the external method.

As for the internal methods, both temperature correlations and adimensional numbers were characterized by presenting a greater number of cases with representative results. For this purpose, the approach of convection and radiation was used, as the approach of convection was characterized by presenting a lower number of representative results. Thus, the percentage contribution of the convective heat flux in comparison with the total significantly varied according to the experimental correlation used, with some of them being characterized by presenting a greater contribution than that of radiation in some case studies, as those included in cluster *g*.

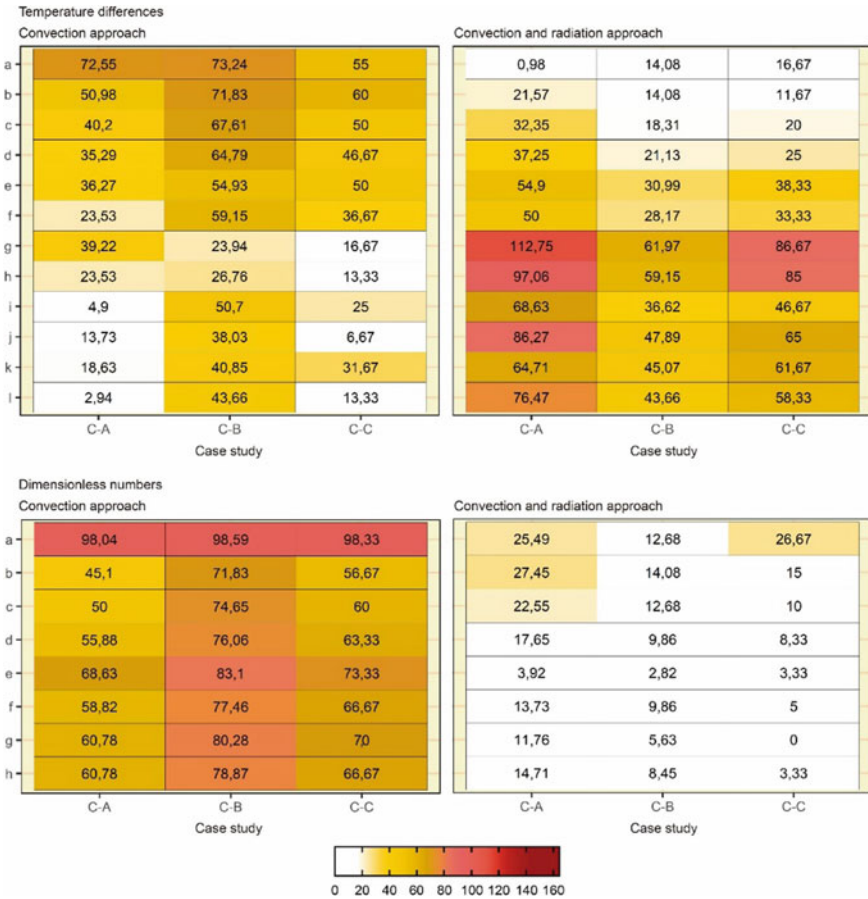


**Fig. 4** Percentage deviations obtained by the internal methods for the two types of correlations (temperature differences and adimensional numbers). *Source* Own elaboration

Similar results of the proportion of the convective term of adimensional numbers were obtained in all cases studies. Thus, the percentage deviations between the various groups of expressions obtained similar results.

The results of the two typologies of experimental correlations used for the internal methods were compared, and the correlations of adimensional numbers presented greater roughness as a greater number of cases with low percentage deviations was obtained.

The results therefore showed that the best approach for quantitative infrared thermography methods are the tests performed from the interior and whose formulation is based on correlations of adimensional numbers. In this regard, the differences between the two approaches were very significant and, although the external method could present some advantages to be applied (because thermographies could be

made from the exterior, affecting as less as possible dwellings' users), their use is not recommended due to the limitations. Thus, performing tests under controlled conditions has implied that the expressions of adimensional numbers obtained an adjusted result.

## 4 Conclusions

The analysis of the convective term in quantitative infrared thermography methods showed that the place where the test is performed (exterior or interior), the data analysis approach, and the convective term strongly affect the results.

As for external methods, the various expressions analysed for the external convective heat transfer coefficients correlated with wind speed obtained different results according to both the test and the approach adopted:

- For the convection approach, valid results were obtained in the 3 types of walls analysed with the equations of Watmuff et al. (Eq. (28)), of Lunde (Eq. (31)), of ISO 6946 (Eq. (46)), and of Liu and Harris (Eqs. (51) and (52)).
- For the convection and radiation approach, the equations that belong to clusters "a", "b", "c", "e", "f", "g", "h", "k", "l", and "o" obtained valid results in the wall without insulation, whereas the use of the equations of clusters "r", "s", and "t" obtained valid results in walls with insulation.
- For the simplified convection and radiation approach, valid results were obtained in walls without insulation or with insulation of low thickness. Also, similar results were obtained between the different equations of the external convective heat transfer coefficient when wind speed was low.

However, the index of repeatability of the valid results of these equations was low. Likewise, the use of the average wind speed or the wind speed measured in each instant as an input variable in the calculation procedure significantly modified the thermal transmittance results obtained in each test. According to this aspect, a greater variation was obtained in the results of those tests in which the deviation presented by the instantaneous wind speed was high with respect to the mean value.

As for adimensional approaches, none of the external convective heat transfer coefficients obtained representative results for the convection approach, whereas the convection and radiation approach obtained representative results in two tests, with a behaviour similar to Albatici and Tonelli's simplified approach.

Given both the differences in the various approaches and the low repetition of results, establishing an appropriate coefficient or approach to use these correlations in the external method was not possible.

As for the internal methods, the different expressions analysed were characterized by showing greater roughness. Regarding the correlations of temperature differences in the convection approach, only those correlations characterizing a high convective flux obtained a larger number of representative results, whereas that, in the approach of convection and radiation, the equations of Alamdari and Hammond (Eq. (72)), of

Min et al. (Eq. (65)), of Holman (Eq. (77)), and of Fohanno and Polidori (Eq. (85)) obtained valid results in the 3 walls analysed. However, the correlations of adimensional numbers obtained a larger number of representative results. In this regard, only 1 out of 20 equations did not obtain representative results, and the rest obtained adjusted results in most tests.

The results showed therefore the advisability of using internal methods with the use of correlations of adimensional numbers as the most acceptable methodology to apply the quantitative infrared thermography method. These results are in accordance with the last research studies on the method carried out by Tejedor et al. [18] in relation to the use of adimensional numbers, thus marking the development of the method for further research works.

## References

1. Kurtz F, Monzón M, López-Mesa B (2015) Energy and acoustics related obsolescence of social housing of Spain's post-war in less favoured urban areas. The case of Zaragoza. *Inf. La Construcción*. 67:m021. <https://doi.org/10.3989/ic.14.062>
2. Adhikari R, Lucchi E, Pracchi V (2012) Experimental measurements on thermal transmittance of the opaque vertical walls in the historical buildings. In: PLEA2012—28th conference, opportunities, limits and needs towards an environmentally responsible architecture
3. Waddicor DA, Fuentes E, Sisó L, Salom J, Favre B, Jiménez C, Azar M (2016) Climate change and building ageing impact on building energy performance and mitigation measures application: a case study in Turin, northern Italy. *Build Environ* 102:13–25. <https://doi.org/10.1016/j.buildenv.2016.03.003>
4. Walker R, Pavía S (2015) Thermal performance of a selection of insulation materials suitable for historic buildings. *Build Environ* 94:155–165. <https://doi.org/10.1016/j.buildenv.2015.07.033>
5. Bagavathiappan S, Lahiri BB, Saravanan T, Philip J, Jayakumar T (2013) Infrared thermography for condition monitoring—a review. *Infrared Phys Technol* 60:35–55. <https://doi.org/10.1016/j.infrared.2013.03.006>
6. Balaras CA, Argiriou AA (2002) Infrared thermography for building diagnostics. *Energy Build* 34:171–183. [https://doi.org/10.1016/S0378-7788\(01\)00105-0](https://doi.org/10.1016/S0378-7788(01)00105-0)
7. Kylili A, Fokaides PA, Christou P, Kalogirou SA (2014) Infrared thermography (IRT) applications for building diagnostics: a review. *Appl Energy* 134:531–549. <https://doi.org/10.1016/j.apenergy.2014.08.005>
8. Lucchi E (2018) Applications of the infrared thermography in the energy audit of buildings: a review. *Renew Sustain Energy Rev* 82:3077–3090. <https://doi.org/10.1016/j.rser.2017.10.031>
9. Albatici R, Tonelli AM (2010) Infrared thermovision technique for the assessment of thermal transmittance value of opaque building elements on site. *Energy Build* 42:2177–2183. <https://doi.org/10.1016/j.enbuild.2010.07.010>
10. Madding R (2008) Finding R-values of stud-frame constructed houses with IR thermography. In: *Proceedings of InfraMation*
11. Fokaides PA, Kalogirou SA (2011) Application of infrared thermography for the determination of the overall heat transfer coefficient (U-value) in building envelopes. *Appl Energy* 88:4358–4365. <https://doi.org/10.1016/j.apenergy.2011.05.014>
12. Holman JP (1986) *Heat transfer*, 6th edn. McGraw-Hill Inc, New York
13. Earle RL, Earle MD (1983) *Unit operations in food processing*
14. Albatici R, Tonelli AM (2008) On site evaluation of U-value of opaque building elements: a new methodology. In: PLEA 2008—25th conference of passive and low energy architecture



15. Albatici R, Tonelli AM, Chiogna M (2015) A comprehensive experimental approach for the validation of quantitative infrared thermography in the evaluation of building thermal transmittance. *Appl Energ* 141:218–228. <https://doi.org/10.1016/j.apenergy.2014.12.035>
16. Watanabe K (1965) Architectural planning fundamentals
17. Dall’O’ G, Sarto L, Panza A (2013) Infrared screening of residential buildings for energy audit purposes: results of a field test. *Energies* 6:3859–3878. <https://doi.org/10.3390/en6083859>
18. Tejedor B, Casals M, Gangolells M, Roca X (2017) Quantitative internal infrared thermography for determining in-situ thermal behaviour of façades. *Energy Build* 151:187–197. <https://doi.org/10.1016/j.enbuild.2017.06.040>
19. Bienvenido-Huertas D, Bermúdez J, Moyano JJ, Marín D (2019) Influence of ICHTC correlations on the thermal characterization of façades using the quantitative internal infrared thermography method. *Build Environ* 149:512–525. <https://doi.org/10.1016/j.buildenv.2018.12.056>
20. Bienvenido-Huertas D, Bermúdez J, Moyano J, Marín D (2019) Comparison of quantitative IRT to estimate U-value using different approximations of ECHTC in multi-leaf walls. *Energy Build* 184:99–113. <https://doi.org/10.1016/j.enbuild.2018.11.028>
21. Meng X, Yan B, Gao Y, Wang J, Zhang W, Long E (2015) Factors affecting the in situ measurement accuracy of the wall heat transfer coefficient using the heat flow meter method. *Energy Build* 86:754–765. <https://doi.org/10.1016/j.enbuild.2014.11.005>
22. Nardi I, Paoletti D, Ambrosini D, De Rubeis T, Sfarra S (2016) U-value assessment by infrared thermography: a comparison of different calculation methods in a Guarded Hot Box. *Energy Build* 122:211–221. <https://doi.org/10.1016/j.enbuild.2016.04.017>
23. ASTM International (2014) ASTM E1933-14, Standard Practice for Measuring and Compensating for Emissivity Using Infrared Imaging Radiometers, West Conshohocken, PA. <https://doi.org/10.1520/E1933-14>
24. Maroy K, Carbonez K, Steeman M, Van Den Bossche N (2017) Assessing the thermal performance of insulating glass units with infrared thermography: potential and limitations. *Energy Build* 138:175–192. <https://doi.org/10.1016/j.enbuild.2016.10.054>
25. Hagishima A, Tanimoto J, Narita K (2005) Intercomparisons of experimental convective heat transfer coefficients and mass transfer coefficients of urban surfaces. *Boundary-Layer Meteorol* 117:551–576. <https://doi.org/10.1007/s10546-005-2078-7>
26. Cole RJ, Sturrock NS (1977) The convective heat exchange at the external surface of buildings. *Build Environ* 12:207–214. [https://doi.org/10.1016/0360-1323\(77\)90021-X](https://doi.org/10.1016/0360-1323(77)90021-X)
27. Watmuff JH, Charters WWS, Proctor D (1977) Solar and wind induced external coefficients—solar collectors. *Coop. Mediterr. Pour l’Energie Solaire, Rev. Int. d’Héliotechnique*. 56
28. Palyvos JA (2008) A survey of wind convection coefficient correlations for building envelope energy systems’ modeling. *Appl Therm Eng* 28:801–808. <https://doi.org/10.1016/j.appltherm.2007.12.005>
29. Defraeye T, Blocken B, Carmeliet J (2011) Convective heat transfer coefficients for exterior building surfaces: existing correlations and CFD modelling. *Energy Convers Manag* 52:512–522. <https://doi.org/10.1016/j.enconman.2010.07.026>
30. Nusselt W, Jürges W (1922) Die Kühlung einer ebenen Wand durch einen Luftstrom. *Gesundheits Ing.* 52:641–642
31. Jürges W (1924) Der Wärmeübergang an einer ebenen Wand (heat transfer at a plane wall). *Gesundh. Ing., Beiheft*
32. McAdams WH (1954) Heat transmission. McGraw-Hill, New York
33. Davies MG (2004) Building heat transfer. Wiley
34. Sogin HH (1964) A summary of experiments on local heat transfer from the rear of bluff obstacles to a low speed airstream. *J Heat Transfer* 86:200–202. <https://doi.org/10.1115/1.3687094>
35. Schaak A (1965) Industrial heat transfer. Chapman & Hall, London
36. Jennings BH (1970) Environmental engineering; analysis and practice. International Textbook Co



37. Sturrock NS (1971) Localized boundary-layer heat transfer from external building surfaces. University of Liverpool
38. Mitchell JW (1971) Base heat transfer in two-dimensional subsonic fully separated flows. *J Heat Transfer* 93:342–348. <https://doi.org/10.1115/1.3449829>
39. Lokmanhekim M (1971) Procedure for determining heating and cooling loads for computerized energy calculations. Algorithms for building heat transfer subroutines. ASHRAE, New York
40. Ito N (1972) Field experiment study on the convective heat transfer coefficient on exterior surface of a building. *ASHRAE Trans* 78:184–191
41. Kimura K (1977) Scientific basis of air conditioning. Applied Science Publishers, London
42. Nicol K (1977) The energy balance of an exterior window surface, Inuvik, N.W.T., Canada. *Build Environ* 12:215–219. [https://doi.org/10.1016/0360-1323\(77\)90022-1](https://doi.org/10.1016/0360-1323(77)90022-1)
43. Lunde PJ (1980) Solar thermal engineering: space heating and hot water systems. Wiley
44. Test FL, Lessmann RC, Johary A (1981) Heat transfer during wind flow over rectangular bodies in the natural environment. *J Heat Transfer* 103:262–267. <https://doi.org/10.1115/1.3244451>
45. Sharples S (1984) Full-scale measurements of convective energy losses from exterior building surfaces. *Build Environ* 19:31–39. [https://doi.org/10.1016/0360-1323\(84\)90011-8](https://doi.org/10.1016/0360-1323(84)90011-8)
46. Yazdani M, Klems J (1993) Measurement of the exterior convective film coefficient for windows in low-rise buildings. *ASHRAE Trans* 100:1–19
47. Jayamaha SEG, Wijesundera NE, Chou SK (1996) Measurement of the heat transfer coefficient for walls. *Build Environ* 31:399–407. [https://doi.org/10.1016/0360-1323\(96\)00014-5](https://doi.org/10.1016/0360-1323(96)00014-5)
48. Loveday DL, Taki AH (1996) Convective heat transfer coefficients at a plane surface on a full-scale building facade. *Int J Heat Mass Transf* 39:1729–1742. [https://doi.org/10.1016/0017-9310\(95\)00268-5](https://doi.org/10.1016/0017-9310(95)00268-5)
49. Taki AH, Loveday DL (1996) External convection coefficients for framed rectangular elements on building facades. *Energ Build* 24:147–154. [https://doi.org/10.1016/0378-7788\(96\)00972-3](https://doi.org/10.1016/0378-7788(96)00972-3)
50. Hagishima A, Tanimoto J (2003) Field measurements for estimating the convective heat transfer coefficient at building surfaces. *Build Environ* 38:873–881. [https://doi.org/10.1016/S0360-1323\(03\)00033-7](https://doi.org/10.1016/S0360-1323(03)00033-7)
51. Mirsadeghi M, Cóstola D, Blocken B, Hensen JLM (2013) Review of external convective heat transfer coefficient models in building energy simulation programs: implementation and uncertainty. *Appl Therm Eng* 56:134–151. <https://doi.org/10.1016/j.applthermaleng.2013.03.003>
52. CIBSE (2015) CIBSE guide a: environmental design. [https://doi.org/10.1016/0360-1323\(94\)00059-2](https://doi.org/10.1016/0360-1323(94)00059-2)
53. Liu Y, Harris DJ (2015) Measurements of wind speed and convective coefficient on the external surface of a low-rise building. *Int J Ambient Energ* 36:225–234. <https://doi.org/10.1080/01430750.2013.853204>
54. Xie J, Cui Y, Liu J, Wang J, Zhang H (2018) Study on convective heat transfer coefficient on vertical external surface of island-reef building based on naphthalene sublimation method. *Energ Build* 158:300–309. <https://doi.org/10.1016/j.enbuild.2017.09.092>
55. Khalifa A-JN (2001) Natural convective heat transfer coefficient—a review I. Isolated vertical and horizontal surfaces. *Energ Convers Manag* 42:491–504. [https://doi.org/10.1016/S0196-8904\(00\)00042-X](https://doi.org/10.1016/S0196-8904(00)00042-X)
56. Khalifa A-JN (2001) Natural convective heat transfer coefficient—a review II. Surfaces in two- and three-dimensional enclosures. *Energ Convers Manag* 42:505–517. [https://doi.org/10.1016/S0196-8904\(00\)00043-1](https://doi.org/10.1016/S0196-8904(00)00043-1)
57. Peeters L, Beausoleil-Morrison I, Novoselac A (2011) Internal convective heat transfer modeling: critical review and discussion of experimentally derived correlations. *Energ Build* 43:2227–2239. <https://doi.org/10.1016/j.enbuild.2011.05.002>
58. Obyn S, Van Moeseke G (2015) Variability and impact of internal surfaces convective heat transfer coefficients in the thermal evaluation of office buildings. *Appl Therm Eng* 87:258–272. <https://doi.org/10.1016/j.applthermaleng.2015.05.030>

59. Wilkes GB, Peterson CMF (1938) Radiation and convection from surfaces in various positions. *Trans ASHVE* 44:513–520
60. Giesecke FE (1940) Radiant heating and cooling. *ASHVE J Heat Pip Air Cond* 12:484–485
61. Min TC, Schutrum LF, Parmelee GV, Vouris JD (1956) Natural convection and radiation in a panel heated room. *Ashrae Trans* 62:337–358
62. Churchill SW, Chu HHS (1975) Correlating equations for laminar and turbulent free convection from a horizontal cylinder. *Int J Heat Mass Transf* 18:1049–1053
63. Engineering science data unit, Heat transfer by free convection and radiation—simply shaped bodies in air and other fluids, London, 1979
64. Alamdari F, Hammond GP (1983) Improved data correlations for buoyancy-driven convection in rooms. *Build Serv Eng Res Technol* 4:106–112. <https://doi.org/10.1177/014362448300400304>
65. Li LD, Beckman WA, Mitchell JW (1983) An experimental study of natural convection in an office room, large time results. Solar Energy Laboratory, University of Wisconsin, Madison
66. Khalifa AJN, Marshall RH (1990) Validation of heat transfer coefficients on interior building surfaces using a real-sized indoor test cell. *Int J Heat Mass Transf* 33:2219–2236. [https://doi.org/10.1016/0017-9310\(90\)90122-B](https://doi.org/10.1016/0017-9310(90)90122-B)
67. Hatton A, Awbi HB (1995) Convective heat transfer in rooms. In: **Proceedings of fourth international conference, building simulation '95**
68. Awbi HB, Hatton A (1999) Natural convection from heated room surfaces. *Energy Build* 30:233–244. [https://doi.org/10.1016/S0098-8472\(99\)00063-5](https://doi.org/10.1016/S0098-8472(99)00063-5)
69. Fohanno S, Polidori G (2006) Modelling of natural convective heat transfer at an internal surface. *Energy Build* 38:548–553. <https://doi.org/10.1016/j.enbuild.2005.09.003>
70. Jakob M (1949) Heat transfer. Wiley & Sons, New York
71. Fishenden M, Saunders OA (1950) Introduction to heat transfer. Oxford University Press, Oxford
72. Chartered Institution of Building Services Engineers, CIBSE Guide C3, Heat Transfer, London, 1976
73. Wong HY (1977) Heat transfer for engineers. Pearson Longman, Harlow
74. Welty JR (1978) Engineering heat transfer. Wiley, New York
75. Al-Arabi M, Sakr B (1988) Natural convection heat transfer from inclined isothermal plates. *Int J Heat Mass Transf* 31:559–566. [https://doi.org/10.1016/0017-9310\(88\)90037-3](https://doi.org/10.1016/0017-9310(88)90037-3)

# In Situ Methodology to Assess the Action of Water-Wind on Building Windows



Manuel J. Carretero-Ayuso, David Bienvenido-Huertas,  
and Carlos E. Rodríguez-Jiménez

**Abstract** The chapter describes a new methodology for the evaluation of the in situ water tightness in window openings located in the building envelope, as well as the development process carried out for its real application. It is an innovative non-destructive testing procedure that reproduces the effects of rain combined with wind, which is applicable both during the building construction process and in buildings in use. It is a useful tool for tightness analysis in quality control of elements and constructive pathologies that offers verifiable results in the field of habitability evaluation in buildings.

**Keywords** Window · Water tightness · Blowerdoor · Buildings

## 1 Introduction

Infiltration and moisture are amongst the main pathologies that affect building envelopes [1, 2] and in some cases, such as in Spain, constitute the greatest percentage of lawsuits in relation to this type of construction unit [3]. This fact also affects the thermal behaviour of walls [4], thus influencing the energy demand of heating, ventilation, and air conditioning systems.

Window cavities in envelopes are critical points for moistures [5], where rain and wind are the determinant factors regarding water solicitation [6]. Thus, testing the parameters of water tightness and wind pressure in windows is important, so the respective regulation usually includes verification points for the assessment and quality control of windows. For instance, this issue is widely included in the European standard, and there are standards on water tightness tests for both external windows

---

M. J. Carretero-Ayuso  
Department of Architecture, University of Alcalá, Alcalá de Henares, Spain

D. Bienvenido-Huertas  
Department of Building Construction, University of Granada, Granada, Spain

C. E. Rodríguez-Jiménez (✉)  
Department of Building Construction II, University of Seville, Seville, Spain  
e-mail: [ceugenio@us.es](mailto:ceugenio@us.es)

and doors (EN 1027:2016) and resistance to wind (EN 12211:2016). According to the results obtained by the tests mentioned, this European standard also establishes classification criteria for both water tightness (EN 12208:1999) and resistance to wind (EN-12210:2016). However, this powerful standard on window control is subject to laboratory tests focussed on carpentry samples, in which the ensemble set of the window to the cavity or its construction perimeter (lintels, sills, etc.) cannot be tested. Laboratory results provide the features of the insulated element, dividing their values into various typologies, which is very useful to choose and validate typologies and construction project acceptance, however, these tests cannot prove the construction features of the several units of the building as each has their own factors, such as tolerances and execution failures, adjustment to other elements, and termination accessories. Consequently, in situ tests are considered an essential part to assess windows and their cavities appropriately, but performing a test outside a laboratory and in different locations implies another technical complexity that should be borne in mind as the tools, systems, and procedures used should be adapted to the various spaces and designs. For this reason, there are important limitations to achieve the utilization requests regarding the elements tested.

Aware of this problem, the TEP 970 research group (technological innovation, 3D modelling systems, and energy diagnosis in heritage and building), which is related to the field of production technologies, belongs to the Research Andalusian Plan of the Regional Government of Andalusia (PAIDI) and is made up by a multidisciplinary group of coordinated researchers from the University of Seville, included this issue in the ongoing works, aiming at looking for a transversal solution based on the knowledge acquired. Building façades are continuously subjected to pressure variations because of atmospheric conditions, with the wind pressure being the variable magnitude load that generally affects the exterior surfaces of architectural constructions. Studies on envelope air permeability are amongst the important areas studied by this research group, so the progress in this issue was considered to make a feasible proposal: the combination of wind pressure with rainfall, two meteorological phenomena that usually takes place together. This combination is very interesting to be studied given its impact on envelope elements and its direct influence on pathologies related to moisture and water infiltration, with window cavities being critical points. Thus, window features should be tested in situ against simultaneous water-wind solicitations, so the behaviour of the elements actually executed could be specified, thus solving existing failures and being a learning bank for future performances.

After the contribution of a particular team within the research group responsible for both this aspect and the development of many works and studies for that purpose, a theoretical proposal was obtained in the first stage of works for a testing system that gave response to these issues [7].

In the second stage of the research, the theoretical solution was implemented in many actual cases, in which the method was improved and adapted to be used in building quality control. This chapter describes the final result obtained after that empirical stage applied to existing buildings. Consequently, the current proposal is a new technique, but with proven tests, to assess in situ water and air permeability in

the envelope cavities of any building by simulating in situ various water conditions and wind pressure.

This procedure is based on putting an interior room of a building under variable pressure conditions; at the same time, an artificial rain is caused in the exterior surface of the existing façade cavities. Thus, meteorological conditions caused by driving rain are simulated in an actual building, i.e. the water driven by wind when acting on the envelope, thus testing the behaviour of the construction elements when these actions take place. It has been empirically tested that this system that assesses in situ permeability in façade cavities is fully versatile and universal to be used as its equipment is easy to be adapted and similar to other widely used diagnostic techniques.

## 2 State of the Art

There is no antecedent with these characteristics in the existing techniques. The study of sources to know the current state of the technique in this area reveals the existence of methods focussed only on theoretical and calculation models related to the various physical effects that the phenomenon of water driven by wind causes on façades [8, 9]. In this regard, there is a standard proposal in ISO 15927-3: 2009 called “*hygrothermal performance of buildings. Calculation and presentation of climatic data. Part 3: Calculation of a driving rain index for vertical surfaces from hourly wind and rain data*”. In other cases, measurements have been conducted in buildings to quantify in façades the typical values of these atmospheric phenomena in natural episodes [10, 11]. However, few references have assessed the phenomenon through actual reproduction techniques in view of such environmental conditions. In this regard, José María Pérez Bella’s doctoral thesis should be stressed [12]. His works conclude that the assessment tests included in the current international standards (and therefore marketed) correspond to sample patterns of laboratory tests whose principle, according to the author in page V.1 of the reference work, is: “*someter a la acción de un determinado caudal de agua sobre su superficie y a la acción simultánea de una determinada presión externa... determinando la presión máxima que el cerramiento es capaz de superar para un aporte de agua constante, sin presentar fugas de agua*” [12]. This author, together with other researchers, has studied this issue in several research studies [13–16] and although the method proposed focusses on the numeric calculation to characterize exposure parameters and payback periods, a correlation with the tests used in various international standards is also made. Nevertheless, in all the cases referenced, assessment techniques, together with the reproduction of actual conditions of water and wind pressure, are always limited to samples or graduated cylinders, expressly made for tests in laboratories or specialized facilities, such as those included in UNE-EN 12865: 2012 to determine water permeability in external walls under pulsating air pressure. There is no procedure for in situ (in the actual building) determinations by using air pressure variations.

On the other hand, some texts within the Spanish standard define tests to prove in situ water permeability, usually used to control quality in building works. This is the UNE 85247:2011 standard, called “*Windows. Water tightness. Site test*”, which describes a simple projection test of a constant water volume for 30 min to later verify or not the existence of water penetration to the interior; however, no mechanism for air pressure is included. To reproduce the wind effect, tightness tests should be performed in laboratories using carpentry samples. There are other research studies conducted in other countries, but none of them is similar to the procedure proposed in this study. It is worth mentioning some studies performed in Florida (USA) [17–19], all related to water action under wind pressure (wind-driven rain). Their goal was to approach to the effects of hurricanes as these phenomena are usual in the area and damage buildings. However, unlike the procedure proposed, isolated samples are reproduced and expressly built to be tested through large devices located in facilities adapted for that purpose to perform tests at a large scale with elements that simulate wind (turbines).

It is also worth stressing the study conducted in the Laboratory of Building Physics at the Catholic University of Leuven, in Belgium [20], with the so-called vliet test building, i.e. a test building expressly built to assess envelopes. Within this research, experimental studies were conducted to test the hygrothermal performance of certain building solutions. For this purpose, tests were performed in the building under the natural meteorological conditions taking place during the test and without simulating artificial rain or wind pressure.

To sum up, the previous sources have proven that today, except this research line, there is no in situ assessment technique for built buildings that reproduce water conditions and variable wind pressure to assess the permeability of façade cavities. Moreover, there is no reference on the use of the procedure proposed that combines the several technologies simultaneously used (infrared thermography, blowerdoor systems, sprinkling systems, etc.).

The novelty of the procedure suggested and tested after the empirical stage has been valued thanks to the large number of sources consulted. In addition, there are no similar antecedents in relation to the application versatility and tool simplicity, with a particular reproduction of the solicitations that involve rain water combined with wind.

### 3 Methodology

The technique proposed aims to assess in situ the behaviour of window cavities in building envelopes regarding both their water permeability and the external air from meteorological phenomena called wind-driven rain.

To describe the operative methodology tested by this study, it is worth describing first the equipment used. The simultaneous use of these systems, together with a coordination based on the protocol established and the lines marked, allows valid results to be obtained regarding the characteristics and possible failures of the windows

placed under actual performance conditions. In particular, the instrumental systems used are as follows:

- a. To reproduce the wind effect on the façade in each pressure step defined, pressure differences should be created between the internal rooms of the building where the cavities to be assessed are placed and the external atmosphere.

For this purpose, one or more ventilator equipment were put in one or several ventilators included in blowerdoor devices (N° 9 in Figs. 1 and 2), which were placed at the door of the interior zones to pressurize, so a range of pressure differences, positive or negative, were created through air flows between the interior and the exterior, including equipment to measure those pressure, air flows, and temperature. For this purpose, commercialized blowerdoor equipment were used as they include a management hardware (N° 8 in Figs. 1 and 2) that was useful to control parameters during the test. To reproduce accurately the wind effect on the building façade, the pressure range should be negative, i.e. the pressure jump should be lower in the room tested than in the external atmosphere, so air flows were produced from the exterior to the interior. Thus, all fixed values for test pressure (measured in Pascals (Pa)) were understood as the magnitude that the exterior pressure should exceed in comparison with the interior one through this equipment.

- b. The rain effect was simulated simultaneously to the wind effect, i.e. by using a sprinkling water system directly from the exterior of the building in the whole surface of the cavity or cavities to be tested (N° 4 in Figs. 1 and 2). This water projection, which was conducted through water equipment with variable volume and tools to measure such volume, should cover the window and the junctions

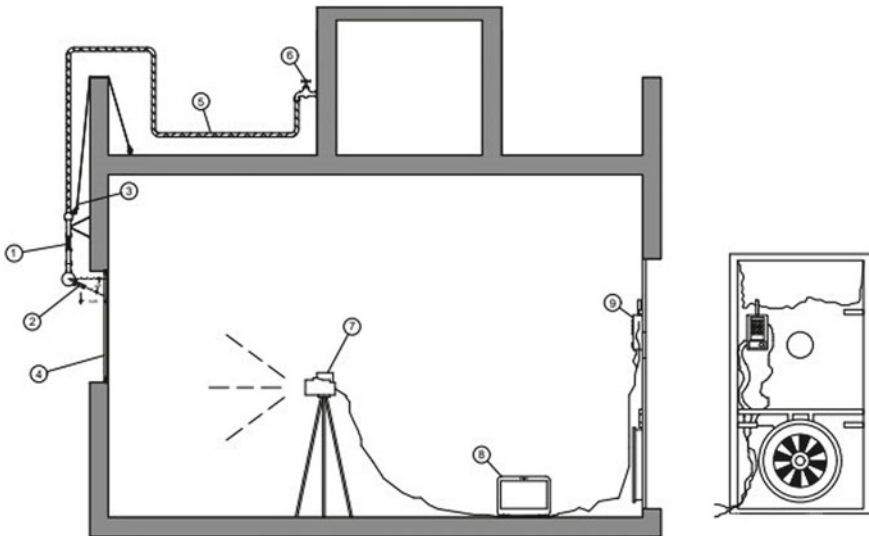
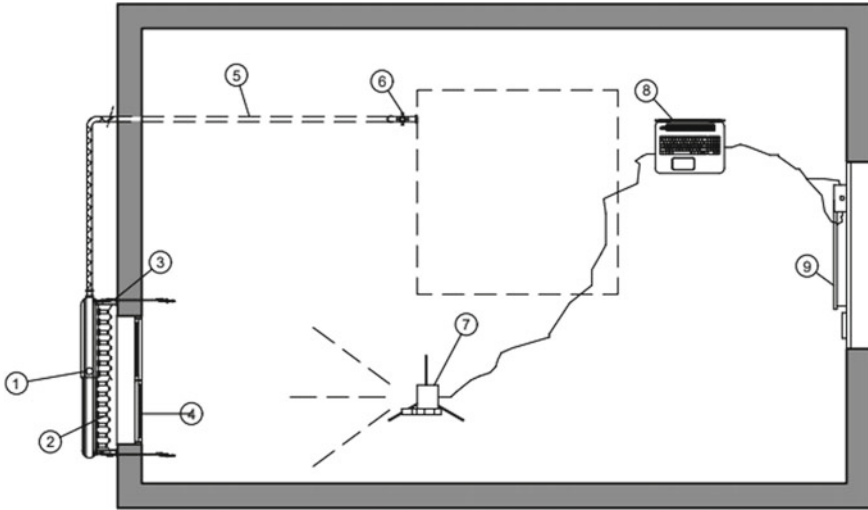


Fig. 1 Sketch of the test. Part I



**Fig. 2** Sketch of the test. Part II

of the various construction elements (woodwork, stonework, cladding, etc.). To set the volume to be reproduced in each test, rainfall criteria included in the respective building standard should be considered, according to climate zones and exposure zones. In Spain, there is a test standard, mentioned in the introduction, to check tightness without pressure (UNE 85247:20118). This standard establishes volume values that could also be used in the test proposed with pressure. For this purpose, a flowmeter of variable area was used (a rotameter) (N° 1 in Figs. 1 and 2), a sprinkling system with circular conical nozzles and a sprinkling angle of 120°, horizontally placed 150 mm above the lintel and separated 400 mm amongst them (N° 2 in Figs. 1 and 2). The flowmeter had a v-bracket so that the system was placed at the vertical position of the façade. Likewise, the flowmeter and sprinkling systems had a clamping system called support anchored to the façade or to the roof of the building (N° 3 in Figs. 1 and 2). Water was supplied by a flexible pipe with a diameter of ½ inch primed by a water intake point (N° 5 and 6 in Figs. 1 and 2).

- c. To complement the assessment of the behaviour of the cavity of the elements unnoticeable by human eyes, a usual infrared camera was used (N° 7 in Figs. 1 and 2) to test the surfaces affected, according to the methodology from UNE-EN 13187:1998.

After defining the tools, it is worth stressing the time sequence required by this methodology. The study of the requirements of each window sample to be tested, together with the analysis of the information that the development of the test provides, leads to a set of specific premises that those responsible for tests should always consider.



The number of windows to be tested in each test depends on the availability of equipment that could be simultaneously used in the several tool procedures described. In principle, there is no maximum limitation of the number of rooms to be pressurized with cavities sprinkled by water, although the experience based on tests for air permeability recommends to divide them into limited areas. If various spaces of a same building are included, the difficulty of maintaining a constant pressure increases due to the increase of the number of internal joints and cavities that produce uncontrollable air flows. However, if equipment is powerful enough, pressurization tests could be performed in spaces such as premises and halls in which the existing cavities could be instrumented with water projection and large tests could be conducted.

Nonetheless, the implementation and development of each test should be adjusted to the specific methodological scheme that has been successfully experimented by the research studies conducted, corresponding to the following steps:

1. Establishment of a protocol before performing each test to establish the number of simulation steps to be reproduced and their values.

Each step consisted of a different combination of pressure and water volume during a specific period of time (no lower than 5 min).

For this purpose, the goals of each test are considered, including both the exposure and the climate conditions required for building walls. For instance, in Spain, the climatic parameters set by the national application standard (The Spanish Technical Building Code) could be used. In addition, values internationally recognized are also useful, such as the Beaufort scale for the wind force. For coefficients and other calculation aspects, the EN-ISO 15927-3: 2011 standard called "*hygrothermal performance of buildings. Calculation and presentation of climatic data. Part 3: Calculation of a driving rain index for vertical surfaces from hourly wind and rain data*" could be used.

2. Preparation of the area. Temporary sealing of the existing gaps in the interior rooms to be pressurized different from those existing in the cavity or cavities of the façade to be assessed. The aim is to remove all the elements that cause controlled air infiltrations, i.e. the infiltrations foreseen in the performance design of the building. Air conditioning grills, ventilation gaps, junctions amongst elements that are not watertight, etc., should be fully sealed to not cause air flows that could alter the development of the test, at the same time, the performance of the ventilator is optimized, thus achieving greater performance of the blowerdoor equipment placed for each case. Only the air pressure could affect the joints and assemblage existing in both the window and its construction perimeter.

In addition, the correct performance of the window to be tested should be verified, i.e. its closure and opening (the window should be fully closed during the test), and all the elements influencing the detection of weird situations should be visually inspected, as well as the shadow elements and the accessories to be placed in the position established by the previous conditions of the tests should be operated.

Likewise, the equipment previously defined is placed and its correct performance should be verified for the test, since it is important to guarantee both the continuous supply of water volume established and the energy sources.

3. The test starts by reproducing rain and wind in situ through the simultaneous action of the tools described and according to the steps pre-established in Point 1. Controlling the correct pressure and volumes in each test phase is crucial.
4. Visual observation to inspect affected surfaces (the window, specially its perimeter junctions, as well as all surface areas of its interior outline and accessories such as shutter boxes and window cranks) during the whole test and after it is finished, for a period of time, no lower than 30 min. Any impact produced should be written down, although it is minimum, to monitor and assess if it is repeated.

Likewise, the infrared equipment should be activated in the inspection to always complement the assessment of elements through this technique, thus detecting the critical points and possible defects unnoticeable by human eyes. This information is useful to mark areas liable to suffer anomalies in the next steps of the test.

After finishing the test and the observation period, all permanent water infiltration and moisture in the interior that affect elements not foreseen to be wet should be considered.

5. The result report will include
  - Situation data of the spaces tested with levels of the existing cavities and their constructive characteristics.
  - Number of steps executed, collecting the following information in each one: time in minutes, pressured measured in Pascals (and equivalent wind speed in m/s) and water volume in l/m<sup>2</sup>h. The maximum values applied are justified according to the climate conditions or specific conditions of the test.
  - Detail of the water infiltration and moisture stains observed, and the step in which they appeared, indicating the wind pressure and speed of the last acceptable step, i.e. the previous to that causing anomalies. These conformance values are useful to tabulate and classify the characteristics of the cavity of the window tested.

Figure 3 includes a flowchart of the methodological process described, whose study and application have been useful for the goals proposed.

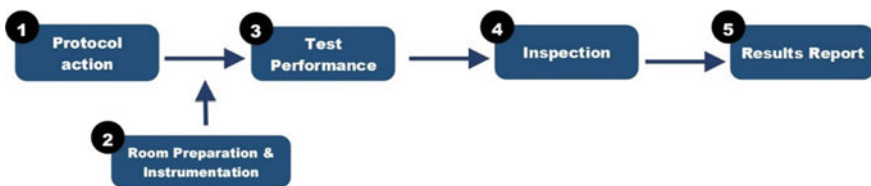


Fig. 3 The flowchart of the methodological process

## 4 Intervention Example

An intervention example developed in the empirical phase of the research is provided. Many applications are conducted in actual cases to quantify values, define specific adjustments, and obtain all the data required to implement the method appropriately. The example is presented as a guide for interventions to be conducted, and based on it, the versatility of the process allows characteristic and detailed parameters to be changed to be adapted to another possible requirement, always considering the initial methodological basis.

This case corresponds to a standard situation amongst all those analyzed. It is a flat located in the second floor of a multi-family residential building in Seville (Spain), where the behaviour of a window cavity is tested. There are no previous requirements, and the test only determines the maximum capacity of the window tested regarding water-wind solicitation. This is a type case conducted by the research team to implement the test system that could be extrapolated to other similar performances in various locations and with other requirements.

After inspecting the dwelling and compiling all the existing information, a window cavity was selected; in this case, it is the only window in the room. It is an aluminium window, with two sliding leaves of total dimensions 145 cm × 205 cm, with a roller blind. The wall is of ceramic brick with double-leaf and internal insulation, and the window is placed in the plan of the interior surface.

The protocol established for the test was based on the following steps:

Assembly of the blowerdoor equipment in the front door of the room chosen as test room in the dwelling. It was previously surveyed and measured according to the procedure of air permeability tests in buildings described by ISO 9972:2015.

Assembly and adjustment of the sprinkling system outside the window as it is described in the methodology and always following the guidelines provided by the UNE 85247:2011 Spanish standard.

Preparation of the infrared camera to take images.

Initial performance verification of the equipment used, as well as the correct closure and lack of anomalies in the cavity to be tested.

Start of the test whose subsequent steps of water pressure (in Pascals) and projection are initially presented with the following rate:

- Water projection without pressure (15 min)
- Water projection + difference air pressure 50 Pa (5 min)
- Water projection + difference air pressure 100 Pa (5 min)
- Water projection + difference air pressure 150 Pa (5 min)
- Water projection + difference air pressure 250 Pa (5 min)
- Water projection + difference air pressure 300 Pa (5 min)
- Water projection + difference air pressure 450 Pa (5 min)
- Water projection + difference air pressure 600 Pa (5 min).

If there are no visible water infiltrations after this test sequence, the series of pressure steps continue with variations of 150 Pa in each.

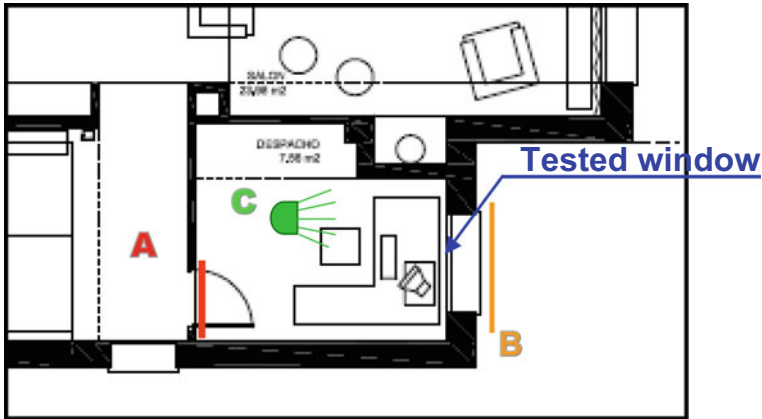


**Fig. 4** Plan sketch of the room tested: (A) blowerdoor; (B) water spray instrumentation, and (C) infrared camera

If there are water infiltrations or constant moisture in surfaces not foreseen to be wet, the test is considered finished. In this case, the maximum acceptable pressure to be considered is that of the step immediately lower than that in which the failure has been detected. This pressure, with its equivalent to wind speed, provides referential parameters to value the maximum capacity of the cavity regarding wind-driven rain, which should be studied from the point of view of meteorology and exposure to the façade in which the window tested is located. Thus, a clear vision of the vulnerability of the window or windows tested could be obtained regarding the appearance of failures due to infiltration or moisture caused by actual rain.

On the one hand, Fig. 4 includes the plan sketch of the room tested and the test layout, and on the other hand, Fig. 5 corresponds to photographs of the equipment used to reproduce wind pressure, and Fig. 6 corresponds to the tested window.

In the case tested, the results showed continuous water infiltrations to the interior in the third step of the test corresponding to 100 Pa (Fig. 7). Consequently, the allowable rating pressure for wind-driven rain was 50 Pa, equivalent to 33 km/h of wind speed.

Based on these results, several aspects are discussed:

- First, the results approve the proposed methodology as the test was fully satisfactory. The reproduction of combined rain and wind phenomena was faithfully simulated.
- Second, the adaptability of the test is obvious as all tools were easily placed, and the protocol established was easily developed.
- Moreover, the practical sense of the test was also shown as interior infiltrations were detected during the water-wind process, thus fulfilling the goal of the procedure, which was to obtain the maximum characteristics with which the window could operate without anomalies in its location and under current conditions. In the case tested, this limit was 33 km/h regarding rain + wind.

**Fig. 5** Equipment used to reproduce wind pressure



**Fig. 6** Tested window



**Fig. 7** Window during test



- Finally, the possible failures to be solved were detected. In the unit tested, the failures were the watertight sealing of the joints between the window and the perimeter of the façade in which it was located.

In addition, other actual applications of the proposed method were conducted in several building typologies and window cavities, obtaining different values regarding their characteristics. Nonetheless, the results of the test performance were always satisfactory.

## 5 Conclusions

The testing method to assess the behaviour of windows regarding water and wind action responds to the following scheme:

1. Means are used to pressurize the building envelope from the interior in one or several rooms. In particular, blowerdoor equipment are used to generate a specific range of constant pressure differences, which are controlled between the exterior and the indoor rooms of the building in which the cavity or cavities to test are placed, by putting a device to make air movements in the interior with measurement of air flow rates and pressures.
2. Similarly, a water sprinkling system is used in the exterior area of the cavity or cavities to be tested and in the perimeter of the façade. Its volume should always be controlled by a metre or flowmeter, and the orientation of the projection system should be adapted to both the configuration of the cavity of the window and the requirements of each test.
3. The test consists in using two equipment that operate in a combined way, thus reproducing identical conditions than that caused by simultaneous water and wind on the façade. Several combinations of pressure and volume could be used according to the climate actions (rainfall and wind) to be tested.
4. Moreover, possible water infiltration or moisture appearance is monitored in the tested zone. To distinguish the aspects related to infiltrations unnoticeable

by human eyes, infrared thermography is used as a simultaneous mean to study and obtain references during tests.

5. Finally, for each of the simulated combinations, the critical points and failures detected are assessed, thus evaluating the maximum resistance of the window to water-wind.

Thus, a tool is defined, and its actual application examples show that it is effective to establish the water-wind solicitations that window cavities could support, as well as to detect their construction or design failures. Using this, method to a great scale will provide useful databases for future decision-making for those responsible for the construction process at a project, execution, or maintenance level.

## References

1. Boudreaux P, Pallin S, Accawi G, Desjarlais A, Jackson R, Senecal D (2018) A rule-based expert system applied to moisture durability of building envelopes. *J Build Phys* 42(3):416–437
2. Pereira C, de Brito J, Silvestre JD (2018) Contribution of humidity to the degradation of façade claddings in current buildings. *Eng Fail Anal* 90:103–115
3. Carretro-Ayuso MJ, Rodríguez-Jiménez CE, Bienvenido Huertas D, Moyano J (2021) Interrelations between the types of damages and their original causes in the envelope of buildings. *J Build Eng* 39:102235
4. Litti G, Khoshdel S, Audenaert A, Braet J (2015) Hygrothermal performance evaluation of traditional brick masonry in historic buildings. *Energ Build* 105:393–411
5. Van Den Bossche N, Huyghe W, Moens J, Janssens A, Depaape M (2012) Airtightness of the window-wall interface in cavity brick walls. *Energ Build* 45:32–42
6. Bomberg M, Kisilewicz T, Nowak K (2016) Is there an optimum range of airtightness for a building? *J Build Phys* 39(5):395–421
7. Rodríguez-Jiménez CE, Moyano J, Carretero-Ayuso MJ, Guillén-Lupión MI (2018) Methodological proposal for on-site watertightness testing with wind pressure on facade windows. *J Perform Constr Facil* 32(2):04017139
8. Sahal N, Lacasse MA (2008) Proposed method for calculating water penetration test parameters of wall assemblies as applied to Istanbul, Turkey. *Build Environ* 43(7):1250–1260
9. Kubilay A, Derome D, Blocken B, Carmeliet J (2015) Numerical modeling of turbulent dispersion for wind-driven rain on building facades. *Environ Fluid Mech* 15:109–133
10. Kubilay A, Derome D, Blocken B, Carmeliet J (2014) High-resolution field measurements of wind-driven rain on an array of low-rise cubic buildings. *Build Environ* 78:1–13
11. Chen C, Zhang H, Xuan Y, Qian T, Xie J (2022) Analysis of wind-driven rain characteristics acting on building surfaces in Shanghai based on long-term measurements. *J Build Eng* 45:103572
12. Pérez Bella JM (2012) Tesis doctoral: parametrización de la exposición a la humedad y de los ensayos de estanquidad en cerramientos de edificación: caracterización prestacional de su comportamiento higrotérmico. Departamento de Ingeniería Mecánica, Universidad de Zaragoza
13. Pérez-Bella JM, Dominguez-Hernández J, Rodríguez Soria B, del Coz-Díaz JJ, Cano-Suñén E (2013a) A new method for determining the water tightness of building facades. *J Build Res Inform* 41(4):404–414
14. Pérez-Bella JM, Dominguez-Hernández J, Rodríguez Soria B, del Coz-Díaz JJ, Cano-Suñén E, Navarro-Manso E. (2013b) An extended method for comparing watertightness tests for facades. *J Build Res Inform* 41(6):706–721

15. Pérez-Bella JM, Dominguez-Hernández J, Cano-Suñén E, del Coz-Díaz JJ, Alvarez-Rabanal FP (2014) Improvement alternatives for determining the watertightness performance of building facades. *J Build Res Inform* 43(6):723–736
16. Pérez-Bella JM, Cano-Suñén E, Alonso-Martínez M, del Coz-Díaz JJ (2020) Equivalence between the methods established by ISO 15927-3 to determine wind-driven rain exposure: reanalysis and improvement proposal. *Build Environ* 174:106777
17. López C, Masters FJ, Bolton S (2011) Water penetration resistance of residential window and wall systems subjected to steady and unsteady wind loading. *J Build Environ* 46:1329–1342
18. Bitsuamlak GT, Chowdhury AG, Sambare D (2009) Application of a full-scale testing facility for assessing wind-driven-rain intrusion. *J Build Environ* 44:2430–2441
19. Baheru T, Chowdhury AG, Bitsuamlak G, Masters FJ, Tokay A (2014) Simulation of wind-driven rain associated with tropical storms and hurricanes using the 12-fan Wall of Wind. *J Build Environ* 76:18–29
20. Desta TZ, Roels S (2010) Experimental and numerical analysis of heat, air, and moisture transfer in a lightweight building wall. In: Thermal performance of the exterior envelopes of whole buildings XI international conference, Leuven, Belgium, December 2010



# Outdoor Microclimate Influence on Building Performance: Simulation Tools, Challenges, and Opportunities



Victoria Patricia López-Cabeza, Jesus Lizana, Eduardo Diz-Mellado, Carlos Rivera-Gómez, and Carmen Galán-Marín

**Abstract** This chapter reviews the different approaches that currently exist to evaluate outdoor microclimates and their influence on building performance. Considering specific outdoor microclimates in building design flow can enable additional passive cooling strategies to mitigate climate risks in buildings and cities, improving their resilience capacity under extreme heat events. The available methods are defined and compared through different case studies of buildings with an inner courtyard, a traditional microclimate for passive cooling in hot climates. The results show the advantages and disadvantages of the different approaches and highlight the high interest in hybrid simulations coupling building energy simulation (BES) and computational fluid dynamics (CFD) tools for early design stages.

**Keywords** Courtyard microclimate · Heat mitigation · Urban heat island · Urban simulation · Climate-resilient design · Climate responsive design

## 1 Introduction

Buildings have an important role in minimizing climate change, given that they are responsible for approximately 40% of energy consumption in the EU [1] and 35% in the world and increasing [2]. Furthermore, they not only affect climate at a global scale but also at a local scale through the urban heat island effect (the higher urban temperatures in the city in comparison to rural areas), which is related to urban compactness and energy performance of buildings [3]. In the last decade, regulations that aim to reduce the energy consumption of buildings have been developed, especially in Europe. The European Directive 2018/844 of the European Parliament is one example [4], conducting net zero energy consumption requirements for buildings.

---

V. P. López-Cabeza (✉) · E. Diz-Mellado · C. Rivera-Gómez · C. Galán-Marín  
Departamento de Construcciones Arquitectónicas 1, Instituto Universitario de Arquitectura y Ciencias de la Construcción, Universidad de Sevilla, Avda. Reina Mercedes, 2, 41012 Sevilla, Spain  
e-mail: [vlopez7@us.es](mailto:vlopez7@us.es)

J. Lizana  
Department of Engineering Science, University of Oxford, Parks Road, Oxford OX1 3PJ, UK

© The Author(s), under exclusive license to Springer Nature Singapore Pte Ltd. 2022  
D. Bienvenido-Huertas and J. Moyano-Campos (eds.), *New Technologies in Building and Construction*, Lecture Notes in Civil Engineering 258,  
[https://doi.org/10.1007/978-981-19-1894-0\\_7](https://doi.org/10.1007/978-981-19-1894-0_7)

Researchers have studied the cost-effectiveness of different energy-saving measures for many years through building simulation tools and computer technology. However, there are still many challenges to be considered in ensuring high quality and useful building simulations: the importance of weather data selection, the need to include passive performance and thermal comfort indices in design processes, and the consideration of the potential benefits of specific microclimates on building performance. This last point is critical since these microenvironments have been proven to provide thermal benefits to buildings, especially in hot and warm climates. Enclosed courtyards are spaces surrounded by buildings and open to the sky. Their geometry, materials, water, vegetation, or shading elements produce thermodynamic effects that help to temper the extreme outdoor conditions. However, the courtyard performance is not considered in the existing building energy simulation (BES) tools and procedures [5]. This is due to two facts: It needs multi-outdoor climate conditions, which is not an option in most BES tools, and courtyard performance is hard to compute, given the multiple factors that have a role in it. The research aims to identify and compare existing and new procedures to account for the benefits of these specific microclimates, discussing advantages and drawbacks, and highlighting future needs toward a more accurate climate-resilient design process.

In the next section, a review of existing tools and approaches is shown, and in the rest of the chapter, some case studies using different approximations are analyzed, providing some challenges, opportunities, and recommendations.

## 2 Existing Tools and Approaches Review

Currently, different approximations to estimate the energy performance of buildings are available. They can be divided into two groups: white box models, which are based on the laws of physics that govern a system (e.g., conservation of mass, energy, and momentum) [6, 7], and black box or data-driven models which are based on statistical methods using machine learning [8]. For the simulation of outdoor microclimate, both models have been used.

### *White box models*

Physics-driven models were the first to be developed, and most of the existing tools and methodologies rely on this approach. BES and computational fluid dynamics (CFD) are two of the main numerical approaches in this area:

- **Building Energy Simulation Tools (BES)**

BES estimates the physical parameters in one single node per zone, representing a uniform profile of parameters in the region. This allows for long-term unsteady analysis although it simplifies too much, and the differences in the area represented by a single node cannot be considered. For that reason, outdoor simulation can be done only in a simplified way. Some examples of software of this kind are EnergyPlus, TRNSYS, or DesignBuilder, among many others. These tools have been used to

predict the influence of semi-outdoor spaces on energy consumption and indoor comfort. However, these models underestimate the potential benefits of these spaces, given that BES tools cannot simulate the microclimatic effects that occur outside. The temperature in the transitional space is assumed to be the same as outside, which is inaccurate most of the time. A study analyzing the impact of urban geometry on the energy consumption of buildings using TRNSYS concluded that if the microclimate is not included; this software can lead to inaccuracies [9]. In the last years, some tools, such as CitySim or UMI, have been specifically developed to account for the urban form on the energy consumption of districts. However, they still rely on microclimate simplifications.

- Computational Fluid Dynamic Tools (CFD)

In contrast to BES, these tools account for the whole volume of the space being considered, which is meshed in a few thousand to a few million control volumes, and the conservation equations are then applied to each of them. The basic that uses the CFD approach is the resolution of the Navier–Stokes’s equations which can be solved using finite element or finite volume methods for each control volume. This means that this approach requires considerable computing power to analyze unsteady states for a longer period than one day. However, they achieve high accuracy in the results.

COMSOL Multiphysics, ANSYS FLUENT, OpenFoam, or FreeFEM++ are some of the many choices of CFD tools available. They provide a variety of numerical solutions, which are not limited to building simulation. For the specific case of urban microclimates, the most widely used CFD software is ENVI-met. It can analyze small-scale interactions between soil, water, air, vegetation, and buildings at different scales. This software has renounced some of the broader capabilities of non-specific CFD tools to simplify the simulation analysis process. For example, the meshing options in ENVI-met are greatly limited.

- Hybrid workflows

There are currently many approaches that combine BES and CFD approaches to take advantage of the benefits of each one. In the hybrid workflows, one software outputs become inputs for another software. The aims of combining tools are diverse. First, to achieve higher accuracy in the simulation predictions. Second, to improve the workability of these tools to make them appropriate for the different design phases. Third, to add some other capabilities to the simulation from one tool, for example, the calculation of comfort indexes. For this reason, the hybrid workflows generally combine one BES tool with CFD software or comfort-calculation-specific tools. For example, EnergyPlus or Trnsys are combined with ENVI-met in many studies [10–12], or with Ladybug Tools [13–16], which are a set of plugins for Grasshopper that link the simulations engines, such as EnergyPlus or TRNSYS, with climate analysis, CFD procedures, and some comfort components.

*Black box models*

This approach, also called data-driven models, is based on statistical predictions using machine learning techniques. No physical model is required, but only large sets of input data to train a selected machine learning model to obtain the predicted outputs. Nowadays, these methods are recognized for their exceptional performance describing the overall behavior of a system based on its input–output relationship without needing any physical knowledge.

Machine learning methods can be classified into supervised or unsupervised. In supervised models, the learning is based on input–output pairs to guide the process. Examples used in building simulation are the artificial neural network (ANN) or the support vector machine (SVM). In unsupervised learning methods, there is no outcome, and the goal is to describe the associations and patterns among a set of inputs. Unsupervised methods are more practical and promising in discovering novel knowledge given limited prior knowledge than supervised methods. For this reason, it is preferred in mining building operational data, when many inputs are not known.

Despite a large amount of research into data-driven models, recently, its application by professionals of the building sector is more limited, and no specific simulation tool is based on this modeling approach. Still, they are a promising tool with many advantages that will be later analyzed. The following section shows some case studies using each of the previously described methods for the simulation of courtyard buildings.

### 3 Courtyard Simulation Studies

In this section, different examples of courtyard performance simulation are analyzed. The case studies selected share the same general methodology, which is represented in Fig. 1. First, a monitoring campaign is carried out to gather weather data used as

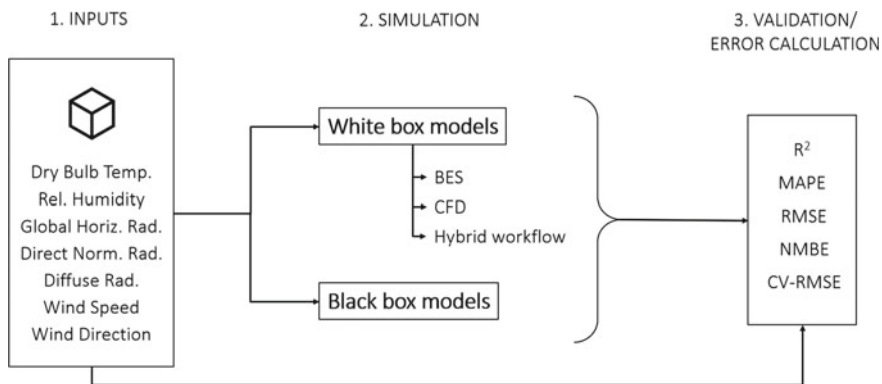


**Fig. 1** General workflow methodology followed in all the case studies

inputs for the simulations and courtyard data to validate the simulations. Then, the simulations are performed, each case using one of the previously described tools or approaches. Then, statistical parameters are calculated in order to measure the accuracy of the simulations and validate the results. The section is structured according to the classification previously used.

*BES*

Many researchers have used building energy simulation to analyze the performance of courtyard buildings [17, 18]. However, few studies have considered the courtyard as a different microclimate to outdoor conditions. This means that the benefits of the courtyard in these simulations are limited to the self-shading that the courtyard provides to the building. Recent studies have acknowledged that the courtyard has a singular microclimate, totally different to the outdoor climate, and they have found a way to include multi-nodal outdoor conditions in the simulations. Lizana et al. [5] quantified the effect of an inner courtyard microclimate on building performance using TRNSYS. The case study was analyzed with two outdoor weather conditions, an inner courtyard, and a local urban climate, as the most realistic case. Then, the building performance was compared to three single outdoor weather conditions associated with the urban climate, weather data from a rural station, and a typical year weather file. The selected case study was a dwelling unit on the sixth floor of a multifamily building in Seville, with one façade to an inner courtyard and the other to the outdoor. The outdoor and inner courtyard environments were monitored using weather stations and data loggers to get information for the microclimatic conditions. The building was numerically modeled as a multi-zone in TRNSYS. Information about geometry, external shadings, constructive elements, internal gains, infiltration, natural ventilation, thermal bridges, and internal heat capacity was required by the software. Surfaces linked to the courtyard microclimate were numerically modeled as an equivalent resistance layer with a boundary condition linked to the courtyard temperature, where courtyard solar radiative and convective gains were previously obtained and introduced per zone. An iterative calibration process was performed using the monitored air temperature data in four rooms and the standard statistical indices for model validation recommended by ASHRAE Guidelines [19] (Table 1). The results were analyzed using two building performance indicators, illustrated in Fig. 2: the percentage of indoor discomfort hours in free-running conditions (Fig. 2a) and the cooling energy demand using an idealized cooling system (Fig. 2b).

The results showed that the simulation considering two outdoor microclimates (the local weather file and the courtyard) mitigates severe hot hours by 88% compared

**Table 1** Statistical indices for model validation following ASHRAE Guidelines

	NMBE (%)	CV-RMSE (%)	R <sup>2</sup>
Bedroom 1	-2.0 (<±10%)	3.9 (<30%)	0.77 (>0.75)
Bedroom 2	-0.5 (<±10%)	2.0 (<30%)	0.93 (>0.75)
Bedroom 3	-1.5 (<±10%)	3.0 (<30%)	0.84 (>0.75)
Corridor	-1.2 (<±10%)	3.5 (<30%)	0.76 (>0.75)

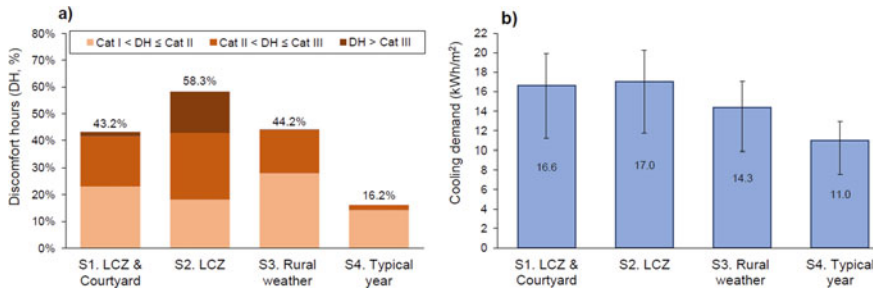


**Fig. 2** Discomfort hours and cooling demand results per simulated scenario in [5]

to the simulation with only the local climate. The discomfort hours were reduced by 26% during the measured period. Additionally, it can be noted in Fig. 2 how the comfort period in the courtyard microclimate ( $S_1$ ) is similar to the simulation where the rural weather file is used. These results demonstrate that the courtyard benefits the building and can mitigate extreme urban heat events.

In terms of cooling energy balance, the courtyard was able to reduce the impact of urban overheating by 15%. This is very influenced by cooling-related occupant behavior patterns, as shown in the bars chart (Fig. 2b), with the possibility of a reduction up to 29% in the case of a low energy consumption pattern.

Another study aimed to quantify the benefits of the courtyard in terms of cooling demand reduction in a building in Seville (Spain) [20]. This time, the simulation was performed with the Spanish BES software HULC and using a university office building with a courtyard as a case study. In this study, only two scenarios were analyzed: a reference case, in which it was assumed that the air temperature throughout the whole building envelope was the outside monitored temperature (Fig. 3a) and the proposed methodology, varying the boundary conditions in the courtyard according to the monitoring campaign (Fig. 3b), thus, considering the effect of the courtyard on air temperature.

The results showed a reduction of the cooling demand in the simulated case considering the monitoring results in the courtyard that reached 10% in adjacent rooms located on the ground floor of the courtyard. For the whole building, the cooling demand obtained was 7% in the spaces adjacent to the courtyard. The variation in cooling demand reduction according to the level of the room is because of the characteristic stratification effect of the courtyards (Table 2).

The results from these studies emphasize the importance of selecting an accurate weather file in the simulation. Local climate weather file increases discomfort hours and cooling demand in comparison to the scenario with the rural weather file, which is not considering the urban heat island effect. Moreover, the unsuitability of the typical year weather file to evaluate the climate resilience of buildings is demonstrated. The analysis of climate resilience building design requires the use of weather files that includes the extreme events that will happen more often in the future. It is also demonstrated how it is needed to include multi-nodal outdoor conditions in order

**Fig. 3** Section of the building showing the boundary conditions considered in the reference case **a** and the proposed methodology, **b** for thermal simulation of a building including a courtyard

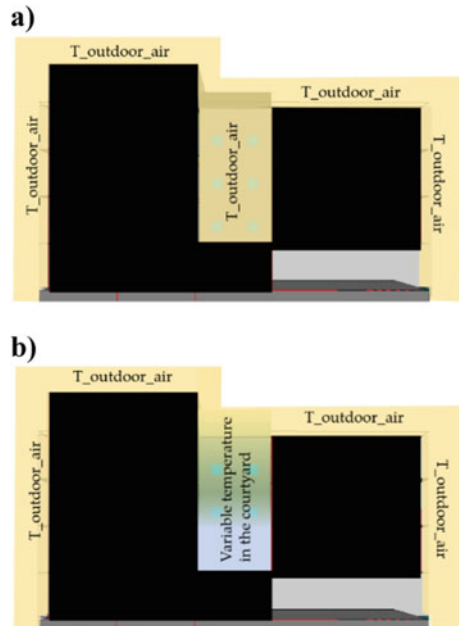


**Table 2** Accumulated cooling demand reduction in the case study by Sanchez de la Flor et al. [20]

Room	Case study (kWh/m <sup>2</sup> )	Reference case (kWh/m <sup>2</sup> )	Absolute difference (kWh/m <sup>2</sup> )	Percentage difference (%)
Third floor room 1	23.67	25.74	2.07	9
Fourth floor room 1	18.38	20.17	1.79	10
Fifth floor room 1	27.62	29.27	1.65	6
Third floor room 2	15.47	15.96	0.49	3
Fourth floor room 2	16.09	16.65	0.56	4
Fifth floor room 2	17.20	17.75	0.55	3

to account for the benefits of passive strategies associated with urban microclimate strategies, such as the use of courtyards. However, this is not straightforward for two reasons. First, the introduction of different boundary conditions for the building envelopes in the simulation has been possible following different assumptions, which are even not possible in other tools. And second, in these studies, the courtyard

temperature introduced had been previously monitored, but for the energy simulation of the early design, this is not possible. Courtyard temperature needs to be also simulated, which is impossible using BES software. For that reason, other kinds of tools are needed, which are discussed in the following sections.

### CFD

Computational fluid dynamic is needed when accuracy is required in the simulation of courtyards, given the thermodynamic effects that govern their performance. Inside a courtyard, not only geometry is a deterministic factor but also the thermal properties of the surface materials, the presence of vegetation, shading, water, etc. They influence the thermodynamic effects inside, associated with the temperature stratification, convection, and flow patterns [21], which are impossible to predict without CFD software.

Several studies use CFD software to predict the thermodynamic performance of courtyard buildings. One of them is ENVI-met, maybe the most widely used for urban microclimate analysis [22]. The suitability of this software for the simulation of inner courtyards is analyzed by Lopez-Cabeza et al. [23], contrasting simulation data with monitoring results. The objective of this study was to find a tool that can predict the temperature of courtyards accurately to be used in the energy simulation of buildings. Three case studies with different aspect ratios<sup>1</sup> were analyzed, all of them located in Seville. Monitoring data from the weather station were used as inputs for the simulations, and the courtyard temperature to validate the results. The three case studies were modeled in ENVI-met, following other researchers' recommendations. Then, results were numerically evaluated using the coefficient of determination ( $R^2$ ) and the root mean square error (RMSE) as statistical parameters.

Results indicated that ENVI-met was able to simulate a reduction in the temperature inside the courtyards. However, the difference between outdoor and courtyard temperature was much higher in the monitoring campaign than in the simulation results, as shown in Fig. 4. The statistical parameters, reported in Table 3 shows that although outdoor temperatures showed high accuracy, the courtyard temperatures did not, and the RMSE reached 3.35 °C.

The results state that ENVI-met accuracy when simulating small inner courtyards is not enough to consider the results in a building energy simulation. The lack of accuracy of the software can be due to different factors: the insufficient resolution of the software for the scale of this kind of spaces and simplification done by the software in terms of radiative fluxes [24]. Moreover, another problem of the software is the large amount of computational power required and the time needed to simulate a short period. This makes it impossible to couple ENVI-met results with a whole-year simulation in a BES software in an acceptable time.

For these reasons, other CFD options have been analyzed. One of the reasons why ENVI-met takes so long is the large amount of data it provides, much of it not required for the later energy simulation of the building. For that reason, one

---

<sup>1</sup> The aspect ratio is the relation between the width and the height of the courtyard, following the equation  $AR = \text{Height/Width}$ .



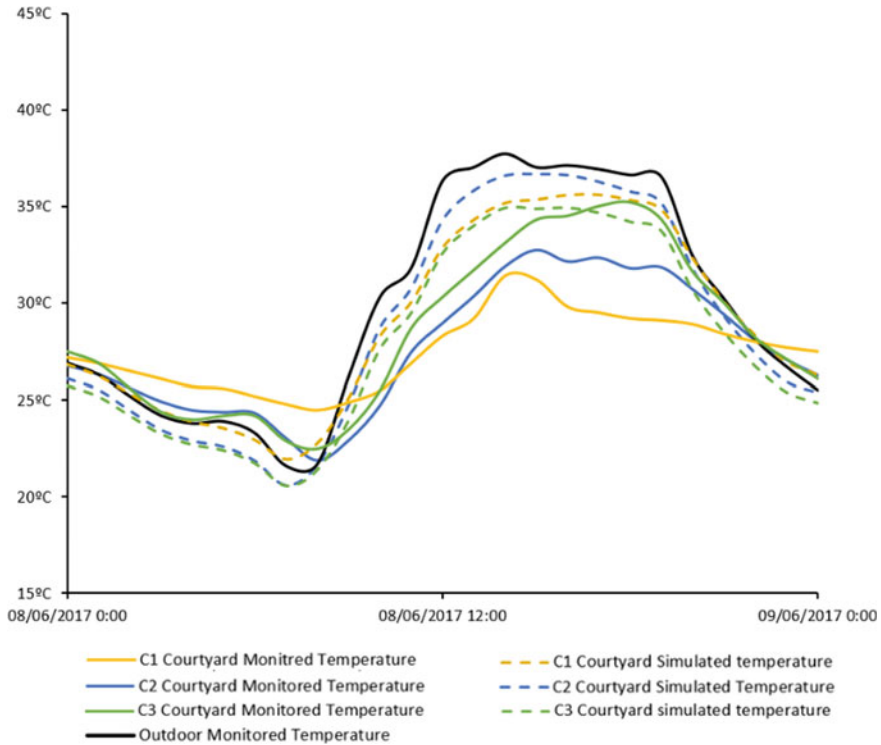


**Fig. 4** Monitored and simulated air temperature outside and inside the courtyards in the three case studies by Lopez-Cabeza et al. [23]

**Table 3** Statistic parameters for the validation of the simulations with ENVI-met

	$R^2$	RMSE (°C)
Case 1	0.84	3.35
Case 2	0.88	2.92
Case 3	0.93	1.52

option to make CFD calculation faster is to design a numerical model that optimizes the courtyard calculation. That is done by Lopez-Cabeza et al. [25], developing a new methodology for the simulation of courtyards, coupling a CFD model with a system of equations at the walls to calculate the surface and inner wall temperatures, providing an accurate courtyard thermal performance evaluation. The results were contrasted to monitored data in order to validate the model. The novel coupled model for courtyard simulation was computed using the FreeFEM++ software and validated in a case study located in Seville. Moreover, the results were compared with the simulation performed by other CFD software, in terms of accuracy in the air temperature inside the courtyard predictions and computational time. This last one is another critical indicator, especially if the simulation results are used in annual

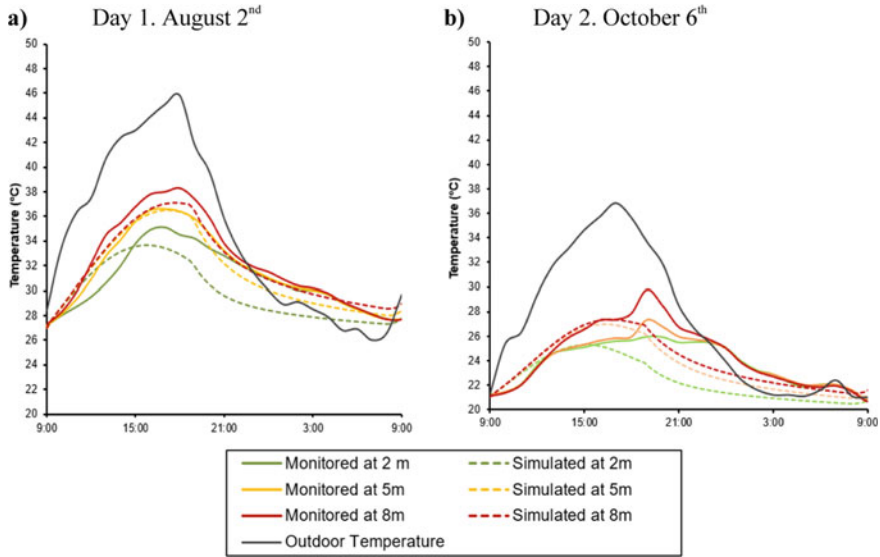


**Fig. 5** Air temperature simulation results using FreeFEM++

**Table 4** Statistical parameters for the validation of the simulation using FreeFEM++

Date	$R^2$	RMSE (°C)	CV (RMSE) (%)	NMBE (%)
August 2nd, 2018	0.88	1.19	3.75	1.72
October 6th, 2017	0.64	1.59	6.59	3.69

performance simulation or early design. Two different days were simulated, one in August and another one in October, to test the model under different solar positions and weather conditions.

Simulation results showed high accuracy in reproducing the thermal patterns inside the courtyard. The model was able to predict a thermal gap<sup>2</sup> close to monitoring data and the stratification effect inside the courtyard, which is the variation of temperatures at different heights (Fig. 5). The statistical parameters for error calculation were the best of the three simulation methodologies used in this courtyard, as shown in Table 4. This methodology was also the fastest in terms of simulation time, requiring only a few minutes for a simulation that other software required hours.

This study showed a methodology that is very promising in comparison with other previously analyzed. However, it needs to be further tested and coupled with modeling and visualizing software in order to make the process accessible for designers. The simulation time is very short in comparison to other CFD methods, given that the methodology is designed and optimized for the simulation of temperature and wind

<sup>2</sup> Thermal gap is defined as the difference between the outdoor temperature and the temperature inside the courtyard, as follows:  $TG = T_{outdoor} - T_{courtyard}$ .

patterns inside the courtyard. Thus, no other results are consuming time and computational resources. The model is also limited to the courtyard space, also reducing the size of the mesh being calculated.

*Hybrid workflows*

The coupling of BES and CFD tools has been studied by different researchers, to combine the advantages of each other. It can be argued that from a designer perspective, a methodology of courtyard simulation should fulfill some requirements. The method should be easy to implement in the early design stage of projects; CFD is highly recommended to achieve accuracy, including the interrelations between building, soil water, and vegetation; moreover, it should be possible to measure comfort indexes and energy consumption in buildings; finally, it would be ideal if the method is open source to understand the process behind the calculations. With all those requirements, it can be said that using one single software is not possible. A hybrid, or a combination of software, is required.

Lopez-Cabeza et al. [26] developed and validated a methodology for the simulation of courtyards in buildings that combines BES and CFD simulations using the Ladybug Tools. The aim was to simulate the temperature of courtyards in a suitable way for the early design of buildings. The results achieved higher accuracy than other existing methodologies. The study developed a script that included a CFD simulation with the Butterfly plugin in Grasshopper to combine courtyard temperature results with outdoor comfort analysis in Ladybug. The workflow is represented in Fig. 6. It was applied in three case studies of building with courtyards of different geometries, and the results were compared with monitored data to validate them.

The results of air temperature inside the courtyard obtained from the simulation are shown in Fig. 7. These values were then used to obtain the Universal Thermal Climate Index, an outdoor comfort index that can be understood as the “feels like” temperature equivalent to the environmental conditions. Monitoring data were used

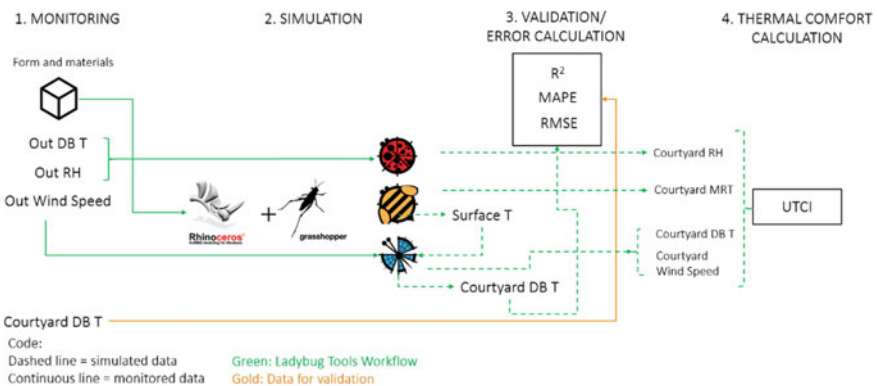


**Fig. 6** Hybrid simulation workflow proposed by Lopez-Cabeza et al. [26] (DBT = Dry bulb temperature. RH = Relative humidity. UTCI = Universal Thermal Climate Index)

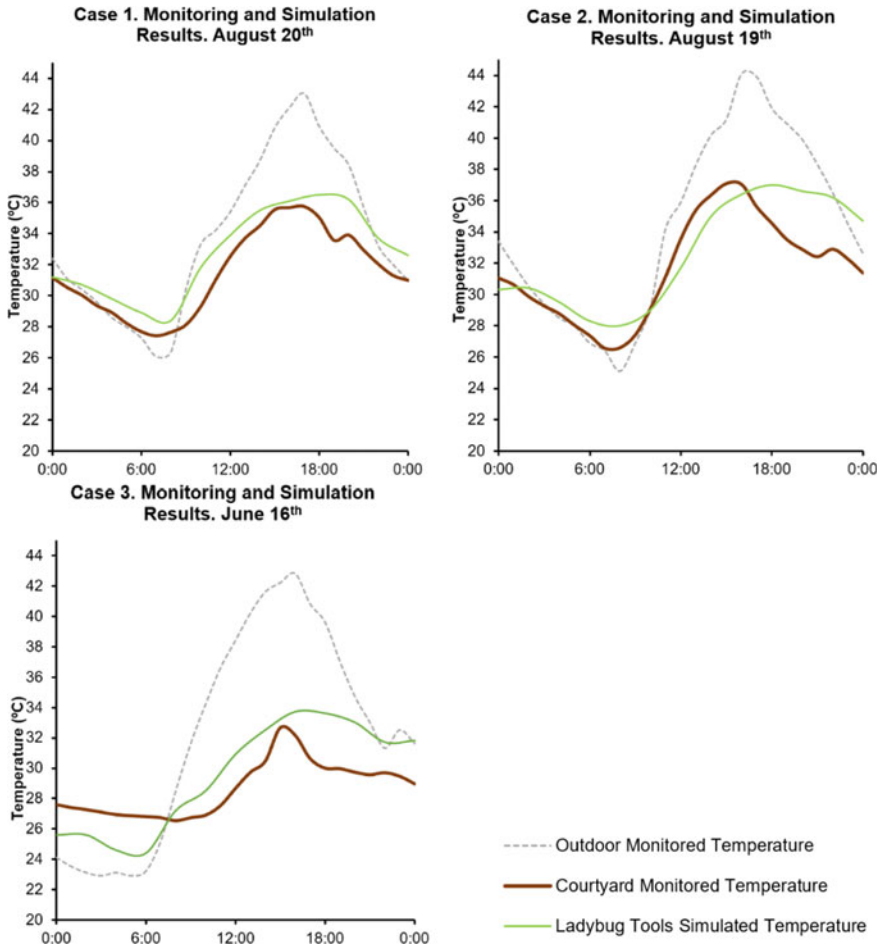


**Fig. 7** Hybrid simulation results for the three case studies by Lopez-Cabeza et al. [26]

to validate the simulations, obtaining a mean absolute percentage error from 3.81 to 7.55% and a root mean square error from 1.37 to 2.29 °C (Table 5), results that can be considered highly accurate in comparison with other studies and methodologies.

**Table 5** Statistical parameters for the validation of the simulation using Ladybug Tools

	AR	$R^2$	MAPE (%)	RMSE (°C)
Case 1	0.9	0.9	3.81	1.37
Case 2	1.5	0.7	5.07	2.00
Case 3	4.6	0.8	7.55	2.29

This methodology was analyzed following three criteria: accuracy, computational resources, and ease of use and access.

- **Accuracy:** The simulation methodology proposed achieves good accuracy in the cases analyzed. However, it has one major limitation, which is that it is not possible to include the evapotranspiration effect of the vegetation. There is no Ladybug Tools component able to do that. On the other hand, given that is an open-source software supported by a large community, this shortcoming may be overcome soon.
- **Computational resources:** Simulation time depends on many factors in terms of computational resources and simulation configurations. This method requires a long simulation time similar to other CFD software like ENVI-met (a few hours are required to simulate a whole day). However, it has one advantage: Given that it is a steady-state solver, it does not need an initialization time to get accurate results. This means that the simulation can focus on specific hours (e.g., extreme temperatures or specific occupation hours), making the simulation time shorter. This is not possible with transient solvers like ENVI-met, which need to calculate all the hours in a run. Moreover, the possibility of connecting all the results in one interface (Grasshopper) and their visualization in the Rhino interface used for design makes the process much suitable for the early design stage of projects.
- **Ease of use and access:** The use of the Ladybug tools has one advantage for the design, the easy connection between the simulation software and the design software, especially for people already familiarized with the Grasshopper tool. Furthermore, there is a major advantage with many other tools: All the simulation software used are open source and free, thus available for everyone.

### *Data-driven method*

Although some of the physical models provide accurate results for the simulation of courtyards, their main disadvantage is the impossibility of calculating long periods using CFD without spending a long simulation time. BES and CFD calculations time differ enormously (from minutes to hours). For that reason and trying to make the prediction of courtyard performance easier, the use of data-driven models has been also analyzed. Diz-Mellado et al. [27] aimed to implement an accurate machine learning methodology to predict thermal patterns in courtyards accurately based on their geometry and outdoor temperature. The study trained the algorithm with the monitored data of 32 other case studies using the support vector regression method and MATLAB interpolations. Using the library of data predicted by machine learning, the temperature inside two other courtyards was forecasted according to their climatic zone and geometry. The simulation was validated contrasting results with monitored data. Figure 8 shows an example of the results obtained in the temperature prediction. The simulation showed good accuracy, particularly on days with higher outdoor temperatures.

This research evaluated the errors in the two case studies for validation, one with monitored and predicted temperatures similar to the outside (CS1) and the second case study with a larger thermal gap to the outside (CS17). The graphic on the left

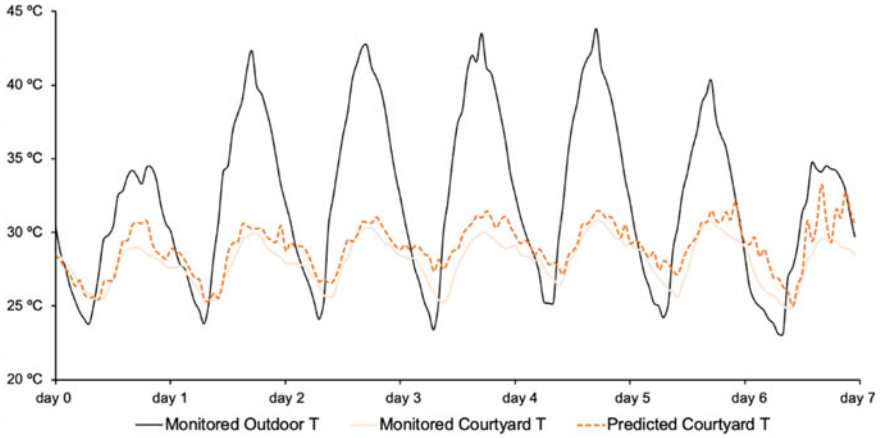


**Fig. 8** Example of air temperature simulation results from the data-driven model by Diz-Mellado et al. [27]

(Fig. 9a) corresponds to the relative error of the predicted thermal gap and is always under 8%, and the graphic on the right (Fig. 9b) corresponds to the relative error of the predicted temperature inside the courtyard, providing results under 0.1% in the two cases.

The values confirm that the strategy used is quite accurate compared to other, more computationally expensive CFD model simulations. In addition, the results show more accuracy than other existing commercial tools. The root mean square error (RMSE) of this investigation is in a similar range to the values obtained with the CFD model in FreeFEM++ described before (1 °C) and lower than in other commercial tools that are around 3 °C. The new methodology proposed for the ML

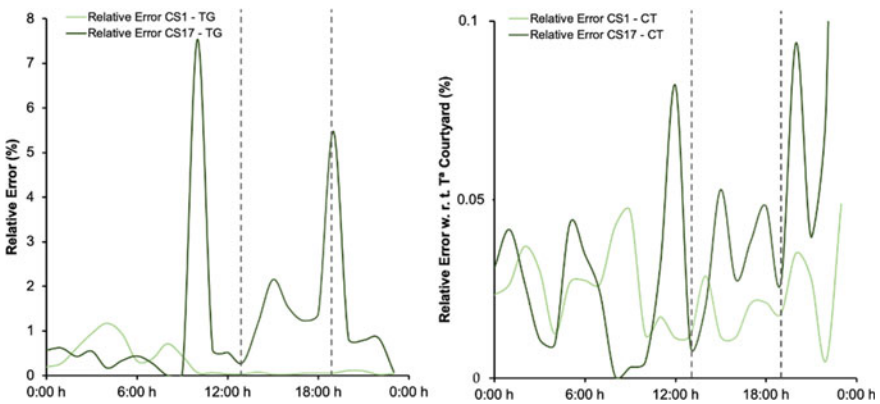


**Fig. 9** Relative error calculated for the validation of the data-driven methodology by Diz-Mellado et al. [27]

method in this research is helpful for developing design tools capable of modeling the complex microclimate of semi-outdoor spaces such as courtyards without the complexity of defining a physical model. Other advantages of using ML techniques are related to the identification of fundamental variables, simplifying the calculation process, and better accuracy by including a more significant amount of training datasets.

## 4 Discussion of Challenges and Opportunities

The previous section analyzed different approaches to simulate the thermal performance of buildings with courtyards. From that analysis, some general conclusions about the strength and weaknesses of each methodology are discussed here:

- BES models are the tool commonly used to simulate the energy performance of buildings. The nodal approach allows for quick computing time when simulating dynamic evolutions throughout the whole year. However, BES models cannot be used to analyze outdoor microclimate influence on building performance if that data are not manually included as boundary conditions. This means that BES needs to be coupled with other simulation approaches that can predict microclimates in order to measure their influence on the building performance. For that reason, the use of hybrid workflows is needed when analyzing passive strategies to enhance the resilience of buildings facing climate change.
- CFD allows performing a detailed analysis of fluxes inside and outside a building on a small scale, being one option to obtain the microclimate data to be coupled in the BES simulations. However, this methodology has some weaknesses. First, these tools are difficult to implement without previous knowledge of fluid dynamics. Some of them are easier but rely on simplifications, leading to a lack of accuracy. And they require a high computation time. We have seen that it is possible to optimize the simulation model for specific simulations, but this has not been implemented yet in a tool accessible to the public, so currently, programming knowledge is also required to do this.
- Data-driven models are a promising alternative to CFD models for the prediction of courtyard performance based on ML. They have another advantage, which is the possibility of being applied even without detailed information of the model. However, their accuracy depends on the quality of the training datasets, and large and representative data are required. This is a novel approach that is currently limited to researchers with programming knowledge of ML.

This analysis highlighted how the best choice depends on the objectives of the analysis and the available data. For example, when speed and easily accessible feedback is needed for the early design, hybrid options using currently available tools are probably the best option. However, research is still needed to improve the connectivity among tools. On the other hand, data-driven models could be the best option if an analysis is to be done about an existing building from which there is not much

constructive information. Being this said, future research on this field should still focus on some essential challenges that are not yet overcome:

- The integration of evaporative effects on the simulations is limited to very few software applications currently available for professionals, like ENVI-met. This means that the evapotranspiration effect of vegetation and the evaporative cooling of water are not being considered in many other tools, but experimental research shows that they are effective passive strategies against urban heat. For that reason, it is important to work on this issue to improve our analysis of urban mitigation strategies.
- The simulations can be further optimized, aiming to reduce computational time and increase accuracy in all methods. For the data-driven models, improving the datasets to train the algorithm or developing other ML techniques applied to urban microclimates is ways of future research. For the CFD and hybrid methods, much research exists that can be applied to the development of new CFD algorithms. As an example, reduced-order modeling (ROM) is a strategy that provides reductions of several orders of magnitude in the computational cost of numerical simulation of parametric design processes and problems. This is an option to reduce computing time that is currently under research [28].
- Finally, although many options and tools have been presented here, better accessibility to the professional sector is still required. Some methodologies are still not incorporated into existing commercial or open-source tools accessible for architects, designers, or city planners. Others require advanced knowledge that makes them difficult to apply practically. This is a problem that needs to be addressed in order to transfer research knowledge into society.

## 5 Conclusion

This chapter presents an overview of the different methods to simulate outdoor microclimates and their influence on building performance. They were tested, discussed, and compared through various case studies based on a very common microclimate, the traditional inner courtyard. Although the examples presented in this chapter focused on courtyards, these methodologies apply to a large variety of small-scale or medium-scale urban outdoor spaces capable of generating microclimates.

The results demonstrate the lack of capabilities of current building energy simulation (BES) tools to consider the benefits of these specific microclimates on building performance. Furthermore, despite different computational fluid dynamics (CFD) software that can predict the performance of these urban environments, the high computational effort and the lack of accuracy limit its potential application for preliminary design stages.

The analysis in different case studies also shows how multi-nodal outdoor climate simulations considering these microclimates can present high benefits in building performance. These specific microclimates can solve the problem of the urban overheating effect, for example, mitigating peak daytime temperatures. The consideration



of these benefits in design workflow can enable additional passive cooling strategies in the building design, and BES tools should be improved to account for them.

In this sense, the potential of hybrid simulations coupling a variety of software (BES and CFD) has been described and tested, presenting a novel promising approach to combine the benefits of different methods in early design stages. However, it is still essential to enable better accessibility to the professional sector to promote a better climate change adaptation of the built environment. The optimal integration of these microenvironments in urban planning can enable new actions to mitigate climate risks in cities and buildings. From a practical view, the most important issue is to make it simpler to incorporate the microclimate data in decision-making processes. Only then it will be possible to broader analyze urban resilience strategies under climate change projections.

**Acknowledgements** This work was supported by the grant RTI2018-093521-B-C33 funded by MCIN/AEI/ 10.13039/501100011033 and by “ERDF A way of making Europe” and the Spanish Ministry of Education, Culture, and Sport via a pre-doctoral contract granted to V.P. L-C. (FPU17/05036) and E. D-M (FPU18/04783). The research was also supported by the European Union’s Horizon 2020 research and innovation program under the Marie Skłodowska-Curie grant agreement No 101023241.

## References

1. Eurostat. Database—Eurostat. <https://ec.europa.eu/eurostat/en/web/main/data/database>. Accessed 14 December 2021
2. Global Alliance for Buildings and Construction. 2020 Global Status Report For Buildings And Construction Towards a Zero-Emissions, Efficient and Resilient Buildings and Construction Sector, 2020. [www.globalabc.org](http://www.globalabc.org). Accessed 14 December 2021
3. Santamouris M, Papanikolaou N, Livada I et al (2001) On the impact of urban climate on the energy consumption of building. *Sol Energy* 70(3):201–216. [https://doi.org/10.1016/S0038-092X\(00\)00095-5](https://doi.org/10.1016/S0038-092X(00)00095-5)
4. Directive (EU) 2018/844 of the European Parliament and of the Council of 30 May 2018 amending Directive 2010/31/EU on the energy performance of buildings and Directive 2012/27/EU on energy efficiency (Text with EEA relevance). *Official Journal of the European Union*, 2018
5. Lizana J, Lopez-Cabeza VP, Renaldi R, Diz-Mellado E, Rivera-Gomez C, Gal C (2021) Integrating courtyard microclimate in building performance simulation to mitigate extreme urban heat impacts. *Sustain Cities Soc* 2021:103590. <https://doi.org/10.1016/j.scs.2021.103590>
6. Li Y, Neill ZO, Zhang L, Chen J, Im P, Degraw J (2021) Grey-box modeling and application for building energy simulations—a critical review. 146
7. Coakley D, Raftery P, Keane M (2014) A review of methods to match building energy simulation models to measured data. *Renew Sustain Energ Rev* 37:123–141. <https://doi.org/10.1016/j.rser.2014.05.007>
8. Hamdaoui M-A, Benzaama M-H, El Mendili Y, Chateigner D (2021) A review on physical and data-driven modeling of buildings hygrothermal behavior: models, approaches and simulation tools. *Energ Build* 251:111343. <https://doi.org/10.1016/j.enbuild.2021.111343>
9. M’Saouri El Bat A, Romani Z, Bozonnet E, Draoui A (2021) Thermal impact of street canyon microclimate on building energy needs using TRNSYS: a case study of the city of Tangier in Morocco. *Case Stud Therm Eng* 24:100834. <https://doi.org/10.1016/j.csite.2020.100834>

10. Yang X, Zhao L, Bruse M, Meng Q (2012) An integrated simulation method for building energy performance assessment in urban environments. *Energy Build* 54:243–251. <https://doi.org/10.1016/j.enbuild.2012.07.042>
11. Natanian J, Auer T (2020) Beyond nearly zero energy urban design: a holistic microclimatic energy and environmental quality evaluation workflow. *Sustain Cities Soc* 56. <https://doi.org/10.1016/j.scs.2020.102094>
12. Perini K, Chokhachian A, Dong S, Auer T (2017) Modeling and simulating urban outdoor comfort: coupling ENVI-Met and TRNSYS by grasshopper. *Energy Build* 152:373–384. <https://doi.org/10.1016/j.enbuild.2017.07.061>
13. Mackey C, Galanos T, Norford L, Roudsari MS (2017) Wind, sun, surface temperature, and heat island: critical variables for high-resolution outdoor thermal comfort. In: *Proceedings of the 15th IBPSA conference San Francisco, CA, USA*, pp 985–993. <https://doi.org/10.26868/25222708.2017.260>
14. Soflaei F, Shokouhian M, Tabadkani A, Moslehi H, Berardi U (2020) A simulation-based model for courtyard housing design based on adaptive thermal comfort. *J Build Eng* 31:101335. <https://doi.org/10.1016/j.jobe.2020.101335>
15. Evola G, Costanzo V, Magri C, Margani G, Marletta L, Naboni E (2020) A novel comprehensive workflow for modelling outdoor thermal comfort and energy demand in urban canyons: results and critical issues. *Energy Build* 216:109946. <https://doi.org/10.1016/j.enbuild.2020.109946>
16. Elwy I, Ibrahim Y, Fahmy M, Mahdy M (2018) Outdoor microclimatic validation for hybrid simulation workflow in hot arid climates against ENVI-met and field measurements. *Energy Procedia*. <https://doi.org/10.1016/j.egypro.2018.10.009>
17. Asfour OS (2020) A comparison between the daylighting and energy performance of courtyard and atrium buildings considering the hot climate of Saudi Arabia. *J Build Eng* 30:101299. <https://doi.org/10.1016/J.JOBE.2020.101299>
18. Soflaei F, Shokouhian M, Abraveshdar H, Alipour A (2017) The impact of courtyard design variants on shading performance in hot- arid climates of Iran. *Energy Build*. <https://doi.org/10.1016/j.enbuild.2017.03.027>
19. ASHRAE (2014) ASHRAE Guideline 14-2014. Measurement of energy, demand, and water savings. <https://energywatch-inc.com/ashrae-guideline-14/>
20. Sánchez de la Flor FJ, Ruiz-Pardo Á, Diz-Mellado E, Rivera-Gómez C, Galán-Marín C (2021) Assessing the impact of courtyards in cooling energy demand in buildings. *J Cleaner Prod* 320:128742. <https://doi.org/10.1016/j.jclepro.2021.128742>
21. Rojas JM, Galán-Marín C, Fernández-Nieto ED (2012) Parametric study of thermodynamics in the mediterranean courtyard as a tool for the design of eco-efficient buildings. *Energies* 5(7):2381–2403. <https://doi.org/10.3390/en5072381>
22. Toparlar Y, Blocken B, Maiheu B, van Heijst GJF (2017) A review on the CFD analysis of urban microclimate. *Renew Sustain Energy Rev* 80:1613–1640. <https://doi.org/10.1016/j.rser.2017.05.248>
23. López-Cabeza VP, Galán-Marín C, Rivera-Gómez C, Roa-Fernández J (2018) Courtyard microclimate ENVI-met outputs deviation from the experimental data. *Build Environ* 144:129–141. <https://doi.org/10.1016/j.buildenv.2018.08.013>
24. Huttner S (2012) Further development and application of the 3D microclimate simulation ENVI-met. Johannes Gutenberg-Universität in Mainz, Mainz. <http://ubm.opus.hbz-nrw.de/vol1texte/2012/3112/>
25. Lopez-Cabeza VP, Carmona-Molero FJ, Rubino S et al (2021) Modelling of surface and inner wall temperatures in the analysis of courtyard thermal performances in Mediterranean climates. *J Build Perform Simul* 14(2):181–202. <https://doi.org/10.1080/19401493.2020.1870561>
26. López-Cabeza VP, Diz-Mellado E, Rivera-Gómez C, Galán-Marín C, Samuelson HW (2022) Thermal comfort modelling and empirical validation of predicted air temperature in hot-summer Mediterranean courtyards. *J Build Perform Simul* 15(1):39–61. <https://doi.org/10.1080/19401493.2021.2001571>

27. Diz-Mellado E, Rubino S, Fernández-García S, Gómez-Mármol M, Rivera-Gómez C, Galán-Marín C (2021) Applied machine learning algorithms for courtyards thermal patterns accurate prediction. *Mathematics* 9(10). <https://doi.org/10.3390/math9101142>
28. Azañez M, Chacón Rebollo T, Gómez Mármol M et al (2021) Data-driven reduced order modeling based on tensor decompositions and its application to air-wall heat transfer in buildings. *SeMA* 78:213–232. <https://doi.org/10.1007/s40324-021-00252-3>

# Identifying and Describing Energy-Poor Household Groups. A Comparison Between Two Different Methods: Conventional Statistical Characterisation and Artificial Intelligence-Driven Clusterisation



Ana Sanz Fernández, Miguel Núñez Peiró, José Antonio Iglesias Martínez, Agapito Ismael Ledezma Espino, Carmen Sánchez-Guevara Sánchez, and Marta Gayoso Heredia

**Abstract** In recent years, numerous indicators for measuring energy poverty have been identified. Some of them are used officially or have a certain standardisation vocation, being relatively common among energy poverty studies for the identification of the phenomenon. This identification is an essential element for a first approach to the problem, but it is necessary to take a further step in characterising the phenomenon. This step necessarily involves characterising the households that suffer energy poverty. Identifying what these households are like, what are the characteristics that define them and the features that make a household more at risk of suffering energy poverty, and whether there are different types of households and whether they can be grouped together, are some of the questions that continue to be relevant in the study of energy poverty. This research compares two different methods of approaching the above-mentioned questions, starting from an analysis based on the income and expenditure approach. In the first, more traditional method, the characterisation of these households is carried out using conventional statistical tools, allowing a general identification of the most prevalent characteristics of households in energy poverty belonging to different vulnerability groups. In the second, artificial intelligence techniques are used to go a step further, not only characterising households but also subdividing the vulnerability groups to which they belong, identifying common characteristics that go beyond those defining the energy poverty phenomenon. The use of artificial intelligence in the study of energy poverty, by unravelling the specific characteristics and needs of the different subgroups affected by the phenomenon, can enable the personalisation of the construction solutions applied to the housing stock in which these households live. This favours a better

---

A. Sanz Fernández (✉) · M. Núñez Peiró · C. Sánchez-Guevara Sánchez · M. Gayoso Heredia  
Universidad Politécnica de Madrid, Madrid, Spain  
e-mail: [ana.sanz@upm.es](mailto:ana.sanz@upm.es)

J. A. Iglesias Martínez · A. I. Ledezma Espino  
Universidad Carlos III de Madrid, Getafe, Spain

coverage of their needs, with greater cost efficiency and results that are better adjusted to the initial conditions, both sociodemographic and constructive.

**Keywords** Households · Artificial intelligence · Energy poverty

## 1 Introduction

The first definition of energy poverty was established three decades ago. Boardman [1] considered that a household suffers from energy poverty when it is unable to have adequate energy services for 10% of household income. Several approaches have been used since then, some of them related to that first definition (the income and expenditure approach) and others, as the consensual approach, which use not only economic indicators. Nevertheless, despite those approaches have been useful, next steps towards a more specific and group focused description of energy-poor households are needed to move forward.

The causes of energy poverty include a wide range of circumstances and can be caused by several factors, such as low-income levels, high-energy needs, high-energy cost or a combination of them, and may appear in diverse household situations (leading to diverse solutions). The identification of the cause or causes is crucial to undertake the phenomenon.

Historically, the analysis of these households has been carried out by characterising them by means of indicators that have made it possible to identify the most common features. For example, some inhabitant types or household compositions are more prone to experience energy poverty. As it can be seen in recent research, among those groups, pensioners, unemployed, those with low levels of education, women as main breadwinners or tenants can be found [2].

The gap which needed to be addressed was the identification of the different groups formed by the energy-poor households. Categorising these characteristics is key to the previously pointed out needs: accurately depict energy poverty, identify the causes and suggest specific and adapted solutions to each group (or subgroup).

For this end, the incorporation of digitalisation and the technologies associated with this process could be an important development. Specifically, artificial intelligence (AI), a ground-breaking technology, may represent a key transformational impulse for this field. The increasing research and applicability of AI during the last few years are due to the increase in the processing capacity of computers, the improvement of algorithms and the exponential growth in the volume and variety of digital data [3]. One of the most relevant features of artificial intelligence is its capacity to emulate human performance, typically by learning, coming to its own conclusions, appearing to understand complex content, engaging in natural dialogues with people, enhancing human cognitive performance or replacing people in performing non-routine tasks [4].

During the last years, AI has been applied in almost all knowledge fields, and, finally, it is becoming fundamental due to the improvement it brings in comparison with previous techniques. In addition, it eases and enhances research activities. There is a wide variety of AI techniques and methods, from machine learning and evolutionary algorithms to deep neural networks.

Since AI had not been broadly used to assess energy poverty, this paper proposes a comparison between a traditional approach to describe energy poverty (using conventional statistical characterisation) and an approach which includes AI to tackle the phenomenon. The aim of this comparison is to identify the strengths and weaknesses of each of the approaches, highlighting what their differences are and what may make the use of one approach or the other more relevant.

To this end, the “Methodology” section presents how households in energy poverty have been identified and grouped so far in previous research. Based on this grouping, the approaches used to characterise these vulnerability groups (conventional statistical characterisation and AI-driven clusterisation) are described. In the “Results” section, those are presented, again differentiating between the two approaches and comparing them with each other. The “Discussion” section includes the strengths and weaknesses of each of these approaches, as well as their possible synergies, in order to delimit their field of application and identify the cases in which each of these methods may be more suitable or appropriate. Finally, the conclusions of the research are presented.

## 2 Methodology

### 2.1 *Identifying Energy-Poor Households*

Both methodologies presented in this paper use the Spanish Household Budget Survey (HBS) [5] as starting point (the data set for 2019 is the one used for the analysis). Household Budget Survey has been broadly used to detect energy poverty, despite it was not designed for that purpose, and partially due to the absence of a more specific statistical data regarding energy poverty. In addition, it has been considered a reliable source since it is annually updated. Additionally, it includes information regarding household incomes and expenditure on energy bills, useful to quantify the effort made by the households to meet their energy needs.

This information can be cross-reference with other characteristics of the households (also included in the database) such as family composition, activity and/or employment of the main breadwinner and the rest of the family members, characteristics of the main breadwinner (such as gender, education level and age) and housing stock characteristics (year of construction, size, type, heating systems availability, tenure status, etc.). The microdata of this database, with a specific data set for each respondent household, is available. Therefore, analysing the specific features of every household is possible. The total sample size in the Community of Madrid (the case

of study in this research) is 345 households. Each of these households has a demographic elevation factor, which may vary for each of them. These factors reflect how many households are represented by each household, and with the use of different elevation factors, the entire population of the region is represented.

To initially divide the households, the energy-poor household's classification developed by Sánchez-Guevara et al. [6] is used (which is also included in the long-term strategy for energy rehabilitation in the building sector in Spain [7]). This methodology classifies households according to their income and energy expenditure, following four thresholds (see Fig. 1):

- The energy poverty line is defined as twice the median value of the last five years' median energy expenditure in Spain [8]. This value is around the 10% of the income.
- The energy poverty vulnerability line is fixed as half the energy-poor threshold (5%).
- The monetary poverty baseline is set, in compliance with Eurostat methodology, as the 60% of the median income.
- Monetary vulnerability stands between monetary poverty and the median income value.

Based on these thresholds, households are classified as follows:

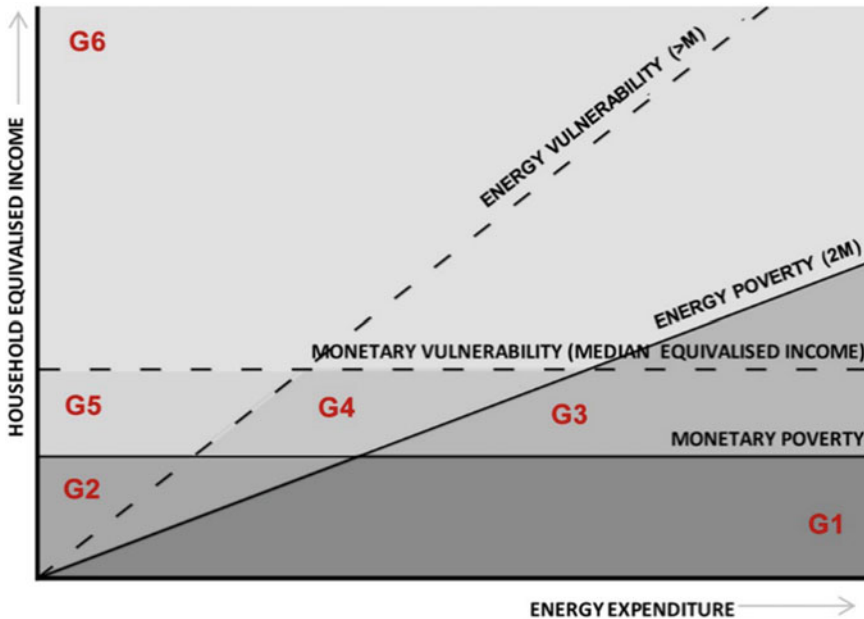


Fig. 1 Schematic energy poverty evaluation chart

- Group 1 (G1): these households are located below the monetary poverty line and below the energy poverty line, due to their high- energy expenditure.
- Group 2 (G2): these households' income is below the monetary poverty line but above the energy poverty line. Previous research has demonstrated that these households are at risk of energy poverty as they are likely suffering from inadequate temperatures due to the lack of heating services [6].
- Group 3 (G3): these households are considered energy poor, being below energy poverty line but over the monetary poverty line.
- Group 4 (G4): these households are considered vulnerable, given their close position in regard to both energy and monetary poverty thresholds.
- Group 5 (G5): these households are vulnerable towards monetary poverty due to their close position to this threshold.
- Group 6 (G6): these households are considered not vulnerable.

## 2.2 *Characterising Energy-Poor Households*

The characterisation of households suffering from energy poverty was carried out using the Spanish HBS indicators themselves, for each of the vulnerability groups identified in the previous section. First, a battery of 50 indicators related to the characteristics of the dwelling, the tenure status of the household, the composition of the household and the socio-economic situation of the main breadwinner were selected.

The level of incidence of each indicator was then estimated for each one of the vulnerability groups, either by estimating the percentage of total households under some condition (e.g. % of households without heating) or by calculating the average levels within each group (e.g. housing floor area). Distinctions were also made as to whether the main breadwinner was male or female in order to detect gender disparities. The groups with the highest rates for each of these indicators were then identified and compared with the average for all groups.

This part of the analysis provides details on households that would be common to each vulnerability group as a whole. This approach assumes, however, a certain intra-group homogeneity, attributing the same characteristics to all households contained in each of these groups. This can be problematic if, as noted in previous studies [2, 9] within the same vulnerability group, there are two or more household typologies with clear differences between them (e.g. single-person households of over 65s, and households with four or more members including minors).

Ignoring these intra-group heterogeneities could lead to a misleading characterisation of these households. To avoid this, an intra-group analysis is proposed to detect and characterise subclusters of households. This analysis is supported by artificial intelligence tools and is described in the following section.



### 2.3 *Subclustering Energy-Poor Households*

The previously done division leads to the next step: clarifying whether those groups are homogeneous or different clusters are formed within them. In this research, the groups G1, G2 and G3, which correspond to those households that are more likely to suffer from energy poverty, were selected for a detailed analysis.

Since the groups are classified using income and expenditure-related indicators, those are not considered for subclustering due to a possible redundancy. Nonetheless, the other database information (which includes family composition, activity and/or employment of the main breadwinner and the rest of the family members, characteristics of the main breadwinner and housing stock characteristics) is considered to be essential for the creation of different types of subclusters.

Machine learning (ML) can be defined as a set of methods that can automatically detect patterns in data. Within the field of ML, two main paradigms can be considered: supervised and unsupervised learning. The main difference is that supervised learning uses labelled data to classify labels, while unsupervised does not. Clustering is one of the most common tasks related to unsupervised learning, as a data mining technique it allows to group unlabelled data based on their similarities or differences. As it can be seen in previous research, several clustering algorithms have been taken into consideration [10, 11]. Within the diversity, some of them are more common and widely used for very different tasks, such as K-means or EM [12]. One of these popular algorithms is the probabilistic method expectation–maximisation (EM) [13], probably due to its simplicity and ease of implementation. It also guarantees to converge to a local maximum, which could not be the same as the global one. For this reason, there is a need to repeat the whole algorithm several times with different initial parameters (specially, the seed). For this research, the Weka's default seed has been the only one used. This aspect, which has not been considered in this research, is expected to be considered in more depth in further research.

As previously explained, the HBS has several indicators (more than one hundred) that could be used to describe households. From that extensive set, 50 indicators were selected for the clustering process (and afterwards for describing the obtained clusters). Those can be seen in Table 1. The selection of those 50 indicators was done after evaluating the clustering results in a recurrent manner, and afterwards they were classified into six classes, relevant to energy poverty vulnerable groups features.

Three different sets of data were established (corresponding the three first groups: G1, G2 and G3). Afterwards, in each of them, the algorithm EM was executed, 4 times per set of data, defining a specific number of clusters (from 2 to 5 clusters). Subsequently, the final number of clusters was selected considering their corresponding likelihood. Finally, the selected number of clusters is as follows: five clusters in G1; three clusters in G2; and four clusters in G3.

Once the number of clusters was established, the application of the algorithm C4.5 was needed to characterise the features of each cluster. In this research, C4.5 is applied by using different subsets of attributes, and, therefore, the description (decision tree)

**Table 1** Indicators used for the description of the clusters classified by class

Class of indicators	Indicators included
General information	Household sequential number, Province capital, Size of the municipality, Population density, Main breadwinner sequential number, Elevation factor of the household
Household characteristics—composition	Equivalent size of the household, Number of members, Size of the household, Number of members under 18, Number of members between 65 and 84, Number of members above 85, Number of students, Number of non-students, Type of households
Household characteristics—activity	Number of active members, Number of non-active members, Number of employed members, Number of unemployed members, Situation of the household regarding employment, Situation of the household regarding activity
Main breadwinner—sociodemographic features	Age, Sex, Country of birth, Nationality (Spanish, foreign or both), Region of the nationality (for non-Spaniards), Level of education
Main breadwinner—employment situation	Employment situation the previous week, Situation regarding activity, Was the main breadwinner employed the previous week?, Type of working day, Have you ever worked before?, Previous or current employment, Type of activity of employing company, Professional situation, Activity sector, Existence of employment contract, Type of employment contract, Socio-economic situation
Features of housing stock	Tenure status, Type of building, Type of housing area, Type of house, Number of bedrooms, Year of construction, Inhabitable area, Hot water availability, Hot water energy source, Heating system availability, Heating systems energy source

Source Compiled by the authors using HBS [5]

of the cluster considers only some specific attributes at a time. These main indicators which were key to define the characteristics of the clusters are reflected in Table 2.

## 2.4 Studying the Characteristics of Each Subcluster

The comprehensive and thorough description of each cluster is one of the objectives of this work. For this matter, decision trees are used to allocate each household (or unit, or database element) into the cluster it belongs to [14]. There was a need to describe each cluster, for this task, a set of five decision trees will be generated per group (G1–G3). Each decision tree is generated only with a subset of attributes that

**Table 2** Key attributes of each class of indicators

Class of indicator	Key attributes
Household characteristics—composition	Number of members and members above 65
Household characteristics—activity	Number of active and unemployed members
Main breadwinnersociodemographic features	Age and sex of main breadwinner
Main breadwinner—employment situation	Was the main breadwinner employed the previous week?
Features of housing stock	Tenure status, type of building, type of house, year of construction, inhabitable area

Source Compiled by the authors using HBS [5]

correspond to the family of attributes presented in Table 1. In a decision tree, each branch represents a choice between several values of a specific attribute. This way, all branches which predict a specific cluster can be used as an explicit description of that cluster.

The algorithm used in this work to generate the decision tree is the well-known C4.5 [15] (Weka's implementation-J48), which, at each node of the tree, chooses the attribute of the data that most effectively splits its set of samples into subsets. C4.5 is used because the obtained models are easily interpreted, the algorithm is easy to implement, and it can deal with noise.

The rules of each decision tree were processed and grouped by clusters. This helped to identify the most relevant indicators and which would differentiate and characterise each of the energy-poor clusters. When an indicator leads to a larger number of households, it is considered to be more relevant to the characterisation of the cluster. Additionally, confusion matrices were used to identify those families of attributes for which two or more clusters could not be differentiated from each other. This made it possible to identify meeting points between different clusters, which provides information on how far apart these energy-poor subgroups might be from each other.

### 3 Results

#### 3.1 Identification of Energy-Poor Households

After the use of HBS and the first subdivision of the households included in the database into groups, six different groups are identified within the Community of Madrid, presenting different degrees of vulnerability towards energy poverty (Table 3).

**Table 3** Description, number and percentage of households and people in each group (regarding energy poverty)

Group		Household		People	
		Number	%	Number	%
G1	Monetary poverty and risk of energy poverty due to a high expenditure	152.684	5.8	380.295	5.8
G2	Monetary poverty and risk of energy poverty due to lack of adequate temperatures	217.714	8.3	721.762	10.9
G3	Risk of energy poverty due to a high expenditure	177.067	6.7	332.045	5.0
G4	Monetary and energy vulnerability	357.682	13.6	954.928	14.4
G5	Monetary vulnerability	351.471	13.3	989.056	15.0
G6	No vulnerability	1.381.569	52.4	3.233.687	48.9
Total		2,638,190	100	6.611.775	100

Source Compiled by the authors using 2019 HBS [5]

### 3.2 Characterisation of Energy-Poor Household Groups

The characteristics of the households contained in each vulnerability group, and carried out directly through the HBS indicators, reveal substantial differences between the groups. The vast majority of these characteristics are well known and are coincident with previous studies carried out at the local, regional and state levels [2, 7, 9]. These characteristics can be seen in Table 4, which highlights their concentration across 24 indicators.

A cross-sectional analysis of the characteristics of each group provides some insights about the configuration of their households. Since previous research has pointed out that groups 1–3 present the most energy poverty-related features [6], these will be the ones described below.

For example, in group 1, households mostly live in small dwellings located in multi-family buildings and are, in spite of their age, generally equipped with natural gas for heating. They are mostly single-person or two-member families, and single-parent and female-headed households are relatively common. A high percentage of the main breadwinners are unemployed or houseworkers, while a high percentage of employed people have a temporary contract. However, this level of precarity may be alleviated by the tenure status, given that a high percentage of them own their home without a current loan or mortgage. This situation could explain the high-level of expenditure on domestic energy in this group.

In group 2, housing is largely also small in size and located in old, multi-family buildings. However, in contrast to dwellings in group 1, a high percentage have

**Table 4** Households' characteristics per vulnerability group. Derived from the Spanish HBS indicators

	G1	G2	G3	G4	G5	G6
<i>Households' characteristics</i>						
Single-family house			●●	●		●●●
Old housing stock	●●	●		○	●●●	
Lack of heating system	●	●●●			●●	
Electrical heating system		●●	●●●		●	
Large size			●●	●		●●●
Large size/inhabitant	●		●●●			●●
<i>Households' tenure regime</i>						
Rented	●	●●●	●●			
Property without loan	●●●		●	●●		
Property with loan				●	●●	●●●
(Semi-) free leasing		●●●	●●		●	
<i>Households' composition</i>						
Single-person households	●●●		●●			●
Households > five members	●	●●●	●●			
Households with children under 16		●●●		●	●●	
Households with people over 65	●●		●●●	●		
Single-parent households	●●	●●●	●			
<i>Socio-economic status of the main breadwinner</i>						
Under 35 years old		●●●	●●		●	
Woman	●●●		●●			●
Migrant (outside Europe)	○	●●●	●		●●	
Low educational attainment	●●●	●	●●			
Unemployed or with no econ. activity	●●●	●●		●		
Retired		●	●●●	●●		
On temporary contract	●●●	●●			●	
Part-time	●●●	●●			●	
Self-employed without employees		●●		●●●	●	

●●● Group with the highest percentage of households. ●● Second highest incidence group. ● Third highest incidence group. ○ Group with a higher incidence than the average for the municipality

no heating or use electricity as fuel. Despite having the smallest housing stock, the size of the households tends to be large. The presence of people under 35 as main breadwinners is noteworthy, as well as the presence of people from outside Europe. Although precarious work levels seem lower than that observed for group 1, it is still well above the average. The presence of self-employed workers with no employees in this group stands out, which could be linked to precarious jobs

(i.e. false self-employment). Also noteworthy is the high presence of single-parent households headed by women. One in three households is rented, which, together with precarious employment and the state of the building stock, points to a group that is unable to meet the minimum domestic energy expenses.

Households belonging to group 3 also mostly live in multi-family buildings, although there is a high percentage of them living in single-family dwellings. These are, in any case, relatively new buildings, but where the presence of electricity as a heating energy source is very high. In terms of household composition, it seems that at least two subgroups can be distinguished. On the one hand, there are two-member households, mainly associated with people where at least one of them is 65 or older and where the main breadwinner is retired. On the other hand, households with three or more members, where the main breadwinner is employed indefinite and full time, are also frequent. The risk of energy poverty in these groups therefore seems to be associated with the type of building and, above all, the type of fuel being used. The solution to this problem should, in any case, be differentiated and adjusted to the reality of the two subgroups mentioned.

### 3.3 Subclusters of Energy-Poor Households

The optimal subdivision of G1 yields five clusters. These five clusters can be described, using the decision trees outputs (e.g., see Fig. 2), as follows:

- G1 Cluster 0 [G1–C0]: single-person household generally headed by a woman over 55 who is a housewife with a dwelling of less than 76 m<sup>2</sup> owned without a mortgage
- G1 Cluster 1 [G1–C1]: household with young or middle-aged adults, whose main breadwinner is employed and in rented house
- G1 Cluster 2 [G1–C2]: middle-aged adult household with an unemployed male main breadwinner and tenancy-ownership status
- G1 Cluster 3 [G1–C3]: high variability (not clearly defined)



**Fig. 2** Example of one of the decision trees. This one was obtained for G2 in relation to the households' activity characteristics

- G1 Cluster 4 [G1–C4]: household of two persons or more with a retired male main breadwinner in a medium-sized dwelling.

Some of the most relevant features are related to age, age, number of household members and ownership and employment status.

Regarding G2, the results show three well-differentiated clusters for almost all indicator categories with these specific features for each of them given below:

- G2 Cluster 0 [G2–C0]: medium to large households with middle-aged adults and/or young people with children in some cases, at least one employed person and a majority of properties with mortgages (and a minority without)
- G2 Cluster 1 [G2–C1]: small households with older adults and a variety of tenure arrangements and housing types
- G2 Cluster 2 [G2–C2]: retired people who own their own home without a mortgage, in a more than 25 years old multi-family building.

Finally, G3 has been divided into four clusters, which can be described as shown below.

- G3 Cluster 0 [G3–C0]: household with an employed main breadwinner in a dwelling of more than 98 m<sup>2</sup> owned with a mortgage
- G3 Cluster 1 [G3–C1]: households without members over 65, with at least one employed person (usually the main breadwinner, with a contract) in rented or mortgaged houses of less than 100 m<sup>2</sup>.
- G3 Cluster 2 [G3–C2]: households living in dwellings larger than 98m<sup>2</sup>, in many cases detached, owned without mortgage
- G3 Cluster 3 [G3–C3]: small households with persons over 65, not occupied in dwellings of less than 98 m<sup>2</sup> owned without mortgage.

The specificity of the results leads to the thorough description and the possibility to, accurate, identify the differences within each group and, remarkably, also similarities between clusters from different groups.

### ***3.4 Brief Comparison of the Results***

The first methodology, conventional statistical characterisation, provides us with a general overview of the most common features of the households included in each group; whereas, the second, AI-driven clusterisation, identifies and describes the clusters within each group. Since the universe described and the indicators used are the same, similar findings, some overlaps as well as some differences are supposed to appear when analysing the results obtained from both methodologies. To accomplish this comparison, a close look to the results group by group is taken.

Some of the characteristics depicted in the general overview of G1 are featured in some of the clusters, for example, small dwellings (in G1–C0), single-person and female-headed households (in G1–C0), unemployed breadwinner (in G1–C1)

or ownership without mortgage (in G1–C0). But other characteristics, such as multi-family building, single-parent households or temporary contract, do not appear in cluster characteristics. On the other hand, some relevant characteristics of the clusters, as age or rental status, are not reflected in the general features of the group.

In G2, the number of group features seen in the cluster's definition diminishes, and only large households (G2–C0) and old multi-family building (G2–C2) are included in the outputs of both methodologies. Meanwhile, some other highly relevant characteristics at group level do not describe clusters, for example, small size of the dwelling, the absence of heating system, relatively young and foreign breadwinners, rental tenure system and single-parent household headed by women.

The clusters within G3 which include some group features are G3–C0 (large households), G3–C2 (large, detached houses) and G3–C3 (retired members over 65). On the contrary, electricity as energy source, size of the household or employment situation are not reflected in the clusters description despite being key for the group.

Finally, it is worth highlighting that some clusters from different groups are quite similar. They do not share all the features but can be considered to have relevant coincidences. For example, G1–C0, G1–C4, G2–C2, and G3–C3 where the members are usually old and/or retired occupying owned dwellings without a mortgage; or G1–C1, G2–C0 and G3–C1, which are households with middle-aged adult members, employed breadwinner and cost associated with their dwelling (by the payment of the rent or the mortgage).

## 4 Discussion

Analysing the results of both approaches, which shed light to different aspects of the energy poverty household description, the first question to be highlighted is the two methods that could be understood as complementary. The conventional statistical characterisation provides the general framework and a first-level approach to the identification of the main features of the groups. On the other hand, the AI-driven clusterisation shows relevant and consistent results and allows to demonstrate significant intra-group heterogeneities (within the original groups identified by the income and expenditure approach). These differences were already intuited by conventional analysis but has been confirmed by AI techniques.

One limitation which is common to both methodologies is the level of disaggregation of the database. The absence of sub-regional information (local and infra-municipal) that allows the territorial location of households is a barrier to understanding the spatial distribution of the phenomenon. Both methodologies could benefit from a potential improvement in the degree of spatial disaggregation of the statistics used.

Regarding to how the methodology is applied, some considerations should be done. Instead of including all the indicators in one decision tree, the decision of preselecting and grouping the indicators allows several decision trees to be obtained in order to identify household characteristics by theme. Additionally, it is important



to point out the relevance of subject expertise to oversee the process of selecting and grouping indicators.

It is worth noting the difference in meaning of the indicators highlighted by the conventional method and the IA method. While the former allows us to identify the most relevant indicators that characterise households within a vulnerability group (e.g. by pointing out that a large number of households do not have heating systems), the latter highlights the indicators that best differentiate the subclusters within each group. Thus, although some indicators have not been used for this differentiation, this does not mean that they are not relevant or characteristic of these households.

The aim of the comparison between the results of the two methodologies and, therefore, between group and clustering features is to identify the strengths and weaknesses of each of the approaches, highlighting what their differences are and what may make the use of one approach or the other more relevant. The comparison reveals that not all of group features are relevant to cluster generation and not all the cluster features are reflected in the group depiction. This may imply that some of the features of the group could be homogeneously distributed among the clusters, without being a characteristic that helps describe or create the clusters, but conforming a majority in the group when the clusters are aggregated. On the other hand, it also points out that the clustering generation reveals features that would be, otherwise, concealed in the general characterisation of each group. Those indicators highlighted by the conventional method but not pointed out when describing the subclusters are most likely to correspond to indicators common to all subclusters of a group (e.g. availability of heating). In other cases, it is also possible that an indicator that was not highlighted as relevant during the conventional characterisation may come to the fore during the characterisation of the subclusters. The synergies between the two methods seem clear.

## 5 Conclusions

As it has been seen in the analyses carried out in this research, using the proposed methodologies, the incorporation of AI as a complementary technique can be an instrument that allows better processing of statistical databases and provides additional knowledge thanks to the identification of subclusters and their characterisation.

Nevertheless, prior knowledge of the phenomenon and a complex vision of fuel poverty is necessary to complement these techniques, in order to be able to correctly discriminate the most appropriate steps and interpret the results obtained.

Focusing on the results, it can be said that one of the characteristics that has emerged as significant is the unemployment situation, while significant differences have been identified with regard to the characteristics of the building stock. Also, several similarities have been found between clusters which belong to different

groups, pointing out the possibility that different income and energy expenditure levels share household composition, dwelling features and tenure status (and therefore may need some shared solutions).

This is an undeniable step forward as it identifies the different situations, allowing measures to be adapted and personalised as needed. This will be possible as long as the characteristics and needs of the end-users are known, which can be done with greater precision using these AI techniques.

**Acknowledgements** This research project was supported by the EPIU-Getafe Project (UIA04-212), co-financed by the European Regional Development Fund. This project was also supported by the Spanish Ministry of Science, Innovation and Universities (RTI2018-096036-B-C22) and by Universidad Carlos III (PEVAUTO-CM-UC3M).

## References

1. Boardman B (1991) Fuel poverty: from cold homes to affordable warmth. London
2. Sánchez-Guevara Sánchez C, Sanz Fernández A, Núñez Peiró M, Gómez Muñoz G (2020) Energy poverty in Madrid: data exploitation at the city and district level. *Energy Policy* 144:111653. <https://doi.org/10.1016/j.enpol.2020.111653>
3. Craglia et al M (eds) (2018) Artificial Intelligence: a European perspective. Publications Office of the European Union, Luxembourg
4. Sage (2019) Artificial intelligence in 2019: a handbook for business leaders, p 222019.
5. Instituto Nacional de Estadística (2019) Encuesta de presupuestos familiares
6. Sánchez-Guevara Sánchez C, Sanz Fernández A, Hernández Aja A (2015) Income, energy expenditure and housing in Madrid: Retrofitting policy implications *Build Res Inf* 43(6):737–749
7. Government of Spain (2020) ERESEE 2020. Update of the long-term Strategy for Energy Rehabilitation in the Building Sector in Spain
8. Ministerio para la Transición Ecológica (2019) Estrategia nacional contra la pobreza energética 2019–2024
9. Sánchez-Guevara Sánchez C, Sanz Fernández A, Núñez Peiró M (2020) Feminisation of energy poverty in the city of Madrid. *Energy Build* 223
10. Xu R, Wunsch D (2005) Survey of clustering algorithms. *IEEE Trans Neural Netw* 16(3):645–678
11. Saxena A et al (2017) A review of clustering techniques and developments. *Neurocomputing* 267:664–681
12. Jung YG, Kang MS, Heo J (2014) Clustering performance comparison using K-means and expectation maximization algorithms. *Biotechnol Biotechnol Equip* 28(sup1):S44–S48
13. Dempster AP, Laird NM, Rubin DB (1977) Maximum likelihood from incomplete data via the EM algorithm 39(1)
14. Witten IH, Eibe F, Hall MA, Pal CJ (2017) Data mining: practical machine learning tools and techniques. Morgan Kaufmann
15. Quinlan R (2014) C4.5: programs for machine learning. Morgan Kaufmann

# **Design and Modelling**

# BIM Technology in Green Buildings: Integrating BIM with Greenery Systems



Mitra Manouchehri, Mercedes Valiente López, and Joaquín Santiago López

**Abstract** The importance of Building Information Modelling (BIM) in achieving sustainable goals is well recognized in the global construction industry. Several studies on BIM have been conducted in the past decade. However, a considerable gap exists regarding the integration of BIM with greenery systems. Greenery infrastructural systems provide a great opportunity in this respect by connecting buildings to the urban environment thereby integrating greenery into increasingly densely populated cities. They may also influence microclimate conditions and contribute to enhancing life quality in urban spaces in various ways. It is to be expected that greening of the building surfaces will be mandatory in an increasing number of cities in the future, in the form of converting a specific area of the building's facade into green space. In this context, the simulation can be used to carry out the obligatory planning of the facade greening. The integration of the concepts of greenery systems and BIM technology could promote the digitalization process in the building sector by offering solutions to improve environmental quality whilst reducing costs. This study explores ways in which BIM and greenery systems can be integrated through an analytical review of evidence from both academic research and case studies; it will also address present challenges towards this green development. In addition, the most significant simulation factors for modelling existing greenery systems and their associated key performance parameters will be analysed and prepared for application in BIM tools. This research could provide great potential by simplifying the decision-making process for the implementation of greenery systems in buildings and can therefore serve as a crucial interface to guide building and greenery researchers and practitioners.

**Keywords** Building Information Modelling (BIM) · Greenery systems · Buildings · Decision-making process

---

M. Manouchehri (✉) · M. Valiente López · J. Santiago López  
Universidad Politécnica de Madrid, Madrid, Spain  
e-mail: [mitra.manouchehri@alumnos.upm.es](mailto:mitra.manouchehri@alumnos.upm.es)

© The Author(s), under exclusive license to Springer Nature Singapore Pte Ltd. 2022  
D. Bienvenido-Huertas and J. Moyano-Campos (eds.), *New Technologies in Building and Construction*, Lecture Notes in Civil Engineering 258,  
[https://doi.org/10.1007/978-981-19-1894-0\\_9](https://doi.org/10.1007/978-981-19-1894-0_9)

141

# 1 Introduction

The Architectural, Engineering, and Construction (AEC) professionals and industry researchers, as well as policymakers, have agreed on the positive influence of the development of greenery systems to overcome the rising concern about global warming caused by the extreme growth of urbanization.

The greening of the building envelope has been formerly used as an aesthetic and protective feature in buildings. However, the concept of greenery systems has been introduced and promoted extensively over the past years. Greenery systems stand out amongst the wide range of passive and low energy building systems available, and they are responsible for incorporating vegetation into architecture on a massive scale. The current technology used in these systems can contribute to sustainable improvement in the building industry. It can also increase the functional benefits of plants to the building performance level [1].

The terms Greenery Systems, Greening Systems, Green Infrastructural Systems, and Building Integrated Vegetation (BIV) are often used in this context. Building-integrated vegetation is formed by green roofs and vertical greenery systems applied to both exterior and internal walls. The existence of vegetation means roofs and walls are living systems that breathe. Thus, the vegetation is encouraged to develop a relationship between concepts of nature and the built environment [2].

Green roof is an established technology in the construction sector, and public and private stakeholders are recently growing more interested in vertical greening systems. The reasons are not only related to their ability to create unique patterns over the building envelope, but also clear energy and environmental benefits. Vertical greenery systems are subdivided into two main categories: Green Facades and Living Wall Systems (LWS). There is a further distinction between green facades and LWSs. As in green facades, climbing plants grow along the wall covering it, whilst LWS is a more recent concept which includes materials and technology to support a wider variety of plants that create a consistent growth along the surface. In LWSs, plants receive water and nutrients from vertical support instead of from the ground. Despite the fact stakeholders recognize the benefits of vertical greening systems, there are some obstacles for large-scale deployment, one being the lack of a consistent standardization to assess their performance [2].

To counteract climate change, big cities are promoting buildings with greenery systems. A good example is the Santalaia building in Bogotá. According to the design team, this green wall can provide oxygen to more than 3000 residents and clean up the equivalent of carbon emissions produced by 745 cars. Bogotá has a temperature ranging 3°–4° higher in areas of higher urban density. The adoption of greenery systems contributes to reducing the urban heat island effect that exists in the urban area compared to the suburbs [3].

Another revolutionary technology proposed as an innovative solution in a wide range of AEC research projects is Building Information Modelling (BIM). BIM emerged as a solution to promote the integration and management of information throughout the building life cycle by offering the possibility of making the best use

of the existing design data for sustainable goals and performance assessment. Since both BIM and green building are gathering momentum, an increasing number of AEC companies are beginning to develop technology on “green BIM” [4].

One famous example of the use of BIM technology is in the Disneyland buildings in Shanghai. In order to keep users safe and protect the environment, over 70% of the buildings were developed using BIM tools. The application of BIM technology gave the project teams access to the same resources and support, and at the same time offered extra advantages such as reducing work, sharing models, increasing the level of details in the design, and thus keeping timelines and objectives [5].

The application of greenery systems in architectural projects has grown substantially over the last few years, but their implementation has little to do with computational control methods or design. It is necessary to integrate the greenery system within BIM tools to overcome the limitations of the potential green architecture. Various research papers have suggested the benefits of greenery, ranging from creating a conducive environment for social activity, promotion of positive effects on mental health, acoustics dampening, to the cooling of the surrounding microclimate. However, literature reviews show there is limited research regarding the incorporation of BIM into the creation stages of greenery systems [6].

In this chapter, we delve into how BIM is applied in greenery system projects and the reasons for its apparent lack of use. Moreover, we discuss the possibility of modelling facade greening systems using BIM tools. Next, we search through the important criteria and factors that should be considered in the application of BIM in greenery system design and simulation stages. And finally, we gauge the advantages and limitations of BIM integration into greenery systems.

The research focus is on the existing greenery systems in Madrid, Spain. To this purpose, we studied the landmarks of facade greenery systems in Madrid landscaped over the past years. Research demonstrates there is no specific BIM implementation in the design and construction stages of these greenery systems. Additionally, results from the systematic analysis of the samples clearly show the limited use of BIM in the development of greenery systems. Moreover, influential factors in the design and other important aspects of the greenery systems simulation are discussed to identify challenging areas and thus facilitate BIM use in the greenery design.

As we have explained above, the combination of BIM and the digital planning process in this field has received little attention. This chapter presents and evaluates the existing approaches towards the integration of BIM and Green Infrastructure Systems and their implications for urban development in the future.

## 2 Background and Literature Review

### 2.1 *Building Information Modelling (BIM) Technology*

The concept of sustainable development was first introduced in 1987 in the World Commission on Environment and Development's Brundtland Report to align economic development with social and environmental balance. Since then, various efforts have been made in support of this concept. Various commissions have been organized and the European Union (EU) has ever since launched different plans to move towards sustainability [7].

BIM was presented as a viable solution to achieve sustainability goals. BIM technology, as an innovative approach that includes diverse tools, can effectively evaluate energy performance in urban facilities. The application of BIM assists in the conversion of two-dimensional drawings into three-dimensional visualization renderings and also can provide architectural information about the building life cycle [8].

The use of computer technology can significantly contribute to facilitating and improving the result. The development of an architectural information model provides technical platform support for all project participant units to share the essential information of the project at all phases, so that different experts, such as design department, construction units, facility operators and operation and maintenance units can work collaboratively on the BIM 3-D model [9].

BIM technology can generate virtual environments identical to real work situations; hence it could detect potential problems at the earlier phases of the project. In construction projects, BIM can serve as a comprehensive method that can enhance performance, preserve practical resources; lower building costs reduce design discrepancies and optimize architectural design procedures to obtain sustainable results. BIM contains a complete process of information modelling including the ongoing technological development, as well as the incorporation of simulation and virtual technology based on parameterisation and computerisation of traditional architecture [9].

A BIM model could comprise individual 3-D models of each building component, with all associated properties such as weight, material, length, height. Beyond the inherent information, BIM also includes external associations between building components. BIM has been applied in the areas of structure, energy, disaster prevention, construction planning and scheduling, project control, construction safety, and maintenance [10]. Amongst the advantages of using this technology, we should mention clash detection in early design stages, automatic design regulatory inspection algorithm and Augmented Reality (AR) visualization to improve the productiveness of on-site work. Moreover, BIM provides a collaborative work environment [11].

Because of the fast growth of BIM in the AEC industry, both at academic and professional level, new approaches based on BIM have been proposed to address the needs in this area. For instance, Building Energy Modelling (BEM) is a tool for energy analysis that can be used with BIM programmes and allows experts to simulate and

analyse energy processes in buildings to further improve energy performance through modelling parameters such as heating, cooling, ventilation, lighting, and plug and process loads as well as water use in buildings. The experts believe its application will increase soon due to its ability to provide a high return on investment and improve sustainability standards [12].

Another approach to the application of BIM in buildings is Historic Building Information Modelling (HBIM). This term involves a new way of modelling existing buildings based on a BIM process that would produce intelligent models containing and managing information. Such models pertain to project components and include their geometric and identifying features, as well as all the physical properties that best describe them. HBIM was designed to generate a BIM model of historical and monumental buildings including a database of model information such as simple geometric reconstruction of volumes or thermal analyses to be inserted into the simulation tools. The application of HBIM was later extended to all existing building models, not only in terms of digital and geometric 3-D reconstruction, but also as a method involving intelligent models with added information. More specifically, this technology can replicate an existing building in order to provide a more feasible way for upgrading its features [13].

The information types in BIM tools are divided into three major categories according to Schlueter and Thesseling [14] research, namely, geometric, semantic and topological. Geometric information shows the 3-D modelling of a building, and semantic information includes the properties of components. Topological information describes the dependence relationship between properties and components [10]. In the present research, we consider all these three types of information for the definition of influential parameters.

BIM adoption in many countries such as the United Kingdom is going from being led by innovators and early adopters towards becoming a more mature market. There is also academic research on adopting BIM in other countries such as China, Finland, Iceland, and India [15]. Regarding Spain, no such project had been undertaken until 2017 [15].

In 2017, the QBIMInvest project [15]—supported by the Universidad Europea de Madrid—conducted a survey on the implementation of BIM in the Spanish AEC industry. The study showed that BIM tools are being used in the design phases. However, the use of BIM tools in the construction stage is insignificant and the BIM model of the project is not generated until it has become a model developed solely for operation and maintenance purposes. It should be highlighted that these are the phases that profit most from the utilization of these tools [15].

Additional challenges of BIM implementation are associated with software and hardware issues. Interoperability is one of the problems in the AEC industry. The former problem happens because dynamics and adaptability are necessary to work in this sector and that users often use different applications and systems [15]. The existing technical issues and interoperability problems between different BIM software packages will be hopefully solved by the package providers over time. Nevertheless, it is more complicated to solve issues regarding people's agreement on common IT platforms and cooperation to share their BIM data models. Restrictions on data



flow towards and from other parties is another key problem, especially as far as license and intellectual property ownership of BIM-generated output is concerned [15].

Overall, the importance of BIM is widely known today. Alongside the importance of cost–benefit analysis, more awareness-raising and up-skilling in the sector are required. Hence, senior managers in building companies will need to invest in BIM education and staff training. Apart from existing general limitations that hinder BIM employment, timelines, levels of expertise and cost also remain barriers to BIM adoption. Moreover, there is lack of transparency in the industry and many practitioners are uncertain about claims to the application of BIM in new and existing projects [15].

## ***2.2 Overview of BIM Software Programmes***

Since BIM is widely used around the globe, there are many options for the software available today. Some of the most widely used BIM software in the AEC industry are Autodesk Revit, ArchiCAD by Graphisoft, Autodesk BIM 360, AECOSim Building Designer for Bentley Systems company, Allplan Architecture, BIMobject, IrisVR, Navisworks, ACCA software Edificius, Tekla BIMsight, Tekla Structure; Trimble Connect, Vectorworks Architect and Rhinoceros VisualARQ. Each of the programmes mentioned focuses on one aspect since the BIM environment is highly open to developer implementations and interpretations. For example, the Tekla Structure is oriented to structural projects, and Vectorworks focuses on architectural rendering and interior design [16].

Amongst the existing BIM programmes, Autodesk Revit and ArchiCAD are the leading ones. These software tools have extensive 3-D object libraries and attribute tables containing useful information to help through the design, construction, and maintenance stages. Objects in Revit contain physical parameters and analytical properties. However, these tools do not provide intelligent plant libraries containing plants' attributes, environmental factors, or their relationship to the environment, which could help designers and planners understand the plant-environment relationship and manage that information in a BIM environment [6].

The existing plant families in REVIT include the geometric components such as height, which only reflects a fully mature plant, whilst the rest of properties such as appearance, model, manufacturer, and cost, are like any other building component. ArchiCAD offers the possibility to alter more geometric properties like height and diameter, and plants can be selected depending on the real-time site conditions. However, critical environmental factors such as light, temperature, and spacing are not considered. Comparably, Vectorworks BIM introduces some additional parameters, however they are not enough to support through BIM design process [6].

Furthermore, a number of plug-ins has been developed for specific BIM authoring software to address the existing issues of plant-based modelling. These include

CS ArtisanRV, ENVIRONMENT plugin for Autodesk Revit, Lands Design for Rhinoceros and Autodesk AutoCAD, and Land F/X for Autodesk AutoCAD. In addition, Vectorworks developed a variant called Vectorworks Landmark specifically for greenery and landscape design. One important limitation of these solutions is the need to subscribe to one particular software, preventing a conformed practice at the national level with a centralized database [17].

Considering the existing limitations, various research approaches present their work through the Industry Foundation Classes (IFC) standard for data exchange regardless of the BIM authoring software used, which provides architects with a more efficient means for creating and using a unified vegetation library. The benefit of a neutral information format is the reduction of the problems that may occur when information is exchanged and converted to a different format. Furthermore, all the units involved in a project can choose to use the BIM software they prefer, as long as the software supports the IFC interface [18].

### ***2.3 Standards and Regulations***

Standardization is growing continuously in the BIM area, as it is considered a key factor in an industry with such a high and diverse number of agents. In 2014, the European Union (EU) urged countries to consider the need for BIM technology to improve public procurement processes. The European Parliament advised the Member States to address modernizing procurement regulation and public tenders. Currently, many countries in the EU, including Spain, have implemented BIM strategy at the national level, thus promoting the demand for the use of this tool in public projects [19].

Governmental bodies in Spain have decided to take the lead in the process of adopting BIM methodology throughout the infrastructures' life cycle. Specific actions involve monitoring public administrations to adopt BIM criteria in infrastructure tenders, drawing a roadmap to adopt the regulations for general use, and developing national standards that allow widespread adoption [19]. The Spanish construction industry has been subject to EU Directive 2014/24/UE. This directive allows member states to encourage, specify and even require the use of Building Information Modelling (BIM) in construction projects financed by EU public funds as of 2016 [15, 20].

Since 2009 individual attempts to incorporate BIM processes as required in international projects were undertaken in Spain by some companies. However, it was only in December 2018 that the use of BIM became mandatory for public building tenders [20, 21]. Making the use of BIM mandatory was a milestone towards a more digitalized construction industry. According to the reports published by the European Commission (EC) in March 2019, 75% of companies that adopted BIM reported a positive return on their investment with shorter project lifecycles and savings in paperwork and material costs [22].

As regards standards and regulations, there have been several committees and organizations in charge of providing comprehensive data and regulations for AEC in Spain over the last years:

The International Committee, [ISO/TC 59 Buildings and Civil Engineering Works](#), works on the standardization of BIM methodologies. There is also a European Committee, CEN/TC 442 Building Information Modelling, whose scope of application is life cycle standardization for the built environment in the field of structured semantic information [22].

The [Spanish Association for Standardization, UNE](#), has been working since 2011 on the standardization of BIM activities. UNE is a subdivision of AENOR, designated to carry out standardization activities nationwide (UNE standards) and to take part in international standardization procedures (EN and ISO standards). The Subcommittee on Organization of information models related to building and civil works was created in the same year. This subcommittee, chaired by a representative of the [Building Smart Spanish Chapter](#) and whose secretariat is held by [Spanish Institute of Cement and Applications \(IECA\)](#), includes 40 entities belonging to both the industrial and research fields. The subcommittee regularly collaborates with international counterparts [22–24].

In 2014, the BuildingSMART Spanish Chapter Association was officially set up to promote BIM through open standards. Additionally, a standardization initiative called uBIM was proposed within the framework of the EUBIM 2013 Conference. The initial objective of uBIM was to develop a guide in Spanish for BIM users. This document was designed to be accessible so as to provide constant support, and to ensure effective actions are taken in the sector. The first 13 documents that make up uBIM guide have been adapted from the Finnish COBIM (Common BIM Requirements 2012) prepared by BuildingSMART Finland in 2012. The development of this guide has been carried out collaboratively with the participation of around 80 independent professionals [25].

In 2015 the Ministry of Public Works established the esBIM Commission. It was made up of different agents and organizations belonging to both the public and private sectors in pursuance of European Directives in Spain. The esBIM draws periodic reports on the progress of the BIM strategy in the Spanish context. In 2015, The [EUBIM-Spain](#) Conference was held in Barcelona, where several Catalan institutions outlined the current situation in terms of initiatives to promote the nationwide use of BIM. In May 2016, the Interdepartmental Commission for BIM implementation in public works was set up and later in 2017; IFC standards were adopted for spreading BIM processes in all phases of the construction process [21].

The Spanish versions of the [UNE-ISO 19650-1](#) and [UNE-ISO 19650-2 Standards](#) set the principles for business processes in the construction sector. This standard specifies the requirements for information management in the form of a management process in the context of the asset development phase and the information exchanges within that phase, using building information modelling. This document can be applied to all types of assets and all sizes of organizations, regardless of the procurement strategy chosen. The National Committee is currently working on

the adoption of the PNE-EN ISO 16757-1 Standards Data Structures for electronic catalogues of products for construction services [22].

It seems clear that intelligent facades, including greenery wall systems, could be one of the options to generate a dynamic and clean urban context. Considering the existing standards and regulations towards BIM adoption and their evolution, it is possible to track down the application of BIM in buildings with greenery systems to analyse the development of their design and function over the past decade.

## ***2.4 The State-of-the-Art in BIM and Greenery Systems***

Integrating vegetation into the built environment can mitigate the negative effects of growing urbanization. In recent years in countries like Singapore and Austria, government policies support the inclusion of sky-rise greenery into new and existing buildings whilst constitutional BIM submissions in AEC industries have been promoted. However, landscape projects are still excluded from these BIM submissions due to the absence of an organized database for vegetation and the lack of a unified BIM platform for greenery structures [25, 33].

As the demand for greenery systems is increasing due to the growing demand for climate resilience in cities, a false branding image of sustainability may be accompanied by such architectural claims. “Green-slapping” is a term devised by Allan et al. to describe the overuse of green systems, whereby buildings are overloaded with greenery to produce an illusion of sustainability, whereas the project’s specifications do not support its sustainability claims [26].

The application of a 3-D information model for plants lies on a quite different level from the information modelling of the buildings. The parametric factors of a plant contain a huge amount of data due to the plant being a natural element. Plants foliage does not react quite like a solid wall surface, as they are not always in a fixed state and their element properties are constantly changing due to factors such as constant growth or external factors like wind and light [27]. Considering the existing differences and limitations, in this study, the term “Greenery Information Modelling” (GIM) is proposed for the process of 3-D information modelling of greenery systems.

The usual complexity of 3-D models with regards to plant materials is further pursued by the lack of a comprehensive material database for greenery system-related 3-D models. Whilst there are usually predefined settings for architectural components like concrete, masonry, or timber materials, there is little systematic information concerning plant materials. Existing vegetation libraries within BIM authoring software are either too limited in terms of species variety or lack specific species. Although it is possible to customize vegetation models or adopt third party libraries in certain software tools, the need to do research and establish various parameters to better define the materials requires additional time and effort to question its practicality for the designers. Without any governing BIM standard, it might not be possible for an extended period [17, 27].

For example, the National Building Specification (NBS) National BIM Library of the United Kingdom, which hosts thousands of BIM objects according to the NBS BIM Object standards, does not comprise a single plant object, whilst other online libraries with individually modelled trees and shrubs are limited to a small number of pre-generated species [17].

At present, Singapore has a centralized public vegetation library maintained by the National Parks Board (NParks) Flora and Fauna Web (FFW). The library contains exceptional botanical details of over 4000 plant species; however, it lacks spatial information. Along the same line, it is to be expected that the FFW database, or other similar vegetation databases, can be extended to include more spatial attributes to generate specific 3-D BIM vegetation models for the industry [17].

Another example is the workflow proposed by Gobeawan et al. [17]. They introduced a methodology in the context of Singapore also applicable to other cities given their species spatial parameters obtained by field measurements or observations. They produced lightweight simplified BIM vegetation models for a computationally efficient means to model these objects with special attention to trees and shrubs. Their workflow comprises four interrelated modules, namely, the vegetation library compilation, BIM authoring workflow, IFC interface, and 3-D vegetation model generation.

Other researchers have also contributed to shed light on the relationship between BIM and greenery systems. The next paragraphs provide highlights of their work:

Krygiel and Nies [28] claim that the goal of BIM is to provide an endless range of possibilities targeted to a design project through a combination of functionalities. They developed a BIM roadmap to show the connection between such features and their functions. They believed the core idea behind BIM is to digitalize the ongoing and interlinked construction process, incorporating all the segments, from design to construction and details like building services and landscape. However, in the case of greenery systems, the omission of greenery is a common occurrence during the digital design model process [26].

Allan and Kim [26] studied the extent of accuracy and efficiency of sustainability claims that BIM can provide during the digital process of vertical greenery design. They established the feasibility of applying vertical greenery systems as part of the BIM process to assess building performance during a project's design stage. The intention was to advance tropical architecture alongside technological improvements in building design.

Briscoe [29] analysed a design process that stems from an extensive green wall pilot project along a 260' × 70' west-facing parking garage facade in Austin, Texas. The project team charted viable precedents and commercial products of both living and facade modular applications and included current parametric, modular plant, and habitat research and they further explored factors at the scale of landscape and of material for formal pattern making and instantiation.

Izlam et al. [27] investigated the possible workflow for architects and architectural engineers to incorporate digital simulation-based energy performance analysis in the design of living wall integrated facades. Their study focuses on living walls (the

plant, substrate, and structural support are directly integrated within the building wall).

According to a study conducted at the Queensland University of Technology [30], choice of vegetation type, substrate geometry, facade orientation aspect, and other factors can negatively influence the energy consumption outcome of vertical greenery system (VGS). The studies also reveal the importance of considering Leaf Area Index (LAI) in plant selection. LAI represents the amount of leaf surface area per unit of wall or ground area and allows to measure the vegetation and different plant canopies effects [26]. Furthermore, the research shows that plants with greater LAI (typically larger than four) can contribute to more significant savings than plants with LAI lesser than two. This fact may produce an adverse effect and instead consume more resources like water and energy [26].

The study by UMD shows that the amount of cooling, heat flux, and reduction in environment temperature provided by a green facade is directly related to the amount of leaf area present in the VGS. Therefore, in order to conduct greenery systems simulation studies in BIM, the acquisition of LAI data is a necessary step [26].

Allan and Kim [26] also claim in their study that a difference of two centimetres within a plant growing average thickness can cause drastic variations in the result of energy savings (from 2 up to 18%). Hence, it is important to consider this for BIM simulation in large-scale tropical architecture projects. Greenery systems without well-considered design parameters may not only fail to achieve their expected sustainable values but also requires additional energy and maintenance costs.

Previous studies based on cost–benefit analysis of greening systems indicate that since the effects of greening are complex and manifold on different levels on groups of people and areas, consideration of private costs and benefits is not sufficient to reflect the actual value of greening. They also show that additional criteria need to be considered in the future assessments for us to be able to make general statements about the actual profitability of the systems [31].

Besides, there is scarce evidence to predict the success of greenery systems prior to the design phase, during construction and even after the project completion. Currently, it is only after a specific amount of time conducting to the growth and maturity of plants that the success or failure of the project can be evaluated, so it is important to note that design decisions can significantly impact energy consumption levels [26].

Despite the progress made in green architecture over the last years, the implementation of greenery systems remains on a superficial level of aesthetics. Most greenery system projects to date are showpieces devised to create an outstanding installation with a positive image [22, 27]. There is a lack of established simulation tools for quantitative analysis of design. Most of the studies on thermal benefits are experimental or mathematical model-based, and not suitable for architects and designers. The findings of scientific studies are rarely combined with digital design platforms such as BIM or 3-D modelling to specifically test in the building context [31].

Furthermore, for greenery systems, there is insufficient advancement concerning BIM utilization that would support decision-making. To integrate the present

greenery systems into future planning methods of sustainable cities and continue the digital development in the construction industry, integration of these systems into BIM is needed, and appropriate methods to implement automated planning should be adopted.

To consider the diverse influence of greenery systems, various criteria must be considered. Thus the possibility of automated creation of different greening variants for certain circumstances is required. Consequently, through the incorporation of these two innovative features into the greenery for buildings and information modelling for simplification, it is possible to minimize efforts in the planning processes, explore numerous variables, and thus facilitate decision-making for the improvement of sustainable cities [31].

### 3 Approach and Methods

In order to obtain a holistic view of an optimal BIM model for greenery systems application, we developed a parameter-based classification that could be used to generate vegetation-based models into the BIM authoring software. Various parameters need to be considered during the BIM process so that the simulation can be performed with maximum accuracy. A range of key parameters for greenery systems is defined in this work through the review of existing standardizations. Besides, the information on websites and product datasheets from manufacturers was used in this phase of the study.

Through the analysis of the existing greenery system elements, their features, and challenges from the pre-design to the maintenance phase, we determined parameters that played a significant role in the process of greenery information modelling for achieving an optimum GIM model. Eventually, the selected parameters were classified into eight main groups according to their functions and impact. The focus was on the parameters to be later modelled into REVIT, as REVIT allows parametric modelling through “families.” This classification could then be applied to all the BIM authorizing systems. (In REVIT, properties of elements are labelled as “parameters”, which are further divided into different categories such as family parameters, system parameters, shared parameters, global parameters, project parameters, etc.)

In the next step, once the identification and classification of the parameters had been completed, research was conducted to know how much BIM technology had been used in the design and construction phases of greenery. To this purpose, we performed an analytical review of the existing literature on BIM integration into greenery systems worldwide. Due to the wide range of approaches, it was necessary to narrow down the scope of our research. In pursuance of regulation on sustainable strategies for BIM application in public and private projects, an increasing number of buildings have been developed in Spain over the past years benefiting from BIM technology. Madrid and its metropolitan area have a Mediterranean climate with hot summers and cold to mild winters, so converting the capital city to a suitable environment for implementing greenery system projects seemed a fair goal.

Ultimately, six vertical greenery systems in the different parts of Madrid were selected. The main criteria for the selection of the case studies were their dimension and type. The greenery systems were chosen considering the quality of design and complexity in construction. Since the application of BIM requires cost, time, and expertise, private buildings of limited size and area offered poor implementation prospects. Therefore, the greenery systems with a surface area lower than 100 m<sup>2</sup> were excluded from this analysis.

Only living wall systems (LWS) were considered, since LWSs can be characterized as self-sufficient vertical greenery systems that are attached to the exterior or interior surfaces of a building. The LWS is a more recent and modern approach in comparison to green roofs and traditional facade greenery systems and needs more complex consideration of design factors, calculations, and equipment for design, installation, and maintenance. The environmental properties of LWSs are remarkable, for this reason, the existing regulations are encouraging architects to use them extensively. In this research, the main focus is on the buildings with exterior greenery systems, since the majority of interior greenery systems are small-scale.

Data were collected from technical information, the website of architectural and construction companies, and existing research papers. Analysis of selected case studies was performed according to the year of implementation so as to compare their specifications to the existing standards and regulations up until the year of the specified LWSs construction.

## 4 Results

### 4.1 Results from Parameter Analysis

The representation of greenery systems and BIM application has been limited to certain factors that were potentially apt for modelling and simulation. To be more specific, the geometric subdivisions are adopted in the design phase and the requirements of the plants and systems are taken into account when placing the greening system on the building. To integrate BIM into the greenery systems, it is necessary to develop intelligent BIM objects that are effective not only in the planning phase but also throughout the entire life cycle of the project. Therefore, in addition to the spatial parameters that determine the physical shape of the vegetation objects, other parameters should be embedded into the vegetation BIM objects.

The most regular parameters that should be considered are Type and Classification, which identify the greenery system's general information, and also associate the BIM authoring software with the centralized vegetation library. In order to incorporate a wider range of systems and applications, parameters such as Design Aspects should also be considered. The design aspects include the factors defined in the preliminary stages of the simulation process, and close observation revealed that any change introduced in their attributes could affect the whole system function.



Moreover, variable changes in Plant Parameters turn out to be also relevant. As mentioned before, plants are subject to considerable changes during their life cycle due to their inherent characteristics. Consequently, consideration of factors such as height of the plant and duration of greening in their different phases is important during the simulation and decision-making stages. Other relevant plant specifications like leaf area index and reflectivity should equally be considered in this classification.

The result of our study also shows the importance of including external environmental factors like solar exposure, shadow and wind; furthermore, other parameters such as Irrigation and Care and Maintenance proved to play an important role in decision-making at an early stage. Additionally, including details about biodiversity, effects on the microclimate, edging profiles on building corners and details on substructure, etc. seems to have a positive impact.

Once the simulation process is complete, it is a vital step for the architects to calculate the costs. Hence, the costs are broken down into costs of planning, design, construction, maintenance, etc., thereby they could be later defined as parameters to be modelled into the BIM programmes.

To facilitate handling and application, we classified the key parameters into the following groups according to their function:

1. Type and classification parameters. This includes parameters that contain information about type of greenery system, its components and their dimensions and materials.
2. Facade Design Aspects. It includes influential parameters that need to be considered for planning and design.
3. Irrigation Parameters. Parameters for irrigation system parameters including water pipes, irrigation hoses, their dimension, material and design.
4. Care and maintenance, including parameters for the maintenance phase and its frequency.
5. Plant Parameter, including important vegetation variables.
6. Stress Factors. The external environmental factors that affect the greenery system's functions.
7. Cost information. Cost parameters to be modelled in different phases of the greenery system life cycle.
8. Other Influential Factors. Parameters that could not be classified in any of the previous groups, but equally important for the designers.

Table 1 offers a systematic classification of the parameters described in this section.

This chapter is a part of ongoing research and can only cover the partial development of the classification. By developing the tools used in previous works, it is possible to collect all data available and process them in an integrated way. The more quality data we obtain to illustrate the effects of greenery parameters, the more accurate and reliable the planning will be. Compared to the conventional static planning methods, this is a more dynamic approach. Further design rules for the greenery systems should be considered in the BIM process as well.

**Table 1** Properties and parameter classification. Author: Manouchehri, M

Type and classification parameters	Facade Design Aspects	Irrigation Parameters	Care and maintenance	Plant Parameters	Stress Factors	Cost information	Other Influential Factors
Greenery system type	Placement	Moisture percentage	Accessibility	Plant type	Solar exposure	Planning	Light condition (location, direction and shading from surrounding buildings)
Total dimension of greenery system	Orientation	Irrigation systems (water pipes and irrigation hoses)	Construction	Leaf area index	Shadow stressed area	Design	Substrate
Element dimensions	Coverage pattern selection	Irrigation intervals	Maintenance intervals	Plant height	Wind factor	Construction	Effects on microclimate
Climbing aids	Plant choice		Planting intervals	Reflectivity		Care and maintenance	Biodiversity
Vegetation support structure	Selection of greening combinations			Duration of greening		Demolition and disposal	Growing medium thickness
Substrate	Selection of greening area ratio (percentage)					Substructures	Life cycle assessment parameters
Planting	Material choice						Edging profiles on building corners
	Slope angle						

## 4.2 Results from Greenery Systems Analysis

Table 2 contains information about six vertical greenery systems in Madrid. The table is divided into several sections including general information such as the location of the building, year of establishment, and architect. It also includes information regarding the type of the greenery system and its technical and technological characteristics. The time gap between the development of the oldest one, the Caixa Forum, and the most recent one (Civitatís) is 10 years. Although the greenery systems under study are all living wall systems, they are different in type and design. Results from the analysis of data reveal that there is limited information about BIM in greenery system construction phases and scanty use of BIM tools.

Results at this stage show that the implementation of BIM only exists at a superficial level of 3-D modelling and does not include modelling of the critical influential factors. The corresponding parameters determined for BIM stimulation in Table 1 have not been defined by BIM tools for any of the six buildings under analysis.

Figures 1 and 4, respectively, show the Caixa Forum and the Midori building green walls that according to our study, lack BIM in their design. Figures 2, 3, 5, and 6 are the photos taken from the same walls indicating the problems in their function and maintenance. Figures 2 and 3 show the damage done to the Caixa Forum living wall plants due to the insufficient irrigation and drainage system situation. As can be seen in Figs. 4 and 5, plants in the Midori building have dried out in some parts. They also show an environment for the growth of algae and fungi has been provided. Aside from affecting the appearance of the greenery system, these issues can cause health problems and impose extra costs. These challenges can be predicted to a great degree at an early stage and prevented considerably with sufficient parameters design and BIM technology application prior to implementation.

Causes for the apparent lack of BIM utilization in greenery systems can be split into two groups. The first group is associated with global trends and existing limitations in the Spanish AEC sector. More specifically, (1) effects derived from the inconsistency of the BIM standards, (2) lack of BIM competency identification, (3) BIM maturity level, (4) high cost of hardware and maintenance investment, (5) absence of tariff standards, (6) insufficient formal training and shortage of BIM experts, (7) lack of interactivity, and interoperability problems between the various applications, (8) shortage of analytical information and last but not least, (9) uncertainty of return of investment and potential savings in new technology [6, 15].

The second group is concerned with the barriers that hinder the development and adoption of BIM in greenery. The main reasons for this limited use lie in the existing challenges for modelling plant components. These challenges include (10) the variety of leaf types, (11) changing properties and parameters of plants due to complex biological features, (12) lack of information from producer companies.

**Table 2** Specifications of the greenery systems under analysis. Author: Manouchehri, M

Name	Location	Year of Establishment	Type of greenery system	Area	Architect	Use of BIM	Other facilities
Caixa Forum	Paseo del Prado 36, Madrid, Spain	2008	Hydroponic system	460 m <sup>2</sup> , more than 15,000 plants, 24 m height	Patrick Blanc	No	Polyurethane sheet is anchored to wall of building leaving a gap that allows passage through its interior for monitoring, automated irrigation and fertilization system
Crystal Tower	Paseo de la Castellana, 295 C, Madrid, Spain	2009	Continues Living Wall/ Indirect	250 m height, 600 m <sup>2</sup>	Cesar Peli-Patrick Blanc-Ortiz León Arquitectos	No	Located in the building with A certification, without soil substrate, plants grow on a felt panel irrigated with nutritive substances through a network of tubes controlled by solenoid valves

(continued)

Table 2 (continued)

Name	Location	Year of Establishment	Type of greenery system	Area	Architect	Use of BIM	Other facilities
Hotel Santo Domingo	Calle de San Bernardo 1, Madrid, Spain	2011	Modular pot system	25 m height, 1026 m <sup>2</sup> , more than 110 species the plants	Félix González-Pasquín Agero	No	Uses planter box and soil, the irrigation system utilizes the used water of the 50 rooms, utilizes an advanced illumination system during the night
Midori office building	Calle Antonio González Echarte 1, Madrid, Spain	2012	Continuous living wall	5% of the whole facade that is 175 m <sup>2</sup>	GBIG Buildings	No	Use rainwater for plants to save 50% of irrigation water, the building holds LEED gold certificate 2015
Vertical Garden Ayuntamiento de Getafe	Plaza de la Constitución, Getafe, Madrid, Spain	2012	Modular Green facade	110 m <sup>2</sup> , 3186 plants	Paisajismo Urbano with collaboration of Urbanarbolism	No	Has an ornamental fountain with a waterfall, was renovated in 2019

(continued)

**Table 2** (continued)

Name	Location	Year of Establishment	Type of greenery system	Area	Architect	Use of BIM	Other facilities
Civitatis Building	Calle Montera 32, Madrid, Spain	2018	Continuous Living Wall	200 m <sup>2</sup> , more than 8000 plants, 22 different species	Paisajismo Urbano	No	Vertical Garden System patented by the designing company was used, plant selection adapted with Madrid climate

**Fig. 1** Caixa Forum living wall system. Photo by: Manouchehri, M



**Fig. 2** Rotten plants in Caixa Forum due to the excessive irrigation. Photo by: Manouchehri, M



**Fig. 3** Excess of the substrate moisture in the bottom parts of Caixa Forum LWS due to the insufficient drainage system. Photo by: Manouchehri. M



**Fig. 4** Midori building green wall. Photo by: Manouchehri. M

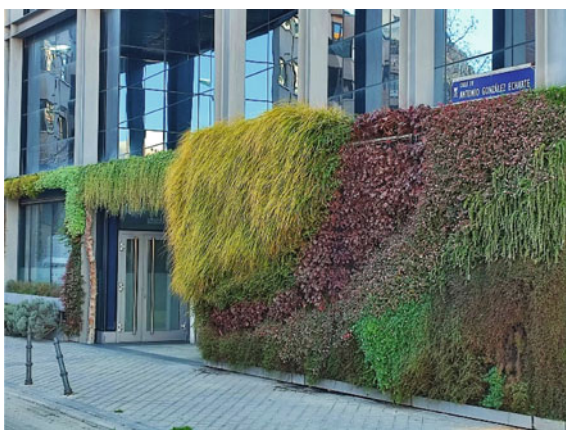




**Fig. 5** Dried plants in Midori LWS caused by problems in irrigation system. Photo by: Manouchehri, M



## 5 Conclusions

BIM is an essential tool that guides us towards achieving sustainable goals in the global AEC industry. The various studies conducted on BIM in the past years demonstrate the positive effects derived from its application. BIM provides the possibility of 3-D modelling in the projects and at the same time coordination amongst all the design disciplines. It also makes it possible to detect errors at the very early stages of the project. BIM technology also allows estimating the costs whilst maintaining timelines and goals. The intelligent (smart) buildings based on BIM use information technology during their creation and operation. As a result, a variety of subsystems that generally operate independently are interconnected, so that the system can share information to optimize the overall performance of the building.

Research reveals the existence of a gap in the integration of BIM with greenery systems. Hopefully, this chapter has shown that integrating greenery systems into BIM is possible and that innovative solutions to existing challenges of sustainable cities can be provided through this implementation. Hence, the process of placing greenery systems in accordance with the buildings and urban development needs

**Fig. 6** Growth of algae in Midori LWS due to the poor maintenance. Photo by: Manouchehri. M



can be facilitated through developments based on various criteria of parameter and algorithm definition. This guarantees a simplification of the design and planning process of greenery placement on buildings and ultimately ensures choosing the best solution.

Greenery systems have a positive impact on urban environments. They can improve air quality, as plants capture  $\text{CO}_2$  and produce oxygen. They also absorb dust and filter up to 85% of the particles suspended in the air. A vegetation cover protects the facade from the impact of extreme weather. Greeneries regulate the temperature; they can help manage energy costs, dampen urban noise, provide solar protection, help ecological balance, and they can also improve appearance in cities by hiding unattractive building parts. Green systems clearly contribute to well-being in occupants, quoting K.L. Wolf “Desk workers who can see a green environment from their desks experience 23% less time off sick than those that have an entirely urban view. Similarly, these workers also report greater job satisfaction” [32].

The reduction rate in environment temperature and heat flux provided by a greenery system is directly related to the amount of leaf area in the VGS. In order to conduct greenery system simulation studies using BIM, LAI data appear to be a

necessary tool. Moreover, a slight difference within a plant growing average thickness can cause drastic variations in terms of energy saving. Hence, it is important to consider these parameters for BIM simulation in large-scale projects.

Greenery systems without well-considered design parameters may not only fail to achieve the expected sustainable values, but they would also involve additional energy and maintenance costs. However, some factors are difficult to model. For example, the moisture level caused by irrigation is related to many other factors, so considering a minimum fixed input value is suggested under these conditions. Research also demonstrates that simplification is imposed in the shape and design of the projects due to software and modelling limitations, which may result in lower accuracy. We have seen how future progress in parameter modelling of greenery systems could solve this problem.

Our study aims to demonstrate that integrating BIM into the greenery system design is still facing many challenges and there are areas for improvement. More particularly, there is a clear lack of BIM objects for greenery systems, which should be supplied by manufacturers and building service connections. This study explores more systematic ways to integrate BIM and greenery systems by detecting influential parameters and classifying them to achieve an optimum model of greenery information. To attain more precise results, building type could be characterized in order to estimate the occupancy level and internal load. Furthermore, building energy performance, local climate area, and impact of living wall in all orientations for different seasons could be included during the simulation process as influential factors.

This chapter proposes an integrative approach for the design of greenery systems, their composition, and their life cycle; a comprehensive approach that involves full-fledged use of BIM technology and widespread adoption of sustainable principles which will hopefully contribute to paving the way towards “our common future”.

## Glossary

**AEC** Architectural, Engineering, and Construction

**AENOR** Spanish Certification Association (Asociación Española de Normalización y Certificación)

**AR** Augmented Reality

**BIM** Building Information Modelling

**BIV** Building Integrated Vegetation

**BEM** Building Energy Modelling

**CBIM** Commission BIM

**COBIM** Common BIM Requirements

**EC** European Commission

**EN** European Norm

**EU** European Union

**FFW** Flora & Fauna Web

**GIM** Greenery Information Modelling

**HBIM** Historic Building Information Modelling  
**IFC** International Foundation Class  
**ISO** International Organization for Standardization  
**LAI** Leaf Area Index  
**LWS** living wall system  
**NBS** National Building Specification  
**NParks** National Parks Board  
**UNE** Spanish Association for Standardization  
**UNEP** United Nations Environment Programme  
**VGS** Vertical Greenery System

## References

1. Manso M, Castro-Gomes J (2015) Green wall systems: a review of their characteristics. *Renew Sustain Energy Rev* 41:863–871
2. Grant G (2006) Green roofs and facades. HIS BRE Press, Berkshire (UK)
3. Santalaia. Available at <https://www.greenroofs.com/projects/santalaia/>. Accessed 14 12 2021
4. Chang YT, Hsieh SH (2020) A review of building information modeling research for green building design through building performance analysis. *J Inf Technol Constr* 25:1–40
5. 8 Inspiring BIM Projects You Need to See. Available at <https://constructionblog.autodesk.com/successful-bim-projects/>. Accessed 14 12 2021
6. Khan R, Aziz Z, Ahmed V (2018) Building integrated agriculture information modelling (BIAIM): an integrated approach towards urban agriculture. *Sustain Cities Soc* 37:594–607
7. Brundtland GH (1987) Report of the World Commission on environment and development: “our common future.” UN
8. Tulubas Gokuc Y, Arditi D (2017) Adoption of BIM in architectural design firms. *Archit Sci Rev* 60(6):483–492
9. Mohammed AB (2020) Collaboration and BIM model maturity to produce green buildings as an organizational strategy. *HBRC J* 16(1):243–268
10. Li J, Wang Y, Wang X, Luo H, Kang SC, Wang J, Guo J, Jiao Y (2014) Benefits of building information modelling in the project lifecycle: construction projects in Asia. *Int J Adv Rob Syst* 11(8):124
11. Cha HS, Jiang S (2020) Special issue on BIM in the construction industry. *Appl Sci* 10(12):4306
12. Gigante M (2019) Building energy modeling: the future of sustainability. <https://www.g2.com/articles/building-energy-modeling-bem-sustainability>. Available at <https://www.g2.com/articles/building-energy-modeling-bem-sustainability>. Accessed 21 12 2021
13. What is HBIM? Let’s find out about BIM applied to existing buildings. Available at <https://biblus.accasoftware.com/en/what-is-hbim-lets-find-out-about-bim-applied-to-existing-buildings/>. Accessed 14 12 2021
14. Schlueter A, Thesseling F (2009) Building information model based energy/exergy performance assessment in early design stages. *Autom Constr* 18(2):153–163
15. Andrés S, del Solar P, de la Peña A, Vivas MD (2017) Implementation of BIM in Spanish construction industry = Implementación BIM en la industria española de la construcción. *Build Manag* 1(1):1–8
16. Martins SS, Evangelista ACJ, Hammad AW, Tam VW, Haddad A (2020) Evaluation of 4D BIM tools applicability in construction planning efficiency. *Int J Constr Manag* 1–14
17. Gobeawan L, Lin SE, Liu X, Wong ST, Lim CW, Gaw YL, Wong NH, Tan PY, Tan CL, He Y (2021) IFC-centric vegetation modelling for Bim. *ISPRS Ann Photogrammetry Rem Sens Spat Inform Sci* 8:91–98

18. Niedermaier A, Robert Bäck R (2016) ALLPLAN BIM compendium theory and practice-guide book 3rd updated and extended edition, December 2016, Document no. 171eng01s38-3-BM1216
19. El Ministerio de Fomento constituye la Comisión para la implantación de la metodología BIM (14 07 2015). <https://www.mitma.gob.es/el-ministerio/sala-de-prensa/noticias/2015/Julio/150714-01.htm>
20. The implementation of BIM in Spain. Available at <https://www.trace-software.com/blog/the-implementation-of-bim-in-spain/>. Accessed 14 12 2021
21. BIM in Europe: national strategy developments in Spain. Available at <https://biblus.accasoftware.com/en/bim-in-europe-national-strategy-developments-in-spain/>. Accessed 14 12 2021
22. Normas en apoyo a BIM en la industria de construcción, December 2019. Available at <https://revista.une.org/20/normas-en-apoyo-a-bim-en-la-industria-de-construccion.html>. Accessed 14 12 2021
23. Historia de AENOR. Available at <https://www.en.aenor.com/conocenos/historia>. Accessed 14 12 2021
24. ASIINDUS Asociación de Ingenieros Industriales del Estado, Se crea UNE, la Asociación Española de Normalización, separándose formalmente de AENOR (03 04 2017). Available at <https://ingenierosindustrialesdelestado.es/2017/04/03/se-crea-une-la-asociacion-espanola-de-normalizacion/>. Accessed 14 12 2021
25. Guías uBIM. Available at <https://www.buildingsmart.es/bim/gu%C3%ADas-ubim/>. Accessed 14 12 2021
26. Allan S, Kim H (2016) A study of workflow for simulations of vertical greenery systems. *Archit Res* 6:142–153
27. Izlam T (2021) Living-wall integrated facades: incorporating energy performance evaluation. Ongoing doctoral thesis
28. Krygiel E, Nies B (2008) *Green BIM: successful sustainable design with building information modeling*. Wiley
29. Briscoe D (2014) Parametric planting: green wall system research + design using BIM
30. Stav Y, Lawson G (2012) Vertical vegetation design decisions and their impact on energy consumption in subtropical cities. *The sustainable city VII: urban regeneration and sustainability [WIT Transactions on Ecology and the Environment, Volume 155]*, pp 489–500
31. Hollands J, Korjenic A (2021) Evaluation and planning decision on facade greening made easy—integration in BIM and implementation of an automated design process. *Sustainability* 13(16):9387
32. Wolf KL (1998) *Urban nature benefits: psycho-social dimensions of people and plants*. University of Washington, College of Forest Resources Fact Sheet, 1

# New Trends in Laser Scanning for Cultural Heritage



Jesús Balado, Ernesto Frías, Silvia M. González-Collazo,  
and Lucía Díaz-Vilariño

**Abstract** The arrival on the market of solid-state LiDAR sensors is generating a series of low-cost devices very attractive to end users. However, the characteristics of low-cost devices do not allow the same use and applications as conventional LiDAR systems. The aim of this work is to compare three LiDAR systems in a typical heritage application: stone individualisation in masonry walls. The system used is one terrestrial laser scanner, Faro X330, and two handheld mobile laser scanners, Zeb-Go and iPad Pro. The case study is an original seventeenth-century gate whose two façades show regular and irregular masonry pattern. Through an analysis of the acquisition process, registration, point density, curvature calculation (for joint detection) and stone individualisation, advantages and disadvantages of each device are discussed. The point cloud acquired with a single scan of Faro X330 was the only one that showed a satisfactory result for stone individualisation, while Zeb-Go and iPad Pro acquisitions were shown to be a fast solution to quickly acquire complete models with a lower level of detail. In the case of the iPad Pro, it is also a low-cost and accessible solution.

**Keywords** Point clouds · LiDAR · Masonry · Terrestrial laser scanning · Handheld mobile laser scanning

## 1 Introduction

Although LiDAR technology was originally developed in the remote sensing community field, its use has been gradually increased in the civil engineering and construction community. But, integration of LiDAR sensors in autonomous vehicles is what has triggered their mass production, the consequent lowering of their prices and reduction in size [1]. This lowering of prices and reduction in size have an influence on the quality of the acquired point cloud and, therefore, on the processing. Point

---

J. Balado (✉) · E. Frías · S. M. González-Collazo · L. Díaz-Vilariño  
Universidade de Vigo, CINTECX, GeoTECH Group, Vigo, Spain  
e-mail: [jbalado@uvigo.es](mailto:jbalado@uvigo.es)

© The Author(s), under exclusive license to Springer Nature Singapore Pte Ltd. 2022  
D. Bienvenido-Huertas and J. Moyano-Campos (eds.), *New Technologies in Building and Construction*, Lecture Notes in Civil Engineering 258,  
[https://doi.org/10.1007/978-981-19-1894-0\\_10](https://doi.org/10.1007/978-981-19-1894-0_10)

167

density, precision and perspective are key characteristics of each point cloud that guarantee the correct replicability of the processing methods.

Point density of point clouds acquired with low-cost devices is usually lower [2]. Since point cloud processing is highly dependent on the geometric and topological relationships between points [3], changes in point density lead to application breakage. Similarly, the precision of new devices is also often lower, leading to noise in the point cloud and in the processing, which requires specific actions to make the algorithm robust [4]. Even so, this noise can still produce false data (roughness, cracks, deformations) in the case of study [5]. Finally, the perspective is a background feature on which the methodological approach is based. Static laser scanning data is not processed in the same way than mobile laser scanning data, not only because density changes, but also due to the number and location of occlusions [6]. It is not all disadvantages with new low-cost LiDAR devices. These new devices are less heavy and bulky, more manageable, allow acquisitions in less time and can even be integrated into a smartphone device. In addition, the quality of the data provided by low-cost LiDAR is sufficient for many of target applications.

In this chapter, data from three LiDAR systems are compared: Faro X330, Zeb-Go and iPad Pro. The object of study is a typical application of heritage studies documentation requiring high precision: the individualisation of stones in a masonry wall. All the process (including acquisition, pre-processing, feature calculation and segmentation) is analysed considering each data source.

## 2 Related Work

This section reviews the evolution of terrestrial LiDAR devices focused on building and infrastructure mapping. The static terrestrial laser scanning (TLS) is the classic setup for using the laser scanner. This mount consists of a tripod, on which the laser scanner is placed and rotates 360° horizontally to cover the surrounding environment. The static position during acquisition allows a higher accuracy (even millimetric) of resulting point cloud with high reality [7]. In addition, being static allows a more durable unattended acquisition over time and a higher frequency of laser rotation, so more points are generated. Between consecutive acquisitions, it is necessary to reposition the TLS equipment. The TLS has been a versatile tool used for the digitisation of buildings, but especially for the detection of surface damages requiring high precision, such as deformations or cracks [8–14]. In some cases, in order to provide TLS equipment's with movement, the TLS was installed on robots or other mobile platforms so that the acquisition became a “stop and go” [15].

Mobil laser scanning (MLS) systems used to acquire linear environments were adapted and mounted on trolleys. The trolleys are pushed by people, and displacement is recorded by odometers, gyroscopes and inertial sensors [16]. This setup allows acquisition in motion, with a minimum loss of accuracy due to the continuous contact between wheels and ground that limits the degrees of freedom. But, this setup also limits acquisition because they need to move over smooth surfaces. Uneven ground



environments, or stairs, limit the movement of the trolleys [17]. LiDAR on trolleys (and the equipment mentioned below) is mainly used for digitising as-built environments [18–21], with the damage control objective depending on the reliability and quality of the equipment in relation to the size/type of damage to be detected.

To overcome the mobility limitations of trolleys, LiDAR was further installed in backpacks. This implied the need to control the weight of the equipment to not injure the user [22]. The heaviest weight is in the batteries for autonomy. Another important change was the elimination of the odometer, which implied less information regarding the relative positioning of the equipment and an increase in the accumulated error [23, 24]. The solution for this was the development of the simultaneous localisation and mapping (SLAM) [25]. As its name suggests, SLAM refers to the problem of locating the position of the equipment while mapping, and it is a common problem addressed in computer vision and widely used in the field of robotics and autonomous driving [26]. However, SLAM algorithms do not work properly when there are abrupt changes in the environment (e.g. in the passage through doors) [27] or in areas with high repeatability, where the algorithm does not find keypoints to take as reference (e.g. corridors or tunnels) [28].

Handheld mobile laser scanning (HMLS) devices work in a similar way to backpacks. When carried in one hand, weight reduction is more relevant, although a backpack is used also to carry batteries and computer components, leaving LiDAR, camera, gyroscopes and inertial sensors strictly for the hand. A positive aspect of HMLS devices is a slightly better positioning and more freedom to move the LiDAR. The procurement of better perspectives reduces occlusions than with using backpacks or TLS [29]. For proof of its feasibility, HMLS is largely employed to digitalize indoor environments and heritage buildings [30–32].

Integration of LiDAR in a pocket device is the latest step in this evolution. The LiDAR integrated in tablets and smartphones is based on solid-state technology, and mechanical moving parts such as rotating mirrors (to orientate the light ray) and corresponding motors are removed. Elimination of moving parts reduces the potential problems of wear or miscalibration [33–35]. The solid-state technology allows a size reduction of the LiDAR until the LiDAR sensor reaches chip size, so that it can be installed in a smartphone without increasing the weight or cost like a photographic sensor. Solid-state LiDAR sensors only acquire data in bidirectional and not in 360° directional ways like conventional equipment. This is a logical evolution since the user can position and orient the equipment towards the object of study, and the SLAM algorithm is to reconstruct and mapping of the scene.

In this work, three devices are compared:

- A TLS, which provides the reference data by generating higher quality density point clouds,
- A handled device, as a specific LiDAR device that allows greater mobility,
- A solid-state LiDAR integrated in a tablet, considerably less expensive.



### 3 Case Study

The selected case study is the Gateway of the Inquisition, in *Salvaterra of Miño*, Spain. The gate is the only remaining part of the palace of *Bartolomé Barbeito y Padrón*, first inquisitor of the Galician censor court in 1677. From the original seventeenth-century building, only the monumental gate remains standing for the most part, and it is one of the best examples of masonry construction in Galicia, both for the quality of the workmanship of excellent silversmithing and for its proportions [36]. The gate is listed in the Spain Heritage Network of Castles and Palaces.

The gateway consists of two sections divided horizontally by a moulded imposition. The lower one is the doorway with a semi-circular arch formed by voussoirs. The upper section is finished with a cornice, also moulded, and is emblazoned with three coats of arms. The right one represents the parental ancestry, while the left one represents the maternal ancestry. The highest central shield indicates the status of inquisitor. In addition, the three coats of arms have the corresponding ecclesiastical seal of the inquisitor: the two cords with six tassels of the bishops hang from the hood. Below the main coat of arms and between the other two, there is the inscription of construction:

MANDOLA FABRICAR ÉL Sr. D. BARTOLOMÉ BARBEITO Y PADRON/ NATURAL DE ESTA FELIGRESÍA/ INQUISIDOR APOSTÓLICO Y ME Las ANTIGUO DE ESTE REINO DE GALICIA/ CORDERO DE 1668/ PARA CLERIGOS DE SU FAMILIA Y VECINOS DE ESTA FELIGRESÍA A FALTA DE AQUELLOS

The translation of which is as follows:

Commissioned by Mr. BARTOLOMÉ BARBEITO Y PADRON/ native of this parish/ Apostolic inquisitor of this Kingdom of Galicia/ Lamb of 1668/ For clergymen of his family and neighbours of this parish in the absence of those.

For the present study, this construction fulfils certain characteristics that will allow the evaluation of the acquisition process, the quality of the point clouds and the methodological processing. The east face (visible façade) is built with regular stones (ashlar fine), and the west face (inside) is made of irregular stones. Fig. 1 shows a picture of both facades. The difference between the compositions of the two faces is remarkable and affects both the acquisition and the thresholds of the presented method. The height can be a limitation for equipment with shorter acquisition range. The roof was not acquired. The horizontal dimensions also allow to compare deviations in the registration of SLAM-dependent devices. And finally, the shields allow a detailed evaluation of very small elements.

#### 3.1 Acquisition Process

The acquisition was performed with three devices: Faro X330, Zeb-Go and iPad Pro 2020. Table 1 contains the technical information of the Faro X330 and Zeb-Go. In

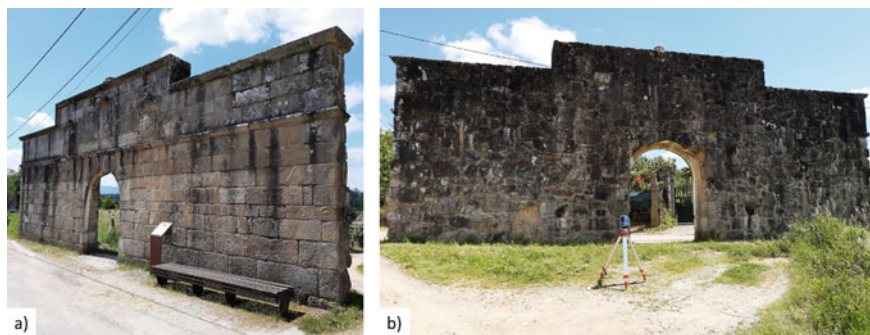


**Fig. 1** Gateway of the Inquisition: **a** Front façade (east side) and **b** Rear façade (west side)

**Table 1** Technical characteristics of Faro X330 and Zeb-Go

	Faro X330	Zeb-Go
Field of view (vertical/horizontal)	300°/360°	270°/360°
Range (m)	330	30
Ranging error (mm)	±2	±30
pts/s	976,000	43,200
Wavelength (nm)	1550	905
Weight (kg)	5.2	1

contrast, Apple does not provide the datasheet of the LiDAR mounted on iPad Pro. The weight of the iPad Pro 2020 is 466 g, and the range of measurement is up to 5 m.

The Faro X330 is a TLS system. Eight scans were performed around the gate (Fig. 2) to obtain the complete point cloud. The distribution of the scanning positions ensures a correct overlap for the subsequent data registration. The resolution was set

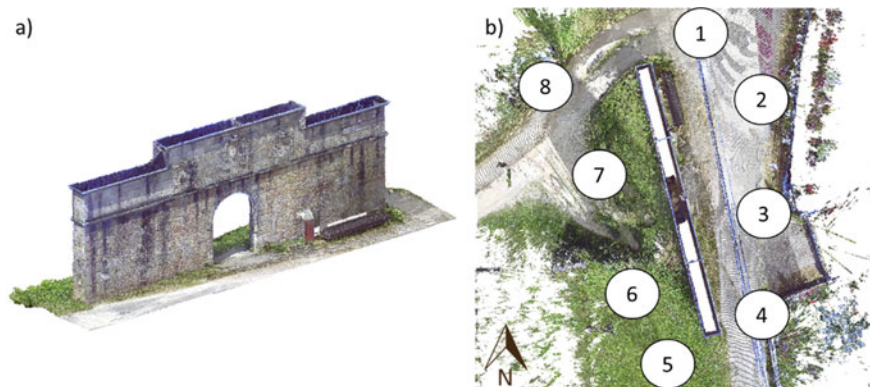


**Fig. 2** Acquisition with Faro X330: **a** Point cloud and **b** Scanning positions

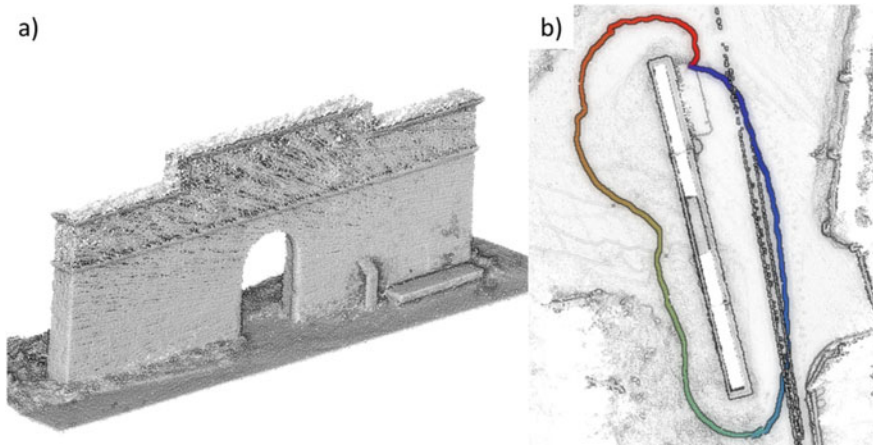


**Fig. 3** Acquisition with Zeb-Go: **a** Point cloud and **b** Acquisition trajectory in colour from red to blue

to 1/16th. Each scan was completed in 1 min 26 s, while taking pictures was in 3 min 20 s min. Colour acquisition is not necessary for processing but provides a more user-friendly visualisation of the point cloud. The total acquisition time was around 50 min, considering the scanning time (LiDAR and photography) at each position and adding few minutes for each repositioning of the TLS equipment for a new scan. The resulting point cloud contained 24.5 million points.

Zeb-Go and iPad Pro are HMLS systems. For the Zeb-Go, since it needs a fixed start and end scanning position, it was initiated on a bench next to the gate. The trajectory of the acquisition and the acquisition cloud are shown in Fig. 3. The scanning time with the Zeb-Go was 3 min. The generated point cloud contained 2 million points. Acquisition with iPad Pro was significantly different. Since the solid-state LiDAR does not acquire in 360°, the device was always oriented towards the gate. In addition, due to the distance limitation (range up to 5 m), the acquisition of the upper areas required a closer approach to the structure, while the mid and low areas were acquired from a more distant position. The acquisition took around 5 min. The app used for the acquisition was *3D Scanner*. No acquisition trajectory was generated. The resulting point cloud (Fig. 4) contains 1.6 million points.

### 3.2 Point Cloud Export

There are multiple formats and standards used for point clouds. Faro X330 exports the point clouds in *fls* format, and Faro SCENE programme is needed to obtain a coloured cloud. It is also possible to open the *fls* files using a CloudCompare plugin. Zeb-Go exports the data in *bag* format. Point clouds can be extracted from a *bag* file using the GEOSLAM programme or a PCL library. The iPad Pro with *3D Scanner*



**Fig. 4** Point cloud acquired with iPad Pro

app, however, allows the export in various formats with or without colour: *obj*, *gltf*, *glb*, *dae*, *stl*, *pts*, *pcd*, *ply* and *xyz*.

### 3.3 Registration

Although the Faro X330 has a GNSS sensor and the acquisition was performed outdoors, the accuracy provided is not sufficient to dispense with the subsequent registration of each scan. For the registration, a minimum of four pairs of equivalent points were selected between the pairs of point clouds, taking as a reference scan no. 7. The point cloud registration induced an RMS error of 2 cm. Zeb-Go and iPad Pro, having a continuous scanning system, do not need to register the point clouds.

## 4 Method

The method for stone segmentation/individualisation in masonry walls is an objective that has been studied with multiple variants based on a common hypothesis: the detection of the joints between stones. This detection can be conducted in 2D images using machine learning [37] or deep learning [38] techniques or by converting the point cloud to a 2D depth map [39]. Depth changes can also be detected linearly (1D) in the wall plane [40]. If point clouds with reflectivity and RGB information are available simultaneously, another alternative is to triangulate the point cloud and search for differences between adjacent nodes based on colour features [41]. Since the aim of this work is not to obtain the best result in a stone segmentation, but to compare the quality and applicability of the point clouds generated by various

devices, a method based on the curvature analysis to locate the joints between stones has been proposed. The curvature analysis is valid and independent of the regularity of the stones and the existence of RGB colour. Then, the high curvature points belonging to the joints are removed, and connected components algorithm is applied to individualise each stone.

#### 4.1 Neighbourhood Calculation

Neighbourhood calculation is a basic operation in the point cloud domain. Since points are not ordered in the point cloud file, it is necessary to identify those points that are closest to each other in space in order to calculate the geometric features of the set. Neighbourhood calculation can be conducted as the *k nearest neighbours* or the *radius search*. Both options are highly influential because of the point density. Taking into account the point densities acquired with each LiDAR device (more information in the results section), the applied neighbour calculation is based on a search radius  $r = 5$  cm. This distance allows the identification of the joints on both façades of the gate and ensures the existence of a minimum neighbourhood even in the point clouds obtained from HMLS devices.

#### 4.2 Calculation of Surface Normal and Curvature

The most straightforward way to calculate the curvature in a point cloud  $P(P_X, P_Y, P_Z)$  is from the variation of the calculation of normal or “Curvature Normal Change Rate”. The surface normal of each point with respect to its neighbours indicates the orientation of the plane containing these points. The plane normal is determined by computing the smallest eigenvalue. The eigenvalues  $(\lambda_1, \lambda_2, \lambda_3)$  are determined from the covariance matrix of each point  $P_r(P_{Xr}, P_{Yr}, P_{Zr})$  with respect to the neighbours within the radius  $r$  [42]. The Curvature Normal Change Rate is estimated following Eq. 1.

$$C = \frac{\min(\lambda_1, \lambda_2, \lambda_3)}{\lambda_1 + \lambda_2 + \lambda_3} \quad (1)$$

#### 4.3 Stone Individualisation

Once the curvature has been calculated, the joints between stones are identified with high values of curvature change. Correspondingly, the points of the joints are extracted from the cloud  $P(P_X, P_Y, P_Z)$  by filtering by threshold value  $h$ . The selection

of  $h$  is done manually for each case study, due to the large variability in the geometrical features of the point clouds acquired with different LiDAR devices. The remaining points are considered as the forming stones of the wall, and connected components algorithm is applied for their individualisation.

The connected components algorithm is based on identifying the different non-connected sets that form an image or graph. In this case, the point cloud is transformed into a graph where the neighbouring points within a distance  $g$  are defined as nodes and connected with an edge. The value of  $g$  must be larger than the resolution of the point cloud in order not to individualise each point, but the value must be smaller than the joint between stones not connecting points from different stones. After converting the point cloud into a graph, the non-connected elements are detected, and an identifier is assigned to each one. Ideally, each non-connected component corresponds to a stone.

## 5 Results and Analysis

In this section, the point density of the acquisitions, the result of the curvature analysis and the application of individualisation are analysed. To improve the precision of the study and given the differences between the front and rear façades, the point clouds of both façades were analysed separately. Given the RMS error produced by the registration (2 cm), the following four acquisitions were evaluated:

- Acquisition with Faro X330 using a single-scan position (no. 3 for the front façade and no. 7 for the rear façade).
- Acquisition with the Faro X330 using two registered scan positions (no. 2 and no. 3 for the front façade and no. 6 and no. 7 for the rear façade).
- Acquisition with Zeb-Go.
- Acquisition with iPad Pro.

### 5.1 Point Density Analysis

One of the distinguishing characteristics of each LiDAR device was the resolution. Figures 5 and 6 show the point clouds coloured according to the number of neighbours for a radius of 5 cm. In the TLS acquisitions, in addition to a higher point density than in HMLS devices, there was a large point density variation. The highest point density was concentrated in areas close to scan positions, more in the rear façade due to the proximity of the scan position 6. Regarding the HMLS devices, the Zeb-Go produced slightly denser point clouds than the iPad Pro (average of 60 points versus 50 points). Although in both devices the point density depended on the speed of the person operating the device, it is very difficult to know this factor prior to a visualisation of the results. The point cloud on the front façade of the Zeb-Go had a higher density area because of the static start/end position of the scanning process. In



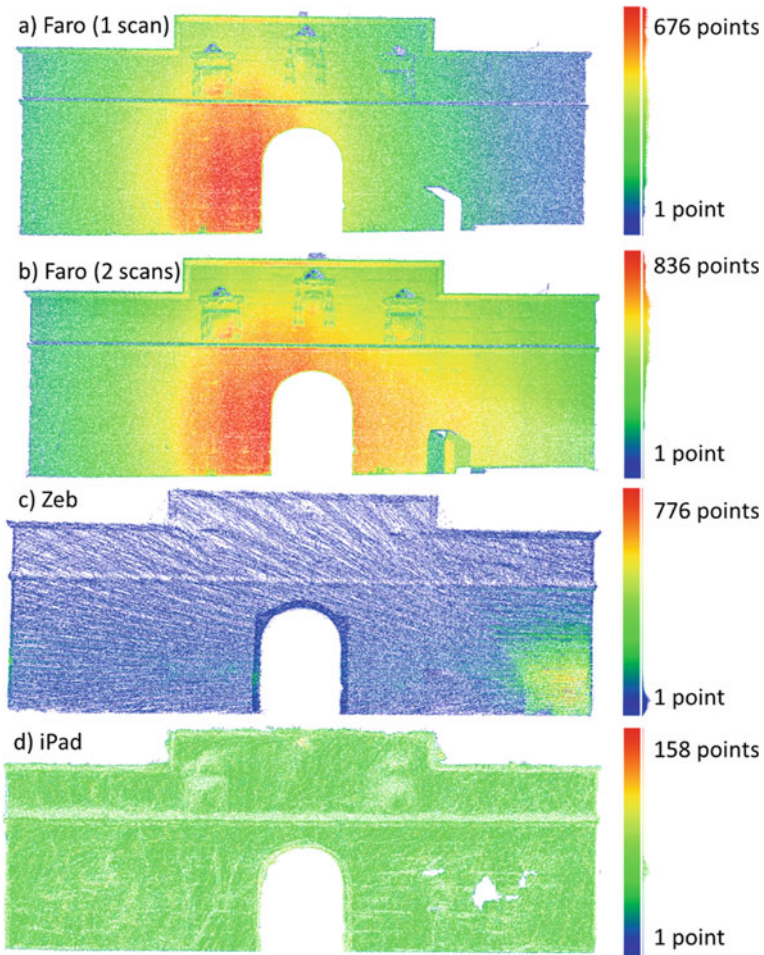


**Fig. 5** Number of neighbours for each point within a radius of 5 cm for the front façade

contrast, the iPad Pro point cloud, despite the visualisation of the acquisition during the process, certain areas in both façades were not acquired despite not having any limiting geometry or building material as it can be seen in Figs. 5d and 6d.

Given the large number of points and density variation, especially in the TLS acquisitions, for the application of the method, we opted to apply a density reduction leaving points at 1 cm. The number of points on each façade before and after the density reduction process is shown in Table 2.

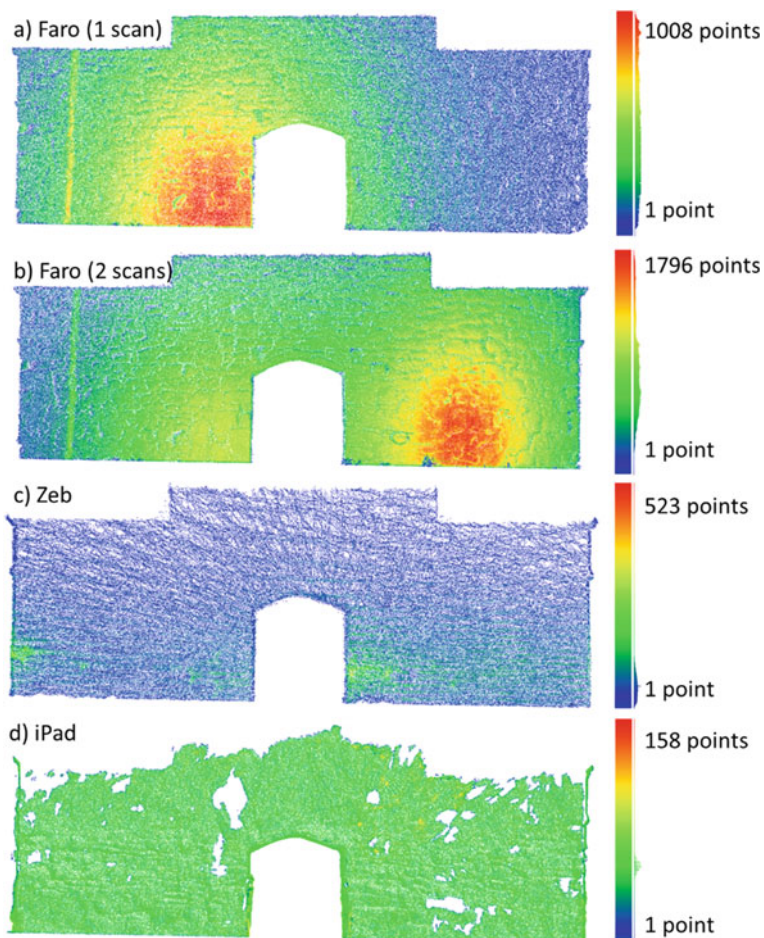


**Fig. 6** Number of neighbours for each point within a radius of 5 cm for the rear façade

**Table 2** Number of points per façade before and after point density reduction

	Acquired		Subsampled (1 cm)	
	Front	Rear	Front	Rear
Faro (1 scan)	2,729,000	2,865,000	420,000	391,000
Faro (2 scans)	4,557,000	6,642,000	518,000	595,000
Zeb-Go	671,000	439,000	390,000	305,000
iPad Pro	532,000	450,000	308,000	263,000



### 5.2 Curvature Analysis

Figures 7 and 8 present the point clouds of the front and rear façade, respectively, coloured according to the calculated curvature. The results of the curvature analysis acquired from each data source were remarkably different. The most accurate values corresponded to the point cloud of the single TLS scan where the joints are visually recognisable, as well as the mouldings and three coats of arms. On the contrary, the case for two registered TLS scans showed errors in the correct registration (lower left and upper right on the front and lower right on the back) that make the correct

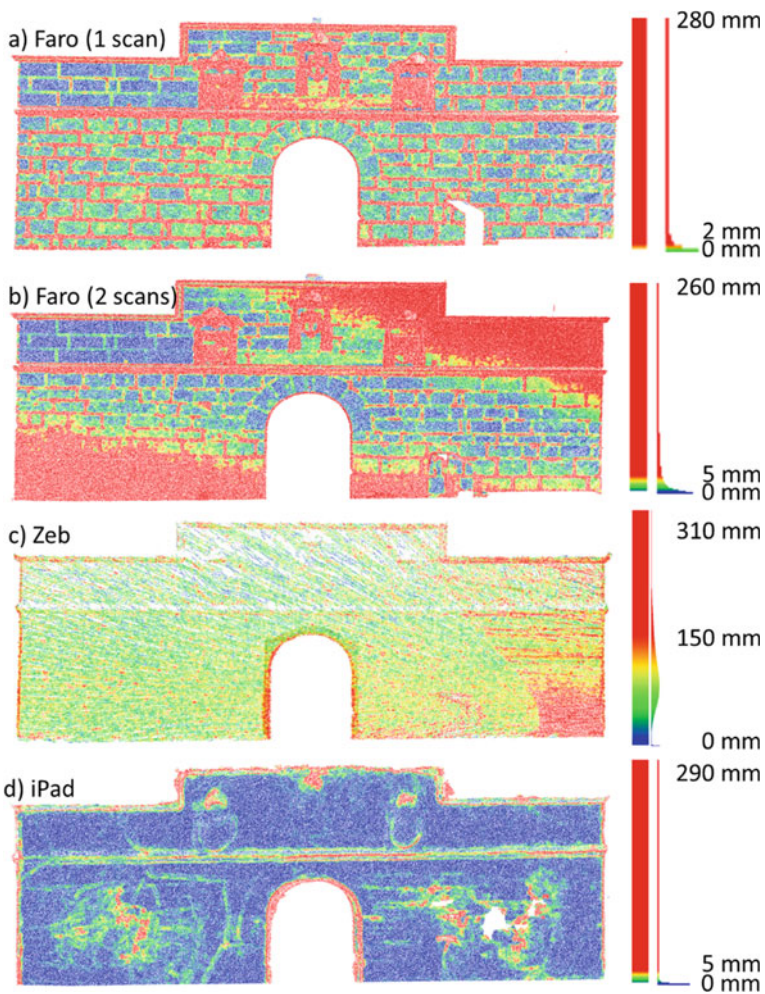


**Fig. 7** Point cloud of the front façade coloured according to curvature values. Saturation (red) value is marked to improve the visualisation of possible joints

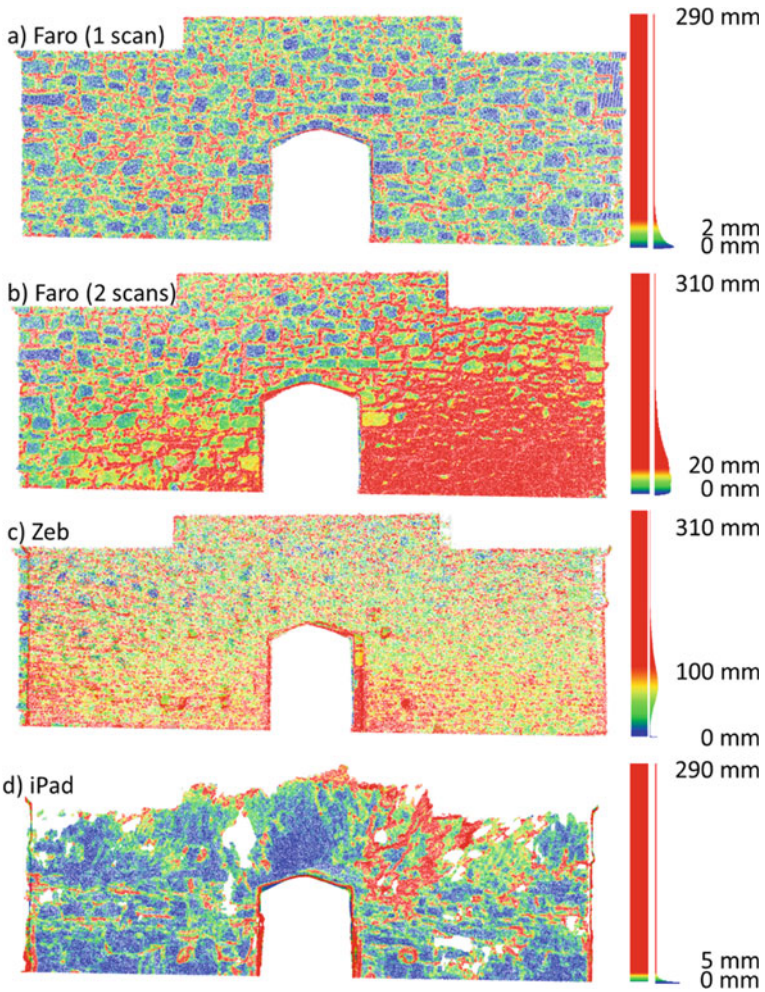


**Fig. 8** Point cloud of the rear façade coloured according to curvature values. Saturation (red) value is marked to improve the visualisation of possible joints

identification of the joints impossible. However, in the central area of the gate, the results are very similar between one scan and two scans.

In the point cloud obtained with the Zeb-Go, it was not possible to identify the joints, neither curvature-based nor visual directly. The cause can be found in the elevate ranging error ( $\pm 30$  mm, Table 1). Points with high curvature corresponded to the area where the HMLS was positioned for calibration at the start/end of the acquisition. A large point generation in this area accentuated the noise generation. The iPad Pro point cloud also did not allow a correct identification of the joints. Although from the curvature analysis of the point cloud with the iPad Pro it was possible to identify mouldings, the curvature of the door edges and the hats of the

coats of arms, wall areas with high curvature values did not correspond to joints. Neither, in comparison with TLS data, these high curvature values could also not be associated with deformations or cracks; therefore, it can be assumed that these are errors in the acquisition with the iPad Pro. The acquisition made with the iPad Pro was also partially incomplete.

The constructional difference between the two façades is remarkable. The front façade, built with irregular stone, has a joint width of approximately 3 cm and a depth of 1 cm. The detection of geometries of this size requires high-precision equipment, such as TLS, and it has been demonstrated that HMLS cannot achieve this level of detail. On the rear façade, on the other hand, due to its irregular construction, the joints between stones have dimensions ranging from similar values to the front façade to reach widths of 10 cm and depths of 5 cm. Although in the most extreme case, the joints are detected by HMLS devices, as shown in Figs. 8c and d, the noise generated by the devices, and the smaller joints hinder the automatic detection.

### 5.3 Segmentation Analysis

In view of the results of the curvature calculation, individualisation was only applied to the TLS point clouds with one single scan and to the rear façade acquired with the iPad Pro. The TLS registered scans were discarded due to RMS error, and the Zeb-Go scans were discarded due to high ranging error. An analysis of the rear façade with the iPad Pro was included due to the correct detection of some joints. The threshold  $h$ -values to eliminate the high curvature points were set manually after a visual assessment. The distance to generate the connected components  $g$  was selected based on the size of the joints and the curvature threshold  $h$ . Table 3 compiles the values of  $g$  and  $h$  used in each case.

Figure 9 shows the result of the stone individualisation by means of connected components. The stone individualisation of the front façade acquired with the Faro X330 was undersegmented. The points of the joints were not extracted correctly, and there was still connectivity between stones. This was noticeable in the upper left block or in the door arch. At the rear façade, due to the larger size of the joints, the undersegmentation was less. Regarding the acquisition of the rear façade with the iPad Pro, the result was noticeably worse than with the Faro X330. In addition to the unacquired areas, there were areas with high curvature that did not always correspond to joints. There was a high undersegmentation of the remaining set of

**Table 3** Values of for split points with high curvature  $h$  and distances  $g$  to break the graph connecting the stones for individualisation

	$h$ (mm)	$g$ (cm)
Faro (front)	0.8	2.5
Faro (rear)	8	1.5
iPad Pro (rear)	0.8	1.5



**Fig. 9** Results of the application of connected components for the individualisation of stones. Individualised stones displayed in random colours

stones. Therefore, neither Zeb-Go nor iPad Pro proved to be a suitable data source for stone individualisation based on point cloud curvature analysis.

All processing (density reduction, curvature calculation and segmentation) was executed in less than 1 min for each point cloud. CloudCompare software was used for processing and visualisation of the results on a laptop with i7-7700HQ 2.80 GHz processor and 16 GB RAM.

## 6 Discussion

The usability of the LiDAR device for the acquisition and generation of the point cloud is a very relevant factor for the comfort of the user. The TLS is the most



precise device, but also the most time-consuming (total for the 8 scans was 50 min) and the heaviest. Fortunately, most of the time it remains static and only needs to be loaded for deployment in a new scanning position. In addition, after acquisition, a registration process between the point clouds and the scan positions are needed to generate a complete final model, which increases the working time and involves registrations errors. However, if the objective is single-scan area, such as one of the gate façades, a single scan can be done quickly in a similar time to HMLS.

The Zeb-Go produces a considerably less dense and accurate point cloud, but the scanning process is the fastest of all. The user does not need to get as close to the case study as with the iPad Pro but must carry a weight of 1 kg in the hand, and the hard drives must be carried on the back. Both Faro X330 and Zeb-Go require software specific to the point cloud exportation.

Advantages of the iPad Pro are: easy handling (lighter than the other two devices), free software and easy export of data in various formats. The iPad Pro also allows a quick acquisition and real-time visualisation during acquisition (the Zeb-Revo RT version also includes a Tablet for visualisation). The visualisation greatly facilitates the acquisition task, although in case studies where both sides are very near, such as the 80 cm of width of this gate, the front and rear visualisation are overlapped and confused, making it difficult to distinguish the acquired surfaces from the second side. Other limitations in the acquisition were found with iPad Pro. It was observed that areas of the gate remained unacquired despite the LiDAR being focused on them. This lack of data is a decisive aspect for obtaining complete models, and it was not observed in the acquisition with Faro X330 or Zeb-Go. Also, the 5 m range limitation, which prevented a correct acquisition of the upper area of the gate.

Regarding data quality for a high-precision application, there are big differences between the three devices. The point clouds of the Faro X330 were the densest. Even with low resolution, in the coloured point cloud, the content of the coats of arms and the inscription at the foot were clearly visible, which was not possible with the HMLS point clouds. However, the TLS point clouds had the greatest variation in point density. The Zeb-Go acquisition showed much more constant densities, although the scanlines in the higher areas of the gate could be clearly identified. Depending on the HMLS acquisition speed, even denser clouds could be produced, although not more precise. The Faro X330 point clouds showed the highest precision of the three devices, although this precision was reduced when registration point clouds. Precision was key to identify the joints between stones (especially the frontal ones), and it is a limiting characteristic for the selection of acquisition device.

Occlusions can be also a determining factor in the choice of a LiDAR device. In this case study, the gate was in an open space and only had the occlusion of an information panel and a bench on the front façade. The occlusion left by this panel can be seen in the single frontal scan with the Faro X330 (Fig. 7a). Registration of point clouds with different scan positions solved this problem. Likewise, the moving acquisition obtained by the HMLS Zeb-Go and iPad Pro also eliminates occlusions. Although in the case of the iPad Pro, there were gaps in the acquisition not caused by occluding objects (Fig. 8d).

The method proposed in this work stone individualisation is highly dependent on the quality of the point clouds. However, and in view of the point clouds generated by the HMLS devices, it is not expected that other methods based on rasterisation would perform better, mainly due to the high ranging error of the Zeb-Go that hinders the identification of the joints even with the naked eye. Also, the gaps in the point cloud generated with the iPad Pro make it impossible to identify stones in empty areas, and the ranging error is considerably high as well.

## 7 Conclusions

In this work, an application for heritage documentation was evaluated by comparing three different LiDAR devices. The object of study was the Inquisition gate in Salvaterra do Miño (Galicia), a building of great relevance at the national heritage level, and with different constructive characteristics between front and rear façades. The acquisitions were conducted using a Faro X330 (considering a case with a single scan and two registered scans), a Zeb-Go and an iPad Pro as a low-cost device. The target application was stone individualisation by means of a curvature analysis and the application of connected components. Only from the single-scan point cloud acquired with the TLS device was possible to achieve the objective.

The choice of the appropriate LiDAR device is largely linked to the objective of the work and the case study. For the generation of a digital model with low resolution, HMLS devices are ideal, particularly the good quality, manageability, versatility and price of the iPad Pro, which can also generate colour point clouds. On the other hand, for high-precision applications, it is still necessary to use TLS devices. The use of TLS with a single scan produces a high-precision and high-density point cloud in an acquisition time comparable to HMLS devices. However, as the number of scans increases, also acquisition time, registration time and the accumulated registration error between scans.

**Acknowledgements** This project has received funding from Xunta de Galicia through human resources grant (ED481B-2019-061) and competitive reference group (ED431C 2016-038) and from the Government of Spain through project PID2019-105221RB-C43 funded by MCIN/AEI/10.13039/501100011033, through project PDC2021-121239-C32 funded by MCIN/AEI/10.13039/501100011033 and “NextGenerationEU”/PRTR and through human resources grant RYC2020-029193-I funded by MCIN/AEI/ 10.13039/501100011033 y FSE “El FSE invierte en tu futuro”. This document reflects only the views of the authors. The statements made herein are solely the responsibility of the authors.

## References

1. Yang K, Bi S, Dong M (2020) Lightningnet: fast and accurate semantic segmentation for autonomous driving based on 3D LIDAR point cloud. In: 2020 IEEE International Conference

- on Multimedia and Expo (ICME), pp 1–6
2. Crommelinck S, Höfle B (2016) Simulating an autonomously operating low-cost static terrestrial LiDAR for multitemporal maize crop height measurements. *Remote Sens* 8
  3. Poux F, Billen R (2019) A smart point cloud infrastructure for intelligent environments. In: *Laser Scanning*. CRC Press, pp 127–149
  4. Huang X, Mei G, Zhang J (2020) Feature-metric registration: a fast semi-supervised approach for robust point cloud registration without correspondences. In: *Proceedings of the IEEE/CVF conference on computer vision and pattern recognition*, pp 11366–11374
  5. Nurunnabi A, West G, Belton D (2015) Outlier detection and robust normal-curvature estimation in mobile laser scanning 3D point cloud data. *Pattern Recognit* 48:1404–1419. <https://doi.org/10.1016/j.patcog.2014.10.014>
  6. Balado J, Arias P, Lorenzo H, Mejjide-Rodríguez A (2021) Disturbance analysis in the classification of objects obtained from Urban LiDAR point clouds with convolutional neural networks. *Remote Sens* 13
  7. Stenz U, Hartmann J, Paffenholz J-A, Neumann I (2020) High-precision 3D object capturing with static and kinematic terrestrial laser scanning in industrial applications—approaches of quality assessment. *Remote Sens* 12
  8. Balado J, Díaz-Vilariño L, Azenha M, Lourenço PB (2021) Automatic detection of surface damage in round brick chimneys by finite plane modelling from terrestrial laser scanning point clouds. Case Study of Bragança Dukes' Palace, Guimarães, Portugal. *Int J Archit Herit* 1–15. <https://doi.org/10.1080/15583058.2021.1925779>
  9. Wojtkowska M, Kedzierski M, Delis P (2021) Validation of terrestrial laser scanning and artificial intelligence for measuring deformations of cultural heritage structures. *Measurement* 167:108291. <https://doi.org/10.1016/j.measurement.2020.108291>
  10. Yang H, Xu X (2020) Intelligent crack extraction based on terrestrial laser scanning measurement. *Meas Control* 53:416–426. <https://doi.org/10.1177/0020294019877490>
  11. Xu X, Yang H (2019) Intelligent crack extraction and analysis for tunnel structures with terrestrial laser scanning measurement. *Adv Mech Eng* 11:1687814019872650. <https://doi.org/10.1177/1687814019872650>
  12. Cho S, Park S, Cha G, Oh T (2018) Development of image processing for crack detection on concrete structures through terrestrial laser scanning associated with the octree structure. *Appl Sci* 8
  13. Yang H, Xu X, Neumann I (2018) Deformation behavior analysis of composite structures under monotonic loads based on terrestrial laser scanning technology. *Compos Struct* 183:594–599. <https://doi.org/10.1016/j.compstruct.2017.07.011>
  14. Yang H, Xu X, Xu W, Neumann I (2017) Terrestrial laser scanning-based deformation analysis for arch and beam structures. *IEEE Sens J* 17:4605–4611. <https://doi.org/10.1109/JSEN.2017.2709908>
  15. Mora R, Martín-Jiménez JA, Lagüela S, González-Aguilera D (2021) Automatic point-cloud registration for quality control in building works. *Appl Sci* 11
  16. Leroux B, Cali J, Verdun J, et al (2017) Assessing the reliability and the accuracy of attitude extracted from visual odometry for LIDAR data georeferencing. *ISPRS - Int Arch Photogramm Remote Sens Spat Inf Sci* 42W6:201–208. <https://doi.org/10.5194/isprs-archives-XLII-2-W6-201-2017>
  17. Nikoohemat S, Peter M, Oude Elberink S, Vosselman G (2017) Exploiting indoor mobile laser scanner trajectories for semantic interpretation of point clouds. *ISPRS Ann Photogramm Remote Sens Spat Inf Sci* IV-2/W4:355–362. <https://doi.org/10.5194/isprs-annals-IV-2-W4-355-2017>
  18. Nikoohemat S, Peter M, Oude Elberink S, Vosselman G (2018) Semantic interpretation of mobile laser scanner point clouds in indoor scenes using trajectories. *Remote Sens* 10
  19. Westling F, Mahmud K, Underwood J, Bally I (2020) Replacing traditional light measurement with LiDAR based methods in orchards. *Comput Electron Agric* 179:105798. <https://doi.org/10.1016/j.compag.2020.105798>

20. Gong Z, Li J, Luo Z et al (2021) Mapping and semantic modeling of underground parking lots using a backpack LiDAR system. *IEEE Trans Intell Transp Syst* 22:734–746. <https://doi.org/10.1109/TITS.2019.2955734>
21. Chen P, Shi W, Bao S et al (2021) Low-drift odometry, mapping and ground segmentation using a backpack LiDAR system. *IEEE Robot Autom Lett* 6:7285–7292. <https://doi.org/10.1109/LRA.2021.3097060>
22. Su Y, Guo Q, Jin S et al (2021) The development and evaluation of a backpack LiDAR system for accurate and efficient forest inventory. *IEEE Geosci Remote Sens Lett* 18:1660–1664. <https://doi.org/10.1109/LGRS.2020.3005166>
23. Filgueira AA, Arias P, Bueno M (2016) Novel inspection system, backpack-based, for 3D modelling of indoor scenes
24. Otero R, Lagüela S, Garrido I, Arias P (2020) Mobile indoor mapping technologies: a review. *Autom Constr* 120:103399. <https://doi.org/10.1016/j.autcon.2020.103399>
25. Zhang D, Gong Z, Chen Y, et al (2019) Slam-based multi-sensor backpack lidar systems in gnss-denied environments. In: *IGARSS 2019—2019 IEEE international geoscience and remote sensing symposium*, pp 8984–8987
26. Taheri H, Xia ZC (2021) SLAM; definition and evolution. *Eng Appl Artif Intell* 97:104032. <https://doi.org/10.1016/j.engappai.2020.104032>
27. Bahraini MS, Rad AB, Bozorg M (2019) SLAM in Dynamic Environments: A Deep Learning Approach for Moving Object Tracking Using ML-RANSAC Algorithm. *Sensors* 19
28. Zhang A, Atia MM (2020) Comparison of 2D localization using radar and LiDAR in long corridors. In: *2020 IEEE Sens* 1–4
29. Bauwens S, Bartholomeus H, Calders K, Lejeune P (2016) Forest inventory with terrestrial LiDAR: a comparison of static and hand-held mobile laser scanning. *For* 7
30. Oniga VE, Breaban AI, Alexe EI, Văşii C (2021) Indoor mapping of a complex cultural heritage scene using Tls and Hmls laser scanning. *ISPRS Int Arch Photogramm Remote Sens Spat Inf Sci* 43B2:605–612. <https://doi.org/10.5194/isprs-archives-XLIII-B2-2021-605-2021>
31. Hu S, Wang D, Xu S (2016) 3D indoor modeling using a hand-held embedded system with multiple laser range scanners. *Proc SPIE*
32. Parent JR, Witharana C, Bradley M (2021) Mapping building interiors with lidar: classifying the point cloud with arcgis. *Int Arch Photogramm Remote Sens Spat Inf Sci XLIV-M-3-2:133–137*. <https://doi.org/10.5194/isprs-archives-XLIV-M-3-2021-133-2021>
33. Poulton CV, Yaacobi A, Cole DB et al (2017) Coherent solid-state LIDAR with silicon photonic optical phased arrays. *Opt Lett* 42:4091–4094. <https://doi.org/10.1364/OL.42.004091>
34. Li C, Cao X, Wu K et al (2021) Blind zone-suppressed hybrid beam steering for solid-state Lidar. *Photon Res* 9:1871–1880. <https://doi.org/10.1364/PRJ.424393>
35. García-Gómez P, Royo S, Rodrigo N, Casas JR (2020) Geometric model and calibration method for a solid-state LiDAR. *Sens* 20
36. Concello de Salvaterra Portal da Inquisición. <https://turismo.concellodesalvaterra.org/pazo-casa-inquisicion>. Accessed 1 Dec 2021
37. Kajatin R, Nalpantidis L (2021) Image Segmentation of bricks in masonry wall using a fusion of machine learning algorithms. In: *Proceedings of ICPR 2020 workshop on pattern recognition in construction and the built environment*. Springer, pp 446–461
38. Ibrahim Y, Nagy B, Benedek C (2020) Deep learning-based masonry wall image analysis. *Remote Sens* 12
39. Valero E, Bosché F, Forster A (2018) Automatic segmentation of 3D point clouds of rubble masonry walls, and its application to building surveying, repair and maintenance. *Autom Constr* 96:29–39. <https://doi.org/10.1016/j.autcon.2018.08.018>
40. Milani G, Esquivel YW, Lourenço PB et al (2013) Characterization of the response of quasi-periodic masonry: Geometrical investigation, homogenization and application to the Guimarães castle, Portugal. *Eng Struct* 56:621–641
41. Sithole G (2008) Detection of bricks in a masonry wall. *Int Arch Photogramm Remote Sens Spat Inf Sci* 1–6



42. Weinmann M, Jutzi B, Mallet C (2014) Semantic 3D scene interpretation: a framework combining optimal neighborhood size selection with relevant features. *ISPRS Ann Photogramm Remote Sens Spat Inf Sci II-3*:181–188. <https://doi.org/10.5194/isprsannals-II-3-181-2014>

# Technological Paradigms for Cultural Heritage. A Scan To BIM Methodology for the Description of Historical Architecture



Cesare Verdoscia, Michele Buldo, Antonella Musicco, and Riccardo Tavolare

**Abstract** The digitalization of Cultural Heritage, important for its preservation and enhancement, helps to keep alive the memory of national communities and their territories and at the same time promote the cultural development. With regard, innovative information and communications technologies have become essential so far for carrying out three-dimensional surveys in the form of point clouds, to obtain texturized and/or parametric models in Building Information Modeling (BIM) environments. Furthermore, using methodologies to support the transition from point clouds to informative models, it is possible of providing an immersive fruition of the scanned object through virtual, augmented, and mixed reality. Many studies have been devoted to the Scan to BIM process, experimenting innovative techniques (such as semantic enrichment, artificial intelligence) with the purpose of enhancing the efficiency of the integration process between point clouds and models, thus creating a cooperative approach that, starting from the survey phase, can end up in a model which is both digital and informative and demands different competences for a more accurate analysis. In the present will be described some experimental approaches, applied to different study cases, that made use of integrated survey techniques (terrestrial laser scanner, close-range photogrammetry), meant to be implemented in the Heritage-BIM.

**Keywords** Building Information Modeling (BIM) · Point clouds · Scan to BIM · Heritage-BIM

## 1 Introduction and State of the Art

In the past two decades, the digital documentation linked to cultural and archeological artifacts has gained a primary role because it is easy to store, access, and save from the threat of material or functional obsolescence and institutional negligence [1, 2].

---

C. Verdoscia (✉) · M. Buldo · A. Musicco · R. Tavolare  
DICATECh, Polytechnic University of Bari, Bari, Italy  
e-mail: [cesare.verdoscia@poliba.it](mailto:cesare.verdoscia@poliba.it)

The use of different and modern technologies for data acquisition, capable of considering the heterogeneity and the complexity of an object, the Level of Details demanded, and the degree of accessibility of the environment, seems therefore to be becoming crucial.

Many progresses have been made in the fields of computer graphics and computer vision, in particular with both the “close-range photogrammetry” and the “structure from motion” (SfM), that define “image-based” approaches able of reconstructing 3D models from 2D images, and “range-based” approaches that imply the use of light detection and ranging (LiDAR) tools, that are highly reliable tools in terms of accuracy and resolution [3–6].

Thanks to the elaboration of point clouds located by means of spatial coordinates and colorimetric characteristics, the integrated survey resulted from laser scans and photogrammetry [7–9] proves to be a methodology that in a short period of time provides accurate results, which can be further implemented through processes like parametric three-dimensional modeling [10, 11], graphic representations of archeological sites [12–14], and multiscale analysis applied to historic buildings in order to document their changes over the years [15].

It is important to notice that in order to merge in the correct way the data collected with different acquisition techniques, a rigorous control on the metric accuracy is mandatory because image-based technologies are not originally intended for the acquisition of the absolute dimensions of objects.

The data obtained can be so implemented in informative systems integrated in BIM [16], where the architectonic components can change their meaning according to the datasets acquired during the survey phase and the archival documents collected. Data can be managed and evaluated by means of platforms integrated in modeling environments through modalities like Open Database Connectivity (ODBC), proprietary interfaces [17, 18], applications of visual programming language—VPL (e.g., Dynamo Studio Autodesk® and Graphisoft Grasshopper®) [19], in cloud platforms for real-time monitoring.

In particular, BIM has obtained remarkable results when it comes to documentation processes, formal analysis, conservation and preservation [20], reconstruction of diachronic models [18, 21], structural analysis [22], and virtual reality enhancement [23].

Nevertheless, finding a way to effectively combine heterogeneous information that help assigning a meaning to the 3D data derived from point clouds, meshes and images, is still a very difficult objective to be attained.

In BIM, the segmentation technique, aimed at the attribution of a semantic class to any of the point detected, is incredibly useful to define an organized and ordered set of geometric points that can be later used for further elaborations, like extrapolating generatrices or erasing the objects that are useless to a specific purpose.

This procedure, in its automatic modality [24, 25], exploits the characteristics and the spatial relations that can be attributed to each point in relation to those adjacent, in order to identify primitive geometrical elements (i.e., sides, edges, planes, cylinders, etc.).

Over the past few years, studies about the semantic segmentation of point clouds in the Cultural Heritage environment have made impressive progresses thanks to the employ of artificial intelligence methods, such as machine learning and/or deep learning, aimed at automatically identifying the architectural elements and their eventual damages.

Providing that the training dataset is correctly arranged, such techniques allow to obtain an automated segmentation according to the criteria and proprieties chosen a priori by the user [26]. In particular, the use of machine learning enables to gather data (points, patches) with similar colorimetric and/or geometric features together in homogeneous subsets [27, 28].

According to some studies, among the most spread methodologies for segmentation and classification of point clouds [24, 29, 30], it is possible to find *edge-based*, *region-based*, *model-based*, *attributes-based*, and *graph-based methodologies* that use algorithms based on clustering of features of data from the point clouds.

Choosing the classes to apply in this process depends on the specific processing or modeling needs. For example, it may be useful to discretize the points belonging to the vegetal elements present during the survey phase so as to be able to ignore them easily in the subsequent modeling phases, thus freeing the user from annoying visual obstacles, or recognizing the elements in the detected area to label them appropriately with metadata, or automatically identifying the rooms making up the building detected by telling their perimeters apart [31].

Since the historical architectural environments are characterized by extremely heterogeneous geometries and it is difficult to obtain a homogeneous training dataset, the automated approach with these algorithms highlights a few more applicational limits and requires often a human intervention for its correct application or verification.

Moreover, although such applications show interesting results in processing point clouds, their integration in HBIM modeling processes is still limited, indeed such operations remain mainly manual.

For this reason, it seems necessary to test a Scan to BIM procedure [10, 11] that, starting from laser scanner and photogrammetric data in form of point clouds, allows the building of *as-built* BIM models, obtaining accurate building parameters, especially from a geometric point of view [32], and guaranteeing a base for the operational planning aimed at the building of a digital informative model, that can be integrated and used for the intended purposes, open, capable of making all the interdisciplinary competences converge in a unique global informative model.

For this purpose, it is fundamental to find the requirements that both the survey and the model should possess and the relative informative proprieties that are destined to integrate them.

At an international level, experts have been trying hard to identify codifications and classifications that can somehow standardize the degree of detail of the object of study, in order to reduce the risk of misunderstandings between customers and designers.

In the meantime, while waiting for an international standardization, each country is striving to elaborate protocols and standards based on LODs, inevitably achieving in this way different procedures.

The American Institute of Architects (AIA) has come up with a protocol known as “G202-2013 Building Information Modeling Protocol” [33] that defines LOD as the Level of Completeness which applies to an element of the model defined in five progressively detailed steps (identified by a numeric scale expressed in hundreds, from 100 to 500).

In the UK, instead, the regulations NBS 1192:2007 and PAS 1192-2:2013 [34] are the point of reference for the information exchange in BIM projects, throughout the identification of Levels of Definition (with a value from 1 to 7), divided in turn into Levels of Model Detail (LOD), that describe, phase after phase, the graphic content of a model and Levels of Information Detail (LOI) that describe the non-graphic content of a model.

The Italian regulation (UNI 11337-4:2017) defines LOD in terms of “Levels of Development”, distinguishing between “Levels of Geometry” (LOG) for all the graphic attributes and “Levels of Information” (LOI) for all the information attributes. It also involves the definition of a LOD scale, codified by means of Latin capital letters (from A to G) that contemplate further intermediate levels that can be defined at the customer’s request [35].

Finally in 2018, with the international regulations UNI EN ISO 19650-1 [36] on the information management in BIM, the definition of “Level of Information Need—LOIN” was first introduced with the aim of overcoming the limits of a rigid classification, based on predetermined classes.

Unlike the other approaches, the LOIN demands a coherent identification of the reading and usability requirements of the model, in order to integrate it effectively in its information processes. A functional classification (based on technology or semantics) gives way to a description which illustrates what the object or the information collected is actually intended for, thus proving the reasons behind certain choices and avoiding to overload the model.

A further application of HBIM can be found in the concept of “Level of Reliability” [37], that tries to face the problem of reliability, considered not only as a formal correspondence between models and point clouds (“Level of Accuracy”) [38], but also as the degree of trustworthiness of the information about materials, construction, etc. [39]

In the Scan to BIM process, apart from defining the geometric and information requirements, guaranteeing both a metric and formal coherence between the digital model and the real one appears to be extremely important, especially when it comes to as-built modeling. In this context, it can be very useful to look at some studies [40, 41] that highlight the surface deviation analysis, easily embeddable in the modeling processes with plug-ins in BIM authoring software, hence giving to the specialists a graphic support for their surveys.

## 2 Methodology and Workflow

In addition to integrating descriptive geometry, the architectonic survey of Cultural Heritage appears to be very useful to computerize the building heritage, especially with knowledge and preservation purposes, by means of modern technologies capable of exploring morphological and material characteristics in a two-dimensional or three-dimensional environments.

The approach adopted by the researchers of the Laboratory of Architectonic and Urban Modelling (MAULab) of the Polytechnic University of Bari is based on a procedure of acquisition and elaboration that derives from range-based (terrestrial laser scanner) and image-based (terrestrial and aerial photogrammetry) scan techniques. It aims at providing a digital documentation and reconstructing a 3D model of the Cultural Heritage thanks to the development of a Scan to BIM methodology made of different subsequent operational phases:

(i) integrated architectonic survey with acquisition of point clouds; (ii) point cloud segmentation; (iii) modeling in BIM environment; (iv) testing of the model.

According to the procedures for digital documentation of Cultural Heritage adopted by international research groups [42–44], an operational workflow was defined for the integrated three-dimensional architectonic survey, briefly summed up as follows (Fig. 1):

- (i) *Planning*: The first phase consists in identifying the requirements and the specific needs of the project, so as to set an efficient work schedule. After that, one of more on-site inspections are to be organized in order to examine the building and define the level of information deepening and accuracy of the morphometric data in relation to quality indicators, like the

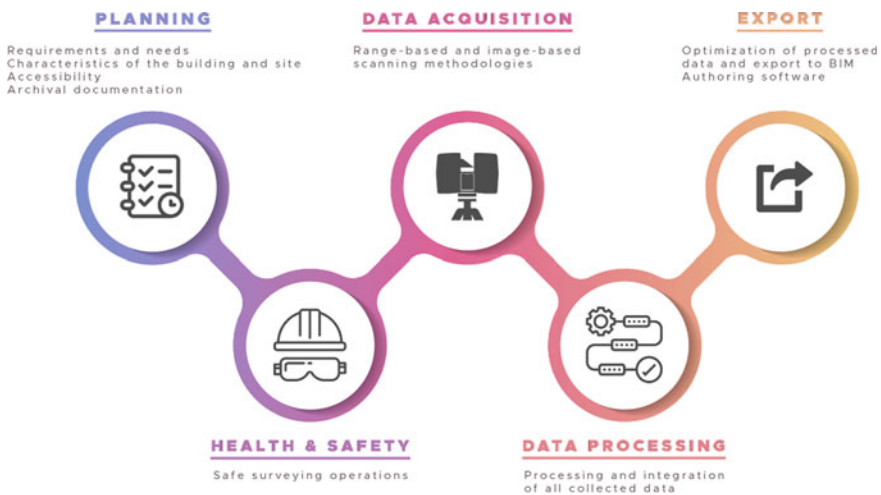


Fig. 1 Scan to BIM methodology workflow

Level of Completeness (LOC), that is the minimum quantity of surface that has to be detected [45]; the Level of Accuracy (LOA), that is the measurement tolerance (expressed in mm) to be apply to the position of every single point of the cloud; and the Level of Density or Detail (LOD), intended as the minimum dimension (expressed in mm<sup>2</sup>) of the object extractable from the point clouds, in other words the density of the point clouds [46].

During this phase, it is also important to evaluate the architectonic characteristics of the building, the morphology of the site, the weather forecasts, and the eventual restrictions to the accessibility of the airspace. Moreover, it is necessary to detect evident issues like occlusions, physical obstacles (e.g., electrical cables, pylons), and zones with reduced visibility and accessibility.

In addition, it is crucial to acquire the bibliographic and archive documents about the building and its vicissitudes throughout the time. At last, it is essential to choose the digital format that will be used to access and share surveys and models, in line with the representational needs.

- (ii) *Health and Safety*: The information acquired allows to plan the survey campaign respecting the security measures defined by the national technical regulation (Legislative Decree 81/2008 known as the “Testo Unico sulla Salute e Sicurezza sul Lavoro”, Presidential Decree 380/2001).

At this stage, it is important to check all the certificates of occupancy, the necessity of specific security measures for the construction site, and the training and preparation of the professionals involved in the survey.

- (iii) *Data acquisition*: The third phase consists in the survey campaign itself, carried out by using *range-based* and *image-based* scan techniques and actions to support the technological equipment (e.g., photographic survey, field notes, placing of targets and light sources, etc.).
- (iv) *Data processing*: Data (instrumental data, bibliographical and archival documentation, photographic surveys, etc.) are processed to elaborate and integrate all the collected data (point clouds, meshes, textures, ortophotos, 360° photos, DEM, etc.), so as to obtain an integrated database.

Hence, the data collected can be processed with a software that generate three-dimensional reconstructions starting from point clouds, employing the potentialities of the algorithms for image processing.

- (v) *Export*: The last phase consists in the optimization of the data processed (e.g., filtering operations, decimation, segmentation), the graphic configuration of the content (e.g., choice of the colors, graphic settings, etc.), and the eventual format conversion of the files (e.g., .RCP,.RVT,.FBX, JPEG, etc.).

### 3 Research Experiences

The so described procedure was later validated in the field with a testing that involved the study of different monumental buildings in Apulia (a region in Southern Italy),

carried out by the Laboratory of Architectonic and Urban Modelling (MAULab) of the Polytechnic University of Bari.

In the following paragraphs, a short overlook on the most important ones will be provided, in order to describe the procedures adopted for each activity of survey and modeling.

### ***3.1 “Civic Museum Romanazzi Carducci” in Putignano (BA)***

The “Civic Museum Romanazzi Carducci” is in the heart of Putignano’s old town, a town southeast of Bari. It was built between the fifteenth and sixteenth century (probably on a place where there once was a Norman building) under the request of Giovan Battista Carafa, a feudal lord of the town.

The building acquired its actual configuration later in time, after the renovation works made throughout the nineteenth century.

In this case (Fig. 2), the survey was carried out by integrating laser scanner acquisitions with phase angle (model: FARO® Focus 3D 120, with a maximum acquisition speed of 976,000 points/s and vertical/horizontal field of view (FOV) of, respectively, 300°/360°) and a drone (model: DJI® Mavic 2 Pro, with a Hasselblad L1D-20c camera and a CMOS 1” 20 MP sensor).

For the laser scanner planning, much attention was given to the positioning of the stations (270 in total), in order to avoid redundancy of data or shadow zones.

As far as the aerial photogrammetric survey is concerned, an overflight with a grid path was defined, calibrating the right front and side overlap and minimizing the number of shots (90 in total) for better managing the point clouds during the alignment phase.

The integration of the data acquired in the two modes was achieved by identifying three recognizable homologous points in both clouds (different in terms of density—LOD and millimeter accuracy—LOA), with an excellent result.

### ***3.2 “Most Holy Trinity Complex” in Venosa, (PZ)***

The “Most Holy Trinity Complex” is a rare example of a medieval building technique (in this case unfinished) that consisted in breaking down an ecclesiastical building only when a new one was ready to fully replace it.

This abbey owes its cultural and historic value to its visible stratification that shows various building phases, which go from the Roman period to the Baroque one, passing through Paleo-Christian, Norman and Swabian-Angevin phases (third century B.C.—eighteenth century A.D.), and the remaining of the monumental “unfinished” church, which is adjacent to the old abbey and is only partially finished.

Three different types of equipment were used to survey the entire complex, which covers an area of approximately 150 \* 60 m<sup>2</sup> (Fig. 3): a terrestrial laser scanner



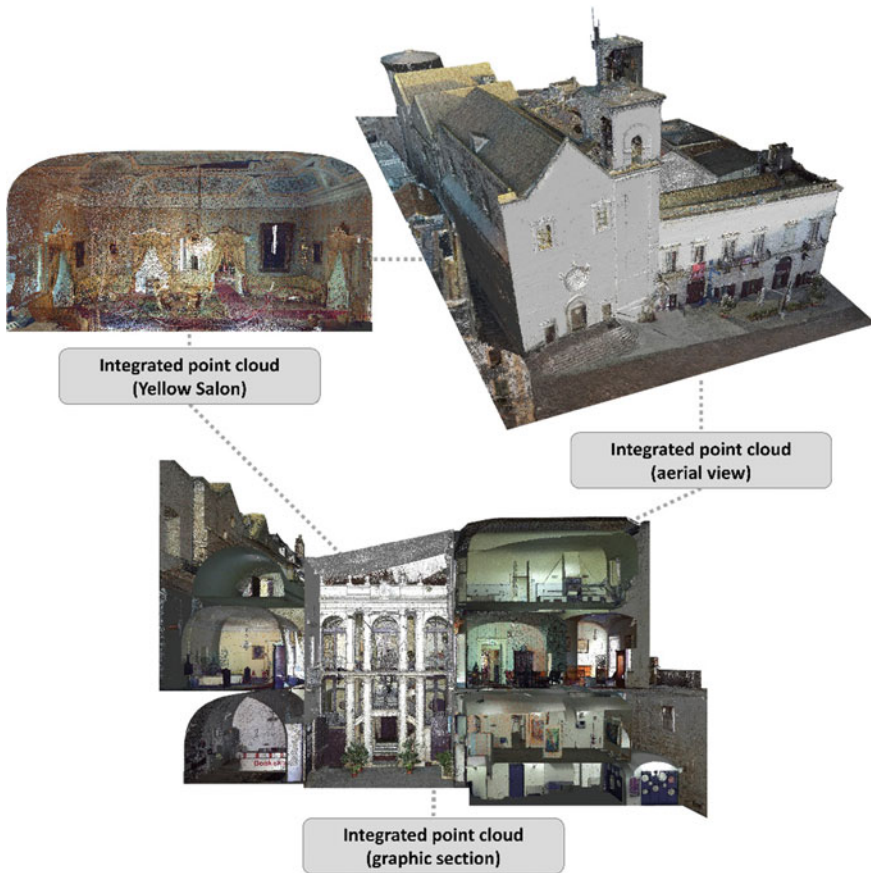


**Fig. 2** Civic Museum Romanazzi Carducci: integrated point cloud

CAM2<sup>®</sup> FARO Focus 3D 120 for the acquisition (with 236 scans) of the internal spaces and the perimeter walls of the abbey; a DJI<sup>®</sup> Phantom 3 Pro drone for the aerial photogrammetric survey (with 618 shots) of the roofs; a reflex digital camera Canon EOS 1200D for an additional photographic survey (for a total of 269 shots) of the facing walls of the entire complex.

The laser scanner stations were carefully identified according to the geometry of the architectural elements (concave/convex, closed/open forms), trying to reduce occlusions and ensuring a correct overlap between the scans.

Specially made targets (dimension: 30 × 30 cm, type: 12-bit, center point radius: 20 mm) were used as ground control points (GCPs) in order to achieve greater geometric accuracy, variable in relation to the distance object sensor, and a better integration with the aerial photogrammetric survey, finally obtained (after splitting the project in four subgroups) by defining couples of homologous points in subsequent scans.

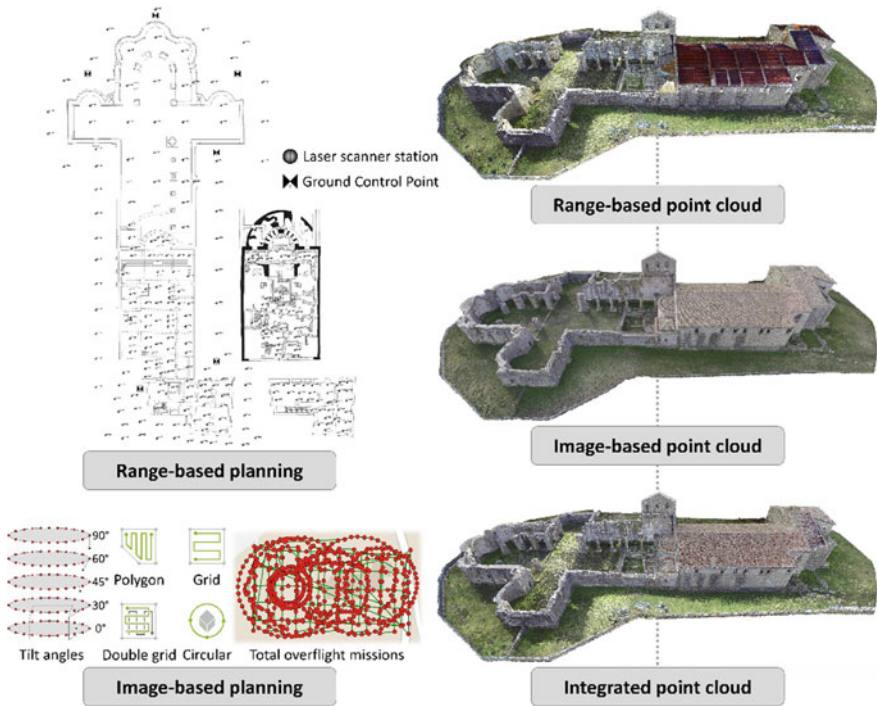


Fig. 3 Most Holy Trinity Complex: survey layouts and integrated point cloud

### 3.3 “Santa Caterina Church” in Conversano (BA)

“Santa Caterina Church” is small rural church built in the twelfth century and made of a quadrilobate plan whose volumes are articulated, with a double symmetry, along the sides of a barycentric octagonal lantern enclosing a central hemispherical dome with a lantern.

The geometry of the isolated building and its accessibility on every side was ideal for the definition of a survey campaign (Fig. 4) easily manageable with different instruments (drone for the roof, laser scanner for the remaining external and internal areas of the church). All this using an alignment type defined by a multi-iterative closest point algorithm (multi-ICP) with the goal of minimizing the distance errors between the points of the two point clouds, taking one as reference.

Furthermore, a polygon mesh model was also developed with the software AWS Thinkbox Sequoia<sup>®</sup>, attributing a radius tolerance value (1.5 cm) and a simplification value for the meshes (20%), in order to define the dimension, the spacing between the points and the number of the faces in the buildings meshes.

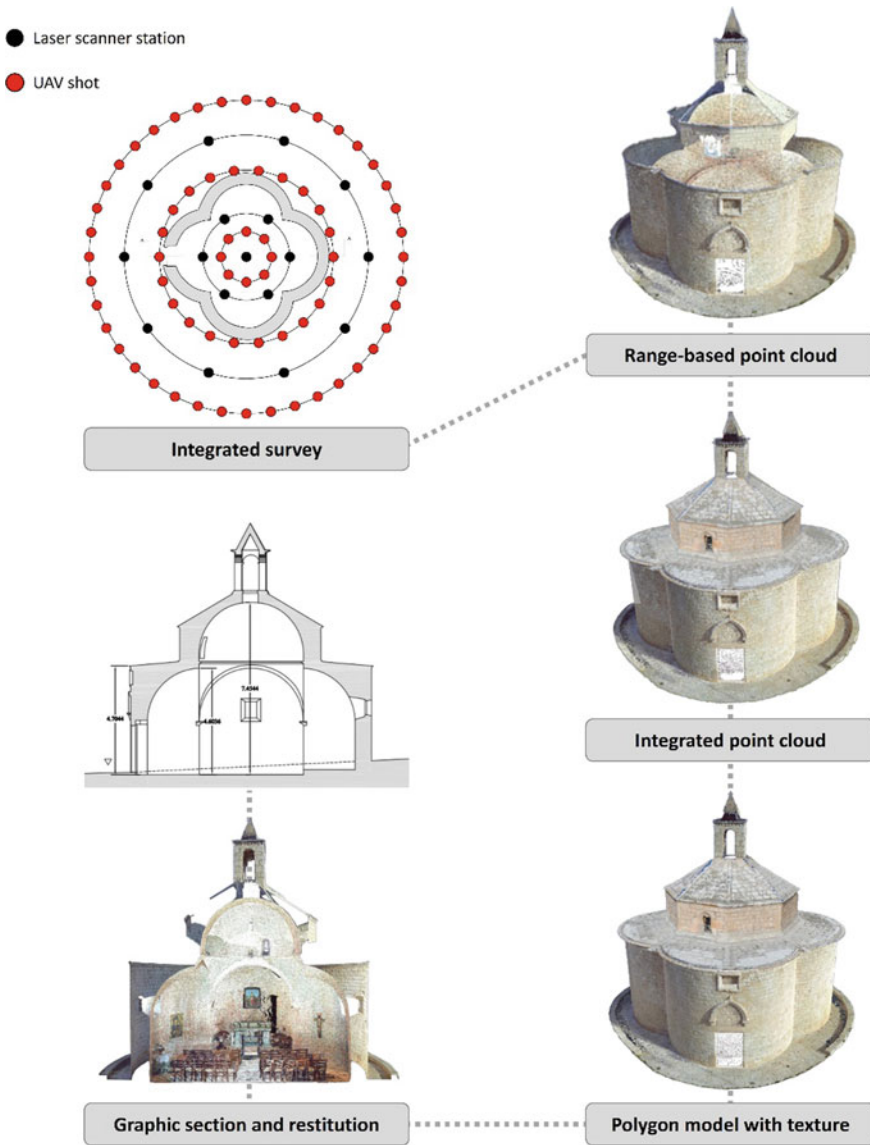


Fig. 4 Santa Caterina Church: 3D integrated survey, point cloud, and polygon model

### 3.4 “Guevara Castle” in Bovino (FG)

The “Guevara Castle” was built on the ruins of a fortress which passed from the Romans to the Byzantines, then to the Normans (in the eleventh century) and the

Swabians, until it lost its original function and became a sumptuous feudal house in the seventeenth century.

The monumental group which develops around the Ducal Castle includes the Norman Castle, the Ducal Palace, the Noble Chapel, the Clock Tower, and the hanging gardens.

In this study (Fig. 5), an aerophotogrammetric survey was carried out with the DJI® Phantom 4 Pro drone programmed for the automatic overflight of the main front of the castle with single, double, and circular grid modes, a longitudinal and lateral overlap equal to 80%, later georeferenced using a Topcon® HiPer II GNSS receiver capable of tracking dual frequency signals (GPS and GLONASS).

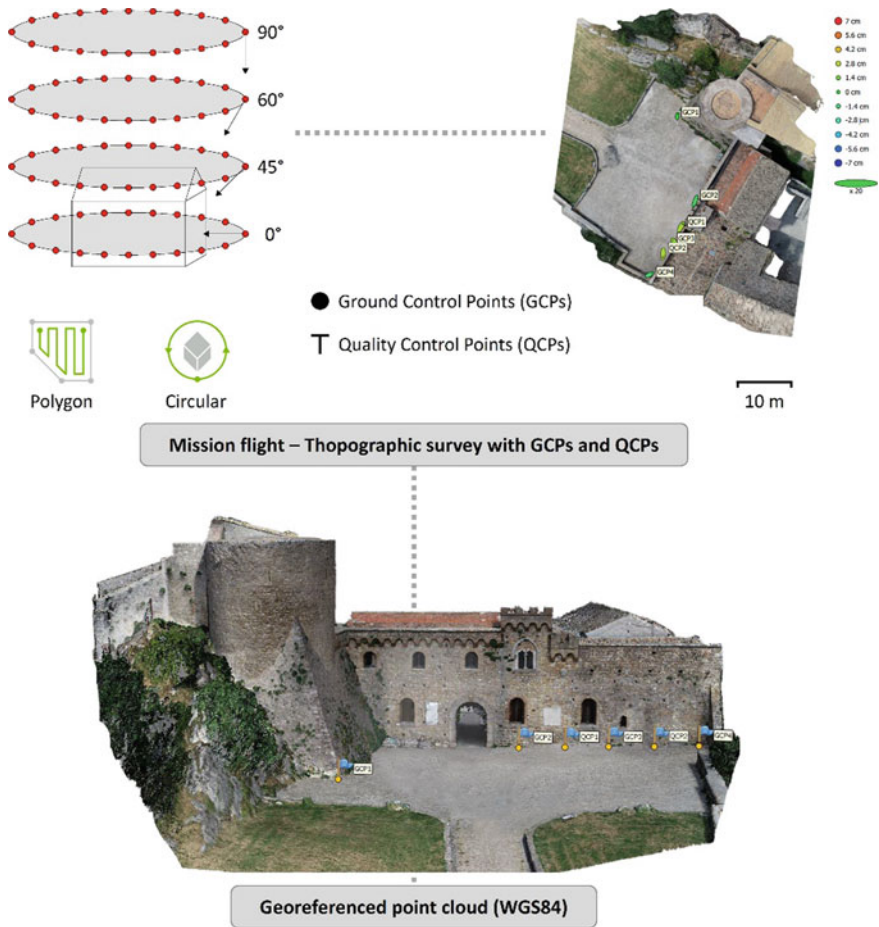


Fig. 5 Guevara Castle: georeferenced aerial photogrammetric survey with GPS

Two types of targets were positioned on the ground and detected by GPS instrumentation: i) ground control points (GCPS) in red/white PVC, with square dimensions of 45 cm per side, used for the alignment, orientation, and dimensioning of the point clouds; ii) quality control points or check points (QCPs) in red/black plywood, of the same size, used to verify the accuracy of the reconstruction and calculating the mean square deviation.

Subsequently, the point clouds were georeferenced in a coordinate system referred to the WGS84 Geodetic Datum. Here, the geolocation point clouds reached an optimal ground sample distance (GSD) spatial resolution of 0.5 mm\*pixel.

### 3.5 “Ognissanti Church” in Trani (BT)

The “Ognissanti Church” is a monument of national interest, built in the twelfth century. It used to be an abbey under Archbishop Byzantium (1142–1150) and then the seat, together with the adjoining hospital, of the order of the Knights Templar. Its interior, without a transept, is divided into three naves by six African granite columns decorated by Corinthian capitals supporting double-ferrule arches.

In this case (Fig. 6), the point cloud was acquired using the FARO Focus 3D 120 laser scanner with a total number of 55 scans (19 of the external perimeter and 36 internal) and segmented it geometrically availing themselves of the model-based random sample consensus (RANSAC) algorithm.

RANSAC—used for the first time to recognize automatically straight lines or circles within point clouds [47] and then implemented [48] to identify objects with

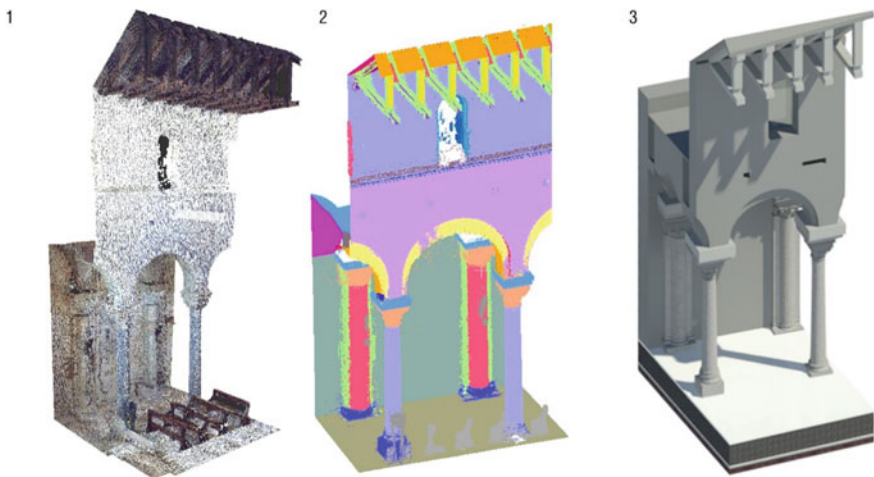


**Fig. 6** Scan to BIM process supported by automatic geometric segmentation: (1) original point cloud; (2) segmented point cloud by RANSAC; (3) BIM model



more complex geometric shapes—allows to create sets of points that conform to the mathematical representation of the primitive shape detected.

In this work, after a morphological analysis of the main architectural components carried out with the CloudCompare software [49] and the “Ransac Shape Detection” plug-in, the experts used RANSAC to identify architectural elements referable to preselected forms such as floors, cylinders, and tori.

It was necessary to split the point cloud into three sections (upper, middle, and lower), to reduce the computation time and limit the recognition to a maximum of three primitives per portion, thus avoiding random selection errors of the minimal sets of points, identified by the plug-in as “minimum support points for primitives”. In this case, a value of 1000 was chosen.

The primitives were automatically compared against all points in the dataset through a recursive procedure that ended with the extraction and selection of the points that best approximated the preselected primitives.

The tolerance of the procedure was managed by applying the “overlooking probability” parameter. It was thus possible for them to isolate architectural components such as columns, capitals, vaults, and moldings, reduce modeling times in a BIM environment, and easily eliminate useless elements such as benches, lanterns, and loudspeakers captured by the laser scanner.

The integration in the HBIM environment of such data made the creation of parametric objects faster.

### 3.6 “Aragonese Castle” in Taranto (TA)

The “Aragonese Castle”, with its quadrangular plan and a large central courtyard, occupies the southeast corner of the island that hosts Taranto’s old town.

Its building started in 780 A.D., during the Byzantine age, but it was later enlarged, modified, and consolidated for defensive purposes.

In 1486, King Ferdinand I of Naples commissioned the military engineer Francesco di Giorgio Martini to give it its current structure.

Also, in this time, an integrated architectural survey was performed (laser scanning and aerial photogrammetry) first, and then the point cloud was manually segmented, on a compositional basis, in eleven macro-sections describing the constituent elements of the entire castle.

The point cloud of the entire building was processed through Geomagic® software to define the three-dimensional meshes of each macro-region (Fig. 7).

Later, two different degrees of definition (according to the UNI 11337 classification) were applied to the model: the LOD B, in which each architectural element is represented by a generic solid with shape, thickness, and approximate position, and the LOD D, in which elements are reproduced with their dimensions, technical, and material characteristics.

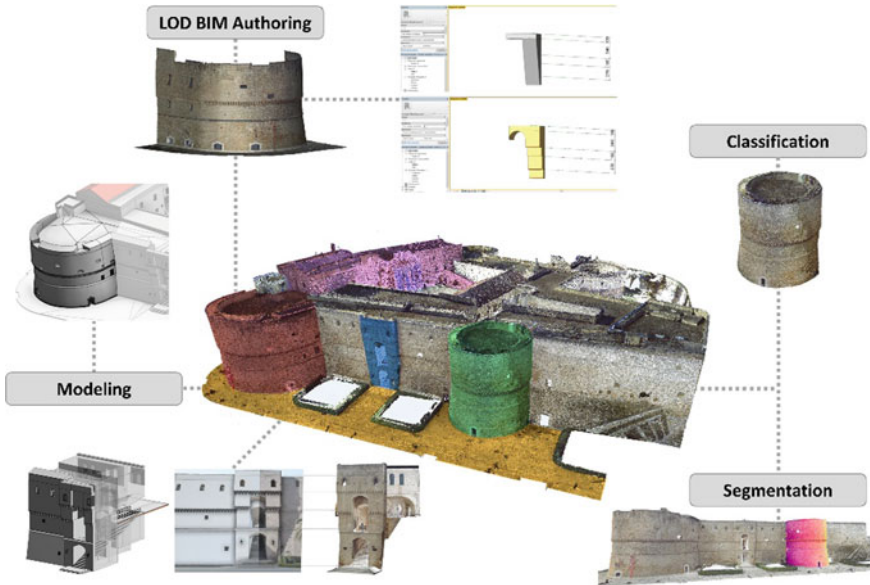


Fig. 7 From segmentation to model LOD definition in a Scan to BIM framework

### 3.7 “Baths of Diocletian” in Rome (RM)

The complex of the “Baths of Diocletian” was built in honor of Diocletian, between 298 and 306 A.D., and extended over on an area of about 13 hectares, between the Quirinale and Viminale hills, reproducing patterns that could be found in the thermal complexes of Traiano and Caracalla.

Here the experts succeeded in creating a computerized three-dimensional model of the rooms VIII, X, and XI of the ancient baths, which now host the Roman National Museum, using a LiDAR point cloud in the context of the Archeological Building Information Modeling (A-BIM) approach, implementing a data link on a relational basis. A geometric model with three levels of detail (*low* with local models created using polygonal generatrices, *medium* through texturing processes deriving from RGB mapping processing and local UV coordinates, *high* thanks to the insertion of the polygonal meshes obtained during the triangulation process applied to portions of the point cloud) was created (Fig. 8).

This approach made it possible to exploit the potential that parametric modeling offers in the geometric synthesis of shapes and the advantage that the automatic extraction of mesh surfaces from the survey output data offers in terms of reproducibility of the irregular surfaces constituting the archeological environments (Fig. 9).

All the information (survey data, monument data, administrative location, georeferencing, sources, and reference documents), organized and hierarchized in Microsoft Access format (structured in tables and reports in XSD format) according

**Fig. 8** Point cloud merged with BIM model for a visual benchmark



**Fig. 9** Point cloud segmentation process represented by a color scheme

to the general catalog of Cultural Heritage, was connected to the BIM model by means of Open Database Connectivity (ODBC) interface (Fig. 10).

### **3.8 “Santa Croce Monastery” in Modugno (BA)**

The “Santa Croce Monastery” is a former convent which dates back to 1618. Its structure, that underwent a series of interventions and transformations over the centuries,



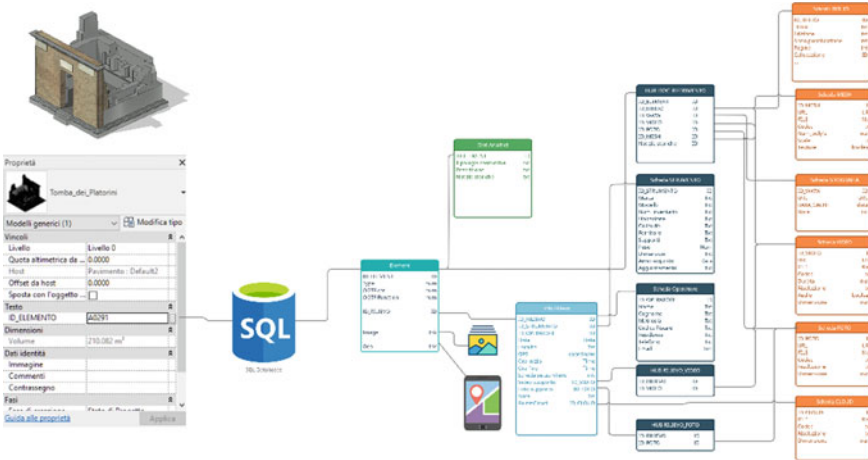


Fig. 10 BIM model relation scheme in DBMS framework

consists today of two buildings positioned around a double-tiered cloister of columns. It currently houses the town hall.

For the HBIM model, the experts chose a unified LOD information modeling (LOD C), attributing to some elements (e.g., capitals) an information link to polygon geometric models, performed with photogrammetric processing.

In order to verify the geometric accuracy of the processed information models, *clash detection* and *surface deviation analysis* were performed (Fig. 11).

The first analysis highlighted the relative positions between the components, noting their architectural, structural, and technological interferences in the 3D model.

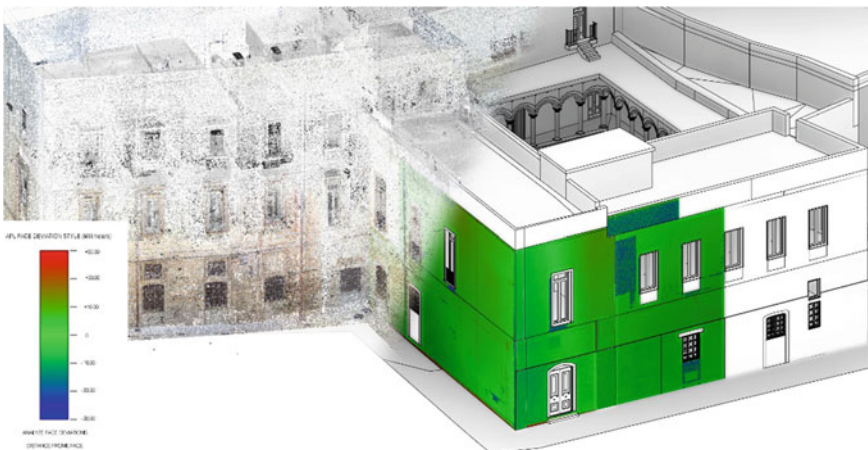


Fig. 11 Clash detection and surface deviation analysis used for BIM model geometric accuracy

The second, on the other hand, detected the errors and their relevance in reference to the point cloud defined as *ground-truth*, through color-coded deviation maps.

## 4 Conclusions

The integration of laser scanning and photogrammetric data into the BIM workflow is a significant advantage for the Architecture, Engineering and Construction (AEC) sector, especially to intervene on existing buildings. They are effective techniques for obtaining accurate geometric parameters of the as-built building, which lead the making of parametric models.

The Scan to BIM process, while involving different technologies and skills, must be based on a coordinated approach that assures a geometric and informative coherence in every operational phase: from the acquisition of survey data to the use of the information model. Each step must be properly dimensioned based on identified requirements, avoiding the recording or processing of superfluous information that can slow down the creation process or even limit the model fruition.

For this reason, taking into account the planning of information needs useful for the complete definition of the architectural survey and for its graphic restitution seems to be a fundamental step, crucial to make appropriate methodological choices.

## References

1. Balzani M, Maietti F, Mugayar Kühl B (2017) Point cloud analysis for conservation and enhancement of modernist architecture. *Int Arch Photogramm Remote Sens Spat Inf Sci—ISPRS Arch* 42:71–77. <https://doi.org/10.5194/isprs-archives-XLII-2-W3-71-2017>
2. Puma P (2016) Editorial. *landscape & archaeology*. *SCIRES-IT—Sci Res Inf Technol* 6:1–6. <https://doi.org/10.2423/i22394303v6n2p1>
3. Tan P (2020) Image-based modeling. *Computer vision: a reference guide*. Springer International Publishing, Cham, pp 1–4
4. Aicardi I, Chiabrandò F, Maria Lingua A, Noardo F (2018) Recent trends in cultural heritage 3D survey: the photogrammetric computer vision approach. *J Cult Herit* 32:257–266. <https://doi.org/10.1016/j.culher.2017.11.006>
5. El-Din Fawzy H (2019) 3D laser scanning and close-range photogrammetry for buildings documentation: a hybrid technique towards a better accuracy. *Alexandria Eng J* 58:1191–1204. <https://doi.org/10.1016/j.aej.2019.10.003>
6. Remondino F (2011) Heritage recording and 3D modeling with photogrammetry and 3D scanning. *Remote Sens* 3:1104–1138. <https://doi.org/10.3390/rs3061104>
7. Aterini B, Giuricin S (2020) The Integrated survey for the recovery of the former Hospital/Monastery of San Pietro in Luco di Mugello. *SCIRES-IT—Sci Res Inf Technol* 10:99–116. <https://doi.org/10.2423/i22394303v10n2p99>
8. Florio R, Catuogno R, Della Corte T (2019) The interaction of knowledge as though field experimentation of the integrated survey. The case of sacristy of Francesco Solimena in the church of san Paolo Maggiore in Naples. *SCIRES-IT—Sci Res Inf Technol* 9:69–84. <https://doi.org/10.2423/i22394303v9n2p69>

9. Beraldin J-A (2004) Integration of laser scanning and close-range photogrammetry. The last decade and beyond. In: Proceedings of the XXth ISPRS Congress, Commission VII
10. Hichri N, Stefani C, De Luca L et al (2015) From point cloud to BIM: a survey of existing approaches To cite this version: HAL Id: hal-01178692 Science Arts & Métiers (SAM)
11. Verdoscia C, Musicco A, Tavolare R (2019) 3D data acquisition and visualisation for implementing cognitive systems. The school building “F. Corridoni” in the old town of Bari. *World Herit Leg*
12. Fiorillo F, Jiménez Fernández-Palacios B, Remondino F, Barba S (2015) 3D surveying and modelling of the archaeological area of Paestum, Italy. *Virtual Archaeol Rev* 4:55. <https://doi.org/10.4995/var.2013.4306>
13. Monterroso-Checa A, Gasparini M (2016) Aerial archaeology and photogrammetric surveys along the roman way from Corduba to Emerita. Digitalizing the ager Cordubensis and the ager Mellariensis. *SCIRES-IT—Sci Res Inf Technol* 6:175–188. <https://doi.org/10.2423/122394303v6n2p175>
14. Willis M, Koenig C, Black S, Castañeda A (2016) Archeological 3D mapping: the structure from motion revolution. *J Texas Archaeol Hist* 3:1–36. <https://doi.org/10.21112/ita.2016.1.110>
15. Russo M, Manferdini AM (2014) Integration of image and range-based techniques for surveying complex architectures. *ISPRS Ann Photogramm Remote Sens Spat Inf Sci* 2:305–312. <https://doi.org/10.5194/isprannals-II-5-305-2014>
16. Pocobelli DP, Boehm J, Bryan P et al (2018) BIM for heritage science: a review. *Herit Sci* 6:23–26. <https://doi.org/10.1186/s40494-018-0191-4>
17. Eastman C, Teicholz P, Sack R, Liston K (2011) *BIM handbook, a guide to building information modelling*, 2nd edn
18. Verdoscia C, Mongiello G, Musicco A et al (2020) 4D-HBIM for the conservation and valorization of cultural heritage. *World Herit Contam* 1000–1008
19. Negendahl K (2015) Building performance simulation in the early design stage: an introduction to integrated dynamic models. *Autom Constr* 54:39–53. <https://doi.org/10.1016/j.autcon.2015.03.002>
20. Diara F, Rinaudo F (2020) Building archaeology documentation and analysis through open source HBIM solutions via nurbs modelling. *Int Arch Photogramm Remote Sens Spat Inf Sci—ISPRS Arch* 43:1381–1388. <https://doi.org/10.5194/isprs-archives-XLIII-B2-2020-1381-2020>
21. Templin T, Brzezinski G, Rawa M (2019) Visualization of spatiooral building changes using 3D web GIS. *IOP Conf Ser Earth Environ Sci* 221. <https://doi.org/10.1088/1755-1315/221/1/012084>
22. Vatan M, Selbesoglu M, Bayram B (2009) The use of 3D laser scanning technology in preservation of historical structures. *Wiad Konserw* 44:659–669
23. Banfi F (2020) HBIM, 3D drawing and virtual reality for archaeological sites and ancient ruins. *Virtual Archaeol Rev* 11:16–33. <https://doi.org/10.4995/var.2020.12416>
24. Grilli E, Menna F, Remondino F (2017) A review of point clouds segmentation and classification algorithms. *Int Arch Photogramm Remote Sens Spat Inf Sci—ISPRS Arch* 42:339–344. <https://doi.org/10.5194/isprs-archives-XLII-2-W3-339-2017>
25. Rabbani T, van den Wildenberg F, Vosselman G (2006) Segmentation of point clouds using smoothness constraint. *Int Arch Photogramm Remote Sens Spat Inf Sci* 36:248–253
26. Brodu N, Lague D (2012) 3D terrestrial lidar data classification of complex natural scenes using a multi-scale dimensionality criterion: applications in geomorphology. *ISPRS J Photogramm Remote Sens* 68:121–134. <https://doi.org/10.1016/j.isprsjprs.2012.01.006>
27. Fatiguso F, Buldo M (2020) Complesso della SS. Trinità di Venosa (PZ). In: De Fino M, Fatiguso F (eds) *La diagnostica per gli edifici storici: Metodi non distruttivi e tecnologie innovative per la valutazione e il controllo*. Collana Architettura sostenibile/Culture costruttive per il recupero sostenibile. EdicomEdizioni, Monfalcone (GO), Italy, pp 169–180
28. Croce V, Caroti G, De LL et al (2021) From the semantic point cloud to heritage-building information modeling: a semiautomatic approach exploiting machine learning. *Remote Sens* 13:1–34. <https://doi.org/10.3390/rs13030461>

29. Nguyen A, Le B (2013) 3d Point cloud segmentation: a survey. In: 6th IEEE conference on Robotic, Automation and Mechatronics (RAM). pp 5–10
30. Sapkota PP (2008) Segmentation of coloured point cloud data. University of Twente
31. Jung J, Stachniss C, Kim C (2017) Automatic room segmentation of 3D laser data using morphological processing. *ISPRS Int J Geo-Information* 6. <https://doi.org/10.3390/ijgi6070206>
32. Badenko V, Fedotov A, Zotov D et al (2019) Scan-to-bim methodology adapted for different application. *Int Arch Photogramm Remote Sens Spat Inf Sci—ISPRS Arch* 42:1–7. <https://doi.org/10.5194/isprs-archives-XLII-5-W2-1-2019>
33. BIMForum, American Institute of Architects (2019) Level of development specification. Part I for building information models
34. BSI (2013) BSI Standard PAS: 1192-2. BSI Stand Publ 1–68
35. Mirarchi C, Lupica Spagnolo S, Daniotti B, Pavan A (2020) Structuring general information specifications for contracts in accordance with the UNI 11337:2017 standard. Springer International Publishing
36. Seyis S, Cekin E (2020) BIM execution plan based on BS EN ISO 19650-1 and BS EN ISO 19650-2 Standards
37. Maiezza P (2019) AS-built reliability in architectural HBIM modeling. *ISPRS Ann Photogramm Remote Sens Spat Inf Sci* 42:461–466. <https://doi.org/10.5194/isprs-archives-XLII-2-W9-461-2019>
38. Antón D, Medjdoub B, Shrahily R, Moyano J (2018) Accuracy evaluation of the semi-automatic 3D modeling for historical building information models. *Int J Archit Herit* 12:790–805. <https://doi.org/10.1080/15583058.2017.1415391>
39. Brusaporci S, Maiezza P, Tata A (2018) A framework for architectural heritage HBIM semantization and development. *Int Arch Photogramm Remote Sens Spat Inf Sci—ISPRS Arch* 42:179–184. <https://doi.org/10.5194/isprs-archives-XLII-2-179-2018>
40. Anil EB, Tang P, Akinci B, Huber D (2013) Deviation analysis method for the assessment of the quality of the as-is building information models generated from point cloud data. *Autom Constr* 35:507–516. <https://doi.org/10.1016/j.autcon.2013.06.003>
41. Verdoscia C, Musicco A, Tavolare R, Buldo M (2021) Evaluation of the geometric reliability in the Scan to BIM process: the case study of Santa Croce monastery. In: Portoghesi P, Gambardella C (eds) *Abitare la Terra/Dwelling on Earth*. Quaderni n.6. Gangemi Editore spa
42. Stylianidis E (2019) CIPA—heritage documentation: 50 years: looking backwards. *Int Arch Photogramm Remote Sens Spat Inf Sci XLII-2/W14:1–130*. <https://doi.org/10.5194/isprs-archives-xlii-2-w14-1-2019>
43. Bryan P, Blake B, Bedford J (2020) Metric survey specifications for cultural heritage
44. Di Giulio R, Maietti F, Piaia E et al (2017) Integrated data capturing requirements for 3D semantic modelling of cultural heritage: the inception protocol. *Int Arch Photogramm Remote Sens Spat Inf Sci—ISPRS Arch* 42:251–257. <https://doi.org/10.5194/isprs-archives-XLII-2-W3-251-2017>
45. Biswas HK, Bosché F, Sun M (2015) Planning for scanning using building information models: a novel approach with occlusion handling. In: 32nd International Symposium Automation Robot Construction Minning Connect to Future Proceedings, 1–8. <https://doi.org/10.22260/isarc2015/0047>
46. Aryan A, Bosché F, Tang P (2021) Planning for terrestrial laser scanning in construction: a review. *Autom Constr* 125. <https://doi.org/10.1016/j.autcon.2021.103551>
47. Fischler MA, Bolles RC (1981) Random sample consensus: a paradigm for model fitting with applications to image analysis and automated cartography. *Graph Image Process* 24:381–395
48. Schnabel R, Wahl R, Klein R (2007) Efficient RANSAC for point-cloud shape detection. *Comput Graph Forum* 26:214–226. <https://doi.org/10.1111/j.1467-8659.2007.01016.x>
49. Girardeau-Montaut D (2011) CloudCompare-open source project. In: *Open Source Projection*. <https://www.danielgm.net/cc/>

# Laser Scanning Intensity Fingerprint: 3D Visualisation and Analysis of Building Surface Deficiencies



Daniel Antón, Manuel J. Carretero-Ayuso, Juan Moyano-Campos, and Juan E. Nieto-Julián

**Abstract** Terrestrial laser scanning (TLS) is a widely used technology in numerous sectors since it enables the recording of both geometric data and colour information of the objects. Moreover, this remote sensing technique allows for producing point clouds enhanced with the reflection intensity of the laser beam. Scientific research has used those data to detect and assess building surface deficiencies. However, the laser scanning intensity fingerprint of a building pathology is yet to be addressed. Thus, this research quantitatively analyses the distribution of point cloud intensities throughout the object geometry to show changes against the general context of the building component surface. This intensity fingerprint reveals the extent of the pathology, which leads to filtering the point cloud by those intensity values to extract and calculate the surface defect. On this basis, TLS is proven to be useful to record, detect, characterise, and examine specific building surface deficiencies and carry out the conservation status analysis of the assets surveyed. The case studies in this chapter are heritage buildings with clear surface pathologies. However, given the relationship between the building surface deficiencies and the point cloud data intensities, this research can also be applied to detect anomalies in modern buildings and constructions.

---

D. Antón (✉)

Research Group 'TEP970: Innovación Tecnológica, Sistemas de Modelado 3D y Diagnóstico Energética en Patrimonio y Edificación', Departamento de Expresión Gráfica e Ingeniería en la Edificación, Escuela Técnica Superior de Ingeniería de Edificación, Universidad de Sevilla, 4A Reina Mercedes Avenue, 41012 Seville, Spain  
e-mail: [danton@us.es](mailto:danton@us.es)

Department of Product Design, School of Architecture, Design and the Built Environment, Nottingham Trent University, 50 Shakespeare Street, Nottingham NG1 4FQ, UK

M. J. Carretero-Ayuso

Departamento de Arquitectura, Universidad de Alcalá, 8 Santa Úrsula Street, 28801 Alcalá de Henares, Spain

J. Moyano-Campos · J. E. Nieto-Julián

Departamento de Expresión Gráfica e Ingeniería en la Edificación, Escuela Técnica Superior de Ingeniería de Edificación, Universidad de Sevilla, 4A Reina Mercedes Avenue, 41012 Seville, Spain

**Keywords** Remote sensing · Terrestrial laser scanning · Intensity fingerprint · Point cloud · Visualisation · Surface deficiencies · Conservation status analysis · Pathology · Heritage building

## 1 Introduction

Building pathologies are diverse in terms of their originating action, their type and extent, and the characteristics of the materials used. These defects or anomalies, being either of a physical–mechanical, chemical or biological nature or a combination of them [23], can occur from the moment the buildings are erected. Not only do these problems arise from the interaction of individual components but also due to the interaction of the building with its occupiers and its environment, as well as because of the exposure time [24]. Likewise, other factors such as malpractice in building design, construction, and maintenance are also the cause of building pathologies [5]. As a consequence of their age, historic buildings and constructions are more likely to present surface deficiencies, but modern buildings are not exempt from this.

In the scientific community, the use of massive data capture technologies [21] has increased in the latest decades. These systems include terrestrial laser scanning (TLS), the structure-from-motion (SfM) photogrammetric technique, mechanical scanning sonar (MSS), infrared thermography (IRT), among others. Being also intended for diverse purposes, remote sensing is used to and capable of recording the deficiencies in a short time and with much more significant detail than using traditional methods. What is more, irregularities inherent to building deficiencies could only be recorded by these means, which in turn enables the as-built modelling and accurate analysis of the geometrical alterations of heritage assets [2, 3, 10]. In this sense, Dias et al. [6] carried out a thorough analysis of the scientific literature on the use of advanced digitisation techniques for the detection and diagnosis of building anomalies. The authors concluded that, although these technologies help the visual assessment building façades, there are still great efforts to make in terms of accuracy and reliability in the analysis.

Previous research publications in the field have addressed the implementation of TLS and unsupervised classification methods into the mapping of defects of historic buildings via the study of point cloud intensities [4]. Having carried out the classification of defects, Kim et al. [16] presented an automatic diagnosis approach based on TLS for the localisation and quantification of concrete spalling on structures. Masiero and Costantino [22] implemented statistical filtering and machine learning to detect and calculate millimetric damages on brick surfaces of façades from TLS point cloud data. Instead of using cloud intensities, the researchers focused on the computation of distances between points of the brick damaged area and a reference plane on the façade surface. Also working on TLS data via machine learning, Valero et al. [28] processed geometric and SfM colour data to automatically identify and classify material loss defects and discolouration on ashlar structures. Suchocki et al. [26] proposed a method to identify and validate construction surface defects by

using TLS radiometric data (laser intensity). The method was also useful to down-size point clouds via eliminating redundant information, which has an impact on both the computational efforts in processing large datasets and the conservation of spatial data of interest. However, subsampling the point clouds to such an extent (5%) implies that the total number of points affected by the pathology cannot be measured as in this research, nor the full pathology can be mapped. More related to the cataloguing of façade materials than to the analysis of building surface deficiencies, Lezzerini et al. [20] used TLS to record the masonry of the Italian St. Nicholas Church in Pisa. Next, using a Geographical Information System (GIS), these authors mapped the façade components with a view to providing essential information as regards their materials and construction techniques. On the other hand, Antón and Amaro-Mellado [1] highlighted the importance of the digital level (digital number, DN) of the images in the analysis of data. Instead of TLS, they focused on a different remote sensing data source, IRT, also called the infrared thermovision technique. Utilising a GIS and 3D point cloud data processing software, these researchers made use of the DN of the infrared images to produce 3D thermal data to represent the thermal behaviour of buildings and bodies.

In view of all the above, considering the capability of TLS to produce intensity data, the research objective is to explore the characterisation of building surface deficiencies through point cloud intensities. In other words, the aim is to analyse the laser scanning intensity fingerprint of building pathologies on surfaces for their detection and quantification.

This chapter is structured as follows: Firstly, the case studies are presented. Next, the Methodology section explains the approach, equipment, technologies, and processes considered. Following the discussion of the results achieved, the conclusions and future work take place.

## 2 Case Studies

This section briefly introduces the case studies through which the research objective will be fulfilled. In this chapter, the focus will be on sectors of building components or constructions with visible surface deficiencies caused by different agents. The description of each case study includes concise and diverse details of their history, features, surroundings, and current conservation status.

### ***2.1 St. Andrew's with Castle Gate United Reformed Church, Nottingham***

The formerly Presbyterian and now congregation called St. Andrew's with Castle Gate United Reformed Church [25], known as St. Andrew's with Castle Gate URC or



**Fig. 1** Colour change in northwest faces of buttresses



commonly and simply as St. Andrew's Church, is registered by the Charity Commission, with the attached former Sunday school, with number 1129944. This institution is based in Nottingham, United Kingdom, in a Grade II listed heritage building (List Entry Number: 1270832), dated 1869 [11]. This church in the Gothic Revival style is surrounded by a wall with railings, also Grade II listed (List Entry Number: 1247549) by Historic England [12]. The church is located opposite the western side of the main buildings of the City Campus of Nottingham Trent University.

In relation to the conservation status of the case study, as shown in Fig. 1, both the church's straight buttresses and the boundary wall evidence a change in the colour of the masonry work in comparison with other areas without this pathology or presenting minor surface deficiencies. In this way, the vertical plane of the buttress and the wall sector on the right (except for the window area) were considered for this research as the affected area and the reference zone for comparison, respectively.

## ***2.2 Bromley House, Beeston, Nottingham***

There are numerous buildings, elements, and parks and gardens, or parts of them, that have been listed by Historic England throughout the country since 1882. A search in the city of Nottingham alone returns 822 results for heritage assets [13]. It is the case of a residential building in the Victorian style called Bromley House, in





**Fig. 2** Bromley House. Efflorescence on the lower part of the western wall. *Source* Google Street View [8]

Beeston, that was the former Board School that can be seen in Fig. 2. This building is located opposite the eastern side of St. John the Baptist Parish Church, also known as Beeston Parish Church, a mid-nineteenth-century Anglican church. This heritage building, listed as Grade II (List Entry Number: 1263823) [14], has undergone several restorations and extensions in the course of its history, such as those of the tower, the bells, the roofs, and the walls [27].

Regarding Bromley House, the building area incorporates the Village Cross, the shaft of the fourteenth-century cross of the village centre, a Grade II listed (List Entry Number: 1263870) heritage asset [15] that was re-erected there in 1929.

The part of Bromley House addressed in this research is the lower section of the ground floor western façade, which is made of traditional red brick. As a result of capillarity humidities, the façade shows efflorescence in diverse degrees, ranging from low-density areas to those with intense white stains, together with a slight loss of mass in some bricks.

### 3 Methodology

The recording and processing of remote sensing data of building surface deficiencies are described in this section. The materials and methods involved consist of the approach adopted in this research, together with the equipment, technologies, and processes implemented. Thus, this section is subdivided into two different stages, *Data collection*, and *Data processing*.

### 3.1 Data Collection

In this way, it is essential to describe the arrangement in the 3D surveys and the setting of parameters. In this subsection, the TLS equipment used to capture the geometry of the two case studies consisted of a tripod-mounted Leica ScanStation P20 [17] 3D laser scanner. The scanner positions (known as stations) and parameters set for each one will be indicated separately.

- *St. Andrew's Church*

The resolution of the laser scanner was set to 3.1 mm at 10 m distance, and the 3D survey was configured as scan only (no images were taken). The number of points (horizontal  $\times$  vertical) for that resolution was 20,107  $\times$  8099. The scan quality was set to 3 out of 4. The 3D survey consisted of two scans. With a view to easing the overlap of scan data, the stations were placed 1.5 m apart at 5.5 and 6 m distance from the buttress vertical plane. Due to the proximity of the stations, no targets were used in the laser scanning. The scanning time was 27 min. The time to set the second station is not considered.

- *Bromley House*

The resolution of the laser scanner was set to 3.1 mm at 10 m distance, and the 3D survey was configured as scan only (no images were taken). The number of points (horizontal  $\times$  vertical) for that resolution was 20,107  $\times$  8099. The scan quality was set to 3 out of 4. The 3D survey consisted of a single scan (no registration process was needed). The scanning time was 13 min and 30 s.

### 3.2 Data Processing

Once the geometric data were recorded, Leica Cyclone 9.4 software [18] was used to produce the case studies' point clouds. To do this, the scan data were imported into the application. As seen in Sect. 3.1, no images were recorded during the 3D surveys, which means that no textures had to be mapped onto the point clouds. This research analyses the laser beam intensities instead of RGB (red–green–blue) coloured textures. In addition, only the St. Andrew's Church case study required scan registration (alignment of scans into the same coordinate system) since it consisted of two stations. This was carried out automatically in the software by creating one cloud constraint, but the optimisation of the alignment was also conducted to minimise the group error.

Besides, it should be noted that the TLS data were recorded and produced in a local coordinate system for each case study. In other words, no geo-referencing process was performed. Given that the analysis carried out focuses on the geometry and the laser beam intensity data on surfaces, the geo-referencing of the point clouds would not make any difference to the results of this research.

After the point cloud data were produced and stored in *.e57* file format, these datasets were manually segmented to select the desired sector to be studied in each case. Using the open-source CloudCompare software [7], this was achieved by conducting manual polygon fencing in the elevation view (*XZ* plane orthogonal view). Thus, the undesired areas were eliminated to extract the segmented point clouds: the pathology sector (1) and the reference zone (2). In addition, the TLS data were subsampled at 20 mm resolution to try to homogenise the unordered datasets, thus reducing their information entropy [9].

The methodology of this research also involved various processes such as: enquiring the TLS data intensities; producing histograms of the distribution of points among intensity intervals; gathering statistical data from those histograms; filtering the segmented point clouds by laser beam intensity values to isolate the affected areas from the rest of the sectors; likewise, presenting the point cloud data intensities in different visualisation modes with a view to highlighting the affected areas. The processes above were also carried out in CloudCompare software.

## 4 Results and Discussion

This section is structured into two different subsections. Firstly, the outcomes deriving from the research objectives are presented and discussed. This involves showing the digitised areas of the case studies, carrying out the analysis of the TLS data and discussing the findings achieved. Secondly, the research limitations are described and included in a separate subsection.

Prior to addressing this section, it is worth providing the main specifications of the computer used to process the data. It was a gaming laptop of the latest generation with an octa-core processor with hyper-threading at 2.30 GHz and a maximum turbo frequency of 4.60 GHz with 24 MB cache, 32 GB RAM DDR4 @ 3200 MHz, a 192-bit graphics card with 3840 cores @ 1425 MHz and 6144 MB GDDR6 dedicated memory @ 14 Gbps, and an NVMe PCIe Gen3x4 SSD (solid-state drive) with 1 TB storage capacity.

### 4.1 *Laser Beam Intensity Fingerprint*

The research objective is to analyse the intensities of point clouds so that building surface deficiencies can be characterised. Given that the reflection of the laser beam varies depending on the surface colour, material, texture, and humidity content, the buttress of St. Andrew's Church and the lower wall sector of Bromley House are suitable case studies to reveal the laser beam intensity fingerprint since they present surface deficiencies.

### 4.1.1 St. Andrew’s with Castle Gate URC

As mentioned before, the change in the buttress colour can be recorded using TLS and next producing the point cloud data enhanced with intensities. Firstly, it is worth specifying the registration diagnostics of the two scans of the St. Andrew’s Church case study:

- Mean absolute error for enabled constraints: 0.001 m
- Overlap point count: 100,266 points
- Overlap error statistics:
  - RMS (Root Mean Square) error: 0.0100678 m
  - Average: 0.00559179 m
  - Minimum: 1.04814e−06 m
  - Maximum: 0.0908525 m.

Based on both the above data and the validity of the alignment, the next step was to use CloudCompare software to enquire the intensity values from the segmented point clouds: (1) pathology sector and (2) reference zone.

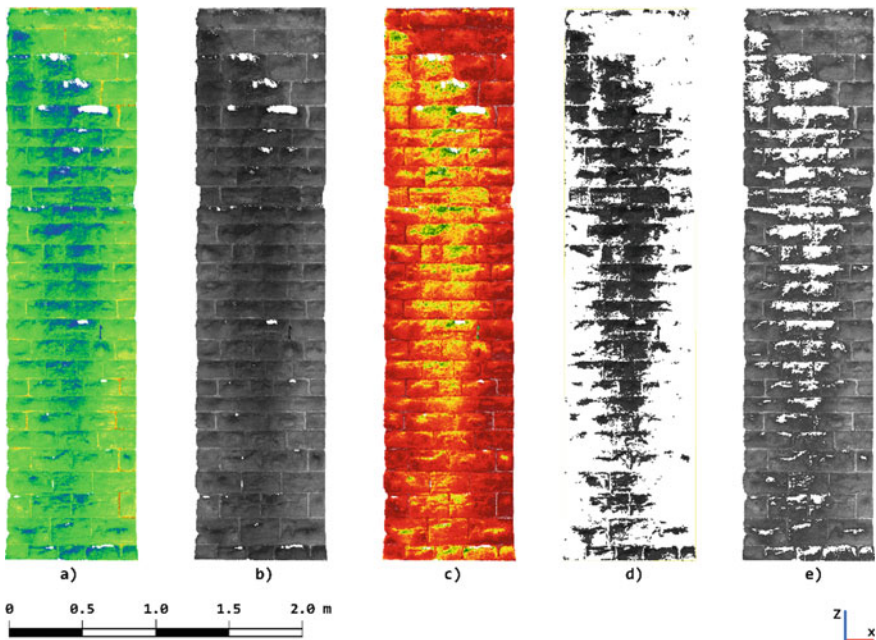


**Fig. 3** Segmented pathology buttress sector enhanced with intensities: **a** blue–green–yellow–red; **b** greyscale (monochrome); **c** high contrast; **d** most severely affected part, in monochrome; **e** the rest of the sector, in monochrome

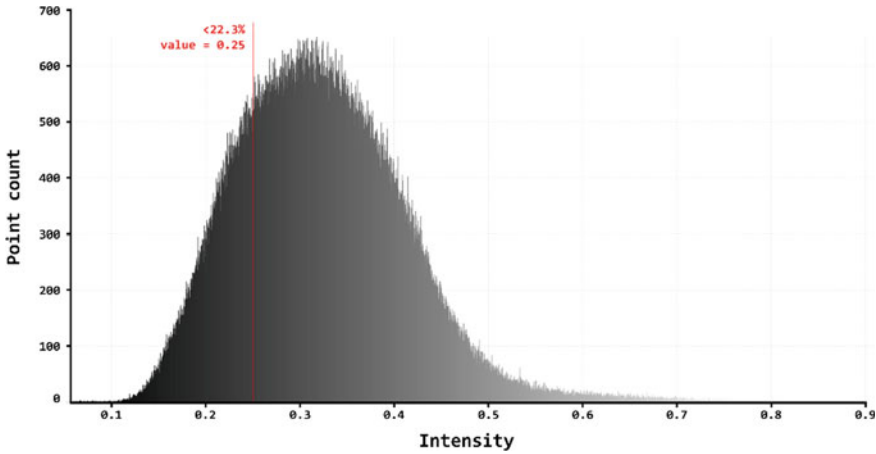


**Fig. 4** Greyscale histogram of points and intensities of the pathology sector (1)

Figure 3 displays the segmented area of the pathology (1) dataset enhanced with intensities—in different visualisation modes—where the most affected parts are shown in blue, dark grey, and green colours.

The analysis of the point cloud intensities was carried out considering 3500 classes or intervals. This amount was chosen so that the width of each interval is reduced in order to increase the accuracy of the graph.

Figure 4 shows the histogram of point cloud data intensities for the pathology sector (1).

The analysis yielded the following data:

- 556,171 values (points displaying intensity);
- Mean: 158.91 points (for each intensity value);
- Standard deviation: 213.56 points;
- Point of Interest (PoI): 0.25 intensity value.

The intensity unit is a coefficient, from 0 to 1 (0 to 100%).

Throughout the histogram in Fig. 4, the point arrangement is not symmetrical; i.e. at lower intensities, the point count rate increases more significantly than it decreases at higher intensities. In view of Fig. 3, that is a consequence of the dark areas on the buttress surface. In this way, by mirroring the highest intensities, the ending intensity value of the pathology was established at 0.25 (PoI) for being the symmetry breaking point. Filtering the TLS point cloud data by the intensity PoI, the dataset is split. The remaining 123,498 points with an intensity value lower than 0.25 correspond to the surface deficiency, which constitutes 22.2% of the total number of points in the pathology sector (1).

On the other hand, Fig. 5 displays the segmented area of the reference (2) dataset enhanced with intensities in the monochrome visualisation mode. The reference sector was rectified for comparison by excluding minor pathological zones on it.

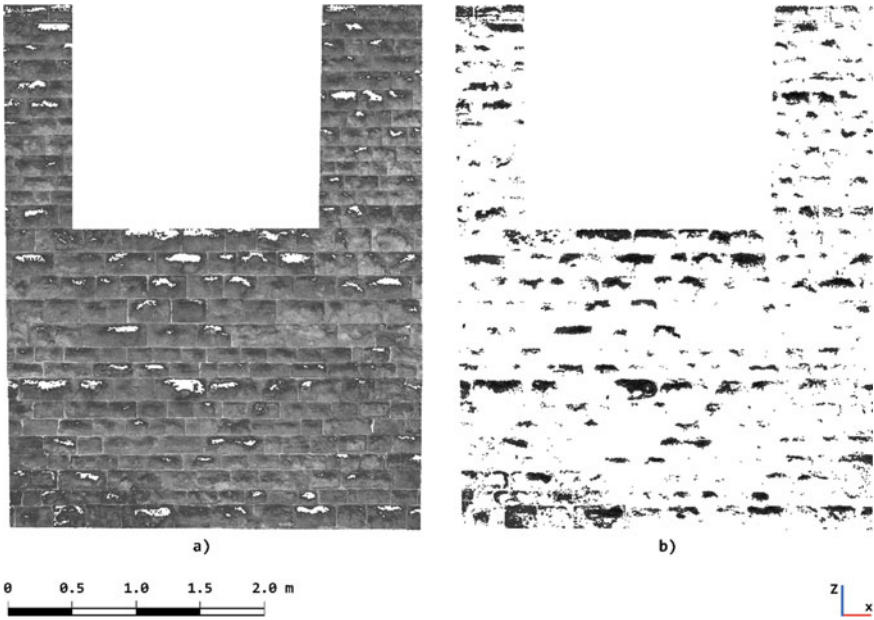


**Fig. 5** Segmented reference buttress sector enhanced with intensities, in monochrome: **a** rectified reference sector; **b** minor pathology in the reference sector

Figure 6 shows the histogram of point cloud data intensities for the reference zone (2).

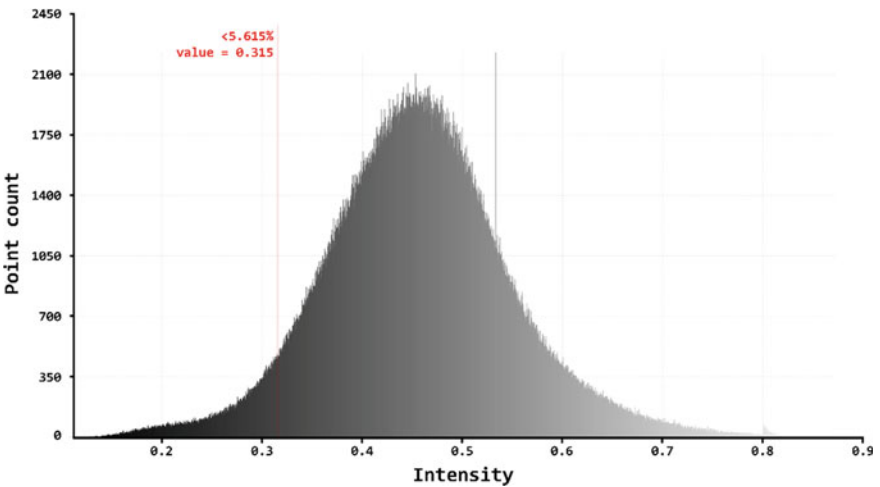


**Fig. 6** Greyscale histogram of points and intensities of the reference zone (2)

Also carried out considering 3500 classes, the analysis of the histogram’s point cloud intensities yielded the following data:

- 1,645,779 values (points displaying intensity);
- Mean: 470.22 points (for each intensity value);
- Standard deviation: 624.32 points;
- PoI: 0.315 intensity value.

As seen in both histograms, the point distribution is more symmetrical in the reference wall zone against the pathology sector. However, in the region of low-intensity values, the curve symmetry starts at 0.315, thus comprising a small portion of the pathology from 0.1 to 0.315. In view of Fig. 1, the reference wall sector also presents dark zones, but minor. By filtering the point cloud by 0.315 intensity value, the reference point set can be rectified (Fig. 5) and be used as a reference for comparison with the pathology sector.

Similarly to the pathology sector (1), when the point cloud is filtered by the intensity PoI, the remaining 91,475 points correspond to the minor surface deficiency in the reference sector (2) for rectification, which is 5.56% of the total number of points.

Finally, considering the pathology (1) and reference (2) sectors, it is worth analysing the distribution of their data. The coefficient of variation (standard deviation divided by the mean) yields values of 1.344 and 1.328, respectively. This reveals a slightly lower dispersion of the data in (2), which indicates that the points not affected by the pathology prevail.

### 4.1.2 Bromley House in Beeston

Regarding the residential Bromley House, the colour change throughout the wall constitutes the second sample to be analysed.

Efflorescences are the result of crystallisation of salts on the material surface [19]. This pathology can be easily identified in a photograph and detected using TLS because of the aforementioned changes in laser beam reflection intensity. Figure 7 displays the segmented area of the point cloud enhanced with intensities, where

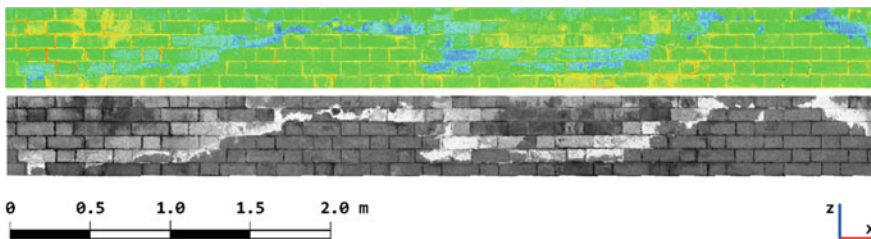
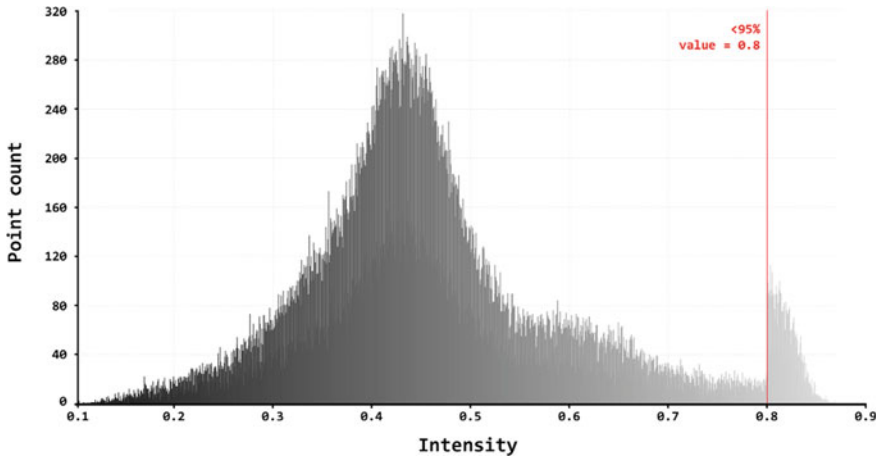


Fig. 7 Segmented wall sector point cloud: top: blue–green–yellow–red; bottom: monochrome





**Fig. 8** Greyscale histogram of points and intensities

the more severe efflorescences are shown in blue and light grey to white colours, respectively.

No scan registration diagnostics are provided in this case because the 3D survey consisted of a single scan.

Given the reduced number of points in comparison with the St. Andrew's Church case study, the analysis of the point cloud intensities was carried out considering 2000 classes. Figure 8 shows the histogram of point cloud data intensities.

The analysis yielded the following data:

- 119,772 values (points displaying intensity);
- Mean: 59.89 points (for each intensity value);
- Standard deviation: 65.89 points;
- Image digital level (Digital Number, DN): from 39 to 223 (dark grey to light grey in the histogram);
- Digital level for 0.8 intensity value: 203.

Unlike the more gradual behaviour of the point count rate in the buttress case study, the histogram above (Fig. 8) presents a breaking point in the distribution of points among the intensity intervals in the region of 0.55 intensity value. Considering Figs. 7 and 8 together, 0.55 could represent the starting intensity value of the pathology (efflorescences), which is on the right side of the histogram, by the highest intensities. However, it is the sudden increase in the number of points for the 0.8 intensity value that causes it to become a PoI in the histogram, leaving 5% of points above.

Next, the relationship between the surface pathology, the point cloud intensities, and the DN of the images should be addressed. In the histogram's greyscale range (image DN from 39 to 223), the starting and ending colours are not black and white, respectively. Therefore, that range differs from the full range [0, 255] (256 levels, 8-bit encoding) of the point cloud intensities in Fig. 7 (from black to white), which makes



it necessary to convert the former values into a comprehensive scale. Considering the current scale:

0.77 #highest value of the histogram intensity range [0.1, 0.87]#  $\rightarrow$  255 (highest DN);

then:

$$0.70 \text{ \#PoIs intensity\#} \rightarrow 231.82 \approx 232,$$

meaning that the DN of the PoI is 232 (starting DN of the remaining 5% points) within the full greyscale range [0, 255].

Scale conversion:

$$232 \div 255 \text{ (highest DN)} \approx 0.91;$$

then:

$$223 \text{ (histograms scale)} \times 0.91 \approx 203,$$

which is the PoI's (0.8 intensity value) DN measured in the histogram.

In view of those results, 5% of the points are within 9% of the intensities, which correspond to the highest values. Therefore, it can be stated that the most affected region of the pathology comprises those DN from 232 to 255 (white). Hence, filtering by intensity value, it is possible to extract that 5% of points (6004) from 0.8 to approximately 0.87 intensity. In this way, the most affected part of the building surface deficiency (0.13 m<sup>2</sup>) can be detached from the rest of the sector (the total area is 2.63 m<sup>2</sup>). It is also worth quantifying the intensities ranging from 0.55 (value where the efflorescences start) to 0.8 (lowest value of the most affected area). In this case, there are 20,369 points affected, 17% of the total number of points in the original segmented sector. Therefore, the complete pathology represents at least 22% of the entire surface area, approximately 0.58 m<sup>2</sup>. The intensity values mentioned above were verified by enquiring the DN of the colour of points in the images, such as the starting and ending value of the ranges, and the PoI. Figure 9 shows the entire pathology subdivided into the affected zone and the most affected area, both filtered by the corresponding intensity values above.

Finally, both case studies should be discussed together. As seen in the results, the arrangement of points of the St. Andrew's Church pathology is gradual, whereas the Bromley House's wall sector presents a clear symmetry breaking point around the 0.55 intensity value and a radical change in the distribution of intensities at 0.8. Besides, the coefficient of variation is 1.10 in the Bromley House wall sector, significantly lower than those in the first case study. By concept, this indicates a lower dispersion of the data; i.e. the distribution of points per intensity interval is more homogeneous. Nevertheless, this means a higher range of intensities corresponding to the pathology; in other words, the pathologies stand out from the reference range of intensities (the rest of the wall sector with no surface deficiency).

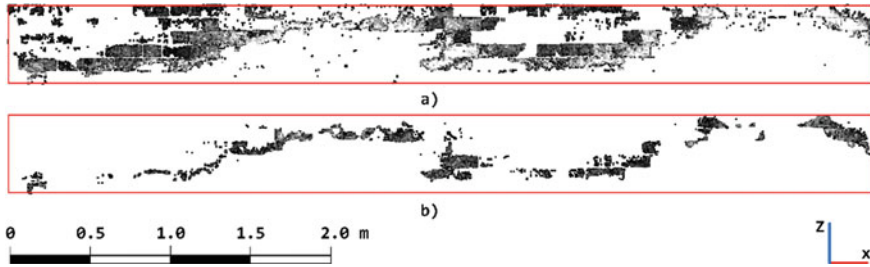


**Fig. 9** Filtered efflorescences, in monochrome: **a** intensity value range [0.55, 0.8]; **b** intensity value range [0.8, 0.87]

In addition to the laser beam incidence angle, it is the surface colours that determine the point cloud intensities. In this way, the values of the dark stains on the buttress differ from those of the light grey to white efflorescence on Bromley House. As per the histograms above, the values of the former are consequently lower than those of the latter. Yet, it is demonstrated that TLS, as a remote sensing technique, enables an accurate level of discrimination of surface deficiencies from the non-pathological zones via the analysis of the point cloud intensities.

## 4.2 Research Limitations

Although the findings of this research derive from a thorough methodology description, and both the qualitative and quantitative analysis of the resulting data, a greater number of samples could provide outcomes of a more robust nature. In relation to the characterisation of pathologies through the laser beam intensity fingerprint, further case studies could lead to a specific analysis of each specific type of deficiency. Besides, the methodology of this research did not take into account the roughness of the surfaces. The produced and filtered intensities were considered to calculate and distinguish between pathologies (most affected points) and reference zones. Finally, some occlusion occurred because of the intrinsic roughness of the masonry blocks of the St. Andrew's Church buttress and the lack of a higher TLS station in the 3D survey. However, the completeness of the dataset has sufficed to draw the above data and the conclusions below.

## 5 Conclusions

Considering their higher efficiency and accuracy in comparison with traditional methods, previous studies in the field of building surface anomalies have relied on massive data capture technologies to detect and analyse these pathologies. In

this sense, TLS constitutes a particularly interesting option because it allows for recording the intensity of the laser beam reflection onto the objects surveyed. In addition, research has addressed the identification and classification of damaged areas via machine learning and the analysis of TLS radiometric data. However, no research has been found on the analysis of the laser scanning intensity fingerprint of building surface deficiencies. For that purpose, this research analyses the distribution of intensities throughout the geometric data of the selected case studies. In this way, specific intensity values reveal an unusual behaviour in the point count rate among the intensity intervals for a specific type of pathology. This, verified by measuring the digital number (DN) of the deficiencies in the images, leads to filtering the point clouds in order to extract the affected areas. Consequently, the pathologies—and their different degrees—can be quantitatively analysed in the general context of the building component surface. Therefore, based on the analysis of the intensity fingerprint, the TLS remote sensing technique is proven to be useful to record, detect, characterise, and examine specific building surface deficiencies and carry out the conservation status analysis of the buildings surveyed.

Finally, according to one of the conclusions drawn by Dias et al. [6], TLS enables the automation of the visual inspection of façades, and the diagnosis of their degradation condition. Nevertheless, this research reveals that future work on this research topic should be carried out to automate the analysis of the intensity data of building surface deficiencies since the process is at best semi-automatic so far. In this way, a software solution should be sought to fully automate the point cloud filtering and pathology mapping to determine the affected area.

**Acknowledgements** This work has been funded by the England European Regional Development Fund (ERDF) as part of the European Structural and Investment Funds Growth Programme 2014–2020, the University of Nottingham and Nottingham Trent University through the Live Experiential and Digital Diversification—Nottingham (LEADD: NG) project (Project Number: 08R20S04177).

The authors also wish to thank the School of Architecture, Design and the Built Environment, Nottingham Trent University, for access to their TLS equipment and workstations for data processing. Special thanks to St. John the Baptist Beeston Parish Church for willingly granting access to their facilities.

## References

1. Antón D, Amaro-Mellado J-L (2021) Engineering graphics for thermal assessment: 3D thermal data visualisation based on infrared thermography, GIS and 3D point cloud processing software. *Symmetry (Basel)* 13:335. <https://doi.org/10.3390/sym13020335>
2. Antón D, Medjdoub B, Shrahily R, Moyano J (2018) Accuracy evaluation of the semi-automatic 3D modeling for historical building information models. *Int J Archit Heritage* 12:790–805. <https://doi.org/10.1080/15583058.2017.1415391>
3. Antón D, Pineda P, Medjdoub B, Iranzo A (2019) As-built 3D heritage city modelling to support numerical structural analysis: application to the assessment of an archaeological remain. *Remote Sens* 11:1276. <https://doi.org/10.3390/rs11111276>

4. Armesto-González J, Riveiro-Rodríguez B, González-Aguilera D, Rivas-Brea MT (2010) Terrestrial laser scanning intensity data applied to damage detection for historical buildings. *J Archaeol Sci* 37:3037–3047. <https://doi.org/10.1016/j.jas.2010.06.031>
5. Delgado JMPQ (2021) Case studies of building rehabilitation and design. Springer International Publishing, Cham
6. Dias I, Flores-Colen I, Silva A (2021) Critical analysis about emerging technologies for building's façade inspection. *Buildings* 11:53. <https://doi.org/10.3390/buildings11020053>
7. Girardeau-Montaut D (2016) CloudCompare: 3D point cloud and mesh processing software. Open Source Project
8. Google Inc. (2021) Street view. In: What is str. view? <https://www.google.com/intl/eng/streetview/>. Accessed 22 Dec 2021
9. He K, Jia MT, Mei-Fang C (2020) Entropy evaluation method for sandstone uranium reservoir characteristics based on convex hull search. *IEEE Access* 8:46307–46323. <https://doi.org/10.1109/ACCESS.2020.2978153>
10. Hichri N, Stefani, De Luca, Veron P (2013) Review of the «As-Built Bim» approaches. *Int Arch Photogramm Remote Sens Spat Inf Sci ISPRS Arch XL-5/W1:107–112*. <https://doi.org/10.5194/isprsarchives-XL-5-W1-107-2013>
11. Historic England (1995) Church of St. Andrew's and attached former Sunday school, Non Civil Parish—1270832. In: Listing. <https://historicengland.org.uk/listing/the-list/list-entry/1270832>. Accessed 6 Aug 2021
12. Historic England (1995) Boundary wall, railings and gates to Church of St Andrew, Non Civil Parish—1247549. In: Listing. <https://historicengland.org.uk/listing/the-list/list-entry/1247549>. Accessed 21 Dec 2021
13. Historic England (2021) Search the list—find listed buildings, monuments, battlefields and more. In: Listing. <https://historicengland.org.uk/listing/the-list/>. Accessed 22 Dec 2021
14. Historic England (1987) Church of St John the Baptist, non civil Parish—1263823. In: Listing. <https://historicengland.org.uk/listing/the-list/list-entry/1263823>. Accessed 7 Dec 2021
15. Historic England (1987) Village cross, non civil Parish—1263870. In: Listing. <https://historicengland.org.uk/listing/the-list/list-entry/1263870>. Accessed 21 Dec 2021
16. Kim M, Sohn H, Chang C-C (2015) Localization and quantification of concrete spalling defects using terrestrial laser scanning. *J Comput Civ Eng* 29:04014086. [https://doi.org/10.1061/\(ASCE\)CP.1943-5487.0000415](https://doi.org/10.1061/(ASCE)CP.1943-5487.0000415)
17. Leica Geosystems (2012) Leica ScanStation P20—industry's best performing ultra-high speed scanner. In: Scanners. [http://w3.leica-geosystems.com/downloads/123/hds/hds/ScanStation\\_P20/brochures-datasheet/Leica\\_ScanStation\\_P20\\_DAT\\_us.pdf](http://w3.leica-geosystems.com/downloads/123/hds/hds/ScanStation_P20/brochures-datasheet/Leica_ScanStation_P20_DAT_us.pdf). Accessed 15 June 2021
18. Leica Geosystems (2019) Leica cyclone—3D point cloud processing software
19. Lerma C, Mas Á, Gil E et al (2014) Pathology of building materials in historic buildings. Relationship between laboratory testing and infrared thermography. *Mater Constr* 64:e009. <https://doi.org/10.3989/mc.2013.06612>
20. Lezzerini M, Antonelli F, Columbu S et al (2016) Cultural heritage documentation and conservation: three-dimensional (3D) laser scanning and geographical information system (GIS) techniques for thematic mapping of facade stonework of St. Nicholas Church (Pisa, Italy). *Int J Archit Heritage* 10:9–19. <https://doi.org/10.1080/15583058.2014.924605>
21. Mallafrè Balsells C, López Besora JM, Costa Jover A, Coll Pla S (2021) Register of dry stone domes. simplified method for point clouds. *Nexus Netw J* 23:493–506. <https://doi.org/10.1007/S00004-020-00533-W/FIGURES/8>
22. Masiero A, Costantino D (2019) TLS for detecting small damages on a building façade. *Int Arch Photogramm Remote Sens Spat Inf Sci XLII-2/W11:831–836*. <https://doi.org/10.5194/isprs-archives-XLII-2-W11-831-2019>
23. Sitzia F, Lisci C, Mirão J (2021) Building pathology and environment: weathering and decay of stone construction materials subjected to a Csa mediterranean climate laboratory simulation. *Constr Build Mater* 300:124311. <https://doi.org/10.1016/j.conbuildmat.2021.124311>
24. Smith M, Gorse C (2021) Building surveyor's pocket book, 1st edn. Routledge, Abingdon, Oxon; New York, NY

25. St. Andrew's with Castle Gate United Reformed Church (2021) St. Andrew's with castle gate United Reformed Church. In: St. Andrew's with castle gate United Reform. Church—living God's love through faith action. <https://standrewswithcastlegate.org.uk/>. Accessed 6 Aug 2021
26. Suchocki C, Błaszczak-Bąk W, Janicka J, Dumalski A (2021) Detection of defects in building walls using modified OptD method for down-sampling of point clouds. *Build Res Inf* 49:197–215. <https://doi.org/10.1080/09613218.2020.1729687>
27. The Southwell and Nottingham Church History Project (2021) Beeston St. John the Baptist. In: Southwell Nottingham Church history project. <https://southwellchurches.nottingham.ac.uk/beeston/hintro.php>. Accessed 7 Dec 2021
28. Valero E, Forster A, Bosché F et al (2019) Automated defect detection and classification in ashlar masonry walls using machine learning. *Autom Constr* 106:102846. <https://doi.org/10.1016/j.autcon.2019.102846>

# The Semantic Discretization of Architectural Heritage as the Basis of a HBIM Restoration and Conservation Project



Juan E. Nieto-Julián, Javier Farratel, Manuel Bouzas Cavada, and Juan Moyano-Campos

**Abstract** In the archeology of architecture, the paramental study requires documentation techniques in order to identify, classify, and document the different stratigraphies that appear in historical buildings. The documentation must be objective, independent, and systematic and must also contain a record that allows the monitoring of specialist technicians in this field. The emergence of technologies based on BIM has opened a new scenario in the 3D registry of heritage buildings. Thus, to reinforce the implementation of the work carried out in heritage, this research carries out an experimentation through a semi-automatic sequence of stratigraphic units in ashlar with complex geometries. The workflow has been developed on the ArchiCAD platform, included in a Teamwork HBIM restoration and conservation project, allowing the sequencing of automatic classification processes, which in the archeology area would be very complex to carry out. To do this, the connection script between ArchiCAD and Python is reconditioned, which works as a Python link for the ARCHICAD JSON interface. The results, although in several initial phases, present classification problems when the stratigraphic units present overlaps, we proceed to improve in such a way that there is a classification in a structured and orderly way. The advantages of obtaining this type of classification in a digital model are innumerable, since each element of ashlar, stone or pilaster contains semantic properties and precise geometric properties that enrich each one of the interventions in a workflow between BIM operators and teams restoration technicians.

**Keywords** HBIM · Paramental analysis · Building archeology · Terrestrial laser scanning

## 1 Introduction

Restoring cultural heritage is one of the great objectives of the scientific community due to its exceptional value and the positive impact that tourism has on economic

---

J. E. Nieto-Julián (✉) · J. Farratel · M. Bouzas Cavada · J. Moyano-Campos  
Departamento de Expresión Gráfica e Ingeniería en la Edificación, Universidad de Sevilla, Sevilla, Spain  
e-mail: [jenieto@us.es](mailto:jenieto@us.es)

growth and development [1]. Heritage is defined as a set of assets worthy of being conserved for the nation for reasons of art and culture (R.D. 1926). In the field of architecture, heritage assets acquire special attention due to their need to control the unique geometry of heritage buildings. The way of modeling architectural heritage has acquired a dizzying advance by the development of technologies for data capture and multi-resolution 3D representation. To these new technologies related to geomatics is added the new operability acquired by BIM platforms. The National BIM Standard-United States [2] defines them as an integrated information model for construction, which acts as a true digital twin in the sense that it has a digital representation of physical and functional characteristics in the field of construction and engineering. Currently the construction sector has assumed the importance of working with BIM, with more and more countries, on a global level, that are developing solid implementation strategies dictated by governing institutions created for this purpose. On the other hand, in the sector of historic buildings, this digital technology is not implemented. As exceptional cases, administrations in Spain admit restoration projects that present Structure from Motion (SfM) or Terrestrial Scanning Laser (TLS) works as data acquisition techniques, and for this civil service sector, it represents a great advance. But public administrations are still unaware of the potential of the BIM methodology and its applicability in Heritage. In this sense, the use of Historic Building Information Modeling (HBIM) allows three-dimensional digital integration and qualitative and quantitative information of the objects that compose them [3]; this information model establishes operating conditions with the technical teams, and this is the key to the technologies supported by BIM platforms and their applicability in architectural and archeological heritage. Some of these technologies go hand in hand with the acquisition of low-cost, high-definition data that put at the service of professionals, researchers, and academics a tool capable of developing elements with complex shapes in a precise and efficient way. In the field of archeology and archeological architecture, the ways of proceeding in a modeling are complex and the heritage has the need of an analysis on the treatment of rehabilitation of facades and envelopes. Many of these works are focused on Infrared Thermography (ITR) technologies to detect façade cracking and degradation, which is why ITR is being used as a non-destructive inspection technique [4]. In this sense, HBIM, as a management system, allows integrating data from scientific analyzes as a data operator in a digital model, where heritage intervention projects contain the phases of intervention design, planning, organization of work, registration of physical data, maintenance, and monitoring of deteriorations that occur in the heritage.

## 2 Related Work

The operators of the conservation and restoration of cultural heritage (CH) can carry out an efficient work, strengthening the dissemination and sharing of specific information with precision techniques and innovative methodologies; today, those provided by geomatics and the Open BIM methodology [5]. Are used, in this line,

numerous studies have been in charge of analyzing which are the best methods for erecting buildings [6–8] but none of the works values establishing a difference in large architectural spaces, simply because there is no single technique that is global to a general survey. Each technique has their specific specificities, for example in Unmanned Aerial Vehicles (AUVs) image captures where they comprise three-dimensional geological model spaces [9] with the combination of BIM, there are numerous case studies with TLS and UAV [10] where the captures of images cannot be made by means of short-range photogrammetry or terrestrial laser scanners, since these do not capture upper levels of buildings, leaving spaces without records. However, precision techniques are necessary to reach BIM platforms, and they are capable of capturing them as auxiliary systems to aid 3D surveys. On the other hand, technical teams, such as restorers, historians, architects, are aware of the need for the historic building to renew its heritage value, but it is not possible to decide what is truly valuable without the mechanisms of historical analysis [11] and have a multidisciplinary intervention protocol facilitating the Archeology of Architecture. In this panorama, the BIM concept is introduced as a mechanism of action and reversal. The area of archeology in stratigraphic issues has its best mentor to the researcher Carandini, who published his book *Store dalla terra* [12] in the 1981 edition. The approach in its research phase gives results on the coordination mechanisms in the world of wealth management. On the other hand, Italian architects such as Treccani et al. [13] defend the adaptation of the stratigraphic registration system to the specifications of the architectural context. Thus restoring means restoring to objects their meaning, the semantic value they had in the past, and their stratigraphic contextualization [14]. So, the stratigraphy remains as the collective memory with its reality and essence. It is a laboratory for the analysis of the reading of facades where the archeological perspective is applied to the architecture itself, such as the work of Blanco-Rotea [15] in the Church of San Fiz de Solovio (A Coruña), medieval paramental analysis. The construction of 3D models in the archeological field represents one of the most complex data, both from a geometric point of view and from the topological level [16]. The availability of a paramental catalog of classified elements and forms enables archeologists and researchers to envision a historical data environment. In a sequence of study of data acquisition techniques, the point cloud is not structured entities, they are recorded without typologies and without semantic discretization [17] on the other hand, BIM requires very defined relationships because they will depend on the elements where they are placed and established semantic units. The first studies on BIM in a paramental analysis scenario that identify stratigraphic units after the intervention of the facades of the RFTS Jail of the University of Seville [11]. Later Diara et al. [18] analyzed a stratigraphic sequence through the FreeCAD software. Angulo-Fornos and Castellano-Román [19] work on associated chronological filtering information assigned to a BIM model. Each of the pieces is assigned to a filtering display of the facing in a Renaissance-style sector of the Seville Cathedral. And on this basis of semantic construction, applied geomatics techniques are essential for semantic discretization, where the 3D virtual model that represents any architectural object implies an organization of digital elements in discretized pieces, that is, segmented into meaningful units. And this process is common to



any workflow applied in BIM [20], it is even possible to analyze what the elements, ashlar, stones or cladding are like depending on the semantic segmentation, be it manual or semi-automatic, since we are far away automatic processes.

### 3 Methodology

#### 3.1 General Framework

In Spain, as in other countries bordering the Mediterranean, we can enjoy a rich Historical Artistic Heritage, which implies the need to protect and preserve it. The Public Administrations of the State are aware that it represents a great asset to strengthen the economy of a country, since it represents economic growth and social development, especially in parts of specific regions and provinces. But interventions have an important intervention decision. According to Harris [21] “... *the act of intervening... causes destruction.*” A restoration project must delimit the actions and meditate extensively on what is discarded, what is maintained, and, consequently, specify the treatment of the materials that remain. Therefore, at the end of the new stage in the restoration, a new architecture will have been defined, establishing a new layer within its constructive evolution. With the BIM paradigm and the recent appearance of Internet of Things (IoT) applications, new opportunities for decision-making are offered; more effective specific applications and tools that, for the present case, will benefit the workflow of a multidisciplinary heritage team, thus reinforcing the interoperability of the technical teams involved; archeologists, architects, historians, engineers, and restorers.

The 3D virtual model involves the organized composition of digital elements. This is a process that, according to Bianchi and Potestá [20], is common to any 3D modeling workflow. But when BIM methodology is applied to historical construction processes, there is a correspondence between rehabilitation processes in the real world and the virtual world. In this framework in a historical building, a 3D model is developed for the HBIM project, which considers the temporary component in the conformation of its architecture, with its singularities, arising from the use of materials and construction techniques typical of the place and that are represented throughout the life cycle of the building. The document exposes a methodology for the automatic identification of the integral elements of the walls, masonry of carved ashlar that close the envelope of a historic building from the sixteenth century. Previously, it has been necessary to develop a segmentation based on a semantic study of the construction systems of its historical architecture.

### 3.2 Case Study

As a case study, the Hermitage of San Antonio, known as Capela de San Brais, in the municipality of O Porriño, an example of religious construction in the province of Pontevedra, Galicia region, north of Spain is chosen. It is a small Gothic-style hermitage dating from 1528 and classified as Cultural Heritage in the category of Religious Architecture. It was rebuilt almost in its entirety in 1738 and today its historical value lies in the plementery of the stone factory that makes up its facades. As can be seen in Fig. 1, the portal presents a double pediment-like arcaded structure, scaled inside and containing the main entrance to the architectural monument. It is adorned with fluted pilasters and topped with small pinnacles at the ends. To cover the top of the front of the facade, there is a bell tower as a temple with clear Gothic features. Another of the artistic elements is the cross from the sixteenth century, protection of walkers on the itinerary to Santiago de Compostela.

Currently, the building intervention project is in charge of the architect Manuel Bouzas, who designed the intervention control instruments based on the collection of historical documentation, including existing texts, drawings, and plans from earlier times. Subsequently, a metric survey is carried out through two campaigns using Massive Data Capture Systems (MDCSs); one by Photogrammetry (SfM) and the other by Terrestrial Laser Scanner (TLS). Then, on the basis of the geometric data provided, the development of an efficient HBIM project is carried out. This project favors the functionality of the structural management of the Chapel, knowledge of the deformations that it has from a comparison between the model and the data bases, and, on the other hand, the integration of the elements of conservation and maintenance in the interventions to be carried out. The building's settlement problems have caused movements of the structural elements that have been moved to the walls and roofs. Dirt is also evident on the surfaces of the stonework on the side of the chapel, as well

**Fig. 1** Exteriors of the San Antonio—San Brais



as specific problems of degradation of the material on the roof, are also evident. It is therefore a building that presents ideal conditions to allow diagnostic.

### **3.3 Data Collection**

3D modeling focused on cultural heritage has two very broad fields of study; one is the area of geomatics engineering and geospatial technology, which we call geomatics, and another that includes computer engineering. The laser scanning technique and the photogrammetry technique are the most relevant and widely used data acquisition techniques for the 3D representation of historical monuments [22]. Although the post-processing chain that consumes resources and time is known, the reality is that a set of data is obtained that explains the success of its work, such as precision, realistic representation, and the possibilities that it has of transfer with the current BIM platforms allowing the adjusted reconstruction of the model. In a first work, published in [23], previous works were carried out on the compilation of historical documents, the auscultation process and the execution of Terrestrial Laser Scanning (TLS) works that were carried out in the entire building and its surroundings. The Structure from Motion (SfM) technique section was dedicated to the façade and niche at the front of the plot. The TLS data set was processed in a single coupling and alignment of the subsets of points obtained by the different stationings of the laser station (BLK360 Leica). The usual procedure of selecting and rotating each scan to a single and common coordinate system, aims to obtain as a final product a faithful 3D geometry of the historic building in the form of points with coordinates  $X$ ,  $Y$ ,  $Z$  and color  $R$ ,  $G$ ,  $B$ . The coupling and alignment of the point clouds are usually carried out by identifying visible homologous points, well marked, or having strategic targets to be identified from different positions of the laser scanner [24, 25].

From the data set, the point cloud is incorporated into a collaborative HBIM “Teamwork” project. The textured point cloud provides accurate measurements of the current state of Capela de San Brais. In addition, it incorporates data related to structural pathologies, be they deformations of the walls or other indicators that allow real-time auscultation of the state of the historic building (Fig. 2).

### **3.4 Database Structure**

The HBIM project is structured in its beginnings from the three-dimensional point cloud acquired by TLS. Thus, a theoretical 3D model is built, where the deformations of the walls can be analyzed. The component in the decision of the geometry of the walls is made through the average of the wall dimensions that appear as main vectors. This faithful model is incorporated into the HBIM collaborative project, together with all the documentation collected to date, and prepared for new adaptations to subsequent studies or future findings. All disciplines that collaborate in



**Fig. 2** Visualization of the imported global point cloud in the Teamwork Project (ArchiCAD Graphisoft)

the management of specific information to be entered into a common “3D database” (CDE) will be taken into account. The structure of the project can be summarized as follows: (i) From the BIM platform used, ArchiCAD V.25, the collaborative rehabilitation project “TeamWork” is managed. The project is shared by the intervening agents: lead architect, execution engineer, BIM manager and modeler, or moderators of the writing team. (ii) The “TeamWork” project “TeamWork” is uploaded to the cloud—BIMcloud Graphisoft [26] to be accessible to all participants, facilitating data interoperability; and that, depending on their assigned role, each member of the team can provide specific information. (iii) In the next phase, to reinforce Open BIM interoperability with technical teams or consultants, the HBIM project will be managed in IFC (Industry Foundation Classes) format, making the information flow more flexible with the created CDE. (iv) The generated IFC model will be approved in each established time phase to be uploaded to the server that supports the data base, marked with a revision ID, and accessible by all members of the team and property. This “Open” system allows the BIM model data to be synchronized with other digital data management, processing and analysis platforms.

### **3.5 Semantic Discretization**

Semantic discretization is a relatively new concept [27], in which semantics refers to the knowledge of the data inherent to the element, so semantic discretization can be applied to the identification, classification, and interpretation of the data. The first time it is used in a scientific text related to HBIM is in charge of Garagnani

and Manferdini [17], and in [28] to refer to the structuring of geometric representations of solid models in 3D meshes. In the process of building a 3D model, the Delivery Level of Development (LOD) must be established, where the minimum level of detail (d) of construction and geometric systems (LOd) is identified, which must be described together with the information (i) characteristic associated with the elements and systems (constructive, evolutionary, installations, among others) (LOi). The intervention proposal must start with an essential model through an LOD (LOd + i)-100 where the walls and roofs of the delimited areas are defined, with their fundamental proportions. Although a specific mixed LOD approach is assumed from the beginning, capable of incorporating the singularities of the architectural, archeological, and artistic heritage of the intervened monument. This degree of knowledge must be endorsed by all participatory disciplines, and a consensus on restoration and preservation actions [29].

These LOD levels explore the definition of the model in a linear process throughout different phases; from the LOD-100 representing a conceptual model, to a LOD-500 representing an “as-built” model. Therefore, the LODt depends on time and its degree of definition [30]. In this research, the HBIM-0 model starts with the insertion of the point cloud in the project, a pedestal for an analysis of its geometry and materiality; and then starts modeling. It is here that more specific geometries of construction systems are established based on parametric elements of the BIM model.

The exposed project has been adapted to the uniqueness of the restoration process of a historic building, enriched with a high Geometry Level (LOG) related to a high Precision Level as a result of the high-resolution survey (TLS + SfM) (Fig. 3).

In addition to LOD levels, different level standards are currently being adapted aimed at knowledge of the modes of action in PH, defined by Castellano-Román

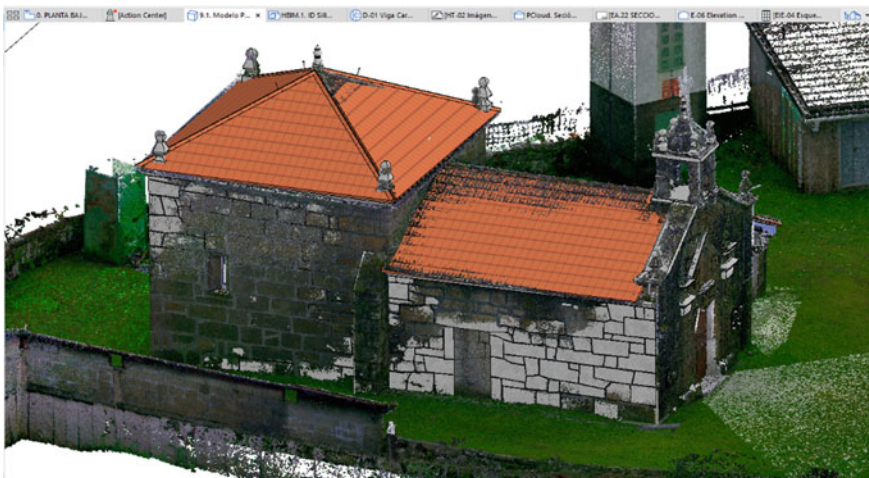


**Fig. 3** Parametric model of the Capela de San Brais, adapted to the precise geometry provided by the global point cloud, imported into the Teamwork HBIM project

and Pinto-Puerto [31] as Level of Knowledge (LOK). It starts from an LOK100, associated with basic identification levels of the architectural asset, up to the LOK500 where comprehensive management is achieved. Therefore, the first study to know the construction systems of the historical architecture of the building is to know that the Hermitage of San Brais was reformed in the eighteenth century, specifically around the year 1738, without much documentation being available, although due to its uniform factories suggest that it was rebuilt in its entirety. This fact certifies the non-existence of a transposition of different techniques in the arrangement of the exterior masonry. The authors estimate that the type of stone used is synchronous, that is, its analysis is under investigation at the time of the study. For this reason, the stratigraphic methodology used has not been complex, since the study provides clear results to determine the temporal evolution of the elements analyzed.

From the point of view of the graphical model, having the HBIM-0 model of the point cloud on the same platform allows the semi-automatic segmentation to be processed directly [30]. An efficient process, where auxiliary work, such as CAD vectoring, has not been necessary to obtain the stratigraphic sequence of the model. Nor has it been necessary to transform the point cloud into mesh or NURBS surfaces, as is the case in the work by Diara and Rinaudo [32] in which a stratigraphic survey of Staffarda's refectory was carried out applying the Harris matrix and using Non-Uniform Rational Basis-Splines (NURBS) on complex surfaces. Other authors [19] determine the surfaces of the walls as an adaptation of photogrammetric digital capture, which constitutes a necessary "mold" to generate volumetric entities, of solid type using CAD applications, which will later be classified in the BIM modeling environment. This "semi-automatic nonparametric" modeling process has been discarded in the HBIM project for the restoration of the Capela de San Brais.

### 3.5.1 Properties Set Definition

All types of elements available in the HBIM project are classified by type based on their constructive property. This property is essential to filter and quantify elements and is later exposed in the BIM ArchiCAD platform schema as: "ElementType": *String, Wall, Column, Beam, Window, Door, Object, Lamp, Slab, Roof, Mesh, Zone, CurtainWall, Shell, Skylight, Morph, Stair, Railing, Opening*.

There are two different types of properties in ArchiCAD software, the first user-defined and integrated. The user-defined properties are those displayed in the Property Manager box. The user can modify the name of these properties and call that name to locate it. Its format can be found in the "UserDefinedPropertyUserId" schema. Instead, the built-in properties are those defined by the BIM software itself. The user cannot modify the name of these properties. They can only be accessed by their internal name. Its format can be found in the "BuiltInPropertyUserId" schema.



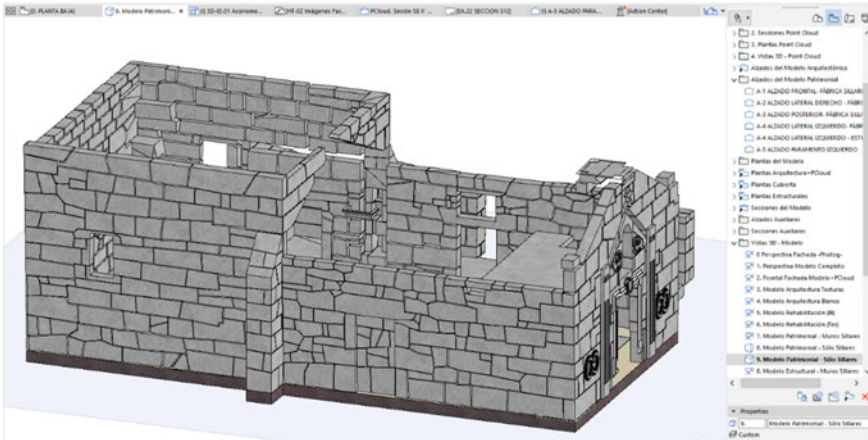


**Fig. 4** Axonometric view of the filtered model with all the elements with the ID “Sillar”

### 3.5.2 Classification

To raise the level of knowledge, it is first necessary to classify the pieces or ashlars by their location or structural function, taking into account the orientation of the container wall and its position. Interactive diagrams are developed that incorporate pre-established items to facilitate this classification of the ashlars. By its orientation of the facade (front, right, rear, left, covered). Due to its location (opening, bell tower, door flange, buttress, cornice, lintel, factory, niche, pilaster, sacristy, drum without cover). Due to its structural function (load element, element without load). Due to the construction material and its surface and finish characteristics. According to the standard classification of the area, region or country; BCCA, GuBIMclass, CYPE, among others, area, volume, and quantity.

As a final result, a total of 842 ashlars have been obtained, distributed by orientation in the outer envelope. Initially, all the pieces of the masonry walls are identified with the ID “Sillar.” The following figures show a perspective of the filtered model showing all the ashlars (Fig. 4), and the scheme of elements classified according to the established fields or items (Fig. 5).

### 3.6 Stratigraphic Identification Automation

The science that studies stratigraphy originally referred to geological and archeological layers had its beginnings with the researcher Roberto Parenti in 1985 [33], in which he contributed the first systematic study of a building from the paramental point of view. Subsequently, the so-called archeology of architecture was configured in which researchers such as Doglioni [34], or Brogiolo and Cagnana [35] were

TOTAL CLASSIFICATION OF SADDLES - SILLARES										
Layer	Fachada	Ubicación	Structural Function	Building Material	Surface	ARCHICAD Classification	BCCA_2017 - 1.0	GuBIMClass E.S - 1.2	Volume (by Story)	Quantity
01 ARQ_FCH_Sillares	Cubierta	Tambor s/Cubierta	Load-Bearing Element	Piedra - Estructural	Piedra - Granto Gris	Stone Masonry	06SS Sillares	20 20 10 30 Muros estructurales	0.99	20
	Fachada Derecha	Contrafuerte	Load-Bearing Element	Piedra - Estructural	Piedra - Granto Gris	Stone Masonry	06SS Sillares	20 20 10 30 Muros estructurales	1.51	29
	Fachada Derecha	Dintel/ Fábrica	Load-Bearing Element	Piedra - Estructural	Piedra - Granto Gris	Stone Masonry	06SS Sillares	20 20 10 30 Muros estructurales	0.19	3
	Fachada Derecha	Dintel/ Sacristía	Load-Bearing Element	Piedra - Estructural	Piedra - Granto Gris	Stone Masonry	06SS Sillares	20 20 10 30 Muros estructurales	0.09	1
	Fachada Derecha	Fábrica	Load-Bearing Element	Piedra - Estructural	Piedra - Granto Gris	Stone Masonry	06SS Sillares	20 20 10 30 Muros estructurales	11.69	231
	Fachada Derecha	Plastrá	Load-Bearing Element	Piedra - Estructural	Piedra - Granto Gris	Stone Masonry	06SS Sillares	20 20 10 30 Muros estructurales	0.61	20
	Fachada Derecha	Poyete	Non-Load-Bearing Element	Piedra - Estructural	Piedra - Granto Gris	Stone Masonry	06SS Sillares	20 20 10 30 Muros estructurales	0.13	4
	Fachada Derecha	Sacristía	Load-Bearing Element	Piedra - Estructural	Piedra - Granto Gris	Stone Masonry	06SS Sillares	20 20 10 30 Muros estructurales	0.52	10
	Fachada Frontal	Fábrica	Load-Bearing Element	Piedra - Estructural	Piedra - Granto Gris	Stone Masonry	06SS Sillares	20 20 10 30 Muros estructurales	7.69	108
	Fachada Izquierda	Cegado Puerta	Load-Bearing Element	Piedra - Estructural	Piedra - Granto Gris	Stone Bricks	06SS Sillares	20 20 10 30 Muros estructurales	0.49	12
	Fachada Izquierda	Contrafuerte	Load-Bearing Element	Piedra - Estructural	Piedra - Granto Gris	Stone Masonry	06SS Sillares	20 20 10 30 Muros estructurales	1.57	29
	Fachada Izquierda	Dintel	Load-Bearing Element	Piedra - Estructural	Piedra - Granto Gris	Stone Blocks	06SS Sillares	20 20 10 30 Muros estructurales	0.22	2
	Fachada Izquierda	Fábrica	Load-Bearing Element	Piedra - Estructural	Piedra - Granto Gris	Stone Blocks	06SS Sillares	20 20 10 30 Muros estructurales	4.86	101
	Fachada Izquierda	Fábrica	Load-Bearing Element	Piedra - Estructural	Piedra - Granto Gris	Stone Masonry	06SS Sillares	20 20 10 30 Muros estructurales	8.41	108
	Fachada Izquierda	Sacristía	Load-Bearing Element	Piedra - Estructural	Piedra - Granto Gris	Stone Masonry	06SS Sillares	20 20 10 30 Muros estructurales	3.88	37
	Fachada Trasera	Fábrica	Load-Bearing Element	Piedra - Estructural	Piedra - Granto Gris	Stone Masonry	06SS Sillares	20 20 10 30 Muros estructurales	9.82	127
										842

Fig. 5 Scheme of “Sillar” elements classified according to the established items. ArchiCAD 25

already present in 2012. Therefore, psychological studies are closely related to stratigraphic units, essentially on the Harris matrix [36] using a scheme or diagram for the graphic representation of the physical units arranged in chronological order. To make this chronological identification sequence effective within a project, HBIM is implemented through the ArchiCAD-Python connection, which works as a Python binding for the ARCHICAD JSON interface. Communication between ArchiCAD and Python occurs over HTTP using JSON messages. It is a language-independent data format, so any other programming language can be used to send commands to the BIM project. The ArchiCAD-Python API interface [37] helps to establish the connection, remaining embedded and always active.

The novelty of the research work is the experimentation of the use of the object-oriented programming language (OOP), a prototype where the data and the operations to be carried out with those data are grouped into logical units, called objects. His way of structuring the code, organizing and reusing it, is what makes it especially effective. The new ArchiCAD connection, V24 and higher, with Python allows one to run automation scripts within the BIM project. Revit also uses applications (API) by programming Python software [38, 39], although the latter does not reach its applicability. The use of predefined scripts, modifying existing types or writing new ones to customize the tasks applied to a specific job, brings benefits in that routine processes are automated that translate into greater effectiveness, time savings, and great productivity.

Python scripts perform a classification task based on the “ID” identifiers that incorporate the chosen parametric elements; it is for this reason that its suitability to apply it in the identification and orderly numbering of the ashlar of the masonry walls that closes the envelope of the Hermitage of San Brais has been appreciated.

Regarding the Identification of objects, in the API interface all objects (type elements, properties, classifications) are uniquely identified by “ID” objects; The



identifier “ElementId” is used for the element, “PropertyId” for properties, and “ClassificationItemId” for classification elements. Although the user will not be able to manufacture or modify said identifier objects, since they are considered black-box objects. With regard to ID recognition, IDs always have their own named object schema, and this name contains the word “ID.” The respective field names will refer to this schema as their own types; most of the time, they are called the same as the schema, purely “lowerCamelCase.”

## 4 Results

One of the objectives of this research is to expose the experimental work that is being carried out through a semi-automatic sequence of stratigraphic units in ashlar with complex geometries. See the enormous opportunity that BIM platforms have to sequence processes that otherwise in the area of archeology would be tedious and extremely complex. Experiments are being carried out in the implementation of the “Python” object programming on the BIM platform, through the ArchiCAD-Python connection, using the ARCHICAD JSON API interface. Adaptations of type scripts have been made, considered for their applicability in contemporary architectural designs and current construction systems, to the peculiarities of a wall of disordered pieces and irregular in size and shape.

For the case study, a panel on the left side has been selected, coinciding with the central nave of the Capela de San Brais, identifying and classifying the stone blocks of the masonry wall. First, each piece has been given an appropriate classification of the element according to its nature, collected in the ArchiCAD database: *Materials > Stone > Stone Masonry > Stone-Fabricated > Stone Block*, and later identified in the script as “ClassificationItemId” (Fig. 6). Other classifications have also been used according to national and international standards (BCCA, GuBIMclass, etc.). In this way, the script contains the ID “Stone Blocks” according to the figure (Fig. 7).

The execution of the script “Stone Blocks.py” has allowed the numbering of the blocks to move along a descending path through rows, from the extreme right to the extreme left and in an ascending direction. The Prefix “S” has been used before the number (three digits) automatically assigned to the element. Note that the first digit establishes the position of the element in relation to its height with respect to the reference level. The script variable “STORY\_GROUPING\_LIMIT” will set the maximum difference between the Z coordinates of the ID elements of the same story. Figure 8 shows the result after automatic numbering.

Specific schemes have also been drawn up for the classification of numbered ashlar. The following figures show the properties assigned to each “ashlar” element identified with a unique ID, also allows the specialist to interact in the stratigraphic study. You can make any change by box, with the correct choice between the different pre-established options in each property, being assigned and registered to the element within the BIM model (Fig. 9).

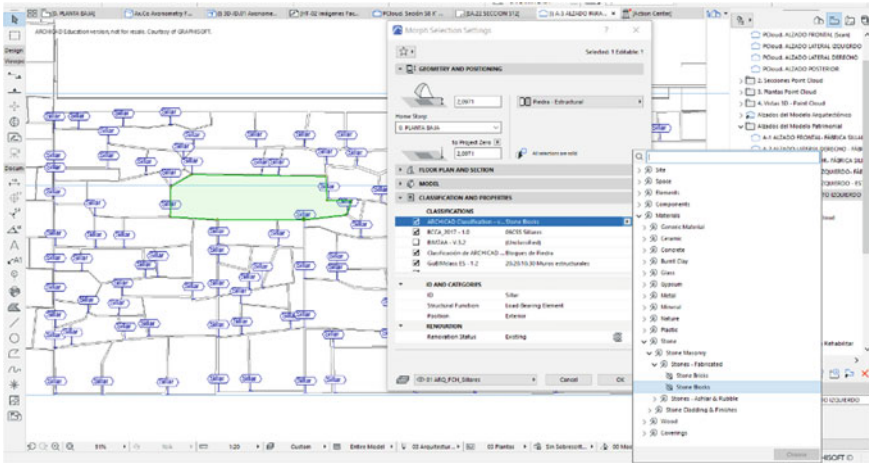


Fig. 6 BIM project interface (ArchiCAD), in the process of classifying a piece of stone masonry (stratigraphic unit), assigning it the classification “Stone Blocks”

```

from ArchiCAD import ACConnection
from typing import List, Tuple, Iterable
from itertools import cycle

conn = ACConnection.connect()
assert conn

acc = conn.commands
act = conn.types
acu = conn.utilities

##### CONFIGURATION #####
propertyId = acu.GetBuiltInPropertyId('General_ElementID')
propertyValueStringPrefix = 'S'
classificationItem = acu.FindClassificationItemInSystem(
    'ARCHICAD Classification', 'Stone Blocks')
elements = acc.GetElementsByClassification(
    classificationItem.classificationItemId)

ROW_GROUPING_LIMIT = 2
STORY_GROUPING_LIMIT = 2

def GeneratePropertyValueString(storyIndex: int, elemIndex: int) -> str:
    return f"{propertyValueStringPrefix}{storyIndex:1d}{elemIndex:02d}"
#####

def generatePropertyValue(storyIndex: int, elemIndex: int) ->
act.NormalStringPropertyValue:
    return act.NormalStringPropertyValue(GeneratePropertyValueString(storyIndex,
elemIndex))
    
```

Fig. 7 Initial script configuration within the JSON interface for the ArchiCAD-Python connection

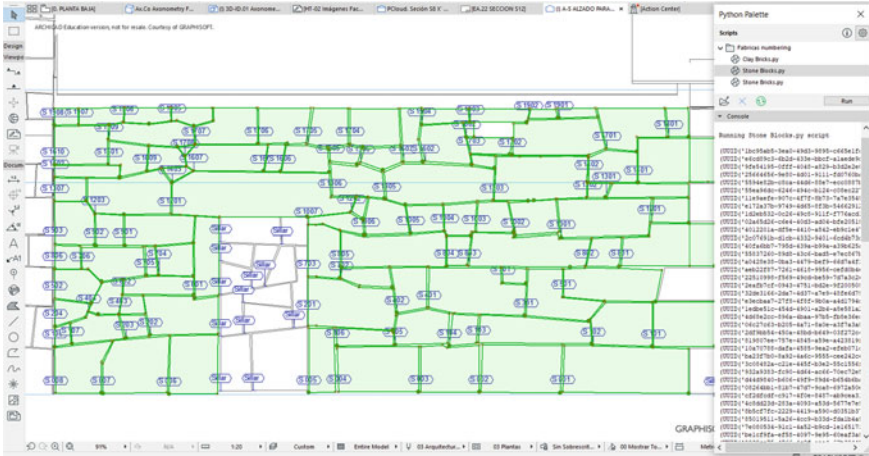


Fig. 8 Ashlar wall with its own ID (Snnn) after executing the Stone Blocks.py script (Python)

## 5 Discussion

The identification results obtained are satisfactory, considering that in several initial phases the procedure has presented problems of correlative numbering when the stratigraphic units present large changes and invade superior rows. Finally, the programming script has been debugged in such a way that there is a more structured and ordered classification, as shown in the results in the figures (Fig. 7). The advantages of obtaining this type of classification in a digital model are innumerable, since each element of ashlar, stone or pilaster contains semantic properties and precise geometric properties that enrich each one of the interventions in a workflow between BIM operators and teams and restoration technicians.

## 6 Conclusions

The initial results of this investigation allow one to determine a workflow of semi-automatic identification of parts in a stratigraphic analysis. This identification favors auscultation in the field of archeology and architecture. It is, therefore, an advance in the field of digitization of archeological and architectural heritage. The contribution in the construction of an HBIM project is recognized in accordance with the norms of the scientific and academic community, pending the applicability by the BIM operators and demanded by the Government Institutions. The use of “Python” object programming, applying a script adapted to the peculiarities of the architectural heritage of the time, has automated the identification of the pieces of the exploded wall. After the automation of routine processes, the intervention and/or preventive conservation actions become more effective for the management of the associated parameters,

Layer	Element ID	Ubicación	Fachada	Structural Function	Building Material	Surface	ARCHICAD Classification	Volume (by Story)	Quantity
01 ARQ_FCH_Sillares	S001	Fabrica	Fachada Izquierda	Load-Bearing Element	Piedra - Estructural	Piedra - Granito Gris	Stone Blocks	0.22	1
	S002	Fabrica	Fachada Izquierda	Load-Bearing Element	Piedra - Estructural	Piedra - Granito Gris	Stone Blocks	0.14	1
	S003	Fabrica	Fachada Izquierda	Load-Bearing Element	Piedra - Estructural	Piedra - Granito Gris	Stone Blocks	0.10	1
	S004	Fabrica	Fachada Izquierda	Load-Bearing Element	Piedra - Estructural	Piedra - Granito Gris	Stone Blocks	0.13	1
	S005	Fabrica	Fachada Izquierda	Load-Bearing Element	Piedra - Estructural	Piedra - Granito Gris	Stone Blocks	0.06	1
	S006	Fabrica	Fachada Izquierda	Load-Bearing Element	Piedra - Estructural	Piedra - Granito Gris	Stone Blocks	0.06	1
	S007	Fabrica	Fachada Izquierda	Load-Bearing Element	Piedra - Estructural	Piedra - Granito Gris	Stone Blocks	0.07	1
	S008	Fabrica	Fachada Izquierda	Load-Bearing Element	Piedra - Estructural	Piedra - Granito Gris	Stone Blocks	0.05	1
	S101	Fabrica	Fachada Izquierda	Load-Bearing Element	Piedra - Estructural	Piedra - Granito Gris	Stone Blocks	0.10	1
	S102	Fabrica	Fachada Izquierda	Load-Bearing Element	Piedra - Estructural	Piedra - Granito Gris	Stone Blocks	0.07	1
	S103	Fabrica	Fachada Izquierda	Load-Bearing Element	Piedra - Estructural	Piedra - Granito Gris	Stone Blocks	0.11	1
	S104	Fabrica	Fachada Izquierda	Load-Bearing Element	Piedra - Estructural	Piedra - Granito Gris	Stone Blocks	0.03	1
	S105	Fabrica	Fachada Izquierda	Load-Bearing Element	Piedra - Estructural	Piedra - Granito Gris	Stone Blocks	0.05	1
	S106	Fabrica	Fachada Izquierda	Load-Bearing Element	Piedra - Estructural	Piedra - Granito Gris	Stone Blocks	0.03	1
	S107	Fabrica	Fachada Izquierda	Load-Bearing Element	Piedra - Estructural	Piedra - Granito Gris	Stone Blocks	0.03	1
	S108	Fabrica	Fachada Izquierda	Load-Bearing Element	Piedra - Estructural	Piedra - Granito Gris	Stone Blocks	0.01	1
	S201	Fabrica	Fachada Izquierda	Load-Bearing Element	Piedra - Estructural	Piedra - Granito Gris	Stone Blocks	0.07	1
	S202	Fabrica	Fachada Izquierda	Load-Bearing Element	Piedra - Estructural	Piedra - Granito Gris	Stone Blocks	0.01	1
	S301	Fabrica	Fachada Izquierda	Load-Bearing Element	Piedra - Estructural	Piedra - Granito Gris	Stone Blocks	0.11	1
	S302	Fabrica	Fachada Izquierda	Load-Bearing Element	Piedra - Estructural	Piedra - Granito Gris	Stone Blocks	0.01	1
	S401	Fabrica	Fachada Izquierda	Load-Bearing Element	Piedra - Estructural	Piedra - Granito Gris	Stone Blocks	0.08	1
	S501	Fabrica	Fachada Izquierda	Load-Bearing Element	Piedra - Estructural	Piedra - Granito Gris	Stone Blocks	0.13	1
	S502	Fabrica	Fachada Izquierda	Load-Bearing Element	Piedra - Estructural	Piedra - Granito Gris	Stone Blocks	0.04	1
	S503	Fabrica	Fachada Izquierda	Load-Bearing Element	Piedra - Estructural	Piedra - Granito Gris	Stone Blocks	0.01	1
	S504	Fabrica	Fachada Izquierda	Load-Bearing Element	Piedra - Estructural	Piedra - Granito Gris	Stone Blocks	0.02	1
	S1801	Fabrica	Fachada Izquierda	Load-Bearing Element	Piedra - Estructural	Piedra - Granito Gris	Stone Blocks	0.09	1
	S1802	Fabrica	Fachada Izquierda	Load-Bearing Element	Piedra - Estructural	Piedra - Granito Gris	Stone Blocks	0.12	1
	S1803	Fabrica	Fachada Izquierda	Load-Bearing Element	Piedra - Estructural	Piedra - Granito Gris	Stone Blocks	0.03	1
	S18	Fabrica	Fachada Izquierda	Load-Bearing Element	Piedra - Estructural	Piedra - Granito Gris	Stone Blocks	0.07	1
	S1805	Fabrica	Fachada Izquierda	Load-Bearing Element	Piedra - Estructural	Piedra - Granito Gris	Stone Blocks	0.05	1
	S1806	Fabrica	Fachada Izquierda	Load-Bearing Element	Piedra - Estructural	Piedra - Granito Gris	Stone Blocks	0.06	1
	S1807	Fabrica	Fachada Izquierda	Load-Bearing Element	Piedra - Estructural	Piedra - Granito Gris	Stone Blocks	0.07	1
	S1808	Fabrica	Fachada Izquierda	Load-Bearing Element	Piedra - Estructural	Piedra - Granito Gris	Stone Blocks	0.00	1
	S1809	Fabrica	Fachada Izquierda	Load-Bearing Element	Piedra - Estructural	Piedra - Granito Gris	Stone Blocks	0.06	1
	S1901	Fabrica	Fachada Izquierda	Load-Bearing Element	Piedra - Estructural	Piedra - Granito Gris	Stone Blocks	0.02	1
	S1902	Fabrica	Fachada Izquierda	Load-Bearing Element	Piedra - Estructural	Piedra - Granito Gris	Stone Blocks	0.00	1
	S2001	Fabrica	Fachada Izquierda	Load-Bearing Element	Piedra - Estructural	Piedra - Granito Gris	Stone Blocks	0.01	1
	S2002	Fabrica	Fachada Izquierda	Load-Bearing Element	Piedra - Estructural	Piedra - Granito Gris	Stone Blocks	0.01	1
	S2003	Fabrica	Fachada Izquierda	Load-Bearing Element	Piedra - Estructural	Piedra - Granito Gris	Stone Blocks	0.03	1
	S2004	Fabrica	Fachada Izquierda	Load-Bearing Element	Piedra - Estructural	Piedra - Granito Gris	Stone Blocks	0.02	1
	S2005	Fabrica	Fachada Izquierda	Load-Bearing Element	Piedra - Estructural	Piedra - Granito Gris	Stone Blocks	0.02	1
	S2006	Fabrica	Fachada Izquierda	Load-Bearing Element	Piedra - Estructural	Piedra - Granito Gris	Stone Blocks	0.02	1
	S2007	Fabrica	Fachada Izquierda	Load-Bearing Element	Piedra - Estructural	Piedra - Granito Gris	Stone Blocks	0.02	1
	S2008	Fabrica	Fachada Izquierda	Load-Bearing Element	Piedra - Estructural	Piedra - Granito Gris	Stone Blocks	0.01	1
									103

Fig. 9 Ashlar scheme with a single ID, hyperlinked to the BIM model. It allows the choice or assignment of the type of property of the "ashlar" element among the different pre-established options

modifying and incorporating new data from the established CDE. The marked aspect of sustainability that a project presents through the Teamwork HBIM workflow in the restoration and conservation of historic buildings, has its importance in the masonry analysis stratigraphy work of archaeologists. The HBIM project provides 2D and 3D digital geometric representation, with millimeter precision after being captured through high-resolution equipment. The auscultation process becomes more effective in determining a logical transposition of elements and construction systems within the evolution of the building.

## References

1. Kim HJ, Chen MH, Jang SCS (2006) Tourism expansion and economic development: the case of Taiwan. *Tour Manage* 27:925–933. <https://doi.org/10.1016/j.tourman.2005.05.011>
2. Annex A, Rules C (2015) National BIM Standard-United States® Version 3
3. Castellano Román M (2015) Generación de un modelo de información del patrimonio inmueble en el momento de su protección jurídica. *EGA Rev Expresión Gráfica Arquitectónica* 20:266. <https://doi.org/10.4995/ega.2015.4060>
4. Bauer E, Milhomem PM, Aidar LAG (2018) Evaluating the damage degree of cracking in facades using infrared thermography. *J Civ Struct Heal Monit* 8:517–528. <https://doi.org/10.1007/S13349-018-0289-0/TABLES/2>
5. Nieto-Julián JE, Lara L, Moyano J (2021) Implementation of a TeamWork-HBIM for the management and sustainability of architectural heritage. *Sustainability* 13:2161. <https://doi.org/10.3390/su13042161>
6. Remondino F, Grazia M, Nocerino E, Menna F, Nex F (2013) Dense image matching: comparisons and analyses. In: *Proceedings of the IEEE digital heritage international congress (DigitalHeritage)*, Marseille, France, 28 Oct–1 Nov 2013, vol 1, pp 47–54
7. Fassi F, Fregonese L, Ackermann S, De Troia V (2013) Comparison between laser scanning and automated 3D modelling techniques to reconstruct complex and extensive cultural heritage areas. In: *International archives of the photogrammetry, remote sensing and spatial information sciences*, vol XL-5/W1, 2013 3D-ARCH 2013—3D Virtual reconstruction and visualization of complex architectures, 25–26 Feb 2013, vol XL, pp 25–26. <https://doi.org/10.5194/isprsarchives-XL-5-W1-73-2013>
8. Teza G, Pesci A, Ninfo A (2016) Morphological analysis for architectural applications: comparison between laser scanning and structure-from-motion photogrammetry. *J Surv Eng*
9. Tian J, Luo S, Wang X, Hu J, Yin J (2021) Crane lifting optimization and construction monitoring in steel bridge construction project based on BIM and UAV. In: *Advances in civil engineering*. <https://doi.org/10.1155/2021/5512229>
10. Martínez-Carricondo P, Carvajal-Ramírez F, Yero-Paneque L, Agüera-Vega F (2019) Combination of nadiral and oblique UAV photogrammetry and HBIM for the virtual reconstruction of cultural heritage. *Case Study Cortijo del Fraile in Níjar, Almería (Spain)* 48:140–159. <https://doi.org/10.1080/09613218.2019.1626213>
11. Nieto Julián JE, Moyano Campos JJ (2014) El Estudio Paramental en el Modelo de Información del Edificio Histórico o “Proyecto HBIM” [The paramental study on the model of information of historic building or “HBIM Project”]. *Virtual Archaeol Rev* 5:73–85
12. Carandini A (1996) *Storie dalla terra. Manuale di scavo archeologico*. Einaudi, Torino
13. Treccani GP, Braga S (Samanta), Cattaneo A (2000) *Archeologie, restauro, conservazione: mentalità e pratiche dell’archeologia nell’intervento sul costruito*. Unicopli. ISBN 88-400-0660-5
14. Azkarate Garai-Olaun A (2002) Intereses cognoscitivos y praxis social en Arqueología de la Arquitectura. *Arqueología de la Arquitectura* 55. <https://doi.org/10.3989/arq.arqt.2002.6>
15. Blanco-Rotea R (2005) The study of mediaeval architecture from an archaeological perspective. In: U. de L.S. du (ed) *Congrès., I.C. of P. and P.S., 14th 2001*. Archaeopress, p 95
16. Gaiani M, Gamberini E, Tonelli G (2002) A framework to use virtual worlds generated from real world 3D models as work tool for architectural & archaeological restoration on the web. [researchgate.net](http://researchgate.net)
17. Garagnani S, Manferdini AM (2013) Parametric accuracy: building information modeling process applied to the cultural heritage preservation. In: *International archives of the photogrammetry, remote sensing and spatial information sciences—ISPRS archives*, vol 40, pp 87–92
18. Diara F, Rinaudo F, Diara F, Rinaudo F (2020) Building archaeology documentation and analysis through open source HBIM Solutions via Nurbs modelling. In: *ISPAR*, 43B2, pp 1381–1388. <https://doi.org/10.5194/ISPRS-ARCHIVES-XLIII-B2-2020-1381-2020>



19. Angulo-Fornos R, Castellano-Román M (2020) HBIM as support of preventive conservation actions in heritage architecture. Experience of the renaissance quadrant façade of the cathedral of Seville. *Appl Sci* 10:2428. <https://doi.org/10.3390/app10072428>
20. Bianchini C, Potestà G (2021) BIM for built cultural heritage: semantic segmentation, architectural stratification and LOD of the baptistry of San Giovanni in Florence. In: Springer tracts in civil engineering, pp 1–15. [https://doi.org/10.1007/978-3-030-49278-6\\_1](https://doi.org/10.1007/978-3-030-49278-6_1)
21. Harris E (1991) *Principios de Estratigrafía Arqueológica [Principles of archaeological stratigraphy]*. Editorial Crítica, Barcelona
22. Grussenmeyer P, Hanke K, Streilein A (2002) Architectural photogrammetry: basic theory, procedures, tools. In: Kasser M, Egels Y (eds) *Digital photogrammetry*. Taylor & Francis, pp 300–339
23. Nieto-Julían JE, Bouzas Cavada M, Moyano J (2021) Un proyecto de rehabilitación HBIM para la Capilla de San Antonio—San Blais, O Porriño, Pontevedra. In: Proceedings of the XV congreso internacional de expresión gráfica aplicada a la edificación, pp 1–12
24. Paul Besl NJ, McKay ND, Besi PJ (1992) Method for registration of 3-D shapes. *1611:586–606*. <https://doi.org/10.1117/12.57955>
25. Yang C, Medioni G (1992) Object modelling by registration of multiple range images. *Image Vis Comput* 10:145–155. [https://doi.org/10.1016/0262-8856\(92\)90066-C](https://doi.org/10.1016/0262-8856(92)90066-C)
26. Graphisoft SE (2021) Introducción a BIMcloud. Available online: [https://help.graphisoft.com/BC/SPA/\\_BIMcloud/\\_10\\_BIMcloudFeatureOverview/10\\_BIMcloudFeatureOverview-1.htm](https://help.graphisoft.com/BC/SPA/_BIMcloud/_10_BIMcloudFeatureOverview/10_BIMcloudFeatureOverview-1.htm). Accessed on 28 Dec 2021
27. Chandrakar O, Saini JR, Bhatti DG (2019) Novel semantic discretization technique for type-2 diabetes classification model. In: *Lecture notes in networks and systems*, vol 74, pp 135–141. [https://doi.org/10.1007/978-981-13-7082-3\\_17](https://doi.org/10.1007/978-981-13-7082-3_17)
28. Shi X, Liu YS, Gao G, Gu M, Li H (2018) IFCdiff: a content-based automatic comparison approach for IFC files. *Autom Constr* 86:53–68. <https://doi.org/10.1016/J.AUTCON.2017.10.013>
29. Brumana R, Della Torre S, Previtali M, Barazzetti L, Cantini L, Oreni D, Banfi F (2018) Generative HBIM modelling to embody complexity (LOD, LOG, LOA, LOI): surveying, preservation, site intervention—the Basilica di Collemaggio (L'Aquila). *Appl Geomatics* 10:545–567. <https://doi.org/10.1007/s12518-018-0233-3>
30. Moyano J, Nieto-Julían JE, Lenin LM, Bruno S (2021) Operability of point cloud data in an architectural heritage information model. *Int J Archit Heritage* 1–20. <https://doi.org/10.1080/15583058.2021.1900951>
31. Castellano-Román M, Pinto-Puerto F (2019) Dimensions and levels of knowledge in heritage building information modelling, HBIM: the model of the Charterhouse of Jerez (Cádiz, Spain). *Digital Appl Archaeol Cult Heritage* 14:e00110. <https://doi.org/10.1016/J.DAACH.2019.E00110>
32. Diara F, Rinaudo F (2020) Building archaeology documentation and analysis through open source HBIM Solutions via Nurbs modelling. In: *ISPAr*, 43B2, pp 1381–1388. <https://doi.org/10.5194/ISPRS-ARCHIVES-XLIII-B2-2020-1381-2020>
33. Tabales Rodríguez MA (1997) Análisis arqueológico de paramentos. Aplicación en el patrimonio edificado sevillano. *SPAL Rev Prehistoria Arqueología Universidad Sevilla* 263–295. <https://doi.org/10.12795/SPAL.1997.16.15>
34. Doglioni F (1988) La Ricerca sulle strutture edilizie tra archeologia stratigrafica e restauro architettonico. In: *Francovich y Parenti*, pp 223–248
35. Brogiolo GP, Cagnana A (2012) Archeologia dell'architettura: metodi e interpretazioni. In: *Archeologia dell'architettura*, pp 1–195
36. Harris E (2014) Archaeological stratigraphy: a paradigm for the Anthropocene. *J Contemp Archaeol*. <https://doi.org/10.1558/jca.v1i1.73>
37. Python-Graphisoft SE (2021) Archicad Python interface (PyPI). Available online: <https://pypi.org/project/archicad/>. Accessed on 29 Dec 2021
38. Charbonneau N, Spiric N, Blais V, Robichaud L, Burgess J, Charbonneau N, Spiric N, Blais V, Robichaud L, Burgess J (2018) 4D modelling of built heritage: a system offering an alternative to using BIM. *Digit Stud [Le champ numérique]* 8. <https://doi.org/10.16995/DSCN.283>

39. Cembranos JR, Fernández JL, Leronés PM, Bermejo JGG, Casanova EZ, Ioannides M (2018) Supporting the automatic extraction of HBIM elements from point clouds. In: Lecture notes in computer science (including subseries Lecture notes in artificial intelligence and Lecture notes in bioinformatics), 11197 LNCS, pp 3–10. [https://doi.org/10.1007/978-3-030-01765-1\\_1](https://doi.org/10.1007/978-3-030-01765-1_1)

# Integrating Artificial Intelligence Approaches for Quantitative and Qualitative Analysis in H-BIM



David Bienvenido-Huertas, Blanca Tejedor, Manuel J. Carretero-Ayuso, Carlos E. Rodríguez Jiménez, and Marta Torres-González

**Abstract** Managing historic buildings is a process in which workers responsible for this task require many time resources. Its optimization through several techniques, such as artificial intelligence, reduces the time related to decision-making. This chapter develops a procedure to generate intelligent GDL objects to predict or estimate the responses required to manage heritage elements in historic buildings. For this purpose, the models developed through data mining procedures in GDL objects in Building Information Modelling (BIM) platforms are combined with their application to historic buildings: Heritage Building Information Modelling (H-BIM). Thus, intelligent BIM models are developed to meet the needs of the technicians responsible for maintaining historic buildings. The responses given by the intelligent objects could be qualitative or quantitative. This methodology would be useful to reduce both the time of decision-making and the data analysis by visualizing them in a three-dimensional model of the historic building. Thus, this is a technique designed to optimize the management of the heritage elements in historic buildings.

**Keywords** H-BIM · Artificial intelligence · GDL

---

D. Bienvenido-Huertas (✉)

Department of Building Construction, University of Granada, Granada, Spain

e-mail: [dbienvenido@ugr.es](mailto:dbienvenido@ugr.es)

B. Tejedor

Department of Project and Construction Engineering, Group of Construction Research and Innovation (GRIC), Universitat Politècnica de Catalunya (UPC), Barcelona, Spain

M. J. Carretero-Ayuso

Department of Architecture, University of Alcalá, Madrid, Spain

C. E. Rodríguez Jiménez · M. Torres-González

Department of Building Construction II, University of Seville, Seville, Spain

© The Author(s), under exclusive license to Springer Nature Singapore Pte Ltd. 2022

D. Bienvenido-Huertas and J. Moyano-Campos (eds.), *New Technologies in Building and Construction*, Lecture Notes in Civil Engineering 258,

[https://doi.org/10.1007/978-981-19-1894-0\\_14](https://doi.org/10.1007/978-981-19-1894-0_14)



# 1 Introduction

## 1.1 *Existing Goals Related to Both the Cultural Heritage of Historic Buildings and the Potential of H-BIM*

The universal values of societies and regions are represented through their cultural heritage (CH). This CH could have a double dimension: tangible or intangible [1]. These two dimensions constitute the legacy of past generations and are the identity and cohesion of nations or cultures. Intangible CH refers to the customs or rituals performed by societies, and the participation and implication of the individuals in each region are crucial to preserve them; however, the circumstances in tangible CH are different, and their appropriate preservation could be limited.

In this regard, tangible CH should be defined. Tangible CH, also known as architectural heritage, is constituted by buildings, monuments or archaeological sites with a historical, cultural or landscape value. These architectural goods are non-renewable resources [2], so their preservation for future generations is among the main society's duties. This requirement is our main goal for future generations; it is actually a moral, ethical and architectural responsibility so that future generations could admire and know the architectural legacy of each region. Likewise, the importance of the symbolism of these constructions is difficult to quantify as, in many cases, these constructions are the most important element representing a region (e.g. the Giralda in Seville or the Hercules Tower in Corunna).

Thus, managing and preserving tangible CH are today among the main activities of the architecture and building sectors, focusing on establishing the maintenance, preservation and restoration actions required for each heritage building [3]. This activity is characterized by the interaction of many specialized disciplines responsible for diagnosing, valuing and monitoring the architectural good, although there could be coordination difficulties in the processes as various professionals (i.e. architects, historians or archaeologists) are involved. Thus, not only the preservation problem is tackled from an architectural perspective (which would be the clearest one), but also the complex character of these buildings as there are other elements not related to the performance scopes of architectural technicians. However, this greater interdisciplinary (a positive aspect from the side of a crossknowledge in the decision-making) could make the consensus on the decision-making process difficult.

Based on the great coordination difficulty among disciplines, the use of computer tools allows the management process to be optimized. Recently, Building Information Modelling (BIM) has become the most effective methodology to manage buildings completely by combining the volumetric and physical characteristics of a building with all the elements defining it [4]. Moreover, its work methodology allows a multi-disciplinary workflow to be carried out, thus optimizing the building management process [5]. However, the use of BIM has been always focused on projects related to new buildings. Despite of this, both the great potential of using this methodology and the great variety of tools (ArchiCAD, Autodesk Revit, Allplan, etc.) have implied that

more and more researchers are focused on searching a logic and consistent application of BIM for preservation tasks. In this regard, the practical application of BIM in relation to tangible CH was called Historic/Heritage Building Information Modelling (H-BIM) by Murphy et al. [6]. The main advantage of this new application of BIM is the modelling of the architectural elements of each building and the compilation of historic, constructive and artistic data [7, 8]. Thus, H-BIM establishes preventive maintenance as a daily requirement, as well as information exchange and knowledge dissemination of tangible CH [9]. In addition, modelling in BIM has other interests for both tourist purposes (as virtual models of historic buildings could be fully and easily viewed in a smartphone device) and volumetric record to have accurate data of an element or part of a historic building if it is damaged in the future (e.g. these models could reconstruct the elements damaged in this type of buildings, such as the roof of the Notre Dame Cathedral after the fire in 2009).

### ***1.2 Three-Dimensional (3D) Historic Building Modelling in H-BIM: Techniques Existing in the Scientific Literature***

Despite the advantages of H-BIM, an essential aspect is the process for the 3D survey of buildings. There are many methodologies that analyse the various approaches existing for the virtual modelling of heritage buildings by using current technologies. This section reviews the most used techniques to acquire, model and study heritage buildings. As there are no maps or any kind of documentation in most buildings, the whole acquisition and modelling process should be carried out. It is difficult to find specific and clear data on the construction project of heritage buildings that could be useful for their modelling. In case these data exist, their use is not widely recommended as there could be deformations in the structural elements. The studies conducted by Antón et al. [10] showed that the existing deformations in buildings could significantly vary the perfect elements (perpendicular vertical and horizontal elements) that are usually modelled in both 2D plans and BIM environments. Thus, the reality of historic buildings is very different from perpendicular environments, so imperfections should be defined in virtual environments.

Thus, all the useful information could be monitored and stored by including the geometric information in H-BIM [11–16]. Data of heritage buildings could be acquired by using two techniques (photogrammetry and laser scanner), and the import of the point cloud into BIM is known as Scan to BIM. Photogrammetry is known as structure from motion (SfM), and the laser scanner is known as terrestrial laser scanning (TLS). The use of one technique or another depends on the element to be digitalized. Thus, the laser scanner is used in a complex, irregular and big object (e.g. the envelope of an historic building or the large open rooms inside it), whereas photogrammetry is used for areas whose colour information is important, apart from its geometry [10, 17, 18]. Photogrammetry is commonly used

to model small elements which can be scanned by photographic shots (e.g. capitals in columns). Given the characteristics of the methods, there could be difficulties on which method should be used. In this regard, the TLS allows 3D as-built environments to be acquired accurately and with no contact [10] and is usually the most appropriate technology to model huge elements. However, photogrammetry could be appropriate to quickly model small elements. Moreover, its technology is simpler, so more technicians are able to use it. For this reason, these two methods are usually combined to take advantage of their individual advantages, thus resulting in both more detailed BIM models and an optimal development [19–21]. Another factor to be considered is the economic cost of the equipment because photography cameras are commonly cheaper than the laser scanning technology [22], whereas low-cost devices have been considered as new alternatives in this context [23]. In this regard, photogrammetry could be used by any device that could take photographs, so any technician having a smartphone could make 3D scans of architectural elements by using this technique. However, using photography cameras with the best features is recommended to obtain 3D models with a mesh more adjusted to the actual conditions of the object.

### ***1.3 Working Platform with H-BIM and Difficulties of the Decision-Making***

Recent research studies on H-BIM have been based on the studies mentioned above. However, the use of a multidisciplinary working platform does not guarantee the optimization of the process because each discipline focused on maintaining CH has its own characteristics and perspectives of the element to be preserved (e.g. the perspective of an historian or an archaeologist does not need to be the same of that of an architect). The workflow among the disciplines requires the proposal of shared hypotheses, the analysis of results and information exchange [24], although there could be problems related to the assessment criterion.

In this context, artificial intelligence (AI) can play an essential role by homogenizing decision-making criteria and quickly predicting a response [25]. In this regard, establishing a priority for conservation performances is crucial because of the budget limitations for conducting restoration works. Thus, having a tool to establish a priority order in performances and to manage architectural elements in an intelligent way constitutes a possibility of study, which has not been previously developed by other research works. In addition, the use of the AI applied to H-BIM as an automation process of the decision-making is among the main gaps of knowledge that could be of great interest for sectors related to the architecture and conservation of historic buildings [4].

In the scientific literature, there are some studies focused on BIM and use optimization techniques through artificial intelligence algorithms [26–28], but none is focused on the preventive management of historic buildings. In the framework of

heritage management, there are some research works focused on the AI application in various case studies. Some of the most important studies are as follows: (i) Silva et al. [29, 30] used the multiple linear regression to predict the useful life and to make performance decisions on the external cladding of building façades; (ii) the studies by Prieto et al. [31–33] and Macías-Bernal et al. [34] were characterized by using the theory of diffuse sets (diffuse logic) to estimate the functional useful life of heritage buildings; (iii) Grishkin et al. [35] developed a prediction model through the support vector machine algorithm to detect biological pollutants on the surfaces of heritage elements; (iv) Bassier et al. [36] also used a classification model developed by the support vector machine algorithm to identify the typology of heritage elements in digitalized environments (e.g. columns, windows or ornaments); (v) Steinbauer et al. [37] developed prediction models through regression tree algorithms to detect factors that stimulate the appearance of plant species in the façades of medieval castles; and (vi) Montoya Obeso et al. [38] and Llamas et al. [39] used convolutional neural networks to effectively classify the images of the architectural heritage. As it is shown, none of these research works have studied the possibilities of implementing appropriate AI models for each conservation approach in an H-BIM model of historic buildings.

#### ***1.4 Goal of the Chapter***

There are some applications in BIM that use optimization techniques through AI. The common aspect is that all the research studies are clearly focused on new buildings or on the industrial maintenance in built buildings, but no study is focused on the preventive management of historic buildings. Consequently, there is no study related to the possibilities of applying this type of technique in an H-BIM environment to obtain an automatic response. In this regard, the great variability of aspects to be determined, of quantitative and qualitative order, together with many factors that could influence these variables forces to establish many approaches to obtain appropriate response routes.

At this point, and as the next sections show, tree prediction algorithms could be a feasible option for the interaction approaches of AI with H-BIM as the algorithms could be easily included in BIM environments. It is important to remind that H-BIM models are models with a personalized level of detail based on the application of points cloud models that have been previously transformed into 3D models. Thus, the typical possibilities of modelling are not considered, and an own virtual model is created by adapting it to the geometric characteristics of the building. The approach of this study goes beyond that own and unique approach of the H-BIM model, since prediction models are developed in the characteristics of the objects and/or models to obtain responses or output values.

This chapter therefore develops the application of AI models in H-BIM based on qualitative and quantitative variables. For this purpose, a theoretical model was used in BIM, and a Geometric Description Language (GDL) object was created in

relation to the floor tiles. This methodology could be used to estimate qualitative and/or quantitative variables in H-BIM models.

## 2 Methodology

The development of the methodology was divided into two sections. Firstly, the most appropriate qualitative and quantitative tree AI algorithms were described in detail to be implemented in H-BIM, and secondly, the next steps to be taken in the implementation process of the prediction model with AI in H-BIM were defined.

### 2.1 Algorithms

The most used tree prediction algorithms are the C4.5 algorithm, the classification and regression trees (CART) algorithm and the M5P algorithm. The use of an algorithm or another will depend on the type of output variable. Thus, the C4.5 algorithm is appropriate for qualitative variables, whereas the CART and M5P algorithms are used for quantitative variables.

#### 2.1.1 The C4.5 Algorithm

Decision trees are a supervised learning technique that develop classification models with the form of a tree, composed by internal nodes corresponding to attributes, arches corresponding to the values of the root node and leaves corresponding to the classification value (Fig. 1). Thus, the response of the system can be determined by the relationships taken place from the root of the tree to one of the leaves. The algorithm operates by dividing the training data set into smaller subsets until determining the

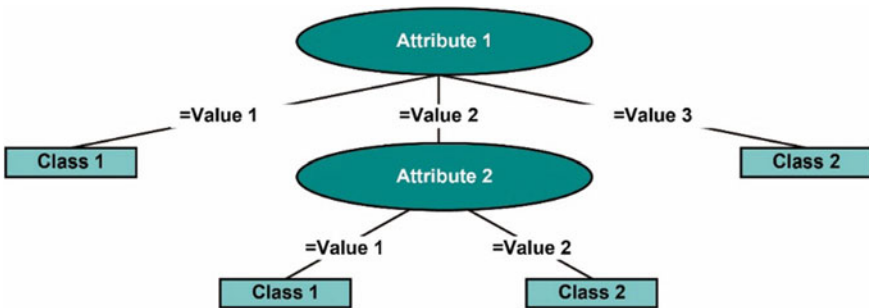


**Fig. 1** Theoretical scheme of a C4.5 model based on two attributes: input variables and output variables

most appropriate configuration. The model is therefore built directly, from up to down, without using backtracking and with resistance to noise as long as the training sample is huge.

Traditionally, this is the most used supervised inductive learning classification technique in the decision-making process in several areas, such as quality control, meteorological predictions or medical diagnosis [40]. However, its use in the field of decision-making related to the management of architectural heritage is an aspect to be studied. In addition, the main advantage of these models is that the connections among nodes could be expressed at a computational level as if-then rules, thus easing their programming in various languages (i.e. if a variable has a value, then the output variable obtains another value). This aspect also allows knowledge on the rules of the model to be obtained as it is a series of rules that could be easily interpreted by any technician. This technique is inherent to tree prediction models and is included in all the algorithms considered in the study.

As for the technique to classify qualitative variables belonging to the decision tree family, two algorithms can be stressed: ID3 and C4.5. The ID3 algorithm was first developed by Quinlan in 1986 [41] and develops decision trees through a training sample. On the other hand, the C4.5 algorithm, published by Quinlan in 1993 [42], is a development of the ID3 algorithm. This new algorithm includes some novelties, such as the pruning of prediction models, thus developing lesser complex systems that are easier to be interpreted.

The decision tree algorithms determine the best attribute or variable at each step through the concept of information gain by using C. Shannon's theory information [43]. For this purpose, it is essential to determine first the entropy, which determines the uncertainty degree of the sample.

### 2.1.2 The CART Algorithm

The CART algorithm develops reverse tree models whose internal nodes correspond to the input variables, the arches correspond to the values of the root node and are useful to connect with other nodes or leaves, and the leaves correspond to the value of the model. These models develop a series of if-then rules that allow the output value to be reached by following the rules indicated in each node. Thus, they are characterized by dividing the input space into subregions, simplifying complex problems with simple models. It is important to stress that the output value included in each leaf is a unique numeric value, with this aspect being different from the C4.5 algorithm. Thus, the scheme of the model is similar to that included in Fig. 1, but with numeric variables in the leaves.

For this reason, CART models have the same advantages as C4.5 models. These models are therefore easy to be interpreted and are useful to understand the solution adopted to the problem, so they have been widely used. However, they have been scarcely used in architecture since the creation of the algorithm.

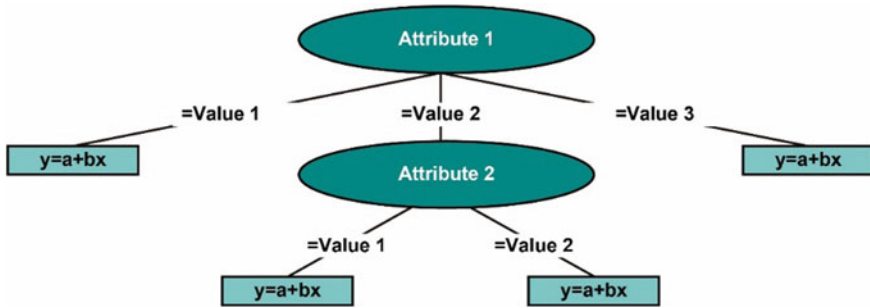


**Fig. 2** Theoretical scheme of a M5P model based on two attributes: input variables and output variables

### 2.1.3 The M5P Algorithm

The M5P algorithm is an evolution of the CART algorithm. The main difference in comparison with the CART algorithm is that the M5P algorithm develops tree models with linear regressions leaves (Fig. 2). Linear regressions are relations through linear equations between the dependent variable (coincident with the variable to be estimated) and the independent variables (coincident with the input variables). Thus, the algorithm develops optimum linear regressions in the various subregions or divisions of the data set. This is an algorithm from which the rules established among the various variables of the data set can be known. Other advantage of the M5P algorithm is that large data sets are effectively managed. These data sets are robust due to the lack of some data in the data set analysed. As for the possible atypical values or noise that the data set could have, its response is appropriate.

To develop the M5P model, instead of maximizing the information gain, the internal variation of the subsets is reduced for the class values of each branch. After the model is built, the pruning (i.e. the removal of ineffective nodes) allows the overfitting to be reduced.

## 2.2 Application Workflow

The methodology used in this study tries to provide a new procedure to develop intelligent H-BIM models by using GDL objects with regression or classification models appropriate to the needs of the technicians responsible for preserving historic buildings. The method consists in

1. Compiling documentary information, obtaining orthophotos, laser scanning and the rest of procedures required to obtain the information required to develop the H-BIM model.
2. Determining the prediction needs that the H-BIM model should carry out. According to such needs, information of the architectural elements of the historic

building should be compiled to generate the data sets required to develop prediction models. This documentary compilation should not include the whole set, and the use of data of similar buildings could be assessed by the technical staff.

3. Developing prediction models by using data mining software or an own code in programming language.
4. Implementing the models in typologies of GDL objects designed for the building. The implementation takes place by programming the script of the object designed.

Although this procedure is susceptible to be differently applied, its particular applications are described here in detail to consider this study as an example of the foundations of the methodology.

To develop intelligent H-BIM models by using GDL objects with regression or classification models according to users' needs, all data required should be first compiled (Section 1 in Fig. 3). For this purpose, historical sources and research works related to the historic building should be consulted to acquire the data required for its survey. Likewise, the 3D survey of certain elements through techniques such as the laser scanner or photogrammetry develops more accurate models, as the analysis of the state of the art in relation to these techniques is shown in Sect. 1.2.

After finishing the documentary compilation, the prediction, estimation or classification needs to which the model should respond must be determined. For this purpose, the technical staff should determine the responses that the various elements of the model should give, as well as the variables to be used. Afterwards, the data sets used should be generated to train the models (Section 2 in Fig. 3). These data sets

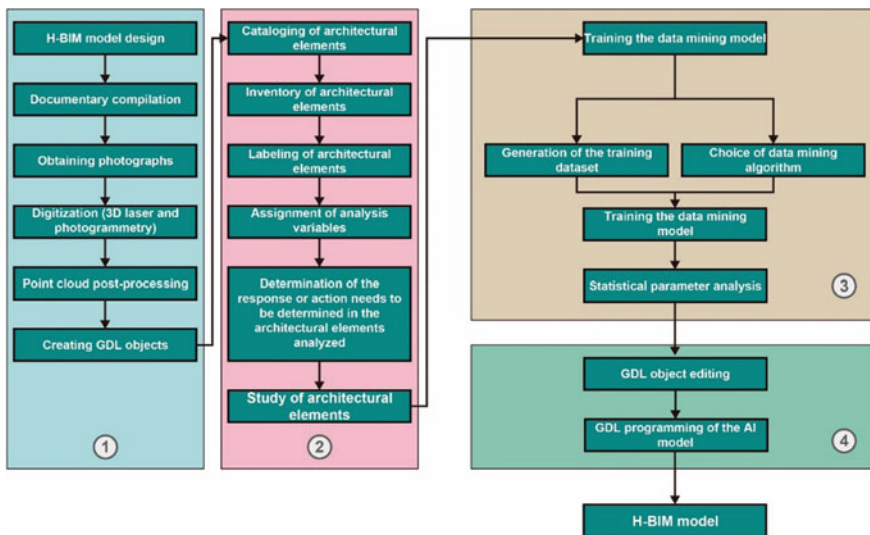


**Fig. 3** Workflow of the methodology to design an H-BIM model with predictive objects based on tree AI algorithms



could be developed by analysing a sample of the heritage elements of the building or by using data from other interventions with similar characteristics. The data set should have an appropriate structure for the data mining approaches, so it should have a series of input variables and one or several output classes or variables. The number of instances of the data set should be enough to develop robust models. In this regard, it is worth stressing that, in the development processes of prediction models, 75% of data is usually used to train the model and the remaining 25% to test it. Thus, as the data set is divided into two subsets, the number of cases should be great enough to not generate ineffective models.

After generating the data sets, models are trained (Section 3 in Fig. 3). For this purpose, the software developed for data mining (e.g. KNIME) could be used or the code designed for a programming language (e.g. R, Java or Python). Given the many possibilities of developing models (as there are many algorithms), the algorithms that develop tree models and are described above should be used. In this regard, it is recommended to use the C4.5 algorithm to estimate qualitative variables, and the CART and M5P algorithms should be used to estimate quantitative variables. When developing models, the ideal would be considering various configurations according to the possibilities of each algorithm. Thus, the approach of various schemes that consider aspects such as the pruning (the removal of ineffective variables), the maximum number of rules, the modification of input variables, the normalization of the value scale or the use of training data sets based on making a fold cross-validation would allow various models to be obtained. The performance is expected to be different in each model. The main aspect is that the performance is as greater as possible to guarantee an appropriate response of the prediction model in H-BIM. Thus, the performance of the models should be analysed by using statistical parameters. In case of inappropriate performances, the technical staff (i.e. the designer, the architect, or the preservation technician responsible for the modelling) should analyse the possibility of increasing the number of instances included in the data set, adding new variables and/or modifying the configuration parameters in the algorithms.

As for the statistical parameters, the type of output variable to be analysed should be distinguished, i.e. if it is qualitative or quantitative. For the qualitative output variables (the C4.5 algorithm), the statistical parameters used in the analysis of prediction models are usually the true positive (TP) rate (Eq. 1), the false positive (FP) rate (Eq. 2), the kappa coefficient (Eq. 3), and the area under the receiver operating characteristic (ROC) curve (Eq. 4). These parameters were used to determine the most appropriate model.

$$TP = \frac{\text{Correctly classified data}}{\text{Total number of data}} \quad (1)$$

$$FP = \frac{\text{Incorrectly classified data}}{\text{Total number of data}} \quad (2)$$

$$K = \frac{p_o - p_e}{1 - p_e} \quad (3)$$

$$\text{Area ROC} = \int_0^1 (1 - G(F^{-1}(1 - t)))dt \tag{4}$$

where  $p_o$  is the relative observed agreement between two observers,  $p_e$  is the hypothetical probability of agreement by chance,  $G$  is the distribution of positive samples,  $F$  is the distribution of negative samples, and  $t$  is a cut point.

As for quantitative variables, the analysis should be based on three parameters: the determination coefficient ( $R^2$ ) (Eq. 5), the mean absolute error (MAE) (Eq. 6) and the root mean square error (RMSE) (Eq. 7).

$$R^2 = 100 \left( 1 - \frac{\sum_{i=1}^n (t_i - m_i)^2}{\sum_{i=1}^n (t_i - \bar{t}_i)^2} \right) \tag{5}$$

$$\text{MAE} = \frac{\sum_{i=1}^n |t_i - m_i|}{n} \tag{6}$$

$$\text{RMSE} = \left( \frac{\sum_{i=1}^n (t_i - m_i)^2}{n} \right)^{1/2} \tag{7}$$

where  $t_i$  is the actual numeric value of the  $i$  datum in the data set,  $m_i$  is the value estimated in the  $i$  datum for the prediction model, and  $n$  is the total number of records or rows that form part of the data set.

After obtaining the appropriate model for the needs of the project, it should be implemented in the GDL object of the H-BIM model (Section 4 of Fig. 3) by programming the model in the GDL object. Figure 4 includes a generic programming example for the GDL object with the various tree-type algorithms. This programming includes both the code to estimate the output variable and the possibility of graphically modifying the visualization of the object according to the value of the output variable. It is recommended to use words without accents due to the incompatibility of the programming language with these elements. Thus, the direct use of words in English

C4.5	CART	M5P	
<pre> if Variable1= "Label1" then   PARAMETERS Class= "Response1" endif if Variable1= "Label2" then   if Variable2= "Label1" then     PARAMETERS Class= "Response1"   endif   if Variable2= "Label2" then     PARAMETERS Class= "Response2"   endif endif if Variable1= "Label3" then   if Variable2= "Label1" then     PARAMETERS Class= "Response2"   endif   if Variable2= "Label2" then     PARAMETERS Class= "Response3"   endif endif                     </pre>	<pre> if Variable1&lt;=2 then   PARAMETERS Class=2,5 endif if Variable1&gt;2 then   if Variable2&lt;=10 then     PARAMETERS Class=3,5   endif   if Variable2&gt;10 then     PARAMETERS Class=4,2   endif endif if Variable3&gt;5 then   if Variable2&lt;=8 then     PARAMETERS Class=2   endif   if Variable2&gt;8 then     PARAMETERS Class=1,47   endif endif                     </pre>	<pre> if Variable1&lt;=2 then   PARAMETERS Class=2,5*Variable1+10 endif if Variable1&gt;2 then   if Variable2&lt;=10 then     PARAMETERS Class=3,5*Variable1+2*Variable3+1,2*Variable4+10   endif   if Variable2&gt;10 then     PARAMETERS Class=Variable1+4   endif endif if Variable3&gt;10 then   if Variable2&lt;=35 then     PARAMETERS Class=2,1*Variable3+1,55*Variable6+2,99*Variable7+0,2   endif   if Variable2&gt;35 then     PARAMETERS Class=Variable3+2*Variable7+1,3   endif endif                     </pre>	<pre> if Class&lt;=10 then   PARAMETERS gs_frame_mat =77   PARAMETERS gs_cont_pen =48 endif                     </pre>

**Fig. 4** Generic programming examples of the various tree algorithms considered in a GDL object. Application using the BASIC programming language in ArchiCAD

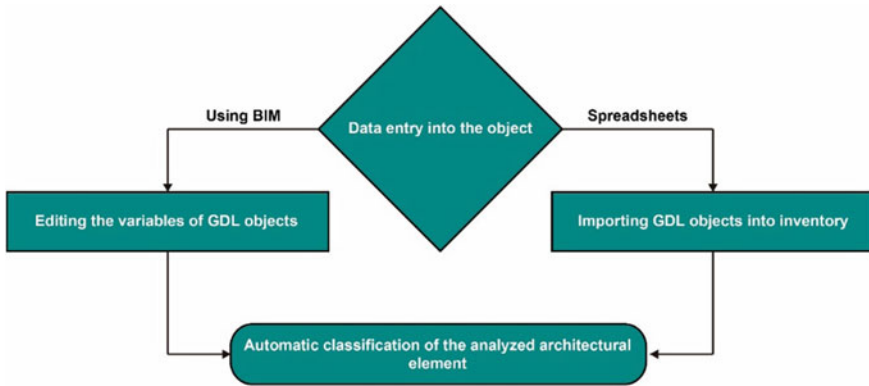


**Fig. 5** Connection flow of the input data in the intelligent GDL objects designed for the H-BIM model

could be useful to avoid this type of error that leads to the impossibility of estimating the response of the system. As graphical 3D environments are used, it is worth stressing that the graphical representation of predictions could ease the performance proposals made by architects and technicians. After configuring the typologies of the GDL object that will be used in the model, the building is modelled.

Finally, after forming the H-BIM model and according to the progress of the intervention or maintenance process, the values of the input variables of the GDL objects designed for the architectural elements should be included. For this purpose, the input values could be included manually in each GDL object or by importing the input values through inventories developed in spreadsheets (Fig. 5). The use of spreadsheets allows the data set to be developed by unqualified people in relation to the management of BIM environments thanks to the possibilities of importing spreadsheets into formats, such as .xls or .xlsx. It is worth stressing that there should be coherence between the input values configured for the prediction models and the data included manually or through the spreadsheet. In case of incoherence (e.g. a label value is written as “Value1” when it is actually “Value 1”), it leads to an error in the model, thus preventing from obtaining an output response. For this reason, it recommended the use of a configuration of the input values of each variable through pull-downs. This aspect is easily configurable in both the GDL objects of the BIM environments and the spreadsheets, so it could be solved in the first implementation stages of the AI models in the H-BIM of the historic building.

### 3 Results and Discussion

An application example of the various tree regression and classification algorithms has been carried out in H-BIM. For this purpose, a theoretical H-BIM model designed

in ArchiCAD (Fig. 6) was used, and the management of floor tiles was analysed. Thus, a GDL object was developed for each element (Fig. 7).

A C4.5 model was used to assess the intervention degree, a CART model to assess the bending strength and a M5P model to assess the rupture load. These prediction

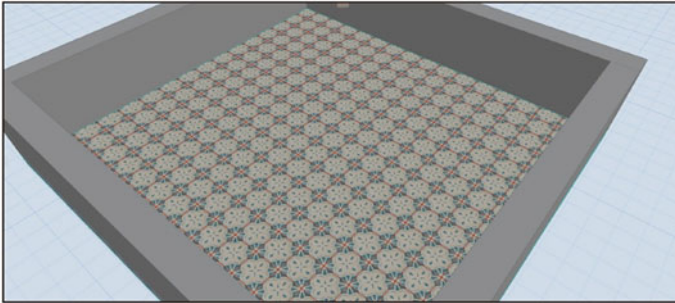


Fig. 6 3D perspective of the theoretical H-BIM model designed for this study

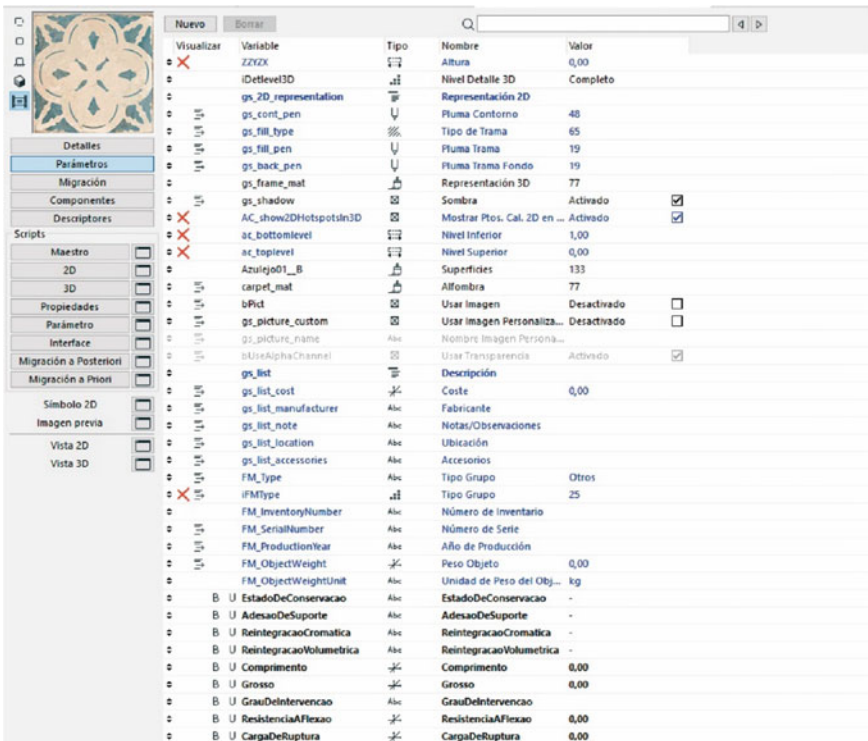
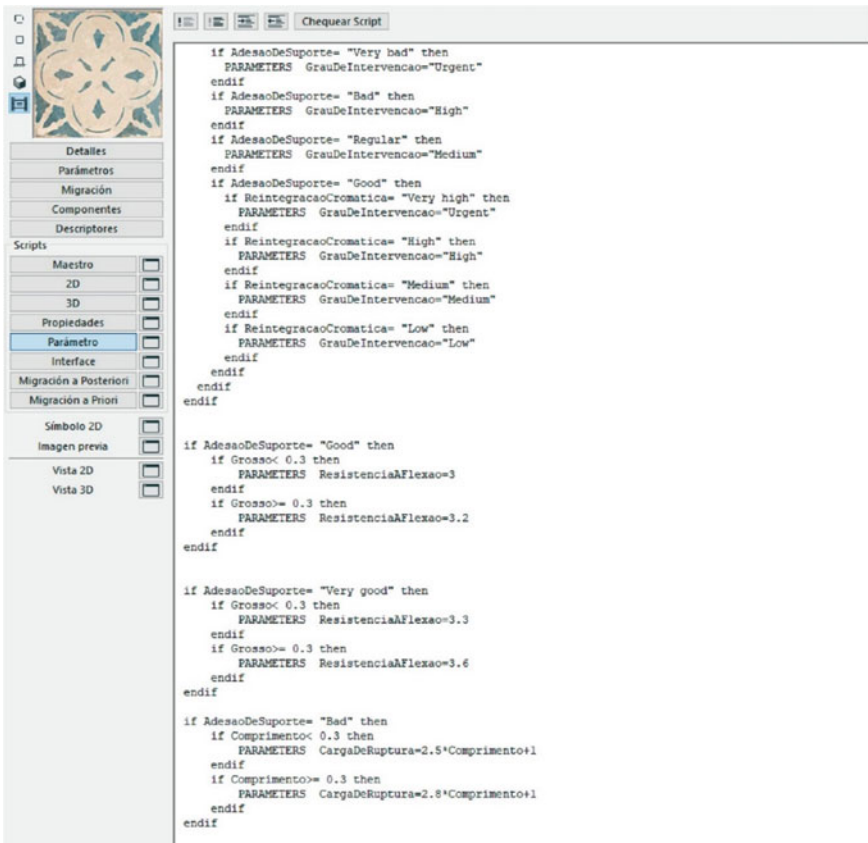


Fig. 7 Interface of the parameters of the GDL object developed to implement tree-type models. The variables created for the models could be seen in the lower part (in bold)

models are theoretical, i.e. they were not designed from a data set due to the limitations to carry out the study. However, under implementation conditions according to the methodology described in the methodology section, models should be validated through statistical parameters, such as the determination coefficient, error parameters, true positive rate and false positive rate. As Fig. 7 shows, in the tap of parameters of the GDL object, the various input and output variables that classification and regression models were going to use were included, also indicating if there were a numeric variable or a text variable (as for the last one, the possible text chains related to the variable could be indicated to avoid errors when it is written according to what the workflow in Sect. 2 indicates). To implement the prediction model developed, the script of the tab of parameters of the GDL object was used, and the if-then rules of the tree-type models were included in the predetermined standard programming (Fig. 8). In this tab, it is possible to combine various prediction algorithms, so the GDL object would not be limited to the use of one prediction model. Figure 8 clearly shows this



**Fig. 8** Extract of the script included in the tab of parameter of the GDL object for the prediction models. The script was configured in English to avoid errors, e.g. accents in words

aspect as the programming of a C4.5 model, a CART model and a M5P model is included. Thus, the model was easily and quickly implemented in the programming language (time resources are usually more focused on the creation of the data set and on the training and validation process of the prediction models).

Moreover, a chromatic codification was implemented in BIM to link the state of conservation of each GDL object in relation to its physical and mechanical properties (e.g. adhesion to support, chromatic reintegration, thickness, length or resistance to bending and compression). Thus, a colour was included in the programming for each possible factor in the output variable to ease both its interpretation at a visual level and the interaction in a 3D model.

The variables of intervention degree (i.e. urgent, high, medium and low) correspond to a colour for each possible response, whereas the numeric variable is shown through ranges (e.g. red colour for values lower than 3 kN in the rupture load). The differences in these parameters of the floor tiles of the model can be graphically seen in the various views of the programming, quickly identifying and limiting the zones or pieces which should require a more urgent performance. Thus, the economic resources available in maintenance and preservation works will be optimized (Fig. 9).

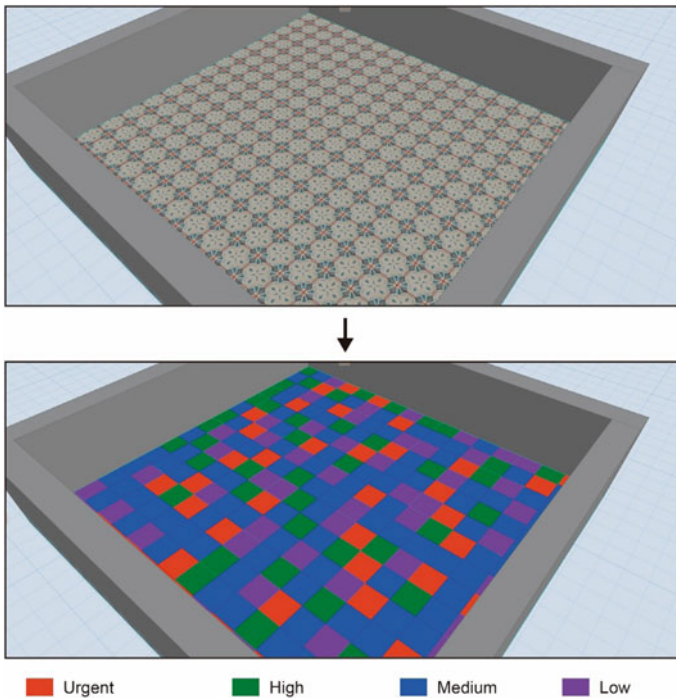


**Fig. 9** Graphic view of the floor tiles of the section analysed with the classification in BIM

## 4 Conclusions

The management of the existing architectural heritage is among the main activities of architects, engineers, conservators and restorers. This activity is characterized by the intervention of various technicians, whose decision-making criteria could be different. Thus, classification or regressions models through artificial intelligence in H-BIM allow to automate decision-making and so optimize the whole process by reducing times and managing intelligently architectural heritage (thus leading to a better preservation of heritage environment).

This chapter develops a solid and practical methodology to implement artificial intelligence in virtual models of heritage buildings in H-BIM, and the steps required to use tree classification and regression models (i.e. C4.5, CART and M5P) in H-BIM have been established. For this purpose, and due to the entity of the study, a theoretical model was used, in which three prediction models (coincident with the three types of tree algorithms) were implemented to manage the floor tiles.

The results showed that these models could be easily programmed, thus being widely used by professionals. For this purpose, a GDL object was created for the floor tiles, and the rules established in each prediction model were implemented through the BASIC programming language. This incorporation was made in the script of the tab of parameters, and it was also configured to visualize graphically in the 3D environment the results estimated in each floor tile.

To conclude, the main advantage by using data mining models is the reduction of time to make a decision on a particular aspect of the element analysed, as well as the estimate of a variable difficult to be valued (such as the resistance of the floor tiles). Thus, the use of artificial intelligence through the proposed methodology is really useful to reach the preservation goals of architectural heritage. This methodology could be applied to many heritage elements that could exist in a heritage environment (friezes, windows, cloths, etc.) as it allows to obtain an interactive and intelligent environment that would contribute to a more optimum preservation of historic buildings and would guarantee the transmission of intangible cultural heritage to future generations.

Nonetheless, this study was limited as it was based on a theoretical model. This aspect was useful to see the possibilities of implementing the methodology based on prediction models in an environment under controlled conditions. However, further studies should implement this methodology in detail. For this purpose, an appropriate case study should be selected and modelled (based on photogrammetry or laser scanner techniques), and a data set should be compiled and implemented in a GDL object to develop prediction models. Likewise, further studies should be focused on a practical application of the methodology. Thus, having a larger number of case studies modelled in H-BIM and implementing prediction algorithms would allow to know the limitations of the methodology among the professionals of the sector and would also be useful to have a larger number of data sets modelled and controlled (this aspect is more related to the transfer possibilities in the professional sector of the methodology). Moreover, artificial intelligence algorithms are not just



limited to the tree-type models. In the data mining and artificial intelligence, a wide variety of algorithms are used to predict quantitative and/or qualitative variables. In this regard, algorithms such as artificial neural networks, Bayesian networks or support vector machines could be an alternative of tree-type algorithms, although their implementation in H-BIM could be an actual challenge as the operation of the models is unknown.

Finally, future studies should focus on the export of the methodology to other scales. In this regard, the similarities between BIM and Geographic Information System (GIS) are clear (incorporation of data in graphical environments), although their approaches and orientations are different. Thus, it is expected that the methodology designed in this study could be extrapolated to GIS as intelligent layers are developed to estimate an output variable. This aspect could be applied for heritage purposes in GIS (e.g. to classify the built environment of heritage buildings in a town, city, region or country) or in other approaches not related to GIS, but of interest for architects, engineers, conservators and restorers (e.g. to predict energy consumption or to characterize the functional useful life of buildings in a region or city).

## References

1. Vecco M (2010) A definition of cultural heritage: from the tangible to the intangible. *J Cult Heritage* 11:321–324. <https://doi.org/10.1016/j.culher.2010.01.006>
2. Krebs M, Schmidt-Hebbel K (1999) Patrimonio cultural: aspectos económicos y políticas de protección. *Perspectivas en Política, Economía y Gestión* 2:207–245
3. Vicente R, Ferreira TM, Mendes da Silva JAR (2015) Supporting urban regeneration and building refurbishment. Strategies for building appraisal and inspection of old building stock in city centres. *J Cult Heritage* 16:1–14. <https://doi.org/10.1016/j.culher.2014.03.004>
4. Bruno S, De Fino M, Fatiguso F (2018) Historic building information modelling: performance assessment for diagnosis-aided information modelling and management. *Autom Constr* 86:256–276. <https://doi.org/10.1016/j.autcon.2017.11.009>
5. Zalama E, Lerones PM (2018) A review of heritage building information modeling (H-BIM). *Multimodal Technol Interac* 2:1–29. <https://doi.org/10.3390/mti2020021>
6. Murphy M, McGovern E, Pavia S (2009) Historic building information modelling (HBIM). *Struct Surv* 27:311–327. <https://doi.org/10.1108/02630800910985108>
7. Dore C, Murphy M (2012) Integration of HBIM and 3D GIS for digital heritage modelling
8. Murphy M, McGovern E, Pavia S (2011) Historic building information modelling—adding intelligence to laser and image based surveys. <https://doi.org/10.5194/isprsarchives-XXXVIII-5-W16-1-2011>
9. Oreni D (2013) From 3D content models to HBIM for conservation and management of built heritage. In: Murgante B, Misra S, Carlini M, Torre CM, Nguyen H-Q, Taniar D, Apduhan BO, Gervasi O (eds) *Computational science and its applications—ICCSA 2013. Lecture notes in computer science*, vol 7974. Springer, Berlin, pp 344–357. <https://doi.org/10.1007/978-3-319-62407-5>
10. Antón D, Medjdoub B, Shrahily R, Moyano J (2018) Accuracy evaluation of the semi-automatic 3D modeling for historical building information models. *Int J Archit Heritage* 12:790–805. <https://doi.org/10.1080/15583058.2017.1415391>
11. Baik A (2017) From point cloud to Jeddah Heritage BIM Nasif Historical House—case study. *Digit Appl Archaeol Cult Heritage* 4:1–18. <https://doi.org/10.1016/j.daach.2017.02.001>



12. Dore C, Murphy M (2012) Integration of historic building information modeling (HBIM) and 3D GIS for recording and managing cultural heritage sites. In: 2012 18th International conference on virtual systems and multimedia, pp 369–376. <https://doi.org/10.1109/VSMM.2012.6365947>
13. Khodeir LM, Aly D, Tarek S (2016) Integrating HBIM (heritage building information modeling) tools in the application of sustainable retrofitting of heritage buildings in Egypt. *Procedia Environ Sci* 34:258–270. <https://doi.org/10.1016/j.proenv.2016.04.024>
14. Logothetis S, Delinasiou A, Stylianidis E (2015) Building information modelling for cultural heritage: a review. In: *ISPRS Annals of the photogrammetry, remote sensing and spatial information sciences*, Copernicus GmbH, pp 177–183. <https://doi.org/10.5194/isprsannals-II-5-W3-177-2015>
15. Sztwiertnia D, Ochalek A, Tama A, Lewińska P (2019) HBIM (heritage building information model) of the Wang Stave Church in Karpacz—case study. *Int J Archit Heritage*. <https://doi.org/10.1080/15583058.2019.1645238>
16. Tommasi C, Achille C, Fassi F (2016) From point cloud to BIM: a modelling challenge in the cultural heritage field. In: *International archives of the photogrammetry, remote sensing and spatial information sciences—ISPRS Archives, International Society for Photogrammetry and Remote Sensing*, pp 429–436. <https://doi.org/10.5194/isprsarchives-XLI-B5-429-2016>
17. Brumana R, Oreni D, Cuca B, Binda L, Condoleo P, Triggiani M (2014) Strategy for integrated surveying techniques finalized to interpretive models in a Byzantine Church, Mesopotam, Albania. *Int J Archit Heritage* 8:886–924. <https://doi.org/10.1080/15583058.2012.756077>
18. Grussenmeyer P, Landes T, Voegtle T, Ringle K (n.d.) Comparison methods of terrestrial laser scanning, photogrammetry and tacheometry data for recording of cultural heritage buildings
19. Pierdicca R, Frontoni E, Malinverni ES, Colosi F, Orazi R (2016) Virtual reconstruction of archaeological heritage using a combination of photogrammetric techniques: Huaca Arco Iris, Chan Chan, Peru. *Digit Appl Archaeol Cult Heritage* 3:80–90. <https://doi.org/10.1016/j.daach.2016.06.002>
20. Magda Ramos M, Remondino F (2015) Data fusion in cultural heritage—a review. In: *International archives of the photogrammetry, remote sensing and spatial information sciences—ISPRS Archives, International Society for Photogrammetry and Remote Sensing*, pp 359–363. <https://doi.org/10.5194/isprsarchives-XL-5-W7-359-2015>
21. Remondino F (2011) Heritage recording and 3D modeling with photogrammetry and 3D scanning. *Remote Sens* 3:1104–1138. <https://doi.org/10.3390/rs3061104>
22. de Reu J, Plets G, Verhoeven G, de Smedt P, Bats M, Cherretté B, de Maeyer W, Deconynck J, Herremans D, Laloo P, van Meirvenne M, de Clercq W (2013) Towards a three-dimensional cost-effective registration of the archaeological heritage. *J Archaeol Sci* 40:1108–1121. <https://doi.org/10.1016/j.jas.2012.08.040>
23. Bolognesi M, Furini A, Russo V, Pellegrinelli A, Russo P (2015) Testing the low-cost RPAS potential in 3D cultural heritage reconstruction. In: *International archives of the photogrammetry, remote sensing and spatial information sciences—ISPRS Archives, International Society for Photogrammetry and Remote Sensing*, pp 229–235. <https://doi.org/10.5194/isprsarchives-XL-5-W4-229-2015>
24. Nieto JE, Moyano JJ, Rico Delgado F, Antón García D (2016) Management of built heritage via HBIM Project: a case of study of flooring and tiling. *Virtual Archaeol Rev* 7:1–12. <https://doi.org/10.4995/var.2016.4349>
25. Chávez-Hernández JA, Recarey CA, García-Lorenzo MM, López-Jiménez O (2012) Utilización de la Inteligencia Artificial en el diagnóstico patológico de edificaciones de valor patrimonial. *Inf Constr* 64:297–305. <https://doi.org/10.3989/ic.11.036>
26. Bloch T, Sacks R (2018) Comparing machine learning and rule-based inferencing for semantic enrichment of BIM models. *Autom Constr* 91:256–272. <https://doi.org/10.1016/j.autcon.2018.03.018>
27. Juszczyk M (2018) Implementation of the ANNs ensembles in macro-BIM cost estimates of buildings' floor structural frames. *AIP Conf Proc*. <https://doi.org/10.1063/1.5030318>

28. Mangal M, Cheng JCP (2018) Automated optimization of steel reinforcement in RC building frames using building information modeling and hybrid genetic algorithm. *Autom Constr* 90:39–57. <https://doi.org/10.1016/j.autcon.2018.01.013>
29. Silva A, De Brito J, Gaspar PL (2012) Application of the factor method to maintenance decision support for stone cladding. *Autom Constr* 22:165–174. <https://doi.org/10.1016/j.autcon.2011.06.014>
30. Silva A, Dias JL, Gaspar PL, De Brito J (2013) Statistical models applied to service life prediction of rendered façades. *Autom Constr* 30:151–160. <https://doi.org/10.1016/j.autcon.2012.11.028>
31. Prieto AJ, Silva A, de Brito J, Macías-Bernal JM, Alejandro FJ (2017) Multiple linear regression and fuzzy logic models applied to the functional service life prediction of cultural heritage. *J Cult Heritage* 27:20–35. <https://doi.org/10.1016/j.culher.2017.03.004>
32. Prieto AJ, Silva A, de Brito J, Macías-Bernal JM, Alejandro FJ (2017) The influence of pathological situations on churches' functionality: an approach based on historical records. *Int J Archit Heritage* 11:566–587. <https://doi.org/10.1080/15583058.2016.1272011>
33. Prieto AJ, Silva A, de Brito J, Macías-Bernal JM (2018) Serviceability of facade claddings. *Build Res Inf* 46:179–190. <https://doi.org/10.1080/09613218.2016.1264808>
34. Macías-Bernal JM, Calama-Rodríguez JM, Chávez-de Diego MJ (2014) Modelo de predicción de la vida útil de la edificación patrimonial a partir de la lógica difusa. *Inf Constr* 66:e006. <https://doi.org/10.3989/ic.12.107>
35. Grishkin V, Kovshov A, Schigorec S (2015) A system for the recognition of biofouling on the surface of the monuments of cultural heritage. In: 2015 International conference on “stability and control processes” in memory of V.I. Zubov, SCP 2015—proceedings, pp 630–633
36. Bassier M, Vergauwen M, Van Genechten B (2017) Automated classification of heritage buildings for as-built BIM using machine learning techniques. In: ISPRS Annals of the photogrammetry, remote sensing and spatial information sciences, vol 4, pp 25–30. <https://doi.org/10.5194/isprs-annals-IV-2-W2-25-2017>
37. Steinbauer MJ, Gohlke A, Mahler C, Schmiedinger A, Beierkuhnlein C (2013) Quantification of wall surface heterogeneity and its influence on species diversity at medieval castles—implications for the environmentally friendly preservation of cultural heritage. *J Cult Heritage* 14:219–228. <https://doi.org/10.1016/j.culher.2012.06.003>
38. Montoya Obeso A, Benois-Pineau J, Ramirez Acosta AÁ, García Vázquez MS (2016) Architectural style classification of Mexican historical buildings using deep convolutional neural networks and sparse features. *J Electron Imaging* 26:011016. <https://doi.org/10.1117/1.JEI.26.1.011016>
39. Llamas J, Lerones PM, Medina R, Zalama E, Gómez-García-Bermejo J (2017) Classification of architectural heritage images using deep learning techniques. *Appl Sci* 7:992. <https://doi.org/10.3390/app7100992>
40. Solarte Martínez GR, Ocampos CA (2009) Técnicas de clasificación y análisis de representación del conocimiento para problemas de diagnóstico. *Sci Tech Año XV* 42:177–182
41. Quinlan JR (1986) Induction of decision trees. *Mach Learn* 1:81–106
42. Quinlan JR (1993) C4.5: programs for machine learning. *Mach Learn* 16:235–240
43. Shannon CE (1948) A note on the concept of entropy. *Bell Syst Tech J* 27:379–423

# Solutions

# Properties of Gypsum Mortars Dosed with LFS for Use in the Design of Prefabricated Blocks



Isabel Santamaría-Vicario, Álvaro Alonso-Díez, Mathieu Horgnies, and Ángel Rodríguez-Saiz

**Abstract** The aim of the present investigation is to determine the suitability of gypsum mortars with mineral additions of ladle furnace slags (LFS) for use in the manufacture of prefabricated blocks. Different dosages of gypsum mortars are designed, and the corresponding tests for their characterization are performed, with the objective of determining their properties, in both the fresh and the hardened state, in accordance with applicable standards. A suitable dosage is then chosen, bearing in mind the optimization criterion on the use of waste in gypsum mixtures, seeking a balance between the quantity of slag that is used and the quality of its properties. Completing the study, a series of complementary tests are performed related to its behaviour in the presence of heat, fire, and both thermal and acoustic transmission. The results showed that the gypsum mortar designs presented similar properties to the conventional mortars and can be approved for use in construction, either as gypsum mortars or as raw material for the manufacture of prefabricated blocks, in compliance with the requirements established in current European standards.

**Keywords** Ladle furnace slags (LFS) · Prefabricated blocks · Gypsum mortar

## 1 Introduction

The deterioration of the environment, global warming of the planet, and climate change are indicators of an uncertain future that we will bequeath to future generations and that is seriously compromising the march towards progress of our civilization [1, 2].

The environmental imbalance that is provoking uncontrolled development, pollution, and huge consumption of natural resources causes the deterioration of ecosystems that, in many cases, can be irreversible [3, 4].

---

<https://www.ubu.es/ingenieria-de-edificacion-giie>

---

I. Santamaría-Vicario · Á. Alonso-Díez · M. Horgnies · Á. Rodríguez-Saiz (✉)  
Grupo de Investigación de Ingeniería de Edificación (GIIE), University of Burgos, Burgos, Spain  
e-mail: [arsaizmc@ubu.es](mailto:arsaizmc@ubu.es)

Our society, understood as a teleological entity, has the duty of rectifying those imbalances and guaranteeing a balanced world, avoiding self-destruction and establishing universal harmony. In this sense, the defence of the environment and sustainable development are concepts that must be compatible with social well-being and the production of goods and services, but guaranteeing in turn the biological balance of the ecosystems [5–7].

One of the factors that has most contributed to environmental imbalance has been industrial activity, understood as a consumer of resources. The consumption of raw materials obtained directly from the natural environment, the expenditure of energy for its transformation, and the generation of water are all critical factors that impact directly on the environment, producing significant imbalance that directly affects the balance of our ecosystems [8].

In an attempt to avoid environmental collapse, awareness of this problem is still growing, albeit very slowly, in our society [9]. At present, there are many investigations that look for solutions, such as the use of alternative raw materials to traditional ones, through the recovery of waste and through the application of more efficient systems of production that consume less energy, avoid gaseous emissions, and contaminating subproducts [10, 11].

The construction sector as a whole is one of the industries with the highest environmental impact, due to the consumption of raw materials, and the energy needed for their extraction, transport, and transformation [12]. Besides, this not-very-innovative and overly rigid sector is still tied to traditional construction systems [13, 14]. Moreover, the life cycle of buildings, especially residential buildings, has a very serious negative environmental impact. The construction of the building, its use, maintenance and demolition, once its useful life is over, affects the ecosystem balance [15, 16].

The need to innovate in the construction sector, incentivizing the use of alternative raw materials to traditional ones, means that both firms and universities research within this area [17, 18]. The design of new materials from industrial by-products is one of the strategic steps to address environmental deterioration and the exhaustion of natural resources [19, 20]. In this sense, the steel making industry, one of the highest consumers of both resources and energy, generates waste and by-products in the form of slags that have been the subject of multiple studies for their recovery [21, 22].

Electric arc furnace slag (EAFS) from primary metallurgical processes has been successfully used in the design of mortars and concretes for construction [23–25]. In addition, more recently, investigations into ladle furnace slags (LFS) generated in secondary metallurgy have also been experimentally used in new masonry mixtures [26, 27].

Today, the recovery of by-products, both separately and jointly, offers us an opportunity for the design of new construction products. In consequence, both the construction and the steel industry, traditionally immersed in a linear economic process, must adapt to the new times, recovering waste as potential raw material, seeking to construct an ecological civilization based on the circular economy of waste, with the subsequent social, economic, and environmental benefits [28–30].

In the following sections, this investigation on the use of gypsum mortars dosed with ladle furnace slags (LFS) will be developed for the design of prefabricated blocks and their use in edification.

## 2 Materials and Methods

The objective of this investigation is the design and the study of gypsum mortars manufactured with ladle furnace slags (LFS), used as a raw material for the manufacture of prefabricated blocks for use in construction.

### 2.1 Raw Materials

- Type B1 gypsum, in accordance with the specifications of standard EN 13,279–1 *Gypsum binders and gypsum plasters—Part 1: Definitions and requirements* [31]. This gypsum was supplied by the firm Yesos Albi S.A. (Grupo CALCINOR), manufactured at its factory in Villalómez, Valle de Oca, Burgos (Spain). Its characteristics are shown in Table 1.
- Ladle furnace slag (LFS) was obtained as a by-product of the steel refining process in secondary metallurgical processes for the production of steel to be manufactured into hot-laminated and cold-pressed steel tubing. It was supplied by the firm *Tubos Reunidos S.L.U.*, Amurrio, Álava (Spain). Its chemical composition is shown in Table 2.

Before use, the slags were subjected to an outdoor weathering and turning process for their stabilization, with the objective of stabilizing the lime and the magnesium oxides for their transformation into portlandite  $\text{Ca}(\text{OH})_2$  and brucite  $\text{Mg}(\text{OH})_2$ , respectively, thereby avoiding expansive effects. Once the slag was

**Table 1** Technical characteristics of B1 gypsum

Granulometry	0–2 mm
Content of $\text{CaSO}_4$	>76.0%
Flexural strength	>2.0 N/mm <sup>2</sup>
Compressive strength	>3.0 N/mm <sup>2</sup>
Water/gypsum ratio	0.40
Onset of setting	>20 min

**Table 2** Chemical composition of LFS (%)

CaO	SiO <sub>2</sub>	Fe <sub>2</sub> O <sub>3</sub>	Al <sub>2</sub> O <sub>3</sub>	MgO	Cr <sub>2</sub> O <sub>3</sub>	TiO <sub>2</sub>	MnO	P <sub>2</sub> O <sub>5</sub>	Others
42.04	15.64	7.88	11.01	19.78	0.45	0.33	0.58	0.10	2.19

**Table 3** Mortar designs

Sample	Volume		Weight (g)		
	B1	LFS	B1	LFS	Water
B1	1	–	1000	–	400
B1:0.2 LFS	1	0.2	1000	166	390
B1:0.4 LFS	1	0.4	1000	332	400
B1:0.6 LFS	1	0.6	1000	498	410
B1:LFS	1	1	1000	829	405

stabilized, it was screened through a 1 mm size mesh. Subsequently, small metallic particles were removed with an electromagnet.

- Water was obtained from the company *Sociedad Municipal Aguas de Burgos, S.A.U.* through the mains water supply of the city of Burgos (Spain).

## 2.2 Mortar Mixtures

The mortars were dosed by adding different quantities of LFS to the gypsum by volume, with the objective of both testing the effect of this recovered aggregate within the mixtures and of determining suitable dosages for its use in the manufacture of prefabricated blocks.

The mixtures were labelled by taking the gypsum (B1) as a reference and the amount of LFS added in volume (0.2; 0.4; 0.6; 1.0), providing four dosages, plus the reference specimen (B1). The mortar designs are shown in Table 3.

The necessary volume of water was added in each dosage to arrive at a diameter of  $160 \pm 5$  mm on the vibrating table, as specified in standard EN 13279-2 *Gypsum binders and gypsum plasters—Part 2: Test methods* [32].

The mixing process began by dry mixing the gypsum and the slag. Subsequently, the water was added and manually mixed for one minute with a spatula, completing the mixing in a Protetic C0087 planetary mixer for a second minute.

## 2.3 Experimental

The gypsum and LFS mortar designs were studied in both the fresh and the hardened state, taking as a reference the tests determined by current European standards.

### 2.3.1 Characterization in the Fresh State

The density in the fresh state is calculated by difference of weights of a recipient of known volume, according to Standard UNE 102042 *Gypsum plasters—Other test methods* [33].

The setting onset time using the Vicat cone method was determined [32], using a standard probe of  $\varnothing$  10 mm and 100 g in weight, performing various successive penetrations with the needle into the body of the mortar, until reaching a depth of around  $(22 \pm 2)$  mm.

### 2.3.2 Mechanical Strength of Gypsum Mortar

The procedure from standard EN 13279-2 [32] was followed for the study of mechanical strength under flexion and compression. To do so, standard specimens ( $40.0 \times 40.0 \times 160.0$  mm) were moulded.

In the first place, the flexural failure tests were performed using a MEM-101/SDC 200 kN universal testing machine, in which the specimens were arranged upon two cylindrical rods, 100 mm apart from each other, subsequently maintaining the pressure on another rod at the centre of the opposite side of the specimen until its breakage into two halves.

The two fragments resulting from the flexural failure test were subsequently tested under compression, placing them on a metallic baseplate to guarantee the downward action of the piston onto a uniform surface of  $(40.0 \times 40.0)$  mm).

The procedure to obtain standardized resistance to the adherence of gypsum mortars is described in the same norm. To do so, a continuous mortar rendering was applied to a thickness of 10 mm on a ceramic brick, previously submerged in water for 60 s, and, in the fresh state, five cylinders ( $\varnothing 50 \pm 0.5$  mm) were marked with a tool.

Once the mortar had hardened, a metallic cylindrical pad was adhered to it, to facilitate the traction effort for removal of the gypsum cylinders, as shown in Fig. 1.

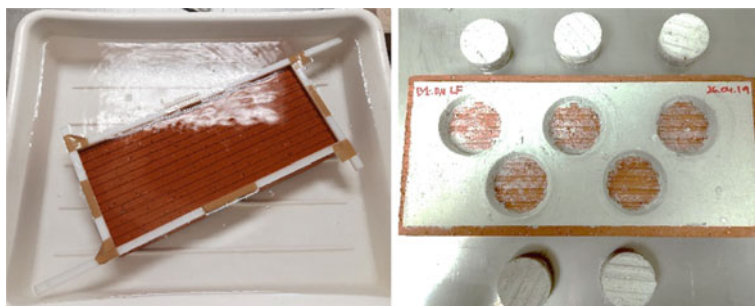


**Fig. 1** Adherence test. Ceramic piece submerged in water (left); final appearance (right)





**Fig. 2** Specimen permeability test (left); suction test (right)

### 2.3.3 Behaviour of the Mortars in Contact with Water

The water vapour permeability and the suction capacity of the gypsum mortars were studied, to understand their behaviour.

The procedure established in standard EN 1015-19 *Methods of test for mortar for masonry—Part 19: Determination of water vapour permeability of hardened rendering and plastering mortars* [34] was followed to establish the water vapour permeability coefficient ( $\mu$ ) of the mortars. Three cylindrical specimens ( $\varnothing$  160 mm  $\times$  16 mm) (Fig. 2) were manufactured and placed in a recipient containing a saturated saline solution. The recipients containing the specimens were sealed and held at a controlled temperature and relative humidity. The flow of water vapour through the mortar specimens was determined through the weight variations under the same conditions of the recipient–specimen.

The water suction capability by capillarity of the hardened gypsum mortars was determined in accordance with the procedure established in standard EN 1015-18 *Methods of test for mortar for masonry—Part 18: Determination of water absorption coefficient due to capillary action of hardened mortar* [35]. To do so, standard specimens (40.0  $\times$  40.0  $\times$  160.0 mm) were moulded and placed upright in a tray in contact with water. The specimens were submerged in water at heights between 5 and 10 mm without touching the tray bottom. The height reached by the water after 10 min of testing was recorded, as was the coefficient of water absorption by capillarity or suction (Fig. 2).

### 2.3.4 Complementary Tests

With the objective of gaining deeper knowledge of the prefabricated blocks and their characteristics, other complementary tests were performed at the given dosages:

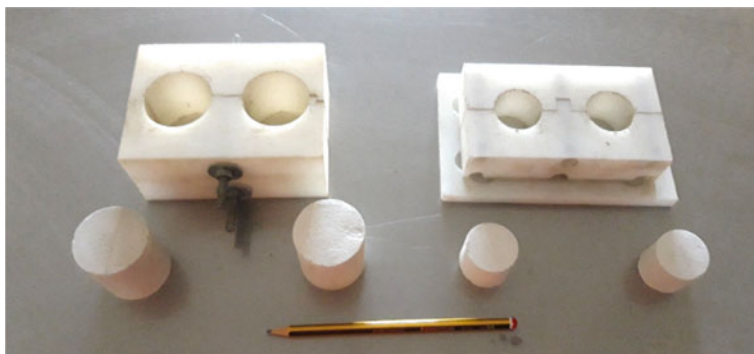


**Fig. 3** Fire test specimens (left); acoustic absorption test specimens (right)

### Thermogravimetric TGA

A thermogravimetric analysis (TGA) is carried out to the gypsum mortar chosen for the manufacture of prefabricated blocks to analyse its thermal behaviour, in other words, the stability of the *gypsum* + *LFS* compound, as the temperature is increased and, in this way, to determine the internal transformations that occur.

To do so, a thermogravimetric analyser TGA Q50 V20.10 Build 36, from TA Instruments, was used with a temperature ramp of 0–800 °C and a gradient of 10 °C/min, in a nitrogen atmosphere.

### Fire-Resistant Behaviour

The non-combustibility test was performed, to establish the fire-resistant behaviour of the selected gypsum mortar, in accordance with the procedure detailed in standard EN ISO 1182:2011 *Reaction to fire tests for products—Non-combustibility test* [36].

To do so, ( $\varnothing$ 45 mm and 50 mm height) cylindrical specimens were moulded (Fig. 3 left), and thermocouples were positioned on them for the purpose of continuous temperature measurements during the fire-resistant test process.

The specimens were placed in a vertical cylindrical oven ( $\varnothing$ 75.0 and 150.0 mm), monitoring the heat with a thermocouple placed at mid-height on the side wall of the oven. A transducer was used to record the temperature sequences reached during the 30-min test, both inside the oven and within the mortar sample.

### Acoustic Absorption

The tests were performed in accordance with the analytical procedure in standard EN ISO 10534-2:2002 *Acoustics—Determination of sound absorption coefficient and impedance in impedances tubes—Part 2: Transfer function method* [37].

Appropriate cylindrical specimens were moulded for testing with the design of the impedance equipment, using, for that purpose, a mechanized mould. This mould produces two cylindrical specimens ( $\varnothing$  31.0 and 30.0 mm) for each mortar studied (Fig. 3 right).

An ACUPRO impedance tube was used for the test, manufactured by Spectronics, administered by a software that analyses the behaviour of the gypsum mortars samples when subjected to different acoustic stationary signal frequencies with a flat spectral density (white noise), generated by a Model DT9837A two-channel spectrum analyser from the firm Data Translation.

The equipment has microphones with Model 46AE pre-amplifiers from the firm GRAS Sound and Vibration. The test instrumentation is sufficient to obtain precise measurements, between 50 and 5700 Hz, of the acoustic properties of the tested materials.

Having laid out the pieces at one end of the impedance tube, noise was generated from a loudspeaker placed at the other end, to generate a set of spectra and its transfer function, which was subsequently analysed with appropriate software.

### Thermal Conductivity

The thermal conductivity of the mortars studied was determined in accordance with the procedure from standard ASTM 1114-06 *Standard Test Method for Steady-State Thermal Transmission Properties by Means of the Thin-Heater Apparatus* [38].

To do so, specimens ( $70.0 \times 110.0 \times 7.0$  mm) were moulded and tested with a Model THA01 thin-heater apparatus, with a model MCU01 measurement control unit, both manufactured by Hukseflux Thermal Sensors.

The Campbell Scientific LoggerNet software with the Thasys version v0909.CR1 was used for data collection and management. Before testing, the equipment was verified with a reference sample of borosilicate Pyrex 7740 glass, at an average temperature of 10.2 °C.

The tests were conducted in an atmosphere at a controlled temperature, guaranteeing an average of  $10 \pm 0.5$  °C.

### 2.3.5 Compressive Strength of Prefabricated Block

A prefabricated gypsum block was designed as a utility model for its use in construction. To do so, an appropriate mould with the dimensions of the piece and the same geometry was machined and then formed.

The prefabricated blocks were tongue-and-grooved pieces ( $340.0 \times 200.0 \times 50.0$  mm) (Fig. 4 left). A 1200 kN hydraulic press was employed for breakage under compression. A load was applied on the area of the piece shown in Fig. 4 (right) until its breakage, in accordance with the specifications of standard EN 772-1:2011 + A1 *Methods of test for masonry units—Part 1: Determination of compressive strength* [39].

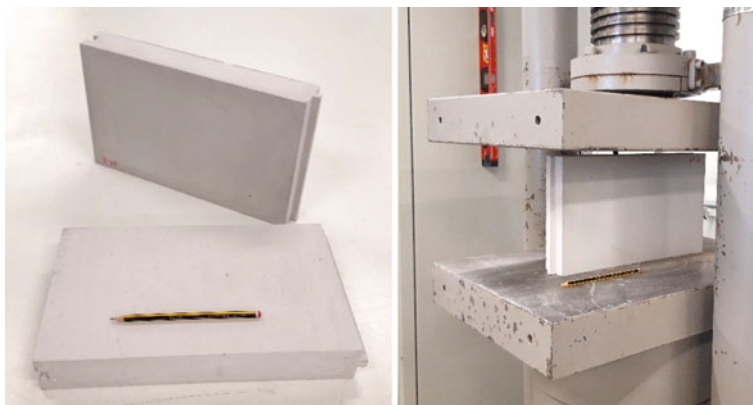


**Fig. 4** Prefabricated block of gypsum mortar and LFS (left); compressive strength test (right)

### 3 Results and Discussion

#### 3.1 Characterization in the Fresh State

The results of the in-fresh characterization are shown in Table 4.

As may be observed in Table 4, there was no significant change in the water/gypsum ratio of the design mortars. A slight increase of the w/b ratio occurred with regard to the corresponding ratio for reference mortar specimen B1, as higher amounts of LFS were added to the mixtures.

The results of adding LFS showed a non-significant reduction of density in the fresh state in comparison with the reference mortar specimen B1. The density reduction of mortar B1:0.2 LFS was 2.85%, and it was 4.28% in the other mortars.

It may be concluded that slag added to the mixtures reduced mortar density in a non-significant way, maintaining stability regardless of the proportion under consideration.

With regard to the setting onset time, the registered results showed that as the proportion of LFS aggregate in the mixtures increased, the setting onset time was

**Table 4** Characterization of gypsum-LF mortars in the fresh state

Sample	Water/binder	Density (kg/m <sup>3</sup> )	Setting onset time (h:min:s)
B1	0.400	1823	0:06:00
B1:0.2 LFS	0.390	1771	0:05:45
B1:0.4 LFS	0.400	1745	0:06:50
B1:0.6 LFS	0.410	1745	0:07:50
B1:LFS	0.405	1745	0:08:40

also lengthier, in correlation with the water/gypsum proportion that was in each case greater.

It can be affirmed that LFS slowed both the setting and the hardening process of the mixture, although within very small proportions of time, because the time difference between the mortars B1:0.2 LFS and B1: LFS was only 3 min.

In the case of the reference specimen B1, the setting onset time practically coincided with mortar B1:0.2 LFS.

### 3.2 Mechanical Strength of Gypsum Mortars

The results from the mechanical strength tests are shown in Table 5.

As may be seen, mechanical flexural strength was weaker in all the mixtures with respect to the reference mortar specimen B1. The reduction was already significant in mortar B1:0.2 LFS, falling to 22.34%, though reaching 55.20% in mortar B1: LFS, with a greater proportion of LFS slag in its composition.

The same behaviour was observed in the case of compressive strength. Strength diminished as the proportion of LFS added to each mixture was increased, being moderate in the case of mortar B1:0.2 LFS (1.63%), but more acute in the case of mortar B1: LFS (54.40%).

It may be concluded that the incorporation of slag reduces the mechanical strengths of gypsum mortars. Nevertheless, the results let us affirm that the mixtures reached very significant strengths, because they were, in all cases, higher than 10.0 N/mm<sup>2</sup>.

The gypsum mortar adherence test results showed that adherence was also weaker as the proportion of LFS in the mixtures was increased.

In the case of mortar B1:0.2 LFS (0.92 N/mm<sup>2</sup>), the reduction was hardly significant with respect to the mortar specimen B1 (1.05 N/mm<sup>2</sup>). As from mortar B1:0.4 LFS, adherence strength underwent a drastic reduction of 50.47%, maintaining very similar values as the amount of slag in the mixtures was increased.

**Table 5** Mechanical strengths (N/mm<sup>2</sup>)

Sample	Flexural strength	Compressive strength Compresión	Adherence
B1	7.70	20.54	1.05
B1:0.2 LFS	5.98	18.59	0.92
B1:0.4 LFS	4.72	14.38	0.53
B1:0.6 LFS	4.05	12.39	0.56
B1:LFS	4.25	11.38	0.54

**Table 6** Behaviour of the mortars in contact with water

Sample	$\mu$	Suction ( $\text{kg/m}^2 \cdot \text{min}^{0.5}$ )	Height (mm)
B1	7	2.61	24
B1:0.2 LFS	4	2.66	30
B1:0.4 LFS	4	2.84	35
B1:0.6 LFS	4	3.24	37
B1:LFS	4	3.65	37

### 3.3 Behaviour of the Mortars in Contact with the Water

The results of the water vapour permeability and suction tests are shown in Table 6.

The results showed a slight reduction of the water vapour diffusion factor ( $\mu$ ) of the mortars with respect to the reference mortar B1.

They indicated that the mortars presented higher water vapour diffusion through the material, probably because of the higher porosity that the slag confers on the mixtures.

Equally, it may be affirmed from the results shown in Table 6 that the mortar designs increased their water absorption by capillarity coefficient when they contain a higher proportion of LFS in their mixtures. Likewise, water reaches a greater height by suction, due to the higher interstitial porosity that the incorporation of slag confers, which produces greater suction capability by capillarity.

### 3.4 Complementary Tests

Having characterized the different mixtures of the gypsum mortars LFS, the dosage corresponding to mortar B1:0.6 LFS was chosen, which shows a reasonable balance between the quantity of LFS that it contains in its dosage and the quality of the test results. The criterion of optimizing the exploitation of waste used in the gypsum mortars designed was followed to achieve performance specifications equivalent to those of a conventional gypsum mortar.

A series of complementary tests on the selected mortar B1:0.6 LFS was performed to complete the research.

#### 3.4.1 Thermogravimetry Analysis TGA

Figure 5 shows the process of mass loss noted in mortars B1 and B1:0.6LFS following a thermogravimetric analysis (TGA). In both graphs, the typical mass loss process in gypsum compounds can be seen.

An important loss of mass was observed in reference mortar B1 when the temperature was between 80 and 100 °C, which is identified with the humidity of the sample.

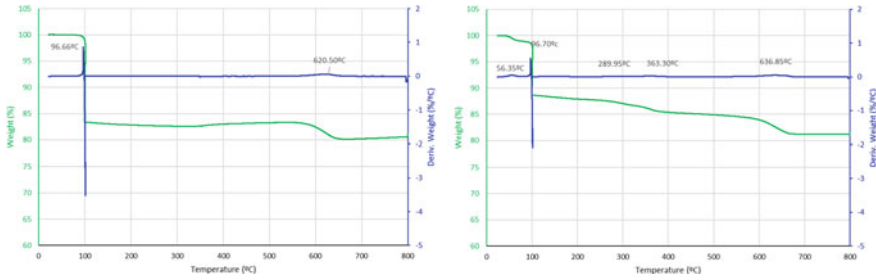
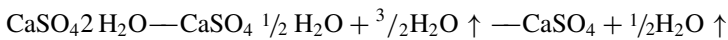


Fig. 5 TGA gypsum mortar B1 (left); TGA mortar B1:0.6LFS (right)

Depending on environmental conditions, the sample humidity is around 3.0% of the dry material weight.

The remaining mass loss corresponded to the transformation process of calcium sulphate dihydrate into calcium sulphate hemihydrate by the effect of heat [40], in accordance with the following expression:



Calcium sulphate dihydrate continues to dehydrate until all the constitutive water is lost, and it is converted into anhydrite. As from 600 °C, a second loss of material takes place, which corresponds to the formation of insoluble anhydrite II and with the transformation of magnesium calcium carbonate or dolomite present in the gypsum into lime oxide or magnesium oxide, respectively, according to the following formula [41]:



In the case of mortar B1:0.6 LFS, the thermogravimetric analysis showed a similar loss of mass at around 100 °C, due to the evaporation of water present in the natural state, and the transformation of calcium sulphate dihydrate.

A second loss took place at around 280–380 °C (3.2%), as a consequence of the transformation of characteristic components present in the LFS slag, such as the magnesium compounds (hydrotalcite or sjögrenita) and the calcium aluminates (mayenite) from reactions when in contact with the water.

The last peak of the curve, at around 650 °C, corresponded to the decomposition of calcium carbonates and magnesium, with a loss of CO<sub>2</sub>.

### 3.4.2 Behaviour in the Presence of Fire

The results obtained in the non-combustibility test are shown in Table 7.

**Table 7** Non-combustibility test

Mortar	$\Delta T^a$ in the oven ( $^{\circ}\text{C}$ )	Persistence of flame Llama (s)	Loss of mass (%)
B1:0.6LFS	5.0	–	18.14

**Table 8** Thermal conductivity

Sample	$T^a$ Avg. ( $^{\circ}\text{C}$ )	Thermal conductivity $\lambda = (\text{W}/\text{m}\cdot\text{K})$
B1	10.1	0.46
B1:0.6LFS	10.1	0.42

The non-combustibility test was applied to mortar B1:0.6LFS, to determine its inflammatory capacity and therefore its contribution to the propagation or otherwise of fire.

From the data registers, it may be confirmed that the selected mortar B1:0.6LFS presented good behaviour when in contact with fire, because, in the development of the test, the temperature increase ( $\Delta T^a$ ) was less than  $30^{\circ}\text{C}$ , and the sample loss of mass was less than 50.0% of the initial test material. For all the above, it may be concluded that in no way did the gypsum mortars contribute to the propagation of fire through its combustion.

The gypsum compounds, by their nature, are classified as A1 Euroclass in accordance with the provisions of Council Directive 89/106/EEC [42], because they withstand the effect of heat and high temperatures well. Nevertheless, LFS slag is a material that requires high temperatures to produce any alteration in its structure.

### 3.4.3 Thermal Transmittance

The results from the analysis of thermal conductivity are shown in Table 8. The values recorded show that reference mortar B1 presented a higher conductivity coefficient than mortar B1:0.6LFS.

The incorporation of the LFS aggregate leaves a lower density mortar ( $1745 \text{ kg}/\text{m}^3$ ), caused by its greater porosity, which is why this type of mortar behaves with greater insulative potential, interrupting the transfer of heat that passes through it.

### 3.4.4 Acoustic Absorption

In Fig. 6, the values of the acoustic absorption coefficients are shown. The records refer to the integrated average for the values recorded in the third octave (100–5000 Hz).

As can be seen, the results indicated that both mortars presented low acoustic absorption, following a similar pattern, which suggests that the LFS produces no effect on this property. As a consequence of this behaviour, its installation as rendering



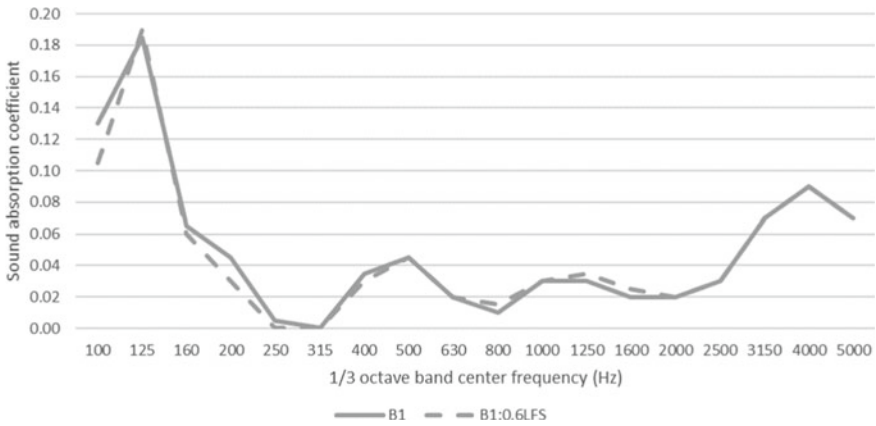


**Fig. 6** Coefficients of acoustic absorption

for interior walls determines the appearance of a reverberant field, hardly appropriate for interior sound quality.

As the values of the curves indicate low absorption, the value of the noise reduction coefficient (NRC) was determined, in accordance with the procedure from standard ASTM C423-17 [43], to establish the amount of energy absorbed by the mortars, when projecting the sound onto their surface.

In Table 9, the absorption coefficient values are shown, obtained from the frequencies in the Hz bandwidth (125/250/500/1000/2000) and the NRC value, as an average of the values in each one.

As may be seen, the NRC values, both of the reference gypsum mortar B1 and mortar B1:0.6LFS, were very close to 0 (0.025; 0.024), a characteristic value of perfect reflection.

This behaviour may be explained by low mortar porosity. The addition of LFS slag produced no modification in this property, with respect to the results of the reference mortar specimen.

**Table 9** Noise reduction coefficient

Sample	Sound absorption coefficient						$\alpha_{NRC}$
	125 Hz	250 Hz	500 Hz	1000 Hz	2000 Hz	4000 Hz	
B1	0.19	0.01	0.05	0.03	0.02	0.09	0.025
B1:0.6LFS	0.19	0.00	0.05	0.03	0.02	0.09	0.024

**Table 10** Compressive strength of prefabricated block

Sample	Average breaking load (kN)	Coefficient of variation (%)	Section (mm <sup>2</sup> )	Form factor (d) [54]	Normalized compressive strength (N/mm <sup>2</sup> )
B1	251,133	2.73	17,000	1.45	21.42
B1:0.6LFS	139,100	2.91	17,000	1.45	11.86

### 3.5 Compressive Strength of the Prefabricated Block

The block designs (340.0 × 200.0 × 50.0 mm) were tested under compression. The results, obtained as the compressive strength measurements of the six pieces, are shown in Table 10.

Standard EN 772-1:2011 + A1 [39] establishes two corrections for average compression test results, to determine the normalized compressive strength: a *coefficient of conditioning* as a function of the environmental curing conditions of the blocks and a *form factor* (d), which depends on the test piece size.

The standard establishes that the *coefficient of conditioning* is 1, for atmospheric curing in a laboratory environment, considering a relative humidity of  $50 \pm 5\%$  and a temperature of  $20 \pm 2$  °C. Moreover, in accordance with the dimensions of the part (height 50.0 and width 200.0 mm), the *form factor* is 1.45.

The results obtained in the compression test of the prefabricated blocks are similar to those obtained in the compressive strength test of the gypsum mortar specimens (20.54 N/mm<sup>2</sup>/12.39 N/mm<sup>2</sup>), following the same trend of decreasing resistance.

However, the results obtained showed a good performance of the prefabricated blocks made with LFS. It can be affirmed that they can be used with guarantees in the construction of interior partitions and internal facade cladding.

## 4 Conclusions

In accordance with the analysis, it can be affirmed that the gypsum mortars manufactured with LFS have properties and characteristics that are similar to traditional mortars. The following conclusions may be drawn from the investigation reported in this paper:

- The incorporation of LFS produces a slight reduction of mortar density in the fresh state and a non-significative increase of setting and hardening times.
- Regarding the mechanical resistance to flexion and compression, the mortars dosed with LFS underwent a reduction of mechanical capacity in all the mixture designs. Nevertheless, in all cases, mechanical strengths higher than 10 N/mm<sup>2</sup> were recorded for the mortars, which mean they are suitable for use in construction.

- The adherence of the mortars to ceramic substrates was also reduced after the incorporation of LFS, and the reduction being greater as the quantity of aggregate in the mixtures was increased.
- The suction capability of the mortars increased with the incorporation of LFS. The height of the water also reached higher levels in comparison with those noted in the reference gypsum specimen B1.

The complementary tests completed with mortar B1:0.6LFS, selected for use as a base material in the manufacture of prefabricated blocks, and yielded the following results:

- The incorporation of LFS slag determines good behaviour against thermal reaction. Because of its nature and composition, slags withstand high temperatures well, a behaviour reinforced by the nature of the gypsum. The reactions that occur, as the temperature is increased are specific to the transformations produced in their components.
- The selected mortar, B1:0.6LFS, showed good behaviour against fire, withstanding high temperatures with insignificant loss of mass. The slag components contributed nothing to the propagation of fire, and, in addition, the selected mortar mixtures can be categorized as Euroclass A1, because of the presence of gypsum.
- The selected mortar showed similar values of thermal transmission coefficient ( $\lambda$ ) as the reference mortar B1. Moreover, its acoustic absorption was very low, which produced intense reflection of the sound and reverberance in the rooms where it was used.

The prefabricated block was tested under compression, which determined the following conclusions:

- The mechanical strength of the block was adequate for the technical requirements of the masonry pieces, in accordance with the applicable norms.

**Acknowledgements** The authors are grateful to the *Consejería de Educación de la Junta de Castilla y León* (Spain) for grants awarded to the *Grupo de Investigación de Ingeniería de la Edificación de la Universidad de Burgos* (GIIE), channelled through funding for the *Proyecto de Investigación Autonomico* GIR D02V.03 2018-2021.

## References

1. Li X (2020) An urgent call for building green civilization: the natural environment is rapidly deteriorating. In: *Green Civilization*. Springer, Singapore. [https://doi.org/10.1007/978-981-15-7812-0\\_1](https://doi.org/10.1007/978-981-15-7812-0_1)
2. Ehrlich PR, Ehrlich AH (2013) Can a collapse of global civilization be avoided? *Proc Royal Soc B: Biol Sci* 280(1754):20122845. <https://doi.org/10.1098/rspb.2012.2845>
3. Appannagari RR (2017) Environmental pollution causes and consequences: a study. *North Asian Int Res J Soc Sci Humanities* 3(8):151–161

4. Tainter JA (2008) Collapse, sustainability, and the environment: how authors choose to fail or succeed. *Rev Anthropol* 37(4):342–371. <https://doi.org/10.1080/00938150802398677>
5. Brown LR (2013) *Eco-economy: building an economy for the earth*. Routledge. <https://doi.org/10.4324/9781315071893>
6. Chen Z (2020) Work together to create a better future for the world's ecological civilization. *Chin J Urban Environ Stud* 8(02):2075001. <https://doi.org/10.1142/S2345748120750019>
7. Ursul A, Ursul T (2018) Environmental education for sustainable development. *Future Human Image* 9(1):116. <https://doi.org/10.29202/fhi/9/12>
8. Basu S, Roy M, Pal P (2019) Corporate greening in a large developing economy: pollution prevention strategies. *Environ Dev Sustain* 21(4):1603–1633. <https://doi.org/10.1007/s10668-018-0121-3>
9. Majeed A, Wang L, Zhang X, Kirikkaleli D (2021) Modeling the dynamic links among natural resources, economic globalization, disaggregated energy consumption, and environmental quality: fresh evidence from GCC economies. *Resour Policy* 73:102204. <https://doi.org/10.1016/j.resourpol.2021.102204>
10. Puskás A, Corbu O, Szilágyi H, Moga LM (2014) Construction waste disposal practices: the recycling and recovery of waste. *WIT Trans Ecol Environ* 191:1313–1321. <https://doi.org/10.2495/SC141102>
11. Sáez PV, Osmani M (2019) A diagnosis of construction and demolition waste generation and recovery practice in the European Union. *J Clean Prod* 241:118400. <https://doi.org/10.1016/j.jclepro.2019.118400>
12. Pacheco-Torgal F (2014) Introduction to the environmental impact of construction and building materials. In: *Eco-efficient construction and building materials*. Woodhead Publishing, pp 1–10
13. Weglarz A, Gilewski P (2019) Innovative technologies in construction sector that meet criteria of sustainable development. In: *IOP conference series: materials science and engineering*, vol 661, no 1, IOP Publishing, p 012058. <https://doi.org/10.1088/1757-899X/661/1/012058>
14. Rakhova M, Nikonorova S (2018) Problems of implementing innovative solutions in the construction sector of economy organizations. In: *MATEC web of conferences*, vol 251. EDP Sciences, p 05013. <https://doi.org/10.1051/mateconf/201825105013>
15. Coelho A, De Brito J (2012) Influence of construction and demolition waste management on the environmental impact of buildings. *Waste Manage* 32(3):532–541. <https://doi.org/10.1016/j.wasman.2011.11.011>
16. Ding Z, Wang Y, Zou PX (2016) An agent based environmental impact assessment of building demolition waste management: conventional versus green management. *J Clean Prod* 133:1136–1153. <https://doi.org/10.1016/j.jclepro.2016.06.054>
17. Lawrence M (2015) Reducing the environmental impact of construction by using renewable materials. *J Renew Materials* 3(3):163–174. <https://doi.org/10.7569/JRM.2015.634105>
18. Huang B, Gao X, Xu X, Song J, Geng Y, Sarkis J, Nakatani J (2020) A life cycle thinking framework to mitigate the environmental impact of building materials. *One Earth* 3(5):564–573. <https://doi.org/10.1016/j.oneear.2020.10.010>
19. Costa C, Monteiro M, Rangel B, Alves FJL (2017) Industrial and natural waste transformed into raw material. *Proc Inst Mech Eng, Part L: J Mater: Des Appl* 231(1–2):247–256. <https://doi.org/10.1590/1980-5373-MR-2020-0043>
20. Sassanelli C, Rosa P, Rocca R, Terzi S (2019) Circular economy performance assessment methods: a systematic literature review. *J Clean Prod* 229:440–453. <https://doi.org/10.1016/j.jclepro.2019.05.019>
21. Oge M, Ozkan D, Celik MB, Gok MS, Karaoglanli AC (2019) An overview of utilization of blast furnace and steelmaking slag in various applications. *Mater Today: Proc* 11:516–525. <https://doi.org/10.1016/j.matpr.2019.01.023>
22. Zhang X, Chen J, Jiang J, Li J, Tyagi RD, Surampalli RY (2020) The potential utilization of slag generated from iron-and steelmaking industries: a review. *Environ Geochem Health* 42(5):1321–1334. <https://doi.org/10.1007/s10653-019-00419-y>
23. Thomas C, Rosales J, Polanco JA, Agrela F (2019) Steel slags. In: *New trends in eco-efficient and recycled concrete*. Woodhead Publishing, pp 169–190. <https://doi.org/10.1016/B978-0-08-102480-5.00007-5>

24. Santamaría-Vicario I, Rodríguez A, Gutiérrez-González S, Calderón V (2015) Design of masonry mortars fabricated concurrently with different steel slag aggregates. *Constr Build Mater* 95:197–206. <https://doi.org/10.1016/j.conbuildmat.2015.07.164>
25. Santamaría-Vicario I, Rodríguez A, Junco C, Gutiérrez-González S, Calderón V (2016) Durability behavior of steelmaking slag masonry mortars. *Mater Des* 97:307–315. <https://doi.org/10.1016/j.matdes.2016.02.080>
26. Alonso A, Rodríguez A, Gadea J, Gutiérrez-González S, Calderón V (2019) Impact of plasterboard with ladle furnace slag on fire reaction and thermal behavior. *Fire Technol* 55(5):1733–1751. <https://doi.org/10.1007/s10694-019-00828-6>
27. Rodríguez A, Gutiérrez-González S, Horgnies M, Calderón V (2013) Design and properties of plaster mortars manufactured with ladle furnace slag. *Mater Des* 1980–2015(52):987–994. <https://doi.org/10.1016/j.matdes.2013.06.041>
28. Yang F (2015) Contemporary construction of ecological civilization: from ecological crisis to ecological governance. *Chin J Urban Environ Stud* 3(04):1550030. <https://doi.org/10.1142/S234574811550030X>
29. Zhu T, Gao S (2014) Promoting circular development and recycling solid waste-In the view of ecological civilization construction. In: *Advanced materials research*, vol 878. Trans Tech Publications Ltd, pp 873–878. <https://doi.org/10.4028/www.scientific.net/AMR.878.873>
30. Ghaffar SH, Burman M, Braimah N (2020) Pathways to circular construction: an integrated management of construction and demolition waste for resource recovery. *J Clean Prod* 244:118710. <https://doi.org/10.1016/j.jclepro.2019.118710>
31. EN 13279-1: 2009 Gypsum Binders and Gypsum Plasters—Part 1: definitions and requirements. European Committee for Standardization Brussels, Belgium
32. EN 13279-2:2014. Gypsum binders and gypsum plasters—Part 2: test methods. European Committee for Standardization, Brussels, Belgium
33. UNE 102042: 2014 Gypsum plasters. Other test methods. Asociación Española de Normalización y Certificación, Madrid, España
34. EN 1015-19:1999 Methods of test for mortar for masonry—Part 19: determination of water vapour permeability of hardened rendering and plastering mortars. European Committee for Standardization, Brussels, Belgium
35. EN 1015-18:2003 Methods of test for mortar for masonry—Part 18: determination of water absorption coefficient due to capillary action of hardened mortar. European Committee for Standardization, Brussels, Belgium
36. EN ISO 1182:2011 Reaction to fire tests for products—Non-combustibility test. European Committee for Standardization, Brussels, Belgium
37. EN ISO 10534-2:2002 Acoustics—determination of sound absorption coefficient and impedance in impedances tubes—Part 2: transfer-function method. European Committee for Standardization, Brussels, Belgium
38. ASTM 1114-06 2019 Standard test method for steady-state thermal transmission properties by means of the thin-heater apparatus. American Society for Testing and Materials. Pennsylvania, USA
39. EN 772-1:2011+A1 Methods of test for masonry units—Part 1: determination of compressive strength. European Committee for Standardization, Brussels, Belgium
40. Ghazi K, Hugi E, Wullschlegler L, Frank TH (2007) Gypsum board in fire-modeling and experimental validation. *J Fire Sci* 25(3):267–282. <https://doi.org/10.1177/0734904107072883>
41. Yu QL, Brouwers HJ (2012) Thermal properties and microstructure of gypsum board and its dehydration products: a theoretical and experimental investigation. *Fire Mater* 36:575–589. <https://doi.org/10.1002/fam.1117>
42. European Union. Council Directive 89/106/EEC of 21 December 1988 on the approximation of laws, regulations and administrative provisions of the Member States relating to construction products. <http://data.europa.eu/eli/dir/1989/106/2003-11-20>
43. ASTM C423-17 (2017) Standard test method for sound absorption and sound absorption coefficients by the reverberation room method. ASTM International, West Conshohocken, PA

# Lightweight Recycled Polyurethane Mortar Placement: A Case of Success



Verónica Calderón, Lourdes Alameda Cuenca-Romero,  
Sara Gutiérrez-González, and Raquel Arroyo

**Abstract** The objective of this case study is based on establishing the real possibilities for the placement of cement mortars lightened with recycled shredded polyurethane, and their performance over a very long period of time, several years. Multiple types of mortars have been designed and dosed to be used as masonry base and resurfacing mortars. On site, therefore, it has been used as joint mortar and rendering mortar in a small shed. Mechanical flexural and compressive strength tests have been carried out on the samples made in the laboratory and on the samples taken from the mortar mixed on site. Adhesion tests have also been carried out on mortars applied as coatings, both exterior and interior. Organoleptic and other aptitude tests complete the study. The results show that this type of material is viable for application as a support for traditional coatings and finishes. This is a good advance in the real viability of reusing inert polymeric wastes in the construction sector, with the consequent environmental benefit, and in the line of contributing to the sustainability of the sector applied to construction materials.

**Keywords** Recycled shredded polyurethane · Performance · Sustainability

## 1 Introduction

Nowadays, different areas are working on actions to raise environmental awareness, reuse and recycling through European, national and regional programs [1], as well as through different studies [2], with the purpose of reducing the existing dependence on raw materials and trying to reuse wastes.

This kind of initiatives has led to the development of new waste recycling techniques, in this case for the construction sector, such as rubber [3, 4], foamed plastic wastes [5], electrical and electronic plastic wastes [6], recycled polyamide [7, 8], polyethylene wastes (PET) [9] or even recycled concrete and mortar wastes [10], as

---

<https://investigacion.ubu.es/grupos/1824/detalle>

---

V. Calderón (✉) · L. A. Cuenca-Romero · S. Gutiérrez-González · R. Arroyo  
Departamento de Cosntrucciones Arquitectónicas e I.C.T, Universidad de Burgos, Burgos, Spain  
e-mail: [vcalderon@ubu.es](mailto:vcalderon@ubu.es)

well as recycled aggregates [11]. In this way, the aim is to reuse wastes as new raw materials, leading to the closing of production cycles toward continuous reuse.

Worldwide, plastic production has grown exponentially in recent decades. However, in Europe, only a third of this material is recycled. About 40% of post-consumer plastic waste is incinerated with energy recovery, and the rest is landfilled or recycled. About half of the recovered and recycled plastic wastes are treated in the European Union; the other half is exported, mainly to China [12].

In 2018, the European Commission published a communication establishing a strategy for plastics in a circular economy. The strategy identifies the main challenges, such as low reuse and recycling rates of plastic waste, greenhouse gas emissions associated with the production and incineration of plastics, and the presence of plastic waste (including microplastics) in the oceans [13].

The construction sector generates 20 million jobs in Europe and accounts for almost 10% of GDP (Gross Domestic Product). The materials used in this sector account for 42% of our final energy demand, approximately 35% of our greenhouse gas emissions and more than 50% of all materials removed. In this way, the use of plastic waste for construction applications can improve environmental sustainability, and can serve as a reliable source of building materials [14].

Concerning construction wastes, numerous experiments are being carried out with the aim of recovering them and diverting them to landfills so that they can be treated at the end of their useful life [15]. In this sense, technologies such as energy recovery, mechanical recycling and chemical recycling are being used to carry out this recycling [16]. Despite these efforts, the need for a collecting, sorting and treatment infrastructure blocks to a certain degree the recycling of these wastes.

In accordance with similar previous studies on the recycling of polymeric wastes [17], on the recycling of polyurethane [18], or on the study of mortars with polyurethane wastes [19], this research is focused on the use of two different polyurethane wastes, obtained from wastes of two different industrial sectors, one from the automotive industry and the other from a factory dedicated exclusively to the manufacture of polymeric foams for construction and refrigeration, valued as a raw material with added value for incorporation into the pre-fabrication industry of the construction sector, which consumes an enormous amount of natural resources (aggregates, cement, energy, water, CO<sub>2</sub> emissions, etc.).

This study is carried out as a proposal for a circular economy network and reuse of a waste that is found in large quantities, and the development in this way of sustainable innovation solutions for cement mortars in construction.

## 2 Materials and Methods

The purpose of this research is the application of mortars made with polyurethane foam, which comes from waste from the automotive industry, partially replacing the amount of aggregates in the mortars with these wastes.

## 2.1 Raw Materials

- Gray polyurethane foam. This is a foam from the automotive industry (Grupo Antolin, Burgos), gray color and semi-rigid (Fig. 1). It was shredded to particle sizes between 0 and 2 mm before being used as a substitute for sand for mortars, since it was considered that this first approximation would provide the most suitable characteristics for the mortars to be manufactured. The density obtained after crushing was  $68 \text{ kg/m}^3$ .
- Cement. Two different cements have been chosen for the dosage and characterization of the mixtures, CEM II/B-L 32.5R and CEM IV/B-V 32.5R, which are two cements commonly used in masonry.
- Sand. The sand used is mine sand, reddish-brown in color, as can be seen in the photograph. A particle size always smaller than 4 mm has been used, with the granulometry shown in the table (Fig. 2).



Fig. 1 Appearance of crushed polyurethane



	%
Sifter 4 mm	0
Sifter 2 mm	5,8
Sifter 1 mm	13,18
Sifter 0,5 mm	34,72
Sifter 0,250 mm	31,01
Sifter 0,125 mm	11,04
Sifter 0,063 mm	3,19
Pass	1,06
Total	100

Fig. 2 Appearance of the sand used and granulometry



## 2.2 Dosages

Samples were prepared by combining polyurethane with 2 different types of cements, with 2 different cement/aggregate ratios (1/4 and 1/6), the aggregate being the addition of sand + polyurethane waste, and substituting 0, 25, 50, 50, 75 and 100% of sand with polyurethane (Table 1).

The manufactured mortars have been characterized both in fresh and hardened state. For this purpose, the dosages indicated previously have been manufactured. The nomenclature of each dosage specifies the type of cement used (II or IV), the cement/aggregate weight ratio for each type of cement (1/4 and 1/6), and the percentage of aggregate replaced by polyurethane (0, 25, 50, 75, 100).

To manufacture the mortars with partial or total substitution of sand by polyurethane waste, the quantities of foam in equivalent volume of substituted sand were weighed and the mixture was mixed, making sure in each case that the quantity of water was adequate for good workability.

Mechanical tests were carried out on all the samples with  $4.00 \times 4.00 \times 16.00$  mm prismatic samples, which were initially broken in two pieces by flexural stress and

**Table 1** Dosages

Series n°	Cement	Cement/(sand + polyurethane waste)	Replacement of polyurethane by sand (%)	Name
Series 1	CEM II	1/4	0	MII-4-0PU
			25	MII-4-25PU
			50	MII-4-50PU
			75	MII-4-75PU
			100	MII-4-100PU
		1/6	0	MII-6-0PU
			25	MII-6-25PU
			50	MII-6-50PU
			75	MII-6-75PU
			100	MII-6-100PU
Series 2	CEM IV	1/4	0	MIV-4-0PU
			25	MIV-4-25PU
			50	MIV-4-50PU
			75	MIV-4-75PU
			100	MIV-4-100PU
		1/6	0	MIV-6-0PU
			25	MIV-6-25PU
			50	MIV-6-50PU
			75	MIV-6-75PU
			100	MIV-6-100PU

then broken by compression according to the UNE EN 1015-11 standard. The results obtained lead us to set the appropriate mechanical compressive strength for masonry mortars at around a minimum of 5 MPa. The use of mortar for coatings requires a minimum compressive strength of 1.5 MPa for all types of interior coatings and 3.5 MPa for exterior coatings, so it is also possible to set the minimum compressive strength condition of 3.5 MPa for coating mortars.

Mortars that meet the minimum compressive strength requirements of 5.0 N/mm<sup>2</sup> are:

- M II-4-50PU
- M IV-4-50PU
- M IV-6-50PU
- M IV-6-75PU

These mortars have been chosen for pilot testing as joint and rendering mortars.

### 2.3 Experimental

Several previous articles have studied the durability of alternative materials such as geopolymeric materials with industrial waste [20], new cement–polymer composites with recycled polystyrene foam [21], or waste polymers (PET, polycarbonate and automobile tires) [22]. The behavior of materials such as geopolymer concrete as an alternative to Portland cement concrete [23], or mortar powder and recycled concrete in concretes [24] have been studied to investigate their behavior, and tests have been carried out on mortars with polymer waste to improve their properties [25].

In this case, masonry mortars have been studied, which are usually used as mortars for masonry base and coating mortars, so that the first application and application on site has been as joint and plastering mortar. In addition, an application has been made as a floor leveling layer to cover pipes and as a base for pavement.

For the mortar application, a rectangular storage shed has been built with external dimensions of 4.25 m by 2.70 m and an average height of 2.25 m. The short walls are facing north and south. The short walls have a north–south orientation and the long walls have an east–west orientation. The roof is one-water. The final use of the shed will be for storage of small products and hazardous products until the work is completed (estimated time 2 years).

The shed has been built in the “Cúpula de la Energía” complex, in the town of Garray, province of Soria, at an altitude of 1011 m.

A lightly reinforced concrete floor has been built on which the walls have been built. Two types of bricks were used. For the two longer walls, a brick with perforations in the head was used, with dimensions of 24 cm of string, 11.5 cm of shear and 9.5 cm of thickness and laid with partition (9.5 cm thickness). The two short walls were built with bricks with dimensions 24 cm of brickwork, 11 cm of brickwork and 10 cm thick and laid with half a foot (thickness 11 cm).

The construction has been laid out and the reinforced concrete slab on which the enclosure walls have been placed has been executed.

The units of work not executed with polyurethane aggregate mixtures were completed with cement mortars and traditional dosages.

### 2.3.1 On-Site Mixing

To make the on-site mixing, the sand was weighed in a plastic container and placed in the concrete mixer. Then the polyurethane was weighed and put into the mixer. The sand and the polyurethane have been previously mixed with the addition of water, approximately 50% of the total water required for the 50 l of mortar. The duration of this mixing is approximately 2 min, producing a quite homogeneous mixture. Finally, the cement has been weighed, introduced into the mixer and the rest of the water has been added to complete the dosage. The whole mixture was mixed for 2 min.

### 2.3.2 On-Site Application

The shed with the mortars used in each area of the shed is shown below (Fig. 3):

The mortars used for each of the applications were as follows:

#### Mortar M II-4-50PU

This dosage has been used as exterior and interior plastering mortar for the walls. The dimensions of this wall are 2.70 m long and 2.25 m high, with a thickness of 11 cm. The brick, with one side with a rough surface and the other side with a smooth surface, has been placed either with the rough side on the inside or the outside. The exterior plastering mortar was applied in two layers of an average thickness of 0.6 cm each, for a total thickness of 1.2 cm. The mortar was finished with a trowel, and a portion of the wall was also burnished with a trowel. Before applying the mortar, the brickwork was humidified.

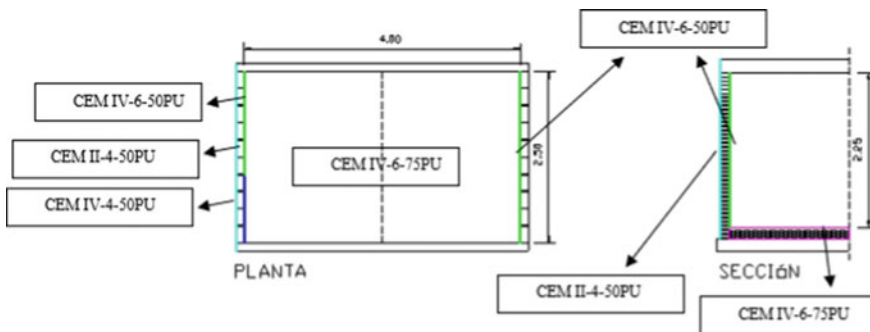


Fig. 3 Mortars used in each area of the building



**Fig. 4** Application of the plaster in the first layer and partial burnishing of the wall. Execution of the 1/2 foot wall

### **Mortar M IV-4-50PU**

This mortar has been used in the execution of the joints of the short wall to the north. The exterior dimensions of the wall are 2.70 m long by 2.25 m of average height and a thickness of 11 cm. The average thickness of the joint between bricks was 1.2 cm, although in some areas the thickness has been increased. Before laying, the brick was humidified by placing it in a barrel with water for just a few seconds to prevent it from saturating.

This wall was then coated on the outside with cement mortar plaster.

### **Mortar M IV-6-50PU**

This dosage has been used in the wall brick bedding. The external dimensions of the walls are 4.25 m long and 2.50 m high, with a thickness of 9.5 cm. The average joint thickness between the bricks was 1.2 cm. The joint thickness has been increased in some of the finishing areas. Before laying the bricks, they were wetted with water.

These walls have been left in the open air without exterior coating.

### **Mortar M IV-6-75PU**

It has been placed as a mortar in a floor leveling layer in the inside (to cover pipes and floor screed prior to the pavement). The dimensions of the leveling layer were 2.52 m long by 1.25 m wide and 6 cm thick.

## **2.3.3 On-Site Placement of Mortars**

Execution of Exterior Plastering. M II-4-50PU

Easy to apply with no perceptible sagging (Fig. 4).



**Fig. 5** Placing and compacting mortar with ruler

#### Execution of Interior Plastering. M II-4-50PU

Mortar similar to conventional mortars, easy to apply and without appreciable sagging.

#### Wall Construction with Joints for Coating. M IV-4-50PU

Behavior and plasticity are similar to conventional mortars.

#### Execution of Wall with Visible Joints. M IV-6-50PU

Behavior and plasticity similar to conventional mortars, producing a very slight flattening of the mortar during compaction, with small bumps on the brick. Slight loss of water in the compaction process, without leaving stains on the brick.

#### Execution of Interior Floor Paving. M IV-6-75PU

Mortar easy to apply on site, without air bubbles and whose handling is similar to a self-leveling mortar (Fig. 5).

#### Ceramic Tile Covering. M II-4-50PU

A medium–high absorption ceramic tile has been placed on the interior plaster of mortar M II-4-50PU. A gray interior tile adhesive cement “Weber Col. Gris,” suitable for medium–high absorption substrates and tiles, was used. It was applied with an 8 × 8 mm trowel according to the manufacturer’s instructions. The substrate has not been wetted.



**Fig. 6** Ceramic tile covering and flooring on both floors

### Ceramic Tile Flooring. M IV-6-75PU

Medium–high absorption ceramic tile has been installed on the leveling floors of the M IV-6-75PU mortars (Fig. 6). A gray glue cement for interiors “Weber Col. Gris” was used. It was applied with an  $8 \times 8$  mm trowel according to the manufacturer’s instructions. The surfaces of the floor screeds were previously cleaned of dust. The substrate was not wetted.

## 3 Results and Discussion

### 3.1 Test Results of Samples Obtained at the Construction Site

#### 3.1.1 Mechanical Tests

Samples of the floor and wall mortars were taken on site to carry out mechanical tests of flexural and compressive strength. The samples of dimensions  $(4 \times 4 \times 16)$  cm<sup>3</sup> were made with the mortar placed in the middle part of the wheelbarrow. The molds with the samples were covered with glass and were kept for the first few hours in a building shed and then moved to Burgos, to the laboratory’s humid chamber. They were demolded after 48 h and cured for 28 days in the chamber.

The results of the flexural and compression tests at 28 days are shown in Table 2, showing on the one hand the results of the samples taken in the laboratory and on the other hand the results of the samples taken from the mortar mixed on site.

The results on the samples collected on site indicate an increase in compressive strength in the tests with type II cement and a 50% replacement of sand, and a decrease in the tests with type IV cement and a 75% replacement of sand by polyurethane. The difference in the results on site compared to the laboratory results may be due to the variation in the water–cement ratio, since the amount of water in the mortar on site was a function of the plasticity required by the workers. Another factor to take into account that may have influenced the results is the compaction done, which

**Table 2** Flexural and compressive strength at 28 days. Mortars placed on site

Mortar	Flexural strength (MPa)		Compressive strength (MPa)	
	Laboratory	Construction	Laboratory	Construction
M II-4-50PU	1.92	2.78	7.01	9.46
M IV-6-75PU	1.15	1.10	4.03	2.84

**Table 3** Adhesion resistance. Mortars placed on site

Mortar	Adhesion strength (N/mm <sup>2</sup> )	
	Laboratory	Construction
M II-4-50PU	0.14	0.18

was somewhat deficient in the mortar with 75% foam. In any case, acceptable results have been obtained, which should be contrasted with the long-term strengths.

### 3.1.2 Adherence Tests of Mortars Placed on Site

Adherence tests have been carried out on the mortar applied as a coating, both exterior and interior. The panel was kept on site for 18 days, until it was ensured that its removal did not involve significant stresses on the mortar. After that, adhesion measurements were carried out in accordance with the UNE EN 1015-12 standard, which are shown in Table 3.

As can be seen from the values obtained, there is greater adhesion on site than in the laboratory. These results are only orientative, since the brick used in the laboratory is different from the one used on site, especially with regard to surface roughness. The site conditions have been different and the mechanics used to take the samples, in a vertical layer and compacted by the workers, differs from that used in the laboratory. However, the results indicate that the adhesion of the mortars is high with a traditional on-site technique.

## 3.2 Test Results on Work Site Units

Certain aspects relating to the behavior of mortars as a coating itself or as a base for a subsequent traditional coating, with ceramic material or paint, have been studied.

### 3.2.1 Organoleptic Tests

The organoleptic tests of the mortar placed on site consisted of a visual evaluation of the coating and leveling mortars and one of the joint mortars.

**Fig. 7** Crack width 2.5 mm.  
Mortar in floor screed M  
IV-6-75PU



## Initial Results

No modifications have been detected in the texture of the plastering mortar, M II-4-50PU, neither has cracking due to plastic shrinkage been observed.

The mortars placed in floors show an important initial cracking by plastic shrinkage a few hours after their placement. The most determining factors that have influenced shrinkage cracking have been the following:

- Thickness of 6 cm of the mortar layer. For thicknesses of this type and floor screed mortars, the use of larger aggregates is recommended, generally of sizes up to 8–10 mm, which would result in the preparation of fine aggregate concretes.
- Richness in binders. In general they do not seem excessively high dosages, although for this type of mortar, of leveling base, dosages of 1/8 or 1/10 are recommended.
- Intense drying shrinkage. The environmental conditions have been of low humidity and temperatures above 30 °C. In addition, a part of the floor was exposed to the sun for more than one hour.

## Results After 28 days

The storage shed has been used since the eighth day for storage and as a stay area for the workers, so that the traffic inside the shed can be considered as important and perhaps similar to that of a leveling floor in a building under construction, taking into account that the execution of the leveling floors corresponds to the final phase of the work.

The stay of the workers inside the building in a seated position means that the abrasion of the floor due to the movement of the footwear has a certain importance. As a result, the M IV-6-75PU screed mortar has suffered a slight surface abrasion. No signs of erosion were observed in the coating mortars.

Direct observation of the mortars placed on site does not differ much from the appearance of the mortar a few hours after placement. The shrinkage cracks in the mortars placed as floor screeds have increased slightly in width and length Fig. 7, and no new surface cracking has appeared.





**Fig. 8** Good adhesion of the mortar to the masonry and adhesive. Homogeneous distribution of the mortar on the surface of the brick

### Suitability Tests

In order to check the suitability of the mortars 28 days after their installation, the following suitability tests were carried out:

- Placement of ceramic tile with adhesive on the interior plaster and on the base screeds for interior flooring.
- Checking the adherence of the base leveling mortar to the concrete floor surface.
- Application of plastic paint on exterior plaster facing.
- Application of coating-finishing paint on mortar floors.
- Estimation of the penetration resistance with the introduction of a nail in the mortars of joints and of floor screeds.

### Ceramic tile adherence

To evaluate the suitability of the interior plaster mortar as a base for traditional coatings, a sample was taken from the enclosure wall of the building with a tile placed 28 years earlier (Fig. 8).

In the extraction of the sample, the homogeneity and continuity of the plaster was checked, in a layer of 1–1.2 mm. Subsequently, a tile was removed by levering it with a fingernail. Due to the good adhesion, the tile was broken into two pieces. Figure 8 shows the good adhesion of the adhesive to the plaster, since the adhesion failed at the adhesive-tile interface.

Once in the laboratory, the homogeneous distribution of the mortar and the good adhesion of the plaster mortar to both the adhesive and the brickwork can be verified.

The adhesion of the adhesive to the M IV-6-75PU mortar floor screed was also tested, with the following results (Fig. 9).

### Adhesion on concrete surface

A sample was taken from the M IV-6-75PU mortar on site to determine the degree of adherence of the mortar floor screed (Fig. 10). You can see part of the surface layer of the concrete screed, darker in color, joined to the mortar, which shows good adhesion between both materials.



**Fig. 9** Good adhesion of the adhesive to floor screed mortars



**Fig. 10** Sample and concrete screed mortar contact plane

### **Penetration resistance**

A steel point has been hammered into the joint mortar M IV-6-50PU and the leveling screed mortar M IV-6-75PU. The test consisted of driving with a traditional hammer. Penetration was not measured with a given number of blows, but simply the resistance was observed when the hammer was struck. The nail was subsequently extracted.

The resistance to the penetration appreciated when hitting with the hammer, in the mortar of joints has been important, even reaching the point of bending the steel nail. Subsequently, the nail has been removed, offering some resistance. The resistance to penetration of the floor has been lower. The M IV-6-75PU mortar has offered enough resistance and the subsequent extraction of the nails has been difficult.

## **4 Conclusions**

Mortars have been made with rigid polyurethane foam residues, previously crushed, partially or totally replacing sand in cement mortars, obtaining workable, homogeneous and plastic mixtures in the fresh state. The mechanical performance of these recycled mortars is lower to that of the reference mortars, but they comply with the specifications of the European standards for their use on site as mortars for masonry

and mortars for rendering and plastering. Mortars that meet the minimum compressive strength requirements have been selected and pilot tests have been carried out with them as joint and plaster mortar. The feasibility of these materials for their application in situ has been tested, verifying that the mixing and application conditions are similar to those of the reference mortars and that they are suitable as a support for traditional coatings and finishes.

The reuse of polyurethane foam waste produces an important environmental benefit, since the volume of mortar used in a building implies a large volume of recycled waste. Recycling is an added value compared to possible energy recovery, and to a greater extent compared to disposal in landfills.

**Acknowledgements** Authors gratefully acknowledge the financial support of BU070P20 Project funded by the Fondo Europeo de Desarrollo Regional (FEDER) of the EU and the Junta de Castilla y León (Spain).

## References

1. Grubert E (2018) Relational values in environmental assessment: the social context of environmental impact. *Curr Opin Environ Sustain* 35:100. <https://www.sciencedirect.com/journal/current-opinion-in-environmental-sustainability/vol/35>
2. Ahmad W, Ayaz A, Krzysztof A, Ostrowski A, Aslam F, Joykladd P (2021) A scientometric review of waste material utilization in concrete for sustainable construction. *Case Stud Constr Mater* 15. <https://www.sciencedirect.com/science/article/pii/S2214509521001984>
3. Amiri M, Hatami F, Golafshani EM (2021) Evaluating the synergic effect of waste rubber powder and recycled concrete aggregate on mechanical properties and durability of concrete. *Case Stud Constr Mater* 15. <https://www.sciencedirect.com/science/article/pii/S221450952101546>
4. de Souza Kazmierczak C, Dutra Schneider S, Aguilera O, Carine Albert C, Mancio M (2020) Rendering mortars with crumb rubber: mechanical strength, thermal and fire properties and durability behavior. *Constr Build Mater* 253:30. <https://www.sciencedirect.com/science/article/pii/S0950061820310072?via%3Dihub>
5. Nwaubani SO, Parsons LA (2021) Properties, durability and microstructure of concrete incorporating waste electrical and electronic plastics as partial replacement for aggregates in concrete. *Case Stud Constr Mater* 15. <https://www.sciencedirect.com/science/article/pii/S2214509521002461?via%3Dihub>
6. Courard L, Michel F, Incarnato L, Scarfato P, Di Maio L (2018) Hygro-thermal and durability properties of a lightweight mortar made with foamed plastic waste aggregates. *Constr Build Mater* 170:200–206. <https://www.sciencedirect.com/science/article/pii/S0950061818305737>
7. Horgnies M, Gutiérrez-González S, Rodríguez A, Calderón V (2014) Effects of the use of polyamide powder wastes on the microstructure and macroscopic properties of masonry mortars. *Cement Concr Compos* 52:64–72. <https://www.sciencedirect.com/science/article/pii/S0958946514000845?via%3Dihub>
8. Dawood AO, AL-Khazraji H, Falih RS (2021) Physical and mechanical properties of concrete containing PET wastes as a partial replacement for fine aggregates. *Case Stud Constr Mater* 14. <https://www.sciencedirect.com/science/article/pii/S2214509520301546>
9. Yanga D, Liu M, Zhang Z, Yao P, Ma Z (2022) Properties and modification of sustainable foam concrete including eco-friendly recycled powder from concrete waste. *Case Stud Constr Mater* 16. <https://www.sciencedirect.com/science/article/pii/S2214509521003417>

10. Fueglein E (2015) About the use of identify—a thermoanalytical database—for characterization and classification of recycled polyamides. *J Thermal Anal Calorimetry* 121(3). <https://link.springer.com/article/10.1007%2Fs10973-015-4583-3>
11. Vitale F, Nicoletta M (2021) Mortars with recycled aggregates from building-related processes: a ‘four-step’ methodological proposal for a review. *Sustainability* 13(5):2756. <https://www.mdpi.com/2071-1050/13/5/2756>
12. Strategy on plastics in the circular economy. EU (Online) (2017). <https://www.europarl.europa.eu/legislative-train/theme-new-boost-for-jobs-growth-and-investment/file-strategy-on-plastics-in-the-circular-economy>
13. Communication on “A European Strategy form Plastics in a Circular Economy” (Online). Available: <https://www.europeansources.info/record/communication-on-a-european-strategy-for-plastics-in-a-circular-economy/>
14. Awoyera PO, Adesina A (2020) Plastic wastes to construction products: status, limitations and future perspective. *Case Stud Constr Mater* 12. <https://www.sciencedirect.com/science/article/pii/S2214509520300024?via%3Dihub>
15. Yang W, Dong Q, Liu S, Xie H, Liu L, Li J (2012) Recycling and disposal methods for polyurethane foam wastes. *Proc Environ Sci* 16:167–175. <https://www.sciencedirect.com/science/article/pii/S1878029612005610>
16. EEA Report No 4/2020 Bio-waste—mainly food and garden waste—is a key waste stream with a high potential for contributing to a more circular economy. This report provides an overview of bio-waste generation, prevention, collection, and treatment in Europe. (Online). <https://www.eea.europa.eu/publications/bio-waste-in-europe>
17. Martínez-López M, Martínez-Barrera G, del Coz-Díaz JJ, Martínez-Martínez JE, Gencel O, Ribeiro MCS, Varela-Guerrero V (2018) Polymer waste materials as fillers in polymer mortars: experimental and finite elements simulation. *Case Stud Constr Mater* 9. <https://www.sciencedirect.com/science/article/pii/S2214509518300421?via%3Dihub>
18. Simón D, Borreguero AM, de Lucas A, Rodríguez JF (2018) Recycling of polyurethanes from laboratory to industry, a journey towards the sustainability. *Waste Manage* 76:147–171. <https://www.sciencedirect.com/science/article/pii/S0956053X18301831?via%3Dihub>
19. Gómez-Rojo R, Alameda L, Rodríguez A, Calderón V, Gutiérrez-González S (2019) Characterization of polyurethane foam waste for reuse in eco-efficient building materials. *Polymer* 11:359. <https://www.mdpi.com/2073-4360/11/2/359>
20. Oliveira L, Azevedo A, Marvilam MT, Pereira E, Fedul R, Vieira C (2021) Durability of geopolymers with industrial waste. *Case Stud Constr Mater*. <https://www.sciencedirect.com/science/article/pii/S2214509521003545?via%3Dihub>
21. Eskandera SB, Saleh HM, Tawfik ME, Bayoumia TA (2021) Towards potential applications of cement-polymer composites based on recycled polystyrene foam wastes on construction fields: impact of exposure to water ecologies. *Case Stud Constr Mater* 15. <https://www.sciencedirect.com/science/article/pii/S2214509521001790>
22. Martínez-López M, Martínez-Barrera G, Coz-Díaz G, Martínez-Martínez J, Gencel O, Ribeiro MCS, Varela-Guerrero V (2018) Polymer waste materials as fillers in polymer mortars: experimental and finite elements simulation. *Case Stud Constr Mater* 9. <https://www.sciencedirect.com/science/article/pii/S2214509518300421>
23. Azarsa P, Gupta R (2020) Durability and leach-ability evaluation of K-based geopolymer concrete in real environmental conditions. *Case Stud Constr Mater* 13. <https://www.sciencedirect.com/science/article/pii/S2214509520300383>
24. Yang D, Liu M, Zhang Z, Yao P, Ma Z (2022) Properties and modification of sustainable foam concrete including eco-friendly recycled powder from concrete waste. *Case Stud Constr Mater* 16. <https://www.sciencedirect.com/science/article/pii/S2214509521003417>
25. Martínez-Barrera G, Martínez-López M, Coz-Díaz J, López-Gayarre F, Varela-Guerrero V (2019) Waste polymers and gamma radiation on the mechanical improvement of polymer mortars: experimental and calculated results. *Case Stud Constr Mater* 11. <https://www.sciencedirect.com/science/article/pii/S2214509519301500>

# Earth as a Sustainable Construction Material. Characterization of Different Mixtures and Implementation Using the Projected Earth System



Ignacio Valverde-Palacios, Raquel Fuentes-García,  
Ana Cervilla-Maldonado, and Ignacio Valverde-Espinosa

**Abstract** The use of the earth as a construction material has been carried out all over the world, in walls, ramparts, fortifications. For this reason, research of this type is necessary to implement current techniques in the restoration of rammed earth constructions with the rammed earth technique. In addition, it can be used for the construction of new works for both walls and cladding. The research of the earth as a construction material is presented here through the characterization of the earth itself, in this case, edaphic soils from the weathering of the Alhambra Formation (Spain), and its mixtures with aerial or hydraulic limes and cement of low resistance. In addition, natural or recycled aggregates and additives such as water repellents and ecological enzymes, to replace binders, and additions of powder rubber and textile from used tire waste have been used. The results obtained in all the mixtures, except the one added with rubber and textile powder, are ideal for use in restoration of earth works and new construction, placed on site using the projected earth system.

**Keywords** Earth · Projected earth system · Restoration of rammed earth · Lime · Ecological enzyme · Powder rubber and textile fiber

## 1 Introduction

Construction materials are considered environmental resources which have been obtained in order to be treated to shape the buildings that surround us. These materials undergo, to a greater or lesser extent, a series of natural processes that help us better understand how they are to be used and used, as well as their behavior throughout their useful life. Throughout history, the methods of extraction and treatment of these have changed, enhancing their virtues and facilitating adaptation to the different requirements to which they are going to be exposed.

All this great variety of materials that we find around us has a common component reinterpreted since the beginning of construction, we speak of a vernacular

---

I. Valverde-Palacios (✉) · R. Fuentes-García · A. Cervilla-Maldonado · I. Valverde-Espinosa  
Department of Building Construction, Technical Upper School of Architecture, University of Granada, Campo del Príncipe, 18071 Granada, Spain  
e-mail: [nachoval@ugr.es](mailto:nachoval@ugr.es)

architecture, an architecture understood and based on the genesis of its environment, in which its components have that authenticity imprinted in their training. One of the materials that most corresponds to this comment is about the earth, this being one of the most used materials throughout history. It is a material present in practically all parts of the world, having been exploited by a multitude of civilizations which have used many techniques. All this set of practices provides us with information about how the land gives identity and shape to the constructions and elements in which it is used, arriving with this statement at the concept of heritage.

However, conserving the heritage built on land is not only considering the construction typology and its limitations, but it also consists of a task of research, rescue, and dissemination of the techniques used, which, since it is traditional architecture, depends on regional wisdom and presents the disadvantage that, since they are knowledge transferred orally, they do not appear in documents. To a certain extent, this problem has influenced the fact that currently the choice of the extraction area for the material is not an easy task, this being one of the main factors for the construction of walls.

The rammed earth is a constructive system used for millennia in places like Egypt, India, China, Syria, Peru, etc. In Spain, the land heritage built using this technique is quite extensive; in fact, it has remains belonging to 820 BC [16]. Specifically, in Granada (Spain) is one of the most extensive monuments built with rammed earth, the Alhambra, as well as domestic houses in the Albaicín and Sacromonte neighborhoods that give the city so much identity and name.

The rammed earth technique consists of filling a formwork with layers of earth of 10–15 cm compacting each one of them with a tamper. The formwork is made up of two separate parallel planks, joined by a crossbar. In compaction with techniques in which the mud is used in a more humid state, the rammed earth technique provides much lower shrinkage and greater resistance. The advantage in relation to adobe construction techniques is that brick constructions are monolithic and therefore have greater stability [20].

This earth system, as we have commented, consists of the tamping of the raw earth by layers inside a wooden formwork where the cohesive property of the clays is complemented by the mechanical compression of the material. Soil compaction is influenced by the degree of humidity. A soil that is too wet cannot be compacted properly just as one that is too dry will not work properly. For this reason, the optimum moisture content is essential so that it is just enough to activate the binding capacity of the clays, which ranges from approximately 0–10% [16]. It is therefore a system in which when using raw earth, the choice of raw material is essential, complementing it with the ideal degree of humidity, and the use of stabilizers to guarantee its durability.

Adobe was used on the Great Wall of China along with stone more than 5000 years ago and was subsequently used in houses and walls about 2700 years ago [18]. On the other hand, in North Africa and the Middle East, the most abundant material was and is earth, for this reason, there are also numerous examples of walls built with earth, a material that was erected as an easy, fast, and inexpensive way to build fortifications.

In addition, throughout the Mediterranean, there are Phoenician vestiges that used the earth in the form of adobe as a construction material, both in North Africa and on the Spanish coasts [3, 4, 17]. There are also descriptions of Roman writers who narrate the construction of clay towers in the invasion of the Iberian Peninsula carried out by the Carthaginians in 218 BC. In the context of pre-Columbian America, there is no evidence of the use of land as a building material, in fact, the first construction on land in North America was carried out by the Jesuit missionary Manuel Da Nobrega in 1549, which sent a request to Europe requesting craftsmen and carpenters to build clay and adobe walls.

In the same way, there is knowledge of earthen constructions carried out in early times in the area of Brazil [13, 22].

In the late Middle Ages, Spain was under Muslim rule, until the Catholic Monarchs, in 1492, took the last Muslim kingdom, the city of Granada (Spain). The Christian Kings implemented the earth building technique by hiring Muslim artisans. Later, the clay was mixed with fired brick, making stronger and more durable fortifications [2].

The proliferation of the earth as a building material was such that there are numerous cities that were built in this way, such as Babylon in Iraq, and the oldest known city, Catalhöyük, as has already been referred to, in Anatolia, from the seventh millennium BC, that it already had the houses built with adobe. In ancient Egypt, adobe, made with silt from the Nile, was frequently used in the construction of houses, tombs (mastabas), fortresses, and even palaces, although the Egyptians were also the first to use the carved stone to erect temples, pyramids, and other monumental buildings. In Peru, there is the citadel of Chan Chan, the largest mud city in America. In Jiayuguan, China, there is a wall partially built with rammed earth, the upper level finished with bricks, built during the Ming dynasty (1368–1644), and giant bearing wall like the Fujian Earth Building (TuLou) of the song-yuan dynasty (800 years ago) [29]. In our temples, this building material finds manifestations such as vestiges that patent its use by various civilizations such as the Roman or Muslim and samples of recent buildings that show that this material is part of a living earthen architecture [14, 19].

Clay, at the end of the Second World War, was once again a widely used construction material in East Germany due to its availability and low price [27]. The same happened in Australia, where his book “Build Your House of Earth” was until recently the accepted standard for construction on Australian soil [21].

All these different readings on the use of land under construction through the ramming technique coincide in one thing, during the development of the technique a series of problems arise about the use of soils of the geological formation of the area that has been used for so long for constructions through this method, since they are considered the best for such construction typology, this has made them be used for a long time, but the cited problems are such as access to extraction of the land and ease of obtaining it. For this reason, in this research, the main objective has been the behavior of colluvial and/or edaphic soils from the Alhambra Formation in Granada (Spain), which has provided a great development to the city, both in application and functionality.



As it has become clear, the use of the earth as a construction material has been carried out all over the world. For this reason, research of this type is necessary to implement current techniques in the restoration of rammed earth constructions with the rammed earth technique. In addition, it can be used for the construction of new works for both walls and cladding.

In this research, earth has been used as the main material, which has been mixed with different binders, aggregates, and additives. On the other hand, the technique of laying by projection has also been presented.

## 2 Materials and Method

### 2.1 Materials

#### 2.1.1 Earth. Colluvial/Edaphic Soils

In this case, the chosen earth corresponds to the B horizon of the edaphic soil of the F. Alhambra (South of Spain, in Granada, Fig. 1) mixed with the roof of the C horizon. These soils are found in situ in the formation itself or accompanying the discharges that have been made in different nearby excavation areas, almost all for building projects.

The most superficial and altered soil formed by angular gravels and sandy silts where the vegetation corresponding to horizon A develops from the extraction zone. In horizon B, there are macroscopic vestiges of the mother material with rounded edges that are much cemented with less organic matter than in the upper level, made evident by the brownish hue of this layer. The C horizon would be the base material that is made up of very different rocks. These are colluvial sediments that make up the Alhambra Formation, characterized by its reddish color. All the results of the study of the physical–mechanical properties of edaphic soils will be compared with those obtained for the Alhambra Formation which is used in many of the surviving

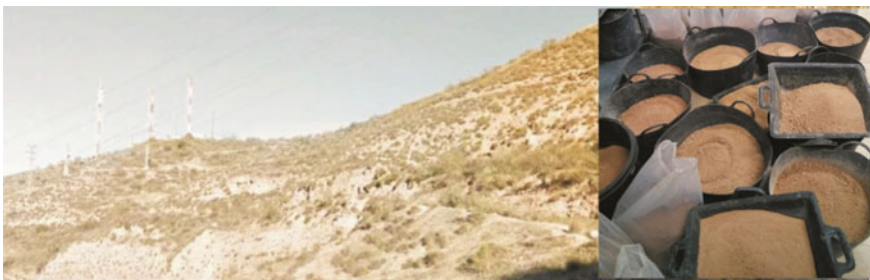


**Fig. 1** General view of the extraction area of the earth used (left) and soil collected in the laboratory (right)



rammed earth constructions in the city of Granada (Spain), including fortifications, dwellings, and walls [15].

The material was extracted in an area near the town of El Fargue, very close to Granada capital. Here, there are lands and orchards of anthropic spills or colluvial soils of the Alhambra Conglomerate that are easily accessible (Fig. 2).

X-ray diffraction tests have been carried out to obtain the mineralogical composition of this soil (Fig. 3), obtaining quartz (46–47%), dolomite (18–39%), and

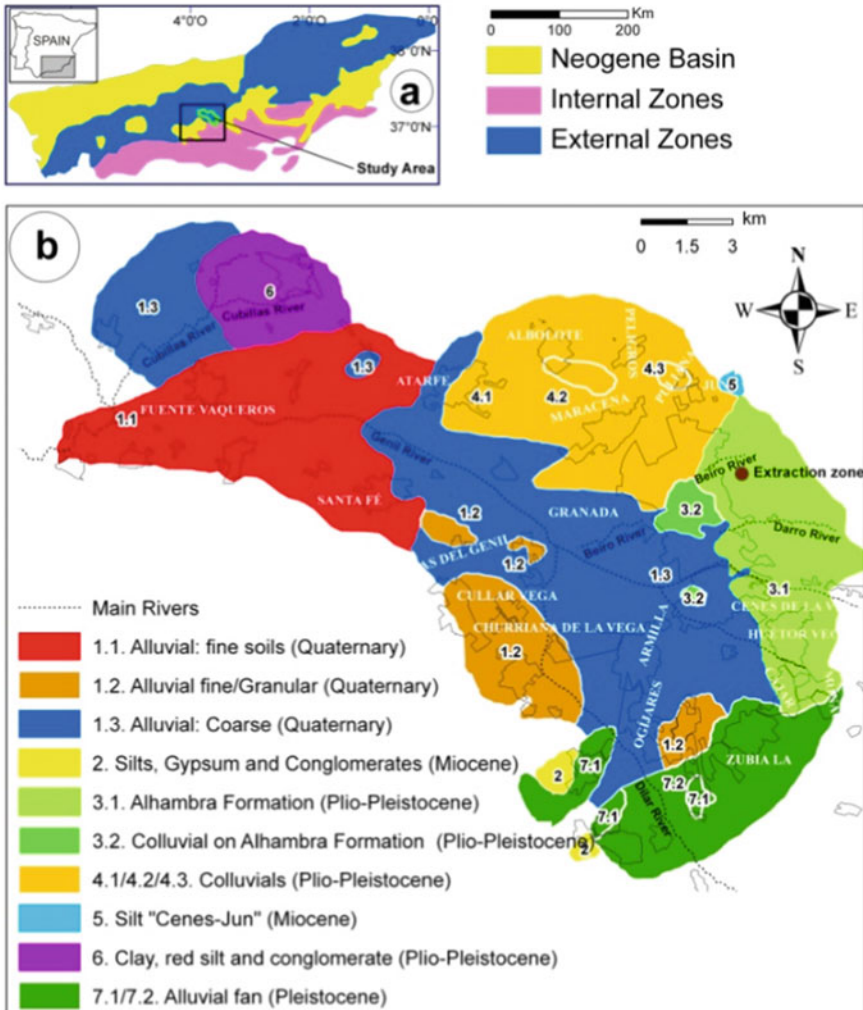


**Fig. 2** General tectonic sketch of the central and eastern Betic Cordillera (a). The remarked zones show the location of Fig. 1b, (b) spatial location of soil units of the metropolitan Area of Granada. Town boundaries are shown with a thin polygonal line. Modified from Valverde-Palacios [28]

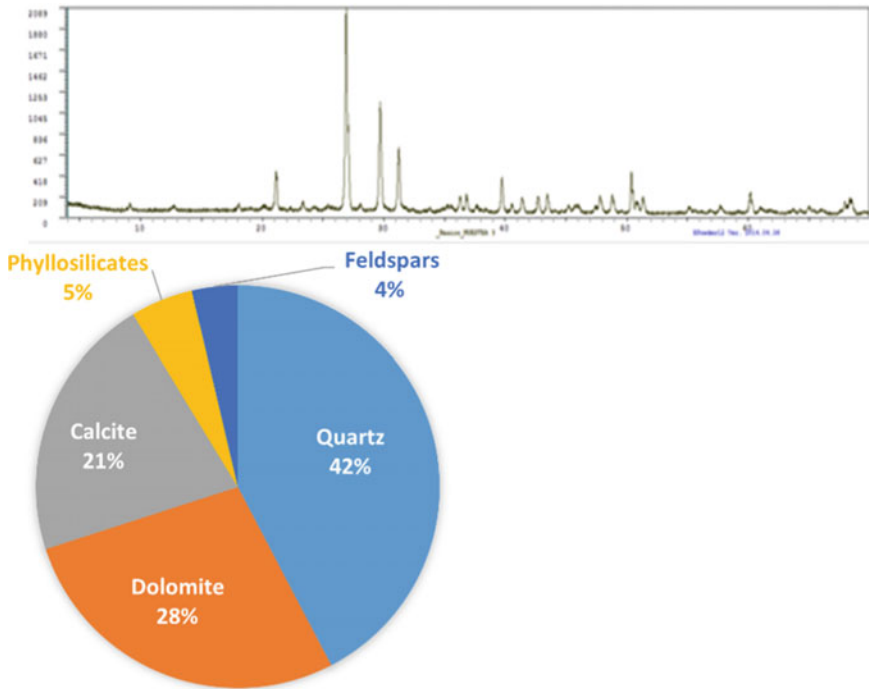


**Fig. 3** Soil-sample powder-X-ray diffraction test results. The mean value of the three samples analyzed is presented

calcite (17–27%) as the dominant mineralogical elements. Feldspars (3–4%) and clay minerals, phyllosilicates (4–7%), such as chlorite and muscovite, are found to a lesser extent.

This mineralogical composition is very similar to the results obtained for soil samples from the Alhambra Formation (Ontiveros 1995, [14]), a result that confirms that the soil presented in this investigation comes from the weathering of level 2 of the F. Alhambra, on its edaphic horizon B with some C.

### 2.1.2 Binders

- CL90-S [7], hydrated calcium lime powder (>90% CaO + MgO). For the rehabilitation and restoration of the interior and exterior of emblematic and old buildings.
- NHL 5 [7], natural hydraulic lime. It is a type of lime widely used in restoration and green building. Its main characteristics include its low tendency to cracking, its great plasticity, and adherence to various surfaces. Regarding the most notable mechanical characteristics, we have a compressive strength of 2.0 MPa at 7 days and 5 MPa at 28.

- BL 22.5X [6], white masonry cement with a compressive strength greater than 10 and 22.5 MPa at 7 and 28 days, respectively, according to EN 413-1: 2011. In the case of cement, no mechanical tests have been carried out since this information was available through a quality certificate from the supplier, to which it must be added that the percentage used, with respect to the weight of the earth, is very low, so its importance as a binder is only in the short term until the main binder, lime, begins to carbonate, providing resistance.

### 2.1.3 Aggregates

- Dolomitic limestone natural aggregate (Fig. 4)

These aggregates come from dolomitic rocks that are basically composed of magnesium carbonate ( $\text{Ca Mg}(\text{CO}_3)_2$ ), not reactive with the alkalis in cement. It is a well-processed material, which presents morphology like that resulting from aggregates from crushing. In this case, the high degree of micro-cracking of the mountain massif, due to tectonic phenomena, allows the rock to disintegrate when executing the extraction process, resulting in an aggregate equivalent to that of artificial crushing.

- Recycled aggregates from construction and demolition waste (Fig. 5)

They are waste from construction and demolitions that are transported to the plant to be treated through crushing and crushing processes, as well as a selection of the ideal material. In our case, we have a mixture of two types of fractions: fine fraction or sand (0/4 mm) and coarse fraction or gravel (4/8 mm). In its composition, we can find the following materials: concrete in a higher percentage, ceramic material, bricks, glass stoneware, porcelain, etc. These aggregates can be coded as 17 01 07 [23] according to the European waste list (Order MAM/304/2002, of February 8. Recovery and disposal operations of waste and European waste list. Chapter 17

**Fig. 4** Dolomitic limestone natural aggregate



**Fig. 5** Recycled aggregates

of the European waste list Annex 2 BOE, no. 43 (ref.: BOE-A-2002-3285)). They comply with the specifications established by the Spanish structural code. It is a well-processed material, with a suitable granulometry to be used in the earth projection technique and compatible with the earth used.

In both cases, their purpose is to correct the granulometric curves of the base material, the earth, in order to achieve greater compactness in the mixture as a whole; in the case of recycled materials, their use also has an ecological function, the elimination of waste.

#### **2.1.4 Additive**

**Waterproofing:** In the case of durability tests against rain, a water-repellent additive from SIKKA, SikaProof L-100, was used.

**Ecological enzyme** as a by-product of sugar cane processing. The product is called COMPAT-TO<sup>®</sup>, produced and provided by nanosystems, and is composed of a mixture of organic enzymes that catalyze a binding action on plastic particles, for which a plasticity index greater than 10 and a content of clay greater than or equal to 20%.

#### **2.1.5 Clays**

The weathered soil of the Alhambra Formation has insufficient fines content for the ecological enzyme to bind the clay material. For this reason, two types of clays (Table 1, Fig. 6), from the company ARGILES COLADES S.A., have been used for the mixtures in which the enzyme has been used.

**Table 1** Chemical composition of the two types of clays used

Chemical composition (%)	Micronized clay pen F gray	Micronized clay pen F beige
Al <sub>2</sub> O <sub>3</sub>	15	18,13
SiO <sub>2</sub>	75,21	55,22
K <sub>2</sub> O	0,64	3,59
CaO	0,40	4,62
Fe <sub>2</sub> O <sub>3</sub>	5,50	6,20

Modified from <http://argilecolades.com/>**Fig. 6** Micronized clay pen F gray (left), micronized clay pen F beige (right)

### 2.1.6 Rubber Powder and Textile Fibers

Material from used tire waste (Fig. 7), which is subjected to a mechanical crushing process in order to obtain different granulometries that serve us in our agglomerate of earth. This mechanical grinding is also responsible for separating all the components of the tires, so that the textiles, steel, and rubber are grouped independently, and the “rubber powder and granules” are free of impurities and can be used.

**Fig. 7** Rubber powder and textile from tire waste



This material is divided into granules, with thicknesses of approximately 4 mm or rubber powder that turn out to be smaller particles, depending on the granulometry, the earth will have one use or another, either to make rammed mud or to use the projection technique.

## 2.2 Methodology

Once all the materials described in Sect. 2.1 had been received, the following tests were carried out:

### Identification tests

- Determination of the particle size distribution by sieving [10]
- Determination of liquid and plastic limits [12]
- Soil type classification according to unified soil classification system [1]
- Qualitative determination of soluble sulfates content in a soil [25].
- Determination of the carbonate content of a soil [24]
- Organic matter content of a soil [26]

### Physical-mechanical tests

- Compaction test. Standard proctor [6]
- Unconfined compression test [11]

One of the innovations of this research consists of the methodology of putting into work by projection of the earth with the proposed dosages. Specifically, a Tigre trademark plasterer (model P4 for walls) has been used. TIGRE™ plastering machines

have been used throughout the world for more than 50 years to spray concrete and mortars on all types of construction systems. The use of plastering machines not only generates significant savings in labor time and material waste, but also does not require specialized labor. The TIGRE™ plastering machine connected to the compressor and loaded with mix in its bucket manages to apply the material at a speed and with adherence impossible to achieve with manual installation.

In addition, accelerated carbonation tests have been carried out, adopting the regulations for the case of concrete [8]. On the other hand, durability tests against rain, with a device designed in the construction materials laboratory of the Department of Architectural Constructions of the University of Granada, have been carried out.

### 3 Results and Discussion

This section presents the most relevant results obtained in the most suitable proportions of each of the mixtures that will be compared with the standard mixture established by only soil for the Proctor tests and resistance to compression or by soil + natural dolomitic aggregate + aerial lime + cement in the case of projection tests. Specifically, the materials that make up the studied mixtures are the following:

- Earth
- Earth + natural dolomitic aggregate
- Earth + recycled aggregate
- Earth + aerial lime + white cement
- Earth + natural hydraulic lime + white cement
- Earth + natural dolomitic aggregate + aerial lime + white cement
- Earth + recycled aggregate + aerial lime + white cement
- Earth + ecological enzymes + clay
- Earth + rubber powder and textile fiber
- Earth + rubber powder and textile fibers + aerial lime + white cement.

However, the results of those mixtures that have finally been used to put them into work through the earth project system are presented here, so the rest of the mixtures should be understood as intermediate tests for better characterization.

#### ***3.1 Size Distribution, Atterberg Limits, Soil Type Classification, Carbonate, and Sulfate Content***

In the case of the base material, the earth, the sample under analysis (Fig. 8) is characterized by having between 6 and 10% in fines (sizes smaller than 0.088 mm sieve), a percentage of gravel that ranges from 3 to 9% (sizes larger than 10 mm sieve). The percentages of sand vary between 53 and 72%, those of gravel between 13 and



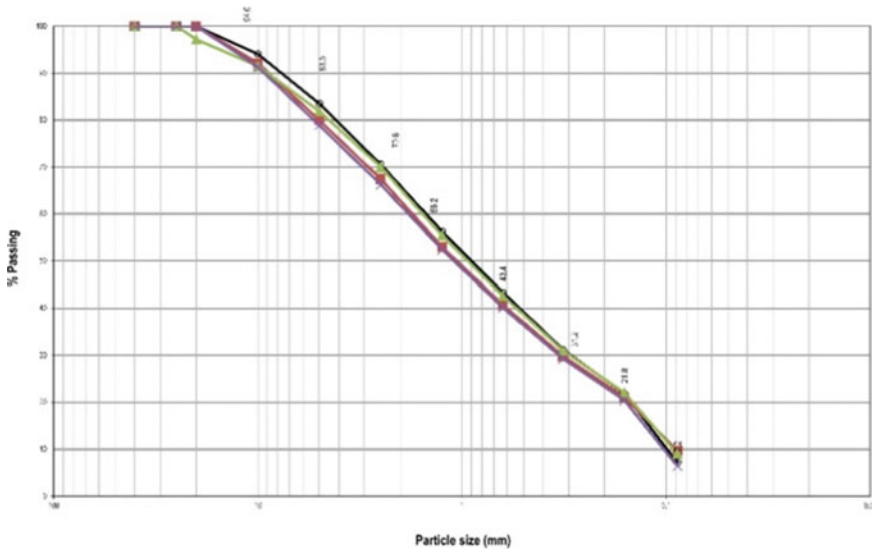


**Fig. 8** Granulometric distribution of the earth used

35% and those under 0.08 (silts and clays) between 12 and 22%. The uniformity coefficient varies between 15 and 18, indicating that it is fairly uniform. As for the curvature coefficient, it is between 1 and 3 classifying it as a well graded soil.

On the other hand, the Atterberg limits for the earth were determined in the laboratory on the fine particles (passing through the ASTM 40 sieve) obtaining the following results: silts and inorganic clays of low-medium compressibility and plasticity, respectively, that is, CL-ML, ML, or CL, with LL between 21–24% and PL between 18–20%.

Both size distribution and Atterberg limits establish an SM or SC-SM classification [1] with different percentages of gravel for the soil used. If we compare with the results in samples from level 2 of the “Alhambra Formation” [15], which corresponds to the parental sample of this edaphic soil, the lack of fines in the soil of this investigation is corroborated, since that we lack samples classified as SC, as well as the significant presence of coarse (gravel) that at the aforementioned level provides GC and GC-GM classifications. Therefore, the edaphic soil in question differs fundamentally from its parent soil in that the clay content is very low, and the coarse sizes are also poorly represented. This is a consequence of the weathering process of the parent soil from which the edaphic soil originates.

The carbonate content varies between 15.50 and 32.50%, resulting in a characteristic average value of 22%, taking into account that two of the dominant components of the soil are carbonates (calcite, dolomite), which explains why the highest values are found between 5 and 16 mm where calcite and dolomite grains should be especially concentrated, also, in the finest particles of this level (0.16–0.18 mm), the carbonate content is also elevated, which is quite normal in the B horizon of



edaphic soils due to the washing out of salts in the upper horizon. Compared to Alhambra Formation (level 2), carbonates range between 13.5 and 17.1%, essentially concentrated in fines [15].

A qualitative determination of sulfates has been carried out, and it has been determined that they are absent. The Alhambra Formation also lacks sulfates in its composition, as does the soil under study (Ontiveros 1995, [15]). The organic matter content is very low, not exceeding 0.13%, so it is a soil with a low-organic content of less than 1%. These results are similar to those obtained for the levels of the Alhambra Formation, which in general tends to be null as it is not affected by edaphogenesis processes.

### 3.2 *Compaction Test. Standard Proctor*

In the standard proctor test (Fig. 9), the maximum density and optimum moisture content, for the earth, vary between 2.01 and 2.17 g/cm<sup>3</sup> and 8.1–8.5%, respectively, and 2.10 g/cm<sup>3</sup> and 8.0% are adopted as the most characteristic values for the edaphic soil of the Alhambra Formation in its B horizon with some mixing of the parent material (C). The Proctor densities of level 2 of the Alhambra Formation [15] vary between 2.0 and 2.06 g/cm<sup>3</sup>. In the case of the research by Ontiveros (1995) and Fuentes et al. [15], the Alhambra Formation presents values of 2.21 g/cm<sup>3</sup> at level



Fig. 9 Pictures show an example of the performance of a standard proctor test

**Table 2** Results of the standard Proctor test (the percentages of binders, aggregates, and rubber are referred to the weight of the earth)

Material or mix	Maximum density (g/cm <sup>3</sup> )	Optimal humidity (%)
Earth	2.02	8.5
Earth + 20% dolomitic natural aggregate	2.02	10
Earth + 8% aerial lime + 1% white cement	2.04	12.7 <sup>a</sup>
Earth + 8% natural hydraulic lime + 1% white cement	2.02	13.5 <sup>a</sup>
Earth + 20% recycling aggregate	1.91	13 <sup>b</sup>
Earth + 6% beige clay	2.05	8.5
Earth + 7.5 ml enzymes	2.03	8.5
Earth + 7.5 ml enzymes + 6% gray clay	2.01	8.5
Earth + 7.5 ml enzymes + 6% beige clay	2.04	8.5
Earth + 10% powder and textile rubber fibers	1.83	11.3

<sup>a</sup>22% (relative to the weight of the cement) more water has been added

<sup>b</sup>4.5% more water has been added

1, 2.16 g/cm<sup>3</sup> at level 2, and 1.87 g/cm<sup>3</sup> at level 3, for optimum moistures of 8.4%, 7.7%, and 9.5%, respectively.

In addition, standard proctor tests have been carried out on the main mixtures, that is, with natural dolomitic aggregates, with recycled aggregates, with enzymes, with enzymes and clays, and with powder rubber and textile fibers from tire waste. Table 2 shows the results obtained for maximum density and optimal humidity.

According to the results shown in Table 2, it is observed that the lowest proctor densities are obtained in the case of the mixtures of soil + powder and textile rubber fibers (1.83 g/cm<sup>3</sup>) and for soil with recycled aggregate (1.91 g/cm<sup>3</sup>), a question that is logical given the low density of used tire dust and textile and the lower density of recycled aggregate. On the other hand, it is observed that in these two mixtures, the optimum humidity increases, an issue that needs to be corrected later with the use of fluidizers that reduce the amount of water to minimize shrinkage cracks for installation using the projection technique. The maximum density of all mixes and additives, earth with aerial lime and white cement, earth with natural hydraulic lime and white cement, hardly varies, ranging between 2.03 and 2.11 g/cm<sup>3</sup> for proctor compaction moistures between 8 and 13%, increasing with the addition of binders and especially for natural hydraulic lime (NHL 5).

On the other hand, it is well known that lime, and especially airborne lime, is a binder that does not provide significant resistance in the very short term, so in this case, it is necessary to complement, for putting into work, whatever the methodology used, with the addition of another type of binder, in this case white cement, which was used in 1% with respect to the weight of the earth; this new addition requires 22% (of the weight of the cement) more water added to hydrate it.

As previously mentioned, the data obtained are like those provided by other works in the tests carried out on level 2 of the Alhambra Formation and to those obtained for the materials of the Alhambra Formation, which have been the most widely used to build part of Granada’s earthen heritage [15].

### 3.3 Unconfined Compression Test

Once the main materials have been characterized in terms of grain size, plasticity, and proctor density, compacted samples have been made at the maximum density and with the optimal humidity that resulted from the referred standard proctor test.

The mean compressive strengths of the earth (maximum density is 2.02 g/cm<sup>3</sup> and optimal humidity 8.5%) are 1.90 MPa (Figs. 10 and 11). These results are low if compared with others belonging to an outcrop of the Alhambra Formation level 2, which indicate that the compressive strengths of this type of material are of the order of 3.7 MPa for a density of 2.05 g/cm<sup>3</sup> and a humidity of 9.55% [15]. However, if we compare it with a fine level of the Guadix Formation, we obtain values of 0.8 MPa for a maximum proctor density of 2.15 g/cm<sup>3</sup> and optimum humidity of 8.46%; this research was carried out for the construction of an information office in a vault, built with soil with walls of 0.40 m thick, in the cave complex of Trópoli in Alcadia de Guadix, Granada, Spain [28].

Comparing the compressive strengths obtained with only earth, in terms of earth mixed with natural dolomitic aggregates and with 10% air lime—CL90S- or natural hydraulic lime (NHL 5) and 1% white cement—BL 22.5 x—(all the percentages of the binders are referred to the weight of the earth) and subjected to seven days of forced carbonation (Fig. 11) (1–3% CO<sub>2</sub>), an increase of the order of 50% is observed. On the other hand, when using recycled aggregates, the problem they have in terms of greater absorption compared to the natural dolomitic aggregate has been

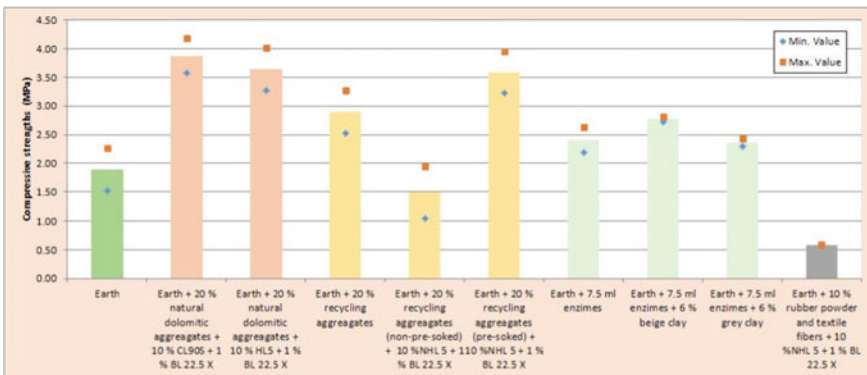


Fig. 10 Compressive strength results in compacted dry samples at standard proctor density



**Fig. 11** Electric compression multi-test machine used (left). Forced carbonation chamber (top right) and sample after unconfined compression test and depth of carbonation test with phenolphthalein (bottom right)

appreciated; for this reason, the low resistance obtained, 26% less, makes it necessary to pre-wet the aggregate with 5% of water with respect to the weight of the dry mass of recycled aggregate added according to the investigations of Cuenca-Moyano et al. [5]; with this pre-wet method, and also after seven days of forced carbonation, an increase in compressive strength of around 47% was achieved.

The mixtures of earth with ecological enzymes, to replace binders, have been very satisfactory in the case of the addition of clay (6% with respect to the weight of the earth), and even more so for the type micronized clay pen F beige in which 31% more is achieved compressive strength compared to ground only.

On the contrary, the use of rubber powder and textile fibers has revealed a notable drop in compressive strengths (~200%), an issue that was to be expected given the low density of the one with this residue. However, this mixture opens up a new line of research for the use of this product as a thermal insulating material put into work using the Projected Earth™ technique.

Regarding the durability in simulated rain test, after 90 min (Fig. 12), the compact specimens at standard proctor density of the different mixtures have a heterogeneous behavior with mass losses of between 10 and 25% for those of only earth, between 2 and 5% for earth + natural aggregate + lime + cement, the most suitable result is aerial lime, a very similar result in the case of substitution of natural aggregate for recycled aggregate. On the other hand, the mass losses measured in the other mixtures, with ecological enzymes and with powder and textile fibers, the weight loss reached 40–50%, an issue that was not later reflected in the projected mixtures that are developed in the next section.

**Fig. 12** Example of cylindrical samples compacted to standard proctor density placed in rain test machine



### ***3.4 Commissioning Test Using the Projected Earth System***

The system presented is a patent and registered trademark owned by the University of Granada (Spain) and by the inventors, Fuentes-Gracia, R., Valverde-Espinosa, I and Valverde-Palacios, I. [14, 15]. However, this technique began with a type of machinery similar to that used to spray concrete by wet means that requires great specialization and high-capacity compressors. For this reason, the projection of four mixes with a Tigre™ plastering machine (Fig. 13) is now presented as an innovation, which does not require much experience and is much more versatile.

Specifically, the mixtures that have been projected are the following (Fig. 14):

- Earth + natural dolomitic aggregate (NA) + aerial lime (CL90S) + white cement (BL22.5X) + water-repellent additive (WRA)
- Earth + recycled aggregate (RA) + aerial lime (CL90S) + white cement (BL22.5X) + water-repellent additive (WRA)
- Earth + ecological enzymes (EE) + beige clay (C) + water-repellent additive (WRA)
- Earth + rubber powder and textile fibers (RPT) + CL90S) + white cement (BL22.5X) + water-repellent additive (WRA)

The mixtures were prepared in a concrete mixer with a pre-established order of filling, according to the previous investigations carried out by Fuentes-García [14], to achieve the greatest possible homogeneity. Tables 3 and 4 show the ideal filling orders for the different mixtures:

The result of the projection of the different mixtures is shown in Fig. 13 in which it can be seen that the texture and adherence to the ceramic support have been very satisfactory. Subsequently, samples were extracted to test them under compression, obtaining as a result, the values shown in Table 5. In this case, durability tests have not been carried out but it should be noted that after two and a half years, in a climate such as Granada (Spain) with annual average temperatures between 0 and 34 °C and



**Fig. 13** a Ceramic brick factory wall that will serve as a support to project the mixtures. b Example of materials dosed by weight prepared for projection. c Tigre plaster sprayer plugged into compressor

a precipitation around 300 mm/year, the projected mixtures are in perfect condition and no mass loss.

Regarding the results of compressive strength on carved samples extracted from the projected mixtures, a decrease of the order of between 46 and 60% is observed with respect to the cylindrical specimens compacted to the density of the standard proctor test. These decrease percentages are consistent with those obtained in the previous research such as Fuentes-García [14]. The concrete results can be seen in Table 5.

## 4 Conclusions

After the results of all the tests that have been presented for the characterization of the proposed mixtures, it can be concluded in a general way that all except the one added with dust and textile from tire waste are suitable for use both in new construction and for rehabilitation of rammed earth-based constructions using the Tapial technique.

In addition, the “projected earth system” laying technique using a plastering machine is viable as a construction technique, achieving adequate strength and durability while saving time and manpower.





**Fig. 14** Result of the projection of the different mixtures. **a** Earth + natural dolomitic aggregate + aerial lime + white cement. **b** Earth + recycled aggregate + aerial lime + white cement. **c** Earth + ecological enzymes + clay. **d** Earth + rubber powder and textile fibers + aerial lime + white cement

**Table 3** Ideal filling order for the case of earth + dolomitic natural aggregate and for earth + recycled aggregate

	Earth + NA		Earth + RA	
	Fill order	Quantity	Fill order	Quantity
1°	Water	All	Water	All
	CL90S or NHL 5	All	CL90S or NHL 5	All
	BL 22,5x	All	BL 52,5	All
2°	Earth	1/2	Earth	1/2
	NA	1/2	RA	1/2
3°	Earth	1/2	Earth	1/2
	NA	1/2	RA	1/2
	WRA	All	WRA	All

**Table 4** Order of filling suitable for the case of earth + ecological enzymes and for earth + rubber powder and textile fibers

	Earth + RPT		Earth + EE	
	Fill order	Quantity	Fill order	Quantity
1°	Water	All	Water	Todo
	CL90S	All	EE	Todo
	BL 52,5	All	Earth	1/2
2°	Earth	1/2	C	Todo
	Cuacho	1/2	NA	1/2
	NA	1/2	Earth	1/2
3°	Earth	1/2	NA	1/2
	RPT	1/2	WRA	Todo
	NA	1/2		
	WRA	All		

The use of construction and demolition waste, specifically recycled aggregate, and rubber powder and textile fibers from tire waste lengthens the life cycle of these products, fully entering the field of circular economy.



**Table 5** Results of the tests of mean resistance to compression of the samples of the different projected mixtures in comparison with those obtained of the compacted samples at the density of standard proctor tests

	Mean value compressive strength (Mpa)	
	Samples standard Proctor tests	Samples from projected mixtures
Earth + 20% natural dolomitic aggregates + 10% CL90S + 1% BL 22.5 X	3.88	1.71
Earth + 20% recycling aggregates (pre-soaked) + 10%NHL 5 + 1% BL 22.5 X	3.59	1.42
Earth + 7.5 ml enzymes + 6% beige clay	2.78	1.25
Earth + 10% rubber powder and textile fibers + 10%NHL 5 + 1% BL 22.5 X	0.58	0.31

**Acknowledgements** This research was partially supported by Research Group TEP942 of the Andalusian Research Plan, funded by the Andalusian Regional Government in Spain and by the Department of Building Construction of Granada University.

## References

1. American Standard ASTM D2487–11. Standard practice for classification of soils for engineering purposes (Unified Soil Classification System)
2. Ballesteros P, Kirchner H, Fernández M, Ortega J, Quirós JA, Retamero F, Sitjes E, Torró J, Vigil A (2010) Por una arqueología agraria de las sociedades medievales hispánicas. Propuesta de un protocolo de investigación. In *Por una arqueología agraria. Perspectivas de investigación en las sociedades medievales hispánicas*, pp 185–202. <http://www.rmoa.unina.it/id/eprint/143>
3. Chazelles CAD (1993) *Savoir-faire indigènes et influences coloniales dans l'architecture de terre antique de l'extrême-occident (Afrique du Nord, Espagne, France méridionale)*. In: *Conferência internacional sobre o estudo e conservação da arquitectura de terra (7a)*. Silves (Portugal), 24 a 29 de Outubro 1993, pp 159–165
4. Costa C, Cerqueira Â, Rocha F, Velosa A (2019) The sustainability of adobe construction: past to future. *Int J Archit Heritage* 13(5):639–647. <https://doi.org/10.1080/15583058.2018.1459954>
5. Cuenca-Moyano GM, Martín-Morales M, Valverde-Palacios I, Valverde-Espinosa I, Zamorano M (2014) Influence of pre-soaked recycled fine aggregate on the properties of masonry mortar. *Constr Build Mater* 70:71–79. <https://doi.org/10.1016/j.conbuildmat.2014.07.098>
6. European standard EN 413-1:2011. Masonry cement—Part 1: composition, specifications and conformity criteria
7. European standard EN 459-1:2016. Building lime—Part 1: definitions, specifications and conformity criteria
8. European standard EN 13295:2005. Products and systems for the protection and repair of concrete structures—test methods—determination of resistance to carbonation

9. European standard EN ISO 17892-1:2014. Geotechnical investigation and testing—laboratory testing of soil—Part 1: determination of water content
10. European standard EN ISO 17892-4:2016. Geotechnical investigation and testing—laboratory testing of soil—Part 4: determination of particle size distribution
11. European standard EN ISO 17892-7:2017. Geotechnical investigation and testing—laboratory testing of soil—Part 7: unconfined compression test
12. European standard EN ISO 17892-12:2018. Geotechnical investigation and testing—laboratory testing of soil—Part 12: determination of liquid and plastic limits
13. Flores R (2005) A construção em taipa de pilão no Brasil: as Casas Bandeiristas de São Paulo. *Arquitectura de Terra Em Portugal*, pp 92–95
14. Fuentes-García R (2010) Construcciones de tierra. El tapial. Nuevo sistema para construcción y restauración mediante la técnica de “Tierra Proyectada”. Tesis Doctoral. Granada, Spain
15. Fuentes-García R, Valverde-Palacios I, Valverde-Espinosa I (2015) A new procedure to adapt any type of soil for the consolidation and construction of earthen structures: projected earth system. *Mater Constr* 65(319):e063–e063
16. Guerrero Baca LF (2007) *Arquitectura en tierra. Hacia la recuperación de una cultura constructiva*. Apuntes: Revista de estudios sobre patrimonio cultural. *J Cultural Heritage Stud* 20(2): 182–201. ISSN 2011-9003. (Ejemplar dedicado a: *Arquitectura en tierra*)
17. Houben H, Guillaud H (2001) *Earth construction. A comprehensive guide*. itdg Publishing, London
18. Keefe L (2012) *Earth building: methods and materials, repair and conservation*. Taylor and Francis, London
19. Marchiori C (2015) *Arquitectura en tierra de la prehistoria y protohistoria en el Próximo Oriente. Estudio arqueométrico del adobe en los yacimientos de Tell Halula, Yumuktepe y Tell Tuqan*. Universitat Autònoma de Barcelona
20. Minke G (2001) *Manual de construcción para viviendas antisísmicas de tierra*. Forschungslabor für Experimentelles Bauen Universidad de Kassel
21. Moor M, Heathcote K (2002) Earth building in Australia—durability research. In: *Proceedings of Modern Earth Building*, Berlin, Germany, 19–21 April 2002, pp 129–139
22. Puccioni S, Lyra CC (1993) O uso da Taipa-de-Pilao em construoões Luso-Brasileiras. In: *Conferência internacional sobre o estudo e conservação da arquitectura de terra (7a)*. Silves (Portugal), 24 a 29 de Outubro 1993, pp 296–298
23. Sanchez-Roldan Z, Martin-Morales M, Valverde-Espinosa I, Zamorano M (2020) Technical feasibility of using recycled aggregates to produce eco-friendly urban furniture. *Constr Build Mater* 250:118890
24. Spanish standard UNE 103200:2021. Determination of the carbonate content of a soil
25. Spanish standard UNE 103202:2019. Qualitative determination of soluble sulphates (in water) content in a soil
26. Spanish standard UNE 103204:2019. Organic matter content of a soil by the potassium permanganate method
27. Steingass P (2004) New chances for modern earth building. In: *Actas del II Seminario Iberoamericano de construcción con tierra [Recurso electrónico]: Escuela Técnica Superior de Arquitectura de Madrid*, 18 y 19 de septiembre de 2003. Mairea Libros, pp 417–425
28. Valverde-Palacios I, Fuentes R, Valverde-Espinosa I, Martín-Morales M, Del Moral Ávila C, Delgado Méndez L, Santos J, Canals Peres E (2012) Projected Earth System®. Aplicación de esta técnica a la construcción de viviendas sostenibles y ecológicas: Ecodome. XI Congreso Internacional de Rehabilitación del Patrimonio Arquitectónico y Edificación (El Patrimonio Ibérico). Cascais (Portugal). Libro de actas digital
29. Zhang PC, Luo K, Liao WB (2012) Study on the material and the structure of Earth building in Fujian. In: *Advanced materials research*. Trans Tech Publications Ltd., vol 368, pp 3567–3570

# Sustainability Challenges in Outdoor Swimming Pools



Miguel José Oliveira, Fátima Farinha, Armando Inverno, Jânio Monteiro, Cristiano Cabrita, and Adelino Venturinha

**Abstract** On a global level there is a significant number of swimming pools, which environmental impact cannot be neglected. The construction and maintenance of swimming pools is comparatively recent within the building sector, but contrary to what would be expected in most cases, this equipment have not improved its environmental performance over the last decades. In this chapter, a review is made of the state of the art in terms of passive and active measures that can be used to improve swimming pools, including suggestions for the main areas of action. Thus, technological suggestions for the thermal insulation of the tank, measures to improve thermal gains, automation system and an intelligent and predictive management platform, are presented and analyzed. The solutions that are available prove that there is a significant set of technological measures, some of them applied in other sectors, which when properly operationalized can decisively contribute to the reduction of the negative environmental impact of swimming pools.

**Keywords** Swimming pools · Sustainability · Passive and active measures · Solution proposals

## 1 Introduction and Motivation

As stated in [1], there are around 13 million swimming pools on a global level, with nearly 29% of these in Europe and 59% in North America, while the rest of the world has only 12% of the global amount. According to [1], France has the highest number of swimming pools in Europe with 34% of the European total, followed by Spain with 27%, Germany with 20%, Italy with 6% and the UK with 5%.

The construction and maintenance of swimming pools is comparatively recent in the building sector, existing on a considerable scale only in the last 70 years. Technologies have been developing significantly and the design and constructing of swimming pools currently requires a high level of expertise. In addition, the high

---

M. J. Oliveira (✉) · F. Farinha · A. Inverno · J. Monteiro · C. Cabrita · A. Venturinha  
Universidade do Algarve, Faro, Portugal  
e-mail: [mjolivei@ualg.pt](mailto:mjolivei@ualg.pt)

competition in the building sector forces companies to provide low-priced and fast construction deadlines, which can bring negative consequences during the construction process and along the life cycle of swimming pools. The design and construction of a swimming pool involves a set of agents and processes that require coordinated efforts. Currently, there are different construction solutions.

In the case of Portugal, for instance, most of the existing swimming pools are small, built in residential zones. In most situations there is little information about the project and the construction methods used. Specifically, in the Algarve region, the execution and maintenance of swimming pools has economic relevancy to more than 500 small and middle companies. Furthermore, swimming pools are also important infrastructures for the tourist offer of the Algarve's region [2].

In general, tourism has important effects on society, with economic benefits for the associated regions and countries. However, the inherent great potential of tourism, comes with serious environmental challenges that require taking proper measures to assure the Sustainable Development Goals (SDGs). Without proper precautions and investments, the expansion of tourism increases pressure on biodiversity and in the ecosystems on which the local communities depend on [3]. An example of this is the pressure that tourism places on water supply, which is a resource, needed to provide services related to basic human needs and for an extensive range of tourism activities [4]. Furthermore, the energy and carbon footprints cannot be ignored.

According to [5], the environmental impact on residential swimming pools in the Arizona state (USA) and on other equivalent warmer regions is very significant. For example, the carbon footprint of the modeled pools was estimated to be  $1400 \pm 50$  kg CO<sub>2</sub>/year/swimming pool. Thus, in addition to the high environmental impacts that swimming pools have, it is also a fact that they are generally used in short periods of the year. In a study by Oliveira et al. [6], based on online questionnaire performed during the year of 2018, about the sustainability of swimming pools in the Algarve region, 72% of swimming pools have no coverage. The coverage is important not only for safety reasons but also to reduce the loss of water by evaporation and to minimize the excessive heat losses from water. The same study also found that 65% of swimming pools have no water heating method. This means that the use of the pool is restricted to the period of time when the water temperature is satisfactory, which for the Algarve region may be a maximum of 5 months a year (between May and September). Accordingly, this equipment is underused, not contributing to the reduction of tourism seasonality—one of the regional's goals.

In this book chapter, a review is made of the state-of-the-art in terms of passive and active measures that can be used to improve swimming pools, including suggestions for the main areas of action.

The rest of the chapter has the following structure. In Sect. 2, a description is made of the sustainability challenges involved in swimming pools. In Sect. 3, a state-of-the-art review is made concerning works that have addressed sustainable swimming pools, but also other areas that can be involved, like automation and smart systems. In Sect. 4 a solution is presented that integrates several of the features considered in different domains to define a model for a sustainable swimming pool. Finally, Sect. 4 concludes the chapter.

## 2 Sustainability Challenges

Swimming pools, whether private or public, in order to assure clean and warm water, have considerable water and energy consumptions with direct environmental impacts.

In a scenario where no refurbishment works take place, and thus no complete drain occurs, a swimming pool may be filled only once in its lifetime. Nevertheless, periodic addition of water is required to compensate for: (1) water losses from evaporation; (2) use; (3) leaks and backwash processes. Backwash processes allows cleaning the filter, but requires water draining to the sewage.

Swimming pool losses due to evaporation [7] are very significant and depend on its surface area, outside temperature humidity and wind. In the case of “infinity pools”, with an edge over which water flows, giving the appearance of the water extending to the horizon, the evaporation increases significantly, depending on the fall height.

In order to keep the water clean and safe, there is a pump working for several hours every day. This requires the consumption of significant amounts of electrical energy. If the swimming pool is heated, the energy requirements is higher to heat the water, depending on the atmospheric conditions, varying inversely with the energy obtained from the solar radiation. While certain regions experience hot weather very frequently, the sun is rarely enough to raise the water temperature to a comfort level across all seasons of the year.

Over the last 30 years, to compensate for the expensive and poorly environmentally friendly nature of traditional swimming pools, designers, constructions and owners have been putting an effort to align swimming pool trends with the sustainable development. Sustainable development, according to [8], is “a development that meets the needs of the present, without compromising the ability of future generations to meet their own needs” with the main aim to assure a quality of life, while minimizing the present impact on the future.

The sustainability challenges in outdoor swimming pools are numerous. The five most important ones are the following:

1. Better insulation: to avoid heat loss, swimming pools structures need to be better insulated and existing pools, which need renovation, have to incorporate insulation;
2. Water surface cover: allows cutting down energy and water usage—most heat loss occurs through the water surface, especially evaporation, so a swimming pool cover has a twofold function, saving energy and water expenditure;
3. Renewable energy: solar and other forms of renewable energy and heat storage systems have a relevant contribution to the energy sustainability of swimming pools, supporting the energy needed in pumping systems to guarantee water quality, as well as, water heating [9];
4. Water efficiency, including leakage detection systems and water reuse: throughout the life cycle of pools, it is possible to have pipe leaks that normally take a long time to be detected since water refilling may be due to other factors, such as, use, evaporation and backwash;

5. **Intelligent Control System:** several elements of swimming pools, as for example, the pool pump, chlorinator, self-cleaning, pool lighting, pool heating and water supply, can be automated; this guarantees that water is constantly safe and warm, with the minimal required energy consumption. It also allows the control from the user of all swimming pool's functions using an app on a smartphone, or tablet.

By using less energy and less water (hence, less chemicals) sustainable swimming pools are far less harmful to the environment ensuring preservation of the resources of our planet for future generations.

### 3 State-of-the-Art

The high number of existing and future swimming pools place challenges associated with water and energy requirements and associated sustainability. There is thus a real need to improve their efficiency.

The design and construction of more sustainable pools require acting in different levels from passive measures to active measures. In following different proposals are described for each of these two levels.

#### 3.1 *Passive Measures*

Passive measures are those where automation systems have small or even no intervention, as well as, human actuation. In the swimming pools context, the first issue is to reduce energy losses in order to avoid water temperature reduction. As water consumption is also a relevant concern, passive measures to avoid water consumption are also analyzed.

Energy losses in swimming pools are mainly due to conduction in walls and floors and to the evaporation process that occurs both in outdoor and indoor swimming pools. Thermal losses by conduction through walls and floors are generally neglected, as they represents only 1–2% of the total losses. Even so in a heated outdoor swimming pool with 1500 m<sup>3</sup> it can represent about 2–7 kWh [10] per day.

On the market there are some thermal insulation solutions that can be applied to the swimming pool tank, such as, the application of extruded polystyrene plates on the outside of the tank, in contact with the ground [11], or the use of modular systems that integrate the structural and insulation function in panels [12] or in blocks [13]. This type of solution, however, is considered for new swimming pools and are difficult to implement or even impractical in existing pools.

Rose [14] proposes, for the thermal insulation of the interior walls and floor of the tank, the use of rigid phenolic panels (high pressure laminates) or cellular glass (material known as FOAMGLAS), together with a rigid waterproof mortar

and PVC coating. This system, which may be also suitable for implementation in existing pools, is not known on the market, nor was it possible to find additional information regarding its effective thermal performance, mechanical strength and durability/longevity. In [14] the authors also considered that due to the rigidity of the insulating panels, the system is also suitable for the application on the floor of the tank, unlike polystyrene or polyurethane panels, which are more compressible, not being suitable for the use inside the tank.

Evaporation causes heat losses and, at the same time, water losses. One way to reduce water loss to zero and heat loss to a minimum is to use a water surface cover during the hours of inactivity. It must be remembered that a surface cover protection also causes a reduction of convection and Infra-Red (IR) radiation heat losses.

The structure of the covers can be diverse, nevertheless, if the swimming pool is outdoor, one must also consider the possibility of getting heat gains to the water, when the swimming pool is not in use, using a cover that is transparent to solar radiation. Thus, water surface covers have a twofold function: (a) reduce heat and water losses and (b) allow heat gains. On average, covers allow turning the energy balance positive when compared with a similar swimming pool without cover, in the same conditions.

The security is another function that can be fulfilled by the water surface cover, but for that purpose, it has to be resistant enough to support a person's weight, although this should be mainly thought to protect children's lives.

Other important passive measures for outside swimming pools must be assured since the very beginning of the design, namely: (1) enforce protection of its water surface from the windward side, as the wind is regarded as the motor for convection and evaporation heat losses. As so, fences or other similar adoptable solution can be considered; (2) deploy the swimming pool in an area where there is no significant shadow projection from adjacent obstacles.

In order to allow energy and water conservation it is also important to control the filter backwashing system since the water required for it is normally lost. Part of the heat, and thus energy [15–18], can be recovered if a wastewater's heat recovery mechanism is used. Regarding the water, it can be diverted to other uses, like outdoor washing, or ultimately collected into a tank, not squandered in the sewage system.

### ***3.2 Active Measures***

Active pool control measures aim to minimize water and energy consumption and cost of operation by means of an optimized control system that assures certain comfort levels for users and water quality levels.

To achieve these objectives, the automation and control systems together, must operate in a combined and coordinated manner, with the following main goals: (1) obtain data from the set of existing equipment; (2) decide, in an optimized manner, what are the best control parameters for the equipment and (3) act on the system to be controlled, reflecting the decisions made by the optimization algorithms.

In its decision process, the optimized management system must take into account different issues. The most relevant are:

1. Number and preferences of users, in terms of daytime hours of utilization and water temperature;
2. Cost of electric tariffs, when a connection exists to the electricity distribution grid;
3. Forecasted and actual levels of photovoltaic generations;
4. Thermal power obtained from installed renewable energy sources;
5. Technical limitations of the existing electrical and thermal equipment.

In order to obtain data from the set of existing equipment and to control it, an automation system must be used. In the following, we describe the main types of automation systems that allow the control of swimming pools, before describing the intelligent control system that can perform the intelligent management of the set of equipment applied to sustainable swimming pools.

### 3.2.1 Automation System

The first industrial automation systems for the integrated management of equipment in swimming pools was created in the decade of the 80s.

During the beginning of the utilization of automation technologies, these frameworks of Centralized Technical Management Systems (CTMS) for large buildings, known as, Building Management Systems (BMS) were implemented in big state offices, sports building, schools and hotels of large sizes.

In swimming pools, the use of field sensors, management algorithms and automation systems permits:

1. A substantial increase in the operational management of heating systems, water treatment, filling and recirculation, allowing a better water and energy efficiency;
2. A reduction in equipment wear due to excessive operating times;
3. A reduction of response times, in case of malfunctioning, through remote alarms;
4. The identification of the source of the problem through the CTMS software;
5. A reduction of specialized labor of the technicians in preventive maintenance procedures, with a quick screening and resolution of malfunctions.

Although these are clear advantages, the utilization of these technologies in the scope of outdoor swimming pools is not common. In this sense, the solutions found in the market commonly focus on the utilization of autonomous systems that depend solely on the information given by the sensing system and react according to the set points of the equipment, without allowing a more exhaustive integration and lacking a holistic view of the management of the different subsystems.

More recently, with the Internet of Things (IoT), it is possible to find equipment from various manufacturers with connectivity and digital platforms set for alarmist and customization definition, however lacking a correlation between performance and parameterization of equipment.



### 3.2.2 Intelligent Control System

Nowadays intelligent control systems are used in a wide variety of applications based in IoT architectures, in some cases with low deployment costs.

In the context of swimming pools the solution proposed in [19], clearly reduces the requirements for human intervention in the maintenance of swimming pools, providing a continuous monitoring system for relevant parameters and integrating alarms, through the definition of set points. Despite these abilities, the system does not allow an automated and effective capacity for automated decision-making regarding the control of the involved systems.

In this field, and to improve energy and water efficiency of swimming pools, solutions exist that based on the storage of time series of data, such as, pressure and water temperature, measured at key points in the hydraulic system, allow the optimized control of the water heating system. At this level, the authors in [20] propose, for indoor swimming pools, a predictive control system in a hybrid control setup that involves solar collectors and a boiler (possibly based on processes of biomass energy utilization) for thermal regulation of temperatures. When compared with a conventional Proportional Integral Derivative (PID) control system, the results show a decrease of nearly 19% in the energy demand of the pool resulting in a reduction close to 43% of the fuel consumption for heating.

The integration of renewable energy sources in swimming pools have been used in sports complexes [21–23]. The generation of electricity that results from renewable energy sources, like solar and wind, is commonly characterized as intermittent, showing a low correlation with the consumption requirements. These impairments impose the use of batteries or storage units. At this level, as described in [24], indoor and outdoor swimming pools have a significant and unused potential. In countries, such as, Germany, these pools are usually heated and thus represent optional deposits of thermal energy. When heating is produced by combined heat and power plants or heat pumps, swimming pools can be used to provide a flexible demand for electricity.

In this context, the work described in [25] focuses on the use of intelligent control systems to perform demand control on indoor pools. In this type of solutions, the integration of renewable energy systems when combined with Building Energy Management Systems (BEMS) present a great potential to reduce electricity and thermal costs. The BEMS specified by the authors in [25], implements strategies to control Heating, Ventilation and Air Conditioning (HVAC) equipment and pump systems, with the aim of reducing electricity demand during peak hours.

To the best of the author's knowledge, none of the works described in literature, have considered the utilization of solutions like machine learning, as for instance Random Forest [26], or Model Predictive Control [27, 28] in swimming pools. These methods have been applied with great advantage in different systems, including industrial and agricultural fields, and thus might stand as a promising solution to improve the energy efficiency of sustainability outdoor swimming pools.

## 4 Proposals for a Sustainable Outdoor Swimming Pool

Given the works and solutions described in the last section, in the following a description is made of a solution that integrates several of these features in order to create a Sustainable Swimming Pool.

### 4.1 *Thermal Insulation Systems Inside the Tank*

In the search for solutions that can be applied in the rehabilitation process of existing swimming pools, or in the design of new equipment, it is intended to demonstrate and ensure that conventional thermal insulation materials, such as, polystyrene, polyurethane or expanded cork agglomerate may still be used. Even though, these are compressible materials, together with a flexible and waterproofing mortar and a ceramic coating, these constitute a system that effectively gives thermal insulation for the interior walls and floor of swimming pools, and above all, has mechanical strength and durability/longevity.

The new thermal insulation system is based on the concept of External Thermal Insulation Composite Systems (ETICS), which are frequently used in the buildings' facade. The ETICS system features numerous advantages from the thermal point of view, with positive consequences in terms of sustainability [29]. The challenge lies in obtaining an optimal ratio of thermal and mechanical performance.

In order to minimize heat losses from the pool area, the application of such a system that integrates thermal insulation, reinforced base mortar reinforced with fiberglass mesh, waterproofing mortar and mortar/cement glue for gluing and grouting the ceramic coating is considered. The mortars that make up the thermal coatings have a paramount role in ensuring the mechanical and hygrothermal performance of the set, specifically when exposed to unusual mechanical, humidity and temperature conditions.

Several studies have been carried out to analyze the hygrothermal behavior of these solutions with authors reporting that as the water reaches the surface of the thermal insulation it migrate through the mortar, leading to an increase in the thermal conductivity [30–32]. This ensures that the porosimetry and microstructure of the mortar play a fundamental role in the hygrothermal behavior of the solution and the finish/coating has a significant impact on the hygrothermal system's performance [33–35].

### 4.2 *Harnessing of Solar Gains*

Solar radiation is a renewable source that is available on large regions and, so, very convenient to use in the context of heating of outdoor swimming pools. Of course, for

this goal to be met the water properties are also very relevant, namely, its absorptivity to solar radiation and its heat capacity. Last but not the least, heat losses must be reduced to achieve efficiency in the whole process.

The first solar collector is the water surface by itself. Significant water temperature differences might be found when comparing a swimming pool which surface can receive solar radiation, to another that is shadowed during long periods of the day.

Solar collectors are a classic and conventional way to bring more heat to the water, increasing its temperature.

The area of solar collectors that should be installed depends on the angle of the collector to the horizontal plane, and also on swimming pool's surface and volume, swimming pool's location, if it has a transparent cover or not, geographical orientation, wind speed and air temperature, as the most important variables. Nevertheless, as it would be wished, it is not possible to heat up more in winter (in the north hemisphere) than in summer, with solar collectors.

At this level, the work referred in [36] comprises the analysis of the thermal behavior of an outdoor swimming pool, in Elche, with 50 m<sup>2</sup>, from June to September that uses flat solar collectors without glass. The emphasis is on the experimentation of several numerical correlations for the calculation of evaporation losses whose results are compared with the measured values, using the temperature of the swimming pool water as a comparative parameter. The authors concluded that the collector's area despite being beneficial in terms of heating, as it contributes to an increase of water temperature, is also responsible for increasing the losses. Thus, they recommend using a swimming pool surface's covering system.

Of course, a quite obvious solution, is to use other processes that could shift the greater "heat availability", due to solar radiation, near solar noon hours, to the end of the day, or to the following morning. This can be done with heat accumulated in the soil around the pool, using pipes at low depths for pool water circulation. A possible handicap of this process can be the area to be reserved to lay the pipe work, which has to receive the solar radiation during the daily periods of highest radiation.

There is not enough work done in this subject, at least published, although there have been some practical examples of similar systems, but without effective results revealing their performance.

Another way to take advantage of time-deferred solar gains is to accumulate heat in Phase Change Materials (PCM), with liquid–solid, phase change temperatures, and vice-versa that are in the range suited in swimming pools, i.e., between 24 and 27 °C. As its known when those materials undergo a phase change, either liquid-to-solid, or solid-to-liquid, its temperature stays almost constant and its heat capacity reach very high values.

There is some work done in this subject. The accumulation can be done incorporating the PCM in the walls and bottom surfaces of the pool where the heat is accumulated, when the temperature of phase change is achieved, what happens always when there are enough solar heat gains by the swimming pool water. Conversely, there is a return of that heat to the water when its temperature drops and, at that instance, the PCM starts to change to its solid phase, giving back the heat to the water, thereby avoiding longer cooling. This is exploited in a model described in

[37], whose authors analyze also the alternative of using a PCM contained in an external Heat Exchanger (HE). In this case a pipe is needed from the swimming pool to the HE. After a simulation for three cities in the North-East of Spain (Catalonia) the authors concluded that using a PCM with a phase change temperature of 28 °C or 29 °C, together with the external HE, constitute the best solution, giving an advance of 20 h to rise the water temperature, so reaching more comfortable values, when the meteorological conditions by itself do not allow it.

The combination of geothermal energy and heat pumps is also used in some systems to heat both outdoor and indoor swimming pools. Generally, geothermal heating is associated with heat pumps to increase the energy potential of both temperature and quantity, unless the available temperature is high enough, allowing direct use. For example, in [38] the author analyses the cooperation of vertical geothermal heat exchangers and heat pumps to avoid the consumption of fossil fuels in public swimming pools, concluding that such solution is feasible, both technically and economically. Another interesting conclusion is found in [39]. In this case the swimming pool's heating is associated with the heating and cooling processes of the house, in various regions of USA. The heating system is based in geothermal heat pumps, one for the control of the temperatures of the spaces inside the house and the other for the swimming pool. The most important conclusion is found for some southern regions, where the swimming pool presence allows a 20% reduction in the ground loop lengths.

The use of the earth heat capacity could be a good mean to accumulate the excess temperature that might exist in swimming pool's water in summer. This can be especially applicable in regions of southern Europe, eventually complemented with some heat coming from solar collectors, if they exist for swimming pool heating purpose, as in summer they are less requested. The accumulated heat can be given back to the swimming pool or, maybe in a more profitable way, used for space heating in a nearby house. This is an unexploited system whose performance must be evaluated, from both technical and economic perspectives.

### ***4.3 Automation System***

The utilization of an automation system in heated outdoor swimming pools for domestic use, particularly for those that integrate renewable energy sources, can be done by reapplying the methodology used in some systems that are already common for water heating and treatment in collective swimming pools. This allows benefiting from the increased competitiveness of technological solutions in the automation, control and sensorization sectors, which have considerably lowered the associated costs during the last few years, making their integration a feasible solution in domestic swimming pools.

Industrial automation and sensorization systems should be subject to a more in depth study, taking into account the hydraulic characteristics and equipment that make up the heating and water treatment systems of the swimming pool. Therefore

it should be designed based on these elements, and use sensorization and control methodologies with standard signals for the control and data collection.

Locally a Swimming Pool Management System (SPMS), is responsible for the communication with these sensors and actuators. It includes interfaces for the integration of Internet Protocol (IP) and Modbus, or KNX automation systems. It can also connect directly with the Home Area Network or use a separate access router to connect to the Internet. This architecture also allows the communication between the SPMS and Cloud-based services on the Internet, through a Web Application Program Interfaces (API) or using the WebSocket protocol. The SPMS also has a web interface where the user can select and configure its preferences.

The Cloud-based service allows the monitoring and control of the swimming pool from anywhere in the World, through an Internet connection.

The utilization of automation systems and industrial sensorization, besides the advantages previously described, also guaranties a high robustness and longevity of the system, given the characteristics and high average robustness that characterize industrial equipment.

#### ***4.4 Intelligent and Predictive Management Platform***

An intelligent management platform must integrate machine learning techniques to replace tasks that are normally done by humans.

Within the scope of model-based predictive control, the system to be controlled is identified through mathematical equations, but it can also result from an “intelligent” model derived from a learning process. In this latter case, learning results from the “active” analysis of the recorded data relating to the behavior of the system subject to the circumstances of the overall control system and the specifications imposed by the system’s user.

In a first instance, it is essential to define the objectives and what data and variables of the system are necessary to obtain. Then algorithms and statistical models should be applied, so that the actions taken might be carried out without specific instructions, but carrying out pattern analysis and statistic inference. An interesting solution is the one proposed by Tao et al. [40] in which Model Predictive Control (MPC) and neuro-diffuse systems are combined to define a model of the system, obtained after the application of optimization algorithms.

In the specific case of heated outdoor swimming pools for private/domestic use, the main variables required for the correct functioning of the management platform are:

- Outdoor air temperature in the area of the pool;
- Superficial water temperature and at various depths;
- Temperature of the outflow of renewable thermal energy systems;
- Water pressure levels of the pumping systems;
- Comfort water temperature

Additionally, in order to enable the effective monitoring and control, the platform shall also give:

- Statistics on monetary savings introduced by the renewable energy sources and optimized control;
- Monthly reports on ecological impact, including CO<sub>2</sub> production values and the corresponding carbon footprint;
- Daily/weekly reports of the water temperature;
- The forecast of the average water temperature over a short time horizon (maximum 24 h) depending on the applicable control scenario;
- The range of permissible values for water temperatures;
- Alarm signals and levels, for example, leakage in the pumping system, indication of values and improper operation of the pumping and heating systems.

The intelligent component of the management platform is fundamental, allowing the replacement of the mathematical equations which define the behavior of the system. To this end, it utilizes the time series records of the variables, which are then used by the optimization algorithms to determine the output of the system in future moments, i.e., thus ensuring that the swimming pool water temperature remains as close to the value set by the user as possible. By only combining the intelligent and the predictive components of the platform in a centralized system, it will be possible to gather the time forecasts and the behavior of the system for the desired goals, while, at the same time, reducing the impacts associated with the energy consumption of the systems, which belong to the global system.

The prediction of the behavior of the water temperature regulation system, does not only depend on the “forecast” of the operation of the various subsystems, but also includes a factor of uncertainty related to the decisions and needs of the different users of the system. In this context, one can resort to models based on “Random Forest” to model human behaviors, as was for example done in [26], in the prediction of services purchased online.

The system can also integrate solutions that allow alarms, specifically for leak signaling, as proposed in [41], where methods are applied to enable the measurement and location of multiple leaks in a network of water pipes. Such methods analyze the variation of pressure sensors, with application in single or double path tubes.

## 5 Conclusions

Swimming pools if not properly dimensioned can cause high economic costs to the owners, as well as significant environmental impacts.

The implementation of sustainable swimming pools requires the combined action of several areas of knowledge. These areas extend from better thermal isolating materials, proper thermal and mechanic sizing of the water heating and filtering system, including the integration of renewable energy sources, and intelligent control of the whole system reflecting user preferences.

In terms of thermal insulation inside the tank several solutions can be used as described in Sect. 4.1, including polystyrene, polyurethane or expanded cork agglomerate, ETICS, reinforced mortars with fiberglass mesh, waterproofing mortar, mortar/cement glue for gluing and grouting the ceramic coating.

Regarding the integration and harnessing of solar gains, as described in Sect. 4.2, in the phase of the project it is important to consider many factors that include: the installation of solar collectors, the introduction of PCM materials to perform time-defer solar gains, combination of geothermal energy and heat pumps, and earth heat capacity.

For the control of the equipment in the swimming pool, industrial automation and sensorization systems should be considered together with a Swimming Pool Management unit that centralizes the communication with these sensors and actuators using standard IP, Modbus and/or KNX protocols. Cloud-based services on the Internet, should also be considered to allow the external monitoring and control of the swimming pool.

For the intelligent control of the system several solutions need to be integrated as described in Sect. 4.4. This includes machine learning techniques to predict user preferences and system behavior. In terms of control, a model-based predictive control, should be considered. This allows the replacement of the mathematical equations that define the behavior of the system.

## References

1. Final report summary—POOLS SAFE (A novel swimming pool water treatment for the detection and elimination of excess cyanuric acid.). Available online: <https://cordis.europa.eu/project/id/604884/reporting>. Accessed on 18 Dec 2021
2. Oliveira MJ et al (2018) SPOOLS—SUSTAINABLE POOLS—main developments of the project. *WIT Trans Ecol Environ* 217. ISSN 1743-3541
3. UNTWO, UNDP, Tourism and the sustainable development goals—Journey to 2030, Highlights, Achim Steiner, UNWTO eLibrary, January 2018. eISBN: 978-92-844-1940-1. ISBN: 978-92-844-1939-5
4. Gössling S, Peeters P, Michael Hall C, Ceron J-P, Du-bois G, Lehmann LV, Scott D (2012) Tourism and water use: supply, demand, and security. *An international review. Tourism Manag* 33:1–15
5. Gallion T, Harrison T, Hulverson R, Hristovski K (2014) Estimating water, energy, and carbon footprints of residential swimming pools. *Water Reclam Sustain* 343–359
6. Oliveira MJ et al (2020) Common typology, durability and pathologies of the swimming pools in the Algarve region—implications in the sustainability. In: Monteiro J et al (eds) *INCREASE* 2019. Springer, Cham. [https://doi.org/10.1007/978-3-030-30938-1\\_70](https://doi.org/10.1007/978-3-030-30938-1_70)
7. Hof A, Morán-Tejeda E, Lorenzo-Lacruz J, Blázquez-Salom M (2018) Swimming pool evaporative water loss and water use in the Balearic Islands (Spain). *Water* (20734441) 10(12):1883. Available: <https://www.mdpi.com/2073-4441/10/12/1883/htm>. Accessed 2 Jan 2022
8. Report of the World Commission on Environment and Development: our common future, UN (1987). Available: <https://sustainabledevelopment.un.org/content/documents/5987our-common-future.pdf>. Accessed 29 Dec 2021

9. Li Y, Nord N, Huang G, Li X (2021) Swimming pool heating technology: a state-of-the-art review. *Build Simul* 14(3):421–440. Accessed 2 Jan 2022. Available: <https://doi.org/10.1007/s12273-020-0669-3>
10. Bernhard M, Marc O, Quilichini E, Castaing-Lasvignottes J (2019) Sensitivity analysis of an outdoor swimming pool under dynamic conditions. *Procedia Manuf* 35:124–129. <https://doi.org/10.1016/j.promfg.2019.05.014>
11. PolyfoamXPSUK. Available: <https://polyfoamxps.co.uk/application-fields/floors/swimming-pool-basins/>
12. HeatForm UK. Available: <https://www.heatform.co.uk/>
13. Styropool DE. Available: <https://www.duw-pool.de/en/products/pools/styropool/>
14. Rose NP (2007) Method of thermal insulation of a pool. US patent 2007/0180603 A1, 2007. Available: <https://patents.google.com/patent/US20070180603>
15. Culha O, Gunerhan H, Biyik E, Ekren O, Hepbasli A (2015) Heat exchanger applications in wastewater source heat pumps for buildings: a key review. *Energy Build* 104:215–232
16. Shen C, Lei Z, Wang Y, Zhang C, Yao Y (2018) A review on the current research and application of wastewater source heat pumps in China. *Therm Sci Eng Prog* 6:140–156
17. Ferreira A, Ribeiro B, Marques P, Ferreira A, Dias A, Pinheiro H, Reis A, Gouveia L (2017) *Scenedesmus obliquus* mediated brewery wastewater remediation and CO<sub>2</sub> biofixation for green energy purposes. *J Clean Prod* 165:1316–1327
18. Piwowar A, Dzikuć M (2019) Development of renewable energy sources in the context of threats resulting from low-altitude emissions in rural areas in Poland: a review. *Energies* 12:3558
19. Simões G, Dionysus C, Glória A, Sebastião P, Souto N (2019) Smart system for monitoring and control of swimming pools. In: *Proceedings of the 2019 IEEE 5th World forum on internet of things (WF-IoT)*, Limerick, Ireland, pp 829–832
20. Delgado Marín JP, Vera García F, García Cascales JR (2019) Use of a predictive control to improve the energy efficiency in indoor swimming pools using solar thermal energy. *Solar Energy* 179:380–390. ISSN 0038-092X. <https://doi.org/10.1016/j.solener.2019.01.004>
21. Zuccari F, Santiangeli A, Orecchini F (2017) Energy analysis of swimming pools for sports activities: cost effective solutions for efficiency improvement. *Energy Procedia* 126:123–130
22. Bailera M, Lisbona P, Llera E, Peña B, Romeo LM (2019) Renewable energy sources and power-to-gas aided cogeneration for non-residential buildings. *Energy* 181:226–238
23. Artuso P, Santiangeli A (2008) Energy solutions for sports facilities. *Int J Hydrogen Energy* 33:3182–3187
24. Stadler I (2008) Power grid balancing of energy systems with high renewable energy penetration by demand response. *Utilities Policy* 16(2):90–98
25. Ribeiro EM, Artilheiro HM, Jorge M, Quintela DAA (2014) Control of indoor swimming pools with potential for demand response. *J Energy Power Eng* 8(1):20
26. Ghosh S, Banerjee C (2020) A predictive analysis model of customer purchase behavior using modified random forest algorithm in cloud environment. In: *2020 IEEE 1st International conference for convergence in engineering (ICCE)*, pp 239–244. <https://doi.org/10.1109/ICCE50343.2020.9290700>
27. Li S, Jiang P, Han K (2019) RBF Neural network based model predictive control algorithm and its application to a CSTR process. In: *2019 Chinese control conference (CCC)*, pp 2948–2952. <https://doi.org/10.23919/ChiCC.2019.8865797>
28. Han H, Zhang L, Hou Y, Qiao J (2016) Nonlinear model predictive control based on a self-organizing recurrent neural network. *IEEE Trans Neural Netw Learn Syst* 27(2):402–415. <https://doi.org/10.1109/TNNLS.2015.2465174>
29. Sulakatko V, Lill I (2019) The economic relevance of on-site construction activities with external thermal insulation composite system (ETICS). *Int J Strateg Prop Manag* 23(4):213–226. <https://doi.org/10.3846/ijspm.2019.7071>
30. Maia J, Ramos NMM, Veiga R (2018) Evaluation of the hygrothermal properties of thermal rendering systems. *Build Environ* 144:437–449. <https://doi.org/10.1016/j.buildenv.2018.08.055>



31. Tadeu A, Skerget L, Simões N, Fino R (2018) Simulation of heat and moisture flow through walls covered with uncoated medium density expanded cork. *Build Environ* 142:195–210. <https://doi.org/10.1016/j.buildenv.2018.06.009>
32. Fino R, Tadeu A, Simões N (2018) Influence of a period of wet weather on the heat transfer across a wall covered with uncoated medium density expanded cork. *Energy Build* 165:118–131. <https://doi.org/10.1016/j.enbuild.2018.01.020>
33. Xiong H, Yuan K, Wen M, Yu A, Xu J (2019) Influence of pore structure on the moisture transport property of external thermal insulation composite system as studied by NMR. *Constr Build Mater* 228:116815. <https://doi.org/10.1016/j.conbuildmat.2019.116815>
34. Matias G, Torres I, Rei F, Gomes F (2020) Analysis of the functional performance of different mortars with incorporated residues. *J Build Eng* 29:101150. <https://doi.org/10.1016/j.jobee.2019.101150>
35. Barreira E, de Freitas VP (2013) Experimental study of the hygrothermal behaviour of external thermal insulation composite systems (ETICS). *Build Environ* 63:31–39. <https://doi.org/10.1016/j.buildenv.2013.02.001>
36. Ruiz E, Martinez PJ (2010) Analysis of an open-air swimming pool solar heating system by using an experimentally validated TRNSYS model. *Solar Energy* 84:116–123
37. Zsembinszki G, Farid MM, Cabeza LF (2012) Analysis of implementing phase change materials in open-air swimming pools. *Solar Energy* 86:567–577
38. Al Kataprakakis D (2015) Comparison of swimming pools alternative, passive and active heating systems based on renewable energy sources in southern Europe. *Energy* 81:738–753
39. Andrew Chiasson PE (2005) Residential swimming pool heating with geothermal HP system. *Geo-Heat Center Bull* 13–17
40. Tao J-L, Wang N, Zhang R-D (2013) GA based fuzzy neural network generalized predictive control method. In: *Proceedings of the 32nd Chinese control conference*, pp 4062–4067
41. Kim SH (2020) Multiple leak detection algorithm for pipe network. *Mech Syst Signal Process* 139:106645. ISSN 0888-3270. <https://doi.org/10.1016/j.ymsp.2020.106645>

# Reality of Photovoltaic Technology Applied to Homes not Connected to the Grid Connected Using to Lithium Batteries Without Generator Set Support



David Marín-García

**Abstract** There are dwellings in which the owner does not have the possibility of obtaining electricity from the grid. The goal of this study is to find out contingencies of a totally autonomous solar energy system that uses photovoltaic panels and lithium batteries, without specific support from generator equipment powered by fossil fuels. For this, the methodology followed focuses on the in situ monitoring of a real installation of photovoltaic panels carried out in a dwelling located in the south of Spain due it is one of the climatic zones of the European continent with the least severity and at the same time with the greatest number of hours of sun exposure. In this way, in addition to knowing the contingencies, it can be deduced that if in these very favorable circumstances they occur, this means that they are likely to occur in any other less favorable. The results indicate that, although the dwelling is supplied, there have been certain contingencies in the supply and in the final cost. This leads to the conclusion that even in dwellings whose users consume little energy, due to their way of life and favorable climatic conditions, there are still some aspects of the technology that produce contingencies and that need to be resolved to make these installations technically and economically comparable to the supply of the electricity grid, in addition to being totally independent from any other source of energy that is not the photovoltaic itself.

**Keywords** Energy · Photovoltaic panels · Houses · Live off the grid

## 1 Introduction

Although the first uses of photovoltaic technology date back to 1950, when NASA used it for certain spacecraft [1], it did not become popular until the end of the twentieth century and the beginning of the twenty-first century.

One of the main reasons for this popularization has been the increase in the cost of energy supplied by the grid [2], and the difficulties posed by the methods

---

D. Marín-García (✉)

Department of Graphical Expression and Building Engineering, Higher Technical School of Building Engineering, University of Seville, 4A Reina Mercedes Avenue, 41012 Seville, Spain  
e-mail: [damar@us.es](mailto:damar@us.es)

of predicting this cost [3]. Thus, although initially the investment remains high, continuous technological advances are increasingly reducing these costs, increasing yields, and improving and solving various problems related to the achievement of zero energy cost dwellings [4] both in the case of hybrid systems such as those that claim to be fully autonomous [5, 6].

An interesting study in this sense is the one carried out by the Polytechnic University of Madrid (ETSIT) in which three real cases (A—consumption as generated; B—with demand control without storage; C—with control of demand and storage) were compared in terms of empirical data obtained from a housing prototype called “Magic Box” [7]. In this study, it is concluded that self-sufficiency can reach 30% in case A, 70% in case B, and 90% in case C. However, regarding energy demand, it is also evidenced that an active management is necessary, as well as an installation of some complexity and costs.

In case C, the best-known weakness of this technology, although not the only one, is “energy storage” [8–10], which at present, if the budget is reduced, is generally carried out by means of gel batteries or, in the case of a bigger budget, lithium. However, it should be noted that lithium batteries have experienced price declines in recent times [11].

To all this, it must also add the advances in policies aimed at promoting the use of solar energy in many countries, taking into account that around 20% of the world’s population lives in 70 countries that have excellent conditions for use of photovoltaic solar energy [12].

On the other hand, it is not the first time in Europe that judicial decisions have resolved a purchase and sale contract due to lack of connection to the electricity supply. Thus, for example, the Spanish Supreme Court upheld this situation in a judgment of November 10, 2016 [13]. Despite this, at present, in addition to the owners who voluntarily prefer not to be connected to the grid, there are other types of homeowners who, due to the circumstances of their building, do not have the possibility of having electricity supply from the supply grid conventional. In these cases, there are different technologies to solve this situation.

Technologies that use the sun’s light and heat directly without changing shape are called passive solar energy technologies, and those that convert it are called active solar energy technologies, such as photovoltaics, which convert radiation directly into electric energy.

As indicated, these photovoltaic systems can be connected to the grid or not, and in the latter case, they can provide total autonomy and energy independence from the grid, even becoming the only source of energy for a home.

These facilities are often referred to as “stand-alone solar energy system”. In these cases, they are basically usually composed of photovoltaic panels combined with batteries for storage, to which is added a control unit (load control) and a DC/AC converter.

The specific characteristics of these systems must be the most appropriate [14] mainly taking into account the climatic conditions, location, needs and behavior of users, and building conditions, such as the energy efficiency of its envelope, which is normally closely related to its thermal insulation.

There are various studies on the choice of installation, execution, commissioning, and even on the monitoring of dwellings in which technologies of these characteristics have been applied in different climatic zones and for different construction characteristics and user needs. Thus, for example, in recent years, studies of applications to dwellings have been detected in various locations, which had a high climatic severity in winter such as Germany [15], not as extreme, although with some severity as Madrid [16] or very hot like Bangladesh [17].

For the climatic severity of the case that will be studied later, the reference to the Polytechnic University of Valencia is interesting, in which various works related to the determination of the number of solar panels and the capacity of the necessary batteries have been carried out by its teachers and students, as well as an analysis of the economic viability and a comparison regarding the price that being connected to the grid would entail [18–24].

However, all these studies consider that it is necessary to install a generator set support, so there are still doubts about whether it is possible with a not excessive investment a stand-alone solar energy system, in such a way that there are no contingencies. In other words, that in its operation, it offers the same stability and results as being hooked up to the electrical grid for the purposes of user perception, without the need at any time to use a generator set powered by fossil fuels, even if it is only as punctual support.

To find out this, in this work, we have chosen to analyze an installation located in one of the climatic zones best classified in the regulations on energy efficiency in Spain, which also initially has basic energy needs, in such a way that if said installation is produced by these contingencies, it could be confirmed that the probability will be much higher in homes located in climatic zones whose climatic severity or energy needs are higher.

## 2 Methodology and Material

In addition to the determination of the state of the art already mentioned in the introduction, the methodology followed has been based fundamentally on the in situ monitoring of a real installation of photovoltaic panels of an independent dwelling in a house located in the south of Spain where the climatic severity both in winter and in summer and it is one of the lowest possible and that initially it has basic energy consumption needs.

### 2.1 Case Study

In order to choose the appropriate area where the dwelling to be analyzed should be located, the information indicated in the Spanish Technical Building Code (CTE), which establishes in its basic energy saving document DB H1 [25], was consulted,

which are the climatic zones into which Spain is divided, identifying them by means of a letter (A, B, C, D, and E) corresponding to the winter climatic severity (A is the least severe) and a number, corresponding to the summer climatic severity (1, 2, 3, and 4).

In Spain, there are only three areas with classification A, and one of them is located in the province of Malaga. The climate of Malaga, and especially in certain areas such as Torrox or Marbella among others, has been declared on several occasions as one of the most pleasant in Europe, since there are very mild minimum temperatures in winter and moderate maximum temperatures in summer.

The average annual temperature in this area is usually around 17–18 °C and rarely reaches temperatures close to 0 degrees in winter or above 28–29 degrees in summer. Precipitation is also low, and there are almost 3000 h of sunshine a year (UTC + 1 or UTC + 2 time zone in summer). The wind is usually light. For this reason, as already indicated, the dwelling chosen for the experimentation is located in one of these areas of southern Spain, specifically in Andalusia, in the municipality of Ojén, bordering Marbella (Malaga).

Regarding the physical characteristics of the house, it has two floors with a porch. It is located on an area of 3000 m<sup>2</sup>. Usually, two people live, although temporary visits from another two more people are foreseen. Access to the electricity grid is not possible given its isolated location in an area far from urban centers. Kitchen and water heater work by gas cylinder.

It is a rectangular building of 7.75 × 5.65 m with a ground floor height of 2.55 m and with walls on the upper floor that range from 1.10 m the lowest and 2.24 m the highest. The window frames are made of aluminum, with two 100 × 110 cm on the ground floor, one of 110 × 85 cm, one of 55 × 50 cm, and one of 65 × 65 cm. On the upper floor, there are two windows of 65 × 65 cm and on the roof two, one of 118 × 78 cm and the other of 98 × 55 cm. The entrance door is double sheet metal.

Regarding the photovoltaic installation guarantee, this is 2 years for the inverter, 5 years for the panels, 12 years (25 years of production, although each year a loss of between 3 and 4% is expected), and finally 5 years for batteries.

As mentioned, the low climatic severity allows almost zero consumption of both heating and cooling, so no electrical devices are used in this sense, and there is only a wood stove and small portable gas cases for specific cases.

On the other hand, to further adjust the home to the objective of meeting only basic electrical needs that cannot be covered by other means, the kitchen and water heater work with gas.

As already mentioned, the electricity consumption for heating and cooling will be practically nil. For this reason, the building envelope, for this study, will not influence excessively given the aforementioned low climatic severity.

However, for merely informative purposes, the envelope is made up of walls, a sheet of concrete block with cement mortar render on the outside and plastered on the inside. Regarding the roof, it is made up of ceramic tiles on a mortar layer supported by a hollow brick board.

The transmittance  $U$  (W/m<sup>2</sup> K) of these elements in a simplified way (the process is really more complex, and various techniques can be used to find out [26, 27]) is  $1/R_t$

where  $R_t$  = total thermal resistance of the element composed of layers ( $m^2 K/W$ ), which is obtained according to Eq. (1)

$$R_t = R_{si} + R_1 + R_2 + R_3 + \dots + R_n + R_{se} \tag{1}$$

where

- $R_{si}$  = internal surface thermal resistance
- $R_{se}$  = exterior surface thermal resistance
- $R_1, R_2, R_3, \dots, R_n$  = thermal resistance of each layer obtained from Eq. (2).

$$R = e/\lambda \tag{2}$$

where

- $e$  = material thickness (m)
- $\lambda$  = material thermal conductivity (W/K m) (according to each material).

From this, the inverse proportionality between transmittance and resistance is deduced, that is, the more the resistance, the lower the transmittance:  $U = 1/R$  or  $R = 1/U$ .

When obtaining our  $U$ -value, normatively speaking, the usual thing is to compare it with the value of the maximum thermal transmittance (or limit) specified for the climatic zone in which our building is located, in winter and in summer.

A summary of the specific characteristics of the building is shown in Tables 1 and 2.

However, as already mentioned, the process of choosing photovoltaic equipment was initially based on the consumption that was going to be produced. According to

**Table 1** Description of the house under observation

Year of construction	1991
$M^2$ built	94 $m^2$
External wall area	112 $m^2$ 1 °F + 35.87 $m^2$ 2 °F
Roof area	73 $m^2$
Window and door glazing area	20.2 $m^2$
Residential part of the usable area of the dwelling	75.7 $m^2$
Occupants	2
Air changes per hour	3

**Table 2** Estimated  $U$ -values [28]

$U$ -value (W/ $m^2$ K)	External wall	2.3
	Roof	1.9

**Table 3** Inventory and characteristics of essential appliances

Electrical devices, appliances, and equipment	Units	Power W/unit	Use time h/day	Days of use days/week
Lighting (LEDs)	10	10	3–5	7
Refrigerator	1	650	24	7
Blender	1	200	0.25	7
Mixer	1	900	0.25	7
Food processor	1	1250	0.25	2
Mobile chargers	2	10	3	7
Laptop/computer	2	100	3	7
Printer	1	15	0.25	1
Router	1	12	12	7
Water pump	1	750	1	7
Washing mach.	1	450	3	4
Dryer	1	600	4	2
Vacuum cleaner	1	750	1	1
Iron	1	2750	1	1
Smart TV	1	66	2–5	5

data from Red Eléctrica de España (REE) [29], the monthly consumption of kWh of a Spanish household is about 270 kWh, for an approximate total of 3272 kWh/year. However, the amount of energy consumed in each home will always vary depending on the following factors: (i) characteristics and dimensions of the dwelling, (ii) electrical appliances, (iii) location of supply, (iv) number of inhabitants, and (v) consumption habits of residents.

Thus, said consumption was calculated based on the minimum essential and usual appliances indicated by the users that they were going to need (Table 3). However, given that in the future these needs could increase, one of the conditions for choosing the elements that make up the system is that in any case it is re-scalable in the future.

These data were simplified in order to introduce them into the simulation application that was used to check the pre-dimensioned (PVSyst) [30].

## 2.2 Features and Circumstances to Be Met by the Installation

These features and circumstances were as follows: (i) It must be an installation completely isolated from the electrical grid, without the need for any external power supply support, not even an auxiliary generator set. However, since there may be the possibility that this is not possible based on the results of the present study, it must be an installation that can be connected to an electric generator that starts automatically and also manually in case of discharge of electricity batteries and insufficient solar

supply. (ii) It must be an easily scalable facility (for future expansion). (iii) There is an annex on the ground floor of the house where the system would be installed (regulator, batteries, inverter, etc.). (iv) The installation must allow online consultation of historical and real-time data. Said online application must be able to consult the load curve, that is, a graphic representation of the energy consumed during a period of time (hours, days, months, or year). Through the load curve and the data, it should be possible to download the application in Excel format and collect all the information necessary to find out the behavior of the system at all times (power consumed, when the highest consumption occurs, when the battery is running charging, and when the system is powered, and to what extent, when the panels are charging the battery and/or powering the system, and to what extent, battery charge levels, etc.). (v) The planned location for the panels is oriented to the south, with no shading elements.

It should be noted that the aforementioned location of the panels is on a tiled roof of about 22 m<sup>2</sup> with an inclination of about 35/30°.

Normally for this type of installations, a shading study is previously carried out since, if there is a uniform irradiance pattern, the voltage and current generation of the cells are the same, if they have identical electrical characteristics.

In order for the energy at the generator output to be used, voltages higher than that of the cell are needed. For this reason, they are usually connected in series. However, if there is a shadow that affects one of the cells and not others, the generation is compromised since the current generated is proportional to the incident irradiance. As all the cells are connected in series, a current limitation occurs, since the output intensity is limited by the lower of the current generated by the cells. In addition, the energy generated by the rest of the cells is dissipated in the form of heat in those less illuminated, the consequence of which is the deterioration of the module. One solution is to divert current flow from partially shaded areas with bypass diodes. In the present case, a parallel connection was chosen.

The checks on solar exposure were based on the solar charts available for specific applications for this purpose such as SunCalc, Sun earth tools, Sun path chart program, Solea-2, among others [31]. Figure 1 shows the one made with software of the Solar Radiation Monitoring Laboratory of the University of Oregon (SunChartProgram).

Regarding the verification of incident solar irradiation, they were calculated based on various databases: Meteonorm [33], NASA [34], and PVGIS [35]. In Fig. 2, you can see the results using the PVGIS application, although Meteonorm was used for the simulation with PVSyst [30].

It should be remembered that the orientation chosen is south and the angle is 30°, the irradiation being between 111.79 of minimum (December) and 229.27 of maximum (August).



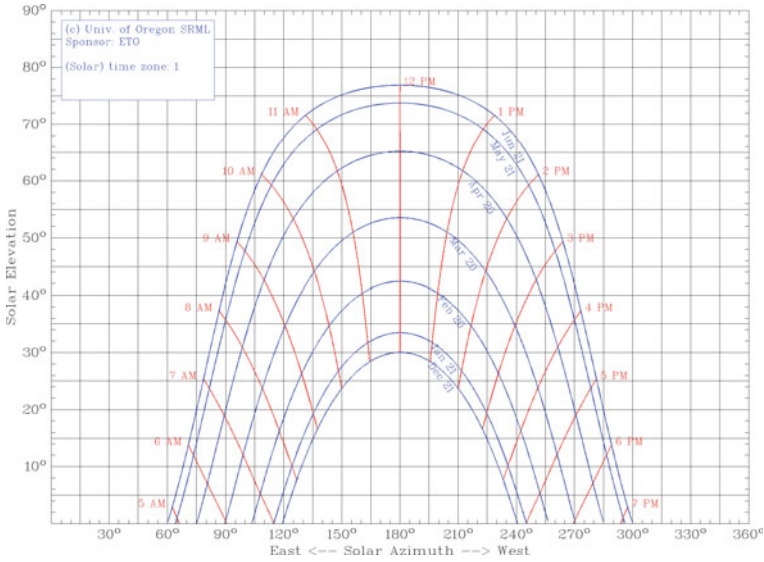


**Fig. 1** Solar trajectory graphs in Cartesian coordinates for the location of the monitored dwelling and for the dates on which the monitoring was carried out. Made with Sun path chart program [32]

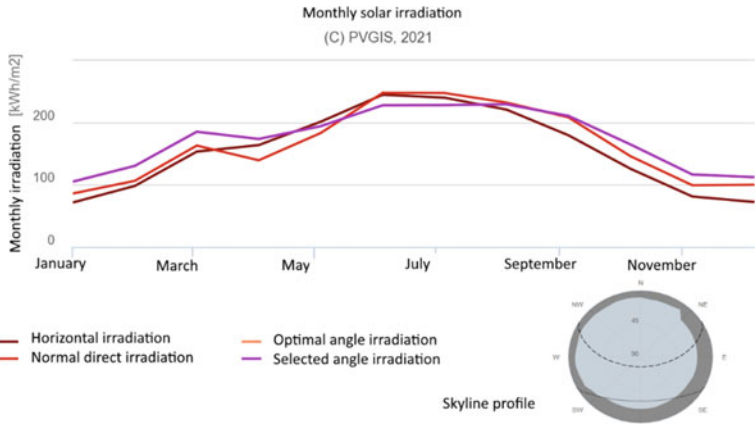


**Fig. 2** Incident irradiation in a plane that forms 30° with the horizontal with east and west inclinations. Fountain: PVGIS

### 2.3 PV System

With all the requirements and information, first of all, the tools provided by PVSyst were used [30].

Without providing any information obtained from all the tools mentioned above, detailed proposals and estimates of the cost of the installation were requested. The

**Table 4** Equipment that make up the system and its characteristics

Elements	Commercial characteristics
Solar panels	10 units of 455 W and 144 monocrystalline cells. JA Solar
Inverter	Storage 1Play 6TL M—6000 W hybrid Monof. Ingenconsun
Batteries	4 units of high voltage Pylontech HV H48050 9.6 kWh
Support	Triangular structure support for 10 panels on sloping roof
Surface panel	With AC and DC protections + wiring and conduits

requests were sent to seven of the closest photovoltaic installation companies with the best Google references. Four responses were obtained, but only two met the aforementioned requirements, discarding those that proposed installing gel batteries given the greater difficulty of making them scalable compared to lithium batteries that usually offer better performance and ease of maintenance according to the technical sheets and bibliography consulted [8].

Regarding the panels, although one of the companies proposed to install 22 panels of 2 × 1 m and 450 W/panel on the roof, the proposal was rejected since this area is not available and it exceeds the electrical needs raised, in addition to having a very high price.

After all the previous process, the selected company carried out the final measurements and verified that the installation was viable. However, several changes were made that included batteries and high-end inverter and a 30° inclined structure, thus theoretically ensuring autonomy of at least 4 days without sun, which caused the total cost of the installation to almost double. Table 4 shows the equipment that make up the system and its characteristics.

Considering the equipment that made up the system, a comparison was made with the results of PVSyst [30] although in this case, it was necessary to make an approximation to said equipment since they were not available in their pre-dimensioning in the application. This is understood because it is a question of equipment whose new models are launched on the market in a novel way and the application is not yet updated in this regard.

### 3 Results

Regarding the comparison between the results of applying PVSyst [30] and the installation carried out by the final installer, given that the actual recorded monthly consumption is low (Fig. 3), in principle, they seem to be correct. The scheme proposed in the application of PVSyst can be shown in Fig. 4.

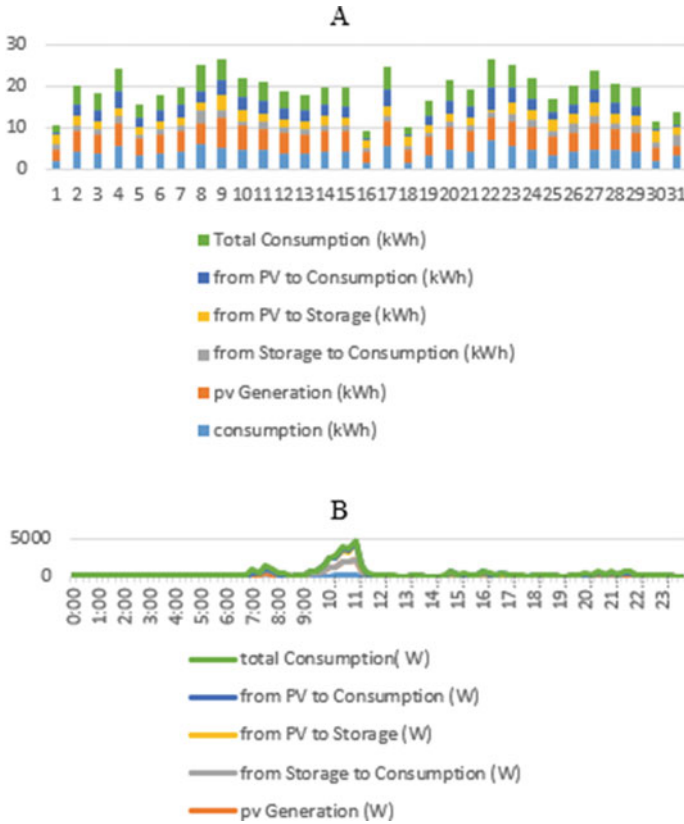


**Fig. 3** **a** Consumption and generation of kWh/month for October and **b** load and consumption curve for a full day of October

Regarding the results of the simulation with PVSyst in Fig. 5, some of them can be seen.

Regarding the execution of the installation, there were no contingencies except for the configuration of the inverter that initially could not be connected to the system, since the equipment’s Wi-Fi did not work and, therefore, could not be configured or activated. After several attempts, it was possible to configure and start-up in a basic mode that at least generated electricity, but without connection. The next day, the situation improved by giving provisional access to investor information. This information is essential as it is needed to organize how and when electricity is consumed. As has already been commented previously, data are obtained from here on: (i) how much electricity the panels are generating; (ii) how much of this electricity is consumed directly; (iii) how much the batteries are charging; (vi) how much energy is being consumed from the batteries; and (v) how much is left in storage.

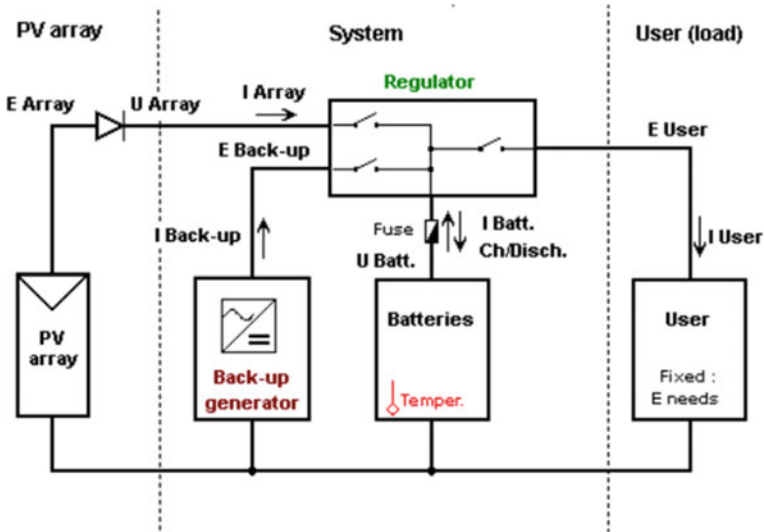


Fig. 4 Simplified scheme of the autonomous system PVSyst [30]

However, this information can only be observed via the web or app, and you need an internet connection or be next to the inverter to connect to its internal network, but there was no physical monitor to access. Also, the inverter does not work with small battery loads or very little generation from the panels. These circumstances must be known in the process of choosing the equipment, and access to said information is understood to be vital since it is not advisable in these facilities not to monitor this control of the inverter information as it is necessary for the electricity supply to function properly.

Regarding the operation of the system, although the supply has covered the established needs, one month after the start-up, around seven in the morning, noises in the form of clicks are detected, the electricity supply is cut off, they become to detect noises, and the electrical flow is restored. After an hour, the whole process is repeated during the day and at night, and at the end, the next day the supply is permanently cut off. The technicians of the installation company indicate that the batteries must be reset because the charges of the different cells are not balanced in the factory. For this, all the batteries must be emptied and recharged, but unfavorable weather means that the batteries do not charge anything for a day and a half, although they should be charged to some extent during that period. Due to the weather conditions, it was necessary to wait 4 days without electricity available, until the batteries were charged and everything worked correctly again.

Despite everything, two months after installation, the contingency described above is repeated. The installation is checked, and it is concluded that lithium batteries often must be discharged more than 50% to function correctly and that since exposure to the sun has been high and a lot of energy has been consumed from the batteries,

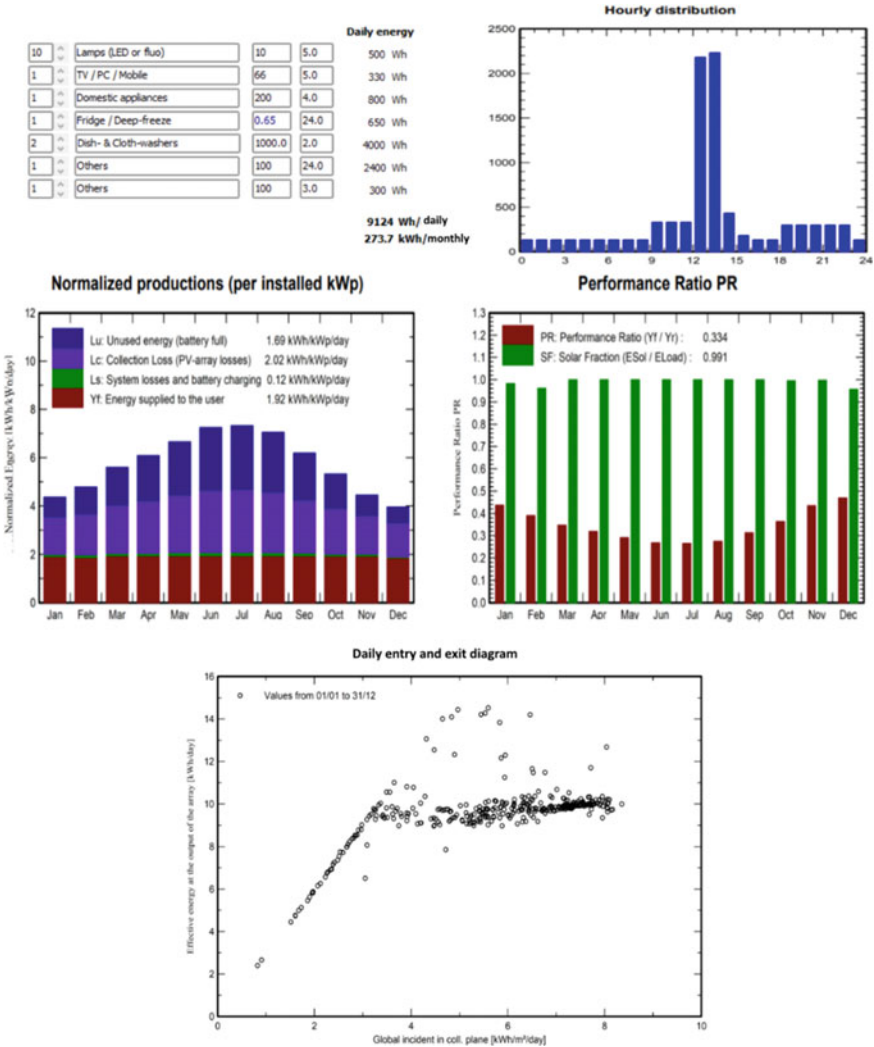


Fig. 5 PVSystem results [30]

the inverter has a security system that automatically disconnects every hour to avoid damaging the batteries.

To offer a definitive solution, it is decided to lower the charge of the batteries to 80%. It is also concluded that the inverter needs a minimum battery charge of 8% for its operation. In other words, for there to be electricity, the autonomy of the batteries must be reduced by 28%.

Before the end of the follow-up period, similar anomalies occurred and it was expected that another electronic device would be installed to resolve the situation, but at the end of this study, there are no data on such a device.

It should be added that the rectification of the battery charge to 80% was carried out remotely, since the user cannot modify this parameter because only the distributor has access to this operation in the inverter.

## 4 Conclusions

From the results of the experimentation carried out, it can be deduced that it is difficult to do without a specific support electric generator, normally powered by hydrocarbons to avoid days without sun and situations such as those described, being also necessary a generator that must have at least the same power than the inverter (6000 W in the case studied), and this is so insofar as, with lower powers, the equipment does not have the capacity to generate electricity to consume and to charge the battery at the same time. Consequently, it will produce energy for household appliances during a few hours the generators can run, but the batteries probably will not charge. The 6000 W generators that can be connected to a photovoltaic system usually cost more than €1500 and require proper installation, not to mention the noise and maintenance of all this.

On the other hand, it should be noted that, if the battery charge limit is not taken into account and consumption is not monitored and attended to, it may happen that energy is not available for consumption with batteries at 8% and the investor is blocked, and this can be extended in time if the weather is not favorable. This means waiting again for there to be enough solar radiation and having to completely reset the inverter.

Regarding the information that the user should know, it is necessary to emphasize that the companies that sell and install this equipment must study in depth the needs of the users to install the most appropriate system and report on all these possible contingencies and how they can make them work correctly, as well as the limitations and how it is necessary to adapt to a certain extent the lives of the users so that these systems work properly, taking special care in the consumption and maintenance that must be carried out.

On the other hand, in the case of experimentation, given that it is a rural building whose characteristics do not allow access to subsidies to help partially finance the installation (a situation that occurs relatively frequently in these properties), it was decided to choose to finance the purchase of the system for 10 years, at 7.17% annual interest, setting monthly payments of €168, that is, in 10 years, the total cost would be around 20,000 euros. This is in principle a high cost for a family with an average economy, also taking into account that most of the equipment will have to be renewed before 10 years, either due to wear (batteries) or due to panel and/or inverter obsolescence. Despite this, the profitability or not of this equipment is strictly comparative with respect to the price of the energy that the grid would

supposedly supply, so if this is at unsustainable levels for users, the profitability of the solar installation would be adequate.

As a final conclusion, it should be noted that for these cases, there does not seem to be a better alternative to the generation of electricity through photovoltaic systems, and although it would have to be studied in greater detail, given the characteristics of the place, the generation of electricity by other means, such as wind energy, for example, is not understood to be viable, although it could be in other cases.

## References

1. Vallèra AM, Centeno Brito M (2006) Meio século d História Fotovoltaica. *Gaz Física* 1:2
2. European Commission (2021) EU Energy prices | Energy. [https://ec.europa.eu/energy/topics/markets-and-consumers/EU-energy-prices\\_en](https://ec.europa.eu/energy/topics/markets-and-consumers/EU-energy-prices_en). Accessed 21 Dec 2021
3. Weron R (2014) Electricity price forecasting: a review of the state-of-the-art with a look into the future. *Int J Forecast* 30:1030–1081
4. Stefanović A, Bojić M, Gordić D (2014) Achieving net zero energy cost house from old thermally non-insulated house using photovoltaic panels. *Energy Build* 76:57–63
5. Akikur RK, Saidur R, Ping HW, Ullah KR (2013) Comparative study of stand-alone and hybrid solar energy systems suitable for off-grid rural electrification: a review. *Renew Sustain Energy Rev* 27:738–752
6. Voss K, Hendel S, Stark M (2021) Solar Decathlon Europe—a review on the energy engineering of experimental solar powered houses. *Energy Build* 251:111336
7. ETSIT U MagicBox. <http://magicbox.etsit.upm.es/>. Accessed 23 Dec 2021
8. Akinyele D, Belikov J, Levron Y (2017) Battery storage technologies for electrical applications: impact in stand-alone photovoltaic systems. *Energies* 10:1760
9. Gurung A, Qiao Q (2018) Solar charging batteries: advances, challenges, and opportunities. *Joule* 2:1217–1230
10. Trahey L, Brushett FR, Balsara NP et al (2020) Energy storage emerging: a perspective from the joint center for energy storage research. *Proc Natl Acad Sci U S A* 117:12550
11. Goldie-Scot L (2019) A behind the scenes take on lithium-ion battery prices | BloombergNEF. <https://about.bnef.com/blog/behind-scenes-take-lithium-ion-battery-prices/>. Accessed 21 Dec 2021
12. Suri M, Betak J, Rosina K, Chrkavy D, Suriova N, Cebecauer T, Caltik M, Erdelyi B (2020) Global photovoltaic power potential by country. *Global photovoltaic power potential by country*. <https://doi.org/10.1596/34102>
13. Supreme Court of Spain (2020) Judgment of nullity of sale due to impossibility of electricity supply
14. Ali W, Farooq H, Rehman AU, Awais Q, Jamil M, Noman A (2018) Design considerations of stand-alone solar photovoltaic systems. In: 2018 International conference on computing, electronic and electrical engineering (ICE Cube), pp 1–6
15. Voss K, Goetzberger A, Bopp G, Häberle A, Heinzl A, Lehmbert H (1996) The self-sufficient solar house in Freiburg—results of 3 years of operation. *Sol Energy* 58:17–23
16. González Carballo A (2021) Diseño de una instalación de autoconsumo fotovoltaico para una vivienda unifamiliar
17. Hossain CA, Chowdhury N, Longo M, Yaïci W (2019) System and cost analysis of stand-alone solar home system applied to a developing country. *Sustainability* 11:1403
18. Melul Campos A (2021) Instalación solar fotovoltaica de autoconsumo para una vivienda rural con baterías
19. Sabater Alemany J (2016) Instalación de energía solar fotovoltaica aislada para una vivienda unifamiliar situada en el campo de 5KW

20. Marchante Pérez C (2015) Instalación solar fotovoltaica aislada para vivienda
21. Teva Caballero A (2021) Estudio de una instalación solar fotovoltaica aislada para una vivienda unifamiliar en Fortuna, 89
22. David A, Quiroga S (2012) Sistema de energía solar fotovoltaica para vivienda unifamiliar aislada, 103
23. Mayor Boronat M (2021) Estudio de una instalación solar fotovoltaica para una vivienda unifamiliar aislada
24. Hernández García E (2020) Estudio de una instalación solar fotovoltaica para una vivienda unifamiliar aislada, 72
25. Ministerio de la Vivienda (2006) Código Técnico de la Edificación (CTE) Documento Básico de Ahorro de Energía (DB-HE). In: BOE. <https://www.codigotecnico.org/>. Accessed 21 Dec 2021
26. Bienvenido-Huertas D, Moyano J, Marín D, Fresco-Contreras R (2019) Review of in situ methods for assessing the thermal transmittance of walls. *Renew Sustain Energy Rev* 102:356–371
27. Teni M, Krstić H, Kosiński P (2019) Review and comparison of current experimental approaches for in-situ measurements of building walls thermal transmittance. *Energy Build* 203:109417
28. Térmica PVGVL de C de C en la EÁ (2015) Catálogo de rehabilitación energética. Herramienta de ayuda para el técnico. *Cercha Rev la Arquitectónica* 62–66
29. Red Eléctrica Española (REE) Publicaciones Red Eléctrica de España. <https://www.ree.es/es>. Accessed 23 Dec 2021
30. PVSyst PVsyst – Logiciel Photovoltaïque. <https://www.pvsyst.com/>. Accessed 23 Dec 2021
31. HelioEsfera Coordenadas y carta solar. <https://www.helioesfera.com/coordenadas-y-carta-solar/>. Accessed 23 Dec 2021
32. Laboratory. USRM (2015) UO SRML: Sun chart program. <http://solardat.uoregon.edu/SunChartProgram.php>. Accessed 23 Dec 2021
33. Meteotest Meteonorm. <https://meteonorm.com/en/>. Accessed 23 Dec 2021
34. NASA Prediction of Worldwide Energy Resources. <https://power.larc.nasa.gov/>. Accessed 23 Dec 2021
35. EU SCIENCE HUB TEC science and knowledge service Photovoltaic Geographical Information System (PVGIS) | EU Science Hub. <https://ec.europa.eu/jrc/en/pvgis>. Accessed 23 Dec 2021



# Extracting Energy from Flooded Coal Mines for Heating and Air-Conditioning of Buildings: Opportunities and Challenges



Amin Al-Habaibeh, Bubaker Shakmak, Anup Athresh, Keith Parker, and Omar Hamza

**Abstract** Extraction energy from flooded coal mines for heating and/or air-conditioning applications could provide a low-carbon and sustainable technology for the future. In heating applications, the implementation normally utilises heat pump technologies to upgrade the temperature of water from a nominal value of normally about 12 to 20 °C to a level above 45 °C. For cooling applications, the water could be used directly or via a heating pump for the cooling process, depending on the temperature of the water. This paper outlines two case studies implemented in the UK at Caphouse Colliery and Markham Colliery. The paper highlights the opportunities and challenges of the technology; it compares between the two systems in terms of configuration, water quality and the need for maintenance. The paper also outlines the commercialisation aspect of the technology and the potential challenges and opportunities captured via a technical workshop and an online survey. The paper also discusses the geohazard prospective of coal mines when used for extracting the thermal energy. The results show that extracting energy from flooded coal mines is unlikely to create any significant geohazard risk, but has the benefits to develop and regenerate the former coal mining areas. The technology can be used to provide low-carbon sustainable energy to homes and businesses in the UK towards zero-carbon future. However, more effort is needed to enhance public awareness and encourage future investments to allow the technology to be utilised in new and existing residential and commercial buildings.

**Keywords** Coal mines · Geothermal · District heating · Sustainability · Heat pumps

---

A. Al-Habaibeh (✉) · B. Shakmak · A. Athresh  
Product Innovation Centre, School of Architecture, Design and the Built Environment,  
Nottingham Trent University, Nottingham, UK  
e-mail: [Amin.Al-Habaibeh@ntu.ac.uk](mailto:Amin.Al-Habaibeh@ntu.ac.uk)

K. Parker  
Project and Programme Solutions, Derbyshire, UK

O. Hamza  
Mechanical Engineering and the Built Environment, University of Derby, Derby, UK

## 1 Introduction

Coal mining in the UK, and in many areas around the world, was one of the main drives for the industrial revolution and for running steam engines and heating applications. However, many coal mines have since been closed in the UK and Europe. When coal mines are closed, they often continue to produce methane, usually referred to as abandoned mine methane (AMM), which can be utilised to generate energy for heating or powering gas engines. Also, with some quality enhancement, it can be fed into the gas grid. In most cases in the UK, however, coal mines will gradually begin to fill with water and the methane will almost entirely disappear. The UK's historic coal mines have a void space of millions of cubic metres. When flooded, the water at this constant temperature could fill approximately 400 thousand Olympic swimming pools, creating another opportunity for energy utilisation which could be used for efficient heating and cooling applications and hence reducing the overall carbon emission. Figure 1 presents a traditional coal mine seam.

Several research papers have been published in relation to extracting energy from flooded coal mines in the UK and Europe. For example, Al-Habaibeh et al. [1] report on the performance of a UK-based system over the winter season and evaluate its long-term benefits. The results show that the system reduces carbon emission and offers an opportunity to regenerate the former coal mining areas. Athresh et al. [2] have reported on the integration of the coal mines with gas engine technology to



**Fig. 1** Typical example of tradition coal mine seam, which overtime will fill with water

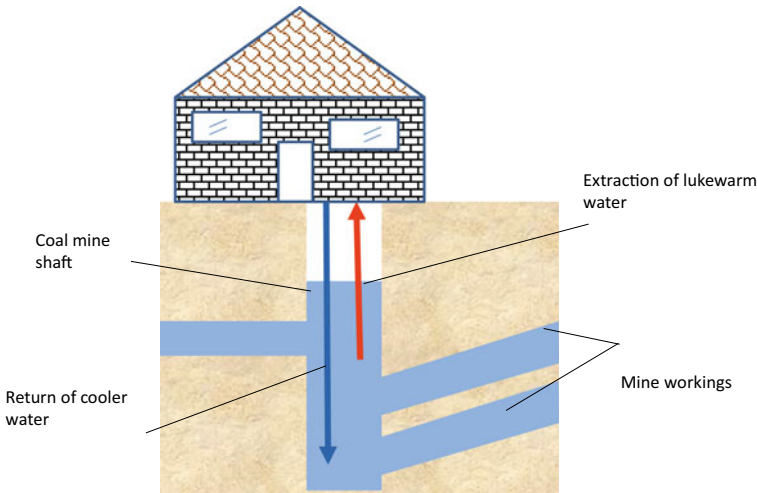


**Fig. 2** Schematic diagram showing the concept of extracting of water for heating or cooling applications; in this figure, the water is returned to the same mine shaft

reduce further carbon emission. Banks et al. [3] have highlighted a several configurations of heat extraction from abandoned and flooded coal mines. They also highlighted the water quality issues and the response of a closed-loop system. A special issue of International Journal of Coal Geology [4] has highlighted a wide range of applications of the technology. Among the applications, the hydrochemical characteristics of a mine water geothermal energy resource in northwest of Spain at Baredo coal mine in Asturias [5]. Figure 2 presents a schematic diagram showing the concept of extracting water for heating or cooling applications, where the water is returned to the same mine shaft. This concept may be applicable to smaller schemes and results in greatly reduced capital costs.

## 2 Energy from Flooded Coal Mines—Case Studies

In the UK, there are several locations that operate with this technology. At the Markham and Caphouse sites, see Fig. 3, monitoring systems have been implemented to evaluate the coefficient of performance (COP) of the heat pumps and the complete systems. Markham site, see Fig. 4a near Bolsover (on the M1 junction 29A), provides heating from coal mine water to two buildings. Caphouse site near Wakefield, see Fig. 4b, which is at The National Coal Mining Museum of England is utilised to heat a building as part of testing process using the water which is already being pumped to keep the museum’s galleries dry for visitors. The two sites, however, have different water quality, see Fig. 5. The iron (Fe-total) concentration is found to be circa 16.5 mg/L for Caphouse and 0.72 mg/L for Markham. Figure 5a presents a

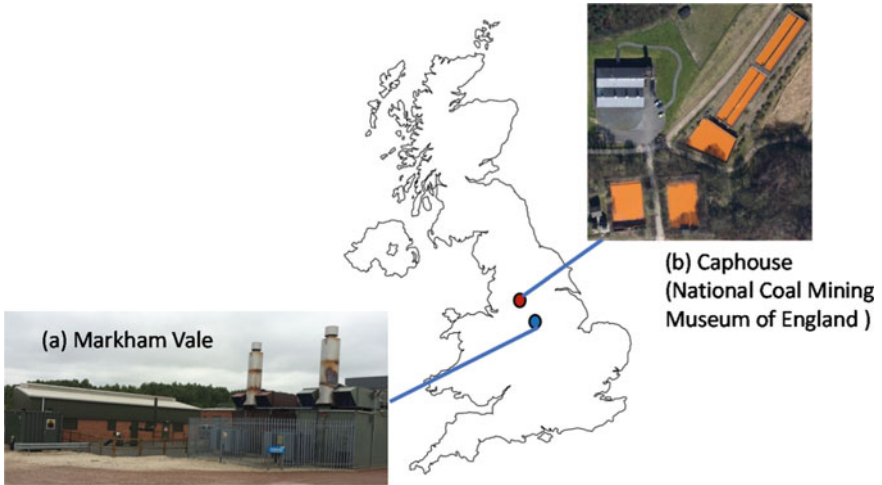


**Fig. 3** Two locations reported in the paper, Caphouse at the National Coal mining Museum of England and Markham Vale (Caphouse image is from Google Earth)



**Fig. 4** Photographs of the system in Markham (a) and Caphouse (b)



**Fig. 5** Difference in water quality, Markham (a) and Caphouse (b)

comparison between tap water and mine water from Markham, while Fig. 5b presents the water quality when pumped out of Caphouse. The pumped water from Caphouse is partially oxidised in the pumping shaft. The pumped water is ochre rich and is treated passively using several settling lagoons and reed beds to remove the ochre to acceptable levels to allow discharge into a nearby watercourse, see Figs. 3, 4 and 5.

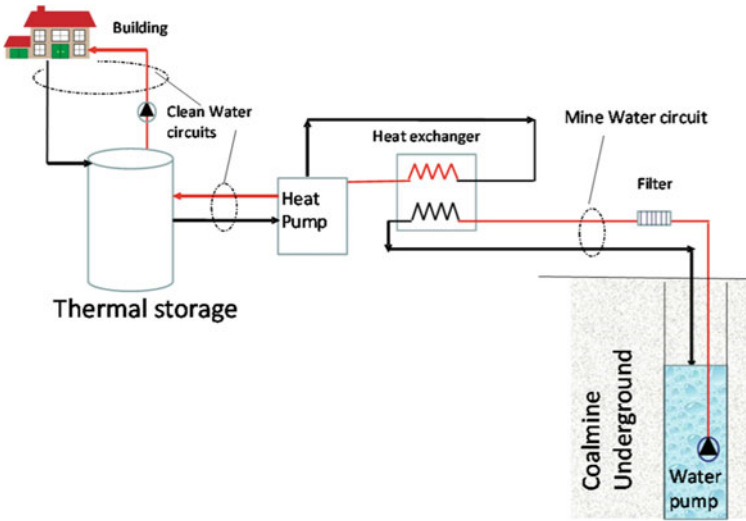
The basic configurations of the two systems are shown in Fig. 6. For Markham, see Fig. 6a, the water is pumped via a heat exchanger before returning to the same mine shaft at different water level. Then, a heat pump loop consumes electricity to upgrade the water temperature to a higher level. The third loop is the building heating system where hot water is pumped via a buffer tank (thermal storage). At Caphouse, Fig. 6b, a small proportion of the pumped water is diverted via the heat exchanger and returned to the treatment lagoon. The rest of the process is similar to Markham site. The key difference between the two systems is that in Markham, the water is returned to the coal mine and limited oxidation process occurs. In Caphouse, the water is pumped to keep the galleries of the museum dry for visitors. The extracted water is treated in different lagoons to allow the iron to settle for removal.

The difference in filters and heat exchangers conditions is shown in Fig. 7. In Markham, the mine water quality has low and dissolved iron content. The filters, pipelines and heat exchangers were examined for any ochre deposition, and very little deposition was found, see Fig. 7a. However, at Caphouse, the water quality is poorer, and this can be seen from the ochre accretion on the filter, Fig. 7b after a limited operational time. Figure 8 presents an infrared image of the water leaving the coal mine (top pipe) and the returning water.

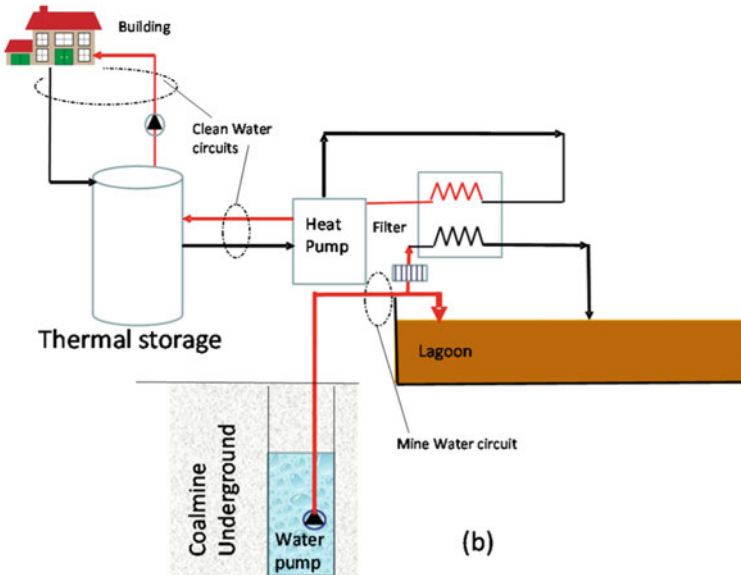
### 3 Commercialisation and Challenges

A workshop for pathway to commercialisation of challenges and opportunities of using water from flooded coal mines for heating and cooling applications was organised at Nottingham Trent University, chaired by Prof. Amin Al-Habaibeh. The workshop has included participants from a wide range of sectors including Nottingham City Council, Alkane Energy Ltd, The Coal Authority, Clean Rivers Trust, Gannet Ltd, UK Community Works CIC (Community Works) and energy researchers, see Fig. 9.

From the discussion, it has been found that energy from flooded coal mines is an opportunity to develop a better peak demand efficiency. The technology is also efficient when compared with standard air heat pumps, due to lack of fluctuation in temperature and the integration of heating and cooling processes. There is an opportunity in many European countries, including the UK, because the water is pumped in many cases for environmental and practical reasons; hence, the underground risk elements have already been overcome. The technology is suitable for low-temperature district heating. In the UK, the coal authority operates over 70 mine water treatment schemes across the UK and treats around 100 billion litres of mine



(a)



(b)

Fig. 6 Basic configuration of both systems in the UK, Markham (a) and Caphouse (b)



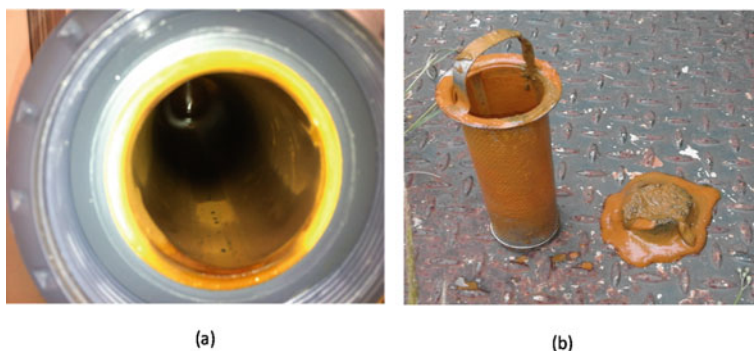


**Fig. 7** Filters and system quality after a considerable running period of more than one year in Markham system (a); After short time of operation of the Caphouse system (b)



**Fig. 8** Heat patterns in Markham (the arrows show the direction of water flow from and to the coal mine); Visual image (a) and Corresponding infrared image (b)



**Fig. 9** Panel discussion and the way forward for commercialisation at Nottingham Trent University, the UK

water per annum to protect the environment. The authority is leading on some initiatives to expand the use of the technology. Data centres and the need for cooling make the water from flooded coal mines a very suitable technology for use in cooling. The technology also allows for improved and localised energy control and reduces strain on national infrastructure. The technology is potentially capable of being integrated with a variety of heat sources and with stratified hot water storage. The concept is simple, being based on a combination of established technologies, and offers long-term benefits in providing a resilience infrastructure. The technology is modular and adaptable to a wide range of applications. It is characterised by low noise and compact infrastructure. Water contamination with metals and chemicals is a very crucial issue in the mine technology. The ambition is to expand the deployment of this technology to provide heat to residential, commercial and industrial users. Many mine water projects in Europe are being operated that aim to demonstrate how the geothermal energy stored by mine water can be used as a safe and ecological way to heat buildings.

Nevertheless, securing investment is one of the main challenges to support the infrastructure of the technology. It is still not a well-known or understood technology for many consumers (see the following section); more effort is needed in this part. There are cultural issues as far as the technology is concerned, particularly with the dependence on gas boilers in most buildings for heating, particularly in the UK. However, the ban on new gas boilers from 2025 should change the dynamics of the market. There is a lack of clear model to follow on all stages and on the long term; this is due to the variation in infrastructure and running costs and the breakeven models. Community acceptance of a new and relatively untried technology may be a barrier to deployment. Lack of assurance regarding the stability of government policies in the EU or a clear subsidiary of the system in most EU countries. Operating cost, particularly maintenance, could be high in some situations. The technology is only possible for areas underlain by flooded coal workings. Fortunately, this includes 25% of the UK populated areas although deployment is still very much dependent on site-specific circumstances where water depth is not too great. Cost of pumping is dependent on the depth of water, which is one of the significant variables in the system. Selling the product is complex, because it is most effectively done via local district heating systems. Many planning hurdles exist, and simplicity is still needed. Effective use of 'Heat networks delivery funding' in the UK or similar schemes in EU countries is required. Heat network delivery unit (HNDU) has been established as part of BEIS (UK Department for Business, Energy and Industrial Strategy) to provide support for those looking to develop district heating schemes. There is also a need to improve public awareness to increase the demand for the technology.

During the technical workshop discussion, it has been agreed that the pathway to commercialisation could be considered for long-term and short-term aspects.



### **3.1 Short Term**

The technology could be feasible commercially for the short term if some conditions are available:

- Infrastructure borehole is available; as this will reduce the cost of drilling which could be significant investment. Also, the availability of the borehole removes the uncertainty of water characteristics such as volume and temperature.
- Water already pumped (for other reasons); this reduces the cost of electricity and at the same time the cost of water treatment; hence, shorter payback period on investment.
- Government organisations can absorb or support the cost of infrastructure; this would encourage the investment from the private sector.
- One main user of energy (e.g. hospital, university, shopping mall), where discussion and decisions can be simplified. This will help in terms of modelling the system, the legal agreements and long-term stability of energy demand.
- Water level is high (low energy for water pumping). This will increase the COP of the system and hence the return on investment.

The above conditions will allow shorter payback period and enhance the commercialisation process.

### **3.2 Long Term**

On the long term, the following measures should be taken:

- Integrate the technology with education and public media. This is to enhance the understanding of the technology and appreciate its advantages.
- More public engagement programmes are needed. If there is a demand from the public or enthusiasm about the technology, this will increase the interest from the commercial sector and investors.
- Educate energy installers companies and provide training courses on how the technology works and its costing process.
- Some legal issues should be resolved regarding the technology, particularly in relation to district heating contractual arrangements including the ability to switch energy suppliers and ensuring competitive pricing of energy.

## **4 Awareness of the Technology**

A short online survey was carried out. The survey had four different questionnaires targeting four different types of audience (energy companies, local councils,

consumers and students/academics). In total, 28 companies responded, 16 local councils, 85 students/academics and 40 from the general public. The objectives is to see if further and wider improvement of the awareness of the technology is needed to enhance the pathway to commercialisation on the long term. The results, see Fig. 10, show that 14% of companies did not hear about the technology and 25% of local councils. The general public and students/academics are 88% and 81% aware of the concept, respectively. These results indicate that more effort is needed to make people aware of the concept of using coal mine water for district heating.

When the people who are aware of the concept are asked about the technology involved, companies had 100% knowledge and local councils had 92% technical knowledge. For the general public and students/academics, their knowledge of the technology was 60% and 50%, respectively.

From the survey (see Figs. 10 and 11), it is clear that the majority of the energy-related companies are aware of the possibility of using mine water as an energy resource. Majority of the local councils who influence the general decision making were also aware of the technology of using mine water as an energy resource. However, the survey showed that the general public which includes customers and general researchers/students was not aware of the technology of using mine water

### Have you heard about the concept of extracting geothermal energy from flooded coalmines?

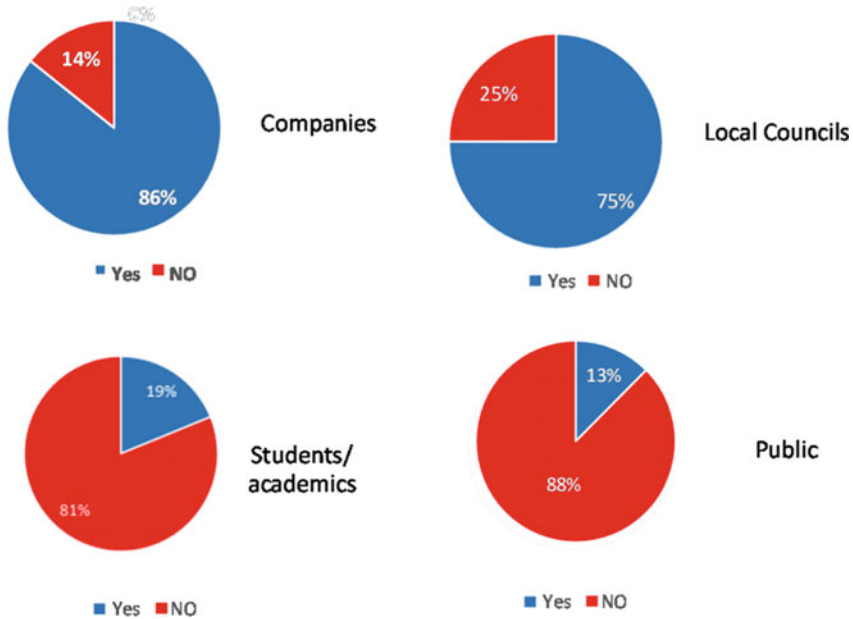
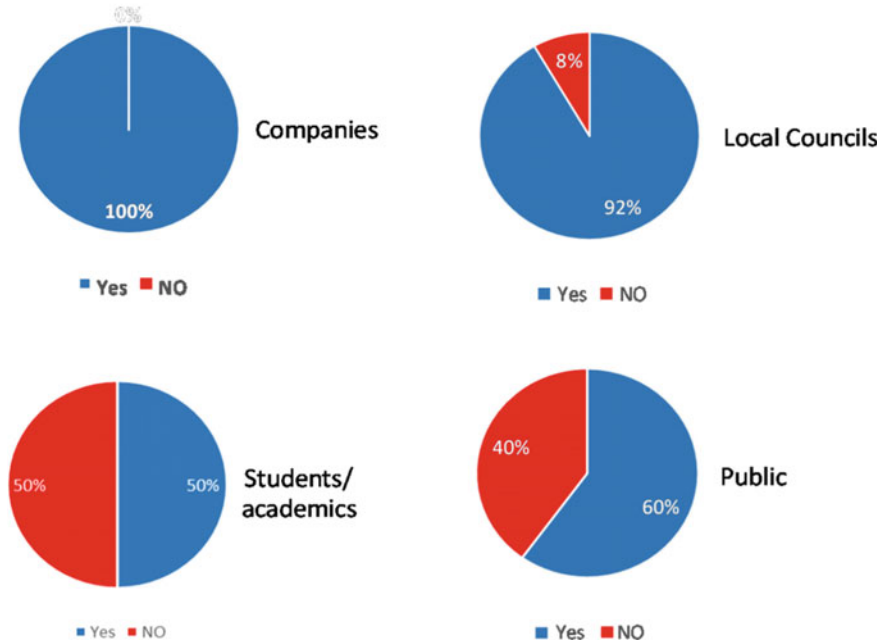


Fig. 10 Familiarity of the concept of extracting geothermal energy from flooded coal mines

If you have heard about the concept of extracting energy from flooded coal mines, are you aware of its technical principles?



**Fig. 11** Awareness of the technology among the respondents who have heard about the concept of extracting energy from flooded coal mines

as a thermal energy resource. This is a cause for potential concern, as without the awareness about the technology, it would be difficult for companies to convince their customers to go for this technology without a clear long-term strategy. The results show that efforts are needed to educate students/academics and the public about the technology to enhance the commercialisation on the long term. However, the results show that most of local councils and energy companies are aware of the technology.

## 5 Ground Movement Hazard Associated with Flooded Mines

The geohazard risk of the technology is expected to be very limited in comparison with the original existence of the coal mines themselves. Large-scale monitoring of surface deformation has shown some changing patterns of ground motion over time [6] in relation to geological conditions and mining history. Subsidence events in most cases take place at the time of active mining but can also occur a long period of time after mining has ceased [7]. However, in some cases, regional patterns of uplift

following coal colliery closure have been observed over several regions in the UK [8] and Europe [9], particularly in flooded coal mines where water pumping has been stopped [10]. The uplift has been attributed to several factors including submerging the previously dry mined area. Submerging of the mined area can reduce the effective vertical pressure and cause decompression of the rock mass, but the main factor for inducing uplift is believed to be the swelling of clay minerals of argillaceous rocks as the water finds its way through open roadways, permeable faults and volumes of loose blocks [11]. Clay minerals are prone to large volume changes (swelling and shrinking) that are directly related to changes in water content.

## 6 Conclusions

This paper has presented two systems implemented in the UK to extract energy from flooded coal mines. The constant feed water temperature could provide a stable source of energy for heating and cooling applications directly or via heat pumps. The geohazard of the technology is considered negligible in comparison with the original mining operations. The commercial success of the technology depends on many factors such as the location, quality of water, depth of water, existing pumping schemes and the availability of consumers. It is expected that the technology will be adopted in many areas in the UK and Europe in the coming years since it provides a sustainable and low-carbon energy opportunity. However, more public awareness is needed about the technology and its benefits. Also, further integration of the technology in teaching and learning processes in further and higher education is critical. However, funding sources compatible with risk appetite for a new technology will be key for success. The general move towards district heating in the UK as well as the ban of gas and oil boilers in new homes from 2025 are expected to create positive drivers for the technology roll out.

**Acknowledgements** The work in this paper is based on research carried out within the frame of research projects: Low-Carbon After Life (LoCAL) financed by the European Commission, Research Fund for Coal and Steel, July 2014–June 2017 (Contract No.: RFCR-CT-2014-00001).

## References

1. Al-Habaibeh A, Athresh A, Parker K (2018) Performance analysis of using mine water from an abandoned coal mine for heating of buildings using an open loop based single shaft GSHP system. *Appl Energy* 211:393–402. ISSN 0306-2619
2. Athresh A, Al-Habaibeh A, Parker K (2017) An innovative and integrated approach for using energy from the flooded coal mines for pre-warming of a gas engine in standby mode using GSHP. *Energy Procedia* 105:2531–2538. ISSN 1876-6102

3. Banks D, Athresh A, Al-Habaibeh A, Burnside N (2017) Water from abandoned mines as a heat source: practical experiences of open- and closed-loop strategies, United Kingdom. *Sustain Water Resour Manag* 2363-5037
4. Younger P (ed) (2016) Abandoned coal mines: from environmental liabilities to low-carbon energy assets. *Int J Coal Geol* 164:1–134
5. Loredó C, Ordóñez A, García-Ordiales E, Álvarez R, Roqueñi N, Cienfuegos P, Peña A, Burnside NM (2017) Hydrochemical characterization of a mine water geothermal energy resource in NW Spain. *Sci Total Environ* 576:59–69. ISSN 0048-9697
6. Banton C, Bateson L, McCormack H, Holley R, Watson I, Burren R, Lawrence D, Cigna F (2013) Monitoring post-closure large scale surface deformation in mining areas. In: *Proceedings of the mine closure 2013, 8th International conference on mine closure 2013*, Australian Centre for Geomechanics, Perth Eden Project, Cornwall, UK, 18–20 Sept 2013
7. Vervoort A, Declercq PY (2017) Surface movement above old coal longwalls after mine closure. *Int J Min Sci Technol* 27(3):481–490
8. Culshaw MG, Tragheim D, Bateson L, Donnelly LJ (2006) Measurement of ground movements in Stoke-on-Trent (UK) using radar interferometry. In: *Proceedings of the 10th congress of the international association for engineering geology and the environment, IAEG2006*, Nottingham, UK, 6–10 Sept 2006. Geological Society, London, UK, pp 1–10
9. Caro Cuenca M, Hooper AJ, Hanssen RF (2013) Surface deformation induced by water influx in the abandoned coal mines in Limburg, The Netherlands observed by satellite radar interferometry. *J Appl Geophys* 88(1):1–11
10. Devleeschouwer X, Declercq PY, Flamion B, Brixko J, Timmermans A, Vanneste J (2008) Uplift revealed by radar interferometry around Liège (Belgium): a relation with rising mining groundwater. In: *Proceedings of post-mining 2008 (GISOS)*. ASGA, Nancy, pp 1–13
11. Herrero C, Muñoz A, Catalina JC, Hadj-Hassen F, Kuchenbecker R, Spreckels V (2012) Prediction and monitoring of subsidence hazards above coal mines (Presidence) RFCS final report 2012. RFCR-CT-2007-00004. EUR 25057 EN. European Commission, Brussels, pp 1–131

# Towards a Simple Cold Box Adapted to Warm Climates: A Case Study in Mediterranean Climate



David Bienvenido-Huertas, Manuel J. Carretero-Ayuso,  
David Marín-García, and Joaquín Durán

**Abstract** The accurate estimation of the thermal transmittance of buildings' envelope is fundamental to study the thermal behaviour of buildings. Thermal transmittance can be determined by means of theoretical and experimental methods. A method known as simple cold box (SCB) was designed in this research work. Such method consists of cooling the internal side of the wall so that a high thermal gradient is generated with the external ambient. To assess the performance of the method, a case study characteristic of the southern part of Europe was assessed with two-dimensional simulation. Time series of the external temperature were also used to guarantee a representative simulation. Based on these simulations, the results of thermal transmittance were analysed, as well as the deviation presented by the results according to a representative value of the façade. Likewise, the energy consumption related to the test was assessed by means of simulation using EnergyPlus. SCB can constitute an opportunity for engineers and architects to ease and hasten the task of improving the performance of buildings.

**Keywords** Simple cold box · Thermal behaviour · Energy consumption

---

D. Bienvenido-Huertas (✉) · J. Durán  
Department of Building Construction, University of Granada, 18001 Granada, Spain  
e-mail: [dbienvenido@ugr.es](mailto:dbienvenido@ugr.es)

M. J. Carretero-Ayuso  
Department of Architecture, School of Architecture, University of Alcalá, 28801 Alcalá de Henares, Spain

D. Marín-García  
Department of Graphical Expression and Building Engineering, University of Seville, 41012 Seville, Spain

## 1 Introduction

In recent years, the establishment of actions to reduce energy consumption and carbon dioxide emissions of buildings constitutes one of the main concerns of the European Union [1], mainly due to their high influence on the progressive environmental degradation [2, 3], which will be greater in future scenarios of climate change [4, 5].

The improvement of the energy behaviour of buildings is therefore crucial to establish a society more sustainable with the environment. In this way, one of the major aspects to be reduced is the energy consumption of heating and cooling systems [6, 7]. If measures to reduce such type of consumption are designed, there would be a significant improvement of the energy performance of buildings [8].

So, the thermal characterization of the envelope elements is essential to establish adequate improvements [8, 9], with thermal transmittance (also known as  $U$ -value) being one of the most studied variables [10, 11] and with the façade being the envelope element with the greatest influence on the thermal behaviour of buildings [12]. This is because thermal transmittance varies the heat losses and influences energy consumption [13]. An adequate assessment of  $U$ -value will contribute to establish the best improvements implying the lowest economic investment for the building's owner [14].

To determine the  $U$ -value, various in situ methodologies are available. Such methodologies can be classified in different typologies according to the variables measured: the heat flow metre method [15], infrared thermography methods [16, 17], and the thermometric method [18, 19]. All of them are usually more accurately characterized than the theoretical methods [13]. However, the experimental methods can present limitations because of the need of a high thermal gradient. In this sense, Desogus et al. [20] concluded that a temperature differential of 10 °C obtains low uncertainties in the  $U$ -value obtained, which can be reduced even more as the thermal gradient increases. Nevertheless, achieving such thermal gradients in real case studies is something of a challenge, particularly in warm climate regions as the Mediterranean.

Because of such difficulty, a methodology combining the advantages of hot box methods [21–24] in in situ tests has appeared in recent years. Hot box methods are a methodology of laboratory tests characterized by controlling the thermal gradient, so it is not therefore limited by climate variations, and the measurement errors are usually low [25]. Meng et al. [26, 27] developed a method of in situ application known as simple hot box heat flow metre method (SHB-HFM). By designing such method, the thermal gradient is only obtained by using heating, and the simple hot box is always placed on the surface area of the envelope at the greatest temperature. Despite this tighter control, the methodology has the disadvantage of being limited used under warm conditions, mainly because of the box is required to be placed at the external side of the façade. Consequently, such methodology could not be used in buildings with variations in the layers of façade at different heights.

A new methodology is therefore suggested in this study: the simple cold box. For this purpose, a box keeping controlled conditions with a low temperature is designed. The box is placed at the internal side of the wall. This new methodology is therefore designed for warm climates in which it could be difficult to obtain a high thermal gradient [28]. Moreover, the energy consumption related to the performance of the test is intended to be low.

The objective of this study is therefore to analyse the possibilities of using such methodology. For this purpose, a temperature profile achieved by the simple cold box in a case study located in the Mediterranean climate was simulated. The analysis was carried out for the period between May and September. Afterwards, transitory simulations were performed to assess the heat flux obtained in different points of the façade and determine the most adequate point.

## 2 Methodology

The device is made up of insulating panels covered with wooden boards or steel sheets. The inside dimensions of the box will vary according to the testing needs. The evaluation of the thermal transmittance of the façade is carried out through two simultaneous operating procedures:

- A. Ensure a high thermal gradient throughout the test. To do this, the device's thermostat must be set with an adequate setpoint temperature according to the outdoor conditions that have been observed in the days prior to the test. In general, the use of a setpoint temperature of 5 °C allows the test to be carried out under suitable conditions throughout the test and with low energy consumption. It must be ensured that the equipment is not disconnected during the entire test to guarantee the correct assurance of the indoor conditions.
- B. Monitoring of the enclosure for a period of three days. To do this, heat flux plates and temperature probes are used to measure three different variables: heat flux, indoor air temperature and outdoor air temperature.

These two procedures follow a three-phase methodology:

1. Installation of the box on the façade to be analysed and configuration of the interior conditions to guarantee a high thermal gradient.
2. Carrying out measurements of heat flux and indoor and outdoor temperatures over a period of three days.
3. Post-processing of the data following the formulation of the progressive average method included in ISO 9869-1.

The test model designed for this study is a box with sandwich panels of 8 cm of thermal insulation, and one of the sides of the box has no wall (see Fig. 1). The internal dimensions of the box are 1.00 × 1.00 × 0.65 m, thereby achieving two aspects: (i) that the internal volume of the box is lower than 1 m<sup>3</sup>, and (ii) that the heat transfer is two-dimensional both in height and longitude because the sides of



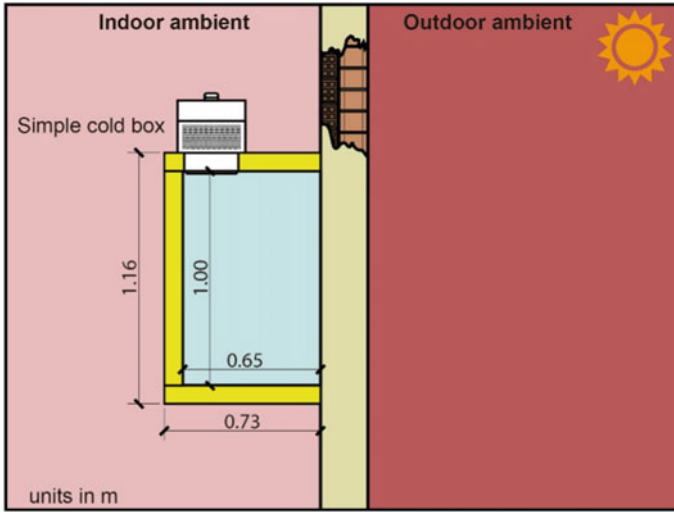


**Fig. 1** Scheme of the simple cold box

the box in contact with the wall and the SHB have the same longitude [26]. The box is cooled by putting a Uniblock equipment for refrigerator chambers on it. This type of equipment guarantees an air temperature of 5 °C inside the box.

To analyse the effectiveness of the methodology, a typical wall of a building located in Seville (Spain) was evaluated. Seville belongs to the Csa climate zone according to the Köppen-Geiger climate classification [29] (dry and hot summers, and smooth winters). Such zone is then characterized by the difficulty of achieving high thermal gradients in winter, as well as by the fact that the days with high temperatures are mostly throughout the year. The theoretical value of the wall (see Fig. 2) was obtained by using the approach included in ISO 6946 [30] (see Eq. 1). The thermal conductivity values were determined by using the constructive elements catalogue of the Spanish Building Technical Code [31].

$$U = \frac{1}{R_{s,in} + \sum_{i=1}^n \frac{s_i}{\lambda_i} + R_{s,out}} \quad (1)$$

where  $\lambda_i$  and  $s_i$  are the thermal conductivity [W/(m K)] and thickness (m) of each layer of the wall, and  $R_{s,in}$  and  $R_{s,out}$  are the internal and external surface resistances [(m<sup>2</sup> K)/W], respectively, obtained by the tabulated values from ISO 6946.

The period of time analysed during the test was between May and September (see Table 1). The internal temperature profile and the energy consumption of the box were performed by using the calculation engine EnergyPlus. Values with an interval of 30 min were obtained. Then, the two-dimensional flux of the wall obtained throughout the test was analysed by means of transitory simulations. Given the variability of the two-dimensional flux along the height of the box, a total of 20 various points

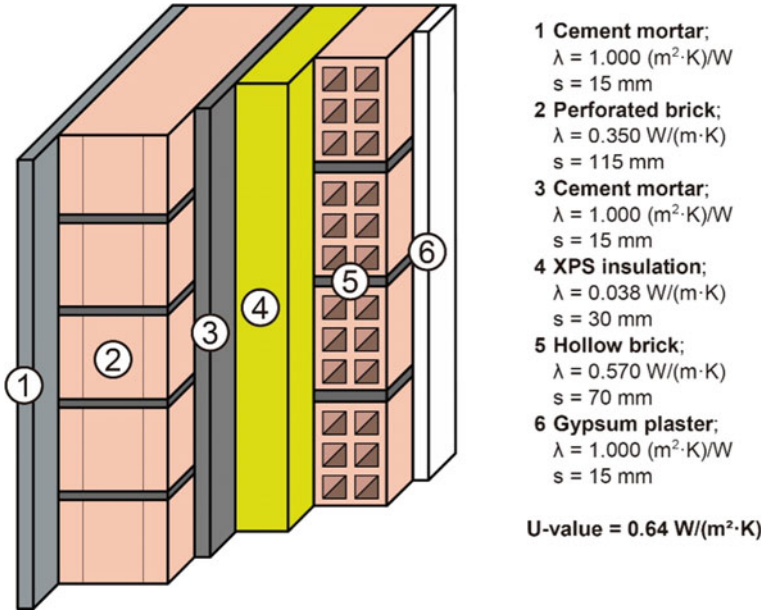


Fig. 2 Scheme of the wall analysed

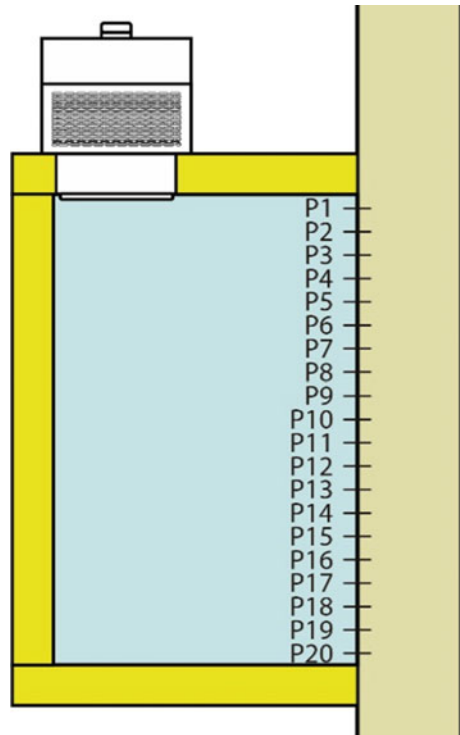
Table 1 Period analysed

Start date	End date	Number of records
May 1st 0:00	September 30th 23:30	7343

was analysed (see Fig. 3). Such points corresponded to zones where the heat flux plates could be placed, with 5 cm among them. The thermal transmittance value was obtained with the formulation from ISO 9869-1 (see Eq. 2). Given that the period of time used (from 1st May to 30th September) widely exceeds the duration advisable (3 days) to conduct transmittance tests, the final value obtained in each point analysed was thought to be the average of all the possible combinations of tests in the period analysed (i.e. the thermal transmittance result obtained at each instant with the measurements of the three previous days).

$$U = \frac{\sum_{j=1}^n q_j}{\sum_{j=1}^n (T_{in,j} - T_{out,j})} \tag{2}$$

where  $q_j \text{ (W/m}^2\text{)}$  is the heat flux of the façade, and  $T_{in,j}$  and  $T_{out,j} \text{ (K)}$  are the indoor and outdoor ambient temperatures.

**Fig. 3** Scheme of the points

### 3 Results and Discussion

Firstly, the temperature profile obtained inside the box was analysed (see Fig. 4). The operative temperature inside the box had an average value of 6.83 °C. In some hours of the period of analysis, a maximum temperature of 7.99 °C was reached, but the thermal gradient was always high. This was due to the radiant temperature of the sides of the box and the wall itself which, although the temperature driven by the equipment was 5 °C, generated a higher operative temperature. In this sense, the radiant temperature of the sides of the box was lower than that of the wall analysed. The internal obtained with the methodology therefore guarantees a high temperature differential with the exterior in warm seasons.

The next step was therefore the analysis of the representation of the results and the adequate points for placing the probes. Table 2 indicates the results obtained in the tests (as indicated above, and the average of the results is obtained by using data of three days in the whole test period). Also, the deviation percentage with respect to the theoretical value of the wall is indicated. As can be seen, the points closest to the sides of the box had a great distortion in the  $U$ -values obtained, with deviations of up to 160.08%, mainly due to the two-dimensionality of the flux in this zone because of both the sides of the box and the slabs of the floor and the ceiling. However, more

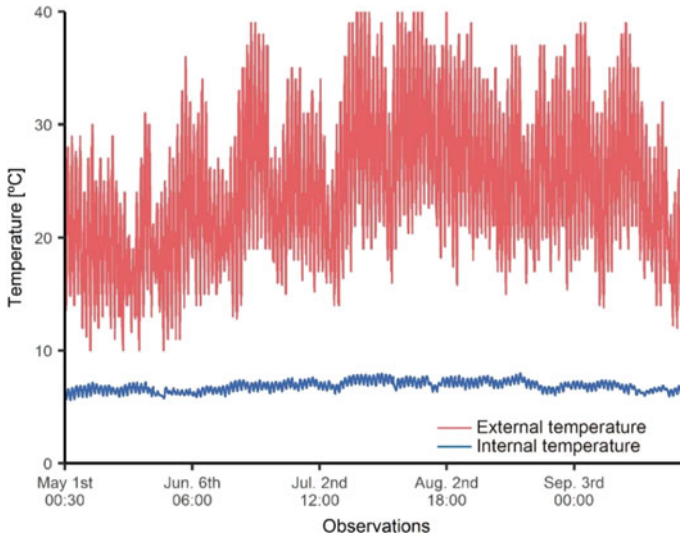


**Fig. 4** Time series of the external and internal temperature

**Table 2** *U*-value obtained in the points analysed

Point	<i>U</i> -value [W/(m <sup>2</sup> K)]	Deviation percentage (%)
<i>P</i> <sub>1</sub>	1.66	160.08
<i>P</i> <sub>2</sub>	1.13	76.31
<i>P</i> <sub>3</sub>	0.88	38.17
<i>P</i> <sub>4</sub>	0.77	19.65
<i>P</i> <sub>5</sub>	0.71	10.33
<i>P</i> <sub>6</sub>	0.68	5.56
<i>P</i> <sub>7</sub>	0.66	3.07
<i>P</i> <sub>8</sub>	0.65	1.78
<i>P</i> <sub>9</sub>	0.65	1.13
<i>P</i> <sub>10</sub>	0.65	0.85
<i>P</i> <sub>11</sub>	0.65	0.84
<i>P</i> <sub>12</sub>	0.65	1.09
<i>P</i> <sub>13</sub>	0.65	1.72
<i>P</i> <sub>14</sub>	0.66	2.97
<i>P</i> <sub>15</sub>	0.67	5.36
<i>P</i> <sub>16</sub>	0.70	9.98
<i>P</i> <sub>17</sub>	0.76	18.97
<i>P</i> <sub>18</sub>	0.88	36.80
<i>P</i> <sub>19</sub>	1.11	73.32
<i>P</i> <sub>20</sub>	1.61	151.78

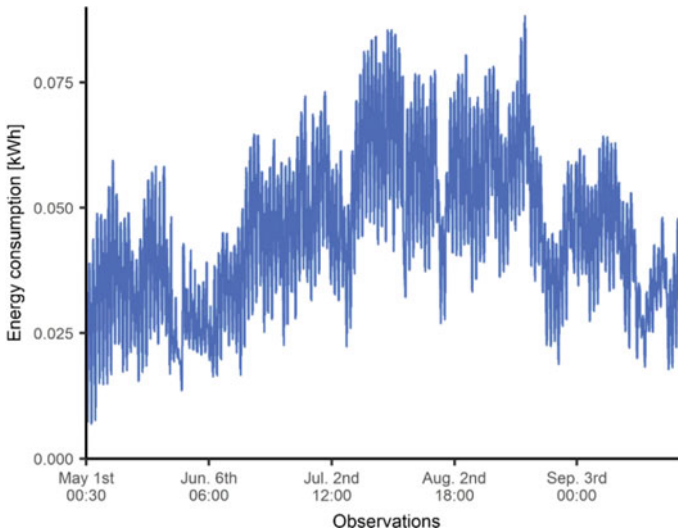


**Fig. 5** Time series of the energy consumption every 30 min

representative results were obtained as the point of analysis was closer to the centre of the box. In this way, the deviation percentage was lower than 5% from  $P_7$  to  $P_{14}$ . This situation corresponds to probes located at 30 cm from the internal side of the box. Likewise, the greatest one-dimensionality in the heat flux was found in  $P_{10}$  and  $P_{11}$ , where a maximum deviation percentage of 0.85% was obtained. The adequate zone for placing the probes will therefore be in the middle of the height of the box.

Finally, the energy consumption of the box should also be analysed. Figure 5 represents the time series of the energy consumption every 30 min. As can be seen, the consumption values obtained every 30 min during the test did not exceed 0.09 kW. By considering the same criterion used to obtain the thermal transmittance values throughout the whole test period (i.e. the values obtained by using the records of the three previous days), the average energy consumption to conduct a test of 3 days was determined to be 33.21 kWh, with maximum values of 4.83 kWh in some tests. The energy consumption required to perform the test is therefore low.

## 4 Conclusions

This study is focused on the preliminary analysis of the use of a test typology called simple cold box to assess the thermal transmittance of façades. The test consists of placing a box with an internal volume lower than  $1 \text{ m}^3$  keeping a low temperature inside it. It is a test typology designed to be applied in warm regions in which obtaining a high thermal gradient limits the practical application of the experimental

methods. From the simulation data of a case study located in Seville between May and September, several aspects have been proved:

- The test methodology keeps an operative temperature between 5 and 8 °C inside it.
- By using data obtained in periods of three days, more representative results were obtained in points located at a distance of more than 30 cm from the internal side of the panels of the box. In this sense, the most adequate zone to put the probes is at the middle of the height of the box.
- The performance of the test for three days had an average energy consumption of 3.21 kWh.

Despite such aspects, the use of the methodology both in various typologies of wall and under different environmental conditions (such as other climates) should be analysed in further studies, thereby analysing the possible limitations to apply the methodology as well as establishing the possible correction measures to be applied in various regions. Moreover, 3D heat transient simulations should be carried out in future works.

## References

1. European Commission (2011) A roadmap for moving to a competitive low carbon economy in 2050. Brussels, Belgium
2. European Environment Agency (2017) Final energy consumption by sector and fuel. Copenhagen, Denmark
3. European Commission (2006) Action plan for energy efficiency: realising the potential. Brussels, Belgium
4. Bienvenido-Huertas D, Quiñones JAF, Moyano J, Rodríguez-Jiménez CE (2018) Patents analysis of thermal bridges in slab fronts and their effect on energy demand. *Energies* 11:2222. <https://doi.org/10.3390/en11092222>
5. Pérez-Fargallo A, Rubio-Bellido C, Pulido-Arcas JA, Javier Guevara-García F (2018) Fuel poverty potential risk index in the context of climate change in Chile. *Energy Policy* 113:157–170. <https://doi.org/10.1016/j.enpol.2017.10.054>
6. Kurekci NA (2016) Determination of optimum insulation thickness for building walls by using heating and cooling degree-day values of all Turkey's provincial centers. *Energy Build* 118:197–213. <https://doi.org/10.1016/j.enbuild.2016.03.004>
7. Vine EL, Kazakevicius E (1999) Residential energy use in Lithuania: the prospects for energy efficiency. *Energy* 24:591–603. [https://doi.org/10.1016/S0360-5442\(99\)00013-4](https://doi.org/10.1016/S0360-5442(99)00013-4)
8. Rubio-Bellido C, Perez-Fargallo A, Pulido-Arcas JA (2016) Optimization of annual energy demand in office buildings under the influence of climate change in Chile. *Energy* 114:569–585. <https://doi.org/10.1016/j.energy.2016.08.021>
9. Invidiata A, Lavagna M, Ghisi E (2018) Selecting design strategies using multi-criteria decision making to improve the sustainability of buildings. *Build Environ* 139:58–68. <https://doi.org/10.1016/j.buildenv.2018.04.041>
10. Natephra W, Yabuki N, Fukuda T (2018) Optimizing the evaluation of building envelope design for thermal performance using a BIM-based overall thermal transfer value calculation. *Build Environ* 136:128–145. <https://doi.org/10.1016/j.buildenv.2018.03.032>

11. Oral GK, Yilmaz Z (2002) The limit U values for building envelope related to building form in temperate and cold climatic zones. *Build Environ* 37:1173–1180. [https://doi.org/10.1016/S0360-1323\(01\)00102-0](https://doi.org/10.1016/S0360-1323(01)00102-0)
12. Adhikari R, Lucchi E, Pracchi V (2012) Experimental measurements on thermal transmittance of the opaque vertical walls in the historical buildings. In: PLEA2012 Conference, Opportunities, limits and needs towards an environmentally responsible architecture
13. Bienvenido-Huertas D, Moyano J, Marín D, Fresco-Contreras R (2019) Review of in situ methods for assessing the thermal transmittance of walls. *Renew Sustain Energy Rev* 102:356–371. <https://doi.org/10.1016/j.rser.2018.12.016>
14. de Luxán García de Diego M, Gómez Muñoz G, Román López E (2015) Towards new energy accounting in residential building. *Inf Constr* 67:1–10. <https://doi.org/10.3989/ic.14.059>
15. International Organization for Standardization (2014) ISO 9869-1:2014—Thermal insulation—building elements—in situ measurement of thermal resistance and thermal transmittance. Part 1: Heat flow meter method. Geneva, Switzerland
16. Bienvenido-Huertas D, Bermúdez J, Moyano J, Marín D (2018) Comparison of quantitative IRT to estimate U-value using different approximations of ECHTC in multi-leaf walls. *Energy Build* 184:99–113. <https://doi.org/10.1016/j.enbuild.2018.11.028>
17. Bienvenido-Huertas D, Bermúdez J, Moyano JJ, Marín D (2019) Influence of ICHTC correlations on the thermal characterization of façades using the quantitative internal infrared thermography method. *Build Environ* 149:512–525. <https://doi.org/10.1016/j.buildenv.2018.12.056>
18. Kim S-H, Kim J-H, Jeong H-G, Song K-D (2018) Reliability field test of the air-surface temperature ratio method for in situ measurement of U-values. *Energies* 11:1–15. <https://doi.org/10.3390/en11040803>
19. Bienvenido-Huertas D, Moyano J, Rodríguez-Jiménez CE, Marín D (2019) Applying an artificial neural network to assess thermal transmittance in walls by means of the thermometric method. *Appl Energy* 233–234:1–14. <https://doi.org/10.1016/j.apenergy.2018.10.052>
20. Desogus G, Mura S, Ricciu R (2011) Comparing different approaches to in situ measurement of building components thermal resistance. *Energy Build* 43:2613–2620. <https://doi.org/10.1016/j.enbuild.2011.05.025>
21. Asdrubali F, Baldinelli G (2011) Thermal transmittance measurements with the hot box method: calibration, experimental procedures, and uncertainty analyses of three different approaches. *Energy Build* 43:1618–1626. <https://doi.org/10.1016/j.enbuild.2011.03.005>
22. ASTM International (2014) ASTM E1933-14, Standard practice for measuring and compensating for emissivity using infrared imaging radiometers. West Conshohocken, PA
23. International Organization for Standardization (1991) ISO 8302:1991—Thermal insulation—determination of steady-state thermal resistance and related properties—guarded hot plate apparatus. Geneva, Switzerland
24. International Organization for Standardization (1994) ISO 8990:1994—Thermal insulation—determination of steady-state thermal transmission properties—calibrated and guarded hot box. Geneva, Switzerland
25. Chen F, Wittkopf SK (2012) Summer condition thermal transmittance measurement of fenestration systems using calorimetric hot box. *Energy Build* 53:47–56. <https://doi.org/10.1016/J.ENBUILD.2012.07.005>
26. Meng X, Gao Y, Wang Y et al (2015) Feasibility experiment on the simple hot box-heat flow meter method and the optimization based on simulation reproduction. *Appl Therm Eng* 83:48–56. <https://doi.org/10.1016/j.applthermaleng.2015.03.010>
27. Meng X, Luo T, Gao Y et al (2017) A new simple method to measure wall thermal transmittance in situ and its adaptability analysis. *Appl Therm Eng* 122:747–757. <https://doi.org/10.1016/j.applthermaleng.2017.05.074>
28. Bienvenido-Huertas D, Rodríguez-Álvaro R, Moyano JJ et al (2018) Determining the U-value of façades using the thermometric method: potentials and limitations. *Energies* 11:1–17. <https://doi.org/10.3390/en11020360>

29. Rubel F, Kottek M (2010) Observed and projected climate shifts 1901–2100 depicted by world maps of the Köppen-Geiger climate classification. *Meteorol Zeitschrift* 19:135–141. <https://doi.org/10.1127/0941-2948/2010/0430>
30. International Organization for Standardization (2007) ISO 6946:2007—Building components and building elements—thermal resistance and thermal transmittance—calculation method. Geneva, Switzerland
31. Eduardo Torroja Institute for Construction Science (2010) Constructive elements catalogue of the CTE



# Information Systematisation Towards Rational Building Maintenance Decisions



Clara Pereira, Ana Silva, Cláudia Ferreira, Jorge de Brito,  
Inês Flores-Colen, and José D. Silvestre

**Abstract** The presented research highlights different ways of collecting, systematising and using data in the field of building maintenance towards rational decisions. First, the harmonisation of the information collected during building inspections is presented. Such harmonisation was developed within a global inspection system for the building envelope, including classification lists of defects, their causes, diagnosis methods and repair techniques, as well as correlation matrices between these items. Using harmonised inspection systems during fieldwork guides the procedures and makes the collected data more objective. With sound information about the degradation of building elements, their remaining service life may be estimated. Different service life prediction methods were adopted, considering their advantages to decide on the best moment to carry out maintenance activities. Computational tools of service life prediction were developed, with different options for users, according to their objectives and available information. Following these methodologies, a condition-based maintenance model was developed, using Petri nets. Different types of maintenance strategies were determined and then compared, according to the progression of degradation, service life, costs and impact on building users. Such a condition-based maintenance model allows better decisions, as more data are available, considering different factors, and not only costs, for instance.

**Keywords** Building inspection system · Condition-based maintenance · Maintenance strategies · Objective information · Service life prediction · Uncertainty

## 1 Introduction

The effective management of a building is associated with the implementation of a maintenance plan that optimises costs and guarantees acceptable performance levels [1]. The development of such a plan requires detailed knowledge about the building

---

C. Pereira (✉) · A. Silva · C. Ferreira · J. de Brito · I. Flores-Colen · J. D. Silvestre  
CERIS, Instituto Superior Técnico, Universidade de Lisboa, Lisbon, Portugal  
e-mail: [clareira@sapo.pt](mailto:clareira@sapo.pt)

elements, including their behaviour, degradation mechanisms, most common defects, estimated service life and maintenance needs. This plan may include proactive (preventive or predictive) or reactive strategies [2].

Preventive maintenance strategies are those that take action before the occurrence of significant changes in the building elements. They are established according to periodic maintenance actions, thus avoiding unexpected defects and additional works. Preventive strategies are based on the theoretical behaviour of the building [3, 4]. As for predictive or condition-based maintenance strategies, in the context of this chapter, they are based on the assessment of the maintenance needs through planned periodic inspections. The results of those inspections determine the degradation condition of each building element, and the maintenance works are carried out according to that condition. In these cases, for an accurate diagnosis of the degradation condition, surveyors must have ample knowledge about the in-service behaviour of building elements [5]. Finally, reactive maintenance strategies are based on corrective actions, which are only carried out in situations of advanced degradation, failure, or in case of emergency, when lives and material goods are at risk.

Building maintenance may be especially complex when compared with factory-made equipment. A building is produced at the construction site, which is always different and is influenced by variable conditions (for instance, topography, weather and the extent of the plot) and by construction workers, which vary throughout the construction stages and from building to building. Besides, the building design is customised, thus requiring the adaptation of construction procedures to the intended specifications (different materials, with different origins, behaviours and degradation patterns). Given such complexity, there is a high degree of uncertainty associated with the adequate moment to perform maintenance actions, as well as with the type and amount of maintenance activities. Since predictive maintenance strategies are based on the collection of data about the degradation condition of building elements, one of the means used to deal with the referred uncertainty is the systematised collection of information.

Nevertheless, a balanced maintenance plan should combine several types of strategies to reach its goals [6]. In that context, inspection activities are essential. For instance, the first step to elaborate a maintenance plan for an existing building is to carry out a detailed inspection of the building, including the identification of each building element and the determination of their actual degradation condition. Additionally, building inspections are also part of a proactive maintenance approach (preventive or predictive), as their results are used to adjust the periodicity of interventions according to observations.

Inspection procedures should be as unbiased as possible, as the accuracy of their results influences the nature and extent of maintenance actions, thus affecting their efficacy and costs. The systematisation of inspection activities improves the objectivity of the procedures, including data collection, thus strengthening the diagnosis' results.

At Instituto Superior Técnico, University of Lisbon (IST-UL), two projects have been developed aiming at more rational building maintenance decisions. Within the project "Service Life Prediction for a risk-based Building Management System"

(SLPforBMS), an inspection system for the building envelope was developed and integrated with service life prediction methods [7]. The project “Buildings’ Envelope SLP-based Maintenance: Reducing the risks and costs for owners” (BEStMaintenance\_LowerRisks) continued the previous research by defining and comparing alternative maintenance strategies based on mathematical models. The results of both projects are the object of this chapter.

First, the process of systematisation of inspections’ information is described. Then, its integration with service life prediction methods and their importance is highlighted. Finally, maintenance strategies are discussed.

## 2 Systematisation of Building Inspections’ Data

The collection of data during building inspections should be based on a well-structured system. In the context of the project SLPforBMS, the IST-UL research team developed an inspection system for the building envelope [7]. It started from a set of individual expert inspection systems with an identical structure, previously developed by the same research team. Each of those systems focused on the pathology, diagnosis and repair of a specific building element/material (Table 1). Therefore, that information had to be harmonised in order to develop a global inspection system, including classification systems, correlation matrices and elements to support the inspection procedures (Fig. 1).

**Table 1** Set of individual expert inspection systems developed at IST-UL—the basis of the global inspection system

Building elements		References
Roofs	External claddings of pitched roofs	[9, 10]
	Flat roofs	[11, 12]
Façade elements	Door and window frames	[13, 14]
Façade claddings	Wall renders	[15, 16]
	External thermal insulation composite systems (ETICS)	[17, 18]
	Painted façades	[19, 20]
	Architectural concrete surfaces	[21, 22]
Façade claddings and floorings	Adhesive ceramic tiling	[23, 24]
	Natural stone claddings	[25, 26]
Floorings	Wood floorings	[27, 28]
	Epoxy resin industrial floor coatings	[29]
	Vinyl and linoleum floorings	[30, 31]

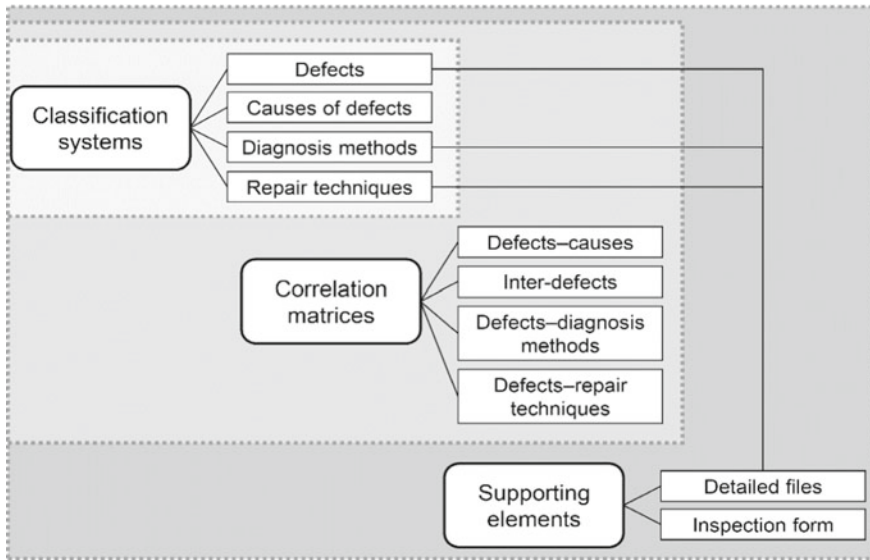


**Fig. 1** Structure of the expert inspection systems

## 2.1 Harmonisation of the Classification Systems

The use of objective classification lists is paramount to an inspection system, as basic tools to organise knowledge and information [8]. In this context, lists of defects, causes of defects, diagnosis methods and repair techniques are considered.

During the development of each individual expert inspection system, a literature review was carried out, including the pathology of the building elements/materials, as well as the applicable diagnosis methods and repair techniques. Such research was complemented by the study of the technology associated with each building element/material, providing fundamental guidelines associated with possible design and execution issues. The information about the pathology resulted in two separate lists (defects and their causes), highlighting the importance of determining identifiable defects and the respective degradation mechanisms.

The literature review performed about diagnosis methods focused on identifying the most adequate tests to characterise the defects and their causes. Those tests can be carried out during the first inspection or in subsequent ones, more detailed. They are needed as complementary sources of information, helping to characterise the severity, extent and progression of defects. They can also help to confirm probable causes, based on qualitative and quantitative data about the pathological process. Often, the comprehensiveness of the results can be improved by combining more than one method, complementing each other [32].

The scope of the diagnosis methods was limited to those that can be carried out on-site, excluding laboratory tests. In situ diagnosis methods tend to be less

expensive, simpler and quicker than laboratory tests. Nevertheless, laboratory tests can be useful in specific contexts (e.g. finding the type of a natural stone), but they were excluded from the classification list. Summing up, that list includes simple, fast, reliable and affordable diagnosis methods performed on-site, using portable, accessible and user-friendly instruments, and allowing an easy interpretation of the results [33].

Furthermore, in situ diagnosis methods can be categorised according to their intrusiveness. They can be destructive or non-destructive [34, 35], the latter being preferable. Destructive methods partially damage the building element (e.g. pull-off test), while non-destructive methods do not affect it (e.g. crack width measurement).

Inspection reports are expected to include the description of the most adequate repair techniques [36, 37] to deal with the identified defects and their causes. The literature review about the best techniques to repair defects and eliminate their causes included an analysis of the current, most recent and proven procedures.

Repair techniques may refer to curative, preventive or maintenance works [38, 39]. Curative repair techniques are reactive actions that allow directly repairing a defect, eliminating or even only disguising it, providing quick results. Preventive repair techniques are commonly advised, as their goal goes beyond an immediate repair of the defect. Instead, they eliminate the causes of the defect to stop the degradation phenomenon, avoiding the recurrence of defects [40]. Additionally, preventive repair techniques tend to minimise the extent of damages due to timely action [39]. Maintenance works may not directly affect the behaviour of building elements, as they are not directed at specific defects or causes. Still, the absence of maintenance works speeds up degradation processes, lowering the performance levels and the expected service life of building elements [38]. Maintenance works are performed regularly to promote stable levels of performance, thus avoiding reactive expensive actions. In different contexts, the same repair technique may be considered curative, preventive or a maintenance work. Preventive repair techniques and maintenance works are usually associated with proactive (preventive or predictive) maintenance strategies [3].

The global inspection system was aimed at supporting the general inspection of the envelope of a building. That scope encompassed all the defects, their causes, diagnosis methods and repair techniques that could usually be associated with specific building elements/materials. In this sense, basing the classification systems on individual expert systems promoted the comprehensiveness of the global classification lists. On the other hand, merging those individual classification systems demanded dealing with a high level of complexity and detail and with occasional repetitions. In the global classification lists, applying to all the considered building elements/materials, the level of detail had to be adjusted, focusing on summarisation, and repetitions had to be eliminated. Such transitional process implied combining and splitting defects, causes, diagnosis methods and repair techniques from the individual expert inspection systems. In this context, shorter lists were considered easier to interpret, but detail could not be neglected.

Each classification list was organised according to specific intelligible categories, which improved the lists' readability. For instance, the classification list of causes of

defects was categorised according to a chronological criterion, following the procedures adopted in the individual expert systems. In this way, the causes were organised according to the stage of the building's life cycle in which they occur, such as causes associated with "design errors" and "execution errors".

The classification systems also had specific codes, which were useful for referring to the defects, causes, diagnosis methods and repair techniques in given contexts. These codes in the classification lists were composed of a combination of letters and digits. Codes referring to the list of defects started with an "A", those referring to the list of causes started with a "C", "D" for diagnosis methods and "R" for repair techniques. Each of these capital letters was followed by a hyphen and another sequential capital letter (A, B, C, D, ...), according to the categories in each list. Within each category, defects, causes, diagnosis methods and repair techniques were numbered (1, 2, 3, 4, ...), thus resulting in codes such as A-A1, C-B2, D-C3 or R-D4, according to the respective list and category (Table 2).

To reach stable harmonised classification lists, all the lists from the individual inspection systems had to be analysed. Each type of classification list (of defects, causes of defects, diagnosis methods and repair techniques) had to go through a process of consecutive iterations, cross merging, combining and dividing entries. In general terms, this process intended to create concise lists, simultaneously ensuring that all items were somehow included in the new global lists. For instance, in the case of the harmonised list of causes, the iterative process of harmonisation started with a list of 300 causes in the first iteration and ended with a final list of 111 causes of defects (Table 3).

**Table 2** Excerpt of the classification list of diagnosis methods of the global inspection system [41]

Code	Category	Code	Diagnosis method
D-C	Thermo-hygrometric methods	D-C1	Measurement of the ambient and/or surface temperature and humidity (NDT)
		D-C2	Measurement of the in-depth humidity (DT)
		D-C3	Infrared thermography (NDT)
D-D	Sound and acoustic methods	D-D1	Ultrasound (NDT)
		D-D2	Percussion (NDT)
		D-D3	Assessment of acoustic insulation (NDT)
D-E	Nuclear methods	D-E1	Nuclear method (NDT)
D-F	Hydric methods	D-F1	Watertightness test (NDT)
		D-F2	Water jet (NDT)
		D-F3	Submersion of the base of window frames (NDT)
		D-F4	Initial surface absorption test (ISAT) and Karsten-tube (NDT)

*NDT* non-destructive test; *DT* destructive test

**Table 3** Excerpt of the classification list of causes of defects of the global inspection system [42]

Code	Category	Code	Cause
C-C	Mechanical actions	C-C1	Deformation of the bearing structure/substrate
		C-C2	Movements of structural nature of walls or foundations
		C-C3	Substrate-cladding differential movements
		C-C4	Movement of people or vehicles over the claddings
		C-C5	Excessive loads on roofs and floorings
		C-C6	Excessive vertical loads on wall claddings
		C-C7	Impacts of heavy objects resulting from inclement weather
		C-C8	Intentional collisions/vandalism
		C-C9	Accidental collisions with the cladding
		C-C10	Stress concentration within the substrate
		C-C11	Fragmentation of the substrate in expansion, peripheral or stone plate joints
		C-C12	Vibrations
		C-C13	Abrasion

To ensure consistency in the described process, specific criteria were defined for each type of classification system, which are described by de Brito et al. [7] and Pereira et al. [41–45]. Of those, some can be highlighted. For instance, on the one hand, each item in the classification list of defects had to correspond to a visually identifiable phenomenon, privileging visual observation as the basis of inspection. On the other hand, items in the list of defects must be clearly different from those in the list of causes of defects. In other words, the listed defects should be visible, identifiable phenomena, independent from possible causations or consequences. Additionally, although all the lists were intended to be as short as possible, in the case of the list of causes of defects, this criterion was less tight, given the large range of different causes of defects. Furthermore, an effort was made to restrict the set of terms used to name the causes. For instance, causes C-A3 to C-A5 all refer to different types of “missing/incorrect design/detailing of ...” [42].

The harmonisation criteria of the classification system of diagnosis methods defined specific rules to guide the combination of different tests in a single diagnosis method. Those rules focused on the functioning principle of the test, type of results, type of instruments and destructive or non-destructive nature of the test [41]. Similarly, the harmonisation criteria of the classification system of repair techniques determined that techniques could be merged according to the repair procedures, the applicability to a single material, the treatment of similar defects and the use of identical repair materials [43].

## 2.2 *Harmonisation of the Correlation Matrices*

Throughout the inspection of a building, defects are visually identified. Diagnosis methods help to confirm their occurrence and to characterise them. In any case, surveyors try to determine causal relationships to pinpoint the origin of a defect. Through simple observation, the most experienced surveyors can identify the probable causes of a detected defect. To speed up that process and make it less dependent on the surveyor's professional experience and knowledge, the individual inspection systems used correlation matrices [33], not only between defects and probable causes, but also inter-defects, defects–diagnosis methods and defects–repair techniques correlation matrices.

Correlation matrices present predetermined relationships, based on knowledge and experience, between the items in the classification systems. For instance, the correlation matrix between defects and their causes guides the surveyor in the diagnosis process, indicating the causes that are more likely to be involved in the pathological process, given the detection of a specific defect. On the other hand, the inter-defects correlation matrix presents the probability of occurrence of a subsequent defect when a given defect is detected.

The harmonisation of the information in the individual system's correlation matrices starts from the harmonised classification lists to create global matrices, applicable to 12 building elements/materials. The range of situations involved in the harmonisation of the classification lists (merging, splitting, combining items) reflects on the harmonisation process of correlation matrices.

Considering double-entry tables as the starting point of the process (the correlation matrices in the individual expert inspection systems), the harmonisation process within the global inspection system implied analysing each row and each column, considering any changes resulting from the respective harmonisation of classification lists. For instance, if the conversion of an individual classification system into the global system implied combining two defects in a single one, the row of that harmonised defect corresponded to two rows in the individual correlation matrix. Likewise, if two causes of defects were combined into one, the column of that harmonised cause corresponded to two columns in the individual correlation matrix.

### 2.2.1 **Incorporation of Two-Dimensional Matrices into a Three-Dimensional Matrix**

Four correlation matrices were included in each individual expert inspection system, namely: defects–probable causes, inter-defects, defects–diagnosis methods and defects–repair techniques correlation matrices. The defects–probable causes correlation matrix helps to determine the origin of the detected defects, as it reflects state-of-the-art knowledge about building pathology. The defects–diagnosis methods correlation matrix assists the surveyor to determine whether further testing may be



useful to characterise a given detected defect. The defects–repair techniques correlation matrix also helps the surveyor during the diagnosis process, but, in this case, it focuses on the work that may be applicable to solve the identified phenomenon. As for the inter-defects correlation matrix, it supplies the surveyor with probabilities of occurrence of a defect when another one is detected. In this way, such a matrix guides the surveyor’s observation process, alerting for highly probable defects that may be going unnoticed.

The correlation matrices in the individual expert inspection systems are double-entry tables that present the most probable relationship between types of defects and types of probable causes, diagnosis methods and repair techniques. The rows of the matrices represent defects, while the columns represent causes, diagnosis methods or repair techniques, according to the type of matrix (Fig. 2). In the intersection between rows and columns, a number determines the correlation level between a defect and the respective cause, for example. To correctly read the matrix (Fig. 2), first, a row (a defect) should be selected. Then, that row is carefully analysed to understand which are the causes (in the columns) related to that type of defect.

In the global inspection system, the correlation matrices become three-dimensional (Fig. 3). Those are similar to two-dimensional matrices, but a third axis is added, which refers to layers of building elements/materials. Those layers are fundamental for the accuracy of the information presented in the matrix, as pathological processes differ according to the type of building element/material involved.

The surveyor should go through the three-dimensional correlation matrices identifying the type of building element/material (layer) first. Then, the type of defect is identified (row) and, finally, the correlation degree between that defect and the probable causes, diagnosis methods or repair techniques (according to the type of matrix) is read (Fig. 3).

	C-A1	C-A2	C-A3	C-A4	C-A5	C-A6	C-A7	C-A8
A-A1	1	1	0	0	0	0	0	0
A-A2	1	0	0	0	0	2	0	0
A-A3	0	0	0	0	0	0	0	0
A-A4	1	0	0	0	1	1	0	1
A-A5	1	1	0	0	1	0	1	1
A-A6	1	1	0	0	0	0	1	1
A-A7	1	0	0	0	0	0	0	0
A-A8	0	0	0	0	0	0	0	0
A-A9	1	0	0	0	0	2	0	0
A-B1	0	0	0	2	1	0	0	0
A-C1	0	0	2	0	0	0	0	0
A-C2	0	0	2	0	0	0	0	0

Fig. 2 Reading order of the defects–probable causes correlation matrix based on an excerpt from the individual expert inspection system of epoxy resin industrial floor coatings

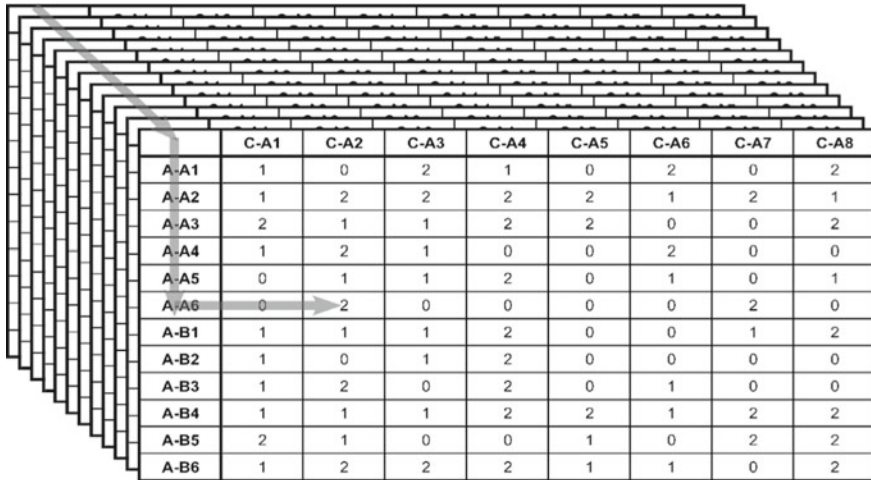


**Fig. 3** Reading order of a simulation of a three-dimensional defects-probable causes correlation matrix

The correlation matrices are filled with three types of indexes (0, 1 or 2), whose meaning is as follows [46]:

- 0: there is no correlation.
- 1: there is a low correlation.
- 2: there is a high correlation.

These indexes assume more specific definitions according to the type of matrix [29]. For instance, in the correlation matrix between defects and probable causes, index 1 refers to indirect causes, and index 2 refers to direct ones.

In the global inspection system, as the correlation matrices are based on the harmonised classification systems, layer by layer, the items in the rows and columns repeat themselves, always referring to the same types of defects, probable causes, diagnosis methods and repair techniques, according to the type of matrix. This reflects a concrete advantage of the global inspection system (standardisation of language/definitions) but implied a process of harmonisation of the correlation matrices, consisting of rebuilding them.

In the case of the inter-defects correlation matrices, the process is similar, transforming two-dimensional matrices into three-dimensional ones, encompassing layers of building elements/materials. However, in this case, the harmonisation process represented the implementation of the method to build inter-defects correlation matrices, as described by Garcia and de Brito [29], layer by layer (based on the harmonised defects-probable causes correlation matrix).

### 2.2.2 Criteria Used to Harmonise the Layers of a Correlation Matrix

The harmonisation of the defects–probable causes, defects–diagnosis methods and defects–repair techniques correlation matrices is based on the respective matrices from the individual expert inspection systems. To make the harmonisation process as unbiased as possible, a set of procedures were defined to guide the harmonisation routines. It should be highlighted that the matrices from the individual expert systems were based on up-to-date knowledge and had been validated through extensive fieldwork [44], thus forming a solid basis for the global inspection system.

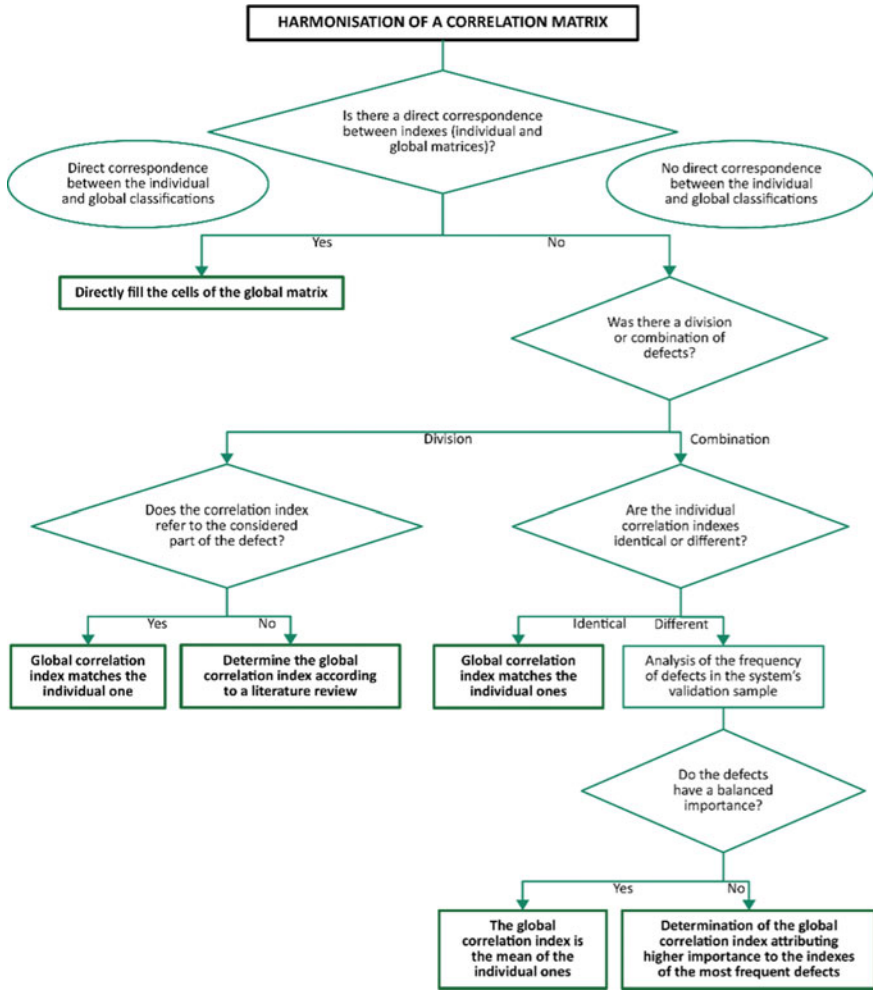
To briefly describe the process of harmonisation of the correlation matrices, the defects–probable causes correlation matrix is used as an example. The methods used for the defects–diagnosis methods and defects–repair techniques correlation matrices are identical.

Figure 4 shows the general workflow of the harmonisation process. Considering the harmonisation of the classification systems, two main situations may occur:

1. Direct correspondence between the correlation index in the individual matrix and that in the global matrix, due to the direct correspondence between the items (defects and causes, diagnosis methods or repair techniques) in the individual and global classification lists;
2. No direct correspondence between the correlation index in the individual matrix and that in the global matrix, due to the lack of direct correspondence between the items (defects and causes, diagnosis methods or repair techniques) in the individual and global classification lists.

The first situation is simpler and the second is more complex. In the first situation, some of the global matrix cells may be immediately filled, while, in the second situation, the harmonisation process of the items under analysis must be assessed (classification lists). The workflow presented in Fig. 4 describes the hypotheses that were formulated in every step of the process. An example is provided below.

In the process of harmonisation of the layer of painted façades of the global correlation matrix between defects and causes, it was observed that there was no direct correspondence between the correlation indexes referring to the relationship between the harmonised defect “A-D4 Finishing colour flaws in painted façades” and the harmonised cause “C-B21 Disregard for the pauses between execution stages”. That fact resulted from the harmonisation of defect A-D4, as it stemmed from the combination of two defects from the individual expert inspection system of painted façades, namely “A-Co2 Lapping” and “A-Co3 Bleeding”. Then, in the individual correlation matrix, the correlation indexes between these defects and the equivalent to the harmonised cause C-B21 were different (2 and 0, respectively) [20]. With that in mind, the frequency of detection of both defects in the validation sample of the individual expert inspection system was analysed [19], leading to the conclusion that there was unbalanced importance of the original defects—“A-Co2 Lapping” was more prevalent than “A-Co3 Bleeding”. For this reason, higher importance was attributed to the correlation index associated with A-Co2 in the individual expert



**Fig. 4** General workflow of the harmonisation of the correlation matrices (based on the example of the consequences of the harmonisation of the classification list of defects)

inspection system, resulting in the global correlation index of 2 between A-D4 and C-B21 in the layer of painted façades.

After the harmonisation process of the correlation matrices, four global matrices were obtained, each one with 12 layers. In Tables 4 and 5, excerpts of two layers of the correlation matrix between defects and causes are presented. It should be highlighted that, in different layers, the correlation indexes between the same defects and causes tend to be different.

**Table 4** Excerpt of the layer of external claddings of pitched roofs of the defects—causes global correlation matrix

	C-C1	C-C2	C-C3	C-C4	C-C5	C-C6	C-C7	C-C8	C-C9	C-C10	C-C11	C-C12	C-C13
A-C1	1	0	0	2	2	0	2	2	0	0	0	0	0
A-C2	1	0	0	2	2	0	2	2	0	0	0	0	0
A-C3	1	0	0	2	2	0	2	2	0	0	0	0	0
A-C4	0	0	0	0	0	0	0	0	0	0	0	0	0
A-C5	0	0	0	0	0	0	0	0	0	0	0	0	0
A-C6	0	0	0	0	0	0	0	0	0	0	0	0	0
A-C7	2	0	0	2	2	0	2	1	0	0	0	0	0
A-C8	0	0	0	0	0	0	0	0	0	0	0	0	0
A-C9	1	0	0	0	0	0	0	0	0	0	0	0	0
A-C10	1	0	0	0	0	0	0	0	0	0	0	0	0
A-C11	0	0	0	0	0	0	0	0	0	0	0	0	0

Notation of defects: "A-C1 Mapped cracking"; "A-C2 Oriented cracking on the current surface"; "A-C3 Fracture or splintering on the current surface"; "A-C4 Cracking and/or splintering adjacent to joints/edges"; "A-C5 Wear or scaling of the finishing coat"; "A-C6 Scratches/grooves and deep wear"; "A-C7 Warpage, swelling, deformation and other flatness deficiencies"; "A-C8 Material gap/puncture"; "A-C9 Detachment"; "A-C10 Loss of adhesion"; "A-C11 Bending and rupture of metallic fastening elements."

Notation of causes: see Table 3

**Table 5** Excerpt of the layer of door and window frames of the defects-causes global correlation matrix

	C-C1	C-C2	C-C3	C-C4	C-C5	C-C6	C-C7	C-C8	C-C9	C-C10	C-C11	C-C12	C-C13
A-C1	0	0	0	0	0	0	0	0	0	0	0	0	0
A-C2	0	0	0	0	0	0	0	0	0	0	0	0	0
A-C3	2	0	0	0	0	0	2	1	2	0	0	2	0
A-C4	0	0	0	0	0	0	0	0	0	0	0	0	0
A-C5	0	0	0	0	0	0	1	1	1	0	0	0	0
A-C6	0	0	0	0	0	0	0	0	0	0	0	0	0
A-C7	2	0	0	0	0	0	2	1	2	0	0	0	0
A-C8	0	0	0	0	0	0	0	0	0	0	0	0	0
A-C9	0	0	0	0	0	0	1	1	1	0	0	0	0
A-C10	0	0	0	0	0	0	0	0	0	0	0	0	0
A-C11	0	0	0	0	0	0	0	0	0	0	0	0	0

Notation of defects: see Table 4

Notation of causes: see Table 3

## **2.3 *Elements that Support the Inspection Procedure***

### **2.3.1 Detailed Files**

To use the expert inspection systems on-site, a set of elements were defined to support the procedures. Each defect, diagnosis method and repair technique included in the respective classification system corresponds to a detailed file that could be consulted to complement the surveyor's knowledge about each item.

The detailed files of defects provide information that allows for: better understanding of the origin and consequences of the pathological process; being more alert towards specific characteristics of the phenomenon; and determining the urgency of repair of the defect according to objective parameters. The detailed files of diagnosis methods supply information to help recommend further testing, presenting the materials needed, the test's procedures and its main advantages and limitations. Similarly, the detailed files of repair techniques present a large range of information about the repair works, including materials needs, procedures, efficiency and reference costs. Consulting these files, the surveyor is better informed during the diagnosis' decision process.

To recap, the individual expert inspection systems included detailed files of defects, diagnosis methods and repair techniques. Likewise, the global inspection system includes the same type of detailed files, as per the harmonised classification systems.

The development of the detailed files of the global inspection system also implied a harmonisation process. The structure of the files in the individual expert inspection systems was followed with the necessary adaptations. For instance, the files in the global system include a section referring to the "field of application", indicating the building elements/materials that item is applicable to. The global detailed files were filled with information from the individual expert inspection systems, filtered to avoid repetitions and to standardise the format.

### **2.3.2 Inspection Form**

Another important element to support the inspection procedures is the inspection form. It should be used during fieldwork to ensure that all important data are collected. The inspection form includes predetermined fields to be filled with information about the building and its context, and the inspected building elements and their defects. The standardisation of the collection of information enables a more objective diagnosis process.

The inspection form is a long document divided into different parts and sections, according to the type of information to be collected. The inspection form of the global inspection system was developed based on the inspection forms of the individual expert inspection systems. In the latter, the inspection form was divided into two forms: the inspection form (for data about the building, its surroundings and the

building elements) and the validation form (for data about the defects). In the global inspection system, those two forms were merged.

The harmonisation of the inspection form consisted of defining a well-structured model, applicable to the 12 types of building elements/materials included in the global inspection system. Therefore, some parts of the inspection form need to be repeated to characterise the different elements that are inspected.

### 2.3.3 Building Inspection Software

After the development of the global inspection system to be used on paper, a Web application was developed to allow using this system in portable devices (e.g. tablets) [45]. That transition aimed at reducing the time invested in fieldwork and post-processing data, while making the inspection procedures easier.

This Web application was based on the inspection form, which was transposed to a set of Web pages, whose data fields are used to build a database of the collected information (Fig. 5). The elements that compose the global inspection system are embedded within the Web application's code, including the classification systems and the correlation matrices.

Collecting information on-site using the global inspection system's Web application enables inputting data directly in a database. Additionally, the Web application allows filling interactively the collected information, as data fields dynamically adapt to inputs, using the elements of the global inspection system (e.g. correlation matrices). These new features help to reduce the number of possible errors during the collection of data.

## 3 Using Inspection Data in Service Life Prediction Models

The inspection of buildings and their components is a decisive part for the adoption of rational maintenance policies. Additionally, the success of a maintenance strategy relies on accurate and reliable knowledge regarding the components' expected service life, in order to compare the available maintenance strategies and their impact on the components' life cycle [47].

The lack of standardised tools for inspection and diagnosis often leads to a time-consuming process [48] and to misdiagnosis, which usually entails the implementation of needless or unsuitable works, thus compromising the future behaviour of the buildings' components [49].

The automation of the inspection processes through the adoption of Web applications as the one described previously, and illustrated in Fig. 5, allows systematising the logical steps for the diagnosis of defects, at a premature stage, in buildings' components. The knowledge obtained from these diagnosis protocols and the inspection data is crucial for the definition of service life prediction methods.



SLPforBMS    Menu -    Logout

### Characterisation of the building element - WR

Year of construction:	1984	Type of render:	Traditional
Floor starts in:	Ground floor	and ends in:	Ground floor
Type of façade:	Side	Façade orientation:	N
Area of the whole surface (m²):	90	Area of the cladding (m²):	30
Reinforcement mesh?	No	Surface protector?	Yes
Type of finish:	Smooth		
Colour:	white		
Type of substrate:	Traditional masonry		
Joints?	- Select a type of substrate -		
Windows?	Reinforced concrete		
Parapet walls:	- Select an option -		
Balconies:	- Select an option -		
Eaves or upper protection?	- Select an option -	Lower protection?	- Select an option -
Flowerbeds and jutting elements?	- Select an option -		
Proximity to heat source:	- Select an option -		
Contact with objects, people or animals:	- Select an option -		
Notes:	Complementary information...		
	Save	Cancel	

**Fig. 5** Example of a page of the Web application of the global inspection system—page of characterisation of the building element (wall render)

Service life must be estimated based on knowledge of the material and its deterioration state, using as indicators some measurable properties [50]. The use of methodologies supported by service life prediction data is still incipient both at the design/execution and service stages of the buildings. In most situations, stakeholders adopt absolute values for the service life of a given component, not considering the uncertainty and variability associated with the degradation agents and their synergy. Knowing the service life expectancy of buildings/components at the design stage is extremely useful, with several practical applications, namely to evaluate the environmental and economic impact of buildings. This information (when attributes and environmental conditions of the buildings are well known) is relevant to manufacturers to set warranty periods for materials and designers to select the most suitable material for a given application.

Consequently, models are needed to relate the service life of building components and the set of conditions that characterise and influence it (inspection data). Using this type of information, it is possible to develop maintenance strategies for existing buildings and at the design stage, estimating their remaining service life, which is essential for building managers, insurers and users. There is an increasing demand

for simple tools to estimate the service life of building components, thus enabling more rational management of the built environment.

### 3.1 Standardisation of Information

Different service life prediction methodologies have been developed considering the inspection and diagnosis data provided by the global inspection system described in Sect. 2. Therefore, a service life prediction computational tool was created, applying the inspection data obtained through fieldwork assessment (collected through the Web application shown in Fig. 5).

This service life prediction Web tool considers the importance rating of the construction elements, the rating of the defects (some defects are more serious than others), the area affected by them and the definition of the condition parameters associated with the defects. This information is converted into a numerical index that expresses the global performance of any construction element. This indicator, called severity of degradation, is determined by the ratio between the weighted degraded area, considering the extent and condition of the defects detected, and a reference area, equivalent to the maximum theoretical extent of the degradation for the element analysed [51, 52]. This numerical index (Eq. 1) is used to express the overall degradation of the elements analysed, considering that it represents the reality observed on-site. The service life prediction methodologies are defined to minimise the differences between the predicted values of the severity of degradation and the observed values (obtained by the numerical index).

$$S_w = \frac{\sum (A_n \times k_n \times k_{a,n})}{A \times \Sigma(k_{\max.})} \quad (1)$$

where  $S_w$  represents the severity of degradation of the façade, as a percentage,  $A_n$  the area of the cladding affected by a defect  $n$ , in  $m^2$ ,  $k_n$  the defects' "n" multiplying factor, as a function of its condition (between 1 and 4),  $k_{a,n}$  the weighting coefficient corresponding to the relative importance of each defect considering the cost of repair or risk ( $k_{a,n} \in R^+$ ) (if no further instructions are provided,  $k_{a,n} = 1$  is assumed),  $k_{\max.}$  the weighting factor equal to the highest condition level, and  $A$  the total area of the cladding, in  $m^2$ .

For the application of the severity of degradation index, the classification system of defects is standardised, through making the information obtained through the building inspection software compatible with the information required for the definition of the service life prediction models. In this sense, a categorisation system of defects was created for each building component, establishing a harmonised degradation rating to express the physical and functional degradation of the elements under analysis. These categorisation systems consist of a scale of discrete variables that varies from the most favourable condition level (no visible degradation) to the least

favourable one (extensive degradation or loss of functionality). Each level of degradation corresponds to a set of reference characteristics based on comparisons with real situations analysed in the fieldwork. For each element of the external envelope of buildings, it is possible to identify main groups of defects, with different levels of severity. The weighing of the group of defects is based on current market costs of repair techniques associated with the various defects in comparison with the cost of executing a new envelope's element.

A detailed analysis was performed to scrutinise in which way the data collected in the inspection and diagnosis software could be directly used in the modelling of the service life, identifying the need for particular adaptations of the two systems.

### ***3.2 Adopted Service Life Prediction Models***

Once the information collection system is harmonised, and once guaranteed that the data collected in the field allow a reliable prediction of the building components' service life, it is necessary to define the prediction methods to be used. Depending on the user's perspective, a given reality can be represented in different ways and by different mathematical models. In this sense, different service life prediction models have been proposed, based on advanced statistical and mathematical tools.

Initially, these methods were classified in four categories [53, 54]: (i) deterministic models (regression analysis: simple nonlinear regression; multiple linear regression; and multiple nonlinear regression); (ii) stochastic models (logistic regression and Markov chains); (iii) computational methods (artificial neural networks and fuzzy systems); and (iv) factorial methods (classical and probabilistic approach).

Deterministic models are expedient and easy to learn and apply [55]. Simple regression models represent the loss of performance of the building's envelope over time. Using these methods, it is possible to estimate graphically the service life of building components through the intersection between the degradation curves and the maximum acceptable degradation level. These models only relate the severity of degradation to age and individually to other characteristics of the building's envelope. Multiple linear and nonlinear regression models include more than one variable in the mathematical description of the envelope's degradation and allow identifying, out of all the characteristics of the envelope's elements, those that best contribute to the variability of its degradation. Using these models, it is also possible to analyse causal relationships between the characteristics of the elements under analysis.

The implementation of stochastic models (logistic regression and Markov chains) allows evaluating the service life of the building envelope by probabilistic distribution functions [56, 57]. The wealth of information produced is superior to that of data obtained by purely deterministic models, allowing dealing with the uncertainty associated with the degradation phenomenon. Moreover, these models allow estimating: (i) the probability of the building envelope's elements having a given degradation condition depending on their age and their characteristics, (ii) the probability of failure at a given age; (iii) the average time of permanence in a given degradation

condition; and (iv) the probability of reaching the end of their service life after a period of time and according to their characteristics.

Artificial intelligence-based models (neural networks and fuzzy logic) will also be implemented [58, 59]. They are obtained using computational techniques that intend to simulate and automate intelligent behaviour. These methodologies use previously acquired knowledge about reality, which is intended to be modelled, and are able to transform raw data into knowledge and easily applicable models. Computational methods allow estimating the degradation and service life of the building envelope, according to the explanatory variables considered.

Finally, factorial methods are defined to estimate the service life of the building envelope. The determinist approach is easy to apply and provides the service life of elements under analysis according to their characteristics [60]. The stochastic approach results in the estimated service life for each case study within the sample, given by a probability distribution [61].

These models were used to create a user-friendly software capable of estimating the service life of a wide range of building envelope's elements (coatings and claddings). This software is an internationally innovative tool, allowing the user (planner, designer, constructor, engineer, architect, manager and insurance company) to predict the service life of a building element based on a set of simple steps: (i) choose the case study; (ii) select in the software the envelope's element to be analysed; (iii) decide on the service life prediction model (considering the intended output's accuracy and complexity); and (iv) define the maximum degradation level that establishes the end of service life of the elements (depending on the users' demands target level).

In this software, the different methods are grouped in four categories, considering the type of information that is required from the user and the type of result obtained: (i) single-parameter deterministic models; (ii) multi-parameter deterministic models; (iii) single-parameter stochastic models; and (iv) multi-parameter stochastic models.

The single-parameter methods require that the user provides only the age of the element and, if this information can be obtained (it is not mandatory to determine the element's service life), the severity of degradation index of the element under analysis. On the other hand, multi-parameter models require that the user provides a set of relevant information about the element (e.g. distance from the sea, type of finishing, exposure to humidity, among others) in order to determine the estimated service life of the element. The quality of the information provided by the user is crucial for the reliability and accuracy of the service life estimated by the computational tool (this indication is shown in the software, to warn the users).

Figure 6 shows an example of a single-parameter deterministic model applied to wall renders. This model is a polynomial regression between the severity of degradation index and the walls' age, representing the loss of performance (considering the walls' physical degradation) over time. This degradation curve was defined for a large set of specimens analysed through fieldwork surveys.

The service life estimations are dependent on the users' level of demand. By default, a conventional limit of 20% of severity of degradation is considered to establish the end of service life of wall renders. This limit was established according

**Fig. 6** Example of the degradation curve obtained for 100 wall renders (mean curve and confidence interval at 95%)

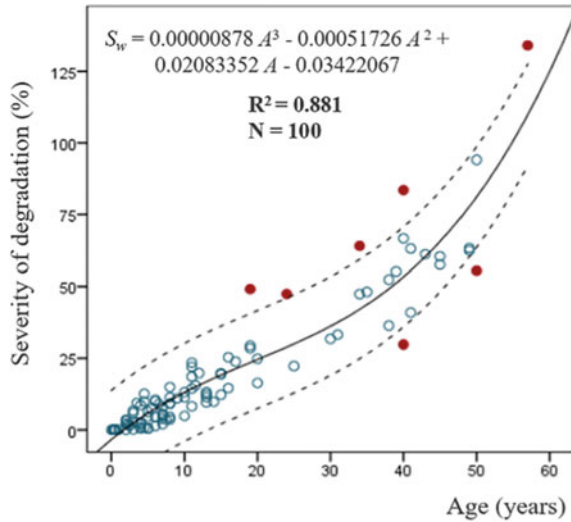


**Table 6** Average estimated service life of wall renders, based on the overall degradation curves as a function of various maximum acceptable degradation levels

Building material	Maximum acceptable degradation levels				
	10%	15%	20%	25%	30%
Wall renders	8	11	16	20	25

to several years of experience in service life prediction and in the analysis of different building elements [53–57]. Nevertheless, in the service life prediction software developed, the user can select another limit to establish the end of service life, being warned about the repercussions of such change. Table 6 presents the average estimated service life of wall renders, based on the degradation curves and according to various maximum acceptable degradation levels.

The single-parameter probabilistic models provide mathematical equations to estimate the probability of a given element reaching the end of its service life, according to its age and for the various service life limits considered (Table 7).

In this research, it is considered that the elements of the building envelope analysed follow a natural degradation process, without any maintenance action during their service life period. In this sense, the age of the buildings’ envelope elements corresponds to the date since their construction or since the last intervention (maintenance or rehabilitation action) up to the time of inspection. There are, generally, in the analysed samples, few case studies at the highest levels of degradation.

The accuracy and effectiveness of the equations depend on the number of examples that have reached the end of service life, for a given level of performance. This characteristic of the models implies that it is more difficult to model the probability of reaching higher levels of severity of degradation. For example, if none of the

**Table 7** Probability of a wall render reaching the end of its service life, according to its age and for the various limits of service life

Maximum acceptable degradation level (end of life) (%)	Probability of reaching the end of service life	% of case studies that reached the end of service life for this limit (%)	Accuracy of the model (%)
10	$P(Y = \text{reach the EndSL}) = 1 - \frac{1}{1+e^{-4.864+0.516.Age}}$	51	90.0
15	$P(Y = \text{reach the EndSL}) = 1 - \frac{1}{1+e^{-7.263+0.531.Age}}$	37	92.0
20	$P(Y = \text{reach the EndSL}) = 1 - \frac{1}{1+e^{-7.767+0.467.Age}}$	31	96.0
25	$P(Y = \text{reach the EndSL}) = 1 - \frac{1}{1+e^{-8.178+0.400.Age}}$	26	95.0
30	$P(Y = \text{reach the EndSL}) = 1 - \frac{1}{1+e^{-7.304+0.276.Age}}$	22	97.0

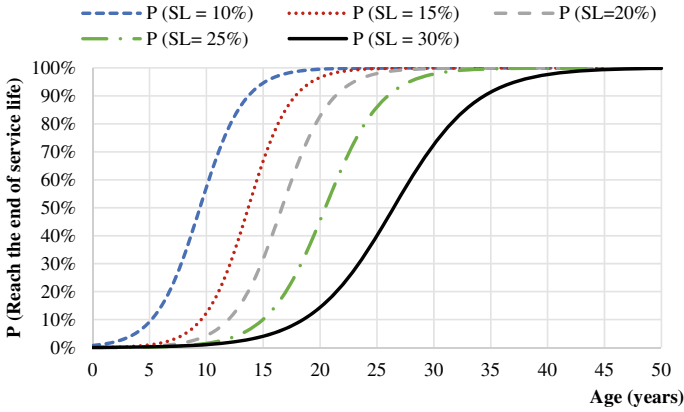
case studies has a severity of degradation of 30%, it is not possible to obtain the mathematical equation for calculating the probability of reaching the end of service life for this limit. In other words, when there are few case studies with these degradation values, the prediction model obtained must be analysed with some caution. Nevertheless, all the logistic regression models proposed for the buildings’ envelope elements analysed, to assess the probability of reaching the end of their service life for a given maximum level of degradation, have an accuracy greater than 80% (generally, greater than 95%).

Figure 7 illustrates the representation of the cumulative probability distribution functions, given by the equations in Table 7.

This visual information is provided to the user, in the software developed, allowing a more expeditious analysis of the probability of a wall render reaching the end of its service life over time. In addition to this information, a summary table must be provided indicating the ages for which there is a probability of 5, 50, 75, 90 and 95% of reaching the end of service life. Table 8 presents the results obtained for wall renders, as a function of different end-of-life limits.

Concerning the multi-parameter models, various methodologies were applied [53, 54]. Table 9 shows some results obtained for wall renders, based on the proposed models.

The probabilistic multi-parameter model is based on a stochastic approach to apply the factor method, originally proposed in the international standard for the durability of buildings and components (ISO 15686). Equation 2 and Table 10 show an example of the application of this model to predict the service life of a specific wall render, according to its characteristics. This model, although more complex, produces more reliable and less generic information regarding the service life of the



**Fig. 7** Probabilistic distribution of a wall render reaching the end of its service life according to various service life limits

**Table 8** Probability of a rendered façade reaching the end of its service life

	Estimated service life (in years), with a given probability of being exceeded				
	5%	50%	75%	90%	95%
$P (ESLL = 10\%)$	4	9.5	12	13.7	15
$P (ESLL = 15\%)$	8	13.7	16	18	19
$P (ESLL = 20\%)$	10	17	19	22	23
$P (ESLL = 25\%)$	13	21	23	26	28
$P (ESLL = 30\%)$	16	27	30.5	35	37

ESLL represents the end of service life limit (maximum acceptable degradation level)

**Table 9** Estimated service life obtained through the application of the deterministic multi-parameter models proposed, applied to wall renders (maximum acceptable degradation level: 20%)

Model	$R^2$	Average estimated service life (ESL)	Standard deviation of the ESL	Confidence interval (95%)
Polynomial model	0.904	15.823	2.982	$\pm 0.587$
Gompertz curve	0.872	21.960	4.262	$\pm 0.839$
von Bertalanffy curve	0.872	21.980	4.286	$\pm 0.844$
Richards curve	0.872	21.970	4.294	$\pm 0.846$
Morgan-Mercer-Flodin model	0.902	15.778	2.776	$\pm 0.547$
Weibull curve	0.902	16.101	2.866	$\pm 0.565$
Brody model	0.905	15.960	2.972	$\pm 0.586$
Exponential model	0.875	21.960	4.157	$\pm 0.819$

**Table 10** Estimated service lives and weighting coefficients for each durability factor considered in the service life prediction of wall renders

Durability factors			Average ESL (DCs)	Average ESL (GMs)	Weighting value ( <i>k</i> )
A1	Render type	Lime-cement renderings	13	15	0.90
		Current cement renderings	17	19	1.00
		Renderings with crushed marble	19	23	1.10
		Single-layer renderings	17	24	1.10
B1	Colour	White	12	18	0.95
		Light colours	14	19	1.00
		Dark colours	16	19	1.00
B2	Building geometry	Compact	13	19	1.00
		Irregular	17	18	0.95
B3	Eaves' protection	Without protection	12	20	1.00
		With protection	15	18	1.00
B4	Platbands copings	Without copings	14	17	1.00
		With copings	16	24	1.00
B5	Balcony copings	Without copings	13	18	1.00
		With copings	18	20	1.10
B6	Ground floor protection (socle)	Without protection	14	20	1.00
		With protection	14	19	1.00
B7	Detailing/design level	Inferior	14	16	0.90
		Medium	14	20	1.00
		Superior	19	22	1.10
E1	Façade orientation	East/SE	15	19	1.00
		North/NE	13	7	0.90
		West/NW	14	20	1.00
		South/SW	17	21	1.10
E2	Distance from the sea	Less than 5 km	13	17	0.80
		More than 5 km	14	19	1.00
E3	Exposure to damp	Unfavourable	12	17	0.90
		Normal	12	17	0.90
		Favourable	16	20	1.00

(continued)



**Table 10** (continued)

Durability factors			Average ESL (DCs)	Average ESL (GMs)	Weighting value ( <i>k</i> )
E4	Distance from pollution sources	Unfavourable	14	19	0.90
		Normal	14	19	0.90
		Favourable	16	22	1.00
E5	Façade protection level	Without protection	13	18	1.00
		Normal situation	15	18	1.00
		With protection	16	20	1.10
F1	Type of property	Private	14	19	1.00
		Public sector	14	15	0.90
		Commerce and services	22	24	1.10
G1	Ease of inspection	Normal	14	18	1.00
		Unfavourable	15	19	1.00

*ESL* estimated service life; *DCs* degradation curves; *GMs* graphical methods

element under analysis, as the stochastic approach associates probability distributions to each durability factor.

$$ESL = RSL \cdot A1 \cdot B1 \cdot B2 \cdot B3 \cdot B4 \cdot B5 \cdot E1 \cdot E2 \cdot E3 \cdot E4 \cdot E5 \cdot F1 \cdot G1 \quad (2)$$

where *ESL* represents the estimated service life, *RSL* the reference service life (equal to 16.1 years), *A1* the render type, *B1* façade colour, *B2* building geometry, *B3* eaves' protection, *B4* protection of parapets in roofs and terraces, *B5* protection of balcony parapets, *B6* ground floor protection (socle), *B7* detailing/design level, *E1* façade orientation, *E2* distance from the sea, *E3* exposure to damp, *E4* distance from pollution sources, *E5* façade protection level, *F1* in-use conditions, and *G1* ease of inspection of the façade.

Therefore, uniparameter models require a smaller amount of information but only provide the user with an estimate that is less adjusted to the specific reality of the building's component under analysis, and more adjusted to an average service life value, considering an extensive sample previously analysed. Multi-parameter models require a larger amount of data to be able to provide an estimate that is more adjusted to the construction element analysed by the user. Within these two types of models, deterministic models only provide an average value of the estimated service life of the component, while stochastic models allow evaluating the probability of a component reaching the end of its service life after a given age and depending on its characteristics.

Based on these models, the software allows the user to predict the service life of a building element based on a set of simple steps: (i) choose the case study (building) and characterise it (the user can also use information collected during the

inspection, which is available in the software described in Sect. 2.3.3); (ii) select the envelope's element to be analysed; (iii) characterise, in general terms, that building element; (iv) characterise the degradation of the building element, or choose to apply a standard prediction, according to the age of the building element (Fig. 7); (v) obtain a deterministic service life prediction of the building element; (vi) define the maximum degradation level that establishes the end of service life of the elements (depending on the users' comfort target level) to obtain different deterministic predictions; and (vii) decide on using other models of service life prediction (considering the intended output's accuracy and complexity), according to a chosen maximum degradation level.

Both computational tools are Web-based applications (to collect data and predict the service life), which can be accessed by a Web browser on a personal computer, tablet or smartphone. The results obtained through the software can be easily interpreted and can be directly used in the service life prediction of the elements without the need of further mathematical modelling. The service life prediction software is extremely useful since: (i) the models are based on advanced statistical models, with an estimated service life given by a characteristic value associated with a probabilistic distribution; (ii) the models are based on artificial intelligence, capable of generalising for new case studies; (iii) the models are created with information based on a specialised data acquisition system that is constantly fed; (iv) the models are adapted to the quality and quantity of available data; (v) the output of the models is adjusted to user's needs (prescribers, designers, contractors, maintenance managers, insurance companies); and (vi) it is possible to quantify/simulate the influence of design, exposure and use conditions on the life cycle of the building envelope's elements. Both software are user-oriented tools, learning from experience and providing useful suggestions for practitioners, with practical advantages in the maintenance/rehabilitation context, aiding the optimisation of maintenance policies.

## 4 Maintenance Strategies Based on Systematised Data

In the building maintenance field, the efficiency of maintenance plans has a direct relationship with the level of uncertainty and risk considered. In this context, risk can be understood as the expected consequences associated with the maintenance activities (or the lack of them). Therefore, in addition to the risk associated with the uncertainty inherent to the real-world phenomena, the risk is also associated with limitations of the mathematical/numerical models implemented. Furthermore, errors, defects and/or neglected events can considerably increase the risk [62]. Based on that, only through detailed knowledge about the buildings and their elements, and deep awareness of the associated errors and defects, from the earliest stages, it is possible to reduce uncertainty and risk in the planning of the maintenance activities.

In the models where uncertainty is not considered [1, 63, 64], the future behaviour of the building elements is neglected from the decision problem. In those models,

the initial application cost is often chosen as a selection criterion [64]. The introduction of uncertainty in the definition of maintenance plans allows systematically computing the costs and benefits of each alternative and using these data to aid the decision-maker to select the most rational and economical alternative over a given time horizon, increasing the durability of the building elements with a reasonable investment. The main disadvantage of these methodologies is the need of complex mathematical/numerical tools to model the degradation and maintenance processes, making decision-makers sometimes hesitant to trust in the recommendation from these new methodologies [65].

However, the experience gained on the use of those models showed that the uncertainty associated with the deterioration process must be explicitly included in the decision-making process, since the complexity of the phenomena involved and the limited information available make it impossible to model the deterioration with high precision [66]. The main difficulty of this set of methods lies in the fit of the inspection data, which are not absolutely reliable. According to Phares et al. [67], visual inspections are an unreliable method for the evaluation of the building degradation condition. Different inspectors, under different conditions, evaluate significantly differently the degradation condition of the buildings, introducing an additional source of uncertainty [68]. Still, the global inspection system presented in Sect. 2 tries to minimise such uncertainty through the use of more objective data, systematisation and standardisation of language, and helping surveyors with additional information (correlation matrices and detailed files, for instance).

In the literature, there are several methods to predict degradation profiles (Sect. 3). However, many of them (such as: regression analysis; simple nonlinear regression; multiple linear regression; and multiple nonlinear regression; logistic regression; Markov chains; classical and probabilistic approach) are not versatile and can offer a gross approximation of the building elements' behaviour. In addition, they have other disadvantages, including the inability to build more complex models, namely referring to inspection, maintenance and environmental conditions, or uncertainty associated with the decision-making. To overcome these limitations, models based on net theory can be useful. Petri nets (PN) are a modelling technique applied successfully in dynamic systems in several fields of knowledge, namely in robotics [69], optimisation of manufacturing systems [70, 71], business process management [72], human-computer interaction [73], among others. This modelling technique has several advantages when compared with other methodologies. The graphical representation can be used to describe the problem intuitively. It is more flexible by allowing the incorporation of more rules to accurately simulate complex situations, keeping the model size within manageable limits. Moreover, this modelling technique is not restricted to one type of distribution to simulate the time. As a disadvantage, there are no closed-form expressions for the probability distribution used and simulation techniques are required.

In the context of the project `BESStMaintenance_LowerRisks`, the IST-UL research team developed a condition-based maintenance model, based on Petri nets, to assess the influence of different maintenance strategies on the overall degradation of building elements [74–78]. This model can be described as a full life cycle model that

includes not only the degradation process but also the inspection and maintenance processes.

#### 4.1 Conceptualisation of the Maintenance Model

Petri nets are considered a mathematical and graphical tool suitable for the formal description of systems whose dynamics are characterised as being concurrent, asynchronous, distributed, parallel, nondeterministic and/or stochastic [79, 80]. As a graphical tool, Petri nets can be used as a visual-communication aid similar to flowcharts, where the tokens are used to simulate the dynamic and concurrent activities of systems. With the mathematical tool, it is possible to set up state equations, algebraic equations and other mathematical models governing the behaviour of systems [80].

A condition-based maintenance model implies that, before any maintenance activity is carried out, the degradation condition of the building element is assessed through an inspection. After that, an intervention is defined based on the current observed degradation condition of the building element under analysis. In this maintenance model, four types of intervention are considered: inspection; cleaning operations; minor intervention and total replacement. The maintenance model is divided into five main parts (Fig. 8):

- (i) **Degradation process (blue):** It allows predicting the degradation of the building components over time. This process is described by a linear sequence of five places ( $p_1$  to  $p_5$ ) and four timed transitions ( $t_1$  to  $t_4$ ). Each place represents a degradation condition, defined in the categorisation system adopted [52]. Places  $p_1$  and  $p_5$  represent the best and worst degradation conditions, respectively. The transition times between degradation conditions are sampled from probabilistic distributions that are fitted through inspection records;
- (ii) **Inspection process (red):** It allows managing the moments in which inspections are performed. The degradation condition of the building elements is not continuously known (the degradation condition is considered unobserved until an inspection occurs). An inspection enables the adoption of the most appropriate maintenance works for tackling existing defects with the appropriate priority. This process is represented through the cycle defined by nodes:  $p_6-t_6-p_7-t_5-p_6$ . A token in place  $p_6$  means that an inspection is not required at this time and enables transition  $t_6$  that manages the time intervals between inspections. A token in place  $p_7$  indicates that it is time to perform an inspection. First, one of the transitions  $t_7$  to  $t_{11}$  is enabled, revealing the true degradation condition. After that, transition  $t_5$  is enabled, allowing the return of the token to place  $p_6$ ;
- (iii) **Maintenance process (green):** It identifies the maintenance activities to be carried out on the building elements, considering the constraints imposed on the maintenance strategy and the results from the degradation process. This

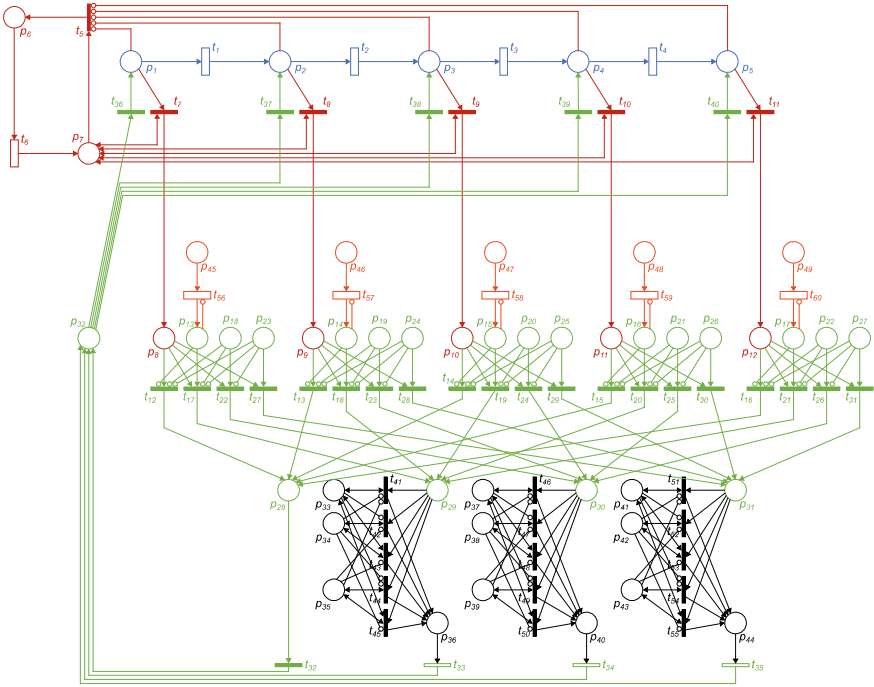


**Fig. 8** Petri net scheme of the maintenance model

process is illustrated by places  $p_{13}$  to  $p_{32}$  and transitions  $t_{12}$  to  $t_{40}$ . According to the observed degradation condition, the intervention that should be performed is selected. Here, three types of maintenance activities are considered: cleaning operations, minor interventions and total replacement. This information is introduced through places  $p_{13}$  to  $p_{27}$ . Tokens in places  $p_{13}$  to  $p_{17}$  mean that cleaning operations must be done, in  $p_{18}$  to  $p_{22}$  that a minor intervention is needed, and in  $p_{23}$  to  $p_{27}$  that a total replacement is required. If there is no token in these places, no interventions should be performed. A token in places  $p_{28}$ ,  $p_{29}$ ,  $p_{30}$  or  $p_{31}$  indicates, respectively, that no intervention, cleaning operations, minor intervention or total replacement is required. After that, the token returns to the degradation process by place  $p_{32}$  and transitions  $t_{36}$  to  $t_{40}$ ;

- (iv) **Modelling of the maintenance activities (black):** Places  $p_{33}$  to  $p_{36}$  and transitions  $t_{41}$  to  $t_{45}$  model the cleaning operations. The marking of places  $p_{33}$ ,  $p_{34}$  or  $p_{35}$  means, respectively, that the cleaning operation, when applied, has the effect of improving the degradation condition, suppressing the degradation process or reducing the degradation rate. Then, depending on the impact of the cleaning operation on the element, only one transition can be fired. For minor intervention (places  $p_{37}$  to  $p_{40}$  and transitions  $t_{46}$  to  $t_{50}$ ) and total replacement (places  $p_{41}$  to  $p_{44}$  and transitions  $t_{51}$  to  $t_{55}$ ), the same methodology is implemented. The impact of the maintenance activity is quantified

based on the historical in situ inspection records and is dependent on the type of maintenance activity and degradation condition;

- (v) **Periodicity of the cleaning operations (orange):** It allows managing the minimum time interval between cleaning operations when these are not adequate to be carried out according to the degradation condition. The indication that the intervention is available, in a given degradation condition, is performed by placing tokens in places  $p_{45}$  to  $p_{49}$ . Transitions  $t_{56}$  to  $t_{60}$  are associated with a delay that allows, at the end of  $\theta$  time units, the tokens present in places  $p_{45}$  to  $p_{49}$  to be returned to places  $p_{13}$  to  $p_{17}$ , allowing cleaning operations to be performed at the next inspection time if the imposed constraints are complied with.

A more detailed description of the maintenance model can be found in Ferreira et al. [74].

## 4.2 Uncertainty in the Maintenance Model

When a maintenance plan is defined, parameters such as the available budget, costs and effectiveness of different maintenance activities, impact on users, environmental exposure, current and future use conditions, among others, are used as decision criteria in the decision-making models [81]. However, in many of these criteria, uncertainties are involved [82]. Mainly, the uncertainties can be associated with the ability to predict future events and/or the intrinsic randomness of the natural phenomena of degradation [82].

In a maintenance model, the most critical parameter is possibly the degradation condition [54, 81]. The accuracy of the direct or indirect prediction of the degradation condition influences the efficiency of maintenance plans. For example, the accuracy of the assessment of the current degradation condition of the building element is fundamental to define the maintenance activities to be carried out, its impact on the degradation condition of the building element and, consequently, to assess the benefits of repairing it or not.

The degradation condition can be obtained in two ways [81]: by measurements or forecasting. Condition measurements involve in situ inspections and allow gathering information on the current degradation condition of the building elements (Sect. 2) while, in forecasting, mathematical/numerical models are used to predict the future degradation condition (Sect. 3). As referred in Sect. 3, these two methodologies are closely linked. The degradation conditions gathered through in situ inspections can either be used in the selection of the maintenance activities for the current period or in the fit of the mathematical/numerical models and in the use of these models to select the maintenance activities for the current period and/or plan future maintenance activities [81].

As can be seen, the accuracy of the assessment of the degradation condition is fundamental in a maintenance model, but these data also have the greatest variability [83]. Both methodologies are characterised by the presence of significant uncertainties, which have substantial life cycle cost implications. For example, in on-site inspections, the errors can derive from: (i) technological limitations, (ii) data processing errors; (iii) errors due to the nature of the buildings' elements inspected; (iv) errors due to environmental effects; and (v) difficult access conditions. On the other hand, in mathematical/numerical models, the error sources are associated with: (i) errors in the variables used; (ii) inherent randomness; (iii) inability to model the true process of deterioration; and (vi) lack of in-service measurements and records [81–83].

The origin of these uncertainties can be either random or epistemic [84]. The random uncertainty results from the variability associated with the physical processes and environmental degradation agents, caused by the random nature of the data [54, 85]. While the epistemic uncertainty is related to the lack of knowledge regarding the phenomenon to be modelled [54, 85]. The former type of uncertainty cannot be corrected [81, 85], but the latter can be reduced through the acquisition of more and better data [54, 85]. Therefore, an appropriate approach to reduce epistemic uncertainty in the maintenance model and, consequently, achieve a more accurate and reliable outcome is through the scheduling of regular inspections and systematisation of building inspections' data (Sect. 2).

In simple way, the maintenance model described allows analysing the degradation process and the impact of maintenance strategies on the durability of building elements. For that purpose, the future degradation conditions and costs are predicted based on historical in situ inspection records. Consequently, the random uncertainty would be the uncertainty associated with the historical in situ inspection records. Moreover, uncertainty also arises from the natural variability of the degradation process, which depends on a large set of factors that act simultaneously, such as: materials' quality; design and execution quality levels; structural typology; environmental exposure conditions; traffic and pollution levels; use and maintenance conditions; among others. On the other hand, the models chosen to describe the degradation process and quantify the impact of maintenance activities will inevitably introduce epistemic uncertainties, mainly due to the limited number of inspection records. Finally, the extrapolation for long periods may also introduce additional epistemic uncertainties. Therefore, considering the different types of uncertainties, the decision on the optimum maintenance strategy can be made based on a cost-benefit analysis. Figure 9 illustrates the presence of the two types of uncertainty in the different layers of the maintenance model.

### 4.3 Outcomes

Figure 10 compares inspection and re-inspection data of seven wall renders with the mean degradation curve obtained through the maintenance model developed by the

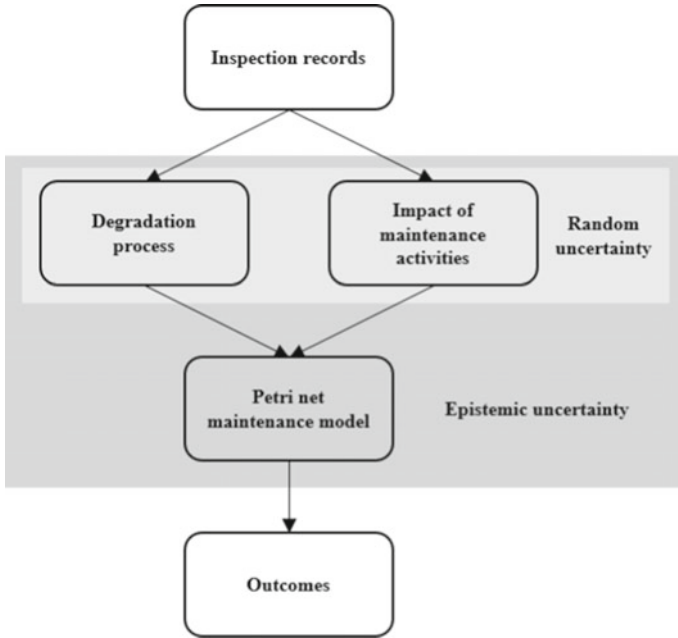
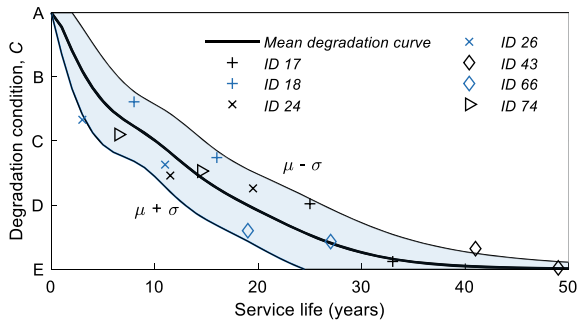


Fig. 9 Distribution of the different types of uncertainty in the maintenance model

Fig. 10 Comparison of inspection and re-inspection data of wall renders with the mean degradation curve obtained through the maintenance model



IST-UL research team. A sample of 100 in situ inspection records was used to fit the mean degradation curve. The main purpose of the re-inspection data is to assess whether the maintenance model developed adequately describes the degradation process of wall renders over time. The time interval between the inspection and re-inspection data is eight years. The inspections were performed in 2008 and the re-inspections in 2016.

The results reveal that the relative error tends to decrease as the age (service life) of the wall render increases. For the year 2008, the mean relative error is 13.7% and, for the year 2016, the mean relative error is 4.7%. Considering the existing conditions, these results are expected. First, the intervals of the categorisation system are not



uniform, so that, in the initial degradation conditions, slight defects cause the element to transition to the next degradation condition. Second, when the defects are close to the transition zone between two conditions, the chosen degradation condition is strongly dependent on the inspector's perception. Both reasons make the uncertainty in predicting the results greater in the first years. In this sense, and considering the subjectivity associated with the visual inspection process, the degradation model adequately predicts the degradation condition of wall renders, allowing considering the future behaviour of the wall render in the maintenance process and in the decision process. Figure 10 reinforces this conclusion. Both inspection and re-inspection data lie within plus or minus one standard deviation of the mean degradation curve.

It is noticed that the maintenance of building's claddings is not yet a priority. By default, maintenance works are not carried out over the cladding's service life. Claddings are only totally replaced when the end of their service life is reached. Therefore, in the decision-making process, this is defined as maintenance strategy 1 (MS1), the alternative most commonly implemented by owners/managers. To highlight the advantages of regular maintenance works, two other maintenance strategies are analysed. In maintenance strategy 2 (MS2), beyond the total replacement of the cladding at the end of the service life, minor interventions are included to delay or mitigate the degradation process; and, in maintenance strategy 3 (MS3), a combination of cleaning operations, minor interventions and total replacement is considered. In MS3, cleaning operations represent the main and most economical maintenance activity applied in wall renders.

The impact of the different maintenance strategies on wall renders is illustrated in Fig. 11 [86]. The results are presented in terms of the degradation curve (Fig. 11a), service life (Fig. 11b), maintenance costs (Fig. 11c), efficiency index (Fig. 11d) and number of replacements (Fig. 11e). The efficiency index measures the ability of a maintenance strategy to maintain the wall renders in a good condition. While the number of replacements intends to measure the impact of the maintenance activities on the users. The results show that the performance of regular preventive maintenance activities (such as cleaning operations and minor interventions) has a significant impact on the service life. In addition, by comparing the three maintenance strategies, the mean degradation curve becomes better as the maintenance strategies become more diversified (from MS1 to MS3). This observation is corroborated by the efficiency index. Finally, if the maintenance costs are analysed, there is an increase in the maintenance costs with the increase of the complexity of the maintenance strategies. The maintenance costs are directly associated with the number of interventions. As the maintenance strategies become more complex, the global number of interventions increases, which implies the increase of their associated costs. Still, the number of total replacements decreases, showing that more complex maintenance strategies are better options when it is important to reduce the users' annoyance and discomfort during the time horizon.

To use the capabilities of the maintenance model to aid the decision-maker to select the most adequate alternative for each specific situation, from a global point of view, three parameters are used in the decision process: C1—efficiency index; C2—maintenance costs (including the inspection costs); and C3—number of total

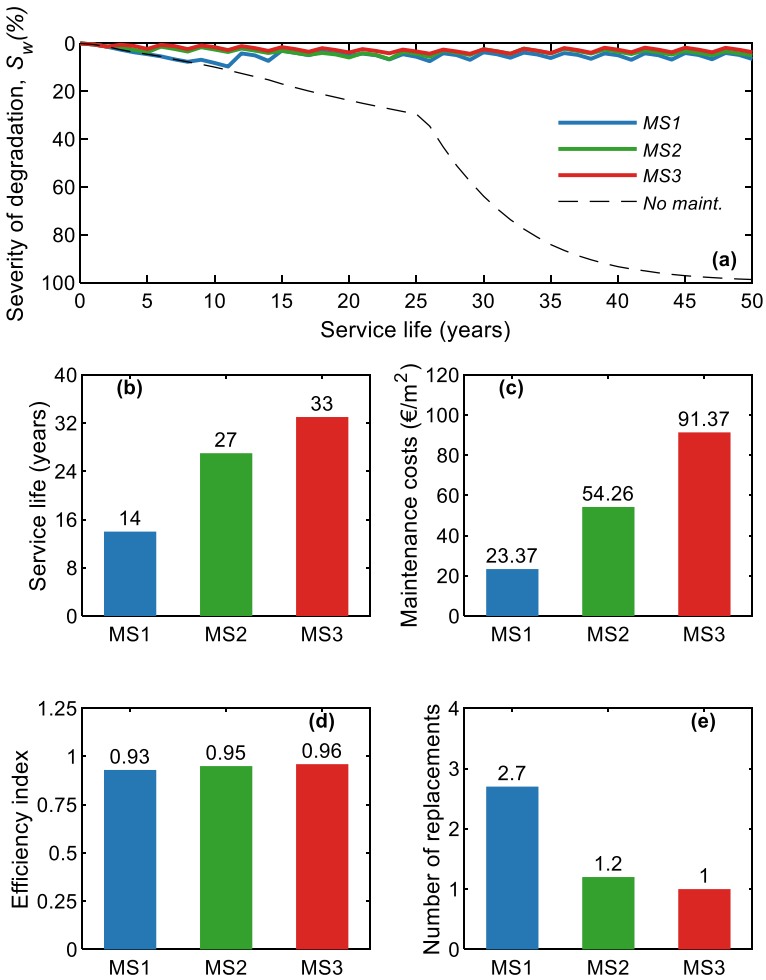


**Fig. 11** Impact of the different maintenance strategies in the wall renders: **a** degradation curves in terms of severity of degradation; **b** service life; **c** maintenance costs (inspection and maintenance activities); **d** efficiency index; and **e** number of replacements

replacements. Using a weighted sum method with subjective weighting methods, to reflect the users’ interests and perceptions, the results presented in Table 11 are obtained. In the four scenarios analysed in Table 11, the results reveal that MS1 (the most common maintenance strategy implemented in wall renders) is the least favourable alternative. Globally, MS2 is the most favourable alternative.

The results confirm that maintenance planning plays an important role to increase the durability of the building elements with a reasonable investment. The use of uncertainty in the maintenance model allows systematically computing the costs and benefits of each alternative and using these data to aid the decision-maker to select

**Table 11** Multi-criteria decision analysis

Scenario	1	2	3	4
Criteria	Weight, $\lambda$			
C1—Efficiency index (%)	33.3	50.0	25.0	25.0
C2—Maintenance costs (%)	33.3	25.0	50.0	25.0
C3—Total replacement (%)	33.3	25.0	25.0	50.0
Maintenance strategy	Standardised global rating, $x$			
MS1	0.00	0.00	0.00	0.00
MS2	1.00	0.87	1.00	0.98
MS3	0.92	1.00	0.00	1.00

the most rational and economical alternative over a given time horizon. In terms of practical application, the maintenance model allows the user to analyse a set of alternatives for a building element in simple steps if there is a sample of previous inspection records. The steps consist of defining: (i) the type and the material of the building element (Table 1); (ii) the time horizon of the analysis; (iii) the initial degradation condition; (iv) the time interval between inspections and its respective cost; (v) the different maintenance strategies, including the cost and the degradation condition of application; and, finally, (vi) the weights of the different criteria in the multi-criteria decision analysis.

The IST-UL research team is currently working on transposing the presented maintenance model to a Web-based application, as a new complement to the previously mentioned software. Such an application is expected to provide access to the maintenance model to decision-makers.

## 5 Conclusions

The research presented in this chapter follows a clear path from the most elemental types of systematisation of information to the complex use of data towards rational decisions. It is expected that such objective information in the field of building maintenance is used by decision-makers to optimise investments considering high levels of performance of buildings. In this way, the building stock is expected to answer the users’ needs, being continuously reused.

Initially, the collection of objective harmonised information was highlighted as a means to fight uncertainty in building inspection. Additionally, the collection of information using an inspection system was emphasised, since it allows obtaining more objective data. A global inspection system for the building envelope (used whether on paper or in a Web application) was presented as a way to guide inspection procedures, helping the surveyor during fieldwork and standardising the type of collected information.

Considering the mentioned objective data, it is possible to provide additional information for maintenance decision-making. That information is based on predictions of the remaining service life of building elements adjusted to their real degradation condition. Therefore, an additional Web-based application for service life prediction was developed.

Service life prediction is carried out based on several types of mathematical models, with varying levels of complexity and accuracy. Decision-makers can choose to use the best method of service life prediction according to their objectives and the available information.

Moreover, following the processes of harmonisation of information and adoption of service life prediction models, a condition-based maintenance model was developed, benefitting of the advantages of Petri nets to assess the influence of different maintenance strategies on the degradation of building elements. Petri nets are a mathematical and graphical tool that, besides analysing problems using a visual component, allows modelling complex information with acceptable accuracy levels. The proposed maintenance model tries to overcome different sources of uncertainty associated with the data used. It is found that the results reveal a good adjustment of predictions to reality.

The condition-based maintenance model includes four types of maintenance works: inspection, cleaning operations, minor interventions and total replacement. These types of works are combined in predetermined maintenance strategies, which typify the interventions carried out over time. Such maintenance strategies allow comparing not only the evolution of the degradation of building elements (according to interventions) but also the associated costs. Additionally, it is also possible to estimate the impact of maintenance activities on building users. The types of presented comparable data enable decision-makers to make better decisions, supported by sound and ample information. In this manner, the maintenance of buildings may be carried out according both to demand patterns and available budget, reaching balanced solutions for all stakeholders, based on objective information.

**Acknowledgements** The authors gratefully acknowledge the support of CERIS (Instituto Superior Técnico, University of Lisbon) and the Fundação para a Ciência e a Tecnologia (FCT) through the FCT project PTDC/ECI-CON/29286/2017 and the FCT Ph.D. Scholarship SFRH/BD/131113/2017.

## References

1. Madureira S, Flores-Colen I, de Brito J, Pereira C (2017) Maintenance planning of facades in current buildings. *Constr Build Mater* 147:790–802. <https://doi.org/10.1016/j.conbuildmat.2017.04.195>
2. Palmer RD (2006) *Maintenance planning and scheduling handbook*, 2nd edn. McGraw Hill, New York, NY USA
3. Flores-Colen I, de Brito J (2010) Discussion of proactive maintenance strategies in façades' coatings of social housing. *J Build Appraisal* 5:223–240. <https://doi.org/10.1057/jba.2009.21>

4. Flores-Colen I, de Brito J (2010) A systematic approach for maintenance budgeting of buildings façades based on predictive and preventive strategies. *Constr Build Mater* 24:1718–1729. <https://doi.org/10.1016/j.conbuildmat.2010.02.017>
5. Pitt TJ (1997) Data requirements for the prioritization of predictive building maintenance. *Facilities* 15:97–104. <https://doi.org/10.1108/02632779710160612>
6. Chartered Institution of Building Services Engineers (2008) *Maintenance engineering and management. A guide for designers, maintainers, building owners and operators, and facilities managers*. Chartered Institution of Building Services Engineers, London, UK
7. de Brito J, Pereira C, Silvestre JD, Flores-Colen I (2020) Expert knowledge-based inspection systems. In: *Inspection, diagnosis and repair of the building envelope*. Springer, Cham, Switzerland
8. CIB W86 (1993) *Building pathology: a state-of-the-art report*. International Council for Research and Innovation in Building and Construction, Delft, The Netherlands
9. Garcez N, Lopes N, de Brito J, Sá G (2012) Pathology, diagnosis and repair of pitched roofs with ceramic tiles: statistical characterisation and lessons learned from inspections. *Constr Build Mater* 36:807–819. <https://doi.org/10.1016/j.conbuildmat.2012.06.049>
10. Garcez N, Lopes N, de Brito J, Silvestre J (2012) System of inspection, diagnosis and repair of external claddings of pitched roofs. *Constr Build Mater* 35:1034–1044. <https://doi.org/10.1016/j.conbuildmat.2012.06.047>
11. Conceição J, Poça B, de Brito J et al (2017) Inspection, diagnosis, and rehabilitation system for flat roofs. *J Perform Constr Facil* 31:04017100. [https://doi.org/10.1061/\(ASCE\)CF.1943-5509.0001094](https://doi.org/10.1061/(ASCE)CF.1943-5509.0001094)
12. Conceição J, Poça B, de Brito J et al (2019) Data analysis of inspection, diagnosis, and rehabilitation of flat roofs. *J Perform Constr Facil* 33:04018100. [https://doi.org/10.1061/\(ASCE\)CF.1943-5509.0001252](https://doi.org/10.1061/(ASCE)CF.1943-5509.0001252)
13. Santos A, Vicente M, de Brito J et al (2017) Inspection, diagnosis, and rehabilitation system of door and window frames. *J Perform Constr Facil* 31:04016118. [https://doi.org/10.1061/\(ASCE\)CF.1943-5509.0000992](https://doi.org/10.1061/(ASCE)CF.1943-5509.0000992)
14. Santos A, Vicente M, de Brito J et al (2017) Analysis of the inspection, diagnosis, and repair of external door and window frames. *J Perform Constr Facil* 31:04017098. [https://doi.org/10.1061/\(ASCE\)CF.1943-5509.0001095](https://doi.org/10.1061/(ASCE)CF.1943-5509.0001095)
15. Sá G, Sá J, de Brito J, Amaro B (2014) Inspection and diagnosis system for rendered walls. *Int J Civ Eng* 12:279–290
16. Sá G, Sá J, de Brito J, Amaro B (2015) Statistical survey on inspection, diagnosis and repair of wall renderings. *J Civ Eng Manag* 21:623–636. <https://doi.org/10.3846/13923730.2014.890666>
17. Amaro B, Saraiva D, de Brito J, Flores-Colen I (2014) Statistical survey of the pathology, diagnosis and rehabilitation of ETICS in walls. *J Civ Eng Manag* 20:511–526. <https://doi.org/10.3846/13923730.2013.801923>
18. Amaro B, Saraiva D, de Brito J, Flores-Colen I (2013) Inspection and diagnosis system of ETICS on walls. *Constr Build Mater* 47:1257–1267. <https://doi.org/10.1016/j.conbuildmat.2013.06.024>
19. Pires R, de Brito J, Amaro B (2015) Statistical survey of the inspection, diagnosis and repair of painted rendered façades. *Struct Infrastruct Eng* 11:605–618. <https://doi.org/10.1080/15732479.2014.890233>
20. Pires R, de Brito J, Amaro B (2015) Inspection, diagnosis, and rehabilitation system of painted rendered façades. *J Perform Constr Facil* 29:04014062. [https://doi.org/10.1061/\(ASCE\)CF.1943-5509.0000534](https://doi.org/10.1061/(ASCE)CF.1943-5509.0000534)
21. da Silva C, Coelho F, de Brito J et al (2017) Statistical survey on inspection, diagnosis and repair of architectural concrete surfaces. *J Perform Constr Facil* 31:04017097. [https://doi.org/10.1061/\(ASCE\)CF.1943-5509.0001092](https://doi.org/10.1061/(ASCE)CF.1943-5509.0001092)
22. da Silva C, Coelho F, de Brito J et al (2017) Inspection, diagnosis, and repair system for architectural concrete surfaces. *J Perform Constr Facil* 31:04017035. [https://doi.org/10.1061/\(ASCE\)CF.1943-5509.0001034](https://doi.org/10.1061/(ASCE)CF.1943-5509.0001034)

23. Silvestre JD, de Brito J (2011) Ceramic tiling in building façades: inspection and pathological characterization using an expert system. *Constr Build Mater* 25:1560–1571. <https://doi.org/10.1016/j.conbuildmat.2010.09.039>
24. Silvestre JD, de Brito J (2010) Inspection and repair of ceramic tiling within a building management system. *J Mater Civ Eng* 22:39–48. [https://doi.org/10.1061/\(ASCE\)0899-1561\(2010\)22:1\(39\)](https://doi.org/10.1061/(ASCE)0899-1561(2010)22:1(39))
25. Neto N, de Brito J (2011) Inspection and defect diagnosis system for natural stone cladding. *J Mater Civ Eng* 23:1433–1443. [https://doi.org/10.1061/\(ASCE\)MT.1943-5533.0000314](https://doi.org/10.1061/(ASCE)MT.1943-5533.0000314)
26. Neto N, de Brito J (2012) Validation of an inspection and diagnosis system for anomalies in natural stone cladding (NSC). *Constr Build Mater* 30:224–236. <https://doi.org/10.1016/j.conbuildmat.2011.12.032>
27. Delgado A, de Brito J, Silvestre JD (2013) Inspection and diagnosis system for wood flooring. *J Perform Constr Facil* 27:564–574. [https://doi.org/10.1061/\(ASCE\)CF.1943-5509.0000342](https://doi.org/10.1061/(ASCE)CF.1943-5509.0000342)
28. Delgado A, Pereira C, de Brito J, Silvestre JD (2018) Defect characterization, diagnosis and repair of wood flooring based on a field survey. *Mater Constr* 68:1–13. <https://doi.org/10.3989/mc.2018.01817>
29. Garcia J, de Brito J (2008) Inspection and diagnosis of epoxy resin industrial floor coatings. *J Mater Civ Eng* 20:128–136. [https://doi.org/10.1061/\(ASCE\)0899-1561\(2008\)20:2\(128\)](https://doi.org/10.1061/(ASCE)0899-1561(2008)20:2(128))
30. Carvalho C, de Brito J, Flores-Colen I, Pereira C (2018) Inspection, diagnosis, and rehabilitation system for vinyl and linoleum floorings in health infrastructures. *J Perform Constr Facil* 32:04018078. [https://doi.org/10.1061/\(ASCE\)CF.1943-5509.0001229](https://doi.org/10.1061/(ASCE)CF.1943-5509.0001229)
31. Carvalho C, de Brito J, Flores-Colen I, Pereira C (2019) Pathology and rehabilitation of vinyl and linoleum floorings in health infrastructures: statistical survey. *Buildings* 9:116. <https://doi.org/10.3390/buildings9050116>
32. Tuna J, Feiteira J, Flores-Colen I et al (2015) In situ characterization of damaging soluble salts in wall construction materials. *J Perform Constr Facil* 29:04014127. [https://doi.org/10.1061/\(asce\)cf.1943-5509.0000616](https://doi.org/10.1061/(asce)cf.1943-5509.0000616)
33. Branco FA, de Brito J (2004) Handbook of concrete bridge management. ASCE Press, Reston, VA USA
34. Almeida Santos L, Flores-Colen I, Gomes MG (2013) In-situ techniques for mechanical performance and degradation analysis of rendering walls. *Restoration Build Monuments* 19:255–266. <https://doi.org/10.1515/rbm-2013-6606>
35. Bungey JH, Millard SG, Grantham MG (2006) Testing of concrete in structures, 4th edn. Taylor & Francis, Oxon, UK
36. Douglas J, Noy EA (2011) Building surveys and reports, 4th edn. Wiley-Blackwell, Chichester, UK
37. Glover P (2009) Building surveys, 7th edn. Butterworth-Heinemann, Oxford, UK
38. Seeley IH (1987) Building maintenance, 2nd edn. Palgrave, Hampshire, UK
39. Van Balen K (2015) Preventive conservation of historic buildings. *Restoration Build Monuments* 21:99–104. <https://doi.org/10.1515/rbm-2015-0008>
40. Houghton-Evans RW (2005) Well built? A forensic approach to the prevention, diagnosis and cure of building defects. RIBA Enterprises, London, UK
41. Pereira C, de Brito J, Silvestre JD (2020) Harmonising the classification of diagnosis methods within a global building inspection system: proposed methodology and analysis of fieldwork data. *Eng Fail Anal* 115:104627. <https://doi.org/10.1016/j.engfailanal.2020.104627>
42. Pereira C, de Brito J, Silvestre JD (2020) Harmonising the classification of the causes of defects in a global building inspection system: proposed methodology and analysis of fieldwork data. *Sustainability* 12:5564. <https://doi.org/10.3390/su12145564>
43. Pereira C, de Brito J, Silvestre JD (2021) Harmonized classification of repair techniques in a global inspection system: proposed methodology and analysis of fieldwork data. *J Perform Constr Facil* 35:04020122. [https://doi.org/10.1061/\(ASCE\)CF.1943-5509.0001529](https://doi.org/10.1061/(ASCE)CF.1943-5509.0001529)
44. Pereira C, de Brito J, Silvestre JD (2021) Harmonising correlation matrices within a global building expert knowledge-based inspection system. *Constr Build Mater* 272:121655. <https://doi.org/10.1016/j.conbuildmat.2020.121655>

45. Pereira C, Silva JN, Silva A et al (2021) Building inspection system software based on expert-knowledge. *J Perform Constr Facil* (accepted). [https://doi.org/10.1061/\(ASCE\)CF.1943-5509.0001700](https://doi.org/10.1061/(ASCE)CF.1943-5509.0001700)
46. de Brito J, Branco FA, Ibañez M (1994) Knowledge-based concrete bridge inspection system. *Concr Int* 16:29–63
47. Shohet IM, Paciuk M (2006) Service life prediction of exterior cladding components under failure conditions. *Constr Manag Econ* 24(2):131–148. <https://doi.org/10.1080/01446190500184535>
48. Mann L, Saxena A, Knapp GM (1995) Statistical-based or condition-based preventive maintenance? *J Qual Maintenance Eng* 1(1):46–59
49. Vicente R, Ferreira TM, Mendes da Silva JAR (2015) Supporting urban regeneration and building refurbishment. Strategies for building appraisal and inspection of old building stock in city centres. *J Cult Heritage* 16(1):1–14. <https://doi.org/10.1016/j.culher.2014.03.004>
50. Sjöström C (1985) Overview of methodologies for prediction of service life. In: *Problems in service life prediction of building and construction materials*. NATO ASI series, vol 95, pp 3–20
51. Gaspar PL, de Brito J (2008) Quantifying environmental effects on cement-rendered façades: a comparison between different degradation indicators. *Build Environ* 43(11):1818–1828. <https://doi.org/10.1016/j.buildenv.2007.10.022>
52. Gaspar PL, de Brito J (2011) Limit states and service life of cement renders on façades. *Mater Civil Eng* 23(10):1393–1404. [https://doi.org/10.1061/\(ASCE\)MT.1943-5533.0000312](https://doi.org/10.1061/(ASCE)MT.1943-5533.0000312)
53. Silva A, de Brito J, Gaspar P (2016) Comparative analysis of service life prediction methods applied to rendered façades. *Mater Struct* 49(11):4893–4910. <https://doi.org/10.1617/s11527-016-0832-6>
54. Silva A, de Brito J, Gaspar P (2016) *Methodologies for service life prediction of buildings: with a focus on façade claddings*. Springer, Switzerland
55. Silva A, de Brito J, Gaspar P (2011) Service life prediction model applied to natural stone wall claddings (directly adhered to the substrate). *Constr Build Mater* 25(9):3674–3684. <https://doi.org/10.1016/j.conbuildmat.2011.03.064>
56. Silva A, Gaspar PL, de Brito J (2014) Durability of current renderings: a probabilistic analysis. *Autom Constr* 44:92–102. <https://doi.org/10.1016/j.autcon.2014.04.002>
57. Silva A, Neves LC, Gaspar PL, de Brito J (2016) Probabilistic transition of condition: render façades. *Build Res Inf* 44(3):301–318. <https://doi.org/10.1080/09613218.2015.1023645>
58. Silva A, Dias JLR, Gaspar PL, de Brito J (2013) Statistical models applied to service life prediction of rendered façades. *Autom Constr* 30:151–160. <https://doi.org/10.1016/j.autcon.2012.11.028>
59. Vieira SM, Silva A, Sousa JMC, de Brito J, Gaspar PL (2015) Modelling the service life of rendered façades using fuzzy systems. *Autom Constr* 51:1–7. <https://doi.org/10.1016/j.autcon.2014.12.011>
60. Silva A, de Brito J, Gaspar PL (2012) Application of the factor method to maintenance decision support for stone cladding. *Autom Constr* 22(3):165–174. <https://doi.org/10.1016/j.autcon.2011.06.014>
61. Silva A, de Brito J, Gaspar PL (2015) Stochastic approach to the factor method applied to service life prediction of rendered façades. *J Mater Civ Eng* 04015130. [https://doi.org/10.1061/\(ASCE\)MT.1943-5533.0001409](https://doi.org/10.1061/(ASCE)MT.1943-5533.0001409)
62. Faber MH (2007) *Risk and safety in civil engineering*. Lecture notes. Swiss Federal Institute of Technology, Zurich
63. Arismendi R, Barros A, Grall A (2021) Piecewise deterministic Markov process for condition-based maintenance models—application to critical infrastructures with discrete-state deterioration. *Reliab Eng Syst Saf* 212:107540. <https://doi.org/10.1016/j.ress.2021.107540>
64. Lair W, Mercier S, Roussignol M, Ziani R (2011) Piecewise deterministic Markov processes and maintenance modeling: application to maintenance of a train air-conditioning system. *Proc Inst Mech Eng O J Risk Reliab* 225(2):199–209. <https://doi.org/10.1177/1748006XJRR347>



65. Løken E (2007) Use of multicriteria decision analysis methods for energy planning problems. *Renew Sustain Energ Rev* 11(7):1584–1595. <https://doi.org/10.1016/j.rser.2005.11.005>
66. Lounis Z, Madanat SM (2002) Integrating mechanistic and statistical deterioration models for effective bridge management. In: Proceedings of the 7th ASCE International conference on applications of advanced technology in transportation, Boston, USA
67. Phares BM, Washer GA, Rolander DD, Graybeal BA, Moore M (2004) Routine highway bridge inspection condition documentation accuracy and reliability. *J Bridge Eng* 9(4):403–413. [https://doi.org/10.1061/\(ASCE\)1084-0702\(2004\)9:4\(403\)](https://doi.org/10.1061/(ASCE)1084-0702(2004)9:4(403))
68. Corotis RB, Ellis J, Jiang M (2005) Modeling of risk-based inspection, maintenance and life-cycle cost with partially observable Markov decision processes. *Struct Infrastruct Eng* 1(1):75–84. <https://doi.org/10.1080/15732470412331289305>
69. Al-Ahmari A (2016) Optimal robotic cell scheduling with controllers using mathematically based timed Petri nets. *Inf Sci* 329:638–648. <https://doi.org/10.1016/j.ins.2015.09.053>
70. Chen Y, Li Z, Barkaoui K (2014) Maximally permissive liveness-enforcing supervisor with lowest implementation cost for flexible manufacturing systems. *Inf Sci* 256(6):74–90. <https://doi.org/10.1016/j.ins.2013.07.021>
71. Uzam M, Gelen G, Saleh TL (2016) Think-globally-act-locally approach with weighted arcs to the synthesis of a liveness-enforcing supervisor for generalized Petri nets modeling FMSs. *Inf Sci* 363:235–260. <https://doi.org/10.1016/j.ins.2015.09.010>
72. van der Aalst WM (2002) Making work flow: on the application of petri nets to business process management. In: Proceedings of the 23rd International conference on application and theory of Petri nets, Adelaide, Australia
73. Tang F, Guo M, Dong M, Li M, Guan H (2008) Towards context-aware workflow management for ubiquitous computing. In: Proceedings of the International conference on embedded software and systems, Sichuan, China
74. Ferreira C, Neves LC, Silva A, de Brito J (2020) Stochastic maintenance models for ceramic claddings. *Struct Infrastruct Eng* 16(2):247–265. <https://doi.org/10.1080/15732479.2019.1652657>
75. Ferreira C, Silva A, de Brito J, Dias IS, Flores-Colen I (2020) Maintenance modelling of ceramic claddings in pitched roofs based on the evaluation of their in situ degradation condition. *Infrastructures* 5(9):77. <https://doi.org/10.3390/infrastructures5090077>
76. Ferreira C, Silva A, de Brito J, Neves LC (2020) Impact of maintenance strategies on the serviceability of architectural concrete surfaces. In: *Life-cycle civil engineering: innovation, theory and practice*. CRC Press, Boca Raton, pp 593–599
77. Ferreira C, Silva A, de Brito J, Dias IS, Flores-Colen I (2021) Definition of a condition-based model for natural stone claddings. *J Build Eng* 33:101643. <https://doi.org/10.1016/j.jobbe.2020.101643>
78. Ferreira C, Silva A, de Brito J, Dias IS, Flores-Colen I (2021) Condition-based maintenance strategies to enhance the durability of ETICS. *Sustainability* 13(12):6677. <https://doi.org/10.3390/su13126677>
79. Marsan MA, Balbo G, Conte G, Donatelli S, Franceschinis G (1994) Modelling with generalized stochastic Petri nets. Wiley
80. Murata T (1989) Petri nets: properties, analysis and applications. *Proc IEEE* 77(4):541–580. <https://doi.org/10.1109/5.24143>
81. Madanat S (1993) Optimal infrastructure management decisions under uncertainty. *Transp Res Part C Emerg Technol* 1(1):77–88. [https://doi.org/10.1016/0968-090X\(93\)90021-7](https://doi.org/10.1016/0968-090X(93)90021-7)
82. Bocchini P, Saydam D, Frangopol DM (2013) Efficient, accurate, and simple Markov chain model for the life-cycle analysis of bridge groups. *Struct Saf* 40:51–64. <https://doi.org/10.1016/j.strusafe.2012.09.004>
83. Ellingwood BR (2005) Risk-informed condition assessment of civil infrastructure: state of practice and research issues. *Struct Infrastruct Eng* 1(1):7–18. <https://doi.org/10.1080/15732470412331289341>
84. Oberkampf WL, Helton JC, Joslyn CA, Wojtkiewicz SF, Ferson S (2004) Challenge problems: uncertainty in system response given uncertain parameters. *Reliab Eng Syst Saf* 85(1–3):11–19. <https://doi.org/10.1016/j.res.2004.03.002>



85. Frangopol DM, Liu M (2004) Life-cycle cost analysis for highways bridges: accomplishments and challenges. In: Structures 2004: building on the past, securing the future, Nashville, TN, USA
86. Ferreira C, Silva A, de Brito J, Dias IS, Flores-Colen I (2021) Criteria for selection of cladding systems based on their maintainability. J Build Eng 39:102260. <https://doi.org/10.1016/j.jobbe.2021.102260>

# Integrated Design of Building Projects: From BIM to Additive Manufacturing



Eric Forcael, Rodrigo García-Alvarado, Jaime Soto-Muñoz,  
and Jesús Alberto Pulido-Arcas

**Abstract** This chapter explores key aspects of integrated project design using the extreme collaboration methodology, which enables the construction of BIM models that integrate architecture, structures, and MEP, using a “war room” or “information room” (i-room) where various project specialists interact in real time. To achieve the highest degree of integration within a project, the BIM model is then sent to a robotic arm that through additive manufacturing techniques, prints concrete elements previously designed in the i-room—in short, total machine–machine integration (BIM-robot).

**Keywords** BIM-robot · Robotic arm · Concrete elements · Total machine–machine integration

## 1 Integrated Project Design

Productivity in the construction industry is a major challenge that makes slow progress and has the potential to speed up and improve process transformation and innovation. According to Barbosa et al. [1], the annual growth of global labor productivity in construction has averaged only 1% during the last two decades, compared to a growth of 2.8% for the total global economy and 3.6% in the manufacturing industry. At the Latin American level, the sector faces the classic difficulties associated with the industry. However, the low degree of technological incorporation is

---

E. Forcael

Department of Civil and Environmental Engineering, University of Bío-Bío, Concepción, Chile

R. García-Alvarado

Department of Architecture, University of Bío-Bío, Concepción, Chile

J. Soto-Muñoz

Department of Construction Science, University of Bío-Bío, Concepción, Chile

J. A. Pulido-Arcas (✉)

Graduate School of Arts and Sciences, Center for Research and Development of Higher Education, College of Arts and Sciences, University of Tokyo, Tokyo, Japan

e-mail: [jpulido@g.ecc.u-tokyo.ac.jp](mailto:jpulido@g.ecc.u-tokyo.ac.jp)

changing, which translates into greater digitalization and innovation every day. In Chile, according to the Chilean Chamber of Construction [2], efforts are being made by companies to ensure excellence along the value chain through integration and collaboration among all the actors involved in the production process. This includes the digitalization and industrialization of building processes to improve resource efficiency.

In this sense, as the development of technologies and software advances expeditiously, multidisciplinary interaction is becoming increasingly close, which improves collaboration between specialists from different disciplines. This is helping to increase coordination to combat building project problems more effectively from the design phase. Thus, integrated design tools are emerging and being put in place to make collaboration more fluid and productive, with greater communication, and therefore better buildings. An interesting result is the example of the BauMax company in Santiago de Chile, which since 2019 has a 40,000 m<sup>2</sup> plant solely dedicated to robotic building and construction 3D printing in concrete, with technology recognized throughout Latin America [3]. In this logic, additive manufacturing and building information modeling (BIM) are emerging trends, and according to Gradeci and Labonnote [4], both increase efficiency and productivity in the construction industry.

### ***1.1 Integration of Stakeholders, Systems, Business Structures, and Practices***

Integrated design is a planned strategy that deals with workflow and brings most of the participants together to interact with the project. However, integration has not progressed easily in the area of additive manufacturing. Compared to the rapidly developing interest in BIM methodology, this trend has not managed to become common practice for professionals. From this perspective, it would seem that more integrative ecosystems are needed to create a workplace where a variety of tools coexist and are supported by good work practices.

In this sense, war rooms or real-time design are a good example of unification in project visualization, as they provide an excellent opportunity for experimentation and the interaction increases confidence in the design for all stakeholders. Collaboration results from precise technical comments and management feedback that continually contribute to a more efficient project model.

However, are war rooms the best multidisciplinary work and performance evaluation strategy? What evidence of productivity improvement is needed to advance integration? Is it possible to incorporate additive manufacturing faster than traditional processes? This paradigm shift focuses on collaboration between project stakeholders interacting through models in the same environment and has the potential to eliminate inconsistencies and the duplication of elements within a project. Currently, a federated model [5, 6] makes it possible for professionals to review and combine in cases

where it is necessary to coordinate several digital models from different disciplines. This increases project consistency at various points in the process. Nevertheless, this is not done instantaneously, and therefore, the concept of the integrated model emerged to improve the design process. This kind of model resolves design conflicts between professionals since the model is developed in real time. Alternately, additive manufacturing or additive layered manufacturing is a form of industrialized construction carried out in a controlled manner through integrated design, thus creating three-dimensional shapes and objects with different materials, generally in layers. It offers a perfect combination of improved performance, complex geometries, and simplified production for parts or a building's construction system.

Collaboration will change the way in which both companies and public institutions develop their projects. Whether from the same site or remotely, several professionals will be able to work collaboratively on the design and construction of the same project simultaneously. The foundation of BIM methodology is conducive to integrated design, and additive construction is the obvious link in the value chain that interests stakeholders. The use of BIM for additive construction works as a single information base that empowers the design and construction team in relation to the owner, regulators, or the community by providing up-to-date information, and enabling them to respond with quick decisions and a high degree of certainty.

## ***1.2 Big Data***

In the construction industry, big data is inherent: building design, construction, and operating processes generate a large volume of data. In both additive manufacturing and building information modeling, information emerges from different processes and does so in an orderly or at times not so orderly fashion. Nonetheless, integration occurs with greater certainty, better data, and more information that will only continue to grow over time.

Then, the focus is no longer on macrodata, but rather on big data, which is an effective input for decision-making that collaborates efficiently in the different stages of the construction process. From this point of view, the most conventional information management systems are based on different applications. However, by planning and designing a project in a war room, many and more important data sets are created. What makes them valuable? First of all, the amount or volume of information requires the development of storage clouds, and consequently, access necessitates organization of the participants. Second, the combinations of data represent the complexity of the variables involved, thus resulting in models, graphs, spreadsheets, and other resources. Also, the potential for growth throughout the life cycle of the building is very high, especially during use. This requires quality controls and data accuracy in specially prepared ecosystems. Unlike other industries, organizations and their analysts in the construction sector often develop their own management, processing, or analysis systems using different technologies. Hence, regarding integrated design,

big data is still receiving unstructured data generated by modern digital design technologies, although there are opportunities to raise the standard of work. It is anticipated that in the coming years, the use of big data will have a significant impact on decisions in the building design process, thereby providing accurate analyses to professionals about buildings, their occupants, and building life cycles.

## 2 Extreme Collaboration Methodology

### 2.1 *War Room and Specialist Integration*

The extreme collaboration methodology (XC) was created by NASA to address the need to accelerate the design of space missions. The Jet Propulsion Laboratory (JPL) was founded to create this methodology [7]. The JPL is NASA's technological center responsible for the development of a number of projects by grouping different disciplines and working together at the same time, which enables information sharing and decision-making [8].

In the Architecture, Engineering and Construction (AEC) industry, the application of this methodology has been studied in building. Following NASA's example, it was implemented in the most reliable way possible, with sessions lasting no more than 3 or 4 h and 3 days a week [9]. For constructive projects, the AEC industry proposes work teams comprised of architects, construction engineers, and engineers from the disciplines required by the project [10, 11].

Although this methodology requires great effort and concentration on the part of the participants, it also has a number of important advantages in the construction industry. They include a shorter design stage, the ideal distribution of information among participants, optimization of estimation of life cycle costs, and improvements in the quality of construction projects. This is the result of detecting errors at an early stage, minimizing poorly performed tasks [10, 12], and reducing and resolving misunderstandings and errors when they arise [8].

There are two active communication networks in this methodology: an electronic network and a human network, which enable the flow of information during XC sessions [7]. The human network is comprised of the team working during the session, in which members participate actively and very close communication occurs between specialists [13]. This generates various kinds of interactions between individuals, since they are continuously coordinating and adapting information to solve the problems that arise in each of their specialties [14].

Alternately, the electronic network consisting of input and output devices, such as computers and monitors, transfers the information during the session, thus keeping the participants informed of each joint decision made in order to update the calculations of each specialist in a timely manner [10]. It also makes it possible to visualize and manage project data and its design instantaneously from each specialist's

computer, which improves the real-time visualization of the project’s development and changes that have been generated together [14].

One of the limitations of working with XC is directly linked to the participants as individuals and as a collective: This methodology requires people with flexible personalities, who adapt easily and are able to tolerate the burden of and stress from conflicts in the sessions [15]. Also, they must be able to withstand the strain caused by the noise from the permanent interaction between participants, and the pressure resulting from time constraints, among other technical difficulties associated with 3D modeling [14]. Additionally, there are other challenges to applying this methodology. In particular, users may have little experience with this manner of work, which can cause delays in decision-making due to conflicts and disagreements between the different disciplines [7].

All of these aspects related to the XC methodology may be implemented in what is known as an information room (i-room) or war room, which is a physical space devoted to integrated project design. The following are some recommendations for implementing an extreme collaboration environment:

First, it is necessary to have a physical space or war room dedicated to integrated project design in which to carry out the actual process, such as that shown in Fig. 1.

Along with an i-room, the work sessions must be planned. To measure the behavior of individuals participating in a project, qualitative and quantitative data may be obtained in each session. The collaborative work sessions are held a certain number of days per week, for a determined number of hours per session. In summary, Table 1 shows an XC methodology proposal.



**Fig. 1** Example of an integrated project design space where the XC methodology can be implemented

**Table 1** Extreme collaboration proposal

Item	Description
Number of participants	Six per session
Place	Integrated design space (i-room)
Hours per session	Three
Number of sessions per week	Three
Number of screens projected	Three
Number of participants per table	Six
Number of worktables	One
Specialists who make up the team	One budget manager
	One structural project manager
	One architectural project manager
	Three MEP project managers

## 2.2 *Dynamic and Effective Collaboration*

Research conducted by García et al. [16] evaluated extreme collaboration with BIM modeling to teach building projects and documented multiple benefits of dynamic, effective collaboration. This experience combined extreme collaboration and information modeling to evaluate cooperation among architecture and engineering students. Student responses via questionnaires and interviews were assessed to improve strategies for teaching BIM models. Although limited to the field of education and a small group of participants, findings suggest certain conditions in order to conduct similar experiences more effectively. Based on the observations and results achieved, it is recommended that a more detailed schedule be available regarding expected production and design requirements, as well as the work sequence, and that a coordinator and/or one of the participants be designated to lead decision-making and planning. Another interesting finding was the different degrees of progress and the lack of coordination between the individuals and the team; in particular, the architectural design showed a weak connection with the MEP and the environmental design, as well as the budget. This demonstrates that processes should be sequential and integrated at all times and enable feedback between the different disciplines required by the project. Likewise, beyond the roles established prior to the activity, a proper balance between the time spent, magnitude, and singularity of each individual assignment was also found to be relevant, as well as participant training and experience. In addition, it was beneficial to provide occasions for critical reflection, which improve design quality and result in projects that are not only comprehensive and effective, but also pertinent and significant.

Notwithstanding the benefits previously mentioned and the potential of the extreme collaboration methodology combined with BIM in the professional and

academic spheres, it is necessary to continue carrying out new XC experiences. They should include not only a greater number of professionals and construction areas, such as industrial, roads, and hospitals, but also address other aspects such as the difficulties of working together in a single space under pressure. This contrasts with the significant benefits of extreme collaboration, specifically the reduction of project development times, among many others.

### 2.3 Log Data Mining

The XC methodology can be employed in log data mining; BIM log file information can provide insights into the behavior and performance of BIM users. Models for collaboration should be created to increase user performance [17]. BIM software like Autodesk Revit creates a database of log files that contains all pertinent information, from computer specifications to user commands. It also functions to coordinate project professionals, which results in fewer execution errors, shorter production times, and lower-related costs [18].

Recently, Forcael et al. [19] studied a group of five professionals from different building project disciplines: civil engineering, building engineering, and architecture. All were trained in both the BIM software employed and how to work collaboratively in different roles. Figure 1 shows how the participants worked in a single environment with modeling technologies. The activity lasted for 3 weeks; time was allocated to 18 sessions, each of which lasted for 3 h. The participants, who were mainly junior professionals, were tasked with designing a two-story educational building together. Roles were assigned to each professional, and all worked on a shared BIM model with different editing permissions. Their contributions were recorded in a log file stored in Revit, which made it possible to establish how they interacted. Finally, an

**Table 2** Total number of commands executed by each designer

		Contributory commands			Non-contributory commands			Contributory versus backwards
		G	NG	C	N	U	B	
Architectural	9430	1770	169	372	3291	3228	657	2150
Structural	6433	1353	203	228	2470	920	1296	1425
Mechanical	5555	1032	121	141	2496	726	1039	1052
Electrical	6523	1296	165	184	2918	994	966	1401
Plumbing	7360	1190	366	165	3101	776	1762	1309

Reprinted from [19]

*G* geometrical modeling; *NG* non-geometrical modeling; *C* collaborative; *N* necessary; *U* unnecessary; *B* backwards



analysis of that information showed relevant trends (Table 2), including the prevalence of geometric modeling from the architect, and the difference in contributory vs backwards commands for all the project professionals.

Such studies allow BIM managers to identify bottlenecks, dysfunctionalities, and lack of coordination between professionals involved in building design, thereby enabling better planning and efficiency in the overall design process of the final product.

### 3 Creation of BIM Models

The creation of BIM models is an essential step toward achieving the effective integration of digital design and its materialization through additive manufacturing. BIM is basically an information management system; a BIM system has two distinctive features: First, the digitized information represents a material reality, and second, since the BIM model is a digital representation of that material reality, all information must be spatially referenced. In additive manufacturing, an automated system interprets the information contained in a BIM database to build a real model. Therefore, the proper coordination of the BIM models with the automated construction system is essential to successfully complete the process.

#### 3.1 *Is BIM Best Information Management?*

BIM is an information management system. The next logical question that arises is whether BIM is the *best* information management system. One of the classic problems in the construction industry, which has been studied by numerous authors, is its low productivity. One of its causes appears to be poor information management during the construction process. The emergence and popularity of BIM systems in the last decade seemed to put an end to this situation. However, since BIM systems were initially developed by private companies, compatibility between different systems has not always been perfect.

In recent years, international and national organizations have implemented initiatives to standardize the exchange and management of information between different BIM systems to effectively make BIM the best possible information management system. At the international level, the International Standard Organization (ISO) [20] has made notable efforts to publish standards that regulate the organization and digitization of building and civil engineering information, including BIM systems. These standards are developed through the collaboration of the national organizations of member countries; in the case of Chile, this work is carried out by the National Standards Institute (INN) [21], through efforts in two areas: first, to provide suggestions

for modifying international standards (ISO) during their drafting process, with a so-called mirror committee, and second, by translating the international standards into Spanish in order to adopt them nationally as the country's official standards.

The classification and organization of information are essential to achieve perfect coordination between all the actors involved in the construction process, but especially in additive manufacturing. In general terms, this set of standards defines a taxonomic model makes it possible to define objects by means of properties and concept groups, as well as to define the relationships between concepts. A concrete example may help to illustrate. Imagine that a designer wants to build a concrete wall using additive manufacturing. The first step is to model the element in BIM. The name of each element must always be recorded in English, e.g., wall, even if the designer names it in his native language when using the BIM system. This avoids discrepancies in the transmission of information. If the wall has a height of 2 m, this information must be recorded in a unit that can be represented by the symbol "m", i.e., meter. In this way, "2 m" will be understood in any context as "two meters", and the system will not accept other expressions that would be confusing, such as "2 mts". As another example, dates must always be given in the form "YYYY.MM.DD". Therefore, May 31, 2021, will be stated as "2021.05.31". This global standardization permits immediate, error-free transmission of information between BIM systems and additive manufacturing machinery in any context and under any circumstances.

The second initiative, in this case at the national level, is the development of BIM standards for the exchange of information between project stakeholders. Additive manufacturing is the last step, but beforehand different actors exchange information at different levels, and this is where discrepancies often arise that delay project progress. In 2018, the Digital Transformation Committee, a public organization belonging to CORFO, the Chilean Production Development Corporation, began drafting a BIM standard for public projects [22], with the aim of facilitating the exchange of information between the clients (the public administration) and the private companies awarded contracts. The project concluded successfully with the publication of the standard in 2019, with versions in Spanish and English.

The scope of application of this national standard is different from that of ISO standards, since the latter focus on communication between a BIM database and an additive manufacturing system and the former on communication between actors. Nonetheless, this standard is also very relevant because of its fundamental objective: to regulate the exchange of information between the intervening agents. The document includes the minimum specifications to be followed by each of the elements of a building project. It also introduces a very enlightening concept: level of development (LOD). Levels of development correspond to the phases of a construction project: planning, design, construction, and operation or use. The levels of development express the degree of information expected for each element: preliminary, general information (LOD-1); basic, approximate information (LOD-2), detailed information (LOD-3); detailed, coordinated information (LOD-4); detailed manufacture and commissioning information (LOD-5); and detailed information on the built elements and their management (LOD-6). Again, the objective is to avoid confusion in the exchange of information by replacing expressions such as "send me a

detailed plumbing plan” to “send me the plumbing at LOD-3 level for the design phase”. Another innovative concept is that of BIM roles, which specify the responsibilities to be assumed by each of the participants in the information management process. There are five basic roles: leadership, validation, modeling, coordination, and management.

In the case of user–machine communication, LOD levels are of utmost importance. A suitable level would be LOD-5, which contains all the details of manufacture and installation. This includes the position of each element in space and its manufacture in time.

### ***3.2 Virtual and Augmented Reality***

The creation of BIM models is associated with the presentation of information in a visual format, which necessitates the development of three-dimensional models. Before the advent of virtual representation systems, buildings were represented with a combination of two-dimensional paper plans and three-dimensional scale models. Since the 1980s, one of the biggest challenges has been the representation of reality in three dimensions on the flat screen of a computer in two dimensions, mainly due to the technical limitations of software and hardware. In the last ten years, the industry’s explosive progress has managed to overcome these limitations and has incorporated new virtual representation technologies that have been implemented in a multitude of fields, among them construction. Two of these technologies stand out: virtual reality and augmented reality.

In a broader framework, virtual reality and augmented reality are a part of the concept of Construction 4.0, which can be defined as the conjunction of two factors: the digitalization of the construction industry and the industrialization of building processes [23]. Construction 4.0 can be divided into seven major areas: Internet of things (IoT), computer-aided design technologies (BIM), 3D printing (additive manufacturing), big data, artificial intelligence and robotics, new materials related to industrialization, and virtual and augmented reality. There are certain differences between virtual reality (VR) and augmented reality (AR). VR is an alternative reality entirely computer generated and not located in real space, whereas AR is a partially computer-generated environment, superimposed on physical reality and located in space. VR can be considered a 100% virtual space and AR halfway between the real environment (RE) and the virtual world (VE) (Fig. 2).

An additive manufacturing process starts with a virtual reality model (VR) and ends with a real object (RE). First, the virtual object is designed in BIM, and then the information is transmitted to a robotic printing system that transforms the virtual object into a real one, thereby giving it a location in physical space. This communication process is complex, and there are still few studies that address this problem.

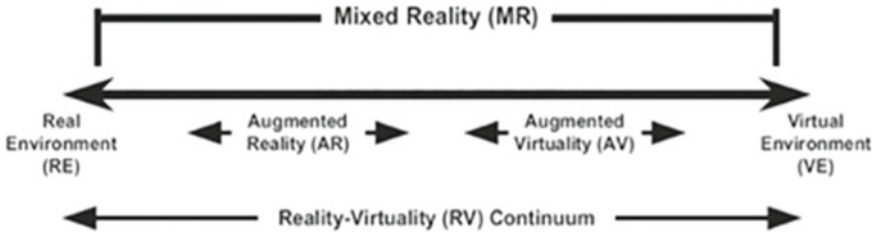


Fig. 2 Reality–virtuality (RV) continuum [24]

In this sense, a noteworthy pilot experience was carried out at the Universidad del Bío-Bío, Chile, a pioneer in Latin America. The main objective was to develop protocols for BIM communication with 3D concrete printing [24]. First, a virtual object was designed using the BIM software Autodesk Revit. Then the data was exported to the point cloud software Dynamo. The next step, perhaps the most laborious, was to translate the Dynamo point cloud to the software that controlled the robotic arm, in this case a KUKATM model. The key steps are obtaining the point cloud that captures the contour of the figure and creating a dynamic 3D printing trajectory, that is to say, one that takes into account the parameter of time, or what is printed first and what is printed next.

### 3.3 Modeling Performance

Once the real model has been printed, it is necessary to evaluate the performance of the whole process. A balance should be sought between rapid manufacture and correctly printing the real object, which accurately reproduces the original model designed in BIM. In this sense, the aforementioned study [21] concluded that considering the printed object’s position and printing speed, the accuracy of the robotic arm was satisfactory, with confidence levels between 98 and 99%. The relationship between printing speed and the spacing of the point cloud elements has a quasi-linear relationship, and speed control is essential, since concrete is a material that needs time to set. Other recent studies on an experimental scale have shown similar results, considering that the balance between printing time and the characteristics of the printed material is fundamental to transmit the information from a virtual environment to the real object [25]. The authors emphasize that the printing time between layers and the robotic arm’s programmed path are essential to avoid the deformation of the final object due to the accumulation of weight on the uncured material. Although experimental studies, these findings are considered significant to address the future debate on the precision and efficiency of robotic construction with additive manufacturing at the commercial scale.

## 4 Additive Manufacturing Techniques

Additive manufacturing is a new process based on the deposition and solidification of material, usually controlled by digital systems, which produces building elements directly from their design. Hence, it is closely related to integrated building modeling. Additive manufacturing technologies consist of nozzles hung from sliding gantries or articulated robotic arms that print different parts or complete constructions in 3D (Fig. 3). Around the world, university teams and entrepreneurs are experimenting with the capabilities of this technology using different machines and materials.

### 4.1 Complex Geometries

The design of a shape for additive manufacturing must decompose the geometric volume into a linear path for the printing nozzle, usually in horizontal layers. Therefore, the volume is first subdivided into slices, known as slicing, and then a path is traced in each layer according to the size of the print filament. The path can either move along the edge of the shape, forming a hollow volume, or complete the whole interior with a mesh, as well as linking the individual layers in a continuous path. This shows that production of the shape is not dependent on additional elements or quantities of material, but rather only on the range of the equipment. Within that volumetric range, different shapes can be created.

This capability is radically different from traditional construction processes that rely on pre-prepared elements, such as boards, panels, and blocks, which have been standardized for large-scale use with orthogonal machinery. In addition, their installation on-site must be coordinated according to their specific dimensions. For this reason, standard installation is the most appropriate, and any variation in this respect generates more work. Thus, the resulting building tends to conform to orthogonal volumes with similar magnitudes, which means that the activities that take place in



**Fig. 3** Printed concrete pieces

the interior spaces, as well as the relationships between them, are subject to standard industrial solutions. This weakens their performance and local identity.

Additive manufacturing makes it possible to reproduce elements similar to those made with conventional construction. However, one of its greatest potentials is the diversity of shape that can be achieved without increased costs or resources involved. In fact, straight edges require greater acceleration of the control motors due to the abrupt change in direction for their production, and horizontal sections are less stable. In contrast, sinuous shapes are easier to manufacture and more stable. Thus, the printing of construction elements promotes greater geometric variety and can produce complex shapes that are more difficult to achieve with traditional building techniques.

3D construction printing permits geometric complexity that is evident from the first examples created [3]. Although some projects reproduce traditional house shapes or elements, most manufacture novel, diverse forms by exploring the new capabilities of this technology. For instance, the Universidad del Bío-Bío, Chile, printed urban architectural elements, vertical and horizontal pieces with different shapes that permit greater diversity of use and are naturally attractive (Fig. 4).



**Fig. 4** Printing at the Universidad del Bío-Bío

## 4.2 *Simplified Fabrication*

3D construction printing is based on the extrusion of a fast-setting fluid material, which is deposited by moving the extrusion nozzle horizontally. This forms a filament that is normally 2–3 cm high by 3–15 cm wide. By placing several successive filaments vertically on top of each other, a three-dimensional volume is formed according to the nozzle's path, which is usually defined by perimeter filaments.

This procedure is quite different from conventional building based on the assembly and reinforcement of pre-cut elements, such as timber framing or ceramic brick masonry. It is similar to pouring concrete into formworks but differs in that, and it does not require these supports to be installed and subsequently removed. Therefore, this technology reduces the processes involved in the elaboration of construction elements and consequently also the time, resources, personnel, transport, and production of materials.

These production advantages simplify the manufacturing process but involve several new steps in the execution phase. The mixtures must be comprised of agglomerates and aggregates that can be pumped and set quickly, several minutes, in order to support the printing of successive layers. Most of the experiences in 3D construction printing have used cementitious mixes with carefully added chemical additives. These include either accelerators, retarders, or plasticizers, and a combination of fine and semi-fine aggregates, with a variable portion of water depending on the relative humidity and volumes, distances or execution times. Various tests have been carried out with fiber reinforcement to reduce refraction, as well as active aggregates that reduce the amount of cement and the mix's environmental load [26]. Successful experiments have also been conducted with mixes based on artificial polymers [27] or natural clays [28]. This opens up the possibility of using soils from the same or nearby construction sites.

In addition, to ensure the mix's open time (between its fluidity for pumping and initial solidification to support successive layers), an adequate "constructability" of the filament must be achieved in terms of its plasticity, continuity, and ability to maintain its dimensions. The expansion generated when leaving the nozzle and the vertical settlement due to its own weight and that of the layers above it must be regulated, as well as that of the whole element to avoid premature collapse. This may occur through displacement of the vertical axis or of the horizontal position of the layers and is usually avoided with sinuous curves or interior reticulation to counteract straight sections.

Likewise, the preparation and pumping of the mix must be managed. Usually, these processes are partially provided on-site, while in printed fabrication a continuous path is created. Furthermore, there is a time delay between control of the mixer and pump, and the delivery nozzle. Therefore, simultaneous regulation must be achieved. Alternately, the positioning of equipment and the provision of supplies at the construction site in relation to the location of the elements to be built require adequate planning and placement in the field. Also, if elements are prepared in a factory, they must be

produced on strong movable platforms and later transported and put in place on-site. In this way, manufacture is becoming more effective.

### ***4.3 Improved Performance***

The design possibilities and process of additive manufacturing result in various opportunities to improve building performance. The geometric flexibility inherent in 3D-printed construction, defined by its capacity for resistance and extended by digital design, optimizes different areas of building performance. For example, this manner of building can improve the configuration of spaces to accommodate the different activities that normally occur in central areas, by reducing the corners or orthogonal perimeters required by conventional construction. Although this may conflict with furnishings and hinder some mechanical, electrical, and plumbing installations, it partially reduces built volumes, concentrating them in central spaces with continuous envelopes. All of this results in a novel interior environment and unique architectural expression.

Also, shape can be optimized according to the resistance requirements of each element, which are normally defined by the most unfavorable conditions. Therefore, the size of structural elements depends on the section that must resist the greatest stress. Thus, a large part of the rest of the piece, which is under less stress, is composed of more material than necessary. The analysis of topological optimization of resistant volumes defines precise shapes according to specific structural requirements. This can reduce material use nearly 50%, which in turn results in decreased costs, production times, and environmental load for the construction. However, the forms created are usually harder to execute and adapt to architectural conditions.

These capabilities apply to homogeneous elements, which can take advantage of additive manufacturing's ability to create diverse shapes to generate strength-optimized forms. Nevertheless, most current buildings combine materials to increase their resistance, as is common in reinforced concrete. This possibility is still under development in 3D-printed construction. A variety of strategies are being explored to produce reinforced elements: from using different mixtures or incorporating fibers to printing around reinforcements or putting them into place during printing. In buildings of greater height or surface area, and especially in earthquake-prone countries like Chile, this is a relevant challenge.

Moreover, employing printed elements as walls, floors, or roofs also requires additional layers to comply with building codes. Additive manufacturing using cementitious mixtures in the normal dimensions usually meets acoustic or fire resistance requirements for habitable buildings, although the thermal conditions must be improved with most construction systems in warm or cold climates. The habitual process of printing walls by means of edge layers generates empty spaces that can be filled with insulation of different types, thereby reducing thermal transmittance. However, the common strategy of interior reticulation produces thermal bridges and must therefore be replaced by supports of another material. Another unique



strategy is to print edges using a material with high thermal resistivity, such as injected polyurethane, and fill the interior with a cementitious mixture and structural reinforcement. It is important to consider that the printed construction process provides continuity in the walls, especially when they are produced on-site. This contributes to the airtightness of interiors, which substantially reduces energy demand and contributes to building sustainability.

The installation of mechanical, electrical, and plumbing is another challenge in 3D-printed construction. Either pieces are removed from elements with interior openings or piping is installed through them or on top of printed components. These strategies require adequate project planning, from the main elements to mechanical, electrical, and plumbing installation that takes advantage of digital control and integrated process modeling. It also promotes the possibility of automating these installations.

Finally, production must be managed in stages, both the integration of the printed parts with the other building elements and printing itself, which consists of a sequence of paths according to the equipment used. A gantry can be used to move a nozzle throughout a building, which requires planning at height and a continuous material supply. One or more robotic arms are also necessary to work on different parts or prepare elements that are assembled on-site. This implies the modulation of parts that must be related to the installation tasks, floors, roofs, structures, etc., through integrated digital modeling.

#### 4.4 Robotic Technologies and Construction 3D Printing

The relationship between BIM modeling, robotic manufacturing, information integration, performance, local adaptation, and reuse is presented in Fig. 5.

3D-printed construction not only incorporates the new process of additive manufacturing elements, but also directly links information between planning and production. Automated technologies require digital control of the extrusion nozzle, which executes the geometry of the design. Thus, a link is established between the project, mainly created in BIM, and the building, through the digital manufacturing of some components. Although different stages, professionals in charge, and tasks exchange

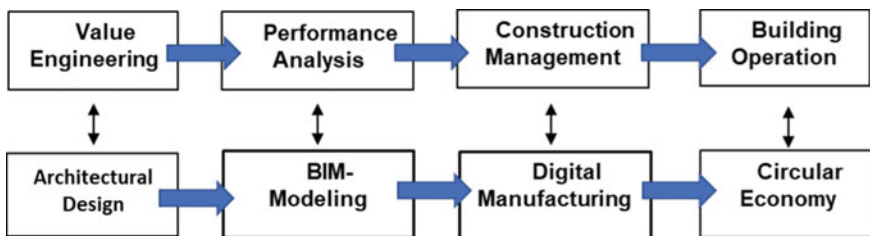


Fig. 5 Relationship between BIM and robotic manufacturing

information in different formats, in the end a logical flow of data is produced (Fig. 5). On the one hand, BIM modeling incorporates the value definitions of the design by integrating the materials and construction processes. On the other, digital production takes project data and relates it with construction management and subsequent building use. Therefore, a flow of information must be managed from the very beginning until construction.

In this digital chain of work, capacity for analysis increases due to feedback from different aspects of the construction process. For example, authors such as Cheng et al. [29] and Martínez-Rocamora et al. [30] reviewed the amount of material needed to ensure the stability of printed walls according to their curvature. They found that in the modeling phase, a number of shape options should be considered, along with the amount of material used and production times with robots, according to cost and construction times. In this way, the most efficient design alternatives and the most appropriate on-site processes can be determined, in addition to achieving greater efficiency that integrates different construction requirements.

This capability can also be attained at the other end of the process. During construction, all the project's digital information is available, and solutions can be analyzed and redesigned in the event of any difficulty or to better address local conditions. For instance, on-site problems, a change in the client, or higher material or process costs can be promptly studied and modified. This facilitates a building's local adaptation, hence ensuring its appropriateness and the flexibility of large investments in equipment and new construction systems.

Additionally, these processes result in better environmental performance. Energy consumption is more efficient for machinery, supplies, and building operation. Materials or elements used on-site can also be reused in preexisting or future constructions. Modeling and automation can be integrated in a circular economy paradigm. These new technologies help to meet productivity goals and imply labor reconversion, along with their construction and sustainable development achievements. They maximize efficiency through information control, but with a social and environmental focus.

## 5 Final Considerations

Finally, a few reflections may be made on the road ahead. With teams of professionals increasingly coordinating projects together synchronously, it is necessary to use a variety of information technologies to maximize the flow of communication and information. The topics discussed in this chapter provide the competitive advantage of efficiency and quality in project coordination. In this framework, the current environment with the greatest technological wealth to foster extreme collaboration is through artificial intelligence. In this context, machine capabilities accelerate and make collaborative work more efficient, which resolves aspects of geometric or semantic reasoning and promotes creative solutions, learning on the part of the designers, and project planning.

So too, design novelty emerges from the process and enables a radical new way for expert project teams to work together. Design processes are changing the priorities of clients and construction professionals, adding power to work with more information in the easiest and fastest way possible. Evidence shows that artificial intelligence uses more advanced technological systems to analyze everyday activities and maximize human capabilities, iterating on the information it collects.

## References

1. Barbosa F, Woetzel J, Mischke J (2017) Reinventing construction: a route of higher productivity. McKinsey Global Institute
2. Cámara Chilena de la Construcción (2020) Impulsar la productividad de la industria de la Construcción en Chile a estándares mundiales. Matrix Consulting
3. García-Alvarado R, Martínez A, González L, Auat F (2020) Projections of 3D-printed construction in Chile Proyecciones de la construcción impresa 3D en Chile. *Rev Ing Constr* 35(1)
4. Gradeci K, Labonnote N (2019) On the potential of integrating building information modelling (BIM) for the additive manufacturing (AM) of concrete structures. *Constr Innov*
5. Solihin W, Eastman C, Lee YC (2016) A framework for fully integrated building information models in a federated environment. *Adv Eng Inform* 30(2):168–189
6. Pärn EA, Edwards DJ, Sing MC (2018) Origins and probabilities of MEP and structural design clashes within a federated BIM model. *Autom Constr* 85:209–219
7. Gu N, London K (2010) Understanding and facilitating BIM adoption in the AEC industry. *Autom Constr* 19(8):988–999
8. Chachere J, Kunz J, Levitt R (2003) Can you accelerate your project using extreme collaboration. A model based analysis. CIFE TR154
9. Kunz J, Fischer M (2012) Virtual design and construction: themes, case studies and implementation suggestions. Center for Integrated Facility Engineering, Stanford University
10. Jara C, Alarcón LF, Mourgues C (2009) Accelerating interactions in project design through extreme collaboration and commitment management—a case study. In: Proceedings of the 17th Annual conference of the international group for lean construction (IGLC-17)
11. Fruchter R (2014) Transformative 3D immersive collaboration environment in support of AEC global teamwork. In: *Computing in civil and building engineering*, pp 1425–1432
12. Becerik-Gerber B, Gerber DJ, Ku K (2011) The pace of technological innovation in architecture, engineering, and construction education: integrating recent trends into the curricula
13. Erdogan B, Anumba CJ, Bouchlaghem D, Nielsen Y (2008) Collaboration environments for construction: implementation case studies. *J Manag Eng* 24(4):234–244
14. Mark G (2002) Extreme collaboration. *Commun ACM* 45(6):89–93; Garcia ACB, Kunz J, Ekstrom M, Kiviniemi A (2004) Building a project ontology with extreme collaboration and virtual design and construction. *Adv Eng Inform* 18(2):71–83
15. Kunz J, Fischer M (2020) Virtual design and construction. *Constr Manag Econ* 38(4):355–363
16. García-Alvarado R, Forcael E, Pulido-Arcas JA (2020) Evaluación de colaboración extrema con modelación BIM para la enseñanza de proyectos de edificación. *Arquitectura Rev* 16(1):137–153
17. Zhang L, Ashuri B (2018) BIM log mining: discovering social networks. *Autom Constr* 91:31–43. <https://doi.org/10.1016/j.autcon.2018.03.009>
18. Bryde D, Broquetas M, Volm JM (2013) The project benefits of building information modelling (BIM). *Int J Project Manag* 31(7):971–980. <https://doi.org/10.1016/j.ijproman.2012.12.001>
19. Forcael E, Martínez-Rocamora A, Sepúlveda-Morales J, García-Alvarado R, Nope-Bernal A, Leighton F (2020) Behavior and performance of BIM users in a collaborative work environment. *Appl Sci (Switzerland)* 10(6). <https://doi.org/10.3390/app10062199>

20. ISO—International Organization for Standardization (n.d.). Retrieved 8 Oct 2021, from <https://www.iso.org/home.html>
21. INN | Instituto Nacional de Normalización (n.d.). Retrieved 8 Oct 2021, from <https://www.inn.cl/>
22. Soto C, Manriquez S, Godoy P (2019) BIM standard for public projects. Plan BIM Chile
23. Forcael E, Ferrari I, Opazo-Vega A, Pulido-Arcas JA (2020) Construction 4.0: a literature review. *Sustainability* 12(22):9755
24. Milgram P, Colquhoun H (1999) A taxonomy of real and virtual world display integration. In: *Mixed reality: merging real and virtual worlds*, vol 1, pp 1–26
25. Forcael E, Pérez J, Vásquez Á, García-Alvarado R, Orozco F, Sepúlveda J (2021) Development of communication protocols between BIM elements and 3D concrete printing. *Appl Sci* 11(16):7226. <https://doi.org/10.3390/APP11167226>
26. Ashrafi N, Nazarian S, Meisel NA, Duarte JP (2021) Experimental calibration and compensation for the continuous effect of time, number of layers and volume of material on shape deformation in small-scale additive manufacturing of concrete. *Addit Manuf* 47:102228. <https://doi.org/10.1016/J.ADDMA.2021.102228>
27. Botsman LN, Strokova VV, Ogurtsova YN (2019) Properties of energy effective concrete based on artificial granulated aggregate. In: *Materials science forum*, vol 945. Trans Tech Publications Ltd., pp 244–249
28. Luhar S, Suntharalingam T, Navaratnam S, Luhar I, Thamboo J, Poologanathan K, Gatheeshgar P (2020) Sustainable and renewable bio-based natural fibres and its application for 3D printed concrete: a review. *Sustainability* 12(24):10485
29. Chen Y, He S, Gan Y, Çopuroğlu O, Veer F, Schlangen E (2022) A review of printing strategies, sustainable cementitious materials and characterization methods in the context of extrusion-based 3D concrete printing. *J Build Eng* 45:103599
30. Martínez-Rocamora A, García-Alvarado R, Casanova-Medina E, González-Böhme LF, Auat-Cheein F (2020) Parametric programming of 3D printed curved walls for cost-efficient building design. *J Constr Eng Manag* 146(5). [https://doi.org/10.1061/\(ASCE\)CO.1943-7862.0001811](https://doi.org/10.1061/(ASCE)CO.1943-7862.0001811)